

**Energy Research and Development Division
FINAL PROJECT REPORT**

**INTEGRATED FORECAST AND RESERVOIR
MANAGEMENT (INFORM)
Enhancements and Demonstration Results
for Northern California (2008-2012)**

Prepared for: California Energy Commission

Prepared by: Hydrologic Research Center and Georgia Water Resources Institute



MARCH 2013
CEC-500-2014-019

PREPARED BY:

Primary Author(s):

Konstantine P. Georgakakos, Nicholas E. Graham, Theresa M. Modrick,
Eylon Shamir, Cristopher Spencer, Jason A. Sperfslage

Hydrologic Research Center
12555 High Bluff Drive, Suite 255, San Diego, CA 92130

Aris P. Georgakakos, Martin Kistenmacher, Huaming Yao, and Dong Ha Kim

Georgia Water Resources Institute
School of Civil and Environmental Engineering, Georgia Institute of Technology, 790
Atlantic Drive, Atlanta, GA 30332

Contract Number: 500-08-033

Prepared for:

California Energy Commission

Joe O'Hagan
Contract Manager

Joseph O'Hagan
Project Manager

Linda Spiegel
Office Manager
Energy Generation Research Office

Laurie ten Hope
Deputy Director
Energy Research & Development Division

Robert Oglesby
Executive Director

DISCLAIMER

This report was prepared as the result of work sponsored by the California Energy Commission. It does not necessarily represent the views of the Energy Commission, its employees or the State of California. The Energy Commission, the State of California, its employees, contractors and subcontractors make no warrant, express or implied, and assume no legal liability for the information in this report; nor does any party represent that the uses of this information will not infringe upon privately owned rights. This report has not been approved or disapproved by the California Energy Commission nor has the California Energy Commission passed upon the accuracy or adequacy of the information in this report.

ACKNOWLEDGEMENTS

The authors thank the California Energy Commission and the California Department of Water Resources for their support of this second phase of the project. Without the foresight of these Agencies to support INFORM, the advances that INFORM incorporates in forecast and management operations would not have been possible at this time.

The authors of this report are grateful for the continuing data and operational hydrologic forecast systems support of Robert Hartman and Pete Fickenschner of the California Nevada River Forecast Center (CNRFC) of the U.S. National Weather Service (NWS), for the support of Stephen Lord, Yuejian Zhu and Suranjana Saha from the National Centers for Environmental Prediction (NCEP) of the NWS with the global forecast system and climate forecast system information and data, and the support of Russell Yaworsky of the US Bureau of Reclamation with the implementation of the river and reservoir temperature models.

Joe O'Hagan, the Energy Commission project Manager for INFORM, supported this project with effective oversight and kept the multi-agency collaboration fruitful for the duration of the project. The authors thank him for his support. Special thanks go to the members of the multi-agency INFORM Project Advisory Committee (PAC) and their home Agencies for their support and assistance with project strategic decisions that were necessary given the ever present and evolving uncertainties in data and models of the operational environment, in which the INFORM demonstration project is conducted. The PAC members are:

John Andrew, California Department of Water Resources (Water Resources Planning)

Beth Faber, US Army Corps of Engineers, HEC Reservoir Management

Paul Fugitani, Bureau of Reclamation – Central Valley Operations

Robert Hartman, NOAA/NWS/CNRFC

Art Hinojosa, California Department of Water Resources (Flood Management)

Joseph O'Hagan, California Energy Commission

Pedro Restrepo, NOAA/NWS/North Central River Forecast Center (NCRFC)

Stuart Townsley, US Army Corps of Engineers, Operations/Safety

Yuejian Zhu, NOAA/NWS/NCEP

PREFACE

The California Energy Commission Energy Research and Development Division supports public interest energy research and development that will help improve the quality of life in California by bringing environmentally safe, affordable, and reliable energy services and products to the marketplace.

The Energy Research and Development Division conducts public interest research, development, and demonstration (RD&D) projects to benefit California.

The Energy Research and Development Division strives to conduct the most promising public interest energy research by partnering with RD&D entities, including individuals, businesses, utilities, and public or private research institutions.

Energy Research and Development Division funding efforts are focused on the following RD&D program areas:

- Buildings End-Use Energy Efficiency
- Energy Innovations Small Grants
- Energy-Related Environmental Research
- Energy Systems Integration
- Environmentally Preferred Advanced Generation
- Industrial/Agricultural/Water End-Use Energy Efficiency
- Renewable Energy Technologies
- Transportation

Integrated Forecast and Reservoir Management (INFORM) for Northern California: System Development and Initial Demonstration is the final report for the Integrated Forecast and Reservoir Management (INFORM) for Northern California: System Development and Initial Demonstration project (contract number 500-08-033) conducted by Hydrologic Research Center and Georgia Water Resources Institute. The information from this project contributes to Energy Research and Development Division's Energy-Related Environmental Research Program.

For more information about the Energy Research and Development Division, please visit the Energy Commission's website at www.energy.ca.gov/research/ or contact the Energy Commission at 916-327-1551.

ABSTRACT

This report describes the results from the second phase of the Integrated Forecast and Reservoir Management (INFORM) demonstration project. The project goal was to use operationally available information to produce reliable ensemble forecasts of reservoir inflow for the major reservoirs of Northern California for lead times from six hours to nine months, and to use these forecasts to generate risk-based trade-offs between multiple objectives such as hydroelectric energy generation, water conservation, flood control and fisheries to inform planning and operational decisions. A full-physics high resolution mesoscale model was implemented for the ensemble prediction of surface precipitation and temperature over the project domain in Northern California with lead times out to 16 days with six-hourly temporal resolution using initial and boundary conditions from the North American Model and the Global Forecast System operational forecast models at the National Centers of Environmental Prediction of the National Oceanic and Atmospheric Administration. An intermediate complexity regional model with high resolution was implemented to downscale the ensemble forecasts from the Climate Forecast System operational model at the National Centers of Environmental Prediction for lead times out to 41 days. Methodologies for model forecast adjustment to comply with the corresponding observations were formulated and tested. Hydrologic models were aligned with the operational flow prediction models of the California Nevada River Forecast Center. Reservoir and river water temperature and river routing models were developed and integrated into the decision model of INFORM and demonstration information was collected and analyzed. A new decision framework to manage forecast uncertainty was also developed and demonstrated.

The project resulted in forecasting precipitation and temperature over the subcatchments of the INFORM domain with high verification skill out to a week in advance. Reservoir inflow forecasts were produced for the shorter lead-times with good verification skill, while reliable long-range ensemble reservoir-inflow forecasts were produced for the decision component of the model that provided useful trade-off information for management decisions. The benefits from including detailed downstream routing and water temperature modeling were also demonstrated.

The project resulted in forecasting precipitation and rainfall over the subcatchments of the Integrated Forecast and Reservoir Management domain out to a week in advance. Reservoir inflow forecasts were produced for the shorter lead-times, while reliable long-range ensemble reservoir-inflow forecasts were produced for the decision component of the model that provided useful trade-off information. The benefits from including detailed downstream routing and water temperature modeling were also demonstrated.

Keywords: California Energy Commission, INFORM, reservoir management, ensemble weather forecasting, ensemble flow forecasting, climate forecasting for hydrology and water resources

Please use the following citation for this report:

Hydrologic Research Center (HRC) and Georgia Water Resources Institute (GWRI). 2013.

Integrated Forecast and Reservoir Management (INFORM): Enhancements and Demonstration Results for Northern California (2008-2012). California Energy Commission.

Publication number: CEC-500-2014-019.

TABLE OF CONTENTS

Acknowledgements	i
PREFACE	ii
ABSTRACT	iii
TABLE OF CONTENTS.....	v
LIST OF FIGURES	viii
LIST OF TABLES	xiii
EXECUTIVE SUMMARY	1
Introduction	1
Project Objectives	1
Project Results.....	2
Conclusions.....	4
Recommendations.....	5
Project Benefits	6
CHAPTER 1: INFORM Project Overview	7
1.1 Introduction	7
1.2 Phase I.....	9
1.2.1 Outline of Development and Main Results.....	9
1.3 Phase II	11
1.3.1 Outline of Planned Development and Intended Outcomes.....	11
1.3.2 Outline of Implemented Enhancements	12
1.3.3 Outline of Report Contents.....	14
CHAPTER 2: Forecast Component Enhancements	15
2.1 Design Overview for Forecast Component	15
2.2 Weather Research and Forecasting (WRF) Model Implementation	19
2.2.1 Mesoscale Model Effects	22
2.2.2 Integration of the Mesoscale Model into INFORM	22
2.3 Intermediate Complexity Regional Model (ICRM) Implementation	24

2.3.1	Introduction	24
2.3.2	Regression-Based Soundings to Produce ICRM Input from CFS1	25
2.3.3	ICRM Input from CFS2	30
2.3.4	Orographic Precipitation Model Updates	31
2.3.5	Surface Temperature Model Updates	35
2.4	Northern California Hydrologic Modeling Enhancements	42
2.4.1	Model Overview.....	42
2.4.2	Hydrologic Model Configuration.....	43
2.4.3	INFORM Hydrologic Model Parameter Values	48
2.4.4	Simulation Performance of the Basin Hydrologic and Routing Model.....	48
2.5	INFORM Web Site Description	55
2.5.1	Graphical Export Post-Processing and Dissemination	55
2.5.2	Accessing the INFORM Dissemination Interface	56
2.5.3	Organization and Navigation of the INFORM Dissemination Interface	56
2.5.4	INFORM Ensemble Median Precipitation Interface Page.....	57
2.5.5	INFORM Ensemble Upper Quartile Precipitation Interface Page	58
2.5.6	INFORM Ensemble Median Temperature Interface Page	59
2.5.7	Data Latency and the Image Unavailable Placeholder	60
CHAPTER 3: Decision Component Enhancements.....		63
3.1	Overview of INFORM Decision Support System.....	63
3.1.1	INFORM DSS Implementation Aspects.....	64
3.1.2	INFORM DSS Enhancements	65
3.2	Uncertainty Management	66
3.2.1	Background and Motivation.....	67
3.2.2	Uncertainty Management Approach.....	68
3.2.3	Mathematical Formulation and Solution Approach	69
3.2.4	Mathematical Formulation and Solution Approach	70
3.2.5	Interactive Management Framework	73

3.3	Reservoir and River Temperature Modeling for Fisheries Management	89
3.3.1	Water Temperature Considerations in the Upper Sacramento River.....	89
3.3.2	Existing Water Temperature Models	90
3.3.3	Water Temperature Simulation.....	91
3.3.4	Water Temperature Optimization	92
3.4	Downstream Routing and Flood Control.....	99
3.4.1	River Routing Models.....	99
3.4.2	Modeling Framework.....	101
3.4.3	Routing Model Identification/Calibration	103
3.4.4	Discrete-Time Linear Quadratic (LQ) Solution.....	105
3.4.5	Application to the Northern California River System	106
CHAPTER 4: Demonstration Results		115
4.1	Forecast Performance Assessment.....	115
4.1.1	Data Processing	115
4.1.2	Statistical Measures.....	118
4.1.3	MAP and MAT Assessments.....	124
4.1.4	Reservoir Inflow Assessments	135
4.1.5	MAP and MAT Bias Adjustment and Impacts	143
4.2	Integrated Forecast-Decision Assessments	152
4.2.1	Long Range Assessments for 2012 Forecasts	152
4.2.2	Water Temperature Assessments for 2012 Forecasts	178
4.2.3	Flood Control Application.....	193
5.1	Introduction	217
5.2	Conclusions.....	217
5.3	Recommendations.....	218
REFERENCES		220
APPENDIX A: Computational Upgrades for INFORM II Forecast Component		A-1
APPENDIX B: ICRM Surface Temperature Model Parameters		B-1

APPENDIX C: Hydrologic Model Parameters and Simulations.....	C-1
APPENDIX D: Feather River Routing Models.....	D-1
APPENDIX E: Comprehensive Statistical Performance Results.....	E-1
APPENDIX F: Comprehensive Statistical Performance Results after Bias Adjustment	F-1

LIST OF FIGURES

Figure 1.1: Northern California Hydrologic Basins for the INFORM Project.	8
Figure 1.2: Northern California Reservoir System.	9
Figure 1.3: Results from Operational Demonstration of INFORM for Years 2006, 2007 and 2008.	11
Figure 2.1: Conceptual Design of the INFORM II Forecast Component.....	16
Figure 2.2: The Computational Grids Used in the WRF-ARW Simulations.....	20
Figure 2.3: The Computational Layers along the Vertical over the Grids Shown in Figure 2.2. ..	21
Figure 2.4: Comparison of GEFS (Left) and WRF-ARW (Right) Forecasts Initialized at 00:00:00 UTC 10 March 2011.....	23
Figure 2.5: ICRM and Links within the INFORM II Forecast System.	25
Figure 2.6: Estimated Air Temperature (T) and Specific Humidity (q) at 700 mbars at Oakland and Eureka Based on CFS1 Input.	29
Figure 2.7: 700 mbar Wind Vectors (m/s) for Oakland and Eureka Based on CFS1 Input.	29
Figure 2.8: Surface Grid of the ICRM for Northern California.....	31
Figure 2.9: Sample CFS-Based MAP ICRM forecasts.....	32
Figure 2.10: Diurnal Distribution of MAP Estimated by CNRFC for the Upper and Lower Portions of the Delta River Subcatchment in the Shasta Drainage.	33
Figure 2.11: As in Figure 2.10 but for the South Fork American River Subcatchment.....	34
Figure 2.12: MAT (at 2 meters) for Three Subcatchments of the Upper Shasta Drainage.	39
Figure 2.13: As in Figure 2.12 but for Lower Oroville Drainage Subcatchments.....	40
Figure 2.14: Location and Elevation of Stations with Observed Air Temperature Data.	41
Figure 2.15: Station Observations of 2-Meter Air Temperature (Black Line), Simulated 2-m Initial Reference Temperature (Blue Line) and Simulated Final 2-m Air Temperature (Red Line).	42
Figure 2.16: Station Observed and ICRM Gridded 2-m Air Temperatures and Regression Fit. ..	42
Figure 2.17: Basin Configuration for Trinity Lake Watershed.....	46
Figure 2.18: Basin Configuration for Shasta Lake Watershed.	46
Figure 2.19: Basin Configuration for Lake Oroville Watershed.	47
Figure 2.20: Basin Configuration for Yuba River Watershed.	47
Figure 2.21: Basin Configuration for Folsom Lake Watershed.....	48
Figure 2.22: Basin Configuration for Downstream Sacramento River Watershed.	49
Figure 2.23: Cumulative Distribution of Daily Flows.....	53
Figure 2.24: Comparison of Daily Observed (Black) and Simulated (Red) Full Natural Inflow to Oroville Reservoir.	54
Figure 2.25: Comparison of Simulated and Observed Snow Water Equivalent (SWE).....	55
Figure 2.26: Window Security Username and Password Authentication.....	56

Figure 2.27: INFORM Dissemination Interface Page – Ensemble Median Precipitation.....	58
Figure 2.28: INFORM Dissemination Interface Page – Ensemble Upper Quartile Precipitation ..	59
Figure 2.29: INFORM Dissemination Interface Page – Ensemble Median Temperature	60
Figure 2.30: INFORM Dissemination Interface Page – Ensemble Reservoir Inflow	61
Figure 2.31: Image Unavailable Placeholder for Data Products Not Yet Processed.....	62
Figure 3.1.1: INFORM DSS Modeling Framework.....	66
Figure 3.2.1: Effect of Inflow Uncertainties on System Trajectories.....	74
Figure 3.2.2: Uncertainty Distributions Resulting from Different Management Policies in a One-Dimensional Reservoir System.	75
Figure 3.2.3: Inflow Forecast Ensembles Issued in January 1922.	76
Figure 3.2.4: Expected Values (Blue) and Standard Deviations (Red) for Monthly (Solid Lines) and Cumulative (Dotted Lines) Inflow Forecast Ensembles Issued in January 1922.....	76
Figure 3.2.5: State Uncertainty Distributions before (Blue) and after (Red) Imposing a Constraint on the Last Time Period Oroville Reservoir Storage Variance.	77
Figure 3.2.6: Decision Uncertainty Distributions before (Blue) and after (Red) Imposing a Constraint on the Last Time Period Oroville Reservoir Storage variance.	78
Figure 3.2.7: State Uncertainty Distributions before (Blue) and after (Red) Imposing a Constraint on the Last Time Period Total System Storage Variance.....	79
Figure 3.2.8: Decision Uncertainty Distributions before (Blue) and after (Red) Imposing a Constraint on the Last Time Period Total System Storage Variance.	80
Figure 3.2.9: State Ensembles before (Blue) and after (Red) Imposing a Constraint on the Last Time Period Total System Storage Variance.	81
Figure 3.2.10: Decision Ensembles before (Blue) and after (Red) Imposing a Constraint on the Last Time Period Total System Storage Variance.....	82
Figure 3.2.11: Trade-off between the Expected Objective Function Value (over the Whole Horizon) and the Total System Storage Variance (at the Last Time Period of the Horizon).	83
Figure 3.2.12: State Uncertainty Distributions before (Blue) and after (Red) Imposing a Constraint on the 9th Time Period South-of-Delta Demand Variance. Both Cases Include a Total Storage Variance Constraint at the Last Time Period.	84
Figure 3.2.13: Decision Uncertainty Distributions before (Blue) and after (Red) Imposing a Constraint on the 9th Time Period South-of-Delta Demand Variance. Both Cases Include a Total Storage Variance Constraint at the Last Time Period.	85
Figure 3.2.14: State Uncertainty Distributions Resulting from Imposing Constraints on the South-of-Delta Demand Variances at Time Period 9 (Blue), Time Periods 8 and 9 (Red), and Time Periods 7 through 9 (Black). All Cases Include a Total Storage Variance Constraint at the Last Time Period.	86
Figure 3.2.15: Decision Uncertainty Distributions Resulting from Imposing Constraints on the South-of-Delta Demand Variances at Time Period 9 (Blue), Time Periods 8 and 9 (Red), and Time Periods 7 through 9 (Black). All Cases Include a Total Storage Variance Constraint at the Last Time Period.	87
Figure 3.2.16: Interactive and Iterative Framework Incorporating User Preferences on the Management of System Uncertainties.	88
Figure 3.3.1: Sample Reservoir Water Temperature Profile.....	96

Figure 3.3.2: Schematic of the Upper Sacramento River Water Quality Model (Adapted from RMA, 2003).....	96
Figure 3.3.3: SRWQM Reservoir Temperature Model Layers and Energy Exchanges	97
Figure 3.3.4: Trinity Releases Temperatures: Comparison between Reduced-Order Model Results (Red) and SRWQM Simulated Monthly Averages (Green)	97
Figure 3.4.1: River Routing Model Concept	109
Figure 3.4.2: Northern California River Network	110
Figure 3.4.3: Northern California River Network	111
Figure 3.4.4: Routing Model Release Function	112
Figure 3.4.5: Simulated (Red) Versus Observed (Blue) Flows (mcf/6-hrs) and Associated Errors (Grey) for the Calibration Period (2004-2006).....	113
Figure 3.4.6: Simulated (Red) Versus Observed (Blue) Flows (mcf/6-hrs) and Associated Errors (Grey) for the Validation Period (2002-2004).	113
Figure 4.1: Diagram Showing the “24-hr Block Average” Verification Scheme	117
Figure 4.2: Sample Forecast Correlation with Observations vs. Lead Time.....	119
Figure 4.3: Example Reliability Diagram.....	121
Figure 4.4: Forecast-Observation Contingency Table	122
Figure 4.5: Example ROC Curve for MAM MAP for 48-hour Lead Forecasts Validating at 00Z for Folsom Sub-Catchment AKYC1.....	124
Figure 4.6: Bias and Correlations of INFORM II Forecasts with Respect to Observations for MAT and MAP in Folsom Subcatchments.	126
Figure 4.7: Smoothed Forecast and Predicted MAP for a Folsom Subcatchment.....	128
Figure 4.8: MAP Observations and Forecasts for an Event in a Folsom Subcatchment	129
Figure 4.9: Subcatchment Distribution of MAP Correlation and Bias Fraction for the GFS-WRF Model.....	130
Figure 4.10: Subcatchment Elevations.....	131
Figure 4.11: Brier Skill Score for MAP and MAT in Oroville Watershed.....	133
Figure 4.12: AROC Values of MAP and MAT Ensemble Forecasts for the Oroville Watershed Subcatchments.....	134
Figure 4.13: Bias Fraction of Reservoir Inflows for the MAM Season.....	136
Figure 4.14: Bias Fraction of Reservoir Inflows for the NDJF Season.....	136
Figure 4.15: Correlations of Reservoir Inflows for the MAM Season	137
Figure 4.16: Correlations of Reservoir Inflows for the NDJF Season.....	137
Figure 4.17: Median Forecasts and Observations for Mean Daily Oroville Inflows	139
Figure 4.18: MAP Median Forecasts and Observations for Upper IIFC1 Subcatchment.....	139
Figure 4.19: BSS for Reservoir Inflows and for the NDJF Season.....	141
Figure 4.20: BSS for Reservoir Inflows and for the MAM Season.....	141
Figure 4.21: AROC for Reservoir Inflows and for the NDJF Season.....	142
Figure 4.22: AROC for Reservoir Inflows and for the MAM Season.....	142
Figure 4.23: Schematic for Bias Factor Estimation Using a Probabilistic Approach.....	143
Figure 4.24: Bias and Correlations of INFORM II Forecasts with Respect to Observations for MAT and MAP in Folsom Subcatchments – Post Bias Adjustment	146

Figure 4.25: Brier Skill Score for MAT and MAP in Oroville Watershed – Post Bias Adjustment	147
Figure 4.26: AROC Values of MAP and MAT Ensemble Forecasts for the Oroville Watershed Subcatchments – Post Bias Adjustment	148
Figure 4.27: Bias Fraction of Reservoir Inflows for the MAM and NDJF Seasons – Post Bias Adjustment.....	149
Figure 4.28: Correlations of Reservoir Inflows for the MAM and NDJF Seasons – Post Bias Adjustment.....	150
Figure 4.29: AROC for Reservoir Inflows for the MAM and NDJF Seasons – Post Bias Adjustment.....	151
Figure 4.30: BSS for Reservoir Inflows for the MAM and NDJF Seasons – Post Bias Adjustment	152
Figure 4.2.1: Long Range Inflow Forecasts.....	155
Figure 4.2.2: Inflow Forecast Comparison, Forecast vs. Historical Mean; Trinity	156
Figure 4.2.3: Inflow Forecast Comparison, Forecast vs. Historical Mean; Shasta.....	156
Figure 4.2.4: Inflow Forecast Comparison, Forecast vs. Historical Mean; Oroville.....	157
Figure 4.2.5: Inflow Forecast Comparison, Forecast vs. Historical Mean; Folsom	157
Figure 4.2.6: Average Basin Inflow Comparisons	158
Figure 4.2.7: Reservoir Storages on March 1st	158
Figure 4.2.8: Monthly Forecast Updates; Trinity and Shasta	159
Figure 4.2.9: Monthly Forecast Updates; Oroville and Folsom	160
Figure 4.2.10: Water Deliveries vs. Carryover Storage Tradeoff.....	161
Figure 4.2.11: Water Deliveries vs. Energy Generation Tradeoff.....	161
Figure 4.2.12: Mean Water Delivery Comparison	162
Figure 4.2.13: Mean Energy Generation Comparison.....	162
Figure 4.2.14: Reservoir Elevation Sequences for the 3rd Tradeoff Point	163
Figure 4.2.15: Reservoir Release Sequences for the 3rd Tradeoff Point	164
Figure 4.2.16: Reservoir Energy Generation Sequences for the 3rd Tradeoff Point	165
Figure 4.2.17: Delta X2 Location Sequences for the 3rd Tradeoff Point	166
Figure 4.2.18: Delta Outflow Sequences for the 3rd Tradeoff Point	167
Figure 4.2.19: Shasta Tradeoff Point #1: Ensemble Forecasts of Release Magnitude/Temperature and the Amount of Reservoir Storage Below 52 F.	181
Figure 4.2.20: Balls Ferry Tradeoff Point #1: Ensemble Forecasts of Release Magnitude/Temperature.....	181
Figure 4.2.21: Jellys Ferry Tradeoff Point #1: Ensemble Forecasts of Release Magnitude/Temperature.....	182
Figure 4.2.22: Bend Bridge Tradeoff Point #1: Ensemble Forecasts of Release Magnitude/Temperature.....	182
Figure 4.2.23: Shasta Tradeoff Point #3: Ensemble Forecasts of Release Magnitude/Temperature and the Amount of Reservoir Storage Below 52 F.	183
Figure 4.2.24: Balls Ferry Tradeoff Point #3: Ensemble Forecasts of Release Magnitude/Temperature.....	183

Figure 4.2.25: Jellys Ferry Tradeoff Point #3: Ensemble Forecasts of Release Magnitude/Temperature.....	184
Figure 4.2.26: Bend Bridge Tradeoff Point #3: Ensemble Forecasts of Release Magnitude/Temperature.....	184
Figure 4.2.27: Shasta Tradeoff point #5: Ensemble Forecasts of Release Magnitude/Temperature and the Amount of Reservoir Storage below 52 F.....	185
Figure 4.2.28: Balls Ferry Tradeoff Point #5: Ensemble Forecasts of Release Magnitude/Temperature.....	185
Figure 4.2.29: Jellys Ferry Tradeoff Point #5: Ensemble Forecasts of Release Magnitude/Temperature.....	186
Figure 4.2.30: Bend Bridge Tradeoff Point #5: Ensemble Forecasts of Release Magnitude/Temperature.....	186
Figure 4.2.31: Shasta: Forecast Averages of Release Magnitude/Temperature and the Amount of Reservoir Storage below 52 F for Tradeoff Points #1 (Blue), #3 (Red) and #5 (Green).....	187
Figure 4.2.32: Balls Ferry: Forecast Averages of Release Magnitude/Temperature for Tradeoff Points #1 (Blue), #3 (Red) and #5 (Green).	187
Figure 4.2.33: Jellys Ferry: Forecast Averages of Release Magnitude/Temperature for Tradeoff Points #1 (Blue), #3 (Red) and #5 (Green).	188
Figure 4.2.34: Bend Bridge: Forecast Averages of Release Magnitude/Temperature for Tradeoff Points #1 (Blue), #3 (Red) and #5 (Green).	188
Figure 4.2.35: Shasta Tradeoff Point #3: Comparison of the Forecast Averages of Release Magnitude/Temperature between Two Scenarios. The Blue Scenario is Based on the Original Temperature Targets while the Red Scenario is Based on Adjusted Targets.....	189
Figure 4.2.36: Balls Ferry Tradeoff Point #3: Comparison of the Forecast Averages of Release Magnitude/Temperature between Two Scenarios. The Blue Scenario is Based on the Original Temperature Targets while the Red Scenario is Based on Adjusted Targets.....	189
Figure 4.2.37: Jellys Ferry Tradeoff Point #3: Comparison of the Forecast Averages of Release Magnitude/Temperature between Two Scenarios. The Blue Scenario is Based on the Original Temperature Targets while the Red Scenario is Based on Adjusted Targets.....	190
Figure 4.2.38: Bend Bridge Tradeoff Point #3: Comparison of the Forecast Averages of Release Magnitude/Temperature between Two Scenarios. The Blue Scenario is Based on the Original Temperature Targets while the Red Scenario is Based on Adjusted Targets.....	190
Figure 4.2.39: Measured Water Temperatures at Bend Bridge from February 2012 to February 2013.	191
Figure 4.2.40: Measured Water Temperatures at Jellys Ferry from February 2012 to February 2013	191
Figure 4.2.41: Measured Water Temperatures at Balls Ferry from February 2012 to February 2013.	192
Figure 4.2.42: Comparison between Average Monthly Forecasted Inflows and Measured Inflows to Shasta Reservoir in 2012.	192
Figure 4.2.43: Daily Measured Inflow to Shasta Reservoir in 2012.....	193
Figure 4.2.44: Oroville Inflow Forecasting Ensemble	195
Figure 4.2.45: River Flow at MRYC1	195

Figure 4.2.46: Oroville Elevation Sequences; Oroville Target Elevation 860 feet.	195
Figure 4.2.47: Oroville Release Sequences; Oroville Target Elevation 860 feet.	196
Figure 4.2.48: River Flow at GRIC1; Oroville Target Elevation 860 feet.	197
Figure 4.2.49: Stage Height at GRIC1; Oroville Target Elevation 860 feet.	197
Figure 4.2.50: River Flow at FLVC1; Oroville Target Elevation 860 feet.	198
Figure 4.2.51: Stage Height at FLVC1; Oroville Target Elevation 860 feet.	198
Figure 4.2.52: River Flow at YUBC1; Oroville Target Elevation 860 feet.	199
Figure 4.2.53: River Flow at Down Stream MRYC1	199
Figure 4.2.54: Stage Height at YUBC1; Oroville Target Elevation 860 feet.	200
Figure 4.2.55: River Flow at FBLC1; Oroville Target Elevation 860 feet	200
Figure 4.2.56: Stage Height at FBLC1; Oroville Target Elevation 860 feet.	201
Figure 4.2.57: Oroville Release; Oroville Target Elevation 862 feet.	201
Figure 4.2.58: Oroville Elevations; Oroville Target Elevation 862 feet.	202
Figure 4.2.59: River Flow at FBLC1; Oroville Target Elevation 862 feet.	202
Figure 4.2.60: Stage Height at GRIC1; Oroville Target Elevation 862 feet.	203
Figure 4.2.61: River Flow at FLVC1; Oroville Target Elevation 862 feet.	203
Figure 4.2.62: Stage Height at FLVC1; Oroville Target Elevation 862 feet.	204
Figure 4.2.63: River Flow at YUBC1; Oroville Target Elevation 862 feet.	204
Figure 4.2.64: Stage Height at YUBC1; Oroville Target Elevation 862 feet.	205
Figure 4.2.65: River Flow at FBLC1; Oroville Target Elevation 862 feet.	205
Figure 4.2.66: Stage Height at FBLC1; Oroville Target Elevation 862 feet.	206
Figure 4.2.67: Oroville Elevation; Oroville Target Elevation 864 feet.	206
Figure 4.2.68: Oroville Release; Oroville Target Elevation 864 feet.	207
Figure 4.2.69: River Flow at GRIC1; Oroville Target Elevation 864 feet.	207
Figure 4.2.70: Stage Height at GRIC1; Oroville Target Elevation 864 feet.	208
Figure 4.2.71: River Flow at FLVC1; Oroville Target Elevation 864 feet.	208
Figure 4.2.72: Stage Height at FLVC1; Oroville Target Elevation 864 feet.	209
Figure 4.2.73: River Flow at YUBC1; Oroville Target Elevation 864 feet.	209
Figure 4.2.74: Stage Height at YUC1; Oroville Target Elevation 864 feet.	210
Figure 4.2.75: River Flow at FBLC1; Oroville Target Elevation 864 feet.	210
Figure 4.2.76: Stage Height at FBLC1; Oroville Target Elevation 864 feet.	211
Figure 4.2.77: Oroville Mean Elevation Comparisons	211
Figure 4.2.78: Oroville Mean Release Comparisons.	212
Figure 4.2.79: Stage Height Comparison at GRIC1	212
Figure 4.2.80: Stage Height Comparison at FLVC1	213
Figure 4.2.81: Stage Height Comparison at YUBC1	213
Figure 4.2.82: Stage Height Comparison at FBLC1	214
Figure 4.2.83: Oroville Mean Energy Comparison	214

LIST OF TABLES

Table 2.1: Surface and Upper Air Variables Available from CFS1 at Each Grid Point	26
---	----

Table 2.2: Surface and Upper Air Variables Required for Upstream Sites for INFORM ICRM ...	26
Table 2.3: Upper Air and Surface Variable Availability for CFS2 Output	30
Table 2.4: Description of INFORM Hydrologic and Routing Model Parameters	50
Table 2.5: Assessment Specifics for Hydrologic and Routing Model Simulations	52
Table 2.6: Statistical Indices Comparing the Daily Simulations and Observed FNF	52
Table 3.3.1: Calibration Mean Squared Errors (MSE) after Sequentially Adding Individual Variables to a Reduced-Order Model. The First Three Variables Were Eventually Chosen to be Part of the Final Reduced-Order Model.	98
Table 3.3.2: Final Reduced Order Dynamic Model Variables for the Trinity Release Temperature and Internal Variables.	98
Table 3.4.1: Routing Model Calibration and Validation Statistics	114
Table 4.1: Time Periods Covered by Observational Data and Forecast System Output.....	117
Table 4.2.1: Monthly Average Inflows for Selected Locations (TAF)	168
Table 4.2.2: Monthly Reservoir Parameters.....	169
Table 4.2.3: Monthly Minimum and Target River Flows	173
Table 4.2.4: Monthly Water Delivery Targets	177
Table 4.2.5: Initial Reservoir Storages on March 1, 2012.....	178
Table 4.2.6: Flow and Stage Height Statistics of River Nodes	215
Table 4.2.7: Oroville Statistics	216

EXECUTIVE SUMMARY

Introduction

Continuing water demand increases and climatic influences on the distribution of water supply require improvement of the management of the existing reservoir system of Northern California to cope with the increasing stress. The Integrated Forecast and Reservoir Management (INFORM) demonstration project was created to develop and demonstrate integrated operational methodologies. These methodologies were designed to allow the utilization of climate and hydrologic forecasts and associated uncertainty to guide reservoir management decisions pertaining to hydroelectric power production, water conservation, flood control and ecosystem health for the large multi-purpose reservoirs in Northern California: Trinity, Shasta, Oroville, New Bullards Bar, and Folsom. INFORM was a prototype demonstration project conceived and applied for the first time in California. The first three years of the INFORM project were funded by the California Energy Commission, the National Oceanic and Atmospheric Administration (NOAA) and CALFED (a consortium of California and federal agencies). This initial work resulted in the development of a prototype integrated and distributed computational system by the Hydrologic Research Center (HRC) and the Georgia Water Resources Institute (GWRI) in collaboration with water forecast and management agencies. These agencies included the California - Nevada River Forecast Center of the U.S. National Weather Service, the U.S. Bureau of Reclamation, the California Department of Water Resources and the California Energy Commission. The system development and initial tests were documented in the Final project report (HRC-GWRI. 2006. *Integrated Forecast and Reservoir Management (INFORM) for Northern California: System Development and Initial Demonstration*. California Energy Commission, *PIER Energy-Related Environmental Research*. CEC-500-2006-109).

The initial tests produced encouraging results and identified a number of refinements to the integrated system that would allow successful and routine application in an operational environment. The next step was the transition to operations and a demonstration of INFORM that utilized present-day scientific observations and forecast information to improve water resources management in Northern California.

Project Objectives

The purpose of the INFORM-II project was to refine the developed system for operational application and to perform the demonstration over the project tenure with real time information and in collaboration with the operational forecast and management agencies. The targets of the refinements and demonstration were increased operational hydroelectric power production, improved flood control, increased water conservation and improved ecosystem health (including fisheries) in Northern California.

The project specific objectives are listed below. Close collaboration between HRC, GWRI, and the operational forecast and management agencies was maintained for all tasks necessary to meet these objectives.

The forecast component was led by HRC and the objectives were to:

- Increase computational power to process all ensembles of GFS by acquiring a multicomputer with 16 processors.
- Ingest CFS output, downscale the data and streamline it with GFS output operations.
- Perform bias adjustment of downscaled mean areal precipitation (MAP) and mean areal temperature (MAT).

The decision component was led by GWRI and the objectives were to:

- Develop an optimization framework that managed system uncertainty.
- Implement an operational monthly river temperature model for addressing fish requirements.
- Align mid-range management with long-range planning by incorporating river routing models.
- Achieve linkage of the INFORM DSS model with other analytical tools used by the state Department of Water Resources (DWR) or the United States Bureau of Reclamation (USBR).

The real time assessments were led by HRC and the objective was to refine operational implementation and perform operational assessments of the INFORM system, including both the forecasting and decision components.

Project Results

The second phase of the project enhanced the INFORM forecast component by implementing: (1) the Weather Research and Forecasting (WRF) model to downscale the ensemble predictions of the Global Forecasting System (GFS) to a 10 x 10 square kilometer (km²) scale with a maximum lead time of 16 days with six-hourly resolution, and (2) an Intermediate Complexity Regional Model (ICRM) to downscale the ensemble predictions of the Climate Forecast System (CFS) to the same scale with a maximum lead time of 41 days with a six-hourly resolution. The ICRM included a land surface energy balance component developed during this phase for ICRM to allow longer lead time surface air temperature prediction for the INFORM snow accumulation and melt model. NCEP transitioned the CFS ensemble predictions from an initial CFS-I version with only limited upper-air atmospheric variable predictions to a final CFS-II version with more complete three dimensional (3-D) atmospheric variable predictions. Adjustments to ICRM were made to accommodate both cases, with the last and more reliable one being operational as of late February 2012. These implementations were made on a dedicated multi-processor computer with adequate computational power to allow twice-a-day starts for the WRF for 20 ensemble members in each start and four-a-day starts for the ICRM for four ensemble members in each start.

The ensemble predictions of the high-resolution surface precipitation and temperature fields produced by WRF and ICRM were used as input to the INFORM adaptation of the operational California Nevada River Forecast Center (CNRFC) snow accumulation and ablation and soil-water models to produce ensemble runoff predictions for the subcatchments of Northern

California that contribute to the reservoir inflow of Folsom, New Bullards Bar, Oroville, Shasta and Trinity reservoirs. Adjustments were made to the precipitation and temperature fields in order to remove biases.

The runoff predictions were then transformed to reservoir inflow predictions through the use of tailored river routing models for the region. The topology of the subcatchments and the hydrologic model parameters for each subcatchment were again aligned to those of CNRFC due to changes made by CNRFC in the operational configurations for more reliable predictions. The CNRFC snow and soil-water model states were assimilated once per day into the INFORM snow and soil-water models to maintain hydrologic model alignment between INFORM and CNRFC hydrologic forecast operations.

CFS long-range ensemble forecasts of surface precipitation and temperature were used in a probabilistic downscaling approach to generate input for the INFORM snow and soil-water models, which were then run to produce ensemble reservoir inflow predictions for periods of one to nine months with six-hourly resolution. The INFORM forecast system consisted of three ensemble prediction sub-systems: the GFS-WRF-hydrology for forecast lead times of 0-16 days, the CFS-ICRM-hydrology for forecast lead times of 0-41 days, and the CFS-Probabilistic downscaling-hydrology for forecast lead times of one to nine months. These ensemble predictions were used as input to the INFORM decision models after adjustment for bias.

Enhancements pertaining to the INFORM DSS component included development and incorporation of: (1) a new optimization framework to manage forecast uncertainties; (2) reservoir and river water temperature models for fisheries management; and (3) river routing models downstream of the main reservoirs to support flood control operations.

A new optimization framework was developed to explicitly address the management of forecast uncertainties system-wide. This DSS enhancement distributed the system forecast uncertainty from climate and hydrology selectively across the system storage projects to mitigate its adverse consequences. Overall system uncertainty is a conservative quantity, much like the conservation of mass. The new optimization procedure determined reservoir release rules that “allocated” uncertainty to system reservoirs that were able to absorb it better, thus mitigating its effects on critical water uses.

The Central Valley and State Water Projects provide a range of services to the environment by maintaining both adequate water quality and water quantity in addition to managing water uses associated with water quantity such as water supply, hydropower and flooding. The previous DSS version incorporated salinity considerations for the Bay Delta and another water quality related requirement was to maintain acceptable water temperatures in the rivers to help sustain local fish populations. A DSS enhancement was implemented to enable the simulation of water temperature in the upper Sacramento reservoirs and rivers and to incorporate it as an additional management criterion evaluated by the INFORM Long Range Planning model. This extension aimed to enable more realistic reservoir storage planning and the development of fish-friendly DSS release rules. Two complementary approaches were explored: (1) A hybrid optimization-simulation approach linking a reservoir and river temperature model to the DSS

Long Range Planning model; and (2) an explicit optimization approach incorporating water temperature criteria into the optimization module of the INFORM Long Range Planning model.

The last DSS enhancement aimed to support flood management operations and short-range decision processes. A new river routing model was developed and tested for several reaches in the upper Feather and Sacramento Rivers. The new model had a mathematical form compatible with INFORM DSS and could be part of the integrated system, unlike existing operational models. The new model was shown to perform effectively despite the marked complexity of the northern California river system.

Evaluation of the INFORM forecast component predictions of subcatchment mean areal precipitation and mean areal temperature as well as reservoir inflow was performed using available data for the periods for which the models had a fixed configuration. The observations used in the evaluation consisted of CNRFC-produced mean areal precipitation and temperature based on observed point measurements and standard operational procedures and of unimpaired (full natural flow or FNF) reservoir inflows produced by California agencies. These data were available through the California Department of Water Resources California Data Exchange Center.

The results indicated that the INFORM forecast component was very effective at reproducing the variability of the subcatchment mean areal precipitation and temperature for the majority of subcatchments in Northern California out to several days in advance and was also very effective at reproducing unimpaired reservoir inflows.

The INFORM DSS component was expanded to include a new optimization framework addressing management of system uncertainty, a reservoir and river water temperature modeling system for fisheries management and new river routing models for downstream flood risk mitigation. All three enhancements were shown to add significant decision support value toward more holistic system planning and management.

Conclusions

The main conclusions of INFORM Phase II for the forecast components were:

- Impressive results were demonstrated for the CFS2-ICRM and especially the GFS-WRF ensemble forecasts for MAP and MAT in the subcatchments of the INFORM domain in Northern California. Clearly these models can be used to provide useful information for the INFORM subcatchments in real time out to two weeks both for the accumulation and the melt period.
- Good forecast results were demonstrated for reservoir ensemble full natural inflows generated by the GFS-WRF forcing and the hydrologic models of INFORM with lead times out to four to six days.
- Low inter-catchment scatter in biases and steady values throughout the range of lead times provided clear evidence that bias corrections for the GFS-WRF model for MAP and MAT will be effective and provide improved flow forecasts. Results of the use of a

probabilistic bias adjustment procedure indicated good corrections for precipitation and air temperature that led to improvements in reservoir inflow predictions for most cases.

- Long-lead capabilities for CFS2-ICRM for large events were found in some cases.

The main conclusions of INFORM Phase II for the decision component were:

- A new uncertainty management framework was implemented and shown to be able to allocate the system forecast uncertainty selectively and effectively across the system storage and release variables. Putting this new capability to practice will require that system planners and managers gain experience with the new framework and assess its value as part of the current decision processes.
- The need and potential to support water temperature management to meet fisheries requirements together with other system objectives were clearly demonstrated. The management of water temperature imposes additional requirements on reservoir storage and release and adds an important dimension to system planning and management tradeoffs. A hybrid simulation-optimization methodology for water temperature management was implemented successfully. A full optimization approach seamlessly integrated with the INFORM DSS was also conceptualized and shown to have good potential for additional operational improvements.
- A new state-space river routing model was developed and demonstrated for the Upper Feather and Sacramento Rivers. This routing model had the advantage of being compatible with the INFORM management framework while exhibiting accuracy comparable to the existing operational routing schemes. Using this model in connection with the INFORM forecast-decision system gave promising results as a means for managing downstream flooding risks. Voluminous data requirements and acquisition delays, however prevented the development of the model for the lower river network reaches.

Recommendations

The following major recommendations emerged from INFORM Phase II:

- Extend the demonstration period of the second-phase final INFORM system configuration in the following three wet seasons to provide additional opportunities for system evaluation and information transfer to agency personnel, managers and planners.
- Work was needed to fine tune the water temperature modeling system within the INFORM decision framework and to allow for more extensive modeling of the numerous river network features to support flood management operations. Researchers also recommended coupling the CFS2 with WRF and evaluating performance for lead times out to one month given the importance of large precipitation producing events and the need for longer lead time to manage them. Researchers recommended that appropriate forecast adjustments be implemented for watersheds with significant

upstream regulation effects based on a recent approach developed by the authors in collaboration with the NOAA River Forecast Centers.

- INFORM may also be used as a screening model for planning studies pertaining to the value of additional data, forecasts, long-range predictions and re-operation strategies towards more integrated assessment and planning of Northern California water resources.

Project Benefits

The results of this project could provide useful information to help increase hydroelectric power production, improve flood control, increase water conservation and improve ecosystem health in Northern California.

CHAPTER 1: INFORM Project Overview

1.1 Introduction

The Integrated Forecast and Reservoir Management (INFORM) Project was conceived to demonstrate increased water-use efficiency in Northern California water resources operations through the innovative application of climate, hydrologic and decision science (*Georgakakos et al. 2005*).

Toward achieving this goal, the particular objectives of INFORM are to (a) implement a prototype integrated forecast-management software system for the primary Northern California reservoirs, both for individual reservoirs as well as system-wide; and (b) demonstrate the utility of climate, weather and hydrologic forecasts through near-real-time tests of the integrated system with actual data and management input, by comparing its economic and other benefits accruing from current management practices for the same hydrologic events. The intent is to align the forecast component of INFORM to operational models and practices in the region as much as possible for an eventual smooth transition to operations.

Figure 1.1 shows the drainage basins of the region of interest in Northern California delineated by the U.S. National Weather Service (NWS) California Nevada River Forecast Center (CNRFC), while Figure 1.2 shows a schematic of the major reservoirs in Northern California. The drainage basins are on the American, Feather, Sacramento and Trinity River and tributaries. The Folsom, Oroville, Shasta, New Bullards Bar, and Englebright reservoirs on the Sacramento River tributaries are included in the INFORM system, together with the Trinity Reservoir (previously called Clair Engle Lake) on the Trinity River. Forecasting of the precipitation and temperature in the drainage basins contributing water to each of these reservoirs together with reservoir inflow forecasting and downstream flow routing is part of the INFORM demonstration project activities.

The project is a joint effort of the Hydrologic Research Center (HRC), a public-benefit research and technology transfer corporation in San Diego, California, and the Georgia Water Resources Institute (GWRI), a federally mandated research institute at Georgia Tech in Atlanta, Georgia. HRC is the lead organization for the forecast components of INFORM and GWRI is the lead organization for the reservoir management components of INFORM. Close collaboration between HRC and GWRI, and between these organizations and operational forecast and management agencies has been established to allow effective integration of system components and to pave the way for its use in Northern California operations. The summary of activities and main findings and recommendations of the first 3-year phase of INFORM are presented in *HRC-GWRI (2006)* and *Georgakakos et al. (2007)* and are summarized below for easy reference. Following this, a summary of the activities and results of the present second phase of INFORM (INFORM II) is presented as an introduction to the main body of the report which provides technical details.

Figure 1.1: Northern California Hydrologic Basins for the INFORM Project.

(Reservoir watersheds are indicated by red line while subcatchments by black line)

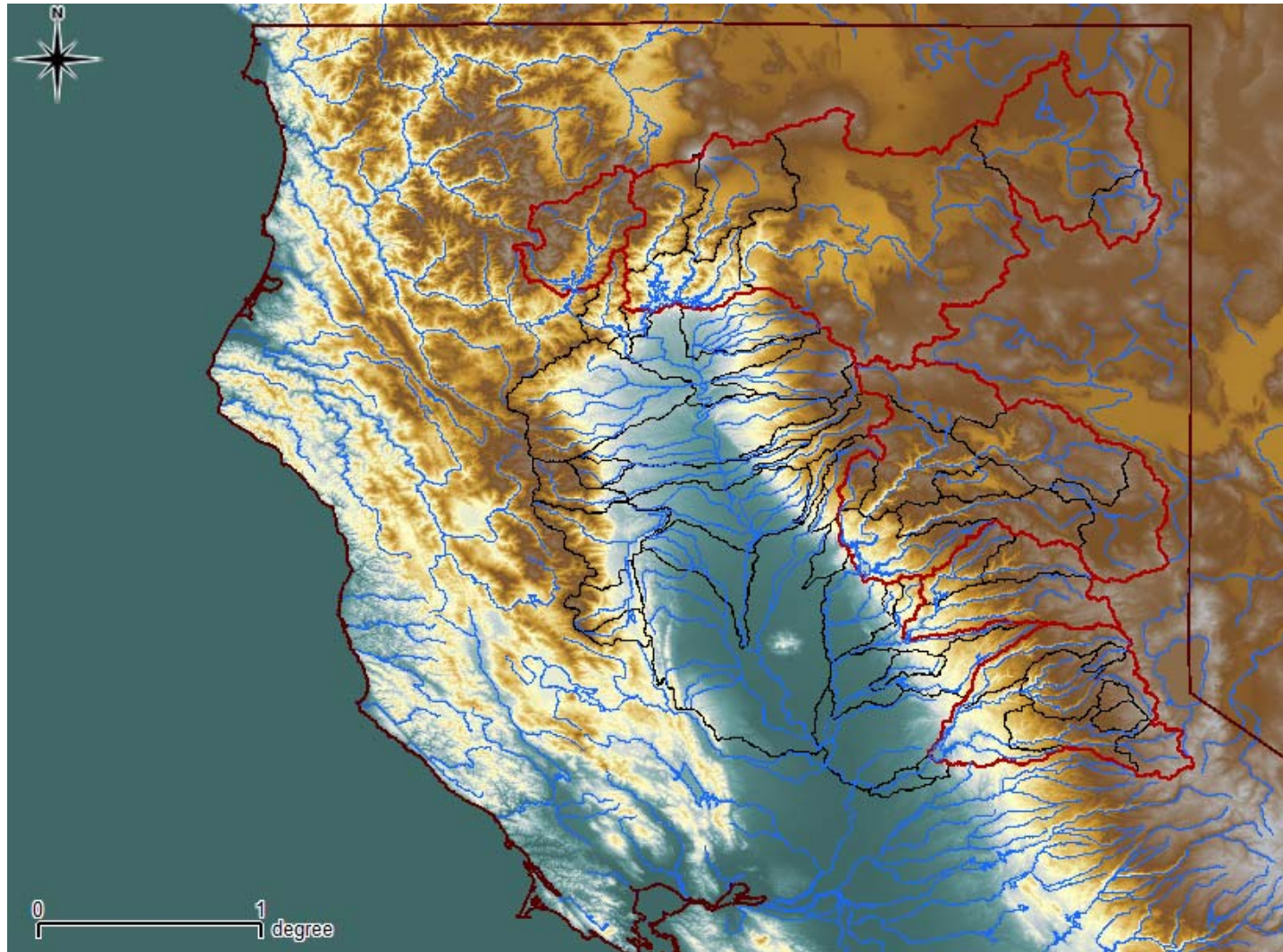
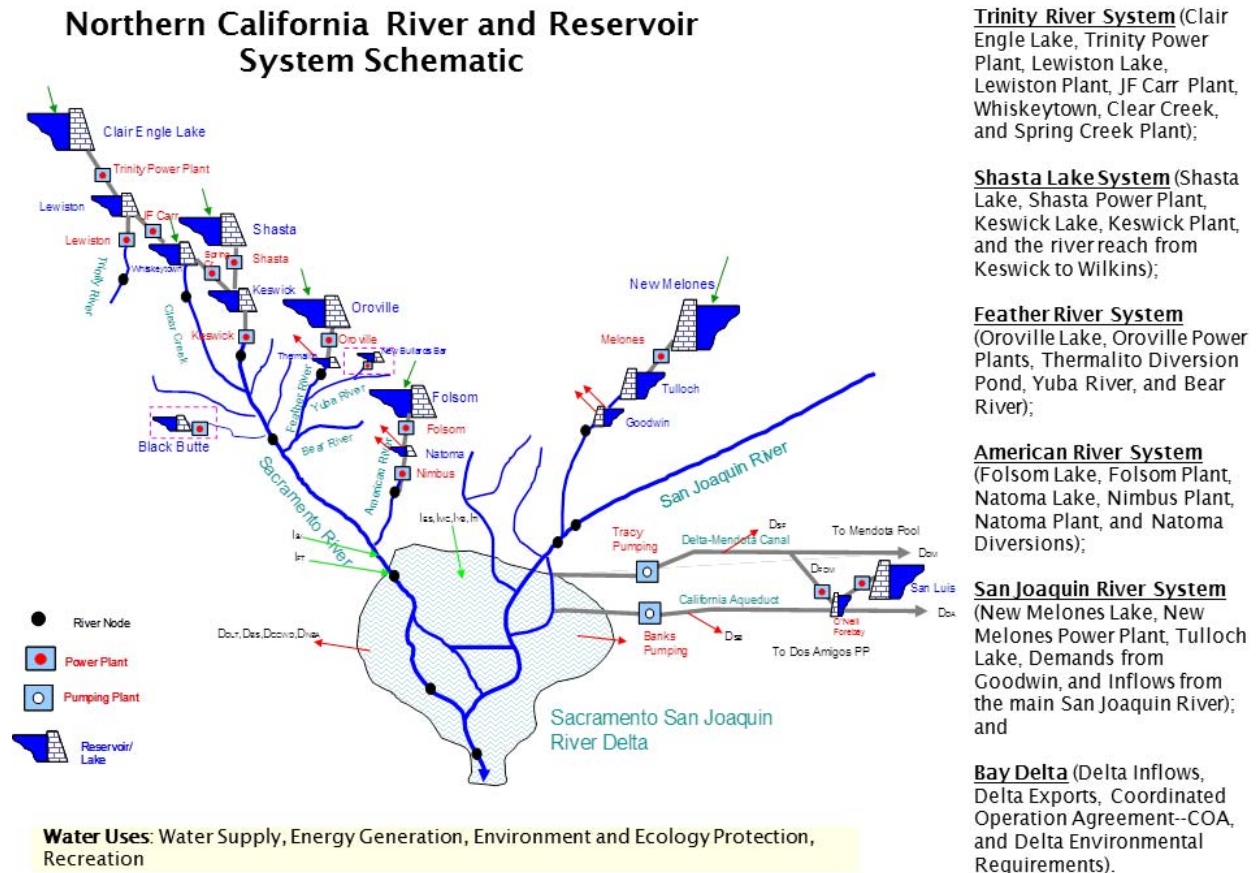


Figure 1.2: Northern California Reservoir System.



1.2 Phase I

1.2.1 Outline of Development and Main Results

During the first phase of the INFORM project, the authors performed the following technical tasks in close collaboration with operational forecast and management agencies in Northern California:

- (a) Created the Oversight and Implementation Committee for project oversight and assistance with system implementation and tests.
- (b) Developed, implemented and performed validation of climate and weather INFORM components for Northern California with historical data and real-time data.
- (c) Developed, implemented and performed validation of hydrologic INFORM reservoir-inflow forecasts with historical and real-time data for all major reservoirs of Northern California.
- (d) Developed, implemented and performed validation of decision INFORM components with historical and real-time data for the Northern California water resources management system.

(e) Integrated INFORM system climate, hydrology and decision components and performed initial operational tests producing real-time ensemble forecasts out to lead times of 16 days four times daily for the wet season 2005-2006.

(f) Performed assessments of the integrated forecast-decision system value via retrospective simulation experiments.

(g) Held INFORM design, assessment and training meetings with operational forecast and management agency staff.

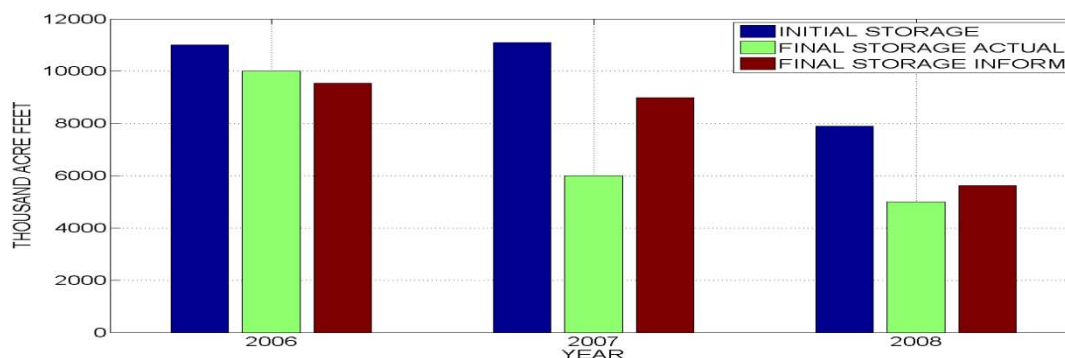
Retrospective runs of the INFORM system were made with historical observations and archived atmospheric forecasts. Assessments were performed between the INFORM system decisions and actual system decisions as regards flood control, water conservation, hydroelectric power production, and ecosystem health metrics. For the 2005-2006 winter real time assessments were made for the short and long range forecasts and for the INFORM decision component performance. With respect to the real time initial demonstration, the INFORM system correctly forecast high likelihood of wetter spring 2006 conditions for the region reservoirs, and the INFORM decision component indicated that, with low risk, additional water conservation would be possible compared to actual reservoir system operations in Northern California. The interested reader is referred to *HRC-GWRI (2006)* for a complete set of results and detailed discussion of assessments performed during this first phase of INFORM.

There was an interim INFORM phase for the period 2006-2008, during which period the demonstration project continued with the evaluation of the long range real-time INFORM forecasts and decisions. Year 2006 was a wet year while Year 2008 was a dry year with water deliveries in California that were almost half of those of Year 2006. Year 2007 was a transition year in terms of inflows to the Northern California reservoirs. For these years ensemble reservoir inflow forecasts were produced for the large Northern California reservoirs on March 1 of each year with a 9-month lead time and resulting risk based trade-offs were produced by the decision component of INFORM. Following preferences indicated by the participating management agencies, decisions were made and the INFORM system assessed the benefits of these decisions for flood control, energy generation, municipal and agricultural water supply, and Bay Delta salinity intrusion levels. Performance was based on the total water in storage in the Northern California reservoir system at the end of the season starting from the known storage at the beginning of the season. The existing system performance was simulated and was compared to that of INFORM in this demonstration project.

Demonstration runs for Years 2006, 2007 and 2008 are shown at the top of Figure 1.3. The columns show aggregate storage estimates in thousand acre feet (TAF) for all reservoirs in Northern California. Shown are (a) the initial storage at the beginning of each year (input on March 1st of each year), and (b) two final storages after 9 months (measures of performance of reservoir management): the final storage at the end of each year with current practice, and the final storage at the end of each year using the adaptive INFORM system. The INFORM-produced final reservoir storage indicates that INFORM allowed for very significant water

conservation for the transitional Year 2007 while it saved more than actual for the very dry Year 2008 and released more than actual in the very wet Year 2006.

Figure 1.3: Results from Operational Demonstration of INFORM for Years 2006, 2007 and 2008.



There are several technical and specific conclusions that have been drawn from the outcomes of the project in the areas of meteorology/climate, hydrology, and decision science. These conclusions are detailed in *HRC-GWRI (2006)*. The most important conclusion of the first and interim phases of the INFORM project is that, with available real-time availability of forecast information from the U.S. National Centers for Environmental Prediction and with real-time observed precipitation and temperature as well as hydrologic model state values from the California Nevada River Forecast Center, integrated forecast-management systems are realizable as effective operational decision support tools for management and planning of California water resources. Such systems assist water managers in translating forecasts and their uncertainty into a range of effective risk-based policies. In addition, these systems can advance current operational practices by (a) incorporating forecast uncertainty in decisions on a range of time scales, and (b) allowing for regional coordination of management decisions.

The first phase recommendation was to continue the demonstration experiment by enhancing the INFORM models with the capability to use the advanced new forecasts that were becoming available at the National Centers for Environmental Prediction (NCEP), and the ability to integrate flood control downstream of the reservoirs and temperature models for fisheries in the INFORM decision component. These enhancements and demonstration results for the second phase of INFORM are the subjects of the present Report.

1.3 Phase II

1.3.1 Outline of Planned Development and Intended Outcomes

The following were identified as main development areas for the second phase of INFORM (INFORM II):

Forecast Component:

Enhance the INFORM forecast component with the ability to ingest and dynamically-downscale the improved GFS and CFS three-dimensional atmospheric-variable forecasts, routinely made available by NCEP, to produce ensemble gridded surface precipitation and

temperature forecasts for the domain of INFORM in Northern California with 6-hour resolution and out to a forecast lead time of 40 days.

Evaluate the ensemble forecasts of mean areal quantities obtained for the drainage basins of interest from gridded precipitation and temperature forecasts and available observations

Continue to maintain the INFORM project secure web site for forecasts produced, with enhancements appropriate for the new development.

Decision Component:

Align mid-range management with long-range planning by incorporating river routing models

Implement an operational monthly river temperature model for addressing fish requirements

Perform integrated forecast-management assessments for the period of phase II after development.

The intended outcome of the development is a INFORM forecast component that is streamlined with operational agency operational products.

1.3.2 Outline of Implemented Enhancements

The forecasting component of INFORM was restructured to ingest and dynamically downscale twice daily Global Forecast System (GFS) ensemble forecasts (20 members) of upper and surface atmospheric variables for the period from 0 to 16 days with six-hourly resolution. The Weather Research and Forecasting (WRF) mesoscale numerical weather prediction model is used to downscale the GFS fields to a grid with a 10 km resolution on the side. This replaces and improves upon the previously used simpler dynamical downscaling of 8-member GFS ensemble forecasts that employed a land surface energy exchange scheme based on the Advanced Regional Prediction System (ARPS) and an orographic precipitation model with potential theory airflow solutions and Kessler microphysical parametrization. The latter, while adequate for orographic regions with significant slopes, had a poorer performance for regions of flatter terrain.

In addition to the enhancements made for the 0-16 day lead times, the forecast component was enhanced with models for producing ensemble forecasts out to 41.5 days with a six-hour resolution. These added forecasts bridge the gap that existed in the first phase of INFORM between the shorter-term ensemble forecasts (0-16 days) and the longer-term ensemble forecasts (1-9 months). The latter (1-9 months) forecasts are based on probabilistic downscaling of the Climate Forecast System (CFS) surface precipitation and temperature ensemble forecasts and have been preserved essentially unaltered in the second phase of INFORM. The added forecasts, with lead times of 0 – 41.5 days and a 6-hourly temporal resolution, use the CFS ensemble forecasts of upper air and surface atmospheric variables and produce dynamically downscaled forecasts of surface precipitation and temperature with a 10 x 10 km² resolution over the INFORM domain. During the tenure of the second phase of INFORM, NCEP has

produced two versions of CFS output (CFSv1 and CFSv2) with varying upper air information content in the ensemble forecasts. Both versions were utilized in INFORM II with the present version (CFSv2) providing 4 ensemble members of upper air information suitable for dynamical downscaling four times daily. In this case, in order to maintain computational efficiency in real time ensemble forecasting and to allow feedback of snow and soil water states from the operational hydrologic models to the downscaling mesoscale models, the orographic precipitation model of the first phase of INFORM and a tailored land-surface energy exchange scheme for surface temperature were utilized. These two components together form what is termed an Intermediate Complexity Regional Model (ICRM).

Bias adjustment methodologies were formulated and tested with real time data for the model ensemble forecasts of precipitation and air temperature. The effect of these adjustments on the ensemble predictions of reservoir inflow was also quantified.

In order to sustain the substantially enhanced computational load of the INFORM forecast component a multi-computer system was purchased and is used for the INFORM system forecast product generation, management and archiving. This computational system also hosts the real-time secure web site with all of the available forecasting products of INFORM. Enhancements of this web site developed in the first phase of INFORM were also necessary due to the forecasting system improvements and added forecast products.

Changes in the hydrologic forecast component of INFORM concentrated on aligning the catchment delineations and associated hydrologic parameter values to those of the operational CNRFC forecast system in order to maintain the real-time assimilation of snow and soil water model state information from CNRFC available once daily.

Enhancements pertaining to the INFORM DSS component include development and incorporation of (i) a new optimization framework to manage forecast uncertainties, (ii) reservoir and river water temperature models for fisheries management, and (iii) river routing models downstream of the main reservoirs to support flood control operations.

A new optimization framework was developed to explicitly address the management of forecast uncertainties system-wide. This DSS enhancement distributes the system forecast uncertainty (from climate and hydrology) selectively across the system storage projects to mitigate its adverse consequences. Much like the conservation of mass, overall system uncertainty is a conservative quantity. The new optimization procedure determines reservoir release rules that “allocate” uncertainty to system reservoirs that are able to absorb it better, thus mitigating its effects on critical water uses.

In addition to managing water uses associated with water quantity (water supply, hydropower, and flooding), the Central Valley and State Water Projects are also operated to provide a range of services to the environment by maintaining both adequate water quality and water quantity. While the previous DSS version incorporates salinity considerations for the Bay Delta, another water quality related requirement is to maintain acceptable water temperatures in the rivers to help sustain local fish populations. A DSS enhancement is implemented to enable the simulation of water temperature in the upper Sacramento reservoirs and rivers and incorporate

it as an additional management criterion evaluated by the INFORM Long Range Planning model. This extension aims to enable more realistic reservoir storage planning and the development of fish-friendly DSS release rules. Two complementary approaches are explored: (1) A hybrid optimization-simulation approach linking a reservoir and river temperature model to the DSS Long Range Planning model, and (2) an explicit optimization approach incorporating water temperature criteria into the optimization module of the INFORM Long Range Planning model.

The last DSS enhancement aims to support flood management operations and short range decision processes. As part of this enhancement, a new river routing model was developed and tested for several reaches in the upper Feather and Sacramento Rivers. The new model has a mathematical form compatible with the INFORM DSS and can be part of the integrated system, unlike existing operational models. The new model was shown to perform effectively, despite the marked complexity of the northern California river system.

1.3.3 Outline of Report Contents

The next chapter describes the updated design of the forecast component and the salient points of model formulation and implementation for the WRF and ICRM, as well as the input GFS and CFS data obtained from NCEP in real time. Adjustments to hydrologic model configuration for alignment with CNRFC model configuration are also described in this chapter along with the updates to the INFORM project secure web site with real time forecasts. Chapter 3 focuses on the decision component design and enhancements, with emphasis on the developed routing model for short term assessments and the water temperature model for longer term assessments pertaining to fisheries. Uncertainty management is also described in this chapter. Chapter 4 describes the demonstration project assessments in terms of quantifying forecast performance for the real time ensemble forecasts of mean areal precipitation and mean areal temperature for the delineated subcatchments of INFORM II and for reservoir inflow for the main INFORM II reservoirs of Northern California. The same chapter also describes the integrated forecast-decision assessments for the short-term and long-term decision horizons pertinent to flood control and water conservation/fisheries, respectively. The main conclusions and recommendations of the second phase of INFORM are in Chapter 5, with Chapter 6 containing the references mentioned in the previous report chapters. Various appendices contain additional results supporting the chapter concepts and assessments. Additional project information with the Phase II Interim Report and summaries of proceedings of Project Advisory Committee Meetings for the first and second INFORM Phase may be found at the website: http://www.hrc-lab.org/projects/dsp_projectSubPage.php?subpage=inform

CHAPTER 2:

Forecast Component Enhancements

This chapter describes the updates in design and implementation of the enhanced forecast component of INFORM II and associated secure web site products.

2.1 Design Overview for Forecast Component

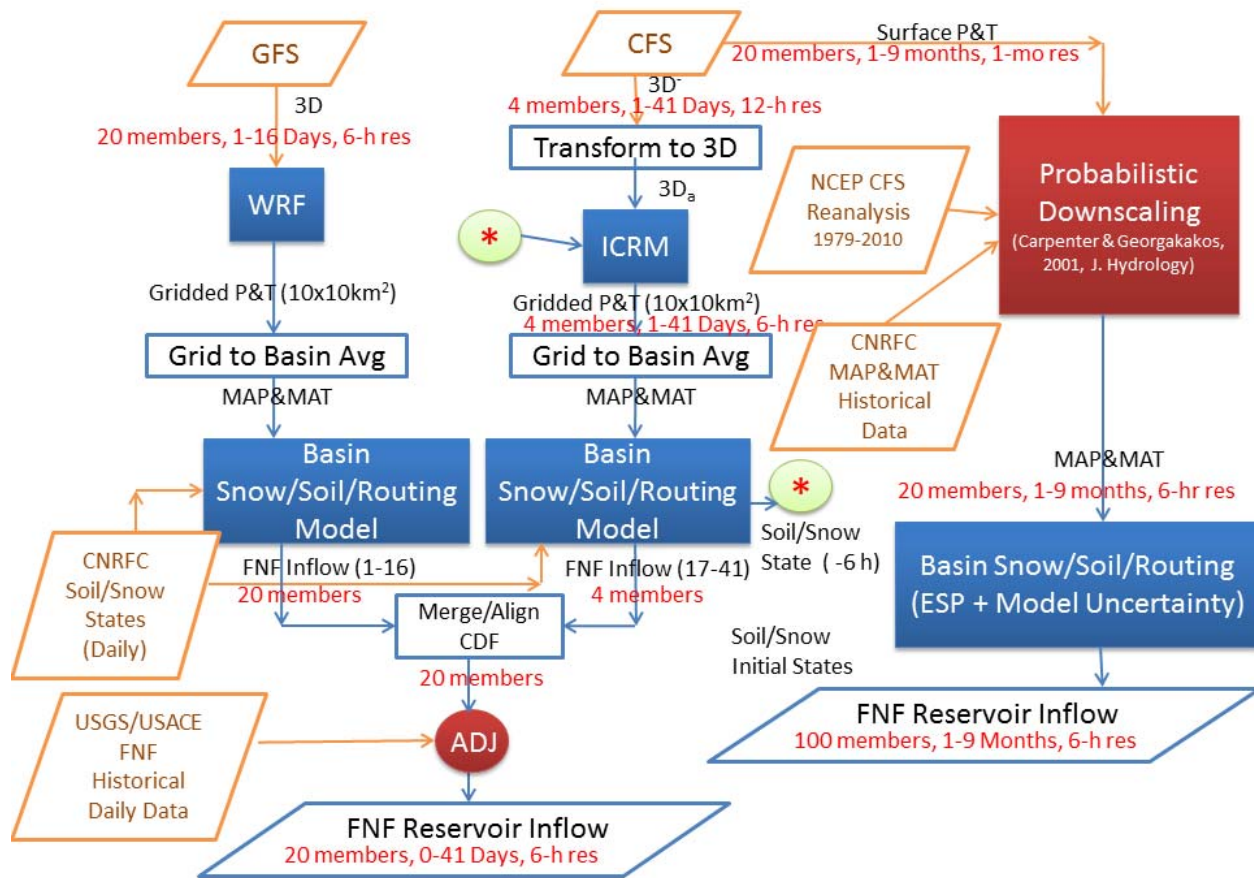
The conceptual design of the INFORM II forecast system is tailored to the data available and to meet the following requirements:

- (a) Ensemble forecasts of mean areal precipitation and temperature as well as reservoir inflow are issued at least twice daily for lead times up to 1 month with 6-hourly resolution based on dynamical downscaling methods;
- (b) Ensemble forecasts are issued for lead times out to 9 months with 6-hourly resolution based on probabilistic downscaling methods off line, with typical starts at the beginning of the winter months through March 1;
- (c) Hydrologic components (snow and soil water models) are used that are adaptations of the operational hydrologic forecast models of the California Nevada River Forecast Center (CNRFC);
- (d) Bias adjustment factors are used for reservoir inflow forecasts based on climatological comparisons of ensemble forecasts and estimated unimpaired inflows based on lake level observations;
- (e) Updated estimates of snow and soil water content states are used once a day to align the INFORM hydrologic forecast system estimates to CNRFC operational forecast system estimates;
- (f) Historical reanalysis data from the National Centers of Environmental Prediction (NCEP) are used together with historical MAP and MAT data from CNRFC in the probabilistic downscaling procedure mentioned in (b) above.
- (g) The final products of the forecast system are ensemble reservoir inflow forecasts: short term forecasts up to a month and long term forecasts up to 9 months, both with 6-hourly resolution and for all the reservoir sites modeled by the decision component of INFORM II.

Figure 2.1 shows a schematic representation of the INFORM II forecast system components and interactions.

There are two main sources of real-time, ensemble, large-scale forecast information for the INFORM II forecast component, both originating at NCEP of NOAA. The first is the Global Forecast System (GFS) and the second is the Climate Forecast System (CFS). The first is used for short term forecasts (1-16 days) and the second is used for longer term forecasts up to 9 months. We discuss next each of the pathways that emanate from these sources in Figure 2.1.

Figure 2.1: Conceptual Design of the INFORM II Forecast Component.



Preliminary runs with the mesoscale forecast model WRF (Weather Research and Forecasting) indicated that the available computing power at HRC on the INFORM II cluster is adequate to support the computations of a 20-member ensemble from GFS and to produce 6-hourly 10x10 km² resolution forecasts out to 16 days for the Northern California INFORM domain within approximately 5.5 hours. On the basis of this finding we use WRF as part of INFORM II for the short-term forecasts that support flood control and hydroelectric power concerns at the reservoir sites. This will result in 20 ensemble forecasts of gridded precipitation and temperature over northern California with a 10x10 km² spatial and a 6-hourly temporal resolution.

A second finding that is pertinent in this discussion is that use of the 3-D (profile) forecasts from the Climate Forecast System (CFS) of NCEP to force the simplified dynamic downscaling model used in the first phase of INFORM predicted the occurrence of heavy rainfall for lead times greater than 16 days out to 30 days under strong synoptic forcing situations in Northern California (Georgakakos *et al.* 2010). It is then appropriate to use the 3-D CFS forecasts to produce dynamically-downscaled precipitation and temperature with a 10x10 km² resolution out to 30-

days for Northern California and to bridge the gap from the short time scales (≤ 16 days) to the 1-9 month time scales.

Initial runs with the WRF model gave execution times that make running this model for the forecast period 0-30 days infeasible on the present HRC INFORM II cluster. In addition and independent of computing power, use of WRF for longer lead times assures divergence of the WRF land-surface component from the operational hydrologic model due to the fact that assimilation of hydrologic model states into WRF is infeasible due to different model physics and structure. For this reason, an intermediate complexity regional model (ICRM) (similar to the one used in the first phase of INFORM with components suitably upgraded), is utilized to provide dynamic downscaling for the 3-D CFS forecasts. ICRM uses a land surface component with soil water modeling that is an adaptation of the operational hydrologic model run at CNRFC. Thus assimilation of operational model states that include any forecaster updates/adjustments is engaged once per day to align the initial conditions of the ICRM integrations with those of the operational hydrologic model.

Two different CFS forecast output streams, CFSv1 and then CFSv2, became available from NCEP. In the latter case, which is the present operational case for INFORM II, there are four CFS starts per day (00Z, 06Z, 12Z and 18Z) each with 4 ensemble members and with maximum lead time of 41 days. It is noted that at present the available 3-D information in the CFSv1 and CFSv2 forecasts is not appropriate for running ICRM directly, so there is a transform module developed to convert the existing 3-D information (indicated as 3D⁻ in Figure 2.1) to ICRM model-ready 3-D information (indicated as 3D^a in Figure 2.1).

At the end of the computations mentioned already, we have 10×10 km² gridded surface precipitation and temperature ensemble forecasts for Northern California and for the period 0-16 days (GFS 3-D based) and 0-41 days (CFS 3-D based). Using these by the hydrologic model of INFORM, requires to convert this information to basin average quantities (MAP and MAT) using the available Geographic Information System (GIS) and the model output grid specifications (see the box with label "Grid to Basin Avg" in Figure 2.1 that applies both to the 20-member ensemble output from WRF and the 4-member ensemble output from ICRM). This conversion gives the MAP and MAT ensemble forecasts for each of the CNRFC sub-catchments of the operational forecast system that is emulated in the INFORM II forecasting component. Adjustment of the ensemble mean areal precipitation and temperature forecasts to comply with the distributional characteristics of the corresponding observations obtained by CNRFC was also made for improved input to the hydrologic models.

The INFORM II hydrologic model is basin-based and uses tailored river routing schemes for all the rivers of interest. It runs both with the WRF and the ICRM ensemble forecast output mentioned above to produce reservoir inflow ensembles for all the reservoir sites of interest with 6-hourly temporal resolution and with forecast lead times that span the range from 6 hours to 41 days (notation in the Figure indicates this by the "1-41 days" indicator). Once daily, CNRFC hydrologic model states for the same sub-catchments as modeled in the INFORM hydrologic models will be downloaded and will be used to provide model state initial conditions for the next run of the INFORM model. In this way the two hydrologic models are

aligned in real time once daily and should not diverge substantially at least in the short term. The decision to make the hydrologic model basin based derives from this requirement of alignment and preservation of the operational hydrologic catchment configuration and the requirement for INFORM to maintain use of operational components to the extent possible. The operational hydrologic forecast models have very good performance (e.g., *Shamir et al. 2007*) and there is no compelling reason to diverge from them in the INFORM system.

Due to the use of different input and models for obtaining the MAP and MAT forcing, it is expected that the error structure of the ensemble reservoir inflow predictions from WRF and ICRM will differ substantially (this is confirmed in the performance assessments of Chapter 4). In addition it is necessary to merge the WRF-based ensemble reservoir inflow predictions (out to 16 days) with those of the ICRM-based ensemble predictions (out to 41 days) and generate the same number of ensemble members throughout the period from 0 to 41 days lead time. To achieve this, it is necessary to align the statistical character of the ensemble predictions from these two operational streams shown in Figure 2.1. This is accomplished using a matching probability method whereby first the 20 predictions at the end of the 16 days from the WRF-based prediction set are used as initial conditions for the ICRM-based predictions, and second quantiles of the cumulative probability distribution functions (CDF) of the ICRM-based ensemble reservoir inflow *volume* predictions for forecast times 0 – 16 days are aligned to the corresponding ones of the WRF-based ensemble reservoir inflow predictions and the same quantile ICRM-based ensemble member is used for each of the 20 members of the WRF-based ensemble as extension beyond the 16 days and out to 41 days. Once aligned (box labeled “Merge/Align” in Figure 2.1) then a unique 20-member ensemble of reservoir inflow predictions is produced that covers the lead times 0 – 41 days with 6-hourly resolution. It is noted that these predictions are for unimpaired flows (not including upstream regulation effects), also called full natural flows (FNFs).

These predictions are expected to contain systematic and random errors due to input, model and parameter biases and random errors for both WRF and ICRM. Climatological bias adjustment factors are estimated for each season and for each lead time by comparing the median of the 20-member ensemble reservoir inflow predictions to historical estimates of the unimpaired reservoir inflow computed on the basis of lake observations and other data by the US Geological Survey (USGS), the CNRFC and the US Army Corps of Engineers (USACOE). The end result is the development of bias-adjusted 20-member ensembles of unimpaired reservoir inflows for the reservoirs of interest in Northern California (see Figure 2.1 circle labeled by “ADJ”).

It is desirable to use the hydrology model snow and soil content states to update the land-surface component of the ICRM (grid based). This was achieved in the first phase of INFORM through a feedback from the hydrologic model to the ICRM (shown in Figure 2.1 through the arrow to the asterisk circle and from the asterisk circle to the ICRM). This same approach is followed in INFORM II with a lag of – 6 hours. Note that ICRM runs four times daily with a 6-hour output resolution for each ensemble member so the assimilation with a 6 hour lag is feasible.

In addition to the CFS 3D ensemble predictions, INFORM receives CFS surface precipitation and temperature predictions that go out to 9 months. This has been useful in the first phase of INFORM to provide ensemble forecast information for the long-range decision model of the reservoir decision support component of INFORM (see Chapter 3). Because good results have been obtained for both wet and dry years (there is evaluation information for years 2006, 2007 and 2008 in Appendix A of *Georgakakos et al. 2010*), INFORM II uses the same approach (described in *Carpenter and Georgakakos, 2001*) to produce long-range ensemble forecasts. The approach uses probabilistic downscaling of the CFS ensemble forecasts of gridded surface precipitation and temperature that cover the Northern California region. On the basis of the CFS real time surface precipitation and temperature ensemble forecasts and an archive of such forecasts that spans several years, the method finds the probability of the next season to be in the upper or lower (or medium) tercile of precipitation and or temperature. This probabilistic assessment is then applied to the historical years of observed mean areal precipitation and temperature (available from CNRFC) to identify the set of years that should be used in the ensemble forcing to the model from the upper, medium or lower tercile of their distribution. These years then are used to provide forcing to the hydrologic model and routing components to produce ensemble streamflow predictions (ESP – as used operationally by the US National Weather Service for hydrologic flow predictions throughout the US). INFORM also accounts for the uncertainty due to model error, so the initial ensemble is enriched to produce more ensemble members in the end.

This probabilistic downscaling procedure combined with the use of the hydrologic model and routing components in an ESP approach is shown schematically in Figure 2.1 right-most computational path produces a total of 100 ensemble members of 6-hourly resolution out to 9 months for all the reservoir inflows used in the decision support component of INFORM II.

2.2 Weather Research and Forecasting (WRF) Model Implementation

The INFORM system employs the Weather Research and Forecasting (WRF) numerical modeling system in the task of generating mesoscale weather forecasts over northern California on the basis of GFS ensemble forecasts with lead times from 0 to 16 days. This system utilizes version 3.2.1 of the Advanced Research WRF (ARW) dynamical core. The WRF-ARW is a state of the art mesoscale model designed for both research and operational applications and is based on the MM5 mesoscale model (*Dudhia 1993*). The equation set used by the model is fully compressible, Euler non-hydrostatic with a terrain following, hydrostatic pressure vertical coordinate. A detailed description of the WRF-ARW can be found in *Skamarock et al. (2008)*.

The application of a mesoscale model to an area of interest is typically made by configuring a system of nested grids, the design of which is strongly influenced by the data available for definition of the model's initial and boundary conditions. An ensemble prediction system was desired for definition of WRF's boundary conditions and NCEP's GFS Ensemble Forecast System (GEFS) was selected. The GEFS system includes a control forecast and 20 perturbed forecasts that are run out to 16 days on a T190L28 horizontal and vertical resolution. Each of the 20 GFS ensemble perturbation forecasts is used to drive a separate instance of WRF, with each of these ensemble perturbations being centered and orthogonal at the initial time. The initial

conditions used for each of the WRF runs are supplied by the analysis time of NCEP's North American Model (NAM). These analyses are on a lambert conformal grid (resolution of approximately 12 km in the horizontal) and are generated by combining model output, i.e. the GFS control run, and observations from various sources.

The WRF-ARW was configured with two nested lambert conformal grids (Figure 2.2) with horizontal resolutions of 30 km and 10 km and corresponding mesh sizes of 30×30 and 52×55 grid points respectively. A two-way interactive communication occurs between the nested grids. Each grid contains 30 computational atmospheric layers with the highest vertical resolution being in the lowest 2 km (Figure 2.3). The highest computational layer is at approximately 50 hPa (nearly 20 km above sea level) and the lowest layer in the atmosphere is approximately 28 m above ground level. Temporal resolutions of 180 and 60 seconds are used on the outer and innermost grids, respectively. Surface terrain features are defined using United States Geological Survey (USGS) terrestrial data with a spatial resolution of 30 seconds (approximately 1 km) which supplies topography, land use, and soil type. General terrestrial input files at a resolution of 1° supply the albedo, greenness fraction, slope category, and deep soil temperature. Parameterizations selected for use within WRF include the Kain-Fritsch convective parameterization and the NOAA land surface model along with the WRF Single-Moment 6-class microphysical scheme.

Figure 2.2: The Computational Grids Used in the WRF-ARW Simulations.

(The coarse outermost grid takes up the entire map with the boundaries of the inner nested grid indicated by the white rectangle labeled "d02".)

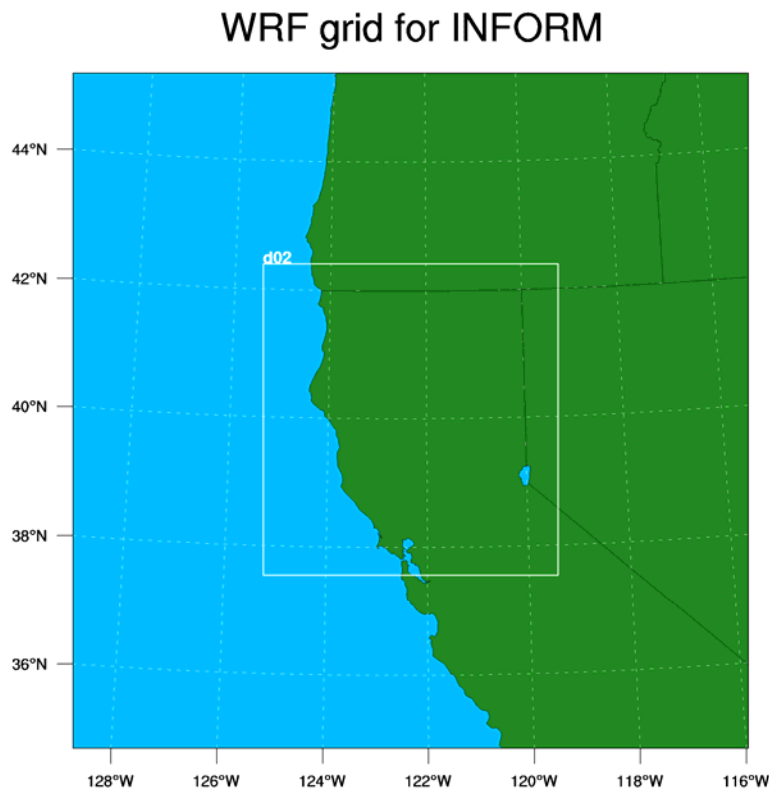
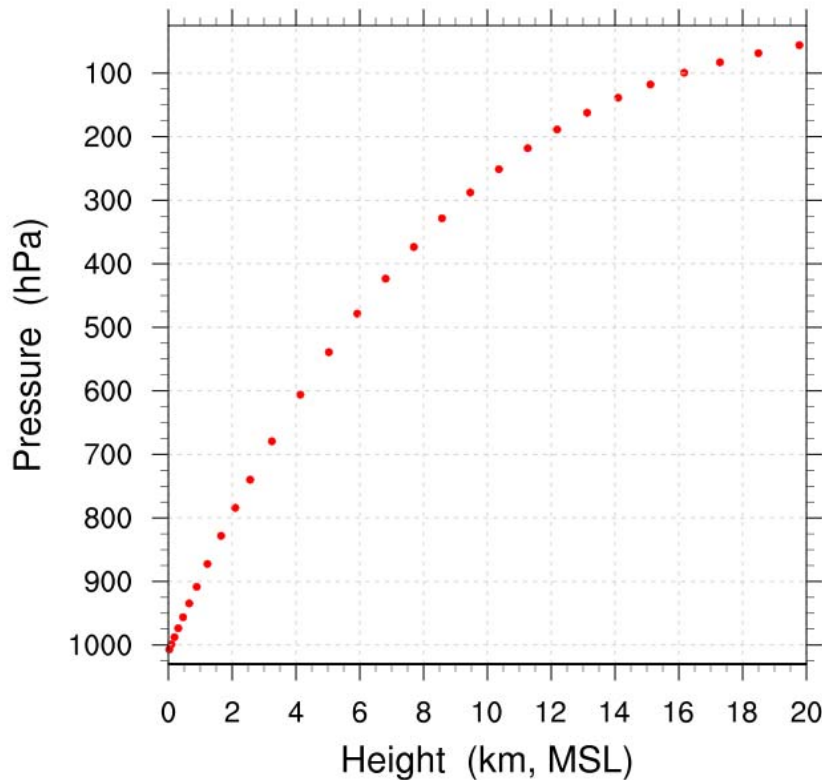


Figure 2.3: The Computational Layers along the Vertical over the Grids Shown in Figure 2.2.

(Each layer is represented by a red dot in the Pressure versus Height graph. These layers are the same over both the outer and inner nested grids.)



The simulations generated by mesoscale models are known to deviate from observed atmospheric states. While these deviations are often small and within the error inherent in meteorological observations they can become amplified as the time period simulated by the model increases. In order to prevent a mesoscale model from deviating or “drifting away” from some reference atmospheric state (in this case, one depicted by the GEFS ensemble perturbations) four dimensional data assimilation (FDDA) techniques are used. FDDA, also known as nudging, is a method of incorporating observations into the calculations from a full-physics model over the course of a single integration. For the simulations presented in this study the FDDA technique of grid- or analysis- nudging is employed. The analysis nudging method introduces a relaxation term in the prognostic equations for wind, temperature, and water vapor to nudge the mesoscale model toward the gridded observations/forecast in time and space at each model grid point (see *Stauffer and Seaman 1990*). Analysis nudging is implemented on the outermost WRF grid (see Figure 2.2) using gridded data interpolated from the GEFS ensemble perturbations; this nudging only takes place above the Planetary Boundary Layer (PBL). The nudging of the model occurs over approximately a one hour time interval centered on the 6 hourly availability of the GEFS forecast.

2.2.1 Mesoscale Model Effects

As part of the validation and testing process the forecasts from the GEFS and WRF were compared. The plots shown in Figure 2.4 compare GEFS and WRF forecasts initialized at 00:00:00 UTC on 10 March 2011 for forecast days three, four, and five. The impact of the higher resolution WRF forecast on the ensemble median of the total accumulated precipitation fields is clearly evident. As would be expected when comparing the results of a mesoscale model to the model used as its forcing, the timing of the precipitation is very similar between the GEFS and WRF-ARW ensemble medians. However, the pattern and magnitude of precipitation differs significantly, particularly over parts of the domain with significant orographic features that can be resolved by WRF (at its 10 x 10 km² spatial resolution).

2.2.2 Integration of the Mesoscale Model into INFORM

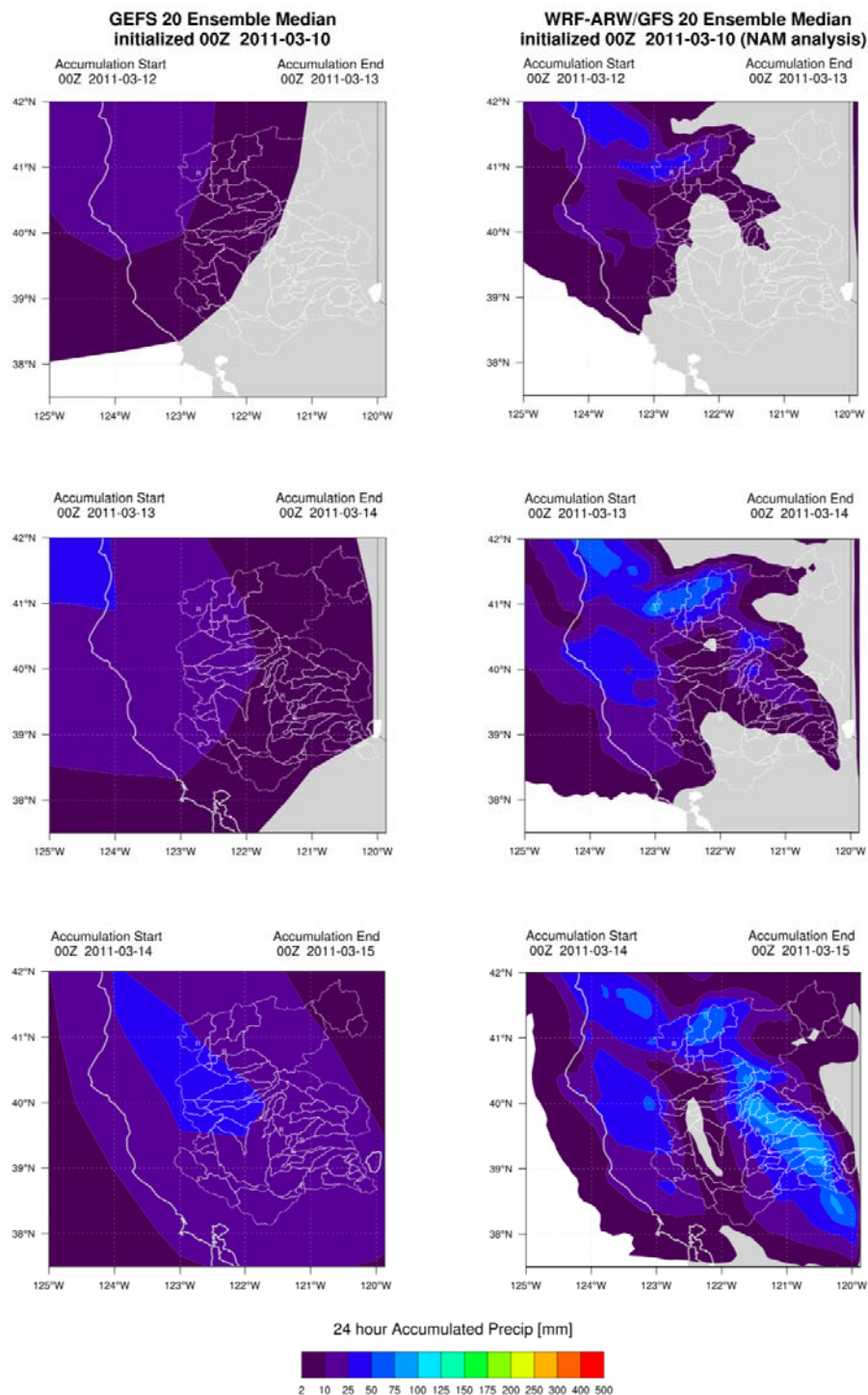
The sequence of events comprising the operational WRF-ARW implementation for INFORM begins with the input data. The 20 GEFS ensemble perturbations and the NAM analysis are downloaded in GRIB format from the NOAA Operational Model Archive and Distribution System (NOMADS) as soon as they become available online. These data are then fed directly into the WRF Preprocessing System (WPS) which decodes the data and interpolates them onto the computational grid used in the WRF calculations. The WPS is executed separately for each of the GEFS ensemble perturbations, resulting in 20 sets of processed input data. Each set of input data is identical to every other set at the analysis (initial) time as these data are defined by the same NAM analysis. In the event that GEFS data is not ready for download by a specified time the processing begins with the data available.

Once the input data have been prepared they are each fed into separate executions of the WRF-ARW dynamical core. These executions are spread across the back-end of the INFORM cluster and are run simultaneously. After the processing of each and every WRF ensemble member is complete the model output data and log files are archived. The post processing sequence begins with the extraction of the meteorological variables of interest from the raw model output. These variables include the air temperature at 2 meters above ground and the total accumulated surface precipitation simulated by the model. The extracted variables are then interpolated from the WRF computational grid onto the cylindrical equidistant grid used by the module that computes mean areal precipitation and temperature and written to separate self-describing netCDF files. The interpolated model output files are then used to generate real-time visualizations for display on the INFORM website. The files are also written to a raw binary format for ingest into the INFORM system and further processing by downstream modules and, finally, are archived.

Significant computational resources are necessary to allow real time ensemble forecasting using WRF and the other models and procedures of Figure 2.1. Appendix A describes the computational platform of the forecast component of INFORM II, mainly pertaining to the computationally demanding WRF processing, and presents an outline of the forecast component computer implementation.

Figure 2.4: Comparison of GEFS (Left) and WRF-ARW (Right) Forecasts Initialized at 00:00:00 UTC 10 March 2011.

(The plots show the ensemble median of the 24 hour total accumulated precipitation over the INFORM watersheds, shown with white boundaries, on forecast days three, four, and five.)



2.3 Intermediate Complexity Regional Model (ICRM) Implementation

2.3.1 Introduction

Phase I of INFORM used an orographic precipitation model and an adaptation of the MM5 land surface component to estimate gridded surface precipitation and temperature for the domain of Northern California from ensemble Global Forecast System (GFS) forecasts issued by NCEP out to 16 days (*Georgakakos et al. 2006; Chapter 3*). In the present Phase II of INFORM (INFORM II), and given the enhanced computational capacity of INFORM II, 10kmx10km-resolution precipitation and temperature ensemble forecast fields out to 16 days are produced by dynamic downscaling GFS ensemble forecasts using the full physics model WRF (see previous section). In addition, discussions with the National Centers for Environmental Prediction (NCEP) that started during the previous phase of INFORM have contributed to NCEP now making available three-dimensional ensemble forecast fields for upper air and surface atmospheric variables from the Climate Forecast System (CFS). Preliminary work (*Georgakakos et al. 2008*) indicated that, under certain conditions of strong and persistent large scale forcing, longer lead time ensemble forecasts of precipitation, temperature and resultant flow fields (out to 30 days) provide useful information after they are dynamically downscaled. In INFORM II the orographic model and surface temperature model of the previous phase are updated and are combined to create a computationally-efficient Intermediate Complexity Regional Model (ICRM) that is used for dynamic downscaling four-times per day of the CFS ensemble forecasts out to 41 days with 6-hour resolution.

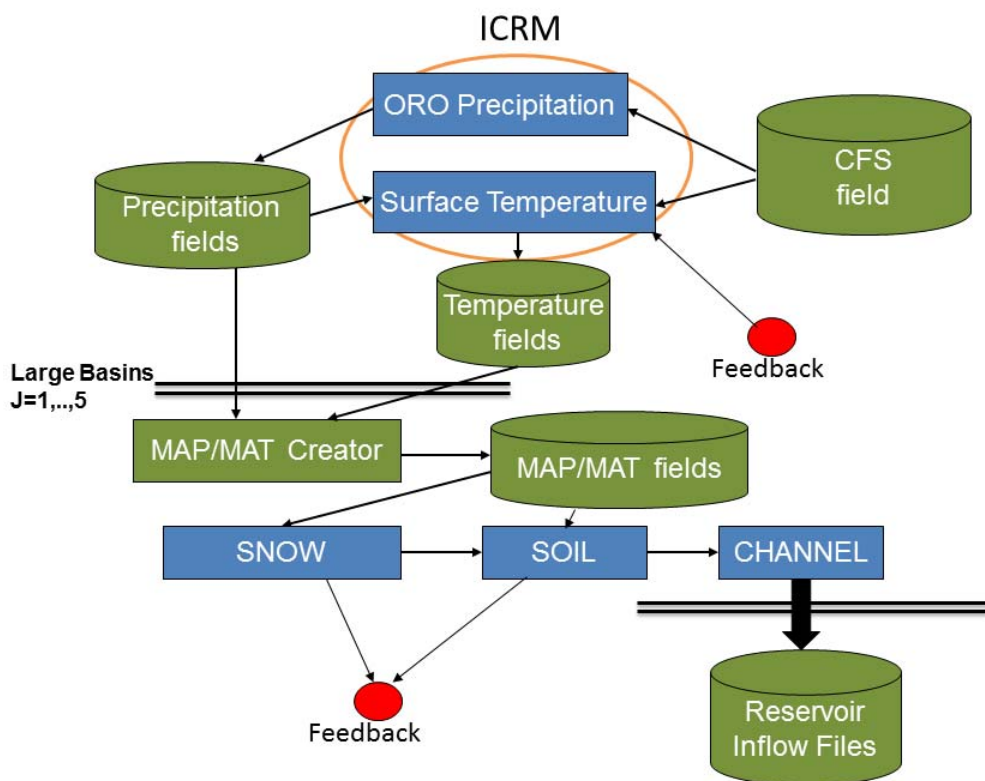
Figure 2.5 shows the ICRM components and their links with other INFORM II forecast components for forcing that is comprised by a single CFS ensemble-member field. The orographic model is invoked first and produces gridded high resolution fields over the INFORM II domain. Given input from CFS and from the orographic precipitation model output, the surface temperature model is invoked and produces high resolution gridded surface temperature and 2-m air temperature fields. For each subcatchment of the five basins (drainages of the major reservoirs of INFORM) and for each 6-hourly time interval, a GIS-based component averages the gridded precipitation and temperature fields over each subcatchment to produce mean areal precipitation (MAP) and mean areal temperature (MAT) time series that are used to drive the snow and soil water models of INFORM II. These models produce snow melt and surface/subsurface runoff which is then input to the routing model of INFORM II for each large watershed to produce reservoir inflow time series. This is done four times per day (see Appendix A for forecast component processing information) and for each of four CFS ensemble members to produce an ensemble of four reservoir inflow forecasts, four times daily. At 1200 UTC each day, hydrologic model states are aligned to those of the CNRFC corresponding operational models. At each time during the execution for a single CFS ensemble member the snow and soil water estimates of the surface temperature model (see description of formulation below) are aligned to those of the INFORM II snow and soil models (feedback indicated in Figure 2.5).

Over the course of INFORM II, NCEP made two versions of CFS three-dimensional ensemble output operationally available for each ensemble forecast member. Initially, a substantially

reduced set of upper air variables was made available once daily with four ensemble members, and then a more complete set for each ensemble forecast was made available four times a day each with four ensemble members. The first CFS forecast output version is referred to as CFSv1 or CFS1, while the second CFS forecast output version is referred to as CFSv2 or CFS2 in this report. During project development, the INFORM II forecast component was enhanced to work first with CFS1 and then with CFS2. The time of the change from CFS1 ingest to CFS2 ingest for the INFORM II forecast component was the 21st of February 2012 at 0000 UTC.

This section describes the ICRM model updates compared to the phase I formulation and presents initial results of real time application as part of INFORM II. In addition, it presents the necessary transformations applied to each version of the CFS output for producing suitable input data to drive the ICRM for dynamic downscaling of precipitation and temperature in Northern California.

Figure 2.5: ICRM and Links within the INFORM II Forecast System.



2.3.2 Regression-Based Soundings to Produce ICRM Input from CFS1

The initial version of the NOAA Climate Forecast System (CFS1) provided a very limited set of high frequency forecast data (few variables, few levels). At a minimum, the orographic precipitation model used in the INFORM ICRM requires a vertical profile (sounding) of meteorological conditions [temperature (T), humidity (Q), winds (U), and heights (Z)] on pressure levels from near the surface to ~200 hPa at representative locations upstream (to the

west) of the Sierra Nevada every 12 hours or less. For instance, Oakland, California is well situated for this purpose, and has a long historical data base of observed radiosonde soundings. In contrast to these requirements, CFS1 provides only a) heights on the 1000, 850, 700, 500 and 200 hPa pressure surfaces, b) winds at 850 hPa, and c) integrated column water content (P_{WAT}). These data are available globally on a 2.5 degree grid. Winds on the 700, 500, and 200 hPa pressure surfaces can be derived via geostrophy. Thus, the required variables available or immediately derivable from CFS1 are as shown in Table 2.1; those required by the INFORM system are as shown in Table 2.2.

Table 2.1: Surface and Upper Air Variables Available from CFS1 at Each Grid Point

("X" indicates a CFS1 output variable; "G" indicates that the winds are derived using geostrophy.)

Pressure (hPa)	Z	U	V	P_{WAT}
1000	X	G	G	
850	X	X	X	
700	X	G	G	
500	X	G	G	
200	X	G	G	
				X

Table 2.2: Surface and Upper Air Variables Required for Upstream Sites for INFORM ICRM

("X" indicates variables available or easily estimated from CFS1 output; "D" indicates variables that must be statistically derived in the present INFORM system.)

Pressure (hPa)	Z	T	Q	U	V
1000	X	D	D	X	X
850	X	D	D	X	X
700	X	D	D	X	X
500	X	D	D	X	X
400	X	D	D	D	D
200	X	D	D	X	X

The basic problem is to develop a statistical model that can produce estimates of the required unknown quantities in Table 2.2 (those marked “D”) when supplied with a single set of the variables in Table 2.1 (those that are available from CFS1). The necessary models were developed using a technique commonly known as “PC regression” (e.g., Jolliffe 2002; here “PC” stands for Principal Components). In PC regression, the predictor and predictand data sets (in this case, the data available from CFS1 and the data required for the INFORM ICRM model, respectively) are expressed in terms of linear combinations of paired orthogonal basis functions known as “Empirical Orthogonal Functions” (EOFs). In this case, these paired functions express different modes of variability in “variable space” (e.g., the 16 predictand variables; these are known as “loadings”) and “time” (e.g., the number of observations; these are the “PCs”). For PC regression, EOF analysis serves to filter noise from the predictor and predictands, and improves the stability of the regression parameters.

For the INFORM system and based on preliminary analysis, separate regression models were developed for locations at Oakland and Eureka. Considering Oakland first, *observed* soundings were available nominally every 12 hours over the period 1981-2004. These soundings provided training sets from which to derive the statistical models. These observations are used to develop a statistical procedure for deriving the unknown variables in Table 2.2 from the variables in Table 2.1 for the sites of interest. This is a relatively simple procedure, but is most easily understood if broken down into steps; do note that separate sets of EOFs and regression models were developed for each month of the year, and that all of the variables are pre-processed to have zero mean and unit variance before any other processing. Thus, estimates of the predictands are initially in “normalized” units and then are “unnormalized” before use.

For a given month (over the 1981-2004 period), assume there are NT soundings that pass an initial quality control step. From these soundings, extract the *predictor* variables (Table 2.1) – this process produces the predictor matrix Y which has dimensions (NT x NY), where NT was typically 1200-1300 (e.g., 24 years x 31 days x 2 soundings per day = 1488; some are missing) and NY is 16 (the number of variables). Using EOF analysis, the predictor matrix Y is expressed in terms of its basis function:

$$Y' = \alpha e^T \quad (2.1)$$

where α is an NT x $N\alpha$ orthogonal matrix (the PCs noted above), and e is an NY x $N\alpha$ orthonormal matrix (the loadings; the superscripted “T” indicates transpose). The superscripted prime indicates that the fraction of the original variance of Y retained in Y' depends on how many modes ($N\alpha$) are retained and how the variance happens to be partitioned among them (in EOF analysis, the modes represent decreasing fractions of variance as the mode number increases; also note that as written here, the variance associated with mode j is retained in PC_j). For this work, $N\alpha$ was set to 10 for all months and at least 97 percent of the original variance was retained in each case.

The same process can be carried out for the *predictand* matrix Z [with dimensions NT x NZ (= 30; Table 3.2)], for which one can write:

$$Z' = \beta f^T \quad (2.2)$$

For the predictand EOFs, $N\beta = 15$ modes were retained, these representing at least 96 percent of the original variance.

With α and β in hand, least squares regression is performed to derive the coefficients A ($= N\alpha \times N\beta$) required to provide estimates of β (β^*) from α . In general, these coefficients are given by

$$A = (\alpha^T \alpha)^{-1} \alpha^T \beta \quad (2.3)$$

In this case, the orthogonality of the predictor PC's α means that matrix $(\alpha^T \alpha)^{-1}$ is a diagonal matrix composed of the inverse variances of each α , obviating the need to formally calculate the inverse.

When applied to the 24-year Oakland sounding training set (i.e., in hindcast mode), the derived model produces skillful results. For example, the correlations between actual and estimated lower tropospheric specific humidity (Q) are 0.80-0.85 for 850 hPa and 0.7-0.75 for 700 hPa. Correlations for winds are very high (~ 0.98) as these are redundant variables.

With the matrix of coefficients (A) computed, a partial sounding from CFS1 (i.e., the data available in Table 2.1) can generate estimates of the full desired sounding (the data in Table 2.2). To accomplish this first the CFS data are normalized (giving Y_{CFS}), then the data are projected onto the predictor loadings to obtain “pseudo-PCs” (as shown below):

$$\alpha^* = Y_{CFS} e \quad (2.4)$$

Next, use A to get estimates of β (β^*) -

$$\beta^* = \alpha^* A \quad (2.5)$$

then project β^* onto the predictand loadings (f) to get normalized estimates of Z

$$Z^* = \beta^{*T} f^T \quad (2.6)$$

Unnormalizing Z^* , using the *observed* standard deviation and mean, gives the values in physical units.

For the site at Eureka, observed soundings are not available, so the necessary training data (as in Table 2.1 and 2.2) were extracted from NOAA North American Reanalysis (NARR) results. These data covered 1981-2003 and were taken at 12 hour intervals (giving ~ 1400 observations per month) to maintain consistency with the Oakland observed sounding database. Otherwise the procedures for developing and applying the statistical model are identical to that described for Oakland. The statistical hindcast skill for lower tropospheric moisture in these results was quite good, with correlations ≥ 0.9 for November-March.

In INFORM II system operational use with up-to-date CFS1 ensemble forecast data, the steps shown above (discussion of Eqs. 2.4 - 2.6) are applied to develop estimated soundings out to a lead time of 60 days with 12-hourly resolution. Examples of CFS1-based estimates of atmospheric variables are shown in Figures 2.6 and 2.7 for the scalar air temperature and specific humidity at 700 mbar level and for the wind vectors at the same level for both Oakland and Eureka and for a period with several storms in the 2010 – 2011 winter season. Analysis and

12-hour forecast results are shown for each day. Higher temperatures (T) are shown for Oakland with higher specific humidities (q) shown for Eureka. Correspondence of wind vectors is good for northwesterly to southwesterly winds (typically causing orographic rainfall development in the Sierra Nevada).

Figure 2.6: Estimated Air Temperature (T) and Specific Humidity (q) at 700 mbars at Oakland and Eureka Based on CFS1 Input.

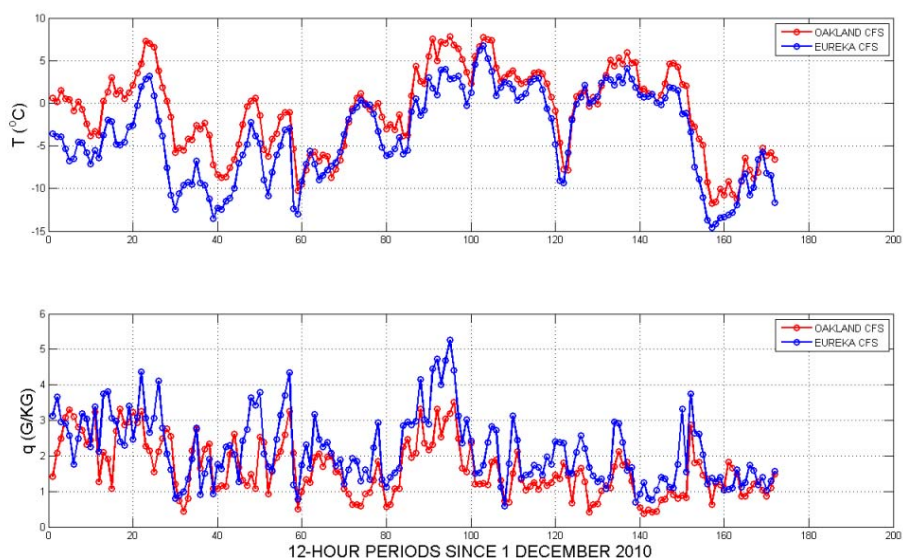
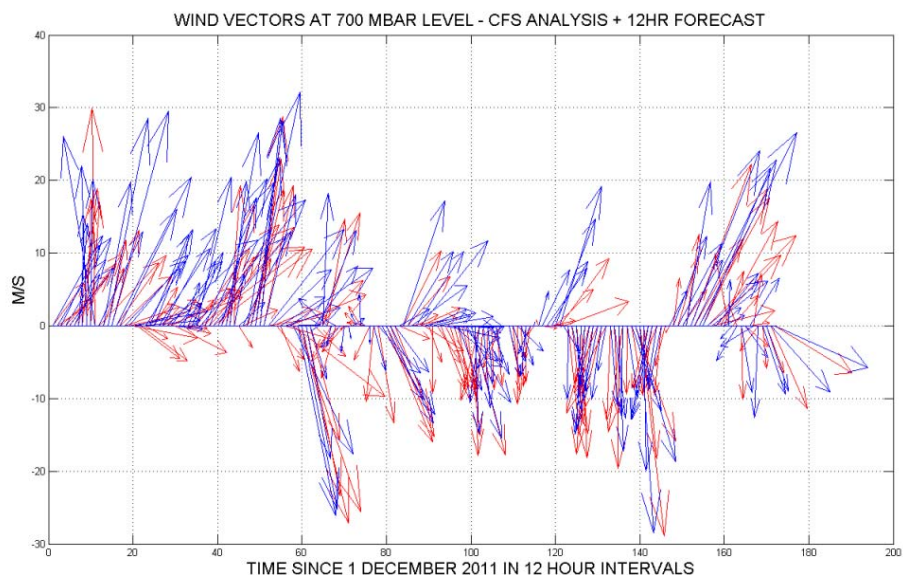


Figure 2.7: 700 mbar Wind Vectors (m/s) for Oakland and Eureka Based on CFS1 Input.



2.3.3 ICRM Input from CFS2

The CFS2 ensemble forecast output is substantially more extensive than that made available initially (CFS1) and described in the previous section. Specifically, the available information for air temperature (T), specific humidity (q), wind (u and v), and geopotential height (Z) is by pressure level (mbars) and at the height from surface (m) as shown in Table 2.3:

Table 2.3: Upper Air and Surface Variable Availability for CFS2 Output

T:		1000		850	700	500	250	200
q:	2m		925	850	700	500		
u,v:	10m	1000	925	850	700	500	250	200
Z:		1000		850	700	500		200

In this case, generation of ICRM input for each time and ensemble member requires interpolation for T and Z to 925 and 250 mbar levels from the neighboring higher and lower levels, for which the values exist, and the estimation of specific humidity for the 1000, 250 and 200 mbar levels. For the first case, the hypsometric equation may be used to estimate T and Z using the 1000 and 850 mbar information from Table 2.3, while in the second case specific humidity may be set at 1000 mbars to be equal to that at 925mbars and to be negligible for the 250 and 200 mbars. The hypsometric equation expresses the value of the geopotential height Z at a certain height (Z_2) as a function of the known geopotential height (Z_1) at a different level:

$$Z_2 - Z_1 = H \ln(p_1/p_2) \quad (2.7)$$

with the scale height (H) expressed as:

$$H = R_d T_v / g_0 \quad (2.8)$$

and with R_d being the gas constant for dry air, T_v is the average virtual temperature in the layer between geopotential heights Z_1 and Z_2 , and g_0 is the acceleration due to gravity at the Earth's surface. The virtual temperature T_{vp} at a given pressure level p may be obtained from:

$$T_{vp} = T / [1 - (e/p)(1-\epsilon)] \quad (2.9)$$

with e representing the partial pressure of water vapor, T is the air temperature, and $\varepsilon = 0.622$. An estimate of e may be obtained from the specific humidity and temperature utilizing saturation vapor pressure empirical functions of air temperature.

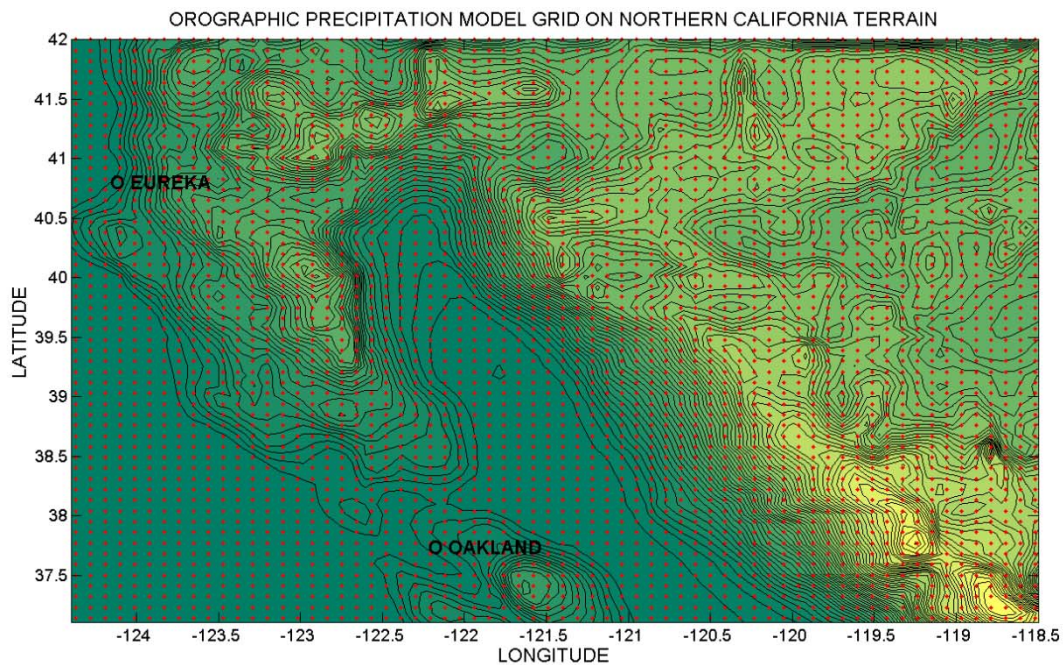
The result of the transformations indicated above is a full matrix of Table 2.3 values for each CFS2 ensemble member, for each time of CFS2 forecast output availability and for each upstream-node input site used in ICRM.

2.3.4 Orographic Precipitation Model Updates

The orographic precipitation model formulation described in *Georgakakos et al. (2006; Section 3.2)* is retained in this phase of INFORM. The surface grid of the model (10kmx10km resolution) as defined for INFORM II is shown in Figure 2.8. In the preprocessor of the input data we made modifications to allow the use of a second site of ensemble input forecasts by the CFS at Eureka (see also discussion in the previous section and Figure 2.8). This was done mainly to provide better resolution of the input for the northern watersheds of the INFORM domain (drainage areas of Shasta and Trinity mainly), particularly under conditions of higher specific humidity at Eureka and northwesterly winds. Figure 2.9 exemplifies the differences between using just Oakland and using both Oakland and Eureka CFS input for the mean areal precipitation (MAP) of the South Fork American River (southernmost subcatchment), the Delta River (in the Shasta drainage), and the Pit River (in the Shasta drainage).

Figure 2.8: Surface Grid of the ICRM for Northern California.

(The two nodes provide CFS three-dimensional ensemble forecast input.)



The three-dimensional ensemble forecasts of CFS have a 12-hour resolution and to maintain a six-hour output for the downstream hydrologic models, an analysis of the distribution of mean

areal precipitation during the day was done for the watersheds of interest. Selected results are shown in Figures 2.10 (for the Delta River subcatchment upper and lower portions) and 2.11 (for the South Fork American River subcatchment upper and lower portions) below. It was concluded that a uniform distribution of 6-hourly precipitation within a day adequately describes the data (values of 0.25 in the plots of Figures 2.10 and 2.11). This was used to distribute the 12 hourly precipitation accumulations produced by ICRM with CFS forcing into 6-hourly accumulation amounts.

Figure 2.9: Sample CFS-Based MAP ICRM forecasts.

(Upper panels use CFS only at Oakland and lower panels use CFS both at Oakland and Eureka.)

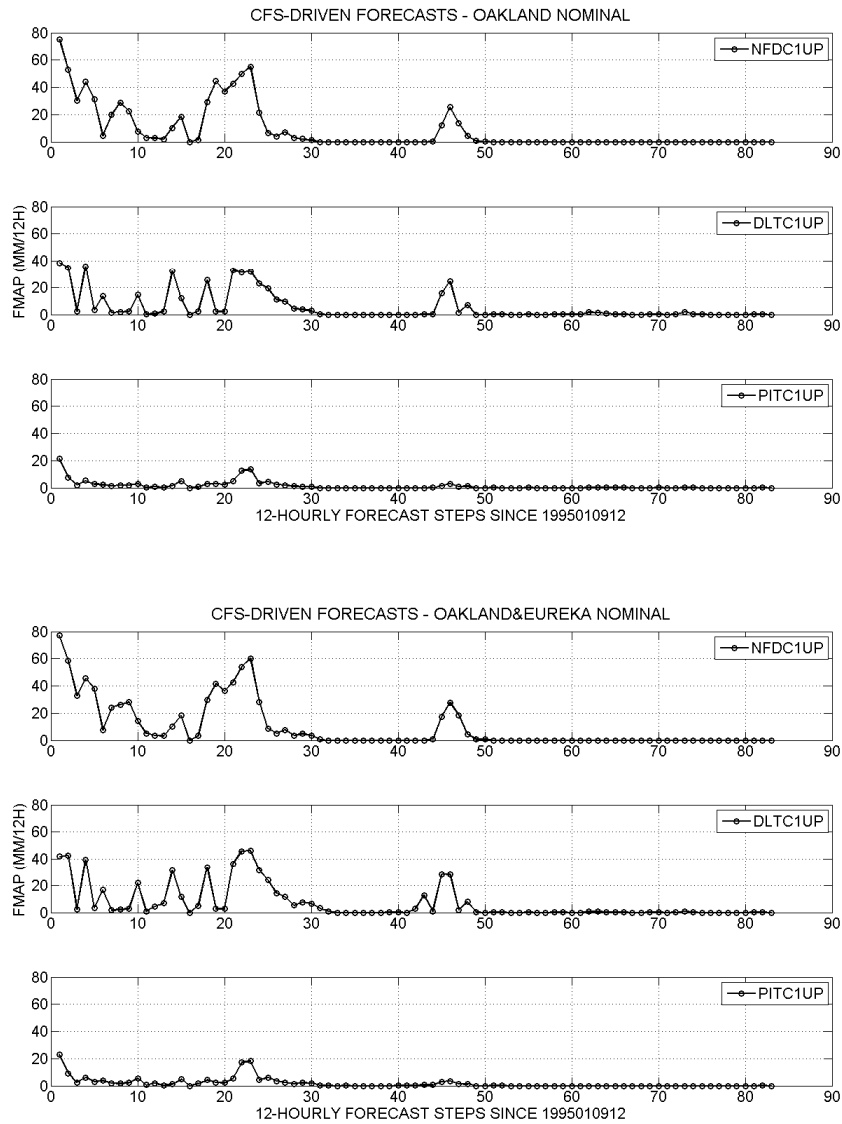


Figure 2.10: Diurnal Distribution of MAP Estimated by CNRFC for the Upper and Lower Portions of the Delta River Subcatchment in the Shasta Drainage.

(The mean areal precipitation is shown as a fraction of the daily total and it is assigned to the ending hour of the 6hour interval (in PST).)

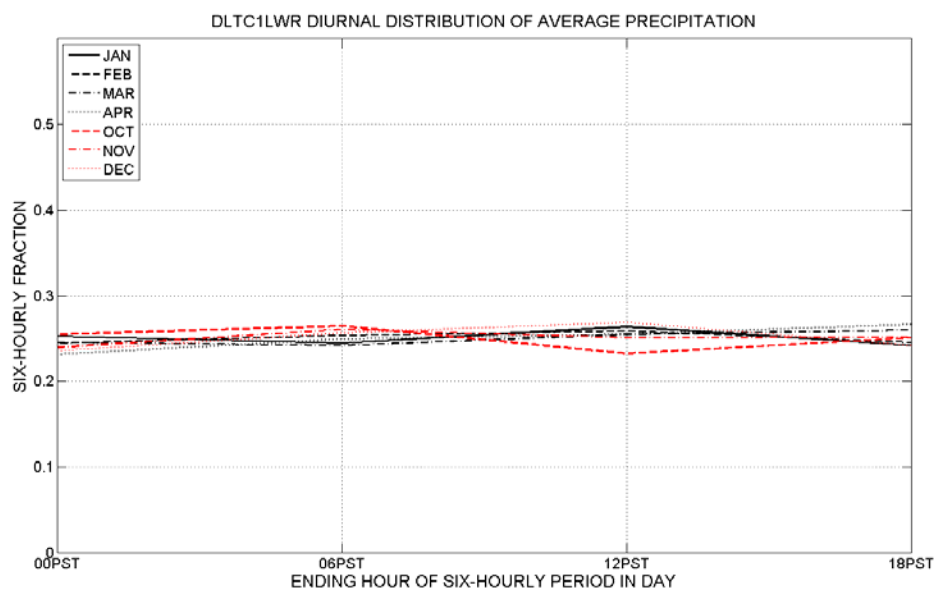
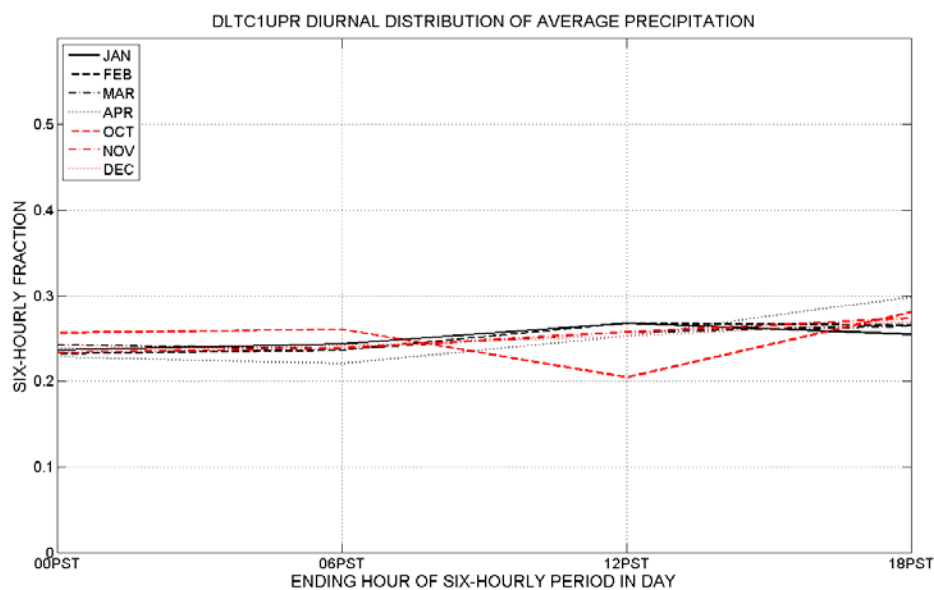
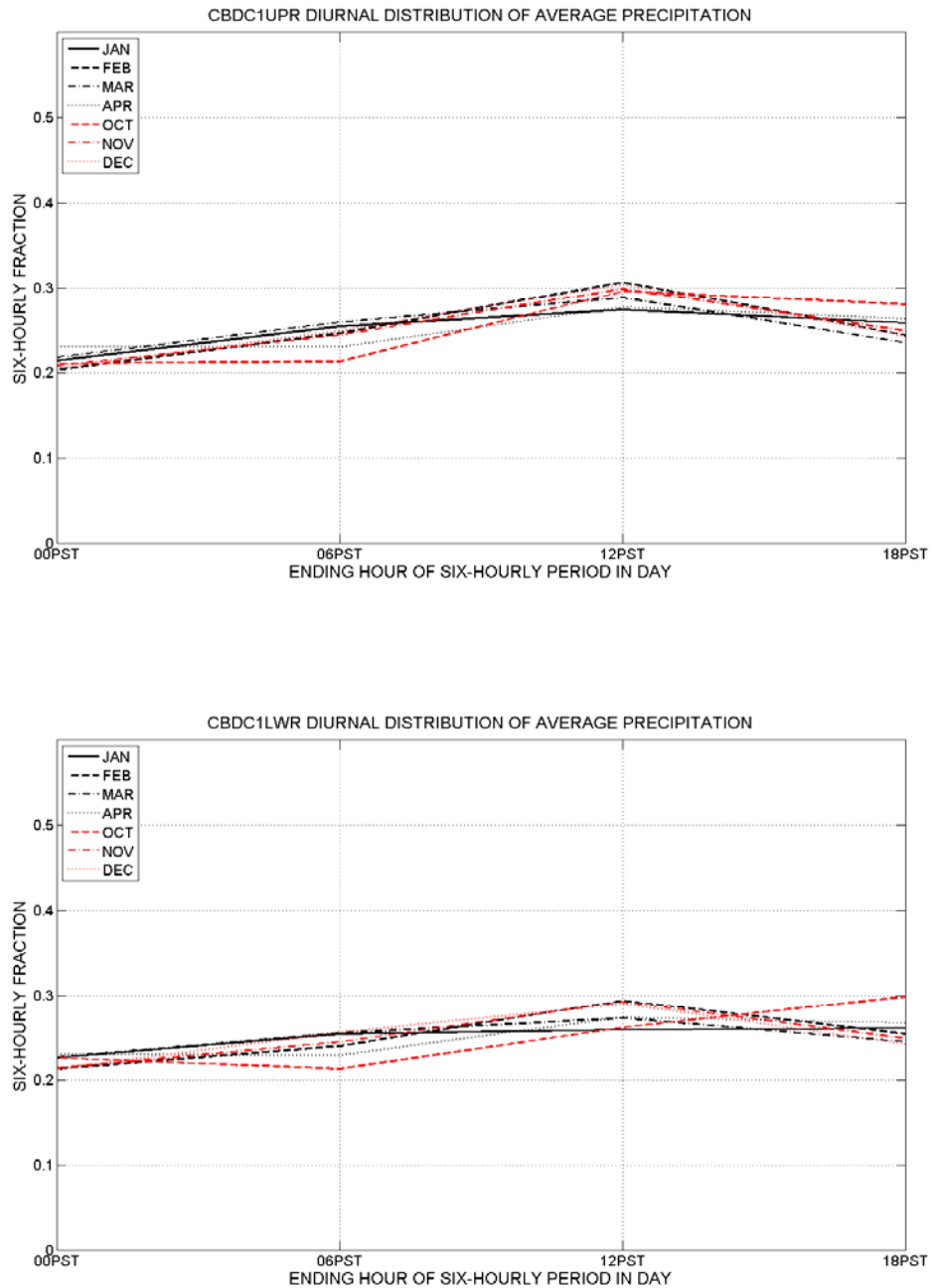


Figure 2.11: As in Figure 2.10 but for the South Fork American River Subcatchment.



The orographic model component of the ICRM is executed first to provide ensemble gridded precipitation estimates with spatial resolution equal to 10km by 10km, vertical resolution of 1000m in mid-troposphere, and with temporal resolution equal to 6 hours and lead times out to 41 days using CFS ensemble input. The model uses a base interval of 112 sec for integration. Once gridded precipitation fields are at hand, mean areal precipitation (MAP) estimates for each subcatchment in the INFORM domain are obtained using a GIS determined basin

boundary map and the gridded model precipitation output for the surface grid. The MAP is used to drive the basin hydrologic and routing models described earlier.

It is important to note that the orographic model component is a simplified dynamical model that generates precipitation estimates due to the interaction of the wind field and the orographic terrain. The model forecasts are thus most usable for sloping terrain in Northern California and underestimation of precipitation is expected in the valley regions with no or little slope. In INFORM II it is used because the domain has substantial orographic precipitation, and the model integration is substantially shorter than that of full dynamical model such as WRF. Earlier evaluation (see *Georgakakos et al. 2006*) showed good performance in estimating the occurrence and amounts of mean areal precipitation, with overestimation in higher elevations and underestimation in lower elevations. The evaluation of the MAP estimates for INFORM II using ICRM with CFS forcing for various lead times is presented in Chapter 4.

2.3.5 Surface Temperature Model Updates

The surface temperature model of INFORM Phase I was the land surface component of the atmospheric mesoscale numerical model MM5. The integration complexity in including an MM5 component within the INFORM system constrains portability. In addition, MM5 is no longer supported but has been transitioned to the WRF-ARW with significant changes in the land surface model. For these reasons, a different model was formulated, tailored for the INFORM purposes to estimate gridded surface temperature for the INFORM II domain (Figure 2.8).

The formulation is based on surface energy balance considerations for the estimation of the surface (skin) temperature at each grid box in a grid of the type shown in Figure 2.8. The surface temperature T_o is computed as the solution of the diagnostic surface energy balance equation, which, for generality that includes melting snow, may be written as (e.g., *Pielke 1984; Liston 1995*):

$$(1-a)Q_{si} + Q_{li} + Q_{lo} + Q_H + Q_E + Q_G = Q_m \quad (2.10)$$

where Q_{si} is solar radiation reaching the surface, Q_{li} is incoming longwave radiation, Q_{lo} is outgoing longwave radiation, Q_H is sensible turbulent heat flux, Q_E is latent turbulent heat flux, Q_G is conductive energy transport (assumed negligible), Q_m is energy available for melt, and a is surface albedo.

For each grid box, the formulation uses parameterizations that employ a reference level temperature in the atmosphere and a surface temperature. The following sections outline important parameterizations used to express the terms as functions of the reference and surface temperatures, reference relative humidity, pressure and wind speed, the presence of precipitating and non-precipitating clouds, the surface soil water saturation level, the presence or absence of snow, and the land surface parameters such as land use type, surface albedo, emissivity and aerodynamic roughness. The second to fifth terms on the left-hand side of Equation (2.10) are functions of surface temperature T_o and thus, given parameterizations of the terms in that expression, T_o may be obtained as the algebraic solution of the aforementioned

equation. After the parameterization sections, the authors discuss the numerical methods for (a) the estimation of surface temperature and (b) of the 2-meter air temperature.

2.3.5.1 Shortwave Radiation

Solar radiation is absorbed and scattered (not emitted). Absorption and scattering are functions of wavelength, incidence angle, and land surface material properties (e.g., snow grain size and surface layer impurities for snow, type of vegetation, etc.). The clear sky incoming shortwave radiation is computed based on the formulation advanced by *Allen et al. (2005)*:

$$Q_{si} = K(z) Q_a \quad (2.11)$$

where Q_a is the extraterrestrial solar radiation, and the function K represents an influence function for effects of atmospheric layer thickness and transmissivity, and water vapor, dust and aerosol content in the atmosphere. Q_a is computed as a function of day of the year, time of the day, longitude and latitude.

The net shortwave radiation requires the estimation of the albedo a (see Equation (2.10)). Spectral measurements are nonexistent at remote sites, so we use a single band, global approach for albedo specification (rather than e.g., visible (0.3-0.7mm) and near-infrared (0.7-2.8mm)). The albedo of the land surface is allowed to vary seasonally, and a single value albedo (=0.5) is used if the grid point of interest has snow cover (no snow age dependence is used). In the presence of clouds, the cloud albedo was computed based on parametric curves produced numerically (*Liou 2002*) and which relate the albedo to the cloud liquid water path (liquid water content x cloud depth) for a given mean water droplet radius. For precipitating clouds a value of 0.85 was used for albedo. The gridded parameter values for shortwave albedo, emissivity, and surface roughness used in ICRM are shown in Appendix B together with the land cover classification.

2.3.5.2 Longwave Radiation

For cloud free conditions, the downward longwave radiation is given by the empirical relationship (*Rockel and Raschke 1994*):

$$Q_{li} = \sigma T_1^4 (0.79 - 0.174 \exp\{-0.095e_1/100\}) \quad (2.12)$$

where T_1 is the reference air temperature, e_1 is the reference vapor pressure, and σ is the Stefan-Boltzmann constant ($= 5.67 \times 10^{-8}$). For cloudy conditions the incoming longwave radiation expression used is (*Liou 2002*):

$$Q_{li} = ((1-\varepsilon)\varepsilon\sigma T_o^4 + \varepsilon\sigma T_c^4) / (1 - (1 - \varepsilon)(1-\varepsilon)) \quad (2.13)$$

In the latter expression, T_c is cloud base temperature; ε is the surface emissivity, and ε_c is cloud emissivity, which is given by (*Stephens, 1978*):

$$\varepsilon_c = 1 - \exp\{-0.158W\} \quad (2.14)$$

where W is liquid water path (g/m^2) (liquid water content x cloud depth near cloud base).

The outgoing longwave radiation from the surface in a cloudless atmosphere is given by

$$Q_{lo} = \varepsilon \sigma T_o^4 \quad (2.15)$$

while in a cloudy atmosphere in correspondence to Equation (2.13) it is given by

$$Q_{lo} = ((1-\varepsilon)\varepsilon_c \sigma T_c^4 + \varepsilon \sigma T_o^4) / (1 - (1 - \varepsilon)(1-\varepsilon_c)) \quad (2.16)$$

The above formulas for cloudy conditions are only applied when the lifting condensation level is estimated to be less than 5000m.

2.3.5.3 Sensible and Latent Turbulent Heat Fluxes

Both these fluxes have been parameterized as in *Liston (1995)* with elements of the formulation traced back to *Price and Dunne (1976)*:

$$Q_H = \rho \zeta c_p D_H (T_1 - T_o) \quad (2.17)$$

$$Q_E = \rho \zeta L_v D_E (0.622[e_1 - e_o]/p_1) \quad (2.18)$$

where ρ is the surface air density, ζ is a non-dimensional stability function given as a function of Richardson's number, c_p is the specific heat of air under constant pressure, L_v is the latent heat of vaporization of surface air, D_H and D_E are exchange coefficients for sensible and latent heat that are functions of the wind speed at the reference height, subscript 1 denotes reference height and subscript o denotes surface, e denotes vapor pressure, and p denotes air pressure.

The Richardson's number is defined as:

$$Ri = - (g/q) (dq/dz) (du/dz)^{-2} \quad (2.19)$$

where g is the acceleration of gravity at the layer considered, q is the layer mean specific humidity, dq/dz is the layer gradient of specific humidity with respect to height, and du/dz is the gradient of the wind with respect to height.

The vapor pressure at the surface is parameterized as

$$e_o = 10^{(11.40 - 2353/T_o)} \beta \quad (2.20)$$

where β is the soil saturation fraction for the upper soil obtained from the hydrologic model.

The vapor pressure at the reference level is given by

$$e_1 = 10^{(11.40 - 2353/T_1)} RH_1 \quad (2.21)$$

where RH_1 signifies relative humidity.

2.3.5.4 Gridded Snow and Soil Models

To obtain estimates of snow cover and soil water saturation levels at the ground surface and to assure consistency with operational hydrologic forecast models (that will use the surface temperature forcing of the energy balance model), gridded versions of the operational snow (SNOW17) and soil water (SACSMA) models were developed. Parameter values for these models were obtained from the initial estimates provided by the Office of Hydrologic Development for their distributed model that uses similar components. Appendix B shows the

values of the major model parameters as applied in gridded form. For real time operation, the relative fraction of water content is estimated over a basin by the basin hydrologic models of INFORM and this fraction is distributed over the grids within the basin to provide initial values for the soil model of ICRM in the feedback process shown in Figure 2.1. The snow fraction and snow water equivalent are similarly distributed prior to each ICRM integration.

2.3.5.5 Method of solution

The numerical solution for the surface temperature T_0 and the 2-meter air temperature T_a over a grid in mountainous terrain is accomplished for a single time period with the application of the following steps:

- Heat flux into the soil at the surface is set (assumed) equal to zero.
- Constant wind profiles are assumed in the mixed layer of the boundary layer and a power law profile in the surface layer of the boundary layer (last 100 meters near the surface).
- Using conservation of potential temperature, and mixing ratio we estimate 100 levels of T , p and RH based on the CFS basic levels (see Tables 2.2 and 2.3 for CFS1 and CFS2, respectively) using vertical linear interpolation.
- Using the same conservation assumptions for potential temperature and mixing ratio, we then interpolate along the horizontal from the CFS grid to the ICRM grid using inverse square distance interpolation for all the levels and all the ICRM grid nodes (two upstream grid points are currently used from CFS). We get T , p , and RH in a three dimensional grid for ICRM.
- We apply adiabatic and pseudo-adiabatic adjustment of the T , p , and RH values at the 2 meter reference level near the surface (parcel ascent given conditions conducive to parcel ascent). The T_1 values obtained are the initial estimates of the reference air temperature that enters the ICRM computations. A sinusoidal curve is fitted to the temperature solution at this point to interpolate from 12 hourly to 6hourly values (the CFS input is in 12 hourly intervals).
- With 6-hourly estimates of T_1 at hand we apply the surface energy balance and we solve for the surface temperature T_0 with a 6-hour resolution.
- An updated estimate of the air surface temperature is a weighted average of T_1 and T_0 : $T_a = T_s w_1 + T_1 w_2$ with w_1 and w_2 being weights that sum to 1.
- The procedure is repeated with T_a used in place of T_1 until there is convergence within a set tolerance. For the purposes of INFORM II, we use one iteration with equal initial weights of 0.5.

It is noted that when there is snow on the ground and the surface (skin) temperature solution is higher than 0 °C, the surface temperature solution is constrained to be at 0 °C and the residual heat flux (resulting from unbalanced terms in Eq. 2.10) is devoted to melting snow.

2.3.5.6 Cloud Influence

The orographic precipitation model provides information pertaining to the development of orographic precipitating clouds. Using just these computed clouds is referred to as the minimal cloud condition. However, clouds exist at other times when precipitation is not occurring. Due to the profound influence that clouds have on surface temperature it is important to account in some way for their development. An important aspect of the computations is the establishment of conditions for the development of clouds through parcel ascent over the mountain barriers in Northern California. Conditions for parcel ascent are that at the 850 mbar level (above the climatological snowline and boundary layer depth) the air is near saturation (relative humidity of 90 percent or higher), the wind speed is greater than 5 m/s, and the wind is from a westerly direction (this to assure that the moist air will be advected over the mountain barrier rather than be blocked); in addition, and based on *Pandey et al. (1999)*, clouds may only develop when and where the 700 mbar temperature is colder than 6 °C.

Several sensitivity analyses were performed using CNRFC mean areal temperature (MAT) data and various conditions for cloud development: minimal cloud condition involving only precipitating clouds, a maximal cloud condition involving unconditional parcel ascent, and a conditional cloud condition involving cloud ascent with the constraints described earlier. A sensitivity analysis example is shown in Figure 2.12 below for three subcatchments of the upper Shasta drainage (Canby, Pit and Delta with elevations above 1,500 meters). The results show that using only precipitation clouds or conditional cloud development using the conditions mentioned above for parcel ascent (better performance) provide best response for this high altitude subcatchments. A second example for lower altitude catchments is shown in Figure 2.13 for the lower Oroville drainage (Indian Creek, Pulga and Merrimac). In this case, the max cloud scenario (green lines) tends to overestimate the temperature, while the other two scenarios (particularly the min cloud scenario in blue) tend to undersimulate the observed temperature.

Figure 2.12: MAT (at 2 meters) for Three Subcatchments of the Upper Shasta Drainage.

(Observations, estimated by the CNRFC, are shown in black, while simulations are shown in green (parcels are free to ascend over the mountains; maximum cloud condition), blue (parcels are constrained and only precipitation clouds are formed), and red (parcels ascend based on the conditions described in the text). CFS1 analysis and 12 hour forecasts are used as ICRM input for these simulations.)

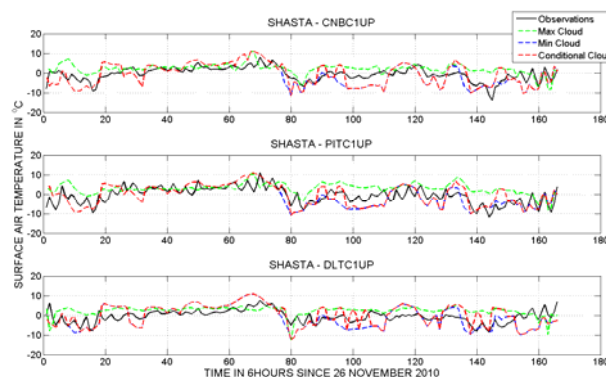
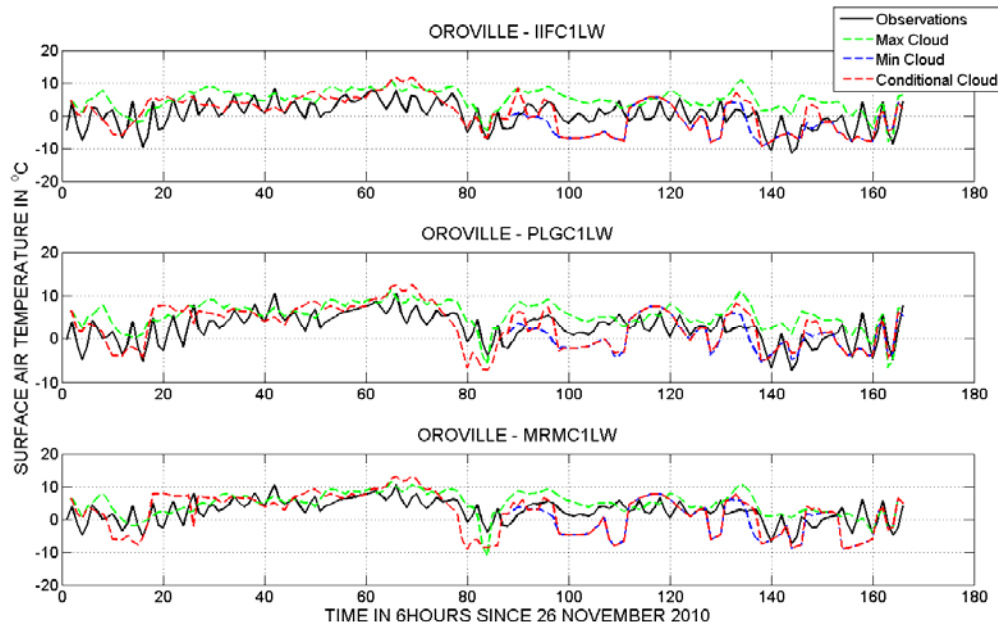


Figure 2.13: As in Figure 2.12 but for Lower Oroville Drainage Subcatchments.



Additional sensitivity analyses results (not shown here) indicate that the conditional cloud development approach gives best results for the subcatchments with elevations above the mean snow line, while for the lower elevations the max cloud approach offers comparable (and even better results in some cases). The decision to use the conditional cloud approach (red lines above) is based on the fact that the ICRM temperature is most significant for predicting snow pack development and melting and it is the snow pack at higher elevations that is most important (higher than the average snow line of 1,500 m) for downstream flow predictions.

2.3.5.7 Sample Results at a Station

A first comparison with mean areal temperature data for INFORM II subcatchments was discussed previously. In this section we present results of comparison of station 2-meter air temperature data to CFS1-driven ICRM model gridded values of 2-meter air temperature for the grid that embeds the station of interest.

Figure 2.14 shows the three stations (Camino, McArthur and Auburn) used in this analysis on a terrain elevation map of Northern California. The station elevations range from 280m to 893m (below the average snow line) and are located in areas of significant slope. For this examples the ICRM ran decoupled from the rest of the INFORM forecast components shown in Figure 2.1 (no feedback was used between the basin hydrologic models and the ICRM hydrologic component). CFS1 input to ICRM surface temperature component consisted of the analysis and 12 hour forecast fields provided twice daily for the period of interest.

Figure 2.14: Location and Elevation of Stations with Observed Air Temperature Data.

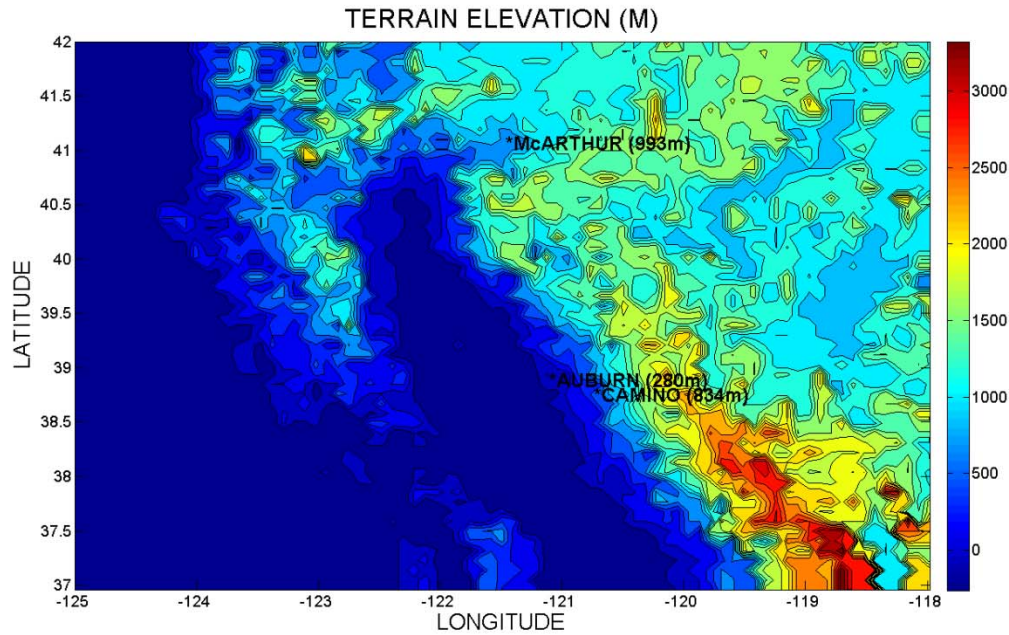


Figure 2.15 shows the observed and simulated (grid average) air temperatures at 2 meters using CFS1 data (analysis and 12-hour forecast). Figure 2.16 displays a scatterplot between simulated and observed data with the fitted regression line (solid line) shown for easy reference. These results indicate that the surface temperature model used reproduces many features of the observed data in spite of the large difference in scale between observations and simulations, and the rather poor-resolution CFS1 input. They also show that for these lower elevation stations (below the average snow line) the ICRM surface temperature model tends to simulate colder 2-meter air temperature than the station observations (as was also pointed out earlier for the comparisons with the CNRFC mean areal temperature).

A more detailed evaluation of the ICRM air temperature estimates is given in Chapter 4 using mean areal temperature observations estimated by the CNRFC for the INFORM II basins.

Figure 2.15: Station Observations of 2-Meter Air Temperature (Black Line), Simulated 2-m Initial Reference Temperature (Blue Line) and Simulated Final 2-m Air Temperature (Red Line).

(Simulated temperatures are averages over a 10km x 10km grid box.)

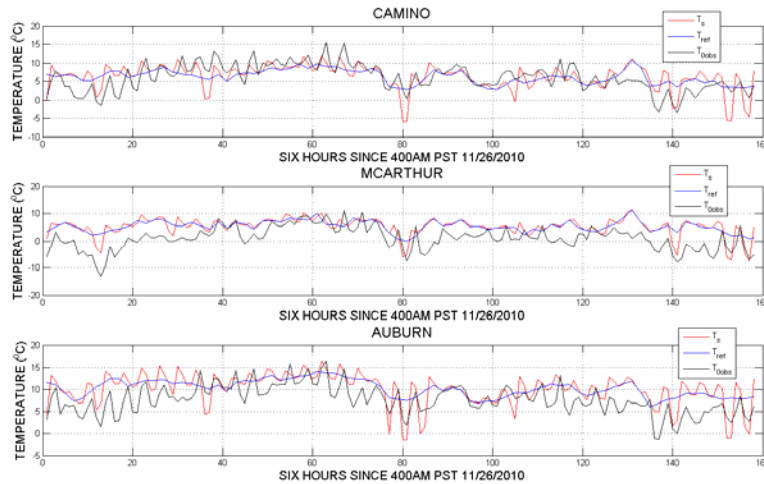
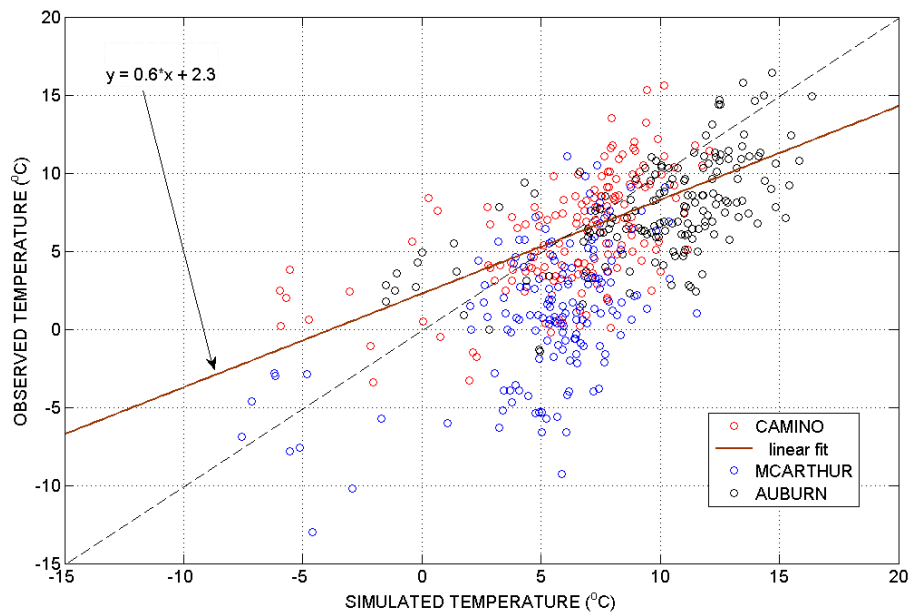


Figure 2.16: Station Observed and ICRM Gridded 2-m Air Temperatures and Regression Fit.



2.4 Northern California Hydrologic Modeling Enhancements

2.4.1 Model Overview

The hydrologic model of INFORM II closely follows the operational hydrologic forecast models used by the California Nevada River Forecast Center (CNRFC). It includes snow and soil water

models adapted from the National Weather Service River Forecast System (NWSRFS), where the hydrologic segments within INFORM are based on CNRFC-defined watershed areas for operational forecasting. Thus the hydrologic model components are basin-based and are updated to align with current CNRFC operations for the five major reservoir watersheds of Trinity, Shasta, Oroville, Yuba, and Folsom. During this second phase of INFORM, an additional component was developed to model the runoff generated for watersheds downstream of these major reservoirs as input to the Sacramento River routing model.

Inputs to the hydrologic model components are basin mean areal precipitation (MAP) and mean areal temperature (MAT). The MAP and MAT estimates are derived from the INFORM forecast system downscaling of large-scale atmospheric forecasts from the Global Forecast System (GFS, 0-16 days with 6 hourly resolution) and the Climate Forecast System (CFS, 0-41 days with 6-hourly resolution and from 1 to 9 months with daily resolution). The snow and soil water model components produce estimates of snow depth, snow melt and runoff during the cold season, along with surface and subsurface runoff for each watershed sub-basin throughout the year. This output is input to channel routing components, tailored for each major reservoir watershed, to produce streamflow estimates at each sub-watershed and an estimate of total reservoir inflow for each of the major INFORM domain reservoirs. As described previously, the INFORM forecast system produces an ensemble of MAP and MAT forecasts over the forecast horizon, and, through the hydrologic and routing models, an ensemble of reservoir inflow forecasts. This ensemble of reservoir inflow forecasts then provide the input to the INFORM decision support component (see Chapter 3). It is noted that the INFORM inflow forecasts are for unimpaired (full natural) flow in all cases.

Model parameters for the snow and soil models are derived from the CNRFC operational hydrologic segment definition input, which is based on CNRFC calibration of natural flows into the reservoirs. Parameters of the routing component for each reservoir watershed were estimated using historical streamflow data and the CNRFC-estimated unit hydrograph at the hydrologic segments. For the INFORM forecast system, initial hydrologic model states are downloaded from CNRFC once-daily (1200 UTC) and are assimilated by the INFORM hydrologic models.

The mathematical basis of the hydrologic models of INFORM (adaptations of the CNRFC operational models SACSMA and SNOW17) has been given in *Georgakakos et al. (2006; Chapter 4)* and will not be repeated here. In the following sections the authors describe the configuration of the hydrologic models. Updates were made during this phase of INFORM (INFORM II) to align with changes in the operational hydrologic model configuration by the CNRFC following input from CNRFC circa 2010-2011.

2.4.2 Hydrologic Model Configuration

The initial INFORM hydrologic model basin configuration and developed parameter files were reported in *Georgakakos et al. 2006* and applied to the INFORM Phase I system in 2005. Several changes in the CNRFC definition of hydrologic segments for forecasts operations were made through 2008. HRC and CNRFC have collaborated to align the models and to develop mechanisms for the near real time exchange of data. The INFORM forecasting system were

updated during Phase II to align the INFORM hydrologic model configuration with the CNRFC operational basins for the five major reservoir watersheds of INFORM. Based on CNRFC hydrologic segment definition input, updated snow and soil model parameters were also incorporated during this latest configuration update. The routing model components for each major watershed were updated to conform to the new upstream basin configuration. The current configurations for the five major reservoir basins, along with the developed configuration for the downstream Sacramento River drainage area are described in the following.

At the end of the second phase of INFORM, CNRFC made additional changes in the basin configuration for the Folsom Reservoir watershed and recalibrated the CNRFC operational hydrologic model for the subcatchments of the American River. There have also been updates in the naming convention for the existing sub-catchments by CNRFC. These additional updates have not been made in INFORM in order to have a consistent set of evaluation results and need be addressed in a subsequent INFORM phase.

2.4.2.1 Trinity Reservoir

The Trinity Lake (formerly Clair Engle Lake) watershed hydrologic model consists of a single basin, as shown in Figure 2.17. No change in the configuration was made for Trinity Lake since 2005. The single basin is labeled CGEC1 (CNRFC's naming convention updated recently to CGEC1H). The area is modeled by upper and lower subcatchment areas to capture differences in higher and lower elevation (relative to the snow line) basin response for snow accumulation and melt, and thus soil moisture. Model input of MAP and MAT is computed for the two subcatchment areas.

2.4.2.2 Shasta Reservoir

The Shasta Lake watershed configuration is depicted in Figure 2.18. The current configuration consisted of 6 hydrologic basins, representing the Pit River at Likely (PLYC1), at Canby (CNBC1), and at Montgomery (PITC1), the McCloud River (MSSC1), the Sacramento River at Delta (DLTC1), and the Shasta Dam local area (SHDC1). Under the new naming convention at CNRFC, these basins are now represented, respectively, as PLYC1H, CNBC1L, PITC1L, MSSC1H, DLTC1H, and SHDC1L. With the exception of the Shasta Local area and for snow and soil computations, the hydrologic basins include upper and lower subcatchment areas based on elevation.

2.4.2.3 Oroville Reservoir

The Lake Oroville watershed configuration is depicted in Figure 2.19. The current configuration consisted of 8 hydrologic basins, representing the North Fork Feather River at Lake Almanor (PLLC1) and at Pulga (PLGC1), Indian Creek (IIFC1), Spanish Creek at Keddies (SCBC1), Middle Fork Feather River at Portola (MFTC1) and at Merrimac (MRMC1), West Branch Feather River near Magalia (WBG1), and the Oroville Dam local area (ORDC1). Under the new naming convention at CNRFC, these basins are now represented, respectively, as PLLC1H, PLGC1L, IIFC1H, SCBC1H, MFTC1H, MRMC1L, WBG1H, and ORDC1L. Each of the hydrologic basins includes upper and lower subcatchment areas based on elevation.

2.4.2.4 Yuba River Reservoirs

The watershed configuration for the Yuba River is depicted in Figure 2.20. The current configuration includes three hydrologic basins: the North Fork Yuba River drainage at Goodyear (GYRC1) and at New Bullards Bar Reservoir (NBBC1), and the Middle and South Fork Yuba River drainage to Englebright Reservoir (HLEC1). The three hydrologic basins include upper and lower subcatchment areas based on elevation.

2.4.2.5 Folsom Reservoir

The Folsom Lake watershed configuration is depicted in Figure 2.21. Several updates were made within the Folsom Lake model configuration during Phase II. The current configuration includes 9 hydrologic basins: the North Fork American River at North Fork Dam (NFDC1), the Middle Fork American River at French Meadows Dam (FMDC1), Hell Hole Reservoir (HLLC1), and Foresthill (MFAC1), the Rubicon River at Gerle (RRGC1), the South Fork American River at Union Valley Reservoir (UNVC1), Kyburz (AKYC1), and Chili Bar Dam (CBAC1), and the local Folsom Dam drainage area (FOLC1). In the current configuration, several of headwater basins represent upper elevation areas only (FMDC1, HLLC1, RRG1, UNVC1, and AKYC1), whereas the main North, Middle, and South Fork hydrologic basins (NFDC1, MFAC1, and CBAC1) are represented with both upper and lower elevation subcatchments. The local Folsom Dam drainage is represented by a single lower elevation subcatchment.

2.4.2.6 Sacramento River Downstream of Reservoirs

For INFORM II additional hydrologic model components were developed to represent to inflow and runoff contributing to the Sacramento River and its tributaries downstream of the major reservoirs. The configuration is depicted in Figure 2.22, with the gray-shaded basins representing the areas of the previously described reservoir watersheds. This model component provides inflows or local area runoff to the Sacramento River routing model component..

The Sacramento River downstream model configuration consists of 18 hydrologic basins including Clear Creek at Whiskeytown (WSHC1) and at Igo (RDGC1), Battle Creek at Cottonwood (COTC1), Cottonwood Creek at Cottonwood (CTWC1), Cow Creek at Millville (CWCC1), Elder Creek at Paskenta (EDCC1), Mill Creek at Los Molinos (MLMC1), Thomes Creek at Paskenta (TCRC1), Deer Creek at Vina (DCVC1), Big Chico Creek at Chico (HKCC1), Butte Creek at Chico (BKCC1), Stony Creek at East Park Reservoir (EPRC1), Stony Gorge (SGEC1) and Black Butte (BLBC1), Honcut Creek at Bangor (HCTC1), Bear River at Camp Far West (CFWC1), Dry Creek at Wheatland (DCWC1), and the Cherokee Canal at Richvale (RCVC1). Many of these basins are represented with both upper and lower elevation subcatchments (exceptions being WHSC1, RDGC1, HKCC1, EPRC1, HCTC1, DCWC1 and RCVC1).

In addition, this component models runoff for the local drainage areas of the Sacramento River at Big Bend (BDBC1), at Tehama (TEHC1), at Vina-Woodson Bridge (VWBC1), at Ord Ferry (ORFC1), and at Sacramento (SACC1), plus the Yuba River at Marysville (MRYC1), Feather River at Yuba City (YUBC1), and American River at Sacramento (SAMC1).

Figure 2.17: Basin Configuration for Trinity Lake Watershed.

(No change in configuration since INFORM Phase I.)



Figure 2.18: Basin Configuration for Shasta Lake Watershed.

(Updated in 2010.)

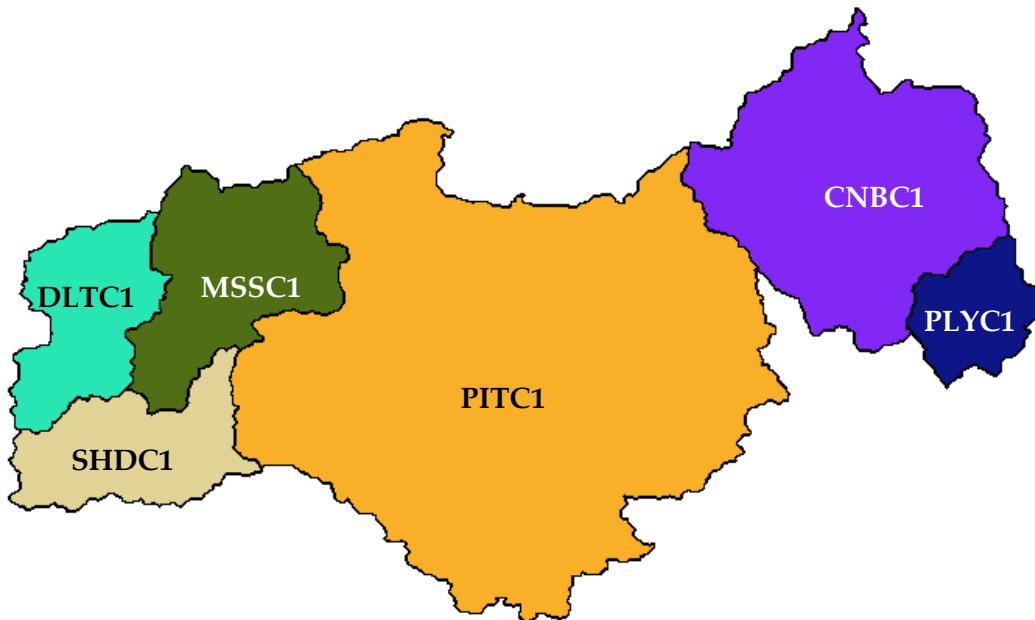


Figure 2.19: Basin Configuration for Lake Oroville Watershed.

(Updated in 2010.)

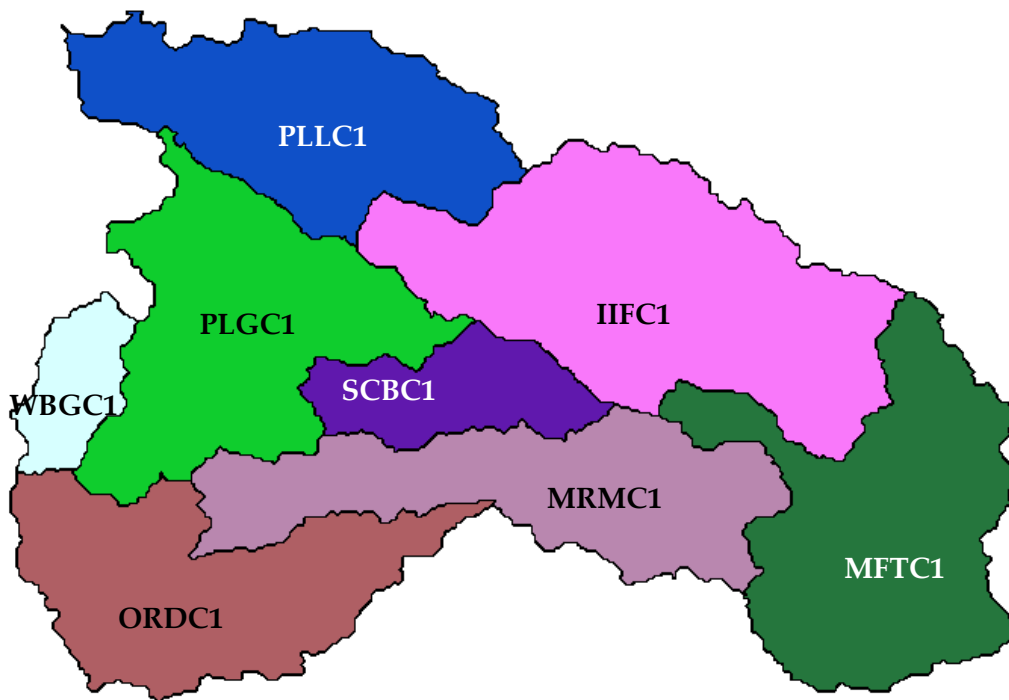


Figure 2.20: Basin Configuration for Yuba River Watershed.

(Updated in 2010.)

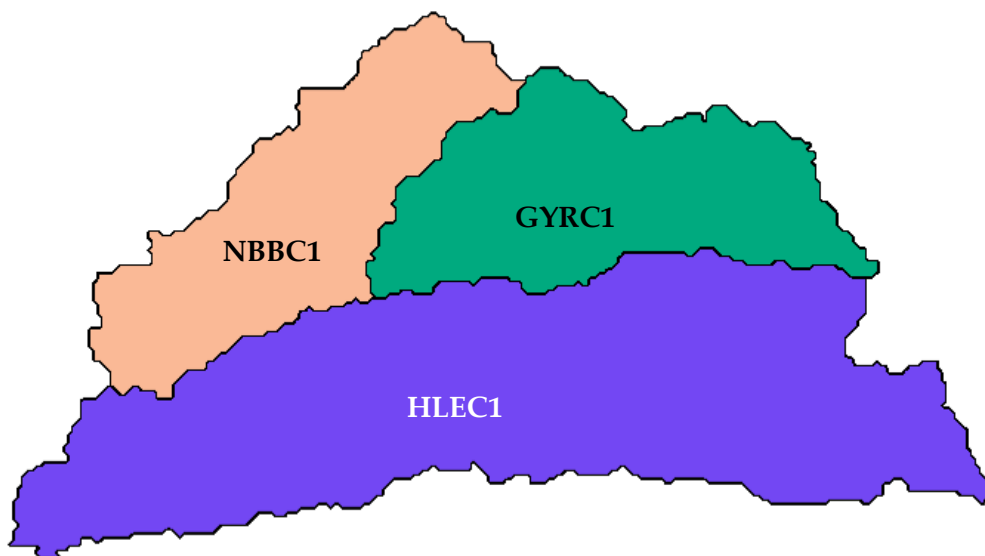
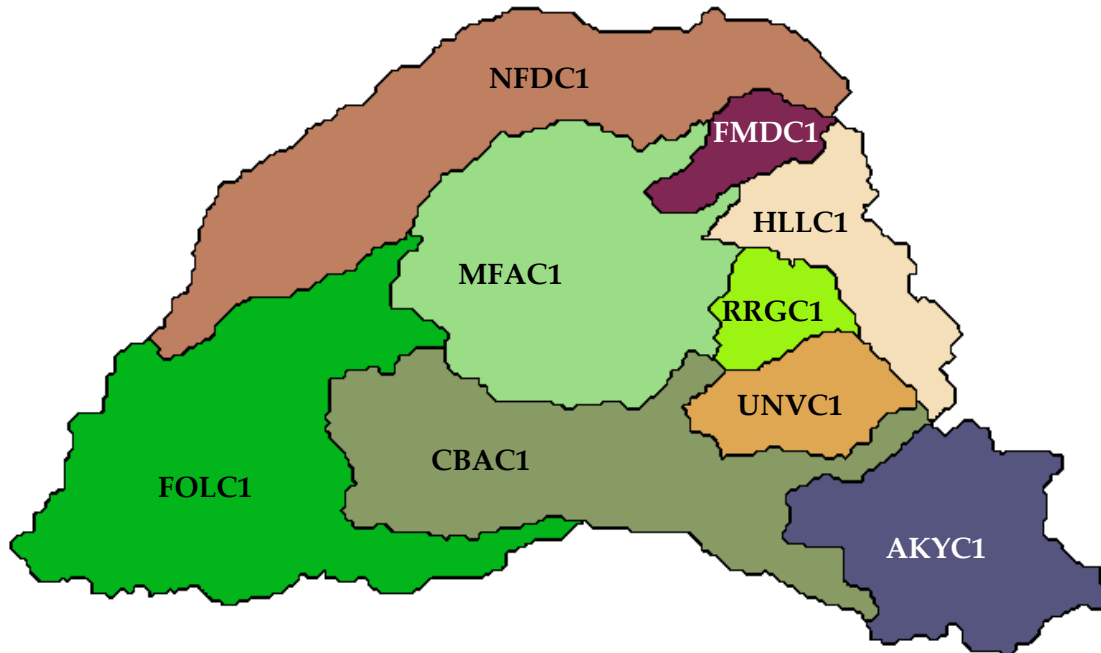


Figure 2.21: Basin Configuration for Folsom Lake Watershed.

(Updated in 2010.)



2.4.3 INFORM Hydrologic Model Parameter Values

Parameters are defined for the adaptation of the CNRFC Sacramento Model (SACSMA) and the snow accumulation and ablation model (SNOW17), and for the linear reservoir routing model of INFORM used for routing in the reservoir watersheds their sub-catchments. Table 2.4, an updated form of that shown in *Georgakakos et al. (2006; Chapter 4, Table 15)*, presents the description of the INFORM hydrologic model parameters for easy reference. The parameter value tables are shown in Appendix C for each watershed defined in the previous section.

2.4.4 Simulation Performance of the Basin Hydrologic and Routing Model

For the INFORM II interim report (*Georgakakos et al. 2011*), the INFORM reservoir inflow simulations were compared to “observed” unimpaired flow estimates provided by CNRFC, for varying periods of record for each of the five reservoirs as indicated in Table 2.5. The simulations for each reservoir were made using historical CNRFC-estimated MAP and MAT for the basin configurations as presented. The unimpaired flows were estimated by lake level measurements and a water balance approach for each reservoir, generally with a 1-day temporal resolution (exceptions for the North and Middle Forks of the American River which have 6-hourly resolutions).

Figure 2.22: Basin Configuration for Downstream Sacramento River Watershed.

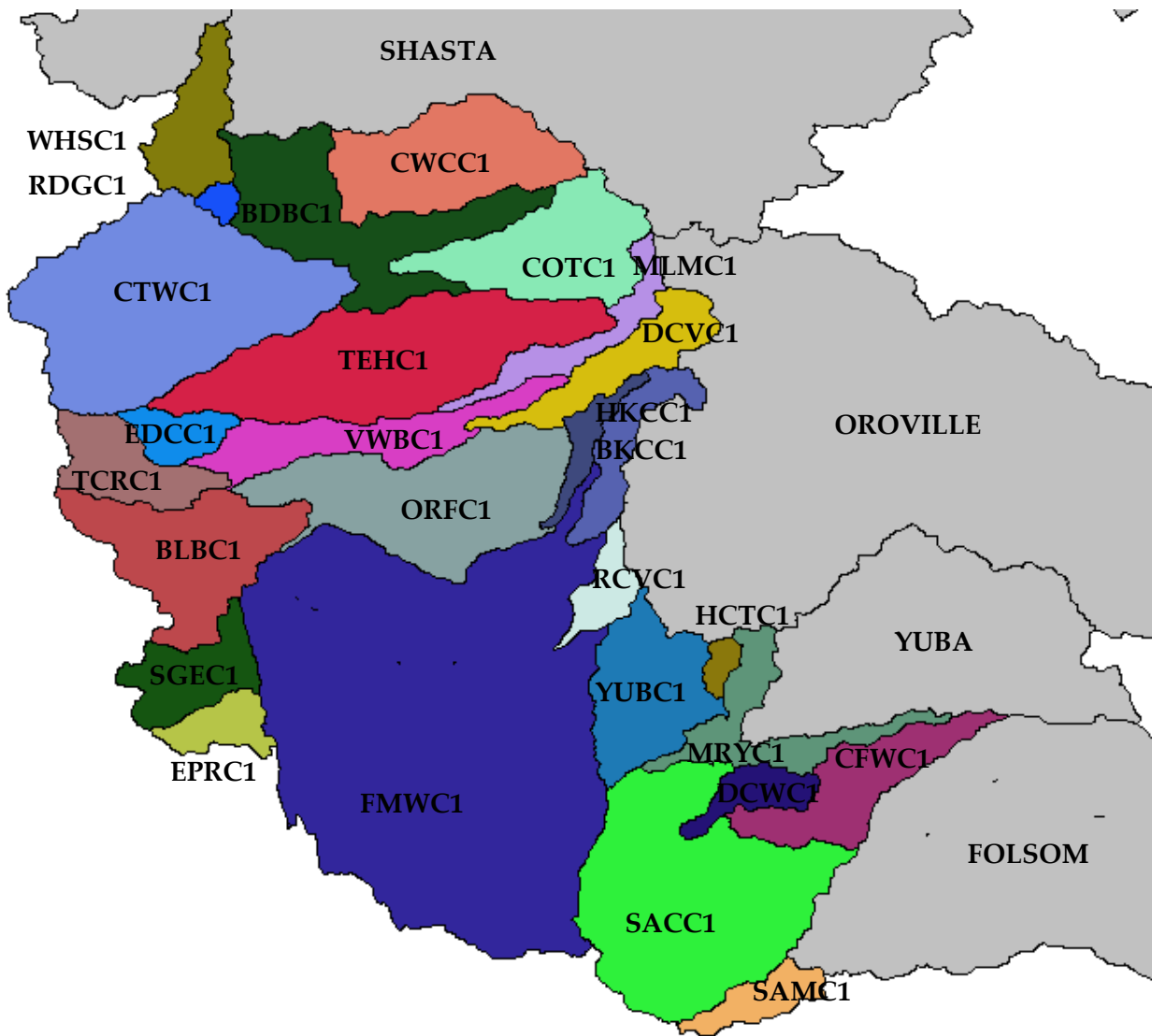


Table 2.4: Description of INFORM Hydrologic and Routing Model Parameters

SNOW MODEL PARAMETERS

<i>SCA:</i>	SNOW CATCH ADJUSTMENT FACTOR
<i>MFMAX:</i>	MAXIMUM MELT FACTOR (MM DEGC ⁻¹ D ⁻¹)
<i>MFMIN:</i>	MINIMUM MELT FACTOR (MM DEGC ⁻¹ D ⁻¹)
<i>NMF:</i>	MAXIMUM NEGATIVE MELT FACTOR (MME DEGC ⁻¹ D ⁻¹)
<i>PLWHC:</i>	FRACTION OF SNOW COVER FOR WATER HOLDING SNOW CAPACITY
<i>TIPM:</i>	PARAMETER FOR ANTECEDENT TEMPERATURE INDEX COMPUTATIONS
<i>MBASE:</i>	BASE TEMPERATURE FOR MELT COMPUTATIONS (DEGC)
<i>UADJ:</i>	AVERAGE DAILY WIND FUNCTION FOR RAIN-ON-SNOW PERIODS (MM MB ⁻¹ DAY ⁻¹)
<i>DAYGM:</i>	CONSTANT MELT AT SNOW-SOIL INTERFACE (MM DAY ⁻¹)
<i>PXTEMP:</i>	TEMPERATURE TO DELINEATE RAIN FROM SNOW (DEGC)
<i>SI:</i> (MM)	MAXIMUM SWE FOR 100 percent COVER IN SNOW DEPLETION CURVE
<i>ELV:</i>	ELEVATION OF CENTROID OF BASIN (10 ² M)
<i>LRMAX:</i>	MAXIMUM LAPSE RATE AT LOCAL NOON (DEGRC/100M);
<i>LRMIN:</i>	MINIMUM LAPSE RATE AT LOCAL MIDNIGHT (DEGRC/100M);
<i>TELV:</i>	ELEVATION OF TEMPERATURE TIME SERIES ESTIMATES (10 ² M)
<i>PADJ:</i>	PRECIPITATION ADJUSTMENT FACTOR

SACRAMENTO MODEL PARAMETERS

<i>UZTWM:</i>	UPPER ZONE TENSION WATER CAPACITY (MM)
<i>UZFWM:</i>	UPPER ZONE FREE WATER CAPACITY (MM)
<i>LZTWM:</i>	LOWER ZONE TENSION WATER CAPACITY (MM)
<i>LZFPM:</i>	LOWER ZONE FREE PRIMARY WATER CAPACITY (MM)
<i>LZFSM:</i>	LOWER ZONE FREE SUPPLEMENTARY WATER CAPACITY (MM)
<i>DU:</i>	INTERFLOW RECESSION (6HRS ⁻¹)

<i>DLPR:</i>	RECESSION COEFFICIENT FOR LOWER ZONE FREE PRIMARY WATER ELEMENT (6HRS ⁻¹)
<i>DLDPR:</i>	RECESSION COEFFICIENT FOR LOWER ZONE FREE SUPPLEMENTARY WATER ELEMENT (6HRS ⁻¹)
<i>EPS:</i>	CONSTANT FACTOR IN PERCOLATION FUNCTION
<i>THSM:</i>	EXPONENT IN PERCOLATIOIN FUNCTION
<i>PF:</i>	FRACTION OF PERCOLATION BYPASSING THE LOWER ZONE TENSION WATER ELEMENT
<i>XMIOU:</i>	FRACTION OF WATER LOST TO DEEP GROUNDWATER LAYERS
<i>ADIMP:</i>	ADDITIONAL IMPERVIOUS AREA MAXIMUM FRACTION
<i>PCTIM:</i>	FRACTION OF PERMANENTLY IMPERVIOUS AREA
<i>ETADJ:</i>	EVAPOTRANSPIRATION DEMAND ANNUAL ADJUSTMENT FACTOR

CHANNEL MODEL PARAMETERS

<i>n_c:</i>	NUMBER OF LINEAR RESERVOIRS REPRESENTING THE CHANNEL SEGMENT
<i>α:</i>	COMMON COEFFICIENT OF LINEAR RESERVOIRS WITH INVERSE DESCRIBING TRAVEL TIME (6HRS ⁻¹)

The interim performance analysis indicated good correlation between simulated and observed inflows for each reservoir. Monthly correlation values ranged from approximately 0.5 during the low flow season (minimum correlation between July and September) to greater than 0.9 for much of the wet season (October through April) at each of the reservoirs. Upstream regulation effects are significant, especially during the period of low flows, for some of the watersheds of the INFORM II domain.

This analysis was updated to consider the performance of the hydrologic model components for the major reservoirs for the two-year period from 1 January 2011 – 31 December 2012. For this analysis, the inflow simulations for each reservoir were extracted from the INFORM database archive and converted to daily flows. These were compared with unimpaired or “Full Natural Flow” (FNF) estimates obtained from the California Data Exchange Center (CDEC). Table 2.6 presents overall summary statistics of daily cross correlation and fractional bias for each of the six major reservoirs. The overall correlation is lowest for Trinity Reservoir inflows (0.77) and is highest (0.92) for both Folsom and Shasta Reservoir inflows. These high correlation values

indicate good agreement between simulations and the FNF observations. The bias statistics indicate an over-estimation of the observed flows by approximately 15 to 50 percent.

Table 2.5: Assessment Specifics for Hydrologic and Routing Model Simulations

<i>Watershed Name</i>	<i>Period of Record</i>	<i>Temporal Resolution (hrs)</i>
FOLSOM		
American River North Fork	19871001 – 19980930	6
American River Middle Fork	19881001 – 19980506 (*)	6
Folsom Lake Inflow	19601001 – 19980930	24
YUBA		
New Bullards Bar Inflow	19881001 – 19990930	24
OROVILLE		
Lake Oroville Inflow	19901001 – 20060531	24
SHASTA		
Lake Shasta Inflow	19601001 – 20060531	24
TRINITY		
Clair Engle Lake Inflow	19630501 – 19990930	24

(*) Note: Only wet season starting in October and ending for some years in March and for some years in May.

Table 2.6: Statistical Indices Comparing the Daily Simulations and Observed FNF

<i>Reservoir</i>	<i>Correlation Coefficient</i>	<i>Fractional Bias</i>
Folsom	0.92	0.24
Oroville	0.89	0.53
Shasta	0.92	-0.01
Trinity	0.77	0.44
New Bullards Bar	0.81	0.15
Englebright	0.87	0.21

Figure 2.23 presents the comparison of the cumulative distribution of daily flow for the observations (FNF, in black) and simulations (in red) for each of the reservoirs. For all reservoirs, good reproduction of the observed daily flow distribution is found. The largest discrepancies are observed for Trinity and Oroville reservoirs; both showing an over-estimation of the observations over a range from mid- to high-flows. This bias is further illustrated in Figure 2.24, which presents the daily inflow hydrographs for the 2-year period for the Oroville Reservoir. This plot clearly shows over-estimation of flows during the spring of 2012. Similar hydrograph plots are included in Appendix C for the remaining reservoirs. The Yuba River, Folsom, and Oroville reservoir inflow comparison indicated over-estimation of flows during the spring of 2012, whereas the comparison for Shasta showed no significant evidence of bias.

Figure 2.23: Cumulative Distribution of Daily Flows

(Simulations in red, observed FNF in black, with the discharge presented in a log scale.)

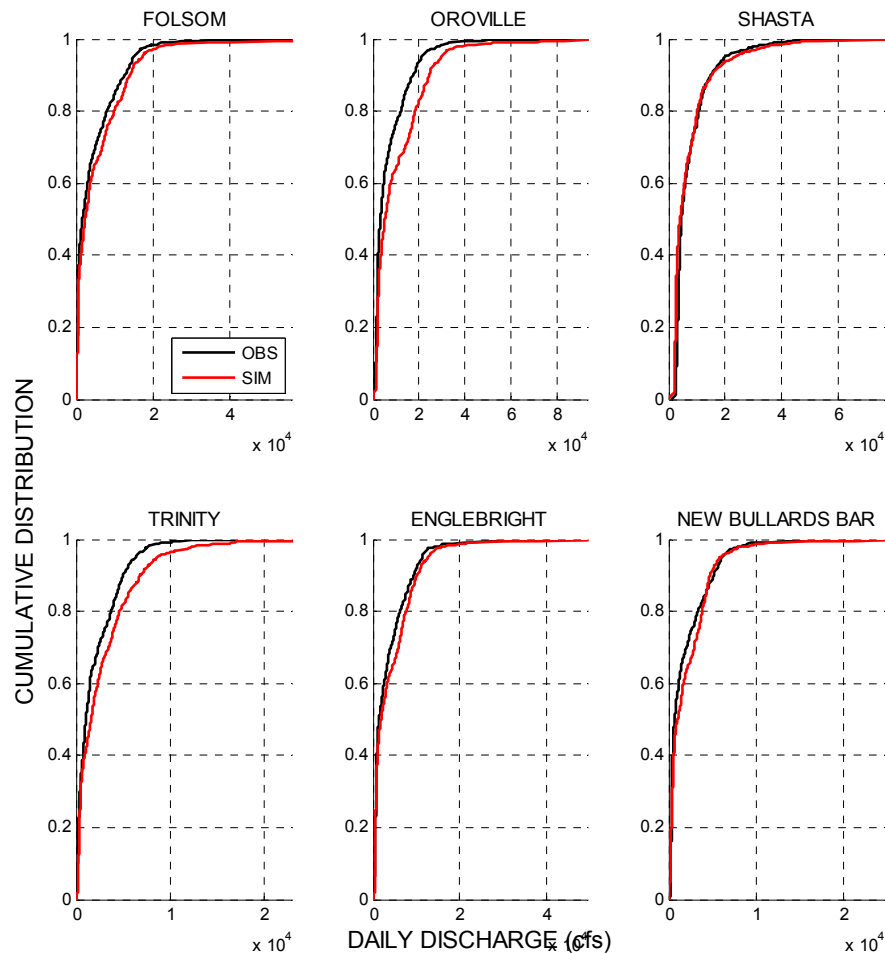
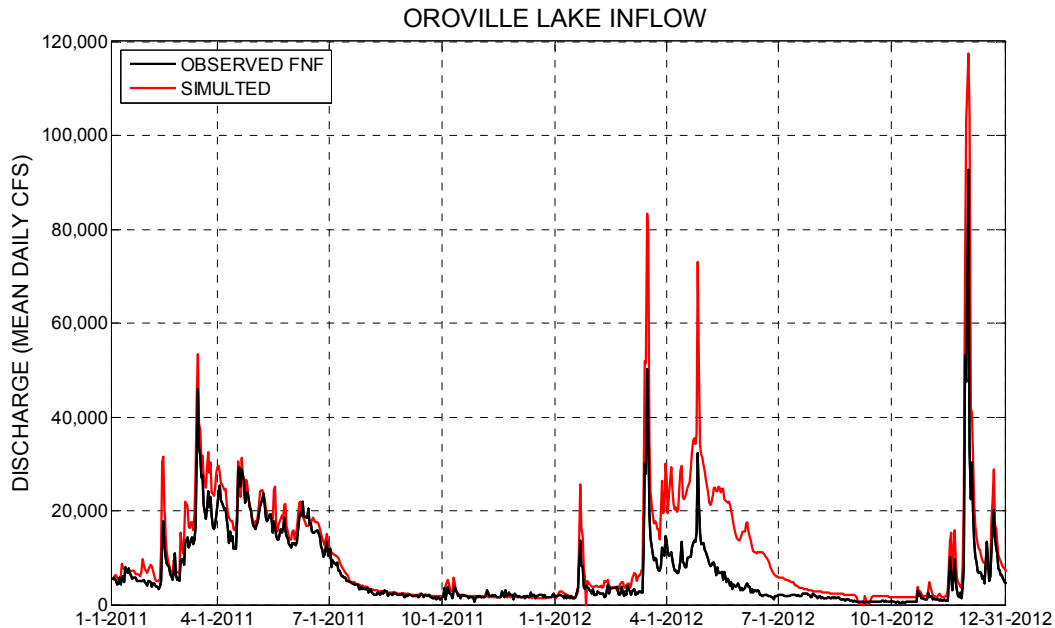


Figure 2.24: Comparison of Daily Observed (Black) and Simulated (Red) Full Natural Inflow to Oroville Reservoir.

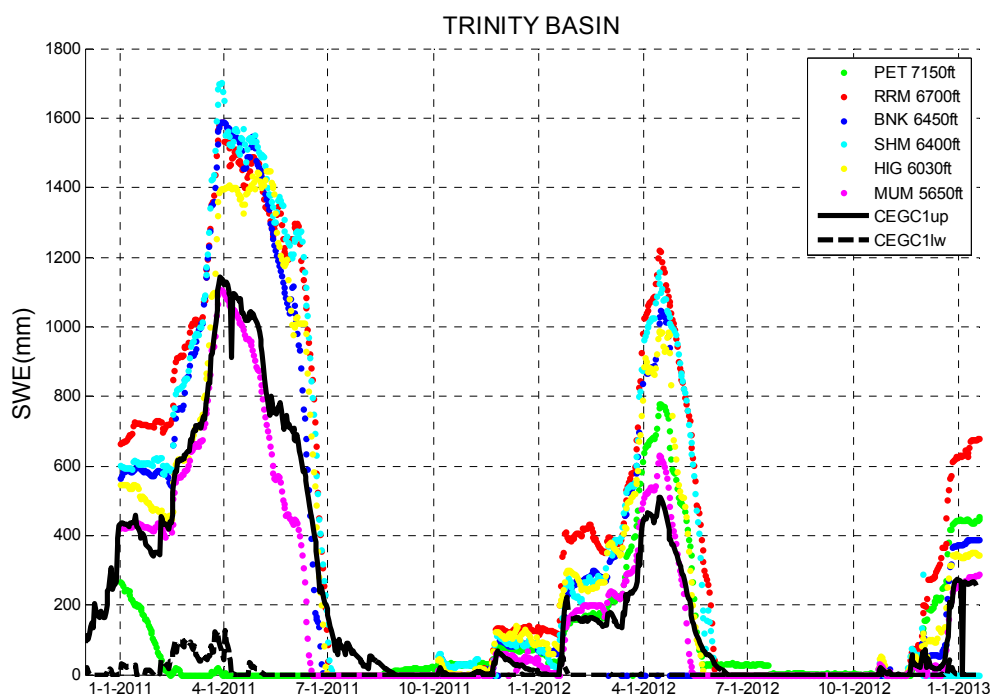


An additional comparison of the simulated snow water equivalent (SWE) with available snow sensors were made to assess the performance of the snow model simulations. It is noted that such comparison between point data (sensors) and the simulations should be interpreted qualitatively as these are at vastly different scales. Snow sensors located in various subcatchments of the hydrologic model components were identified and snow observation records were extracted from the CDEC archive for the period from January 2011 to January 2013.

An example comparison is given in Figure 2.25 for the upper and lower elevation subcatchments of the Trinity Reservoir Watershed. The daily average simulated SWE values for the upper (solid line) and lower (dashed line) subcatchments are shown together with the sensor observations indicated by the colored symbols. The lower elevation subcatchment SWE simulations are low, reaching a maximum of about 100 mm in 2011. The upper-elevation subcatchment simulations (where the bulk of the snow accumulation is expected) follow well the pattern of accumulation and ablation indicated by the snow sensors. Similar plots are included in Appendix C for the remaining reservoirs. Qualitative comparisons indicate that the patterns of accumulation and ablation shown in the snow sensor records are captured by the simulations, especially for the accumulation regions of the upper elevations in the watersheds.

Figure 2.25: Comparison of Simulated and Observed Snow Water Equivalent (SWE)

(Upper and lower elevation subcatchments of the Trinity watershed and six snow sensors.)



2.5 INFORM Web Site Description

2.5.1 Graphical Export Post-Processing and Dissemination

The processed model results are used to produce a set of data product images for review by the INFORM user. The gridded model output from both the ICRM and WRF-ARW is used to create visualizations in real-time for display on the INFORM website. The ensemble median of the air temperature at 2 meters above ground and the total accumulated precipitation simulated by each model is calculated. These median calculations are used to plot the daily total accumulated precipitation for each forecast day and the instantaneous temperature at 2 meters for 06:00:00 and 18:00:00 UTC on each forecast day for each model. Next, the mean of the ensemble upper quartile precipitation is calculated for each model, with plots of the 5-day total accumulated precipitation made in 5-day increments out to the end of each model's forecast period. All of the images also display important information about the model run that created their data: the forcing data used with the model, model initiation time, and the number of ensemble members used.

The flows forecasted by the hydrologic model are plotted as a time series and displayed in real-time on the INFORM website. Separate flow images are plotted for the ICRM and WRF-ARW at the watershed control points at Trinity Lake, Folsom Lake, Englebright Lake, New Bullards Bar Reservoir, Lake Oroville, and Shasta Lake. The individual images for each atmospheric model includes plots of the flow produced by forcing from that model's individual ensemble members, along with the ensemble median; the ensemble median of the other model is also plotted for

reference. To avoid confusion between the ICRM and WRF-ARW ensemble medians, these medians are always plotted in blue and red, respectively.

Once the various data product images have been produced for WRF and ICRM, the image files are uploaded to the web-based secure INFORM Dissemination Interface hosted on the Hydrologic Research Center's website. From this interface, the INFORM user may review and evaluate the WRF and ICRM processing output product images. The next sections provides more information on the INFORM Dissemination Interface.

2.5.2 Accessing the INFORM Dissemination Interface

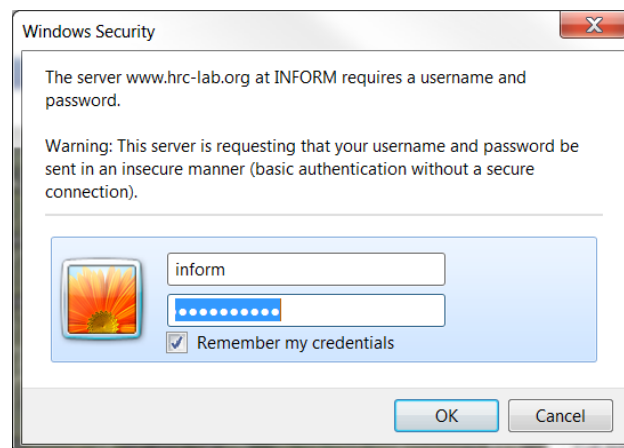
To access the INFORM Dissemination Interface for use as described in the following sections, the user may use any standard web browser, including but not limited to *Internet Explorer* (v8 or later recommended) or *Mozilla FireFox* (v3 and later recommended). Once the browser is directed to the Dissemination Interface URL, the user will be presented with a login dialogue. Here, the user must enter the valid user IDs and password. Examples of the dialogue as presented by *Microsoft Internet Explorer* are shown in Figure 2.26. The URL and user authentication information by which the INFORM Dissemination Interface may be accessed are, at the time of this report, as follows (case sensitive):

URL: <http://www.hrc-lab.org/INFORM/realtime>

Username: inform

Password: xxxxxxxxxxxxxx

Figure 2.26: Window Security Username and Password Authentication



2.5.3 Organization and Navigation of the INFORM Dissemination Interface

The interface displays results for two lines of processing within INFORM. The first line uses the GFS (Global Forecast System of NCEP) ensemble output and the mesoscale numerical model WRF to produce surface precipitation and temperature (and other attendant) fields out to 16 days with 6-hourly resolution. The second line of processing uses the CFS (Climate Forecast Model of NCEP) ensemble predictions and an Intermediate Complexity Regional Model (ICRM)

to produce dynamically-downscaled surface precipitation and temperature fields out to 41 days with 6-hourly resolution. The spatial resolution of the fields is 10mk x 10km. These fields are input to a semi-distributed snow-soil-channel hydrologic and routing model that is an adaptation of the CNRFC operational hydrologic forecast model which produces ensemble inflow forecasts for six major reservoir sites of interest in Northern California: Folsom, Englebright, New Bullards Bar, Oroville, Shasta and Trinity (Claire Engle). Once a day the hydrologic model states are aligned to those of the CNRFC operational models. (See Figure 2.1 for a detailed flow diagram of INFORM forecast component operations.)

Upon successful login, the user will arrive at the INFORM Dissemination Interface seen in Figure 2.27. At the top of this page, links are provided to navigate amongst the various data products available from this interface, including: Ensemble Median Precipitation, Ensemble Upper Quartile Precipitation, Ensemble Median Temperature, and Reservoir Inflow. Clicking on any of these links will navigate to the corresponding page displaying the desired data product. The first interface page that the user will encounter after login is that displaying the Ensemble Median Gridded Precipitation for the current day. Each of these interface pages provide access to a single data product organized into a table with columns for images produced from GFS-driven WRF processing results and images produced from CFS-driven ICRM processing results. Each individual image includes important information about the model run from which it was generated including the forcing data used, model initialization time and the number of ensemble members included in the image. Where applicable, the images will indicate an accumulation start and end time or an instantaneous valid time. The vertical organization of each interface page varies and is detailed in the following sections.

Below the set of links for selecting available data products, the Current Date and the Initialization Date are displayed which indicate the date & time in UTC that the page was last refreshed and the date & time in UTC of model initialization for the products displayed. It is important to note that, when navigating the interface, all data products are organized and displayed according to the Initialization Date and Time. By default, the interface will display data products for the current day when loaded. To view data products initialized, the user may click on the navigation buttons provided below the date and time indicators. The available buttons allow the user to adjust the viewing Initialization Date chronologically forward or backward by one day at a time or, alternatively, reset the current viewing date to that of the current day. When navigating to past dates, the color of the viewed Initialization Date will change from green to red to provide a contrast from the green Current Date, indicating that that the viewed initialization date and time are from the past. The INFORM Dissemination Interface allows for review of data products initialized within the last 5 days. An attempt to navigate beyond five days prior to the current day will result in the user being presented with a message noting the limitation to five days and the interface will reset to the data products for the current day.

2.5.4 INFORM Ensemble Median Precipitation Interface Page

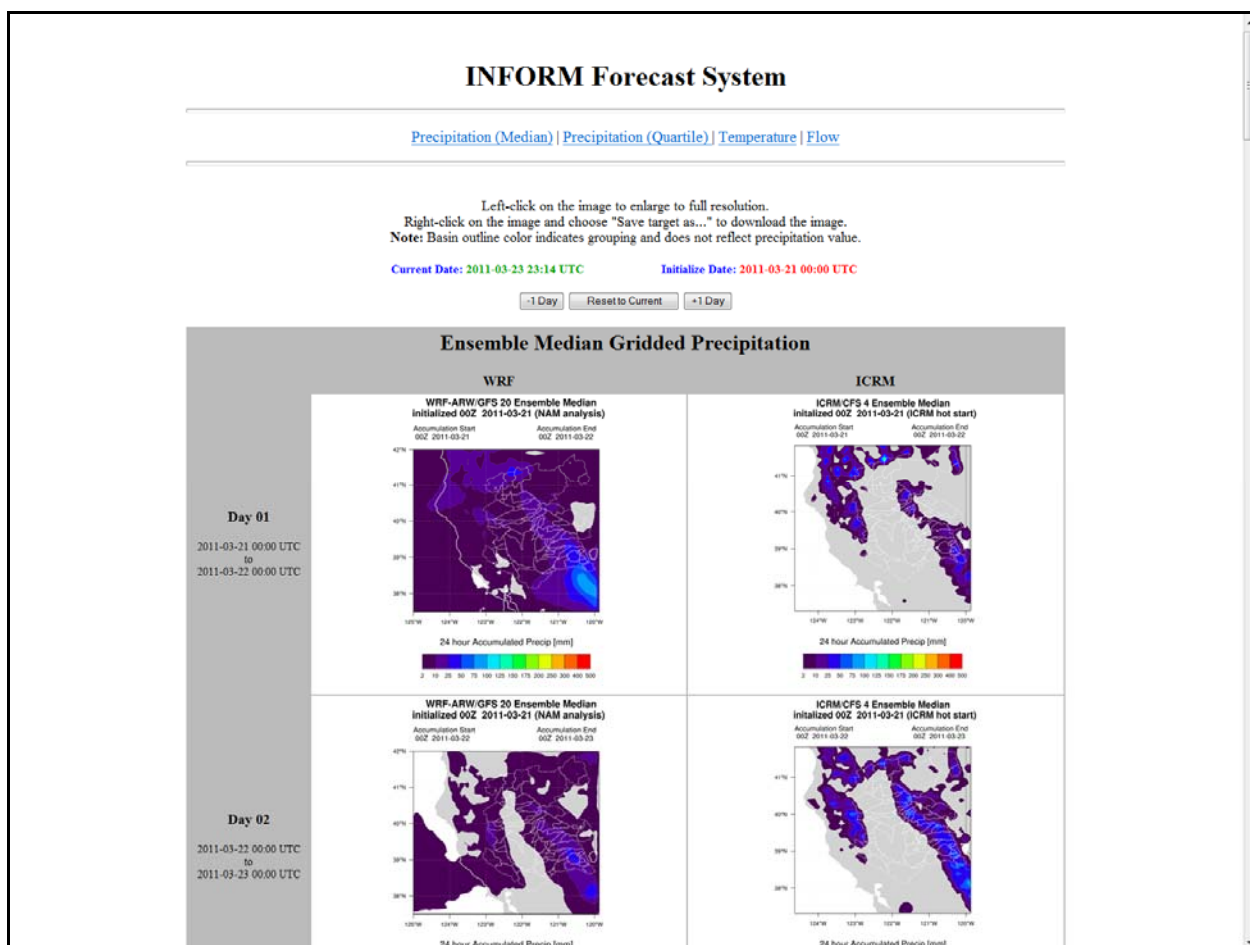
The first page encountered upon logging in to the Dissemination Interface is that displaying the Ensemble Median Gridded Precipitation data product. This page, which can also be accessed by

clicking on the “Precipitation (Median)” link at the top of the page, provides images of accumulated daily precipitation forecasts from the currently viewing Initialization Date out to 15 days for WRF and 21 days for ICRM. Each image represents the median simulated precipitation in millimeters across all ensemble members of the corresponding processing module between the “Accumulation Start” and “Accumulation End” dates listed in the image. The daily accumulation images are organized in chronological order according to valid time as the user scrolls down the interface page with the accumulation start and end date indicated for each row in the table (Figure 2.27).

2.5.5 INFORM Ensemble Upper Quartile Precipitation Interface Page

Clicking on the “Precipitation (Quartile)” link at the top of any interface page will open the display for the Ensemble Upper Quartile Gridded Precipitation data product. This page provides images of the mean five day total accumulated precipitation in millimeters from the ensemble upper quartile from the current Initialization Time out to 15 days for WRF and 20 days for ICRM. The 5-day mean accumulation images are organized in chronological order according to valid time from the current Initialization Date as the user scrolls down the interface page. As with the Ensemble Median Precipitation images, the accumulation start and end dates are indicated at the beginning of the row in the table and in each image (Figure 2.28).

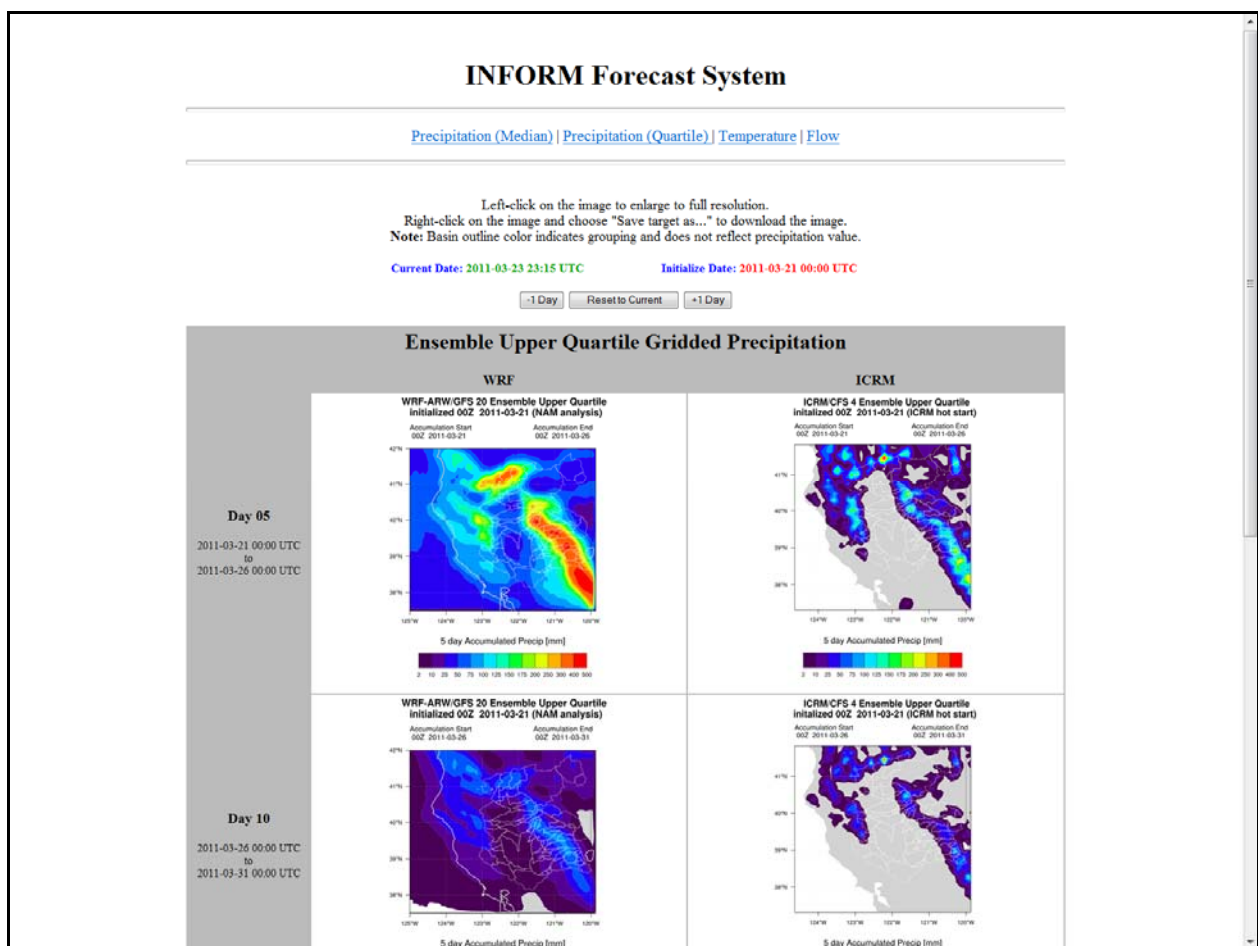
Figure 2.27: INFORM Dissemination Interface Page – Ensemble Median Precipitation



2.5.6 INFORM Ensemble Median Temperature Interface Page

Clicking on the “Temperature” link at the top of any interface page will open the display for the Ensemble Median Gridded Temperature data product. This page provides images of the median instantaneous air temperature at 2 meters above ground across all ensemble members. Images detailing median instantaneous temperature are produced twice for each forecast day, at 06 and 18 UTC, from the current Initialization Date out to 15 days for WRF and 21 days for ICRM. The temperature images are organized in chronological order according to valid time from the current Initialization Date as the user scrolls down the interface page. The Ensemble Median Temperature images each include the forecast valid time, which is also indicated at the beginning of the row in the table and in each image (Figure 2.29).

Figure 2.28: INFORM Dissemination Interface Page – Ensemble Upper Quartile Precipitation

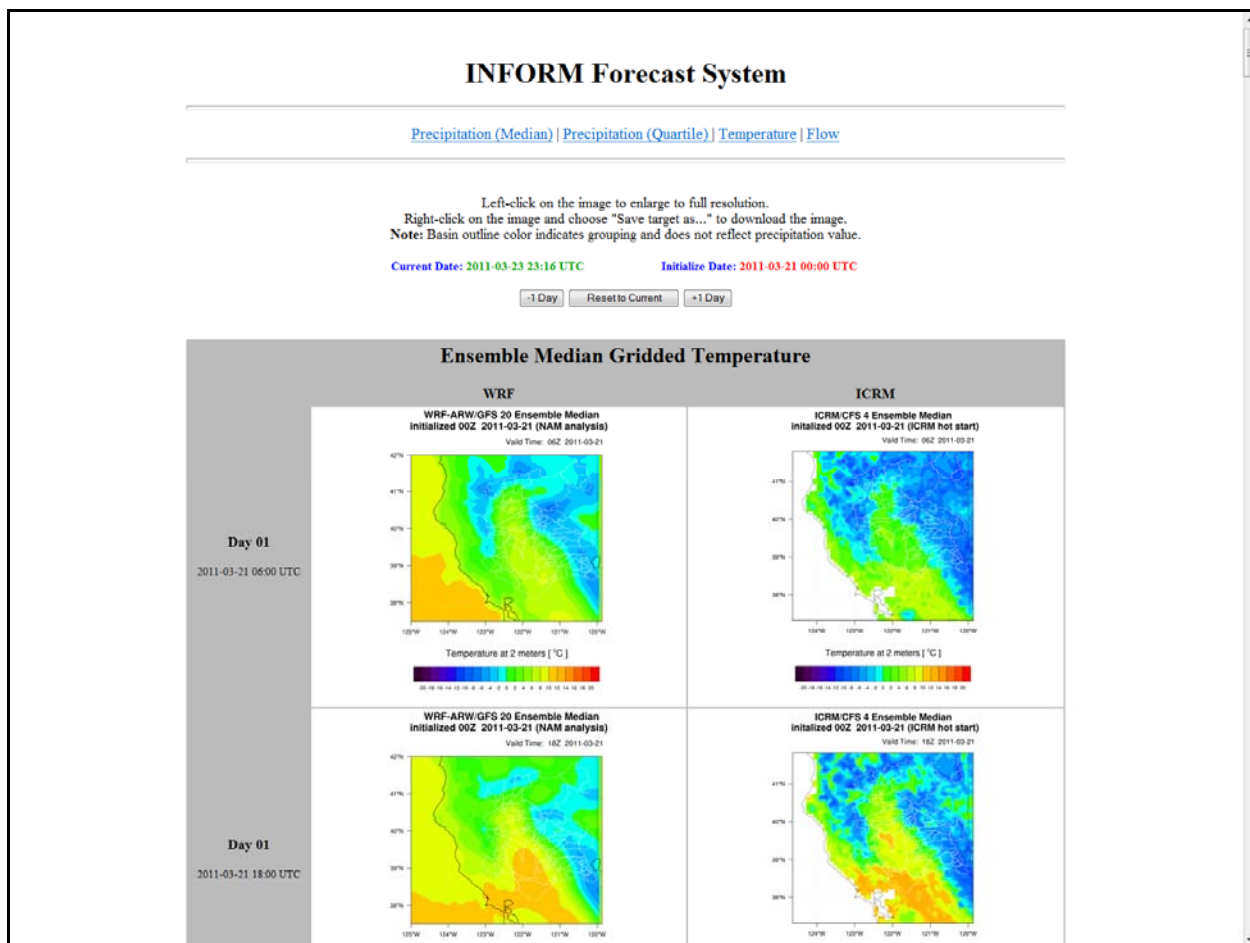


INFORM Reservoir Inflow Interface Page

Clicking on the “Flow” link at the top of any interface page will open the display for the Ensemble Reservoir Inflow data product. The simulated temperature and precipitation fields from the ICRM and WRF-ARW are used to drive a hydrologic model. The flows forecasted by the hydrologic model are plotted as a time-series from the current Initialization Date out to 15

days for WRF and 30 days for ICRM. Separate image products are provided for the watershed control points at Trinity Lake, Folsom Lake, Englebright Lake, New Bullards Bar Reservoir, Lake Oroville, and Shasta Lake. The individual images for each dynamic downscaling regional model include plots of the flow produced by processing forcing from that model's individual ensemble members, along with the ensemble median; the ensemble median of the other model is also plotted for reference. To avoid confusion the ICRM ensemble median is always plotted in blue while the WRF-ARW ensemble median is always plotted in red (Figure 2.30).

Figure 2.29: INFORM Dissemination Interface Page – Ensemble Median Temperature



2.5.7 Data Latency and the Image Unavailable Placeholder

Both the GFS and the CFS input data products have latency on initial availability for acquisition, approximately 5 hours and 12 hours, respectively. Additionally, both WRF and ICRM require multiple hours of processing following product acquisition before results from either processing module can be applied to produce image products. During this time, the Dissemination Interface will display a placeholder image reading "Image Unavailable" in green (Figure 2.31). This indicates to the user that the data products for the current Initialization Date are not processed. In the event that the data product images exceed the threshold for "normal" latency, the "Image Unavailable" placeholder will be displayed in red.

Figure 2.30: INFORM Dissemination Interface Page – Ensemble Reservoir Inflow

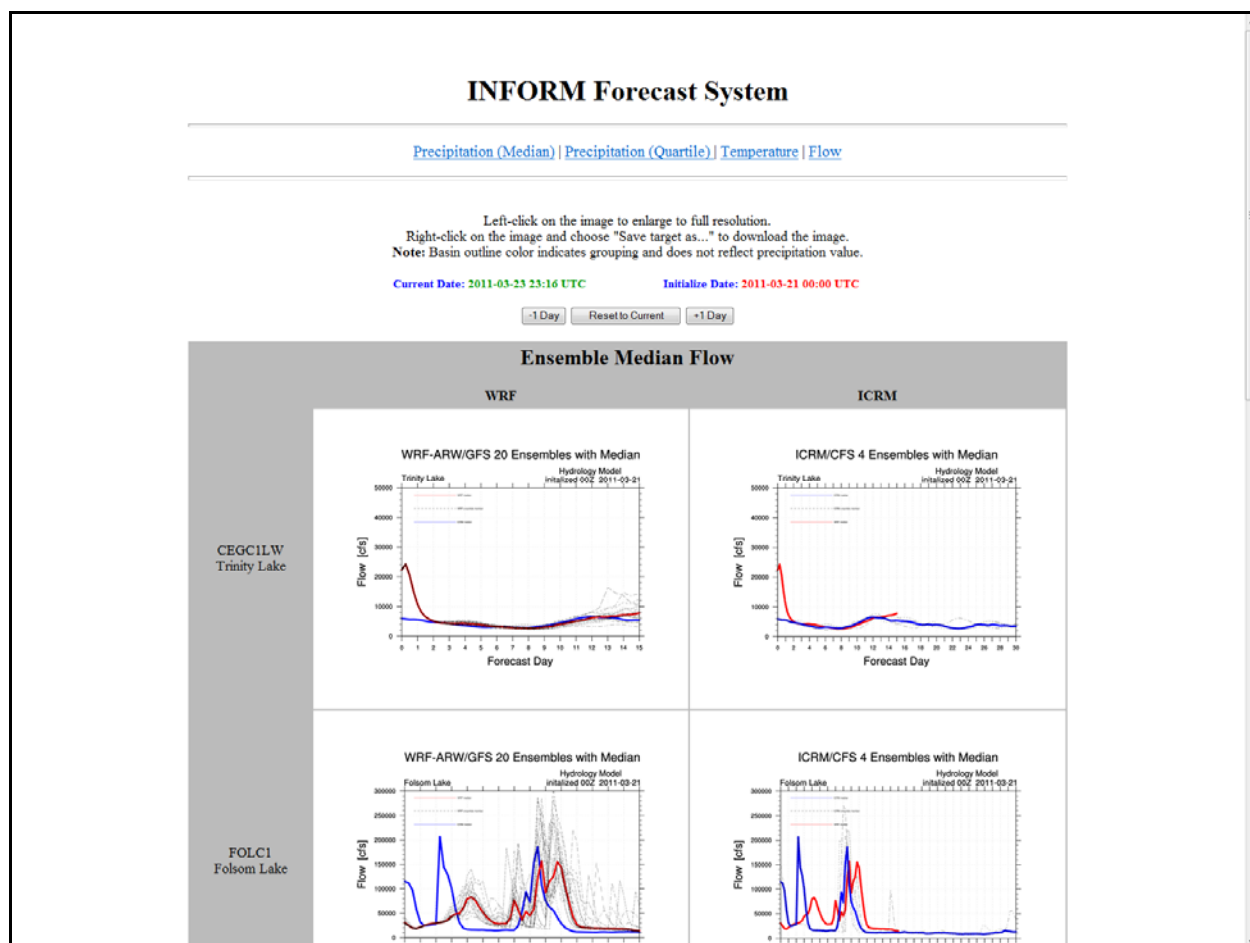
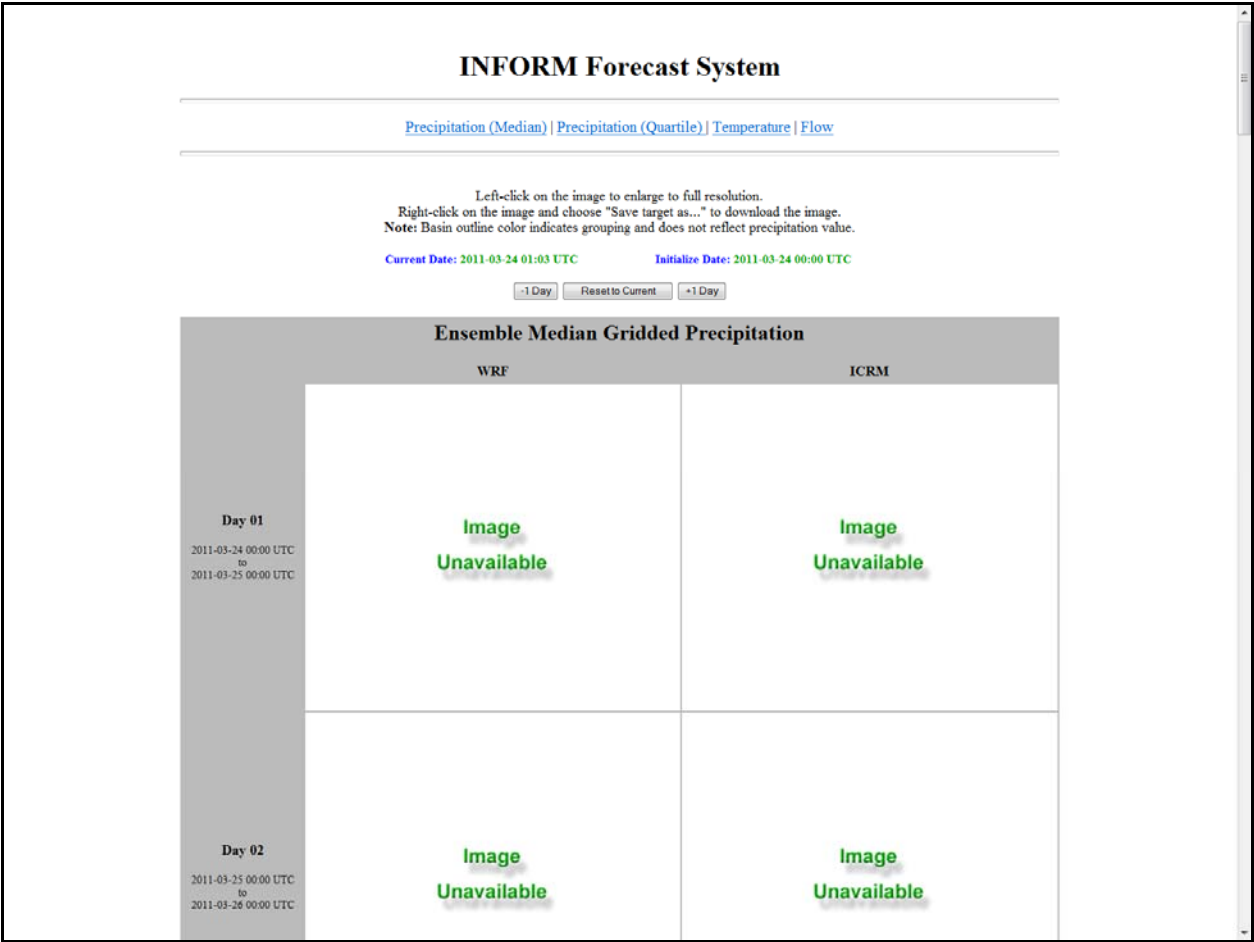


Figure 2.31: Image Unavailable Placeholder for Data Products Not Yet Processed.



CHAPTER 3:

Decision Component Enhancements

3.1 Overview of INFORM Decision Support System

The INFORM DSS modeling framework is illustrated in Figure 3.1.1. The DSS includes multiple modeling layers designed to support decisions pertaining to various temporal scales and objectives. The three modeling layers shown in the figure include (1) short range and near real time operations decision support (which has hourly resolution and a horizon of one day), (2) mid-range reservoir management (which has a daily resolution and a horizon of several months), and (3) long range planning (which has a monthly resolution and a horizon of one or two years). The INFORM DSS also includes an assessment model which replicates the system response under various inflow scenarios, system configurations, and policy options.

The INFORM DSS is designed to operate sequentially. In a typical application, the long range planning model is activated first to consider long range issues such as water conservation strategies for the upcoming year in view of the climate and hydrologic forecasts. As part of these considerations, the DSS quantifies several tradeoffs of possible interest to the planning and management agencies and system stakeholders. These include, among others, assessments regarding relative water allocations to water users throughout the system (including ecosystem demands), reservoir carry over storage, reservoir coordination strategies and target levels, water quality constraints, and energy generation targets. This information is intended for consideration by various planning agencies and other stakeholders as part of their decision process together with other information not readily modeled. After completing these deliberations, key decisions are made on monthly water supply contracts, reservoir releases, energy generation, and reservoir coordination strategies. The INFORM DSS planning level is linked to the INFORM forecast component through the use of the long range forecasts.

The mid-range management model is activated next to consider system operation at finer time scales. The objectives addressed here are more operational than planning and include flood management, water supply, and power plant scheduling. This model uses mid-range forecast ensembles with a daily resolution and is intended to quantify the relative importance of upstream versus downstream flooding risks, energy generation versus flood control, and other applicable tradeoffs. Such information is again intended for consideration by management agencies (the operational departments) and other stakeholders to use it within their decision processes to select the most preferable operational policy. Such policies can be revised as new information on reservoir levels and flow forecasts is acquired. The model is constrained by the long range decisions, unless current conditions indicate that a departure is warranted.

Lastly, the short range and near real time operations models are activated to determine the turbine and spillway operation that realize the hourly release decisions made by the mid-range decision process. The results of this model can be used for near real time operations.

In developing the INFORM DSS, particular attention has been placed on ensuring consistency across modeling layers, both with respect to physical system approximations as well as with

respect to flow of decisions. For example, the mid-range management model utilizes aggregate power plant functions that determine power generation based on reservoir level and total plant discharge. These functions are derived by the short range and turbine load dispatching models which determine the optimal turbine loads for each plant corresponding to the particular reservoir level and total discharge. Thus, the mid-range model has an accurate estimate of the power generation that will actually result from a particular daily release decision. Furthermore, the mid-range model generates similar energy functions to be used by the long range planning model. In this manner, each model has a consistent representation of the benefits and implications of its decisions.

The three modeling layers discussed earlier address planning and management decisions. The scenario/policy assessment model addresses longer term planning issues such as the implications of increasing demands, inflow changes, storage re-allocation, basin development options, and mitigation measures. The approach taken here is to simulate and compare the system response under various inflow, demand, development, and management conditions.

Altogether, the purpose of the INFORM DSS is to provide a modeling framework responsive to the information needs of the decision making process at all relevant time scales and water uses.

3.1.1 INFORM DSS Implementation Aspects

The INFORM DSS runs on personal computers under the WINDOWS operating system. The software includes a graphical interface that provides access to data, activates model runs, and visualizes/manages model results.

Database: The DSS database uses the MS ACCESS engine. All system data and model inputs and outputs are organized in MS ACCESS relational tables. The data in the database are accessible from the DSS interface and can be easily visualized and updated through EXCELL and graphical menu screens. The interface is written in MS Visual Basic. Interface implementation for the database has been completed, and the available data have been incorporated into the database.

Data Processing and Utility Tools: Use of the original data by the various DSS models requires processing. For example, the reservoir management models require analytic forms of the reservoir elevation-storage and elevation surface curves. Such curves can be derived via regression analysis. To automate this process, a regression utility tool has been developed allowing the user to generate the analytic relationships interactively. Other utility tools are also developed to derive optimal power plant functions and daily energy functions.

Interface Functions: As explained earlier, the DSS includes a suite of reservoir management models to support decisions pertinent to long range planning as well as short range scheduling. The management models have a hierarchical structure according to their time resolution. In a typical run, the interface enables the user to select (or generate) the forecast ensemble first, followed by the long range planning model (monthly resolution), the short range management model (hourly resolution), and the turbine load dispatching model. In this execution order, the results of the upper level models are automatically passed onto the lower level models. In addition, the DSS interface also allows the user to run all applications independently. The user

can start with any of the models without previously running any of the upper level models. In this case, however, one would have to prepare the required input data externally. The DSS interface also provides EXCEL templates to assist the user prepare input data externally for all models.

The INFORM DSS has been provided to the INFORM participating agencies. Training and demonstration workshops have been conducted to enable the agency personnel to use it and interpret its results correctly.

3.1.2 INFORM DSS Enhancements

3.1.2.1 Uncertainty Management

The INFORM DSS developed in the previous project phase propagates the climate and hydrologic forecast uncertainty through the system, quantifies the uncertainty of the various water uses, and generates decision rules that manage the reliability with which water uses will be met. In evaluating alternative decision rules, the uncertainty of individual water uses remains the same. A DSS enhancement introduced and demonstrated in this phase distributes the system input uncertainty (from climate and hydrology) selectively across the system storage projects to mitigate its adverse consequences. Much like the conservation of mass, overall system uncertainty is a conservative quantity. The new optimization procedure determines reservoir release rules that “allocate” uncertainty to system reservoirs that are able to absorb it better, thus mitigating its effects on critical water uses.

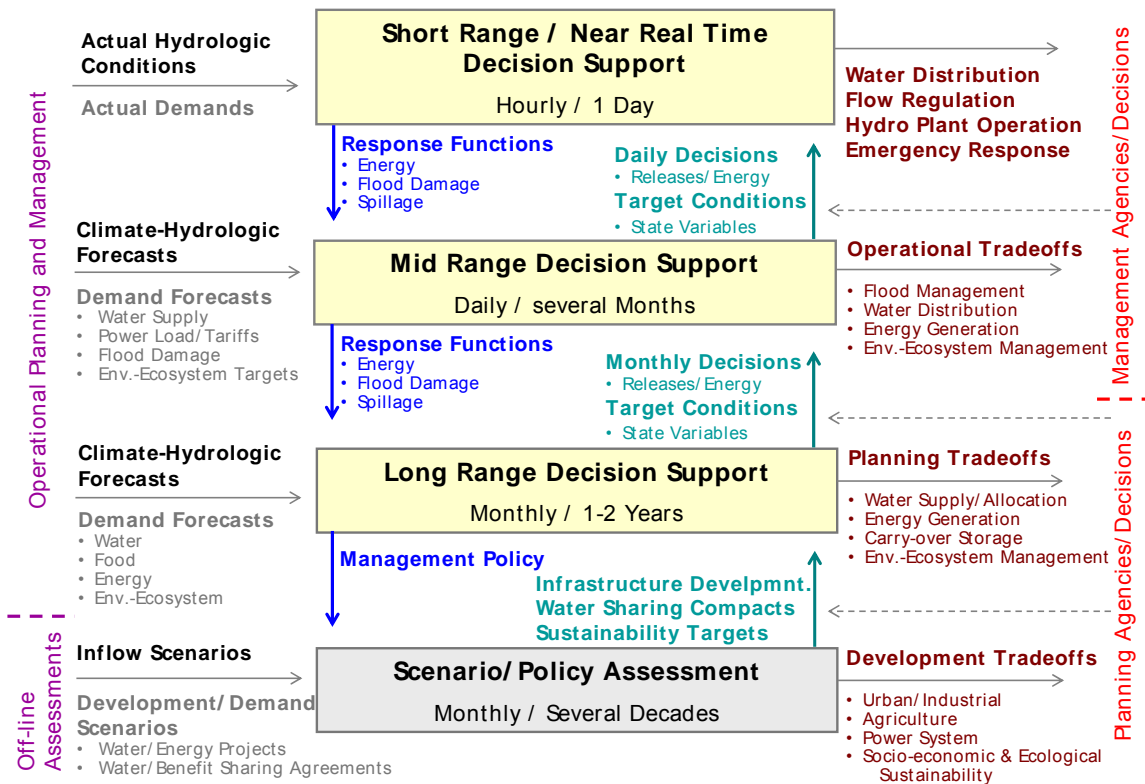
3.1.2.2 Water Temperature Modeling for Fisheries Management

In addition to managing water to deliver water supply for irrigation and municipal uses, generate hydropower, and prevent flooding, the Central Valley and State Water Projects are also operated to provide a range of services to the environment by maintaining both adequate water quality and water quantity. One of these services is to maintain acceptable water temperatures in the rivers to help sustain local fish populations. The purpose of this DSS enhancement is to add water temperature in the upper Sacramento River as another management criterion evaluated by the INFORM Long Range Planning model. This extension aims to enable more realistic reservoir storage planning and the development of fish-friendly DSS release rules. Two complementary approaches are explored: (1) A hybrid optimization-simulation approach linking a reservoir and river temperature model to the DSS Long Range Planning model, and (2) an explicit optimization approach incorporating water temperature criteria into the optimization module of the INFORM Long Range Planning model.

3.1.2.3 Downstream Routing and Flood Control

While the previous two DSS enhancements pertain to the DSS Long Range model, flood control operations is a short range decision process pertaining to daily or sub-daily time resolutions. As the critical flood control areas in the Northern California river system occur downstream of the main reservoirs, supporting this process requires the development and inclusion of routing models for the downstream river reaches. The last DSS enhancement aims to explore efficient ways to accomplish this goal.

Figure 3.1.1: INFORM DSS Modeling Framework



3.2 Uncertainty Management

In water resources systems, the values of several variables may not be known with certainty in future time periods. Even though uncertainties may only be introduced through a few variables, the interconnected nature of the system may result in uncertainties manifesting themselves in other system variables. As shown in Figures 3.2.1, different inflow forecast traces lead to a variety of different possible storage and releases traces. Furthermore, other performance measures such as hydropower production, water deliveries, river water temperature, etc., may also differ from one trace to another. Fortunately, inflow uncertainties can be quantified by ensembles consisting of many different traces. This approach has been adopted in the INFORM Long Range Planning model, whereby inflow ensemble forecasts are issued and then used to generate ensemble forecasts of management variables.

However, the presence of uncertainties complicates the management problem. Managers and stakeholders need to consider a range of possible traces and make decisions that lead to acceptable system performance in light of these uncertainties. Consequently, elements of risk, which can be defined as the “effect of uncertainty on objectives” (Leitch, 2010), are introduced into the decision-making process. Is it desirable to supply higher water deliveries on average even though there it is likely that only small deliveries would be supported under several of the inflow traces? Or would it be better to accept slightly lower average performance in return for greater assurance that a minimum amount of water can be delivered even if the least favorable traces were to materialize? Such questions are not addressed explicitly in most traditional

applications of stochastic methods to the water resources field. Instead, these methods find management policies by trying to optimize one particular statistic: the expected value of the objective function. As a result, little control is provided over how the uncertainty is distributed throughout the system. Once the problem is set up through the definition of the system variables, objective function, and parameter values, an optimization method will compute a particular management policy and application of this policy to the system then results in uncertainty distributions and risks that stakeholders would have to accept.

The INFORM Long Range Planning Model is also based on optimizing with respect to the expected value of the objective function. The model does however provide users the ability to explore several different management policies via tradeoff points that vary the amount of carryover storage that should remain in the reservoir at the end of the management horizon. Nevertheless, efforts were undertaken to explore other ways of generating additional management policies that take into account objectives beyond simply optimizing with respect to the expected value.

3.2.1 Background and Motivation

The opportunities that exist with respect to managing the uncertainty in water resources systems can be elucidated by a few simple examples. Uncertainty is introduced into the system shown in Figure 6.1a by the fact that the inflows are not known beforehand and are described as ensemble inflow forecasts. A simple linear management policy may be constructed to manage such a system:

$$u(k) = u_{\text{constant}}(k) + f(S(k) - S_{\text{constant}}(k))$$

In this policy, u_{constant} represents a constant release quantity, while the second part,

$f(S(k) - S_{\text{constant}}(k))$, introduces a deviation from this constant depending on the storage in the reservoir. Different ways of managing the uncertainty in the system can be explored by altering the value of the slope of the management policy, f . At one extreme, it may be desirable to maintain fairly predictable releases that minimize the risk of deviating from a target. In that case, f can be set to zero, leading to the state and decision trajectories shown in Figure 6.1b, where, for simplicity, the graphs only show the 10th and 90th percentiles of the variable ensembles. The resulting releases are constant no matter what the inflows are, while the reservoir storages contain the uncertainty introduced by the inflow ensemble. On the other extreme, a slope of 1 can be used to keep reservoir storages as tightly contained within a desired range as possible. As shown in Figure 3.2.2, this alters the uncertainty distribution such that the releases are highly variable, whereas the storage can be predicted with certainty. Between these two extremes, different options for distributing the uncertainty among the states and decisions could be explored by varying the slope of the management policy between 0 and 1.

If the management horizon spans multiple future time periods, trade-offs between the variables at several time periods throughout the management horizon may be considered in addition to just investigating trade-offs between the uncertainties at a particular time period. Furthermore, there are even more possibilities for managing uncertainties in multi-dimensional systems.

Besides looking at the interplay between the storage and release of one particular reservoir, the uncertainties could potentially be distributed into different locations of the system.

However, there are limitations to how the uncertainties in the system can be managed. For instance, it is impossible keep both the storages and releases entirely predictable over the management horizon since making one of them certain will introduce uncertainties into the other. The dominant factor is ultimately the magnitude of the uncertainties that are introduced into the system. Unless the inflow uncertainties are reduced by better inflow forecasting models, uncertainties will enter the system and manifest themselves in the other system variables. These uncertainties may be distributed among the states and decisions in a multitude of ways, but they cannot be completely eliminated. A system may be managed to make certain variables predictable, but in return be subject to uncertainties in the other variables. Another limiting factor is the presence of constraints. Revisiting the example in Figure 3.2.2, achieving the goal of managing the system such that the reservoir releases follow the same exact magnitudes under all possible inflow traces may not be possible if there are constraints on the system storages or releases. The system structure and management goals in Figure 3.2.2d are the same as those in Figure 3.2.2b, with the exception that the former is subject to storage constraints. As a result, releases that are higher than the release target may be required for high inflow magnitudes as the storage approaches the reservoir capacity. Conversely, releases may have to be curtailed when the inflows are so small that the reservoir would be emptied under the target release. The uncertainty distribution of the releases in the later time periods is affected by the constraints as there are deviations from the targets that would not have occurred in the unconstrained case.

These concepts can also be expanded beyond states and decisions to include other variables that are dependent on them. For instance, hydropower production is a function of both the reservoir storage and release and its distribution could be altered through different management policies. Additionally, the uncertainties in the objective function values over the entire management horizon, such as total water deliveries over an entire season, could also be managed.

3.2.2 Uncertainty Management Approach

The previous examples show that the distributions of uncertainties in the system variables are a function of the policies that are used to manage it. The management policies also relate to risk management since risks are a function of the uncertainty distributions of the objectives. In order to use these concepts in actual system management, a relationship between the uncertainty distribution and the satisfaction of system managers has to be established such that the best management policies can be identified. One approach involves defining a utility function that takes into account the entire uncertainty distribution and converts it into a scalar value (Karbowski, 1996; Watkins and McKinney, 1997). Different policies can then be compared, with the best policy being the one that yields the highest utility. Unfortunately, it has proven difficult to determine such utility functions. An alternative approach involves only looking at a few characteristic of the uncertainty distribution. An overwhelming number of studies have included just one particular characteristic: the expected value of the objective function distribution.

Ultimately, the types of criteria to be included should be chosen by system managers to address their particular concerns. Unfortunately, an equally important consideration is whether or not a systematic and computationally efficient procedure for finding management policies that meet these criteria can be developed since it is possible to select certain criteria for which there are no solution procedures or only heuristic ones that do not guarantee optimal or near optimal results. It was decided that the question of uncertainty management would be addressed by coupling variance criteria with traditional approaches since a solution procedure could be developed for such a problem. While this does not address every aspect of uncertainty management and risk, the incorporation of variance criteria is still expected to add significant flexibility over traditional approaches. The variance is a very important parameter that has a strong effect on the distribution of uncertainties and will provide managers with a tool to modify this distribution and mitigate risks.

3.2.3 Mathematical Formulation and Solution Approach

The problem being solved is based on the following traditional expected value optimization problem already being used by the INFORM Long Range Planning model (see HRC-GWRI, 2007 for a detailed description of the optimization problem). Additionally, constraints on the variances of different variables are added. The first type of constraints pertain to variables that are additive over multiple time periods of the management horizon. Such constraints can arise when there are management goals that depend on the performance of the system over the entire management horizon. The second type of constraint pertains to variables at individual time periods.

The variance constraints were incorporated into the original optimization problem through a method initially developed by Sniedovich (1980). However, the method was extended to be applicable to multi-dimensional systems and also to allow for several constraints to be added. The problem is formulated by using Lagrangian multipliers to augment the original objective function as follows:

$$L_{new}(\pi, \lambda) = \mathbf{E}_{w(1), \dots, w(N-1)} \left[\sum_{k=0}^N g(k, S(k), \mu(k, S(k))) + g(N+1, S(N+1)) \right] + \sum_{c=1}^C \lambda_c \mathbf{V}_{w(1), \dots, w(N-1)} \left[\sum_{k=0}^N R_c(S(k), \mu(k, S(k))) \right]$$

The first portion of the objective function represents the original objective function that is based on optimizing with respect to the expected value of the system objectives. The second portion represents the variances of the variables to be constrained (R_c) multiplied by Lagrangian multipliers (λ). The formulation is general to allow the variances of several different variables ($c=1, 2, \dots, C$) to be constrained.

With the problem having been formulated, a solution strategy needs to be developed. One possibility is to follow the work of Sniedovich (1980), Karbowski (1996), and Watkins and McKinney (1997) and explore a whole range of management policies and variance values. This

approach consists of fixing the Lagrangian multipliers at certain values and solving the augmented optimization problem for a management policy. This policy is then used to manage the system and find the resulting variances of the variables to be constrained. The policy will be optimal for the original problem with the variance constraints set to these values. Another set of Lagrangian multipliers can then be chosen and a new management policy can be identified. This policy will again be optimal, but with respect to the original problem with the variance constraints set at values resulting from having applied the second management policy to the system. This process can be repeated many times for different choices of the Lagrangian multipliers to generate a host of policies that are optimal for different values of the variance constraints.

While the previous approach can be used to explore trade-offs, it is not the most efficient way of finding management policies that meet a specific set of variance constraints. Even though one could theoretically find such policies by testing out many Lagrangian multiplier candidates and choosing the ones that meet the constraints and provides the best average performance, this process is cumbersome, especially as the number of constraints is increased. Methods that take a more direct approach to searching for management policies that meet certain pre-defined variance constraints and optimize the objective function at the same time would therefore be useful. Such a method was developed by using an outer optimization problem to find those Lagrangian multipliers that result in the most desirable management policy. Nonlinear programming methods were used to identify suitable Lagrangian multipliers that meet the specified variance constraints. The details of this approach are described in Kistenmacher (2012) and Kistenmacher and Georgakakos (2013).

3.2.4 Mathematical Formulation and Solution Approach

The proposed algorithm was tested in a case study using the INFORM Long Range Planning model. The model considers a nine month management horizon starting in January 1922.

3.2.4.1 Variance Constraints

The INFORM Long Range Planning model was expanded to incorporate the following variance constraints:

$$\begin{aligned}
 V[S_r(k)] &\leq \nu_r^{state}(k) \\
 V[u_r(k)] &\leq \nu_r^{decision}(k) \\
 V[u_6(k) + u_7(k)] &\leq \nu^{demand\ met}(k) \\
 V[s_1(k) + s_2(k) + s_3(k) + s_4(k) + s_5(k) + s_6(k)] &\leq \nu^{total\ storage}(k) \\
 &\text{for } k = 1, 2, \dots, 9 \text{ or } 10 \\
 &\text{and } r = 1, 2, \dots, 7
 \end{aligned}$$

The first two constraints pertain to the individual states and decisions while the third and fourth constraints can be used to limit the variances of the south-of-Delta demands and the total system storage, respectively. For the states, subscript 1 refers to storage in Trinity reservoir, 2 to storage in Shasta, 3 to storage in Oroville, 4 to storage in Folsom, 5 to storage in New Melones, and 6 to storage in San Luis. X2 location is another state variable identified by subscript 7. The decisions are releases associated with the same reservoirs as the corresponding storage subscripts, i.e. the Shasta releases would be u_2 . The decision variable u_7 represents the total exports being made from the Delta. Each of the constraints are defined for each time period of the management horizon and, if applicable, for each location.

3.2.4.2 Inflow Uncertainties

A Historical Analog ESP (HRC-GWRI, 2007) model was used to generate an inflow forecast ensemble for each of the six inflow locations within the study area. The 15 member ensembles are plotted in Figure 3.2.3 while ensemble statistics are summarized in Figures 3.2.4. The standard deviations indicate the magnitudes of the uncertainties that are introduced into the system each month throughout the system. The largest uncertainties are introduced in the winter and spring months. These seasons receive more precipitation, while the months with lower variability correspond to the dry parts of the year that are also lower in average magnitude. The same statistics are also plotted for the cumulative inflows.

3.2.4.3 Single Variance Constraint

The first example only considers a single variance constraint: the variance of Oroville reservoir storage at the end of the management horizon, i.e. S_3 (10). After solving the original unconstrained problem, the variance of this variable was found to be 350,000. The problem was then resolved with the variance constraint being set to roughly a third (100,000) of the original variance. The search procedure found an optimal solution after 2 iterations. Figures 3.2.5 and 3.2.6 depict the resulting state and decision uncertainty distributions before (blue lines) and after (red lines) the addition of the variance constraint. For clarity, trajectories corresponding to the 25th and 75th percentiles are plotted instead of each of the individual traces. The effect of introducing the variance constraint can be observed in the plot of the third state since the new distribution is significantly tighter than the original distribution. This simple example can be used to explore how system management is impacted by the imposition of a variance constraint. For one, the uncertainty distribution of the Oroville storage begins to tighten several time periods before the end of the management horizon. The management policies at some of the preceding time periods are therefore also altered to contribute towards meeting the constraint even though the constraint only affects the objective function at the last time period. It appears to be more optimal to slowly reduce the variance over a few time periods than to abruptly make adjustments immediately prior to the last time period.

The response of the remainder of the system to the variance constraint is also noteworthy. The south-of-Delta system (S_6 , u_6 , u_7 , and demands) is almost completely unaffected by the constraint. In order for this to be the case, however, the other upstream reservoirs have to adjust their operations. The variance constraint on the storage at Oroville reservoir is partially met by reducing that reservoir's releases. In order for the south-of Delta system to receive the same

amount of water, the management policies are altered to increase the releases of some of the other reservoirs, a response that also manifests itself in the associated storages by making them more variable.

3.2.4.4 Multiple Variance Constraints and Trade-offs

The next example imposes constraints on the variance of the total system storage at the final time period of the horizon. While each reservoir has its own management goals, the total system storage is an indicator of the combined amount of water that is available to meet water demands throughout the entire system. Maintaining adequate system storage at the end of the management horizon, which happens to coincide with the end of the water year, is important to ensure that enough water is available to meet future demands. In the unconstrained case, the final total system storage variance was 3,900,000. Figures 3.2.7 and 3.2.8 show the state and decision uncertainty distributions that result when the variance is constrained to about a third of the original variance (1,400,000). It took the search procedure 7 iterations to find the optimal solution. The total system storage trajectories before and after the addition of the variance constraint, shown in the bottom right corner of Figure 3.2.7, reveal that the uncertainty range of this variable has indeed been reduced. Furthermore, the reduction again takes place gradually over time. The variances of several of the upstream reservoirs have also been decreased, resulting in a decrease in the total system storage variance.

However, the uncertainty distribution of San Luis reservoir (S6) is increased significantly. At first, this appears counter-intuitive since San Luis reservoir storage also contributes to the total system storage. However, the sum of the individual variances does not necessarily have to correlate positively with the variance of the total system storage. In fact, the opposite seems to be true: as the San Luis reservoir storage variance increases, the variance of the total system storage decreases. The variance constraint actually alters the management policies such that San Luis reservoir storage is used strategically to decrease the variance of the total system storage by storing more water for traces that originally had relatively low total system storage. Figures 3.2.9 and 3.2.10 contain the individual ensemble traces, where the final trajectories (i.e. belonging to the red ensemble) for two particular traces are highlighted by black lines. The solid line corresponds to a trace for which the storages in the upstream reservoirs are relatively low. The capacity of San Luis reservoir is used to store water that would otherwise have gone towards meeting demands such that the total system storage is increased and brought closer the ensemble mean. On the other hand, the upstream storages for the trace depicted with the dotted black lines are relatively large and San Luis reservoir is not really used to affect the total system storage. Instead, the upstream reservoirs release more water, which eventually discharges into the San Francisco bay (as evidenced by the decreased X2 distances), to bring the total system storage closer to the ensemble mean.

The problem was resolved several times by changing the severity of the variance constraint. The results can be used to explore the relationship between the expected objective function value and the variance constraint. The trade-off curve shown in Figure 3.2.11 reveals that tightening the variance constraint decreases system performance. However, this decrease is not very significant, with the costs being in the range of 0-10 percent of the costs resulting from the

unconstrained problem. A possible reason for this is that the constraint only applied to the variance of one particular system variable at one particular time period. While several portions of the system respond to meet this constraint, other portions and the earlier time period are left relatively unaltered.

A more drastic trade-off is expected if the total objective function value were to be constrained instead. However, this requires the addition of another state variable and was not investigated at this time. A closer look at the decision variables reveals that the change in the San Luis reservoir storage is primarily facilitated by a decrease in that reservoir's release. Furthermore, the south-of-Delta demands that can be met are also decreased and their distributions become significantly more uncertain and subject to fluctuations. Adding a constraint on the total system storage variance therefore adversely affects the objective of meeting south-of-Delta demands, which may be undesirable for stakeholders that rely on these demands. The next example takes the previous problem and adds additional constraints on the variance of the south-of-Delta demands. In particular, the variance of the south-of-Delta demands at time period 9 was limited to 200,000 while the total storage constraints at the last time period were constrained to be less than or equal to 2,000,000. Figures 3.2.12 and 3.2.13 show the uncertainty distributions before and after the addition of the additional constraint. The resulting management policies are able to meet the both constraints by adjusting San Luis reservoir operations to store more water earlier in the horizon, allowing the total storage constraint to be met without having to have highly variable releases in the last time period.

While the additional constraint reduced the demand variance at the end of the horizon, the demands in prior time periods continue to exhibit high variability. An additional problem that constrains the south-of-Delta demand variances at time periods 8 and 9 was also solved. Figures 3.2.14 and 3.2.15 show that all of constraints can again be met by management policies that adjust San Luis reservoir storage earlier in the horizon.

Another problem that constrains the final total system variable variance as well as the demand variances from time periods 7 through 9 was also solved. However, the search procedure was unable to find a feasible solution and meeting the demand variances resulted in violations of the total storage variance constraint, and vice versa. In the end, the final management policies wind up slightly violating both the total storage and demand variance constraints. The reason for this appears to be the fact that San Luis reservoir storage is already using its entire capacity and cannot store additional water to help decrease the variance of the total system storage.

3.2.5 Interactive Management Framework

The previous examples identified several different management policies that produce a variety of uncertainty distributions. The search procedure can be used to find policies that meet a pre-defined set of constraints as well to generate trade-offs between different objectives. Given the multi-dimensional, multi-objective, and multi-stakeholder nature of many reservoir systems, it is possible that a large number of different management policies have to be explored. Instead of creating a few general trade-off curves and solving policies corresponding to pre-specified criteria, the interactive and iterative framework shown in Figure 3.2.16 can be used to aid in decision making. Under this framework, an initial run of the management model is used to

generate an initial scenario. The resulting system ensembles are then presented to stakeholders who can evaluate them and suggest desired changes about how the system is to be managed. These suggestions are then transformed into updated inputs to the management model (in the form of variance constraints), which is subsequently used to generate new management policies. This process can be repeated until the model finds a satisfactory management policy. Individual policies can be stored and compared in order to elucidate the trade-offs and dependencies that exist between managing the different system components.

Figure 3.2.1: Effect of Inflow Uncertainties on System Trajectories.

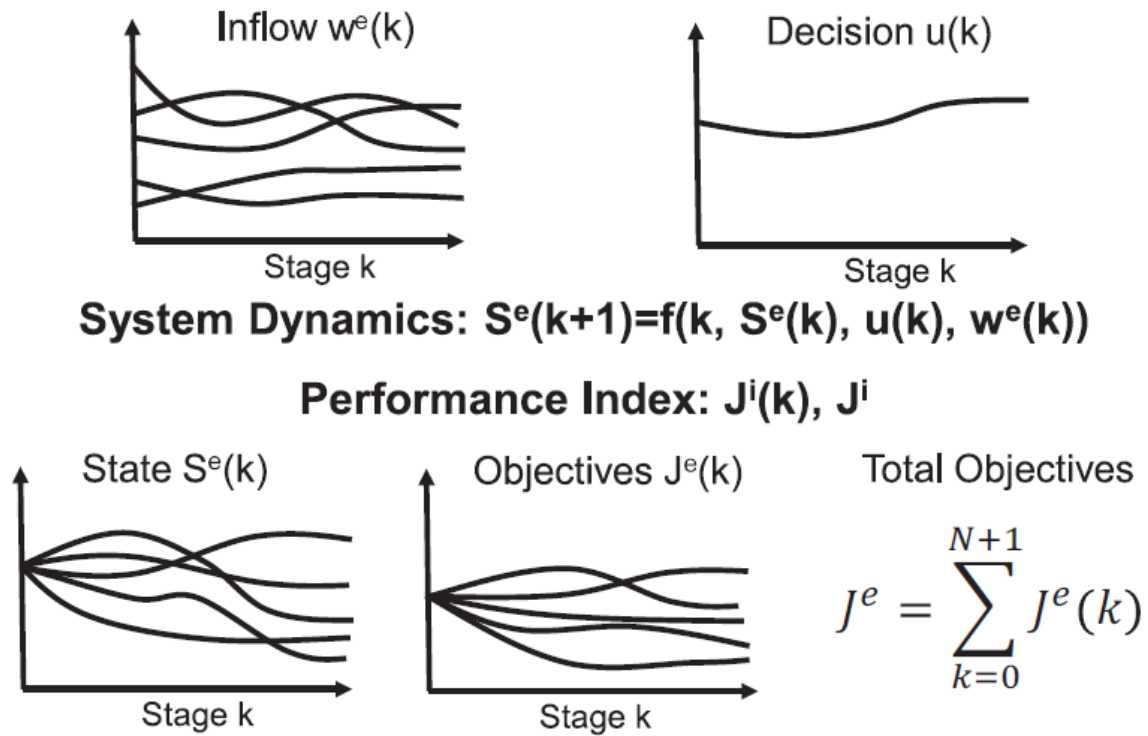


Figure 3.2.2: Uncertainty Distributions Resulting from Different Management Policies in a One-Dimensional Reservoir System.

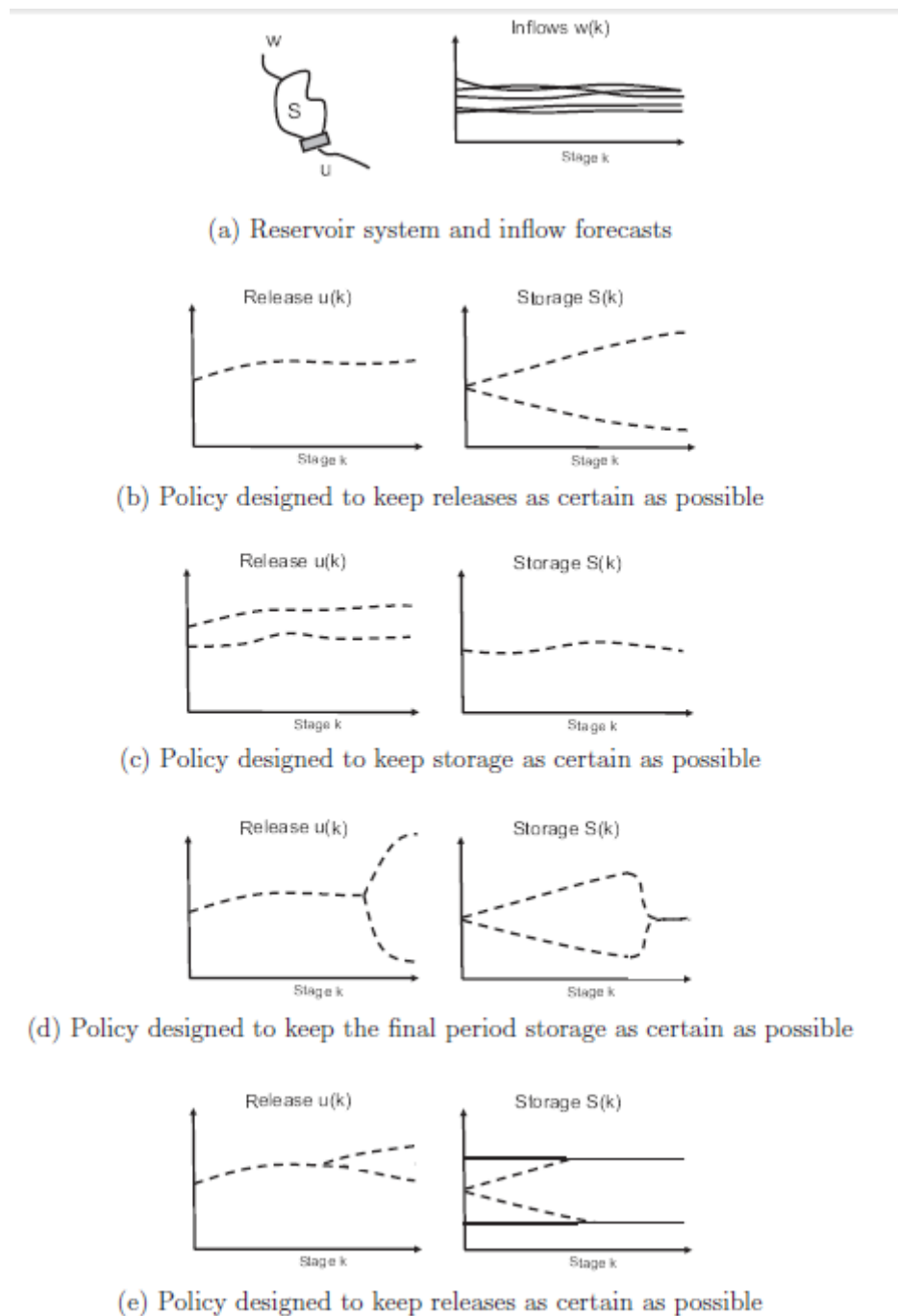


Figure 3.2.3: Inflow Forecast Ensembles Issued in January 1922.

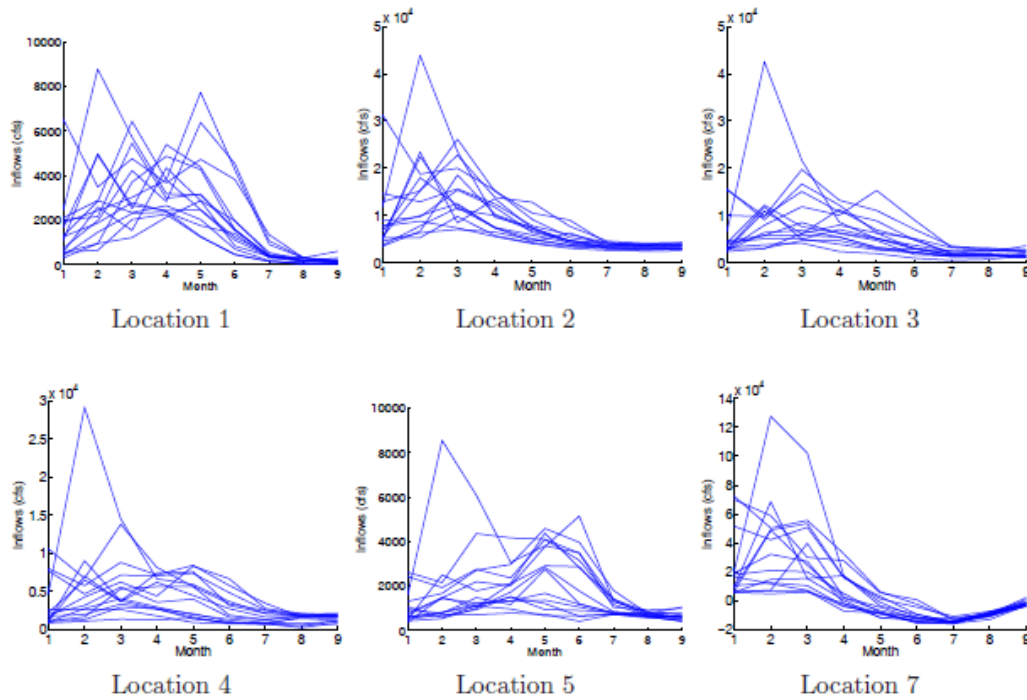


Figure 3.2.4: Expected Values (Blue) and Standard Deviations (Red) for Monthly (Solid Lines) and Cumulative (Dotted Lines) Inflow Forecast Ensembles Issued in January 1922.

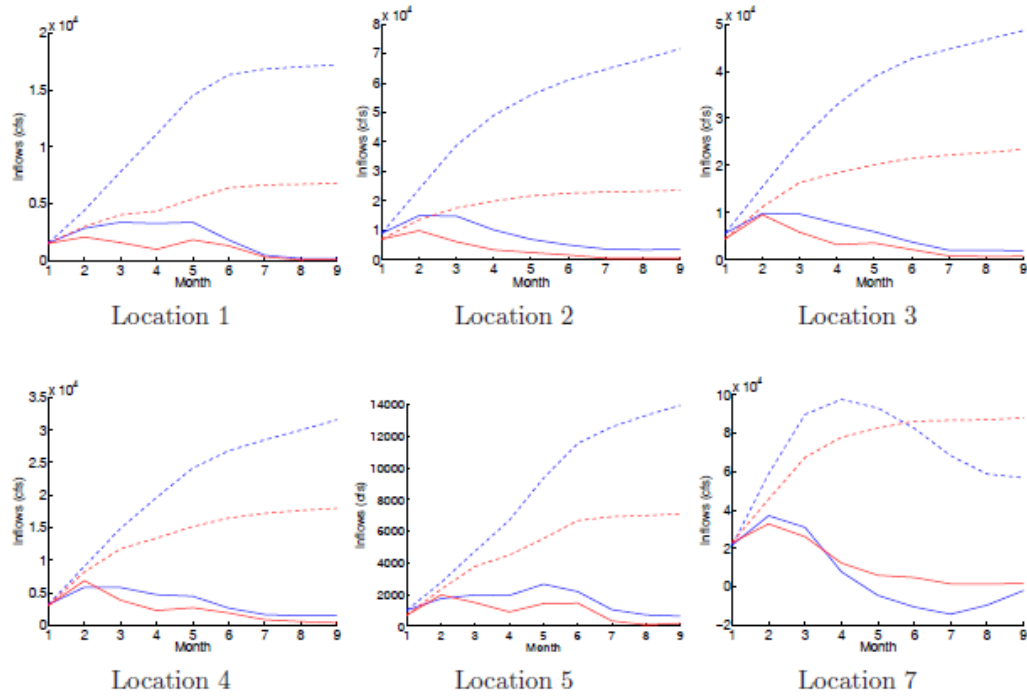


Figure 3.2.5: State Uncertainty Distributions before (Blue) and after (Red) Imposing a Constraint on the Last Time Period Oroville Reservoir Storage Variance.

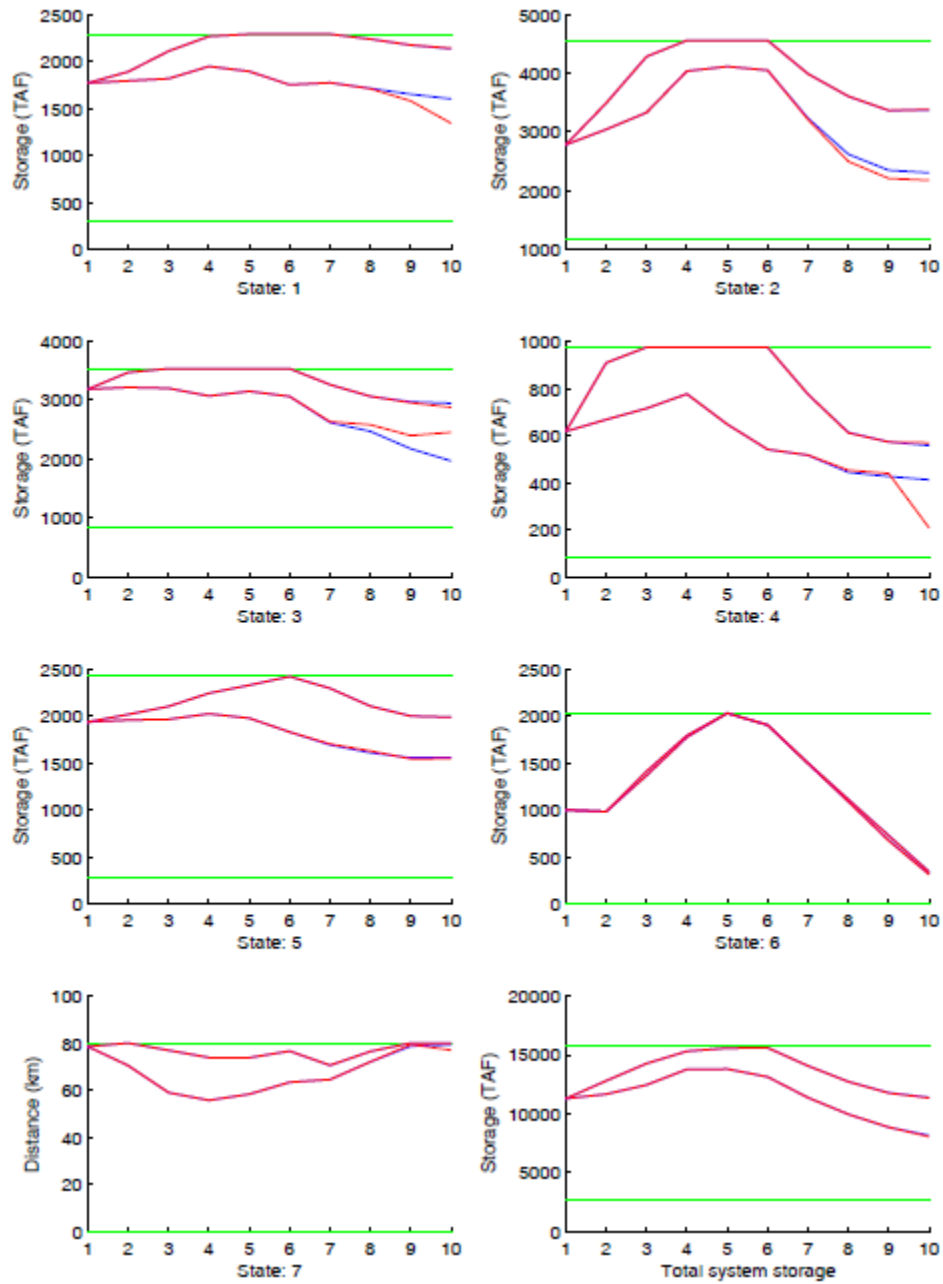


Figure 3.2.6: Decision Uncertainty Distributions before (Blue) and after (Red) Imposing a Constraint on the Last Time Period Oroville Reservoir Storage variance.

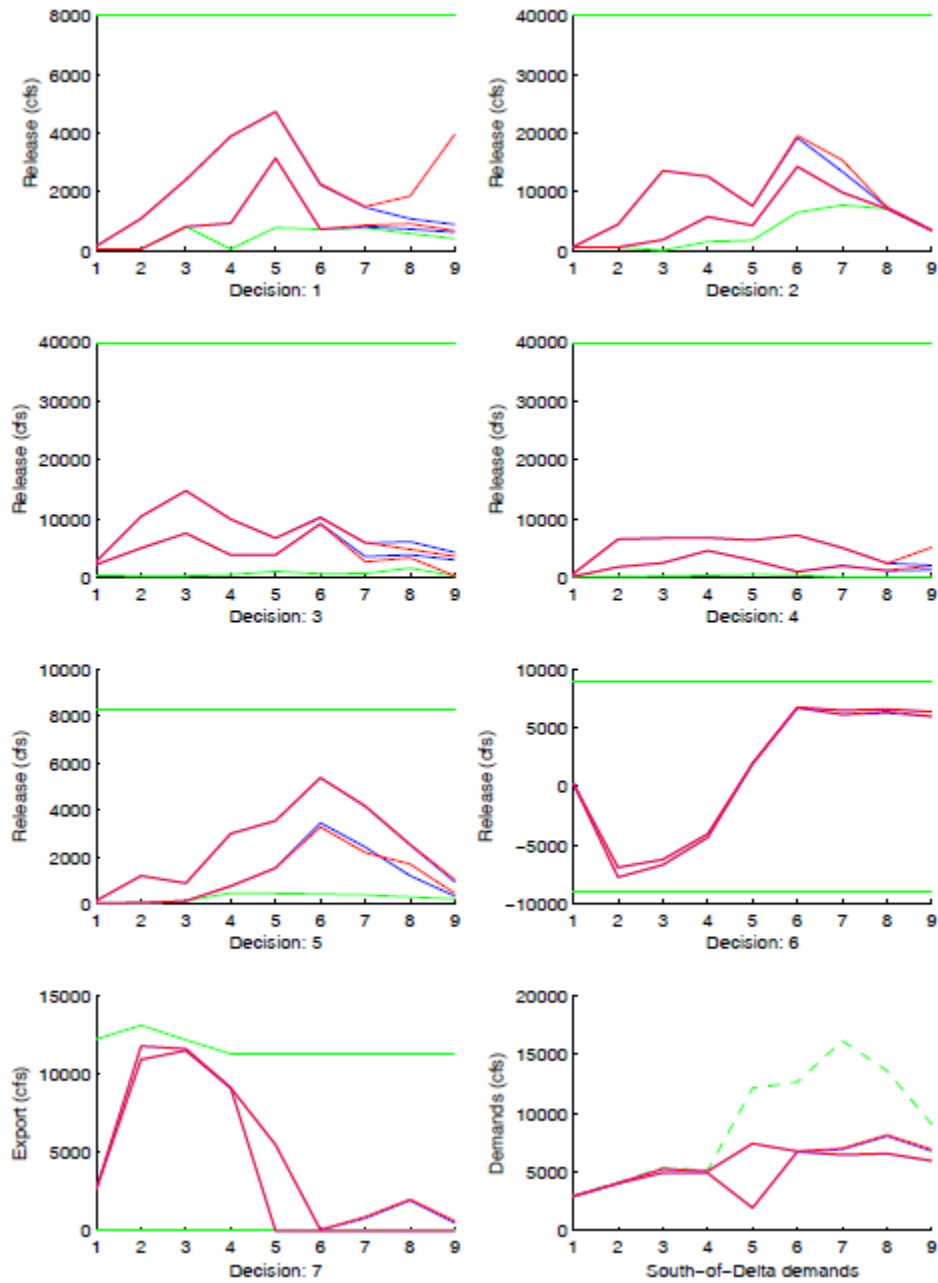


Figure 3.2.7: State Uncertainty Distributions before (Blue) and after (Red) Imposing a Constraint on the Last Time Period Total System Storage Variance.

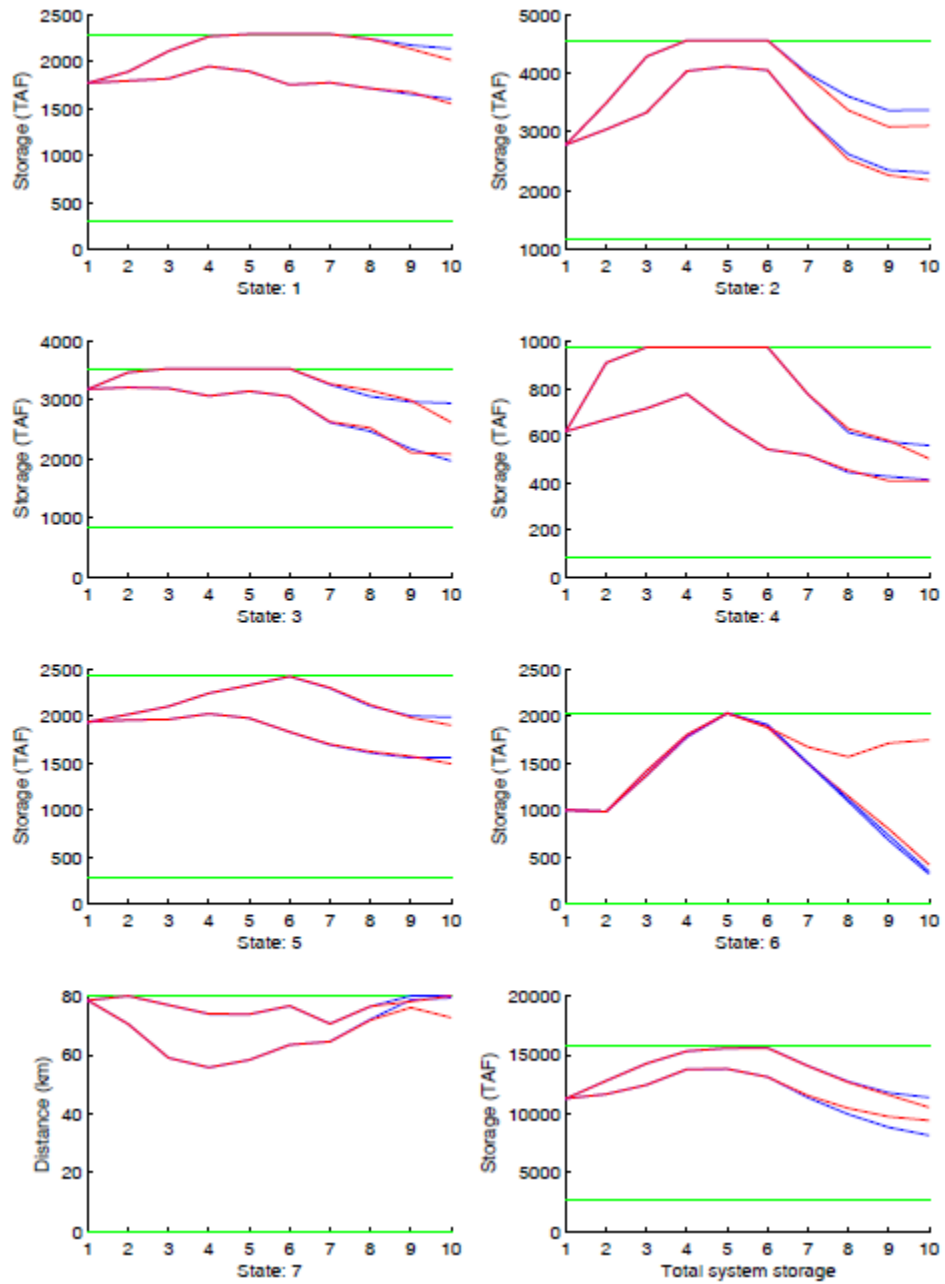


Figure 3.2.8: Decision Uncertainty Distributions before (Blue) and after (Red) Imposing a Constraint on the Last Time Period Total System Storage Variance.

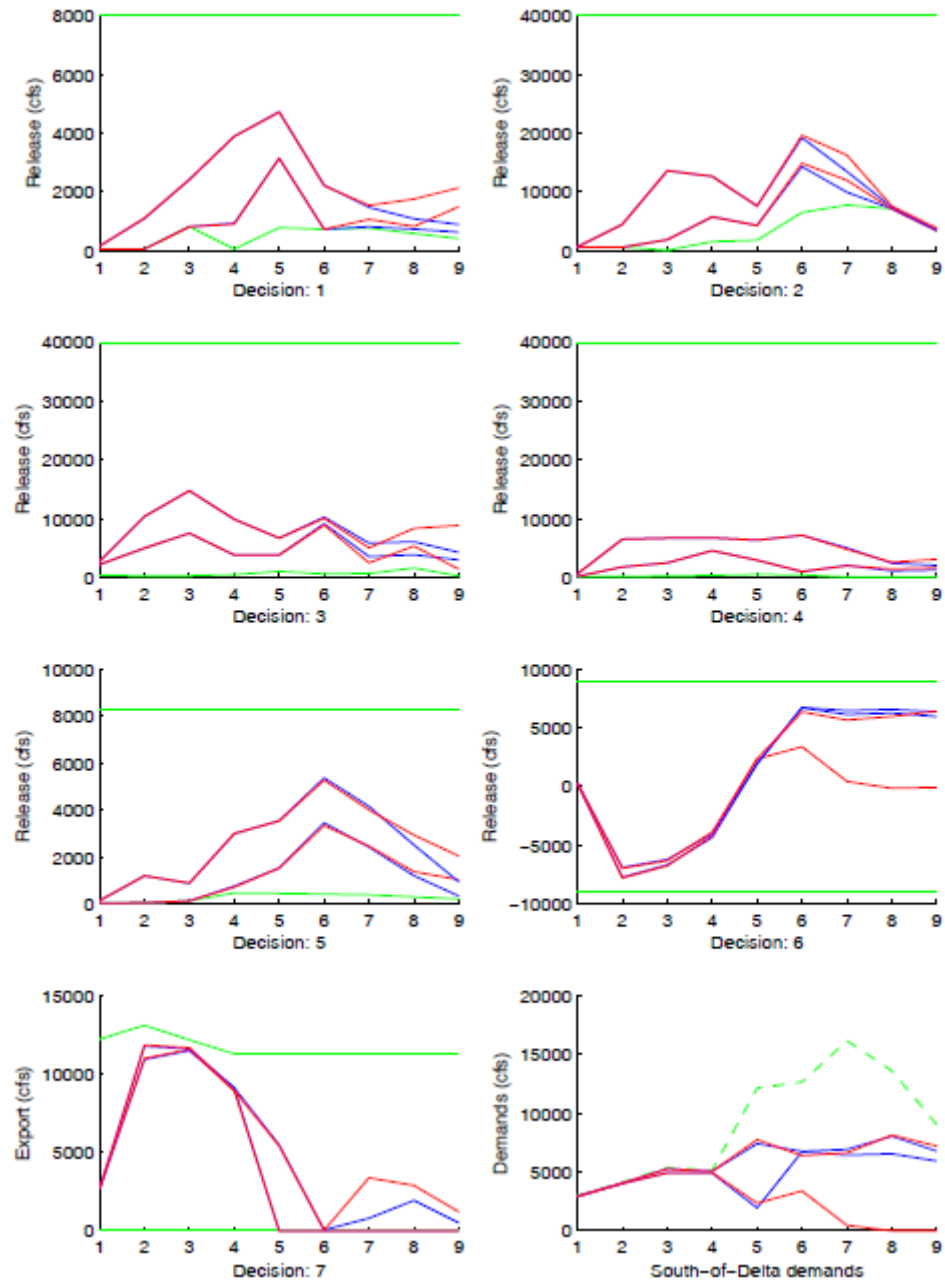


Figure 3.2.9: State Ensembles before (Blue) and after (Red) Imposing a Constraint on the Last Time Period Total System Storage Variance.

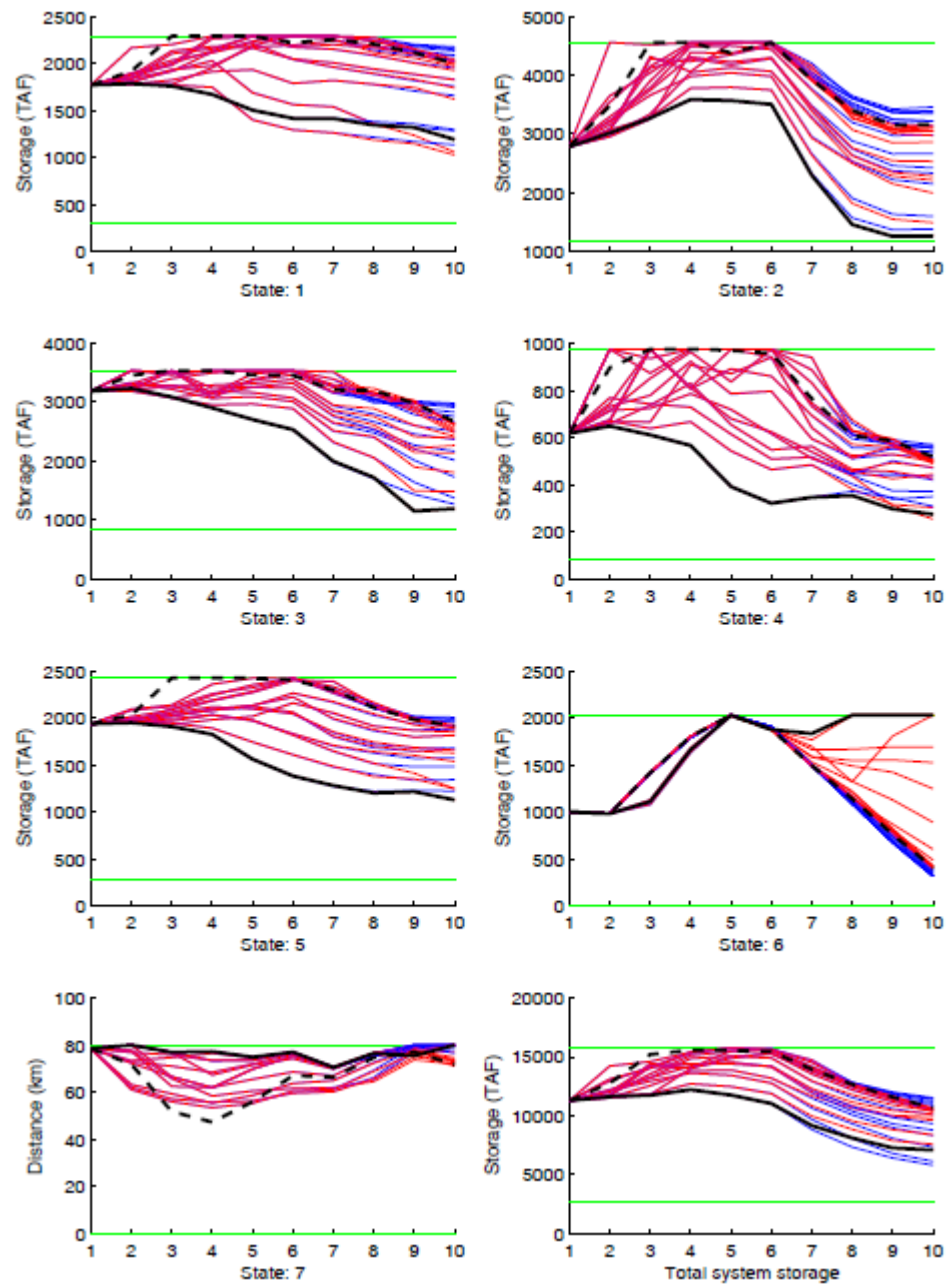


Figure 3.2.10: Decision Ensembles before (Blue) and after (Red) Imposing a Constraint on the Last Time Period Total System Storage Variance.

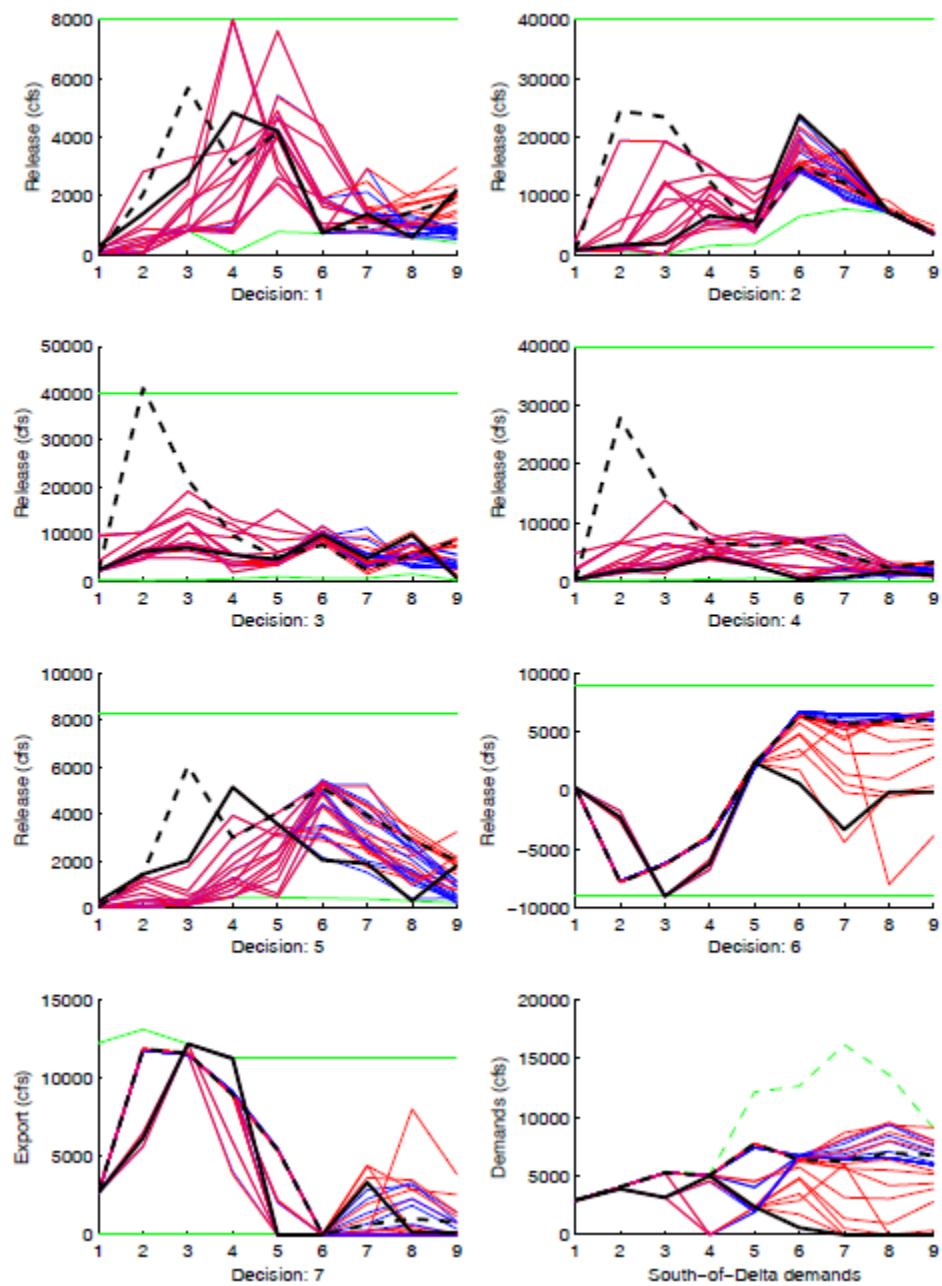


Figure 3.2.11: Trade-off between the Expected Objective Function Value (over the Whole Horizon) and the Total System Storage Variance (at the Last Time Period of the Horizon).

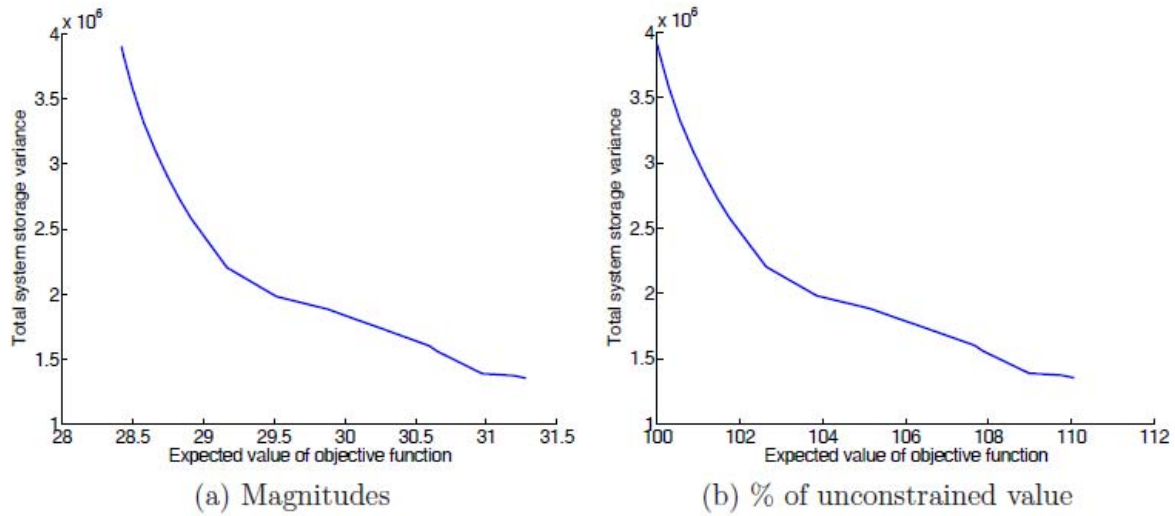


Figure 3.2.12: State Uncertainty Distributions before (Blue) and after (Red) Imposing a Constraint on the 9th Time Period South-of-Delta Demand Variance. Both Cases Include a Total Storage Variance Constraint at the Last Time Period.

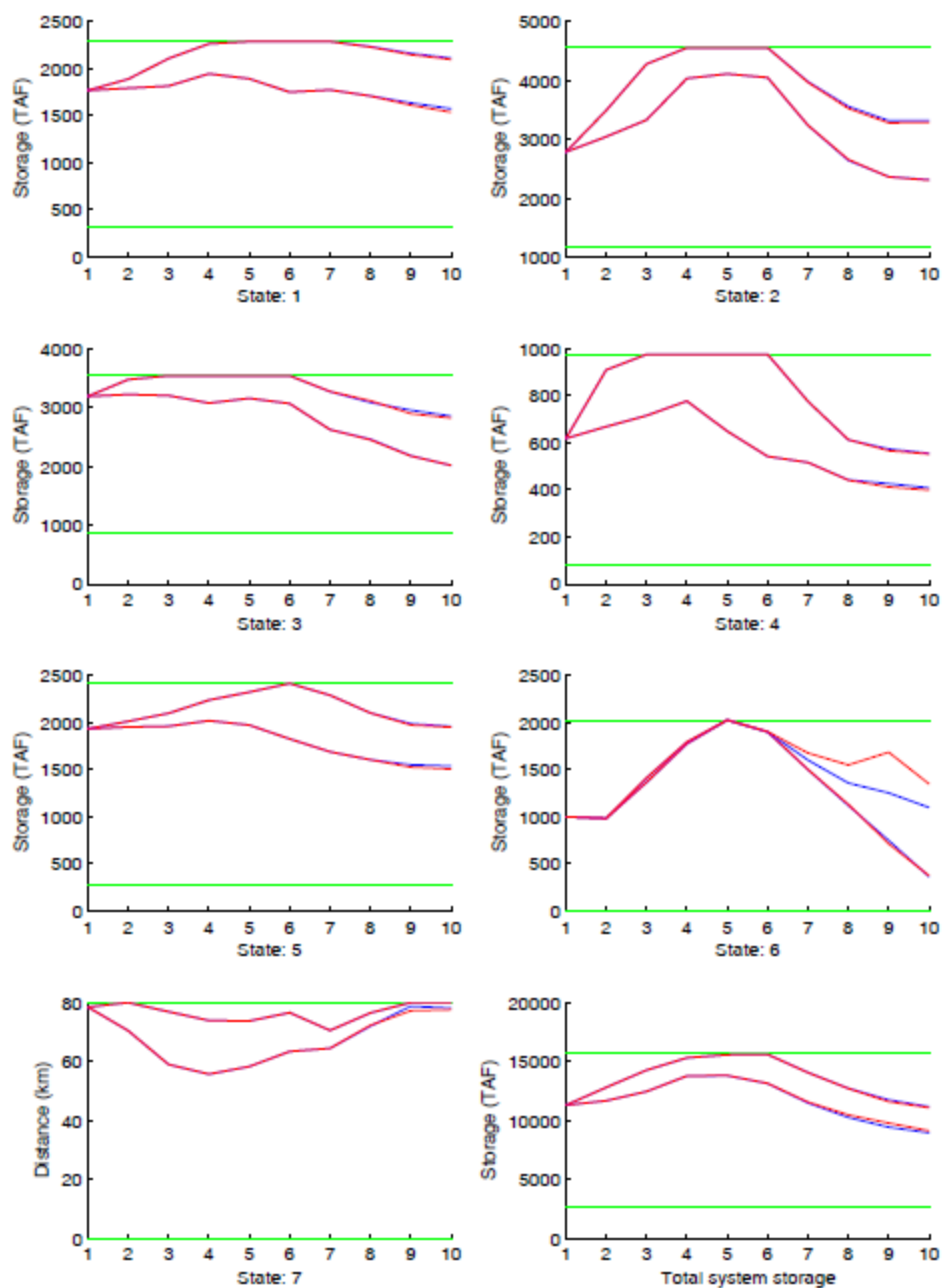


Figure 3.2.13: Decision Uncertainty Distributions before (Blue) and after (Red) Imposing a Constraint on the 9th Time Period South-of-Delta Demand Variance. Both Cases Include a Total Storage Variance Constraint at the Last Time Period.

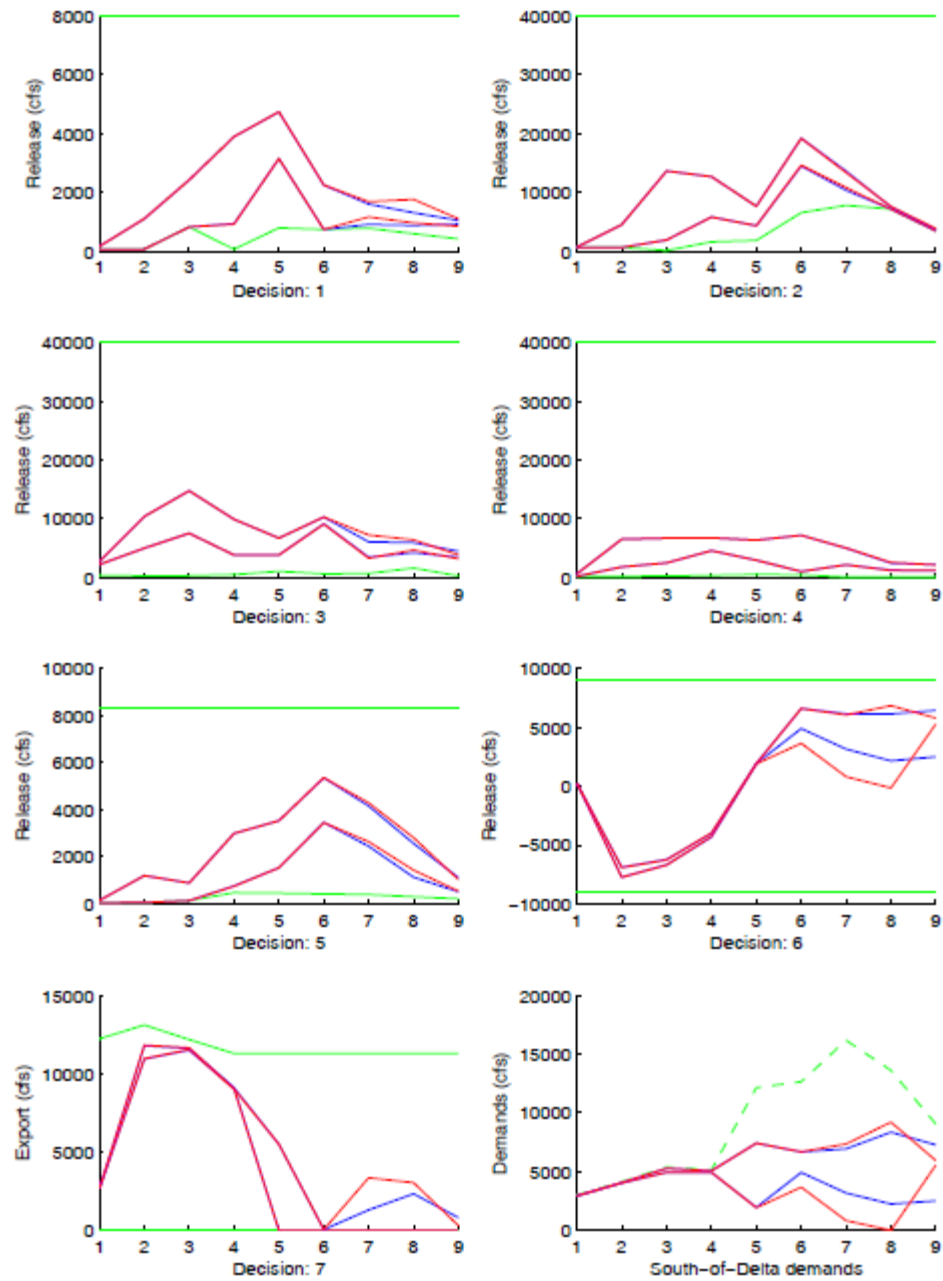


Figure 3.2.14: State Uncertainty Distributions Resulting from Imposing Constraints on the South-of-Delta Demand Variances at Time Period 9 (Blue), Time Periods 8 and 9 (Red), and Time Periods 7 through 9 (Black). All Cases Include a Total Storage Variance Constraint at the Last Time Period.

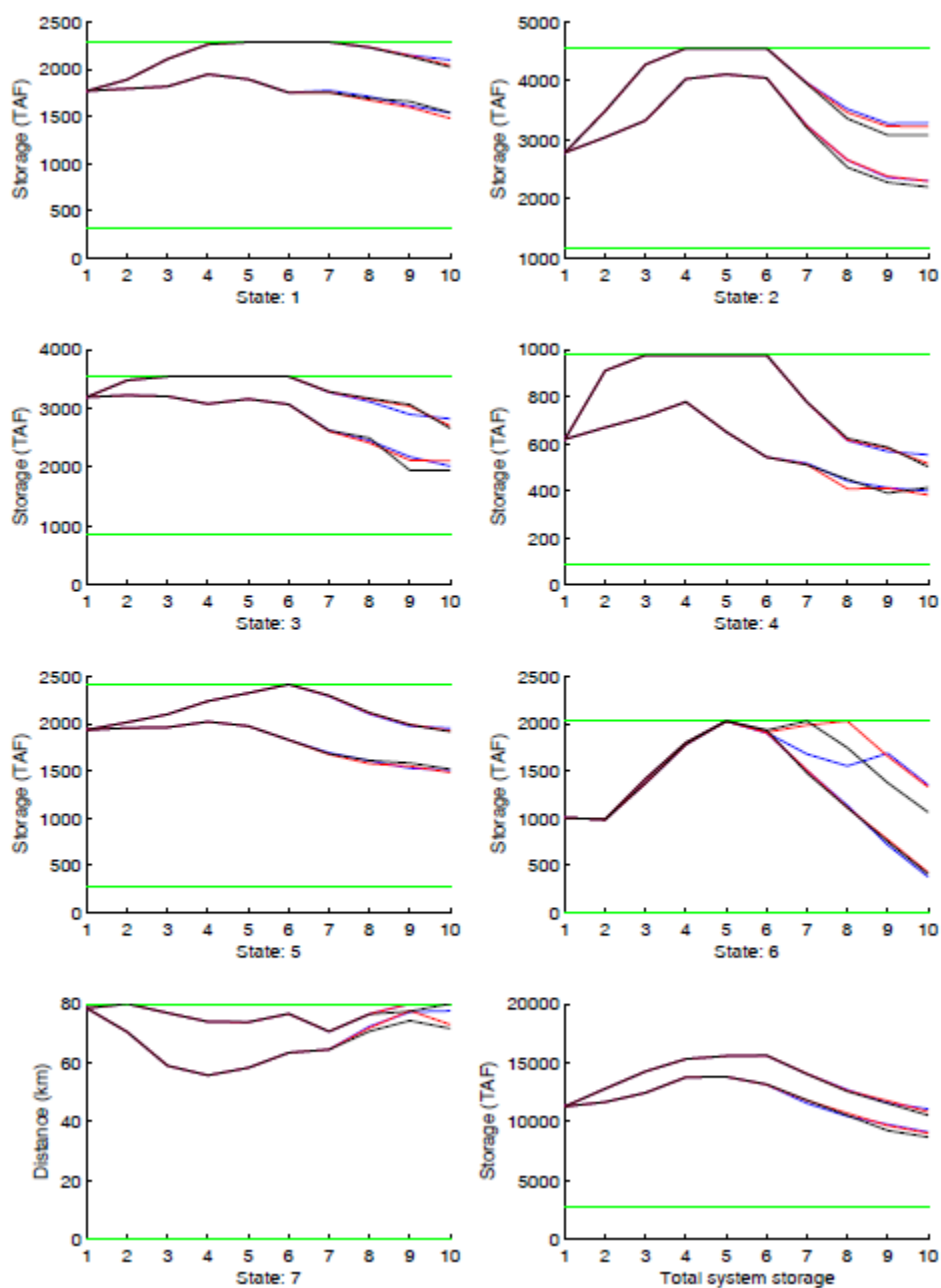


Figure 3.2.15: Decision Uncertainty Distributions Resulting from Imposing Constraints on the South-of-Delta Demand Variances at Time Period 9 (Blue), Time Periods 8 and 9 (Red), and Time Periods 7 through 9 (Black). All Cases Include a Total Storage Variance Constraint at the Last Time Period.

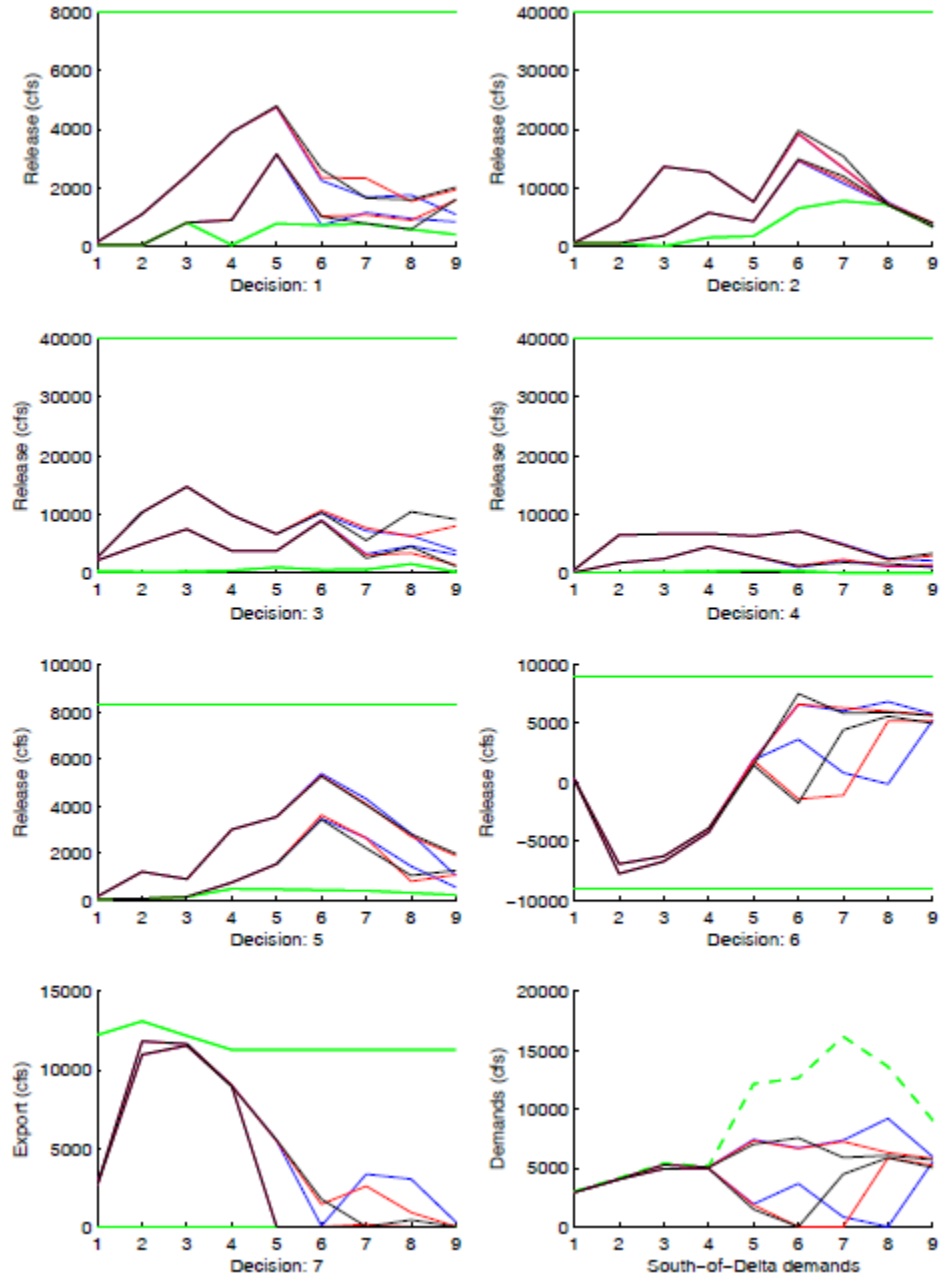
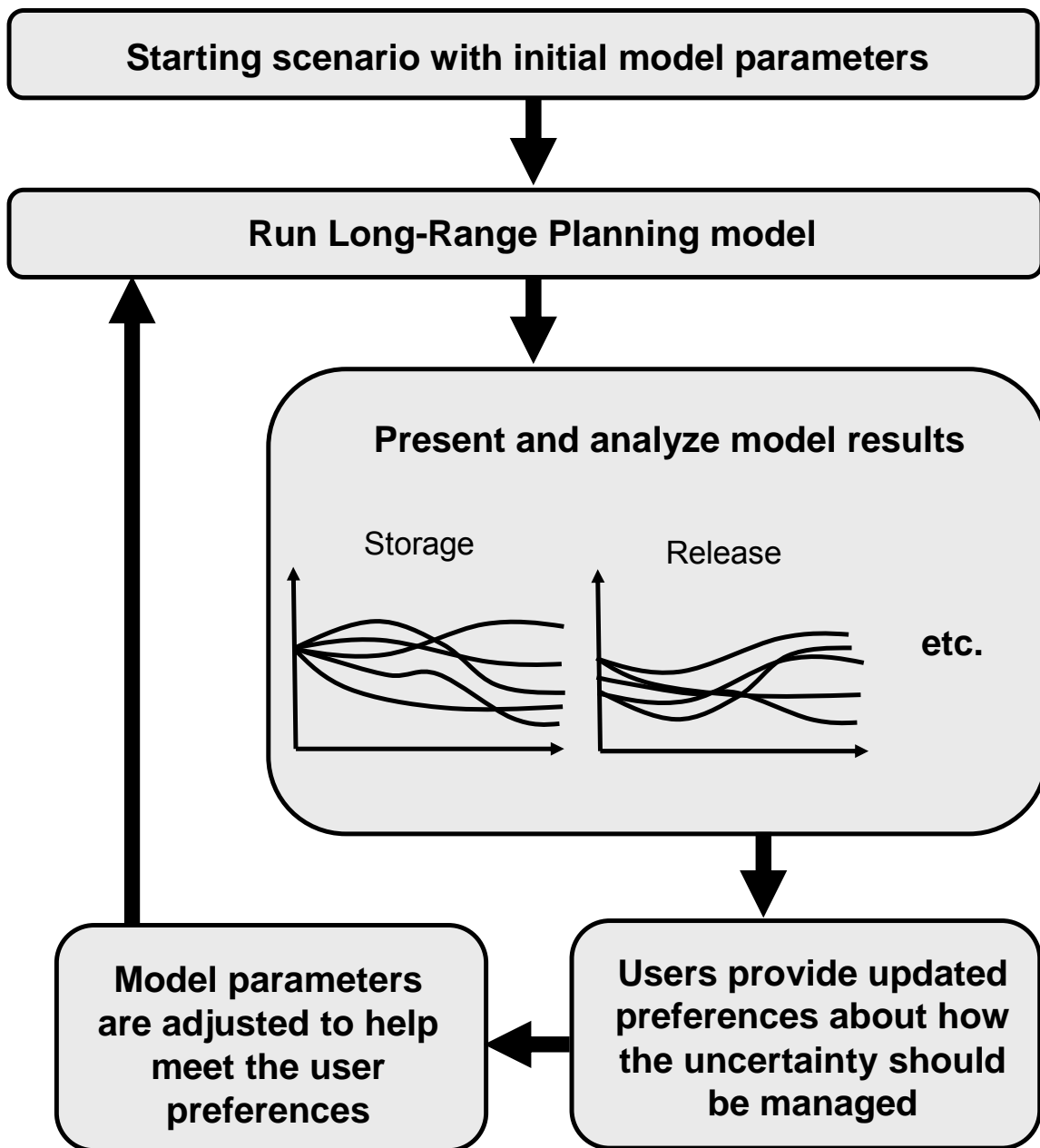


Figure 3.2.16: Interactive and Iterative Framework Incorporating User Preferences on the Management of System Uncertainties.



3.3 Reservoir and River Temperature Modeling for Fisheries Management

In addition to managing water to prevent flooding, generate hydropower, and deliver water supply for irrigation and municipal uses, the Central Valley and State Water Projects are also operated to provide a range of services to the environment by maintaining both adequate water quality and water quantity. One of these services is to maintain acceptable water temperatures in the rivers to help sustain local fish populations. Ultimately, water temperature is a function of the climate and meteorological variables, such as air temperature and solar radiation.

However, the management of water in the system reservoirs can also play a role in maintaining adequate river temperatures. Due to the vertical distribution of temperature (warmer water on top and colder water at the bottom), water stored within the larger reservoirs can be strategically withdrawn to generate releases at a range of temperatures throughout the year.

The purpose of this component of the project is to add water temperature in the upper Sacramento River as another management criterion evaluated by the INFORM Long Range Planning model. Two complementary approaches were explored: (1) simulation of existing INFORM Long Range Planning model strategies to evaluate their effects on water temperatures and (2) direct incorporation of water temperature criteria into the optimization module of the INFORM Long Range Planning model.

3.3.1 Water Temperature Considerations in the Upper Sacramento River

There are several fish species in the upper Sacramento River the health and survival of which depend on the quality and quantity of water in the river system. Water temperatures above certain ranges have been found to adversely impact the species' ability to navigate to spawning sites, as well as considerably decreasing the survival rates of newly laid eggs (NMFS, 2009). Since reservoir management decisions can influence the river water temperatures, ensuring the survival of native fish species is an objective that reservoir managers consider.

Water temperatures in the upper Sacramento River can be influenced by adjusting the release rates of the Shasta reservoir. Additionally, the amount of water entering the upper Sacramento River from the Spring Creek Tunnel and Clear Creek can be adjusted. Another management decision affecting water temperature pertains to the temperature of the releases made from Shasta. Unlike most other facilities in the system, Shasta is equipped with a temperature control device (TCD) that allows withdrawals to be made from several different levels within the reservoir. Due to the water temperature profile that exists in the reservoir (see Figure 3.3.1 for a typical temperature profile), the TCD can be used to release the same volume of water at different temperatures, providing operators with additional flexibility to alter downstream water temperatures. However, the ability to release water at certain temperatures depends on the exact temperature profile in the reservoir at any given time. If the amount of cold water stored in the reservoir is not sufficient, then water temperatures below certain limits may not be attainable.

NMFS (2009) describes a wide variety of water temperature conditions in the upper Sacramento River system favorable for native fish species. For seasonal reservoir release planning, adequate water temperatures along certain stretches of the upper Sacramento River are usually targeted.

Specifically, the area between Balls Ferry and Bend Bridge has in the past been identified as a location for control points where water temperatures should not exceed 56 F during part of the year, with these water temperatures ideally being maintained as far downstream as possible. However, the location of the control point in any given year and season can vary depending on other water management criteria.

The primary challenge to maintaining adequate temperatures is the finite volume of reservoir storage that is available to be released from the upstream facilities. For Shasta, this finite volume does not only correspond to the total reservoir storage, but also the amount of cold water stored in the reservoir. While there is usually sufficient cold water in the reservoir during the winter and spring months, the warmer summer months heat up the water and deplete the cold water storage. When viewed as a stand-alone objective, managers are faced with the challenge of identifying release strategies to manage the cold water pool throughout the water year such that adequate water temperatures can be maintained even during the warmer months. This problem is further complicated by the fact that maintaining acceptable water temperatures is only one management objective that has to be met by operators. As a result, even though a certain release strategy could meet temperature criteria, it might adversely affect other system objectives, such as maintaining sufficient carry-over storage at the end of the water year. Since the INFORM Long Range Planning model has been designed to facilitate exploration of a variety of different management strategies, this project component focused on incorporating water temperature considerations as another management objective to be evaluated.

3.3.2 Existing Water Temperature Models

Water management for temperature criteria is supported through the use of computer models that simulate the change of water temperature in response to management actions and natural drivers. Three monthly temperature models have been developed by the USBR and can be used to estimate water temperatures throughout the CVP and SWP (Roswell, 1979, 1990, and 1997). Their combined scope encompasses the Sacramento, Feather, American, Stanislaus, and Trinity rivers. Due to their monthly timesteps, these models were initially identified as being the easiest to link with the INFORM Long Range Planning model, which is also based on a monthly timestep. However, discussions with USBR staff revealed that these models are being phased out and being replaced by newer models.

In particular, the upper Sacramento River Water Quality Model (SRWQM; RMA, 2003) is currently being used by USBR to support seasonal and long term planning. The model is based on the HEC-5Q software package developed by the US Army Corps of Engineers and simulates the water temperature in the upper Sacramento River. Figure 3.3.2 shows the general spatial extent of SRWQM. The spatial resolution is finer than depicted, with water temperatures and flow rates being computed at numerous additional locations between those shown. SRWQM runs on a 6-hourly time step and computes water temperatures in the Trinity, Lewiston, Whiskeytown, Shasta, and Keswick reservoirs, as well as several river reaches around these facilities. Even though this timestep is significantly finer than the one used by the INFORM Long Range Planning model, it was decided to use this model by employing averaging

approximations to make the time resolutions compatible. GWRI staff met with USBR employees to understand the basic model set-up and obtain a copy of the model.

The model computes vertical water temperature profiles at several major reservoirs, while vertically averaged temperature values are calculated at a few smaller reservoirs as well as many different locations along the river network. The major reservoirs are divided into many horizontal layers, with each layer assumed to be completely mixed. The temperature profiles depend on meteorological forcings, inflow magnitudes and temperatures, and releases from the reservoir. Figure 3.3.3 illustrates the layers and energy exchanges used in the USBR reservoir temperature models. Temperatures within the river network, as well as several smaller and well-mixed reservoirs, are modeled as vertically averaged temperatures at discrete locations. The rivers are divided into longitudinal segments that model water temperature as a function of existing temperature, the temperature and magnitude of upstream and lateral inflows, and meteorological forcings. A detailed description of the underlying equations is given in RMA (1998).

Each model run requires several inputs that specify both natural variables and management decisions. Natural variables include meteorological forcings (equilibrium temperatures, exchange rate, wind, and solar radiation), as well as inflow volumes and temperatures. The required management decisions include (1) the regulation policies used to manage the reservoirs in the form of reservoir releases from each of the facilities being modeled, and (2) a release temperature target for Shasta reservoir. The model therefore does not compute any operation policies, but rather uses policies imposed from external sources. The one exception pertains to the releases made from Shasta reservoir. Since the TCD allows for releases from outlets at multiple elevations, the management decision made at Shasta not only consists of the total release magnitude, but also the individual releases from the different outlets. While the total releases to be made from Shasta and the release temperature target are specified as input variables, SRWQM has an internal algorithm to decide which outlets to use when making the release. The releases from the different outlets are chosen such that the final temperature of the total release is at or below the release temperature target. In general, releases from higher elevations are considered first, with releases from lower outlets only being made when the water temperature at the higher outlets is too high to meet the temperature targets. If the reservoir does not contain any available water at temperatures that are at or below the target, then the target cannot be met.

3.3.3 Water Temperature Simulation

The INFORM Long Range Planning model has previously been designed to generate extensive data and information that can be used to support system-wide reservoir management. Specifically, using ensemble forecasts of reservoir inflows, seasonal forecasts of reservoir releases, reservoir storages, energy generation, river flows, water deliveries, Delta outflows, and X2 location can be produced. Furthermore, several different scenarios can be evaluated by varying the end of season carryover storage requirements. This process facilitates the exploration of tradeoffs among the various management objectives.

This framework was further extended herein to include forecasts for river and reservoir water temperatures by using SRWQM as a simulation model to post-process INFORM Long Range Planning model results. Specifically, the models were linked by taking the outputs produced by the Long Range Planning model and using them as inputs to SRWQM. For a particular inflow ensemble forecast trace, the associated inflow magnitudes and reservoir releases were transferred to SRWQM and used to drive a water temperature simulation run. This process was repeated for every trace in the ensemble forecasts, as well as every tradeoff point. The linkage between the INFORM Long Range Planning model to SRWQM was fully automated so that water temperature forecasts can be generated through the INFORM DSS. A set of batch and data export/import routines were used to transfer data between models and activate the water temperature simulations in SRWQM.

The resulting information consists of water temperature forecasts and tradeoffs that can be used to further support seasonal planning and management. In addition to evaluating tradeoffs between existing variables such as carryover storage and reservoir releases, the ensembles associated with different tradeoff points can be evaluated to determine if water temperature criteria are being met. Detailed assessments using this approach are provided in the following chapter.

3.3.4 Water Temperature Optimization

The linkage between the INFORM Long Range Planning model and SRWQM can be used to determine if the management strategies identified by the planning model also meet water temperature criteria. If the management strategies are found to produce unacceptable water temperatures, the management decisions could be adjusted. Specifically, the magnitude and timing of the reservoir releases could be altered to ensure that the downstream water temperatures remain within acceptable levels. Furthermore, the temperature target for the Shasta releases could be altered to force the TCD to release waters at different temperatures. The INFORM Long Range Planning model and SRWQM would then be run a second time and used to generate new forecasts of reservoir storages, flows, energy production, etc., as well as water temperatures. Several iterations of this could be performed until an acceptable management strategy is identified. This management process is based on a hybrid optimization-simulation approach, whereby the INFORM Long Range Planning model, which is based on optimization, receives updated input from the SRWQM simulation model.

The joint use of the INFORM Long Range Planning model and SRWQM to identify desirable management policies is however based on heuristic adjustments. While this process could be used to identify acceptable management policies, it is possible that a large number of iterations may be required. Furthermore, if tradeoffs between many different variables are to be considered, then it might prove difficult to identify an optimal management strategy. An alternative to the optimization-simulation approach consists of directly incorporating the water temperature model into the existing optimization routine used by the INFORM Long Range Planning model. Water temperature criteria could then be modeled as constraints or objectives that are to be met.

However, the incorporation of detailed water quality models such as SRWQM into optimization models is challenging. For one, SRWQM is based on a 6-hourly timestep, while the INFORM Long Range Planning model uses a monthly timestep. Furthermore, the spatial resolution of SRWQM is much finer. The SRWQM uses finite difference equations to calculate water temperatures in each of the vertical and longitudinal segments of the river basin. Since such a formulation requires solving a very large system of equations it is not possible to directly integrate the SRWQM temperature model into the INFORM system-wide optimization model. As a result, GWRI has been investigating an alternative approach consisting of constructing a reduced-order system by first converting the temperature model on a monthly time resolution. The second approximation consists of altering the spatial resolution of the longitudinal and vertical segments. For reservoirs, instead of modeling the temperature profile through the use of dozens or hundreds of layers, simpler ways of representing the temperature profile were explored. A similar reduction can be performed for the longitudinally arranged river segments by combining several consecutive segments. The final reduced order system, which is to be expressed in the general form of a dynamic model, $S(k+1)=f(S(k),u(k),w(k))$, can then be integrated into the INFORM optimization model.

The first step to developing reduced-order models involves collecting temperature data that can be used to estimate the form and calibrate the parameters of the simplified model. To this end, GWRI first developed a calibration dataset by running SRWQM for a simulation period ranging from 1921 to 2003 using inputs provided by USBR and recording water temperature data for the river segments and reservoirs. To improve the calibration, the inputs to the SRWQM model were slightly altered and used to generate additional water temperature sequences. Specifically, the model was rerun by taking the original input dataset and unilaterally changing individual input types. Additional model runs were based on altering the reservoir outflows, the meteorological variables, and the reservoir inflows (magnitude and temperature). The additional datasets were then combined into one large dataset to be used for calibration purposes.

The second step involves identifying the elements of the reduced-order model. All of the variables used in the detailed SRWQM model are analyzed to identify a smaller subset of these variables that form the basis of the reduced-order model. The goal is to make this subset as small as possible while still retaining the ability to accurately estimate water temperature. Variables can be sub-divided into two general categories: external and internal variables. External variables or inputs ($w(k)$) are variables that affect water temperature but are specified a priori before the model is run, and are not influenced by management decisions ($u(k)$). Examples of external inputs include inflow magnitudes and temperatures, light attenuation rates, and meteorological variables. Internal variables, or states ($S(k)$), are computed dynamically by the model and are a function of the external inputs and management decisions, as well as internal variables at previous time steps. Examples of internal variables include reservoir storage, water temperature in different reservoir zones, and river water temperature. Ideally, the number of internal variables is as small as possible to ensure that the Long Range Planning model remains efficient.

The structure of the reduced-order model is determined by evaluating the importance of each variable in estimating water temperature, as described in Castelletti (2012). Starting with a list of all variables, artificial neural networks were used in conjunction with the calibration dataset to derive reduced-order models that estimate water temperature as a function of each individual variable. The variable resulting in the best performing model is then selected and added to a list of reduced-order model variables. The previous steps are repeated to identify the next variable to be added to the list of reduced-order model variables. In this case, the reduced-order models are based on both the variable being evaluated, as well as on the variables that have been previously added to the list of reduced-order model variables. This process is repeated until the addition of new variables does not significantly improve the performance of the reduced-order model. The reduced-order model can then be used to simulate water temperature. However, if the final list of variables includes internal variables, then a similar process has to be performed for each such variable. The reason for this is that if the reduced-order model is to be used to issue seasonal forecasts over a span of several months into the future, then the values of the internal variables will not be known. As a result, the internal variables will themselves have to be computed from dynamic models. For instance, if the temperature of a reservoir release is found to be a function of the water temperature at a certain elevation within the reservoir, then the dynamic model not only needs to compute the outflow temperature, but also the temperature at that particular elevation within the reservoir.

After a suitable reduced-order model has been identified, the model then needs to be incorporated into the INFORM Long Range Planning model. This process includes expanding the system dynamics to include the reduced-order model, as well as expanding the constraints and objective function to consider water temperature criteria.

The development of a reduced-order water temperature models was first performed at Trinity reservoir. Using results from the detailed SRWQM, a monthly dynamic model estimating release temperatures was calibrated. Table 3.3.1 lists all of the considered variables, which include both external and internal variables. The internal variables considered for the reduced-order model consist of total reservoir storage and reservoir water temperatures at various elevations in the reservoir. Specifically, the range of possible reservoir elevations was subdivided into 5 vertical zones spaced 100 feet apart. This represents a significant reduction of internal variables from those used within the detailed SRWQM model, which employs a much larger number of internal variables (over 100, depending on reservoir storage) spaced less than 4 feet apart.

Table 3.3.1 lists the order in which the different variables were selected. The mean square errors (MSE) between the reduced-order model and the calibration dataset are also shown. The table reveals that the addition of new variables into the reduced order model initially improves model performance. However, after a number of variables have been added, the model performance no longer increases significantly and in some cases may even get worse. Considering a tradeoff between model accuracy and complexity, it was decided that the reduced-order model for Trinity release temperatures was to be based on only the first three variables: reservoir temperatures at elevations 2150 and 2350, as well as total reservoir storage.

Since the elevation related variables are internal variables that are currently not being computed by the INFORM Long Range Planning model (storage is also an internal variable, but it is already being computed by the model), additional reduced-order models describing their dynamics had to be developed by repeating the previously described selection process. The same steps as those used to develop the model for reservoir outflow temperature were performed, with the only difference being that the internal variables were now the variables to be predicted. Table 3.3.2 lists the final variables that were selected as predictors for each of the internal variables, as well as those initially identified for the model used to predict reservoir outflow temperature. The table reveals that the final set of dynamic reduced-order models is based on a total of 5 different variables: 3 external inputs (equilibrium temperature, outflow magnitude and inflow) and 3 internal variables (storage, reservoir temperature at 2150 feet and reservoir temperature at 2150 feet).

Figure 3.3.4 compares the predicted Trinity reservoir outflow temperature (red) with the actual simulated temperatures of the calibration data set (green). When using the reduced-order model to compute outflow temperatures, it was assumed that the reservoir temperature profile was known at the beginning of March of each year. The reduced-order model was then used to compute reservoir temperatures for a horizon of 7 months into the future based on known values of the external values. The MSE during the calibration and verification period was 0.18 F, confirming that the reduced-order model adequately represents average outflow temperature at monthly timescales even though the number of internal variables used by the model (3) is just a fraction of the number of internal variables used by SWRQM (potentially over 100).

Calibration efforts for the other portions of the system are ongoing. Extension of the Long Range Planning model to include explicit temperature optimization is recommended for a follow-up project phase.

Figure 3.3.1: Sample Reservoir Water Temperature Profile

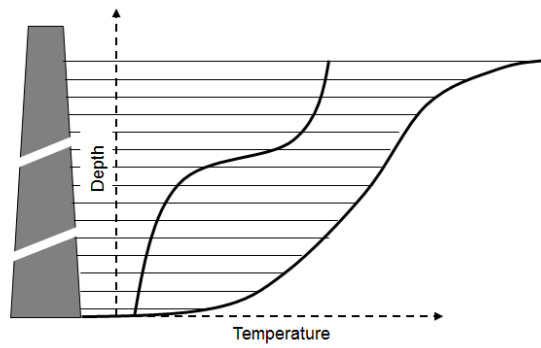


Figure 3.3.2: Schematic of the Upper Sacramento River Water Quality Model (Adapted from RMA, 2003)

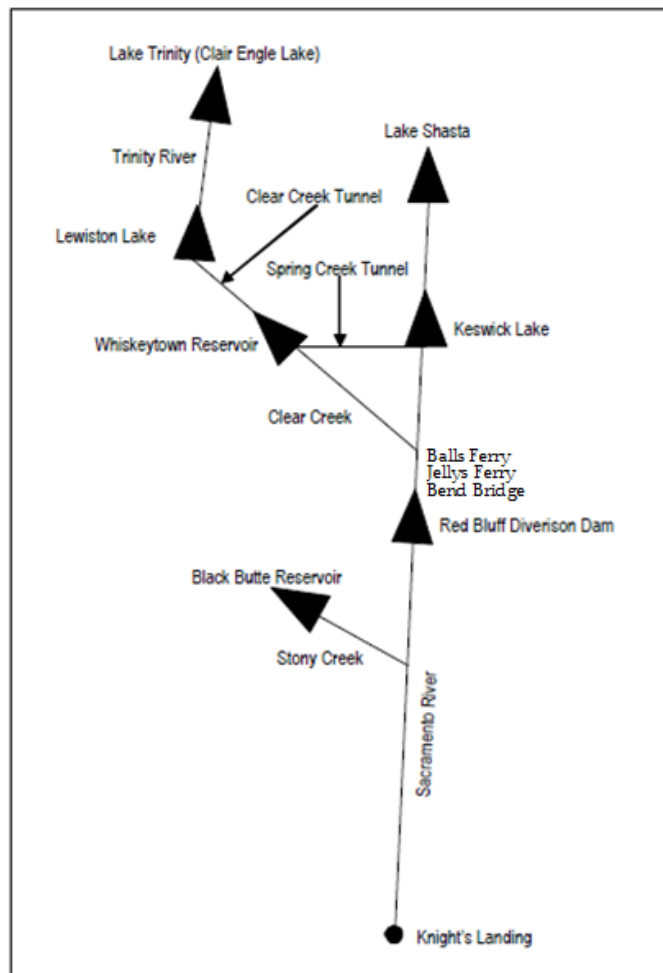


Figure 3.3.3: SRWQM Reservoir Temperature Model Layers and Energy Exchanges

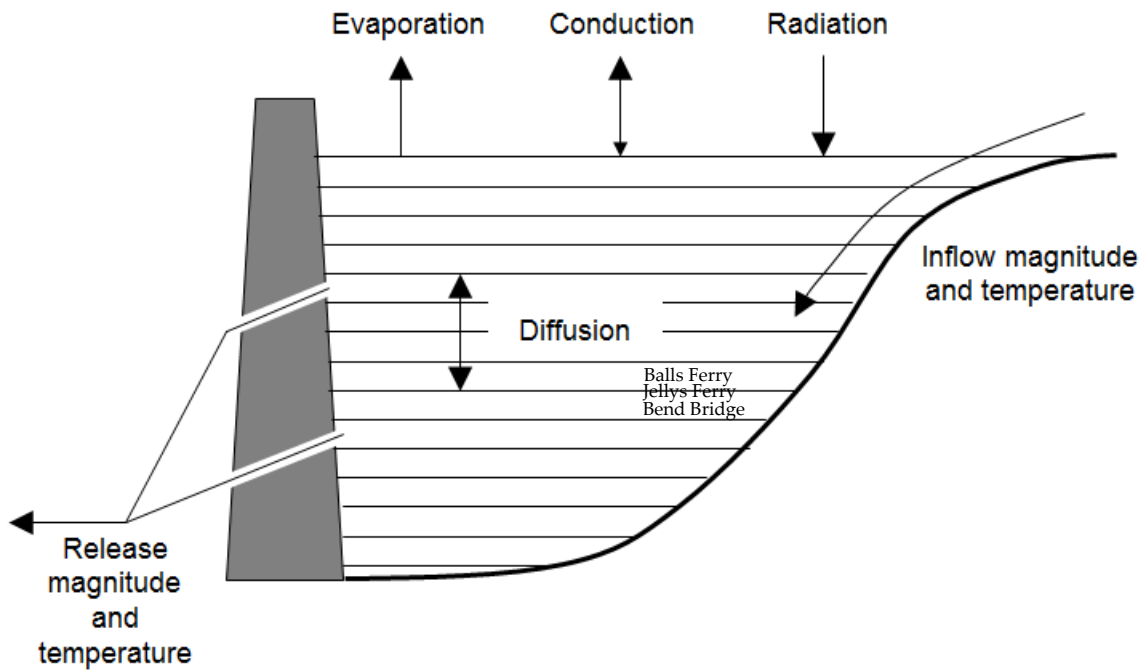


Figure 3.3.4: Trinity Releases Temperatures: Comparison between Reduced-Order Model Results (Red) and SRWQM Simulated Monthly Averages (Green)

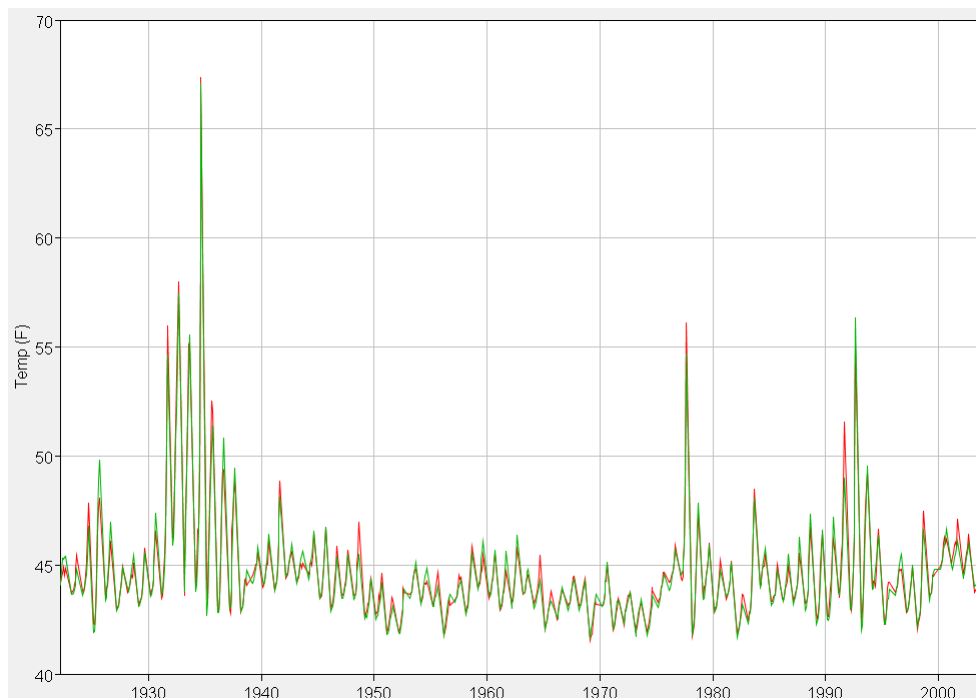


Table 3.3.1: Calibration Mean Squared Errors (MSE) after Sequentially Adding Individual Variables to a Reduced-Order Model. The First Three Variables Were Eventually Chosen to be Part of the Final Reduced-Order Model.

Iteration	Variable	MSE
1	Reservoir Temperature at 2150 feet	0.49
2	Reservoir Temperature at 2350 feet	0.35
3	Storage	0.21
4	Reservoir Temperature at 2050 feet	0.14
5	Light	0.14
6	Month	0.14
7	Outflow	0.18
8	Reservoir Temperature at 2250 feet	0.09
9	Inflow Temperature	0.13
10	Exchange Rate	0.13
11	Inflow	0.12
12	Solar Radiation	0.11
13	Equilibrium Temperature	0.20
14	Wind	0.18
15	Reservoir Temperature at 1950 feet	0.21

Table 3.3.2: Final Reduced Order Dynamic Model Variables for the Trinity Release Temperature and Internal Variables.

Trinity Reservoir Release Temperature
Reservoir Temperature at 2150 feet
Reservoir Temperature at 2350 feet
Storage

Reservoir Temperature at 2150 feet
Reservoir Temperature at 2150 feet (previous time period)
Reservoir Temperature at 2350 feet (previous time period)
Equilibrium Temperature
Outflow Magnitude

Reservoir Temperature at 2350 feet
Reservoir Temperature at 2150 feet (previous time period)
Reservoir Temperature at 2350 feet (previous time period)
Storage
Outflow Magnitude
Inflow
Equilibrium Temperature

3.4 Downstream Routing and Flood Control

Flood control operational decisions require that the short range modeling layer of the INFORM decision system be expanded to incorporate river routing models downstream of the major system reservoirs. This section describes the development of a new river routing model compatible with the decision system and its application to the INFORM river network [Kim and Georgakakos, 2013].

3.4.1 River Routing Models

Hydraulic river routing models are based on the complete St. Venant equations and are the most comprehensive and potentially accurate river routing approaches. However, their application to actual river (and flood) routing requires (1) extensive and high quality flow/channel data; (2) calibration of many computational parameters; (3) significant computational cost; and (4) good modeling experience [Weinmann and Laurenson, 1979; Becker and Kundzewicz, 1987; Garbrecht and Brunner, 1991; Camacho and Lees, 1999]. By contrast, hydrologic river routing schemes are much simpler in terms of the overall model structure and data requirements. The accuracy of hydrologic river routing models is generally less than that of hydraulic models, but it can be enhanced if outflow measurements are taken into account [Wasimi and Kitanidis, 1983; Georgakakos et al., 1990]. Furthermore, hydrologic routing models have the additional advantages that they (1) can be easily expressed in state-space form and conveniently incorporated into reservoir management schemes and (2) can account for input and model uncertainties [Georgakakos et al., 1990].

Muzik [1974] developed a state-space kinematic routing scheme to simulate unsteady non-uniform overland flows in which the overland flow is represented by a series of interacting reaches of uniform flow. Hoos et al. [1989] proposed a flood routing scheme that approximates the diffusion wave equation with lateral inflow using an explicit finite difference scheme. They represented the finite difference approximation in a state-space form to make the deterministic routing model fully adaptable to a stochastic updating procedure, Kalman filtering [Kalman, 1960], to account for modeling uncertainties related to (1) the model structure, (2) model parameters, and (3) observed input/output data. Georgakakos and Bras [1982] developed a statistical linearization technique to convert a nonlinear routing model to an equivalent linear model. To improve the model performance in forecasting (e.g., time to peak discharge, magnitude of the peak discharge), this linear model is represented by a state-space model in

order to use filtering and optimal estimation techniques, utilizing observed hydrologic data in real time. *Georgakakos et al.* [1990] reformulated the Muskingum-Cunge routing scheme into a state-space model that uses real time measurements (on river discharge) to generate unbiased, minimum variance state variable estimates. They applied both linear (constant routing coefficients) and nonlinear (time-varying coefficients) state-space routing models to manmade channels with mild or steep slopes and compared their results with those of a dynamic wave operational model (DWOPER, *Fread* 1978) as benchmark. They showed that when coupled with the state estimation procedure, both the linear and nonlinear models exhibit improved performance for channels with a wide range of slopes.

The movement of floods is an intrinsically nonlinear hydraulic process, so linear flood routing methods such as the Muskingum model [*Cunge*, 1969] and the Kalinin-Milyukov model [*Kalinin and Milyukov*, 1957], have limited ability to describe nonlinear characteristics. In general, in multilinear routing models [*Becker and Kundzewicz*, 1987; *Perumal*, 1992; 1994; *Camacho and Lees*, 1999], the inflow to the system (i.e., river reach) is divided into blocks of constant duration, each subsequently routed through a series of interacting linear routing sub-models. The entire river reach can be thought of as a cascade of interacting conceptual reservoirs in which outflow depends linearly on storage, and the overall output is the combined response of all linear sub-models. This feature of multilinear routing models is effective in simulating the nonlinear flood wave response while maintaining the mathematical convenience of linear routing schemes. *Kundzewicz* [1984] pointed out that these multilinear schemes are not able to take into account significant backwater effects, formation of computational irregularities in the peak discharge of the simulated outflow hydrograph, caused by (1) insufficient partitioning of the inflow hydrograph and (2) the subjectivity involved in selecting the computational inflow ranges. To overcome these limitations, except that of the backwater effect, *Perumal* [1992] proposed the multilinear Muskingum flood routing method. Based on the time distribution scheme with a constantly partitioned time interval equivalent to the routing time interval, this method routes each of the input pulses through the Muskingum-Cunge model, the parameters of which depend upon not only flow and channel characteristics, but also the intensities of the input pulses. In a uniform wide rectangular channel with no lateral inflow, the test results showed that this model was able to simulate the solution of the St. Venant equations closely when the rating curve at the inlet of the reach was characterized by narrow loops. In addition, a “dip” or “reduced outflow” at the beginning of the routed hydrograph, well known to the users of the Muskingum method, was diminished by increasing the number of routing reaches. However, this procedure increases the number of the model parameters from two to three. To overcome this drawback, *Perumal* [1994] proposed a cascade of linear sub-models in a discrete time domain, introduced by *O’Connor* [1976]. This multilinear discrete cascade model is analogous to the Nash model [*Nash*, 1960] in the continuous time domain, which is a conceptual representation of the Kalinin-Milyukov model when its parameter for the number of linear reservoirs in a reach is an integer. The parameters of the discrete cascade model vary at each routing time to account for the non-linearity of flood waves more appropriately. The discrete cascade model is derived by taking finite difference approximation of the governing equations of the Nash model. Each pulsed input from the input hydrograph is routed by the input pulse response of the cascade model. The parameters of the sub-model are estimated by (1) relating

them to the channel and flow characteristics [Dooge, 1973] and (2) using one-to-one relationships between the pulse response of the discrete cascade model and the impulse response of the Nash model. The overall outflow at a certain time $j\Delta t$ is calculated by adding all component outflows estimated at the same time. *Perumal* [1994] tested this model in uniform rectangular channels with a given hypothetical inflow hydrograph and compared it with the solution of the St. Venant equations. The results show that this discrete cascade model can account for flood wave non-linearities better than the multilinear Muskingum flood routing method [Perumal, 1992], and is able to reproduce the solution of the St. Venant equations closely when the rating curve at the channel inlet is characterized by a narrow loop. *Camacho and Lees* [1999] added a discrete linear channel in the multilinear discrete cascade model to lag a routed hydrograph by an explicit time interval specified by the time delay parameter, making it a three-parameter model. The multilinear discrete lag-cascade model was better than the multilinear discrete cascade model in uniform channels with very low slopes and high resistance effects and open looped-rating curves at both their inlet and outlet. In addition, the test results show that a considerable portion of the flood wave advection process can be explained by the explicit time delay of the discrete channel.

A key element of all hydrologic routing models is the storage-discharge relationship assumed to follow a certain mathematical form, usually a linear or a power function, the parameters of which are calibrated based on existing inflow-outflow data function [Cunge, 1969; Muzik, 1974; Georgakakos, 1982; Perumal, 1992]. While this assumption simplifies the model calibration process, it also constrains the models to operate by this function *throughout* their flow range. In view of the complex and nonlinear river flow behavior, this approximation undoubtedly introduces errors. The new nonlinear hydrologic river routing approach introduced herein is not limited by the above assumption. River reaches are modeled as cascades of interacting conceptual reservoirs, with storage-discharge functions identified by the data. A novel parameter estimation approach has been developed to identify these functions and all other model parameters based on control theory concepts. After calibration, these functions indeed exhibit different mathematical forms at different regions of their active variation range. The new approach is applied and successfully demonstrated in the INFORM river network as well as other real world river systems.

3.4.2 Modeling Framework

The new river routing model is based on the assumption that a river reach can be represented as a cascaded series of interacting conceptual reservoirs, in which the outflow and water losses are non-decreasing functions of storage. While this modeling framework uses the cascaded reservoir concept as many other previous studies [Georgakakos and Bras, 1982, Becker and Kundzewicz, 1987; Georgakakos et al., 1990, Perumal, 1994; Camacho and Lees, 1999], it includes the distinguishing difference that the outflow and loss functions are not structurally predefined, but they are identified as part of the model development/calibration process from input-output measurements. The advantage of this modeling feature is that the dynamic river response is not constrained to follow any particular mathematical law (e.g., linear, exponential, or power type), but it is free to change depending on flow conditions. This modeling flexibility is more realistic for actual rivers where the relationship between reach storage, outflow, and losses may change

in irregular (but non-decreasing) ways for low, medium, and high flow conditions based on site-specific geomorphologic and engineering features (e.g., latitudinal and longitudinal cross sections, roughness factors, and cross section modifications).

The model mathematical formulation is elaborated below.

Figure 3.4.1 shows a schematic of a river reach (top graph) with upstream inflow $I(k)=u_0(k)$, local inflow $w_i(k)$, storage $S(k)$, loss $L(k)$, net water withdrawal $D(k)$, and outflow $u_M(k)$. The previous fluxes represent averages over a time interval k , except for the reach storage $S(k)$ which represents the actual water volume at the beginning of time interval k . The bottom graph of Figure 3.4.1 represents the same river reach as a cascade of M conceptual reservoirs. Each i^{th} conceptual reservoir is characterized by its storage $S_i(k)$ at the beginning of time step k , local inflow $w_i(k)$, outflow $u_i(k)$, water loss $L_i(k)$, net water withdrawal $D_i(k)$, if any, and outflow $u_i(k)$ to the downstream $(i+1)^{th}$ reservoir. The water loss term may represent water seepage, net evaporation losses from the water surface, water retention on flood plains, weir-controlled diversions, and possibly other types of losses assumed to be unknown but non-decreasing functions of $S_i(k)$. The river reach response can then be modeled by the following set of coupled discrete-time dynamical equations:

$$\begin{aligned}
 S_1(k+1) &= S_1(k) + u_0(k) - u_1(k) - L_1(k) - D_1(k) + w_1(k), \\
 &\dots \\
 S_i(k+1) &= S_i(k) + u_{i-1}(k) - u_i(k) - L_i(k) - D_i(k) + w_i(k), \\
 &\dots \\
 S_M(k+1) &= S_M(k) + u_{M-1}(k) - u_M(k) - L_M(k) - D_M(k) + w_M(k), \\
 k &= 1, \dots, N.
 \end{aligned}$$

In the above equations, $u_0(k) [= I(k)]$ is the inflow to the first conceptual reservoir, and $u_M(k) [= Q(k)]$ is the reach outflow from the last conceptual reservoir. $I(k)$ and $Q(k)$ are assumed known for all time steps $k=1, 2, \dots, N$, as are the local inflows, $w_i(k)$, and the net water withdrawals, $D_i(k)$, for all reservoirs i . The reservoir release and loss terms, $u_i(k)$ and $L_i(k)$, are only assumed to be non-decreasing functions of the storage at the beginning and end of the time step k , namely, $[\eta_i S_i(k) + (1-\eta_i) S_i(k+1)]$. This weighted storage will hereafter be denoted $S_i(k/k+1)$. The model parameter η_i is in the range $[0, 1]$ and controls the relative influence of the beginning and ending reservoir storage on the release and loss fluxes. The mathematical difference between the net water withdrawals $D_i(k)$ and losses $L_i(k)$ is that the former are not necessarily non-decreasing functions of storage. In cases where the withdrawals *are* non-decreasing functions of storage, they can also be considered and identified as part of the reach losses. Lastly, as long as their form remains non-decreasing, the lower portion of the loss functions may extend into negative values representing water gains from regional groundwater.

The development and calibration of the above-described routing model consists of identifying the required number of conceptual reservoirs M and associated functions $u_i(k) = u_i[S_i(k/k+1)]$ and $L_i(k) = L_i[S_i(k/k+1)]$ such that the model outflow $u_M(k)$ simulates adequately well the observed outflow $Q(k)$ for all k .

3.4.3 Routing Model Identification/Calibration

First, the identification of the required number of conceptual reservoirs is addressed by developing models with progressively more reservoirs and determining the configuration that achieves satisfactory correspondence between $u_M(k)$ and $Q(k)$ based on the principle of parsimony. For each model configuration, the general identification procedure is outlined below:

1. Assume that $\eta_i, i=1, 2, \dots, M$ are equal to some initial values (e.g., $\eta_i=0.5$ for all i) and that $u_i[S_i(k/k+1)]$ and $L_i[S_i(k/k+1)]$, $i=1, 2, \dots, M$, are equal to some initial non-decreasing functions of storage, $f_{L_i}[S_i(k/k+1)]$ and $f_{u_i}[S_i(k/k+1)]$. These initial functions can be linear.
2. Assume that the loss functions $f_{L_i}[S_i(k/k+1)]$ are fixed at their current nominal forms and determine the outflow sequence $\{u_i(k), i=1, \dots, M\}$ that minimizes the following objective function

$$\text{Min}_{\substack{u_i(k), i=1, \dots, M \\ k=1, \dots, N}} \sum_{k=1}^N \left\{ \theta_1 [u_1(k) - f_{u_1}[S_1(k/k+1)]]^2 + \dots + \theta_M [u_M(k) - f_{u_M}[S_M(k/k+1)]]^2 + \theta_{M+1} [u_M(k) - Q(k)]^2 \right\},$$

subject to the water balance relationships,

$$S_i(k+1) = S_i(k) + u_{i-1}(k) - u_i(k) - f_{L_i}[S_i(k/k+1)] - D_i(k) + w_i(k),$$

$$i = 1, \dots, M; \quad k = 1, \dots, N.$$

In the above formulation, $\theta_i, i = 1, \dots, M+1$, are coefficients specified to prioritize the minimization of the last term in the objective function (simulated minus observed outflows) while keeping the decision variables $u_i(k)$ in the vicinity of the initial non-decreasing functions $f_{u_i}[S_i(k/k+1)]$, $i = 1, \dots, M$. The solution of this problem is used to create a new set of non-decreasing release functions $f_{u_i}[S_i(k/k+1)]$ (as described below), and the problem is resolved until no further reduction of the objective function is possible. Namely, this step involves solving a sequence of iterative optimization problems. After each iteration, the release functions $f_{u_i}[S_i(k/k+1)]$, $i = 1, \dots, M$, are updated by ranking each of the sequences $\{u_i(k), k=1, \dots, N\}$ and $\{S_i(k/k+1), k=1, \dots, N\}$ individually and associating the u_i and S_i values of the same rank. If necessary, the functions so obtained can be approximated by analytical functions (e.g., cubic

polynomials). However, such analytical approximations should adhere to the non-decreasing functional requirement.

3. Assume next that the release functions $f_{u_i} [S_i(k / k + 1)]$ are fixed at their current nominal forms (obtained in the previous step) and determine the water loss sequence $\{L_i(k), i = 1, \dots, M\}$ that minimizes the following objective function

$$\text{Min}_{\substack{L_i(k), i=1, \dots, M \\ k=1, \dots, N}} \sum_{k=1}^N \left\{ \theta_1 [L_1(k) - f_{L_1} [S_1(k / k + 1)]]^2 + \dots + \theta_M [L_M(k) - f_{L_M} [S_M(k / k + 1)]]^2 + \theta_{M+1} [u_M(k) - Q(k)]^2 \right\},$$

subject to the water balance relationships

$$S_i(k + 1) = S_i(k) + f_{u_{i-1}} [S_{i-1}(k / k + 1)] - f_{u_i} [S_i(k / k + 1)] - L_i(k) - D_i(k) + w_i(k), \\ i = 1, \dots, M; k = 1, \dots, N.$$

As before, the coefficients $\theta_i, i = 1, \dots, M + 1$, are specified to prioritize the minimization of the last error term in the objective function (simulated minus observed outflows) while keeping the decision variables $L_i(k)$ in the vicinity of the initial non-decreasing functions $f_{L_i} [S_i(k / k + 1)], i = 1, \dots, M$. It is noted that the decision variables of this problem are $L_i(k), i = 1, \dots, M; k = 1, \dots, N$, while releases $u_i(k)$ are obtained from the release functions derived in Step 2. This step involves a sequence of optimization problems, the solution of which creates a new set of non-decreasing loss functions used in the next iteration of the optimization problems until no further reduction of the objective function is possible. After each iteration, the loss functions $f_{L_i} [S_i(k / k + 1)], i = 1, \dots, M$, are updated by ranking each of the sequences $\{L_i(k), k=1, \dots, N\}$ and $\{S_i(k/k+1), k=1, \dots, N\}$ individually and associating the L_i and S_i values of the same rank. As in Step 2, the functions so obtained can be approximated by analytical, non-decreasing functions.

4. Iterate between Steps 2 and 3 until the release and loss functions $f_{u_i} [S_i(k / k + 1)]$ and $f_{L_i} [S_i(k / k + 1)]$ converge to stable forms, and the cumulative square error of the simulated versus the observed outflows achieves a minimum value. Every several iteration cycles, the $\eta_i, i=1, 2, \dots, M$, values can be updated to minimize the objective function in Step 3.

The sequence of optimization problem in Steps 2 and 3 can be solved using any suitable dynamic optimization method. In this work, the solution is obtained using control theory methods for linear systems with quadratic costs. The solution process is described next.

3.4.4 Discrete-Time Linear Quadratic (LQ) Solution

The general LQ solution applies to linear systems of the following form [Lewis and Syrmos, 1995]:

$$x_{k+1} = A_k x_k + B_k u_k + C_k,$$

where the state is an n -dimensional vector, $x_k \in R^n$, the control $u_k \in R^m$, and the system matrices $A_k \in R^{n \times n}$, $B_k \in R^{n \times m}$, $C_k \in R^n$. (To simplify the notation, the time dependence of these quantities is indicated through subscripts.) The objective function to be minimized (also known as cost functional) is quadratic:

$$\begin{aligned} J_1 &= \frac{1}{2} (x_N - \gamma_N)' P (x_N - \gamma_N) + \sum_{k=1}^{N-1} \left(\frac{1}{2} x_k' L_{xx,k} x_k + \frac{1}{2} u_k' L_{uu,k} u_k + u_k' L_{ux,k} x_k + L_{x,k}' x_k + L_{u,k}' u_k + \hat{L}_k \right) \\ &= \phi_N(x_N) + \sum_{k=1}^{N-1} L_k(x_k, u_k), \end{aligned}$$

where the weighting matrices are $L_{xx,k} \in R^{n \times n}$, $L_{uu,k} \in R^{m \times m}$, $L_{ux,k} \in R^{m \times n}$,

$L_{x,k} \in R^n$, $L_{u,k} \in R^m$, and $\hat{L}_k \in R^1$; the terminal matrix is $P \in R^{n \times n}$; the desired final state is $\gamma_N \in R^n$; and “ $'$ ” denotes the transpose of a vector or a matrix. The problem is to find the solution u_k^* which minimizes J_1 and simultaneously satisfies the system equations. This problem is equivalent to minimizing the Hamiltonian functional which incorporates the system equation through the Lagrange multipliers λ_{k+1} :

$$H_k(x_k, u_k) = \frac{1}{2} x_k' L_{xx,k} x_k + \frac{1}{2} u_k' L_{uu,k} u_k + u_k' L_{ux,k} x_k + L_{x,k}' x_k + L_{u,k}' u_k + \hat{L}_k + \lambda_{k+1}' (A_k x_k + B_k u_k + C_k).$$

This transformation frees the dependence of x_k on u_k , and the gradients of H_k with respect to x_k , u_k , and λ_{k+1} can now be calculated independently [Lewis and Syrmos, 1995]. Then, the necessary conditions for the constrained minimum are given by

$$\begin{aligned} x_{k+1} &= \frac{\partial H_k}{\partial \lambda_{k+1}} = A_k x_k + B_k u_k + C_k \\ \lambda_k &= \frac{\partial H_k}{\partial x_k} = A_k' \lambda_{k+1} + L_{xx,k} x_k + L_{ux,k} u_k + L_{x,k}' \\ 0 &= \frac{\partial H_k}{\partial u_k} = B_k' \lambda_{k+1} + L_{uu,k} u_k + L_{ux,k} x_k + L_{u,k}' \end{aligned}$$

$$\lambda_N = \frac{\partial \phi_N}{\partial x_N} = P(x_N - \gamma_N).$$

Assuming that the matrices $L_{uu,k}$ are positive definite and the matrices $L_{xx,k}$ are positive semi-definite, the optimal control and state sequences follow from the necessary conditions for optimality and are calculated recursively as shown below (where the superscript “-1” denotes matrix inverse):

$$\begin{aligned} S_k &= L_{xx,k} + A_k' S_{k+1} A_k - \left(B_k' S_{k+1} A_k + L_{ux,k} \right)' \left(B_k' S_{k+1} B_k + L_{uu,k} \right)^{-1} \left(B_k' S_{k+1} A_k + L_{ux,k} \right), \quad S_N = P, \\ v_k &= A_k' v_{k+1} - A_k' S_{k+1} C_k - L_{x,k} - \left(B_k' S_{k+1} A_k + L_{ux,k} \right)' \left(B_k' S_{k+1} B_k + L_{uu,k} \right)^{-1} \left(B_k' v_{k+1} - L_{u,k} - B_k' S_{k+1} C_k \right), \quad v_N = P\gamma_N, \\ u_k^* &= - \left(B_k' S_{k+1} B_k + L_{uu,k} \right)^{-1} \left[\left(B_k' S_{k+1} A_k + L_{ux,k} \right) x_k^* + B_k' S_{k+1} C_k - B_k' v_{k+1} + L_{u,k} \right], \\ x_{k+1}^* &= A_k x_k^* + B_k u_k^* + C_k. \end{aligned}$$

This recursive solution is in the form of a Riccati equation. With boundary condition $S_N = P$, the solution of the Riccati equation S_k is obtained from the first equation above through backward recursion. As with S_k , the auxiliary sequence v_k (second equation above) is also computed recursively in the backward direction with boundary condition $v_N = P\gamma_N$. The S_k and v_k sequences can be computed off-line even before the optimal controls u_k^* are calculated. Subsequently, u_k^* and x_k^* are computed by alternating in k between the last two equations above using the already calculated S_k and v_k , and a given initial state x_1 . Thus, the optimal controls u_k^* are linear functions of the current states x_k^* .

The LQ solution can be applied to the routing model identification problem, Steps 2 and 3, after local linearization of the release and loss functions in the system dynamics and the objective function.

3.4.5 Application to the Northern California River System

The physical structure of the Northern California river network is depicted in Figure 3.4.2. The network structure is rather complex involving many tributaries, confluences, manmade diversions, returns, and other channel losses and gains. The figure also reflects the routing process carried out by the California-Nevada River Forecast Center (CNRFC) using Lag/k routing models with an hourly time resolution. The routing process is as intricate as the river

system itself using the Lag/k routing models but also historical experience and expert knowledge of the river response at different flow conditions. While this system serves the CNRFC well in their flood control operations, it cannot be directly incorporated in the decision support system.

The purpose of this application is to demonstrate that the routing model introduced in this section has the potential to replicate the river response with sufficient accuracy throughout the range of flows, while having a mathematical form compatible with the INFORM decision support framework. The application of the routing model is described here for the Feather River sub-system, highlighting the model performance but also the complexities of actual flood routing operations. The model has also been implemented for several reaches of the Upper Sacramento River with similar performance. Model implementation and testing for the lower Sacramento reaches are on-going.

Figure 3.4.3 depicts the Feather River network including four main stem river nodes (CRIC1, FLVC1, YUBC1, and FBLC1). The upstream inflow to this reach (at node GRIC1) consists of flows from Orroville (node named ORDC1) combined with other local inflows (from node YUBC1L), while the reach outflow (at node FBLC1) consists of the previous flows routed through the reach combined with other local tributary flows (from node MRYC1). Depending on the relative flow rates in the main river stem and in the tributary coming from MRYC1, the flow stage at node YUBC1 experiences backwater effects. The figure also shows the CNRFC computational routing process (indicated by the routing path arrows), according to which each of the main stem flows (at CRIC1, FLVC1, YUBC1, and FBLC1) are computed directly from Orroville (ORDC1) rather than sequentially.

Model calibration requires voluminous and consistent data, and the data gathering process was time consuming and challenging. It was finally decided to calibrate the routing model against a simulated flow dataset created by CNRFC's CHPS system using historical reservoir sequences and observed tributary flows. This dataset was created jointly by CNRFC, GWRI, and HRC, and required that some routines were customized to extract the local inflow information from the CHPS database. The final simulated dataset covers the period from 10/1/2000 to 1/31/2010 and has a 6-hourly time resolution. The routing models were calibrated using the three-year period from 1/1/2004 to 12/31/2006 and validated using the three-year period from 1/1/2002 to 12/31/2004.

The Feather River reaches required models with only one routing reservoir. The routing model for the first reach from ORDC1 to GRIC1 is described next, while the models for all Feather routing reaches are described in similar detail in Appendix D.

3.4.5.1 Routing Model for Feather Reach ORDC1 to GRIC1:

The routing model equation is as follows:

$$S_i(k+1) = S_i(k) + \text{Units} * [I_i(k) + w_i(k) - L_i(k) - D_i(k) - u_i(k)].$$

The terms in the above equation are defined as follows:

k: Time index corresponding to 6-hour intervals.

$S_1(k)$: Reach storage in billion cubic feet at the beginning of time interval k .

Units: Unit factor to convert reach fluxes from million cubic feet to billion cubic feet,

$$\text{Units} = 1/1000.$$

$I_1(k)$: Upstream inflow in mcf/6-hrs.

$w_1(k)$: Local reach inflow in mcf/6-hrs.

$L_1(k)$: Reach losses in mcf/6-hrs. The losses in this reach are negligible.

$D_1(k)$: Reach intake withdrawals in mcf/6-hrs. The withdrawals in this reach are also negligible.

$u_1(k)$: Reach release to the downstream system as a function of the reach storage, $S_1(k/k+1)$, where $S_1(k/k+1) = \eta_1 S_1(k) + (1-\eta_1) S_1(k+1)$, with $\eta_1=0.4$.

The $u_1(k)$ vs. $S_1(k/k+1)$ function is shown in Figure 3.4.4. The model calibration process generates the non-decreasing function consisting of the individual data points. The fitted analytical curves shown are used in the river routing simulations. The figure shows that the release function exhibits different nonlinear behavior for weighted reach storage values below and above 14.56 billion cubic feet.

Figures 3.4.5 and 3.4.6 depict the routing model performance for the calibration and validation periods. The figures visually show that the model exhibits very good performance in both periods. Furthermore, model performance is quantified through several measures:

- Average Error = $\frac{1}{N} \sum_{k=1}^N \{Error(k)\}$; $Error(k) = Obs.Flow(k) - Sim.Flow(k)$;
- Absolute Average Error = $\frac{1}{N} \sum_{k=1}^N |Error(k)|$;
- Percent Absolute Average Error = $\frac{1}{N} \sum_{k=1}^N \left| \frac{Error(k)}{Obs.Flow(k)} 100 \right|$;
- Mean Square Error = $\sqrt{\frac{1}{N} \sum_{k=1}^N Error(k)^2}$; and
- Percent Mean Square Error = $\sqrt{\frac{1}{N} \sum_{k=1}^N \left(\frac{Error(k)}{Obs.Flow(k)} 100 \right)^2}$.

Table 3.4.1 provides the values of these measures for the model calibration and validation periods confirming that the model is highly effective. The percent absolute average error and the percent mean square error for both periods are respectively less than 2.6 percent and 6.2 percent.

The Feather River routing models are used in the following chapter in flood operations assessments aiming to demonstrate the potential effectiveness of integrated inflow forecasting, reservoir management, and downstream routing approaches.

Figure 3.4.1: River Routing Model Concept

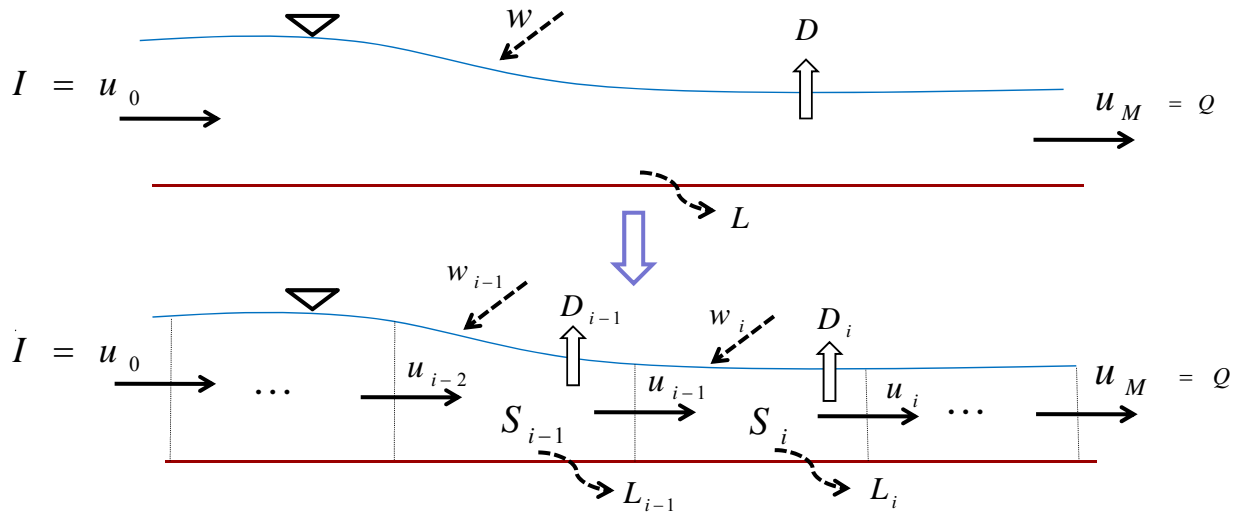


Figure 3.4.2: Northern California River Network

(Source: California Nevada River Forecast Center)

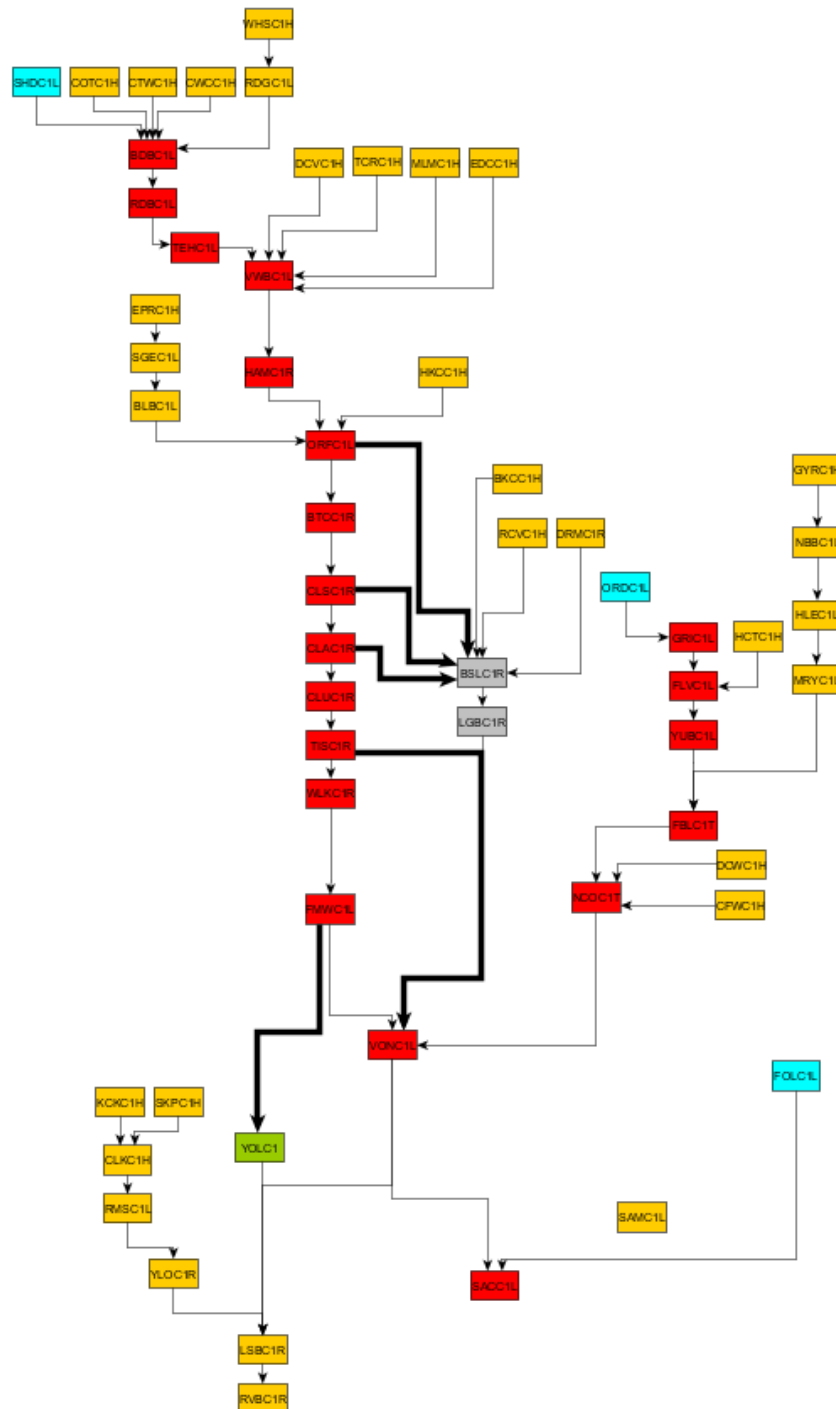


Figure 3.4.3: Northern California River Network

(Source: California Nevada River Forecast Center)

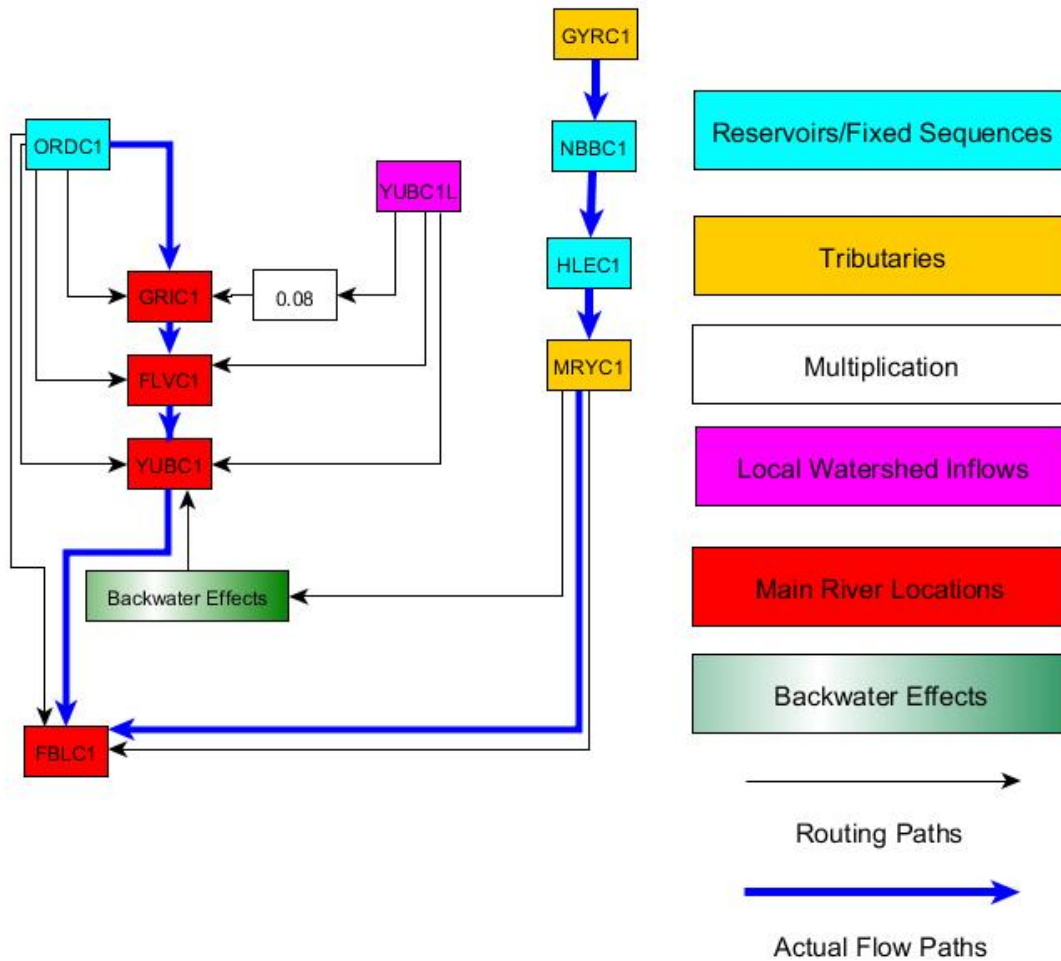
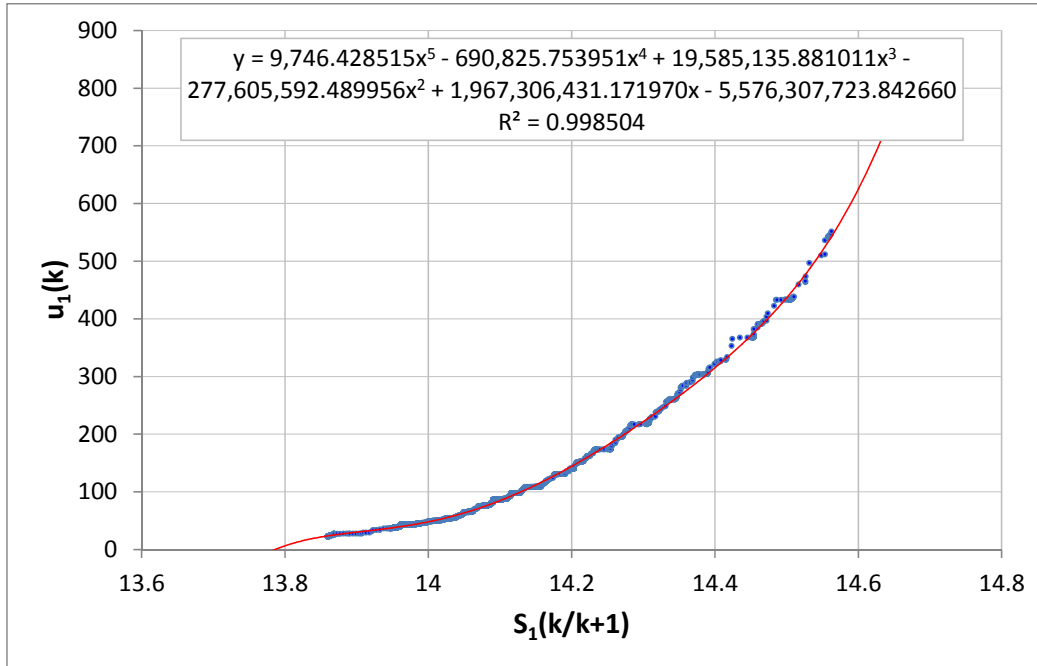


Figure 3.4.4: Routing Model Release Function

(i) $S_1(k/k+1) \leq 14.56$ bcf:



(ii) $S_1(k/k+1) > 14.56$ bcf:

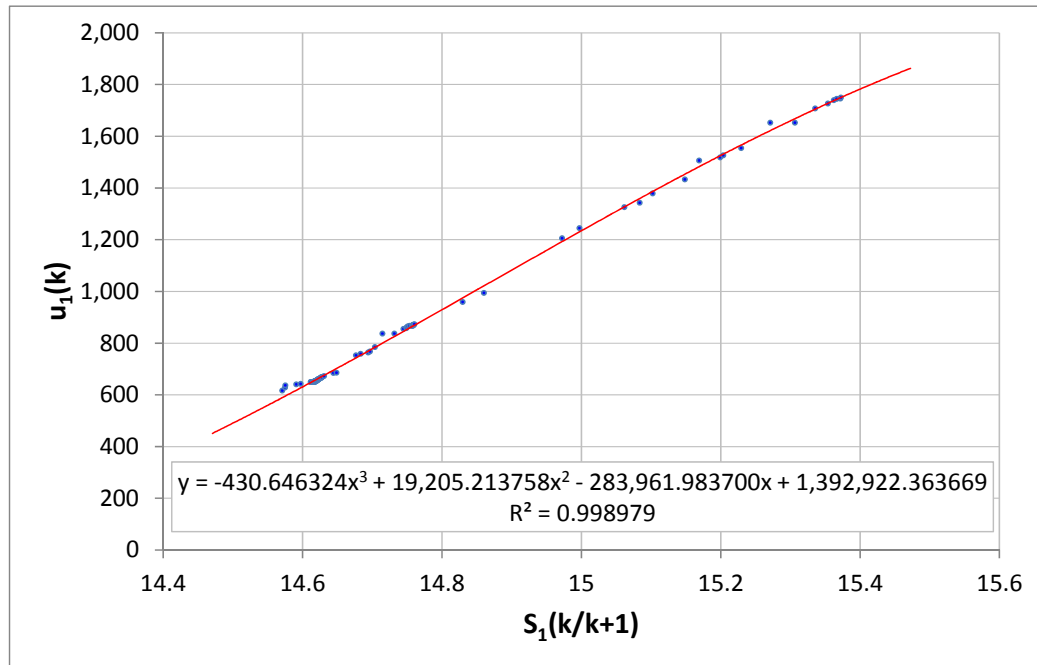


Figure 3.4.5: Simulated (Red) Versus Observed (Blue) Flows (mcf/6-hrs) and Associated Errors (Grey) for the Calibration Period (2004-2006).

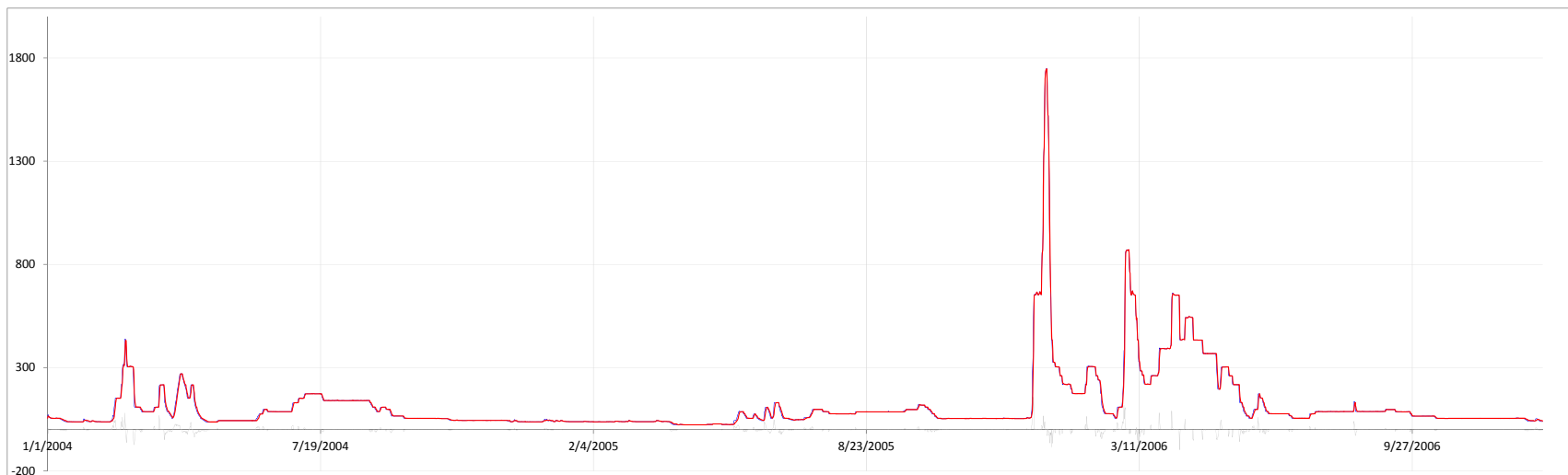


Figure 3.4.6: Simulated (Red) Versus Observed (Blue) Flows (mcf/6-hrs) and Associated Errors (Grey) for the Validation Period (2002-2004).

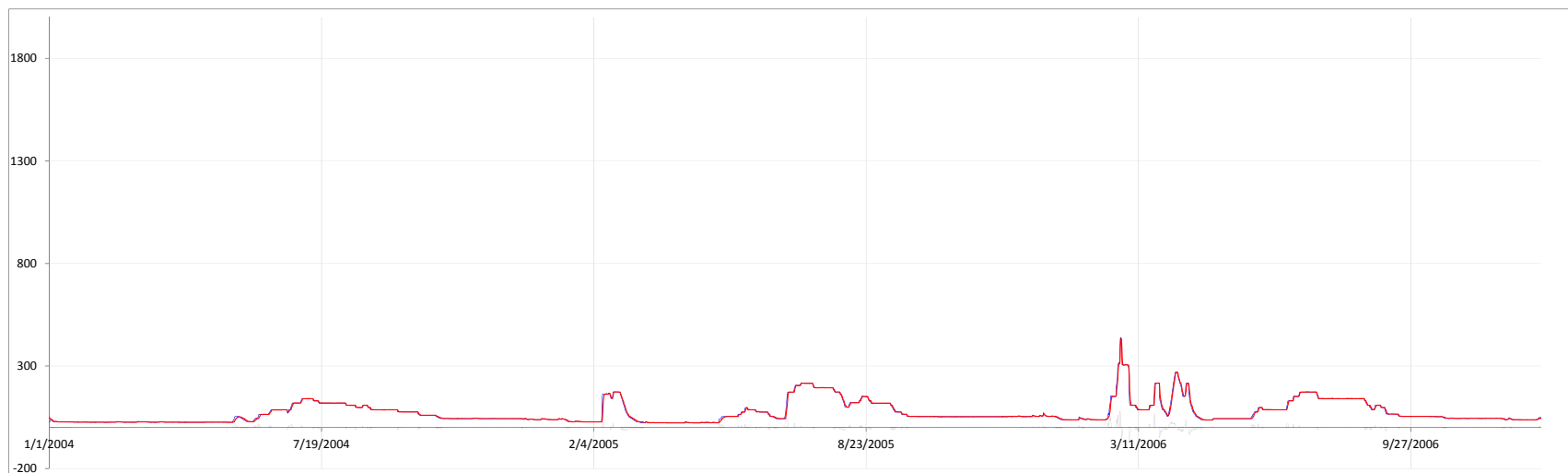


Table 3.4.1: Routing Model Calibration and Validation Statistics

Model Performance Measures	Calibration Period (1/1/2004 – 12/31/2006)	Validation Period (1/1/2002 – 12/31/2004)
Average Error, mcf/6-hrs	0.000	0.018
Absolute Average Error, mcf/6-hrs	2.927	1.817
% Absolute Average Error	2.626 %	2.471 %
Mean Square Error, mcf/6-hrs	9.921	6.085
% Mean Square Error	6.210 %	6.089 %

CHAPTER 4:

Demonstration Results

4.1 Forecast Performance Assessment

This section presents a selection of verification results comparing INFORM II atmospheric and hydrological model forecasts with observations. The results shown here cover the five large watersheds composing the INFORM II system (drainages of the Folsom, New Bullards Bar/Englebright, Oroville, Shasta, and Trinity reservoirs). For the atmospheric model forecasts we compare forecast and observed mean areal precipitation (MAP) and mean areal temperature (MAT), with the later derived by NOAA/NWS CNRFC from *in situ* measurements. For the hydrologic models, the forecast inflows are compared to full-natural-flow (FNF) estimates of the inflows to the primary reservoirs in each watershed. The next section provides a brief outline of how the observational and forecast data were processed and a description of the statistical measures used for performance assessment. The assessments for MAP, MAT and INFLOW follow in separate sections.

4.1.1 Data Processing

4.1.1.1 MAP and MAT Data

Observation-based estimates of MAP (mm 6 hr⁻¹) and MAT (°C) were obtained from CNRFC for each of the 47 sub-basins within the five main watersheds described in Chapter 2. These data have 6-hour temporal resolution and cover 00Z June 15, 2009 through 00Z November 4, 2012 at 6-hour resolution. These data were processed to provide 24-hour averages (MAT) and accumulations (MAP) for each 24-hour period in the record ending at 00Z or 12Z. The MAP and MAT comparisons discussed focus on the time periods ending at 00Z, with some discussion of 12Z results as appropriate, as the results do not change much for different validation times. Figure 4.1 provides a schematic showing the observational processing (in the “00” hour forecast lead time column) for 24-hour time averaging blocks ending at 12Z.

Forecast MAP and MAT were available from ensemble simulations with the three atmospheric modeling systems described in Chapter 2 designated ICRM-CFS1, WRF, and ICRM-CFS2. These data were available for the 47 constituent sub-basins noted above for times described below. Each forecast system produces output for each 6-hour increment through a given forecast run.

The ICRM-CFS1 system provided one four member ensemble forecast per day (initialized at 00Z) going out to a lead time of 41.5 days (996 hours) and operated over the period noted below until the driving climate forecast model (NOAA NCEP CFS-1) was disengaged from INFORM; until October 2012. The limitation of just four ensemble members per day precludes the use of daily probabilistic statistics with ICRM-CFS1.

The ICRM-CFS2 system produces a four-member ensemble four times per day (at 00Z, 06Z, 12Z and 18Z) using boundary conditions from the NOAA CFS-2 climate forecast system. These forecasts run out to a lead time of 996 hours. This system began running on 21 February 2012 and the final forecast used here was produced on 12 November 2012.

The WRF system is driven by NOAA NCEP GFS output and produces two 20-member ensemble forecasts per day (initialized at 00Z and 12Z), these running out to a lead time of 384 hours (16 days). This system produced forecast data from 7 November 2011 through 2 November 2012.

The output from each forecast system contains sizable gaps when some or all of the ensemble members failed to complete, nevertheless the sample sizes are sufficient to provide statistical guidance concerning performance. Table 4.1 summarizes the time period covered by observational and forecast system data.

4.1.1.2 INFLOW Data

The INFLOW observational data was provided as the average discharge rate (CFS) for the 24-hour period ending at approximately 12Z each day (this contrasts with the 6-hourly observational data for MAT and MAP). These data consist of “full natural flow” estimates obtained by the US Geological Survey and the US Army Corps of Engineers and made available via the California Data Exchange Center (CDEC). The forecast INFLOW data was in the same form described above for MAT and MAP giving inflow for each 6-hour lead time increment in CFS.

4.1.1.3 Forecast Averaging

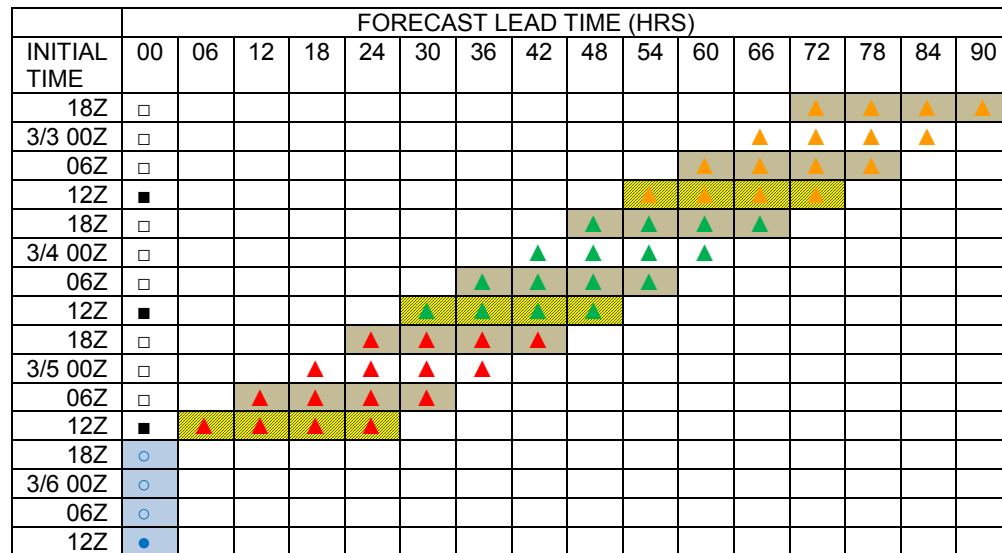
For most of the results described here, the forecast data for WRF and ICRM-CFS2 were processed to provide 24-hour averages from multiple lead times for comparison with the observed 24-hour averages as shown schematically in Figure 4.1 (note that Fig. 4.1 shows the verifying averaging blocks ending at 12Z; this is appropriate for INFLOW data; averaging blocks for MAP and MAT ended at 00Z for the results shown here) The basic idea is to form “super-ensembles” from all of the forecasts that a) validate during the 24-hour observational averaging period of interest, and b) come from separate lead time blocks, each 24 hours in length. For each such block, the 24-hour average (or accumulation) was calculated for each available ensemble member. The average of these ensemble means provided an overall cross-ensemble “grand average”. This procedure provides individual ensemble averages and a cross-ensemble grand average for each 24-hour lead time block going out to a lead time of 720 hours for ICRM-CFS2 and 336 hours for WRF. Referring to Figure 4.1, one can see that what is denoted a “00 hour lead” forecast here is actually available ~24 hours prior to verification time. With ICRM-CFS2 having four-member ensembles and four initializations per day, there are a total of 16 24-hour averages in each super-ensemble. For WRF, with 20 member ensembles and two initializations per day, each super-ensemble consists of 40 24-hour averages. This processing scheme provides both a scalar value (the super-ensemble mean) and a set of equiprobable ensemble outcomes for comparison with the observed data.

An alternative processing scheme was used to incorporate the “single four-member ensemble per day” ICRM-CFS1 data (see Figure 4.1). For this method, only the data from the overall cross-ensemble average final forecast in each 24-hour block was used (yellow shaded in Figure 4.1) to compare with the observations.

Table 4.1: Time Periods Covered by Observational Data and Forecast System Output.

DATA SOURCE	COVERAGE
OBSERVATIONS (MAP and MAT)	06/15/2009 – 11/04/2012
OBSERVATIONS (INFLOW)	01/01/2010 – 01/08/2013
ICRM-CFS1	11/26/2010 – 10/23/2012
WRF	11/07/2011 – 11/02/2012
ICRM-CFS2	02/21/2012 - 11/12/2012

Figure 4.1: Diagram Showing the “24-hr Block Average” Verification Scheme



In the diagram of Figure 4.1, forecast initialization time and observation times are shown along the left side, and forecast lead times are shown along the top. The blue circles (open and filled) indicate the period of time going into one observed 24-hour average (average of 4 6-hourly values for MAT and INFLOW; accumulation from 4 6-hourly averages for MAP), with “validation time” indicated by the filled blue circle (at 12Z March 6 in this case). The colored triangles indicate the “blocks” over which the forecast averages were calculated. Here, the red triangles mark the most recent set of forecasts (covering a 24x24-hour (4x4) initial time/lead time “coordinate” block) validating at 12Z March 6, these would belong to the “00-hour lead” forecast using the notation in the text. The green and orange triangles mark (“24-hour lead”) and (“48-hour lead”) forecast blocks from earlier initializations, all validating on the 24-hour observational period of interest. Black squares (filled and open) mark other possible 24-hour observational averaging periods (ending at the solid black square). The WRF forecast system has initialization times every 12 hours; gray shading indicates forecast initial times not used for that system. The ICRM-CFS2 system was initialized every 6 hours. 24-hour flow FNF “observations” are only available at ~12Z, so validation statistics are for 12Z only. WRF forecasts went out to 384 hours lead time, so the last block having the full complement of forecasts has a nominal lead time of 336 hours (14 days; using the nomenclature used in the text). ICRM-CFS2 forecasts ran out to 996 hours (41.5 days) but were processed to provide statistics out to a nominal lead time of 720 hours (30 days). Note that each forecast is composed

of individual ensembles that are not indicated here. The yellow shaded bar shows an alternative averaging scheme used for the ICRM-CFS1 MAP and MAT forecast output (corresponding results are available for the other INFORM-II models as well, but are not presented here).

4.1.2 Statistical Measures

These measures compare each observation with a single corresponding multi-ensemble mean of forecasts verifying at the observation time at some defined forecast lead time. In the discussion that follows we use the following nomenclature:

O_T – 24-hour average (or accumulation for MAP) observed at time T (“the verification time”).

$F_{T,L}$ – 24-hour average (or accumulation for MAP) “grand average” forecast at lead time L, verifying at time T.

$F_{T,L,E}$ – 24-hour average (or accumulation for MAP) for single ensemble member E at lead time L, verifying at time T.

Symbols with a prime (') indicate departures from the respective mean of a variable (“anomalies”); “NT” is the length of the record, “NE” is the number of ensemble members; “NL” is the maximum lead time; “t” designates a particular verification time, “e” designates ensemble number and “L” the nominal lead time, a single value (0,24,48...) assigned to each “forecast block” (see Figure 4.1). Statistics are generated as a function of lead time (1, NL), variable (MAP, MAT, INFLOW) and season. Two “seasons” were defined on the basis of the verification time to approximately differentiate between non-melt and melt dominated settings; these are November-February (NDJF) and March-May (MAM).

For a given variable, lead time (L), season triplet, corresponding observation-forecast sets were constructed. For example, each observation during NDJF (O_T) was matched (where possible) with the ensemble forecast data for lead L validating at time T, these are $F_{T,L,E}$, $E=1,NE$. The “grand average” of the 24-hour ensemble means is then

$$F_{T,L} = NE^{-1} \sum_{NE} (F_{T,L,E})$$

where $\sum()$ denotes the arithmetic sum of the quantity in parenthesis. An initial calculation gives the overall seasonal mean for the observations

$$O_{BAR} = NT^{-1} \sum_{NT} (O_T)$$

and for the forecast values verifying during that season at lead time (L)

$$F_{bar,L} = NT^{-1} \sum_{NT} (F_{T,L})$$

Some statistics are derived using departures from these mean values and these are indicated with a prime (') in the discussion below.

Most of the statistical measures defined below (correlation, bias, bias fraction, Brier skill score, ROC area) give a single value for i) each basin or sub-basin ii) each season iii) each forecast lead time (in 24-hour blocks) and each variable. Others (reliability and ROC curves) are composed of multiple values defining behavior in probability space (see probabilistic measure discussion below).

4.1.2.1 Non-probabilistic measures

Non-probabilistic measures express the “forecast” for a particular verification lead time as a single value, in this case the “grand average” cross-ensemble mean. The three non-probabilistic measures used in the analyses presented in this section (correlation, bias and bias fraction) are described below.

Correlation [R; recall for given basin or sub-basin, variable, and season, there is one value for each lead time (L)].

$$R_L = C_{OF} / (S_O S_F) \quad (4.1)$$

where

$$C_{OF} = [NT^{-1} \sum_{NT} (O'_T F'_{T,L})]^{1/2}$$

$$S_O = [NT^{-1} \sum_{NT} (O'_T O'_T)]^{1/2}$$

$$S_F = [NT^{-1} \sum_{NT} (F'_{T,L} F'_{T,L})]^{1/2}$$

Correlation gives a useful measure of linear association between the observations and the forecast “grand means”. Correlation does not account for bias, can be sensitive to outliers, and ranges from -1 to 1. Figure 4.2 shows a sample correlation plot from the INFORMII analyses.

Figure 4.2: Sample Forecast Correlation with Observations vs. Lead Time.

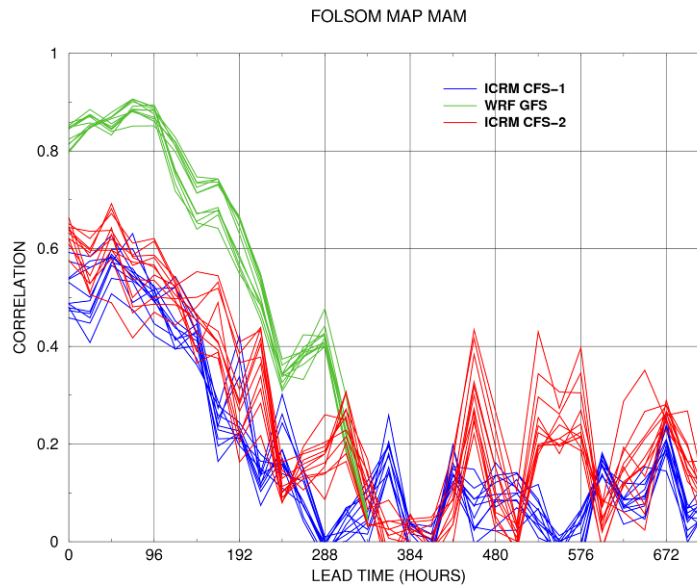


Figure 4.2 is for MAM MAP forecasts validating at 00Z for each of 11 sub-basins in the Folsom basin. ICRM CFS-1 results are shown in blue (these results derived using the alternative averaging scheme described above; results from WRF (green) and ICRM-CFS2 (red) used the block averaging scheme). These results indicate similar and reasonably good performance for the ICRM-CFS1 and ICRM-CFS2 forecasts, with considerably better performance for the WRF forecasts. All forecasts reach a near-zero correlation at forecast lead times of ~two weeks (336 hrs). The relatively tight clustering of the results within each set of model results (for the individual sub-basins) reflects consistent performance between sub-basins. The elevated variability in forecast correlations for longer lead forecasts reflects the relatively smaller sample sizes available for longer range forecasts and the effects of relatively few precipitation events.

Bias [B]

$$B_L = F_{bar_L} - O_{bar}$$

Bias is used for evaluating systematic errors in MAT.

Bias fraction [BF]

$$BF_L = F_{bar_L} O_{bar}^{-1}$$

Bias fraction is used for evaluating systematic errors in MAP and INFLOW.

Bias and bias fraction plots use the same lead time vs. value format shown for correlations in Figure 4.2.

4.1.2.2 Probabilistic measures

In contrast with the non-probabilistic measures, probabilistic measures include information from the individual ensemble means (F) and thus deal directly with questions bearing on the forecast probability of particular outcomes. These measures were not calculated for the ICRM-CFS1 system because its output was limited to four ensemble members per 24-hour period; too few to provide robust probabilistic statistics.

Reliability Diagram and Brier Skill Score

The reliability diagram and Brier Skill Score (BSS) assess the accuracy of forecast probabilities for a pre-defined event to occur (e.g., Hsu and Murphy, 1986). The basic idea is to define a specific “event” of interest, for example, whether measureable rain will fall during the verification time. The ensemble forecasts are grouped according to the forecast probability (P_F) that an “event” will occur; P_F is defined as the fraction of ensemble 24-hour forecast means ($F_{T,L,E}$) that exceed the threshold for an event. For example, in the analyses reported here, the groups covered the ten probability of occurrence categories 0-10 percent, 10 percent-20 percent,...,90 percent-100 percent. For each of these categories, the actual frequency of occurrence of events is calculated from the observations verifying with the forecasts in a given bin.

For example, reliability might assess the question “For the group of forecasts indicating a 70-80 percent chance of rain, how frequently did rain actually occur?” The results of reliability

analysis are typically plotted in the form of a “reliability diagram” giving the forecast probability of an event along the abscissa and the observed relative frequency of events on the ordinate (e.g. see Figure 4.3). The 1-to-1 line on the reliability marks perfect reliability; the forecast probabilities being exactly correct. If the reliability curve is horizontal it implies that the forecast probabilities have no bearing on the observation (guessing), such forecasts are said to lack “resolution”. A curve with a slope less than one implies forecasts that are “over-confident”, with forecast probabilities of more extreme events that are higher than actually occur; in contrast, a curve has a slope greater than one, the forecasts are said to be “conservative” and the forecast probabilities of more extreme events are too low. For our results, reliability diagrams are presented only for 48-hour lead time, with one diagram for each basin, variable, and season. An example of a reliability diagram from the INFORM system analyses is presented in Figure 4.3.

Figure 4.3: Example Reliability Diagram.

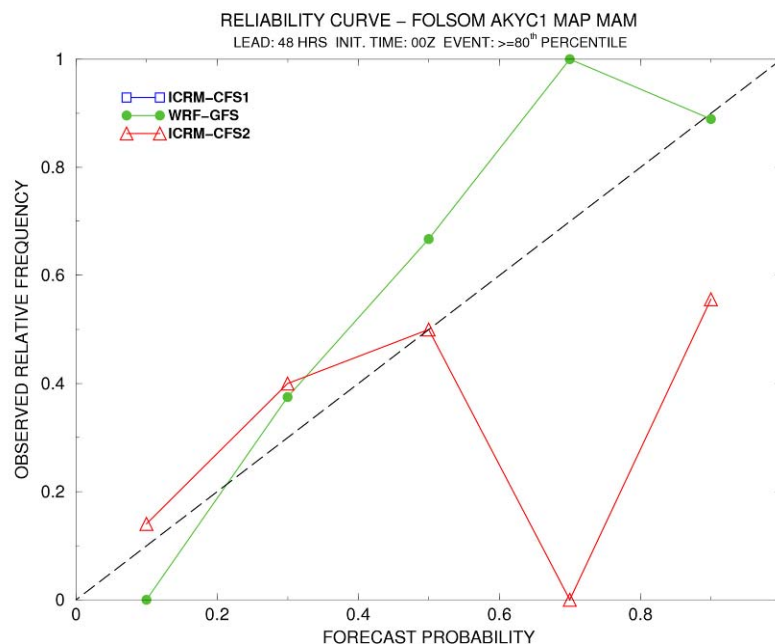


Figure 4.3 is for MAM MAP for 48-hour lead forecasts validating at 00Z for Folsom sub-basin AKYC1. In the reliability diagrams presented in this work, “events” are considered those cases where the variable in question (MAP, MAT, or INFLOW) exceeded the 80th percentile observed value for the sample of observations for that season. Forecast probabilities of events are the probabilities of exceeding the 80th percentile of all ensemble averages of the season, basin and variable in question (thus forecast biases in magnitude are removed for probabilistic assessments). The figure shows results for two forecast systems (WRF-GFS, green; ICRM-CFS2, red; probabilistic results are not available for ICRM-CFS1). In the example, the WRF forecasts indicate good but slightly conservative forecast behavior (forecast probabilities tend to be below

actual probabilities), while the ICRM-CFS2 forecasts suggest good performance for lower probabilities and poor performance for probabilities higher than 0.5.

While reliability is depicted with the reliability diagram showing a value for each forecast probability bin, the Brier Skill Score (BSS) gives an aggregate statistic concerning how close the reliability curve is to the 1-to-1 perfect fit line. BSS is defined as follows for a given set of probabilistic forecasts and observations.

$$BSS = 1 - (BS / BS_{ref})$$

where BS_{ref} is the climatological frequency of occurrence of events (the “base rate”); it gives a score for always forecasting the probability of the event as the base rate. BS is the typically defined “Brier Score” (or “half Brier Score”), and is given by

$$BS = NT^{-1} \sum_{k=1,NT} (y_k - o_k)^2$$

where NT is the number of forecast-observation pairs available, y_k is the forecast probability of an event (the fraction of ensemble means exceeding the event threshold), and o_k is a binary observation value taking the value of 1.0 if an event occurred, and 0.0 otherwise.

BSS gives a measure of the “improvement over climatology” (BS_{ref} being the climatological score) in terms of the forecast system’s actual Brier Score (and hence its overall reliability). Note that BSS can range from 1 (perfect) to $-\infty$. As an aggregate measure, there is a single BSS value for each lead time, basin, variable, and season, so the results are presented as a plot of BSS vs. lead time (similar to Figure 4.2) for each basin, variable and season.

It is important to note that for the performance assessment period of the CFS2-driven ICRM forecasts, relatively few precipitation events are available for the MAM season to compute the observed climatological frequencies given the model forecast. As such the reliability diagrams and the BSS of this model and season contain very large uncertainty and are not used in the performance assessment.

ROC curves and ROC Area.

Like the reliability-based measures discussed above, the Relative Operating Characteristic (ROC) curve and ROC Area measures concern the accuracy of probabilistic forecasts of a pre-defined “event” [e.g. Mason and Graham (2002) and Kharin and Zweirs (2003)] but for these measures the forecast-observations pairs are stratified according to whether or not an event was observed (not whether an event was forecast as in reliability analysis). A common way to introduce ROC concepts is with a contingency table (Figure 4.4).

Figure 4.4: Forecast-Observation Contingency Table

	EVENT OBSERVED	EVENT NOT OBSERVED
EVENT FORECAST (warning)	True Positive (HITS)	False Positive (FALSE ALARMS)

	EVENT OBSERVED	EVENT NOT OBSERVED
EVENT NOT FORECAST (no warning)	False Negative (MISSES)	True Negative (CORRECT REJECTIONS)
TOTAL	TOTAL EVENTS (NE)	TOTAL NON-EVENTS (NE')

As in reliability analysis, ROC analysis begins with the definition of some “event” of interest, with ROC also requiring specification of a warning threshold for the forecasts defining whether or not a warning is issued. Typically, this is determined by the forecast probability that an event will occur. For example, a hypothetical forecaster might issue a flash flood warning when the probability of 24-hour rainfall over 10 cm exceeds 75 percent. In this example, each forecast-observation pair in the available sample is considered and given a count in one of the shaded boxes in Figure 4.4. When all pairs have been considered, the “hit rate” (HR) is calculated as the number of true positives divided by the total number of events (HITS / NE). Similarly, the “false alarm rate” (FR) is calculated as the number of false positives divided by the number of non-events (FALSE ALARMS / NE').

The procedure outlined above would give a single vector “RC” = (HR, FR) for the sample of forecasts and observations, and for the given warning threshold. This vector provides one point on the “ROC curve”. Further points are determined by varying the warning criteria (similar to the stratification used in reliability analysis), the idea being that in a skillful forecast system both the hit rate and false alarm rate will tend to increase (decrease) as the threshold for issuing a warning is decreased (increased). For example, a skillful forecast system might produce an (HR, FR) of (60 percent, 20 percent) with a warning threshold of 80 percent (warnings issued when the forecast probability of an event exceeds 80 percent); the same system might produce RC = (85 percent, 80 percent) when the warning threshold is reduced to 20 percent. By considering a set of candidate warning thresholds (e.g., warning at 0 percent, 10 percent, 20 percent, ..., 90 percent, 100 percent) the “ROC curve is built up. If the forecast system is skillful, most points on the curve will lie in the upper left quadrant of the plot while forecasts consisting of random guesses will fall near the 45° line. A sample ROC curve is shown in Figure 4.5.

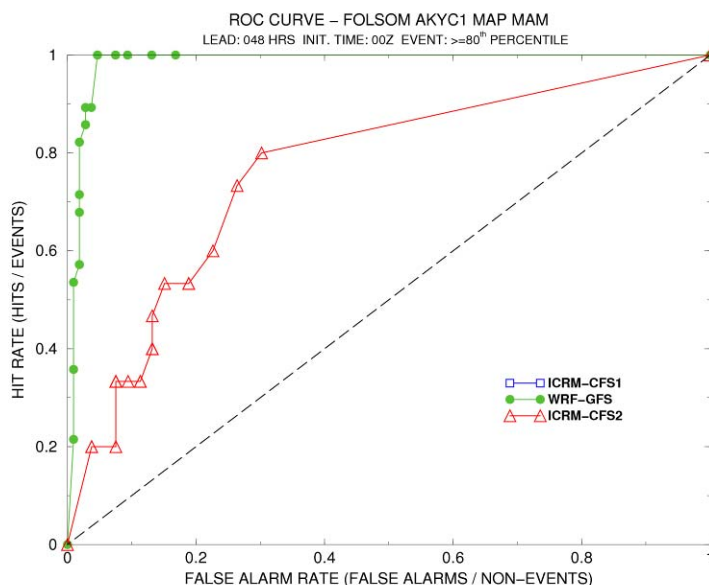
As with the reliability measures, for ROC analyses (Figure 4.5), “events” are considered to be those cases exceeding the 80th percentile observed MAP value in the sample, and warnings are based on the probability of exceeding the 80th percentile of the forecast MAP values in the sample. Results for two forecast systems are shown (WRF-GFS, green; ICRM-CFS2, red; there are no results available for ICRM-CFS1), with the points marking warning threshold probabilities ranging from “always forecast an event” (upper right on both curves), to “never forecast an event” (lower left points) at increments of 5 percent increments (some points plot over each other).

This example indicates both WRF and ICRM-CFS2 are skillful (in the upper left quadrant of the chart) for the 48 hour lead time, with WRF being considerably more skillful. As with reliability diagrams, ROC curves were constructed for 48-hour lead time for each basin, variable and season.

Just as the Brier Skill Score provided an aggregate measure for the reliability diagram, the area under the ROC curve (ROC area, or “AROC”) summarize the information on the ROC curve; AROC above 0.5 (the area under the 45° “guessing” line) is considered skillful. In our analyses, ROC area was calculated using a trapezoid approximation. As an aggregate measure, AROC results are displayed as a function of lead time for each basin, variable, and season classification (analogous to Figure 4.2).

The following sections summarize the demonstration results in terms of forecast performance. These results are presented for each of the variables treated: MAP, MAT and INFLOW. In all cases, a selection of representative results is presented in the main text, with all the results available included in Appendix E.

Figure 4.5: Example ROC Curve for MAM MAP for 48-hour Lead Forecasts Validating at 00Z for Folsom Sub-Catchment AKYC1.



4.1.3 MAP and MAT Assessments

4.1.3.1 Biases and Correlations

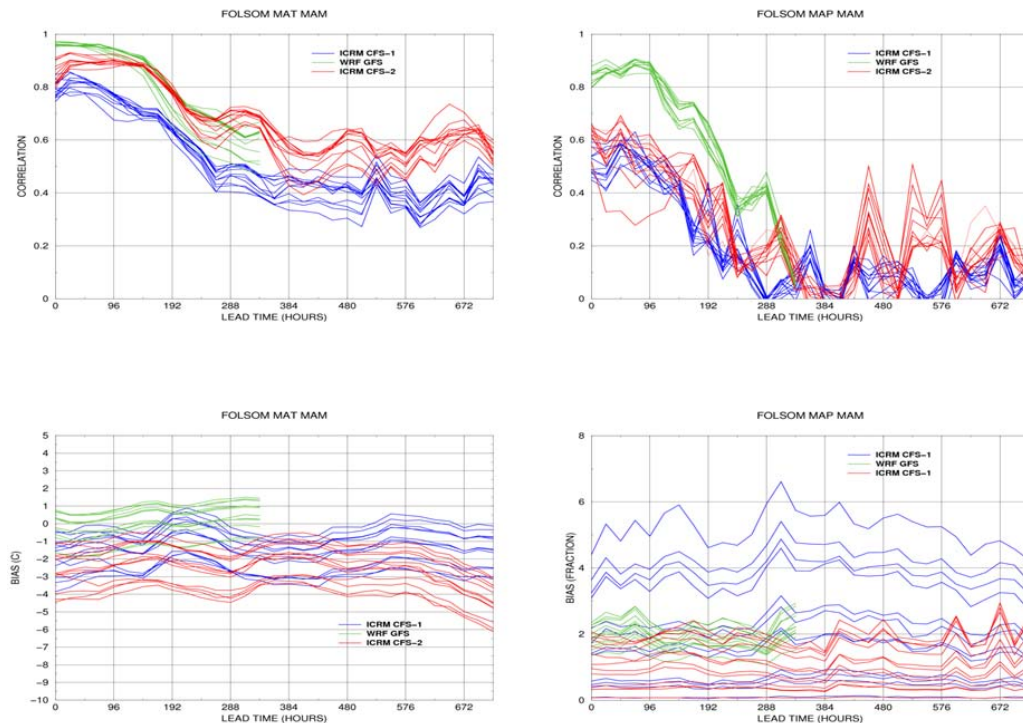
The results are presented in the form of Figure 4.6 (a comprehensive set of such plots is in Appendix E). The figure panels are for bias (fraction for MAP and difference for MAT), and for cross-correlation of daily accumulated precipitation and daily average temperature for the MAM season. Left panels are for MAT and right panels are for MAP. In each panel bias or

correlation is shown as a function of forecast lead time, with green lines representing the GFS-WRF forecast results, blue lines representing the CFS1-ICRM forecast results, and red lines representing the CFS2-ICRM results. Note that the time periods and ensemble members for each case are different as discussed in the previous section. For each case, multiple lines signify results for different sub-catchments within the Folsom watershed.

For Folsom (Figure 4.6) the WRF ensemble MAP forecasts show very high correlations (≥ 0.80) with observations for lead times out to about 5 days (120 hours) and good correlations (≥ 0.60) with observations for lead times out to about 8 days (192 hours). Significantly lower correlations are shown for the ICRM MAP ensemble forecasts for both the CFS1 and CFS2 forcing, with CFS2 forcing showing slightly better results (correlations ≥ 0.6 for lead times up to about 4 days). There are non-negligible correlations shown for CFS2-ICRM forecasts for lead times of about 20 days and beyond. This will be discussed later in this section.

MAP forecast fractional bias is clustered around 2 for the WRF forecasts while it is much greater for the CFS1-ICRM forecasts for a few subcatchments and much lower than 1 (1 indicates a no bias condition) for a few subcatchments (indicating underestimation for subcatchments with low sloping terrain). Fractional bias for CFS2-ICRM MAP forecasts is less than 2 for all the subcatchments and for most of forecast lead times (except for some long lead times for a few subcatchments). Similarly, the ICRM forecasts show that subcatchments with low terrain slope have bias fractions lower than 1 (a few much lower). Apart from the CFS1-ICRM case, the other cases exhibit weak dependence of bias with lead times. This indicates that for those cases of WRF and ICRM bias correction may be effectively applied for each subcatchment.

Figure 4.6: Bias and Correlations of INFORM II Forecasts with Respect to Observations for MAT and MAP in Folsom Subcatchments.



The MAT forecast correlations are high for all cases, with very high values (≥ 0.80) for GFS-WRF and CFS2-ICRM out to about 8 days, while CFS2-ICRM maintains correlations of 0.6 for several subcatchments out to lead times greater than 25 days. CFS1-ICRM also exhibits high correlations, which remains lower than those of both other forecast models for all lead times and catchments. Overall the GFS-WRF has lower biases than the other two forecast models that exhibit a cold bias for most subcatchments and lead times. For a given subcatchment, bias depends again weakly on lead time (up to the maximum lead time for GFS and up to about 25 days or so for ICRM); this indicates that bias adjustment may be done effectively for MAT as well. The high correlations for ICRM MAT at long lead times support the use of the ensemble forecasts for the prediction of melt out to 20-28 days.

Results in Appendix E for the rest of the watersheds of interest, and for the same (MAM) season, are similar qualitatively with those discussed for the Folsom watershed. In all cases, the GFS-WRF model ensemble MAP forecasts have consistently high correlations for lead times less than about 5 days and outperform the ICRM model ensemble forecasts in terms of correlation. They do show high positive bias (bias fraction near or more than 2) for these lead times. Short lead times for CCFS2-ICRM carry correlations near or above 0.6 except for Trinity basin where the highest correlation reaches 0.5. The correlation for the CFS2-ICRM forecasts (and of the CFS1-ICRM forecasts) for lead times 16 – 20 days exhibits anomalously high values that consistently reach or exceed 0.4 in all cases. Biases for ICRM MAP are lower than 1 for several

of the subcatchments for all watersheds. The strength of CFS2-ICRM is exhibited in the MAT ensemble forecast predictions that maintain high correlation to observations for long lead times during this snow melt season (MAM). For most subcatchments, there is a cold bias for ICRM forecasts. The CFS1-ICRM model has lower skill for all lead times but maintains 0.4 correlations even for lead times greater than 15 days for this MAM season. It exhibits less of a cold bias than the CFS2-ICRM for most subcatchments.

The plots in Appendix E also present results for the NDJF season (snow accumulation season for high elevations). There are no CFS2-ICRM results for this season and the plots only show results for GFS-WRF and CFS1-ICRM. The MAP results show consistently high correlations of the GFS-WRF model forecasts for lead times up to a few days with correlations dropping rapidly with lead time. It is notable that the MAM season exhibits substantially longer persistence of high correlations than the NDJF season for the GFS-WRF and to a lesser degree for the CFS1-ICRM. Since both models exhibit this behavior and it is shown for all watersheds, it is expected that this difference has to do with the particular events of the observation period and their measurement. The number of events for the GFS-WRF analysis and for NDJF is 165 while for MAM it is 133 (not very large sample size difference). It may also be that the CNRFC MAP estimates carry more uncertainty in the NDJF than in the MAM season. At this time, the reason for this difference has not been fully investigated.

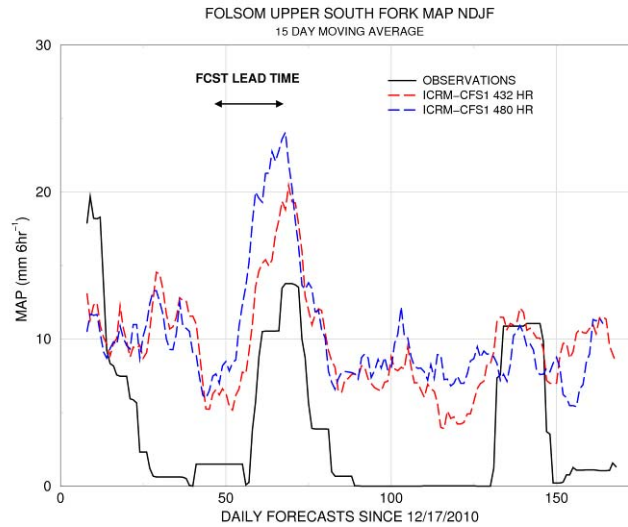
The CFS1-ICRM shows substantially lower correlations for MAP than GFS-WRF, and has a milder slope of decline with lead time. In this season and for this ICRM model configuration too, there is anomalous high correlation in long lead times suggesting skill in the window between 16 and 20 days. The MAT correlations are somewhat lower in the NDJF season than in the MAM season for both GFS-WRF and CFS1-ICRM. Both models indicate broadening of the subcatchment differences in MAT correlation in the NDJF season.

The GFS-WRF maintains high positive MAP bias (near 2) for the NDJF season (as did for the MAM season), but in this case the bias increases with lead time. Subcatchment differences are rather small for GFS-WRF. Very large MAP bias differences among subcatchments are noted for CFS1-ICRM for Folsom and Shasta, while for most of the Oroville subcatchments the ICRM MAP bias is less than 1. Similar to the GFS-WRF behavior, the MAP bias of the CFS1-ICRM also presents an increasing trend for lead times up to about 12 days. GFS-WRF MAT biases range from about -2 °C to about +2 °C for the study watersheds, with a warm bias for most subcatchments of the Folsom watershed and a cold bias for most of the subcatchments of the rest of the watersheds. CFS1-ICRM MAT forecasts exhibit a bias range from about 1 °C to about 3 °C, with an overall warm bias except for the Trinity watershed where a cold bias is shown (-1 to -2.5 °C).

The anomalously high correlations between ICRM MAP forecasts and observations for lead times 15-20 days are a consistent feature in all basins during the MAM season; this raises the question whether these higher values are due to statistical behavior or represent real skill. Although this may not be answered unambiguously with the present limited data, one can test whether there is consistent behavior of the models for these long lead times when there is an event. If there is such consistent behavior then one cannot dismiss the possibility of real

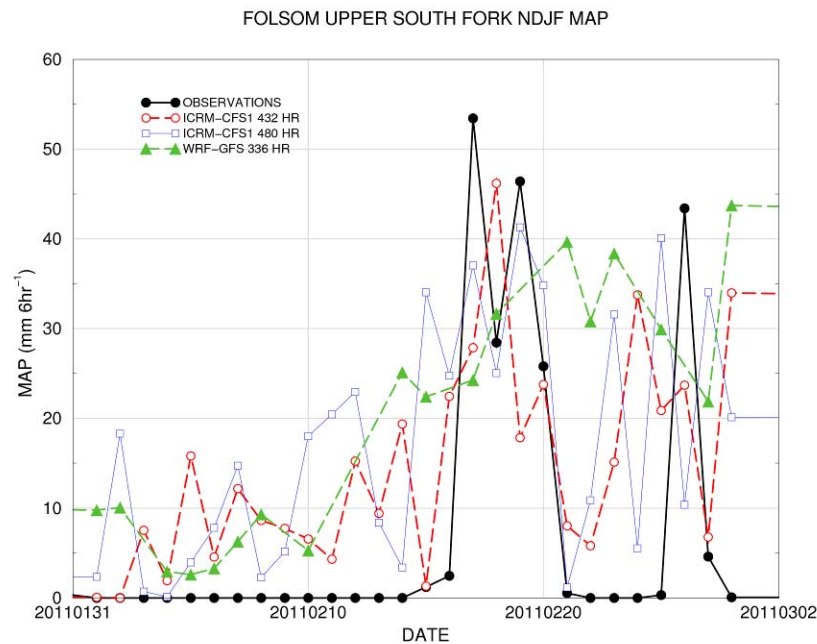
forecast skill for these lead times when there is a significant event. An example of an event apparently forecast at long lead times is depicted in Figure 4.7.

Figure 4.7: Smoothed Forecast and Predicted MAP for a Folsom Subcatchment



The figure (Fig. 4.7) shows the MAP observations (black) and the CFS1-ICRM long lead MAP forecasts (red is for the 432-hr lead time and blue is for the 480-hr lead time) for a time period starting in mid-December 2010. Both forecasts and observations are smoothed by a 15-day smoother for figure clarity. It is clear that the CFS1-ICRM forecasts consistently predict the timing of the mid February 2011 event at these long lead times (432 hours or 18 days, and 480 hours or 20 days). Focusing in on the event more closely, we show in Figure 4.8 the unsmoothed MAP observations and CFS1-ICRM forecasts (both lead times) and the GFS-WRF forecast with a lead time of 14 days. In all forecast cases, there is evidence of skill in predicting this event occurrence, with sharper predictions for the CFS1-ICRM with a lead time of 18 days. This consistency in forecast performance between the same model and different lead times and between different models supports the accretion that there is skill at these lead times. Inasmuch as the GFS system does not use dynamical sea surface temperature forecasts, it is conjectured that this example of skill seen in both GFS and CFS-1-driven long lead forecasts is due to slow internal atmospheric process.. Additional data and analyses are necessary to confirm this conjecture but it is in line with the findings of *Georgakakos et al. (2008)*.

Figure 4.8: MAP Observations and Forecasts for an Event in a Folsom Subcatchment

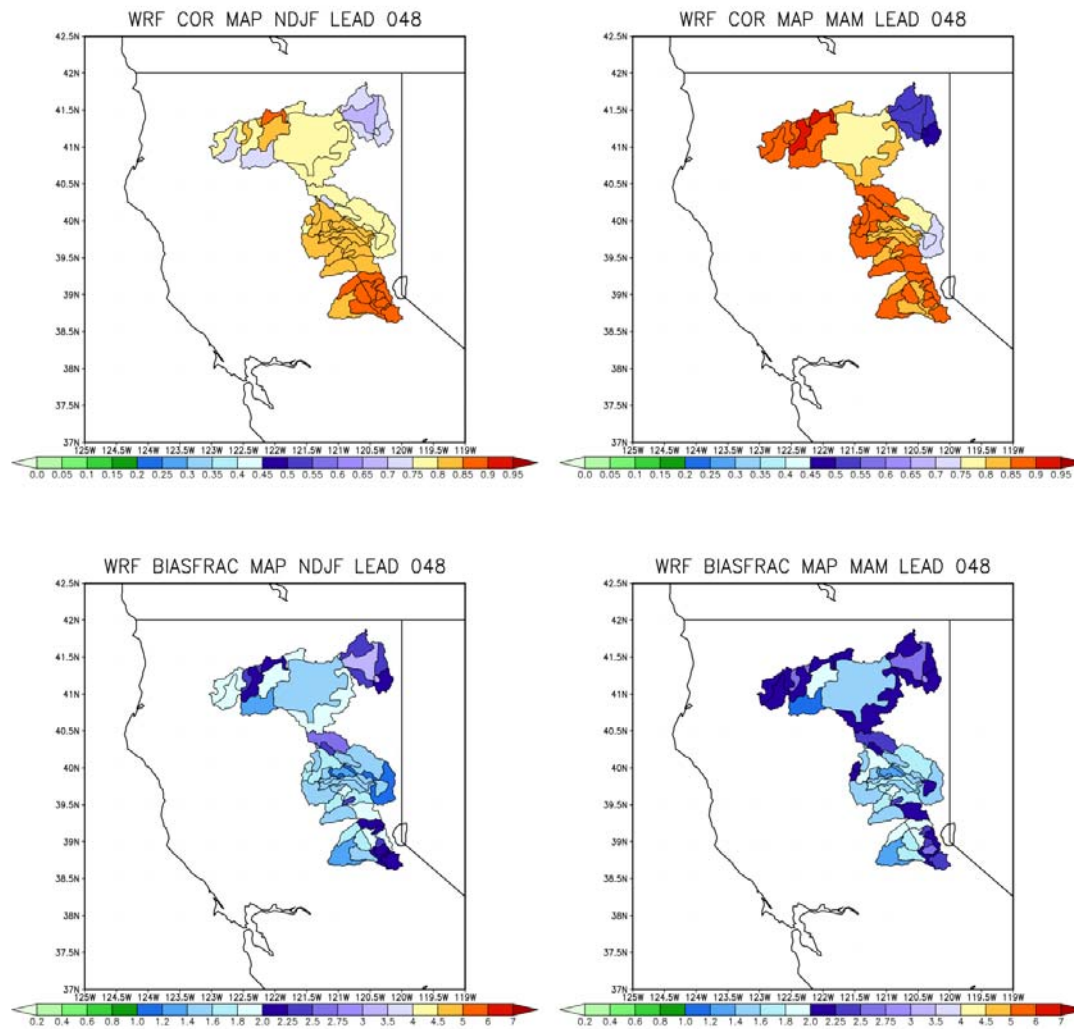


The geographical distribution of the bias and correlations for MAP for a 48-hour lead time and for both seasons is shown in Figure 4.9 for the GFS-WRF model. Similar plots are shown in Appendix E for all three models (GFS-WRF, CFS1-ICRM, and CFS2-ICRM) and for both MAP and MAT. Figure 4.10 shows the subcatchment elevations for easy reference.

Non-uniform spatial distribution in MAP correlation between forecasts and observations is shown in Figure 4.9. For the lead time of 48 hours, the MAM season shows higher correlations for most basins apart from the northeastern subcatchments of the Shasta watershed and the southern subcatchments of the Folsom watershed, which show lower correlation in MAM. Relatively low correlations are shown for both seasons for large subcatchments of the Shasta watershed and certain subcatchments of the Oroville watershed. Comparing to the elevations of Figure 4.10 shows that higher elevation subcatchments have higher correlations in general (e.g., high elevations of Yuba and Folsom watersheds and Shasta watersheds of higher elevation).

High MAP bias fractions are prevalent for most subcatchments for both seasons, with higher biases generally shown for higher elevations (probably also contributed by the lack of reliable precipitation observations). Variability among subcatchments is substantial in both seasons, but with NDJF exhibiting (generally) lower bias fraction for the subcatchments.

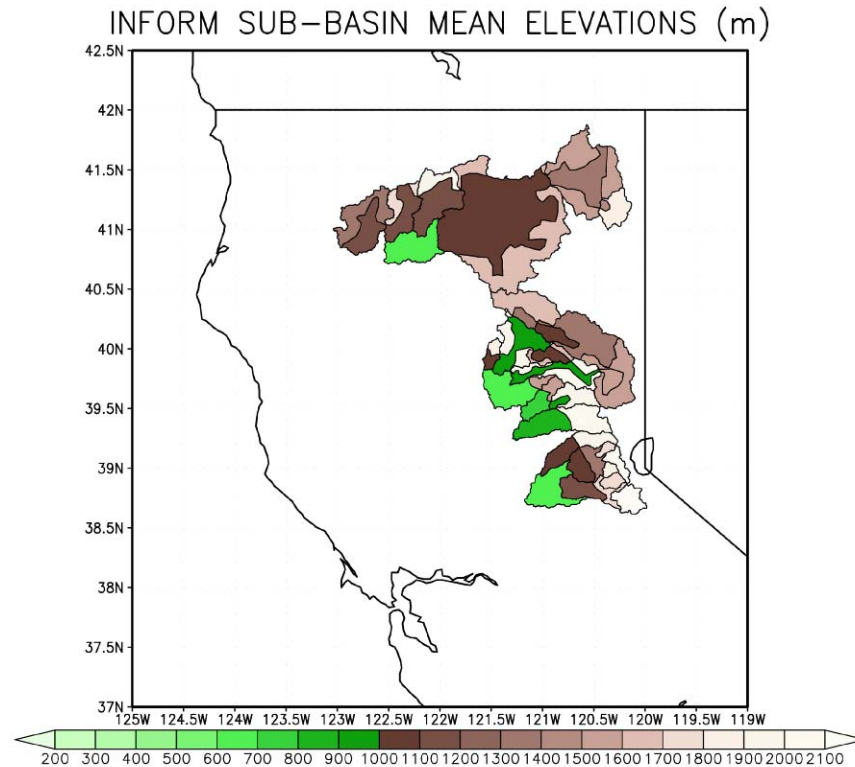
Figure 4.9: Subcatchment Distribution of MAP Correlation and Bias Fraction for the GFS-WRF Model



Results for the CFS1-ICRM and CFS2-ICRM models for MAP forecast are shown as maps (geographic distribution) for 48-hour lead time in Appendix E. As mentioned earlier there is no data for CFS2-ICRM for the NDJF season (maps show values of 0.0 for this case). Both models CFS1-ICRM and CFS2-ICRM show substantial spatial variability in the MAM season, with low elevation basins generally showing lower correlations and high elevation basins showing higher correlations; this is to be expected because ICRM uses of an orographic precipitation model (see discussion of Chapter 2). For most subcatchments, CFS2-ICRM shows better performance in MAP correlation with similar or closer to 1 bias fraction (KOSTA?). For the case of NDJF and CFS1-ICRM, notable increases in correlation are shown in comparison to the MAM season and the same model. Biases are similar between the two seasons except for the northeastern subcatchments of Shasta watershed where the bias fraction for the NDJF season is much higher

(significant MAP over-estimation) than that of the MAM season. These are high elevation catchments (> 1400 m) as shown in Figure 4.10.

Figure 4.10: Subcatchment Elevations



The MAT forecast bias and correlation subcatchment plots for both seasons and for all three models are shown in Appendix E as well for the lead time of 48 hours. Very high correlations are exhibited over all subcatchments in the MAM season by the GFS-WRF while higher spatial variability in correlation is seen for the NDJF season. Bias is generally low for this lead time with cold bias for the higher elevations, more so in NDJF than in MAM. For the MAM season correlations for the CFS1-ICRM and CFS2-ICRM are higher in the southern subcatchments than in the northern subcatchments (especially so for the CFS1-ICRM forecasts). Generally less uniform results for correlations have been obtained with CFS-ICRM (both CFS1 and CFS2 versions) than with the GFS-WRF for the 48-hour lead time. Cold bias is exhibited by both CFS1-ICRM and CFS2-ICRM for the MAM season particularly for some lower elevation catchments (although not all as the example of the lower Oroville local subcatchment shows). For the NDJF season, the CFS1-ICRM MAT forecasts exhibit lower correlations than for the MAM season, and these NDJF results have a rather uniform warm bias even for the higher-elevation subcatchments, apart from the Trinity watershed where they have a cold bias.

4.1.3.2 Probabilistic Performance Measures

The previously discussed performance measures concerned the ensemble mean forecast MAP and MAT values. However, both GFS-WRF and CFS2-ICRM produce ensemble MAP and MAT forecasts, which are used to produce ensemble reservoir inflow forecasts used by the INFORM decision component. It is thus useful to also examine the performance of these ensemble forecasts using probabilistic performance measures as discussed earlier of this chapter.

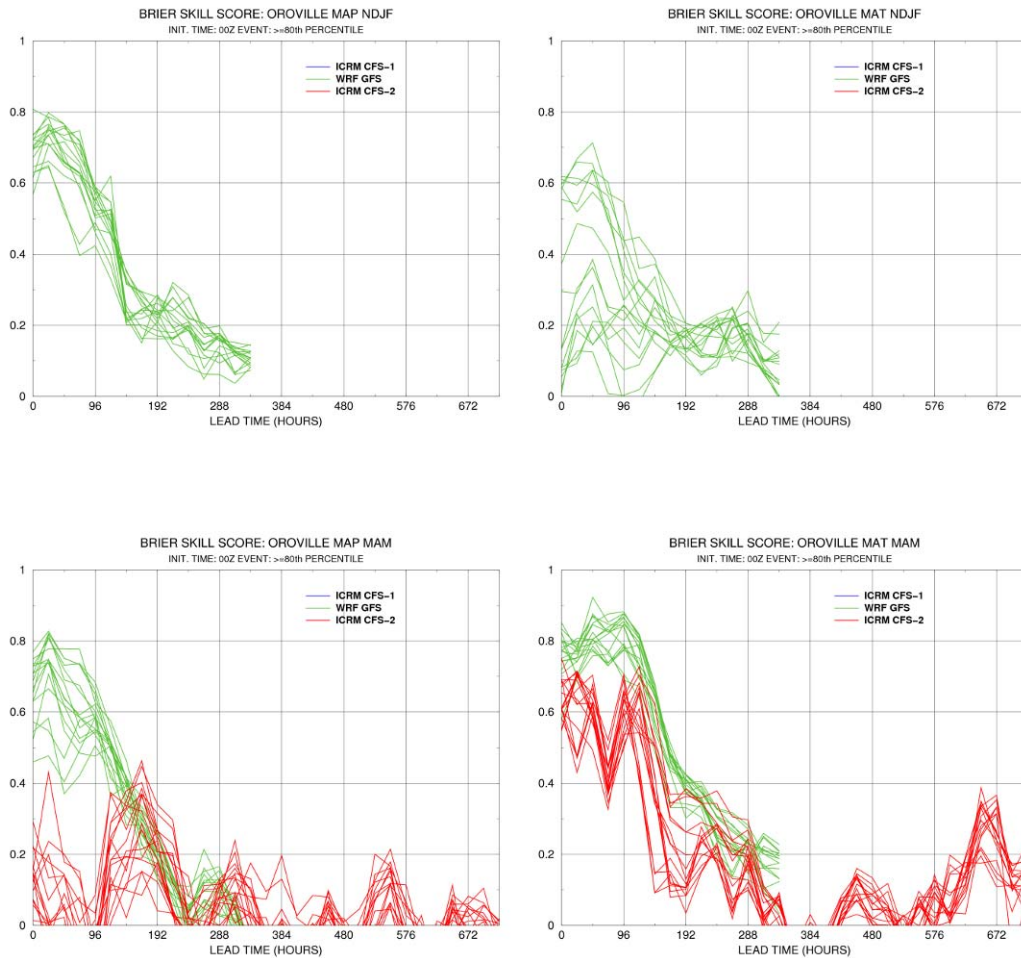
The reliability diagrams and the Brier Skill Score (BSS) have been computed for both seasons and for both the models GFS-WRF and CFS2-ICRM. As noted earlier, the CFS2-INFORM model results are only available for the MAM season and for the single year 2012. This year 2012 did not contain an adequate number of precipitation events to allow stable statistics for the climatological frequencies conditional on a forecast frequency interval that are necessary for the reliability diagrams and for the BSS. Thus, even though the MAP results for this model and season are included in the figures of this section and in Appendix E, they carry large uncertainties and they are not deemed appropriate for deriving conclusions at this time. Therefore they are not discussed, and the emphasis of this discussion is on the GFS-WRF MAP and MAT results that include two years of operation (2011 and 2012) for both, and on the CFS2-ICRM MAT results.

Figure 4.11 shows the WRF MAP and MAT BSS for multiple lead times and for all the subcatchments of the Oroville watershed and for both seasons NDJF and MAM. Positive BSS is indicated throughout the WRF forecast lead time range (maximum lead time of 16 days), with MAP forecasts for NDJF indicating higher reliability than those in MAM and with opposite seasonal performance indicated for MAT forecasts, with substantial degradation of MAT forecast reliability for the NDJF season. Large differences between subcatchments are shown in MAT reliability for the NDJF season and with lower range of differences in MAP reliability for the MAM season. MAP ensemble forecast BSS values are above 0.2 even out to 8 days indicating good reliability, while very good reliability is exhibited by the MAT ensemble forecasts of GFS-WRF out to 4 days lead time (BSS near or above 0.8 for all subcatchments of Oroville watershed). The BSS for the CFS2-ICRM MAT ensemble forecasts (lower right panel of Figure 4.11) shows positive values out to 16 days with a peak of long-range forecast positive values for lead times of about 20 days. The MAT BSS for CFS2-ICRM is lower than that of GFS-WRF for this season for most lead times and subcatchments, reaching maximum values of about 0.7 for most subcatchments. Overall, Figure 4.11 reveals good reliability of the INFORM ensemble forecasts with respect to climatological forecasts of both MAP and MAT out to about 16 days.

Appendix E presents the MAP and MAT BSS results for all the INFORM watersheds. Comments analogous to those made for the Oroville watershed above apply to the other watersheds as well. Notable is the poor reliability performance of the MAT ensemble forecasts for a few catchments of the Folsom watersheds, for short lead times and for the NDJF season. Estimation of the MAT values for that season generally carries significant uncertainty, especially for high elevation areas. The individual reliability diagrams in Appendix E show the performance of the MAP and MAT forecasts of the GFS-WRF model for individual

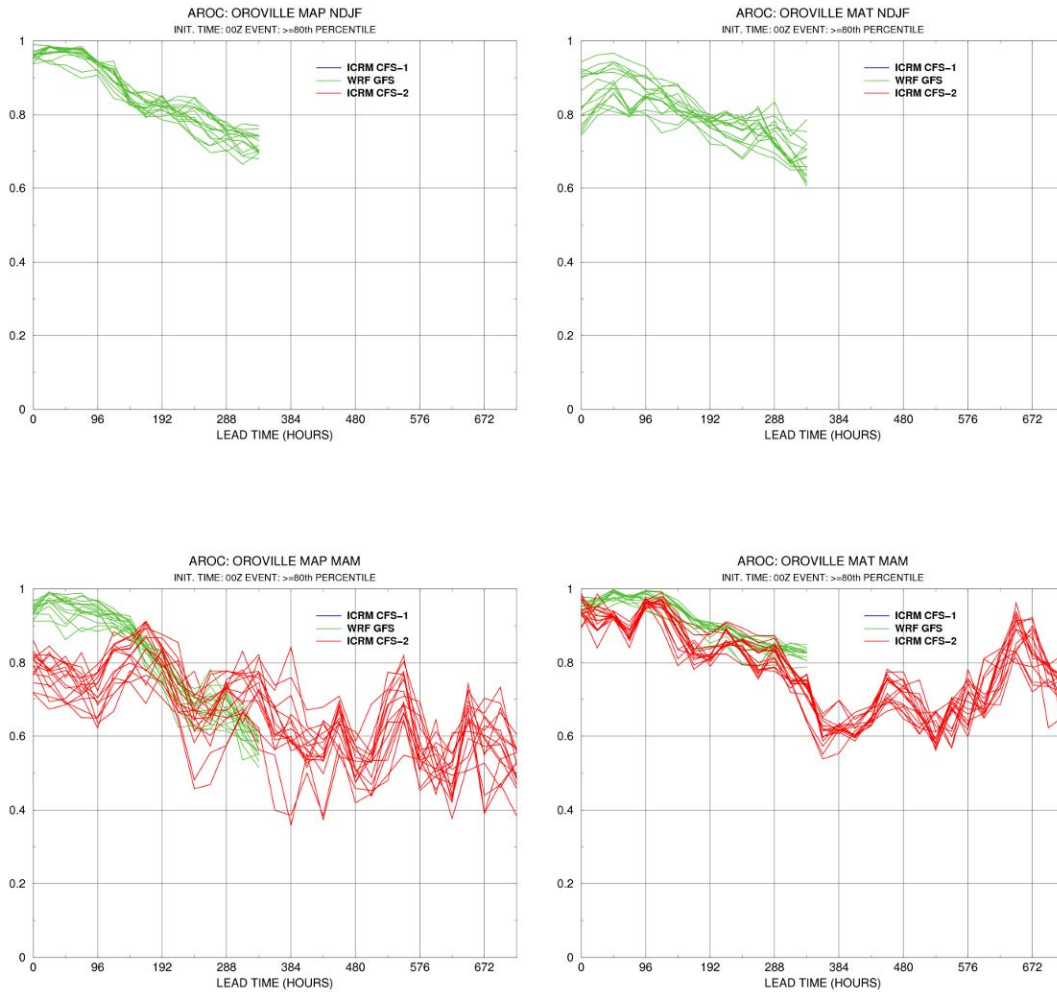
subcatchments (distinguishing upper and lower areas within subcatchments as appropriate). For MAT ensemble forecasts and for NDJF the high elevation catchments (AKYC1, UNVC1, RRG1, HLLC1, and FMDC1) have the poorest reliability diagrams for the Folsom watershed.

Figure 4.11: Brier Skill Score for MAP and MAT in Oroville Watershed



The Relative Operating Characteristic (ROC) curve provides additional insight into the accuracy of the ensemble forecasts, converted to probability forecasts for a specified event. In addition and analogous to the BSS, the area of the ROC curve (AROC) provides a scalar skill measure of the ensemble forecasts as far as the specified event (exceedance of the climatological 80th percentile value) is concerned (see the ROC curve and AROC discussion in the first section of Chapter 4). AROC values greater than 0.5 are considered skillful (ROC curve above the 45 degree line). Figure 4.12 shows the AROC index for MAP and MAT multi-lead forecasts as a function of lead time for all the subcatchments of the Oroville watershed and for the GFS-WRF and CFS2-ICRM models and NDJF and MAM seasons (CFS2-ICRM only available for the MAM season).

Figure 4.12: AROC Values of MAP and MAT Ensemble Forecasts for the Oroville Watershed Subcatchments



The results of Figure 4.12 show skillful forecasts (> 0.5) in all cases and for all leads (< 16 days) for the GFS-WRF model. For the CFS2-ICRM model, MAP forecasts have good skill for all but two subcatchments for lead times out to 18 days, and for most subcatchments out to 30 days. The MAT ensemble forecasts from the CFS2-ICRM model have good skill for all subcatchments out to a 30-day lead time. Generally, for MAM and for shorter lead times (< 10 days) for MAP the GFS-WRF system outperforms the CFS2-ICRM, beyond this the skill is comparable for both models.

Appendix E presents the AROC results for all the INFORM domain watersheds. Comments analogous to those made above for the Oroville watershed apply to the other watersheds as well. Generally, the AROC performance index indicates good skill even out to long lead times for the majority of the watersheds and for both MAP and MAT. The individual ROOC curves for all the subcatchments of the INFORM domain are also given in Appendix E.

4.1.4 Reservoir Inflow Assessments

4.1.4.1 Biases and Correlations

The bias and correlation errors of the reservoir inflows (mean daily flow) for the range of lead times out to a month or so have been examined. Bias is an indication of the volume errors and correlation is an indication of timing and variability errors in the forecast inflows with respect to the observed FNF inflows. These performance metrics have been defined in the first sections of this chapter and concern the overall mean ensemble reservoir inflow forecasts (non-probabilistic) as described there. In the discussion below we refer to the forcing model to distinguish system inflow forecasts (e.g., GFS-WRF model means forcing from the GFS-WRF model MAP and MAT used to drive the snow, soil and routing models). Figure 4.13 shows the bias errors (shown as the fraction of the forecasts over the observations) for both GFS-WRF and CFS2-ICRM and for the MAM season. The biases appear to be weakly varying with forecast lead time (except for Trinity inflows for the GFS-WRF model), and range from about 1.2 (Yuba, New Bullards Bar) to about 2.0 (Oroville) for GFS-WRF and from about 0.7 (Shasta) to about 1.8 (Oroville) for CFS2-ICRM. The bias difference among inflows to different reservoirs is higher for the CFS2-ICRM than for the GFS-WRF model. Lowest bias for GFS-WRF is for New Bullards Bar inflows of the Yuba River (1.2) and for CFS2-ICRM is for Trinity reservoir inflows (0.85), with New Bullards Bar inflows a close second (1.25).

The bias for the NDJF season (for the GFS-WRF model only) is shown in Figure 4.14. There is an increasing trend in the bias fraction for this season for the GFS-WRF. Shasta forecast inflow has the lowest bias fractions, near 1 in short lead times and up to 1.4 at 20 day lead time, while Folsom forecast inflows have the highest bias fraction for lead times longer than 3 days (2.2 to greater than 2.5). New Bullards Bar inflows on the Yuba River have the highest bias for lead time shorter than 3 days (values in the range 1.5 – 2). The accumulation season NDJF has higher biases than the melt season MAM.

The correlation for the MAM (NDJF) season between model forecasts and observations of mean daily FNF inflows is shown in Figure 4.15 (Figure 4.16) for both GFS-WRF and CFS2-ICRM. These show that for the GFS-WRF model and for MAM, Folsom, Trinity and Shasta inflows have the highest correlations, remaining greater than 0.5 even out to 12 days, maintaining values greater than 0.7 out to a 4-day lead time. The correlations for New Bullards Bar forecast inflows on the Yuba River and for Oroville forecast inflows exhibit lowest correlations with values greater than 0.5 maintained only up to a 2-day lead time, dropping precipitously after that to levels of about 0.2.

Figure 4.13: Bias Fraction of Reservoir Inflows for the MAM Season

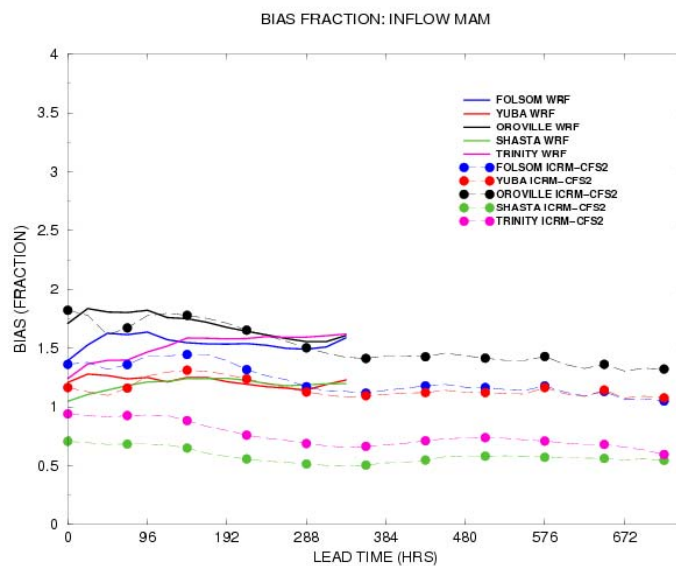


Figure 4.14: Bias Fraction of Reservoir Inflows for the NDJF Season

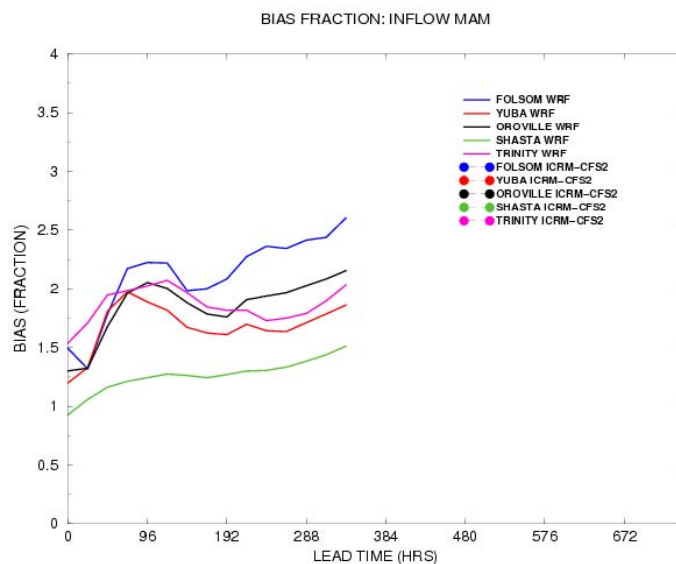


Figure 4.15: Correlations of Reservoir Inflows for the MAM Season

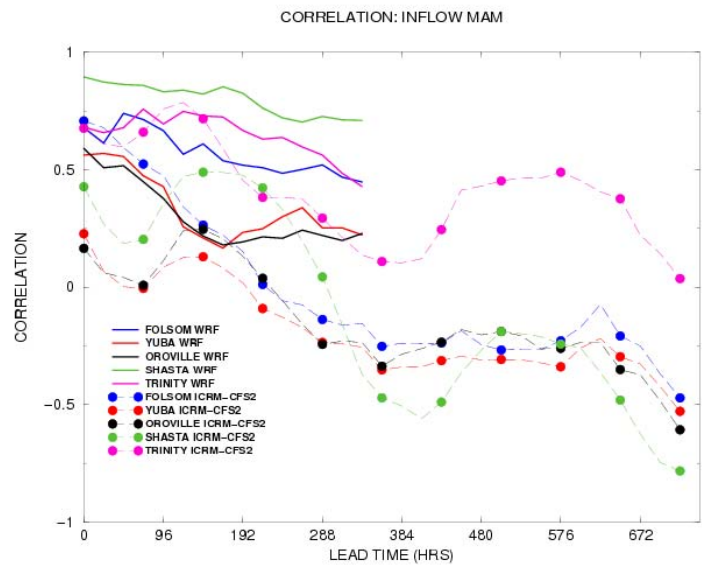
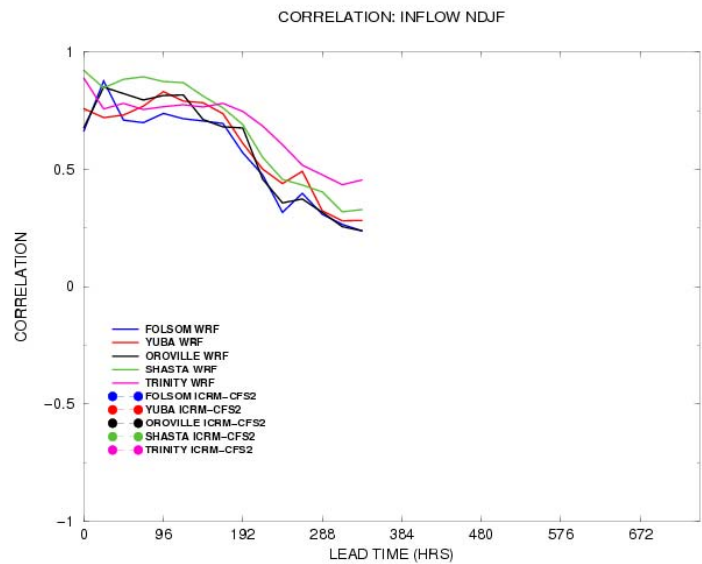


Figure 4.16: Correlations of Reservoir Inflows for the NDJF Season



Significantly lower correlations in reservoir forecast inflows are exhibited by the CFS2-ICRM model and for MAM, except for the Trinity basin for which values of 0.5 are shown for lead times out to more than 20 days. For short lead times (≤ 2 days) Trinity and Folsom forecast inflows exhibit correlations ranging from ~ 0.5 to 0.75. After that lead time the Folsom forecast inflow correlations fall substantially. The behavior of New Bullards Bar, Oroville and Shasta inflows shows an initial dip and then an increase to fall again to negligible levels. For Shasta, the increase brings the correlations to the level of 0.5 for a lead time up to 10 days, while for the other two reservoir inflows the correlations maintain a value less than 0.3 in all cases.

For the NDJF season, the correlations remain above 0.5 (Figure 4.16) for the GFS-WRF model for lead times out to 10 days or so. On average and for lead times out to 8 days, Shasta reservoir forecast inflows exhibit the highest correlations and Folsom reservoir forecast inflows the lowest.

For the interpretation of the results presented, one must consider the development of errors in the integrated forecast system of INFORM, which consists of the large-scale NCEP model forecasts (GFS and CFS), the downscaling model forecasts (WRF and ICRM), and the snow-soil-routing model inflow forecasts. Thus, the development of errors in the inflow forecasts is a combination of MAP and MAT errors for the subcatchments of the watershed of interest, initial condition errors in the snow-soil-routing model for these subcatchments and river segments, and the hydrologic model parameter errors. We present the results here for an event in Oroville inflow on the 16th of March 2012 (in the MAM season) to illustrate some of the important reasons for reservoir inflow error development.

Figure 4.17 shows mean daily Oroville inflow observations and forecasts (lead times from 6 to 24 hours averaged to mean daily flow values) from March through mid-May 2012 as produced by the INFORM forecast component in real time. The observations are shown with black dots, the ensemble mean of the inflow forecasts driven by GFS-WRF are as red triangles, and the analogous median forecasts driven by the CFS2-ICRM are shown as blue squares. Mean forecasts from both models tend to overestimate the observed flows in the period from late March to mid-May, with WRF-driven forecasts showing higher overestimation for this period. The main event however in this period of record is on the 16th of March 2012, and it is rather well predicted by the WRF-driven median forecast (overestimating the peak) while it is underestimated by the ICRM-driven median forecast with a delay in the forecast peak compared to the observed peak. Analysis of the MAP forecasts for the subcatchments of the Oroville watershed showed underestimation of MAP values for this event.

An example is shown in Figure 4.18 for the subcatchment labeled IIFC1UP (area of Indian Creek subcatchments above 1,500m elevation; see Figure 2.19 for the location map of the IIFC1 subcatchment in the Oroville watershed). Both models forecast rainfall in two pulses for the event under consideration. However, Figure 4.18 clearly shows the underestimation of the MAP for this upper area of IIFC1 and for this event by the CFS2-ICRM model (about 10mm/6hrs versus 34 mm/6hrs), as opposed to the GFS-WRF model that predicts the MAP observation well (about 29 mm/6hrs versus 34 mm/6hrs). Examination of the temperature estimates from both models at that time indicated that the precipitation fell as rain for both

models. Also, for both model cases the hydrologic snow and soil model initial conditions were the same as the start time for forecasts is at 1200Z at which point CNRFC hydrologic model states are assimilated.

Figure 4.17: Median Forecasts and Observations for Mean Daily Oroville Inflows

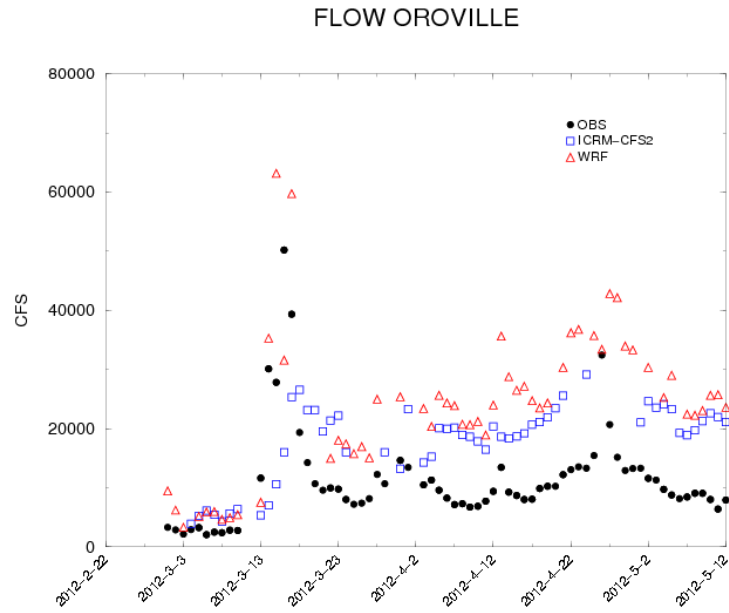
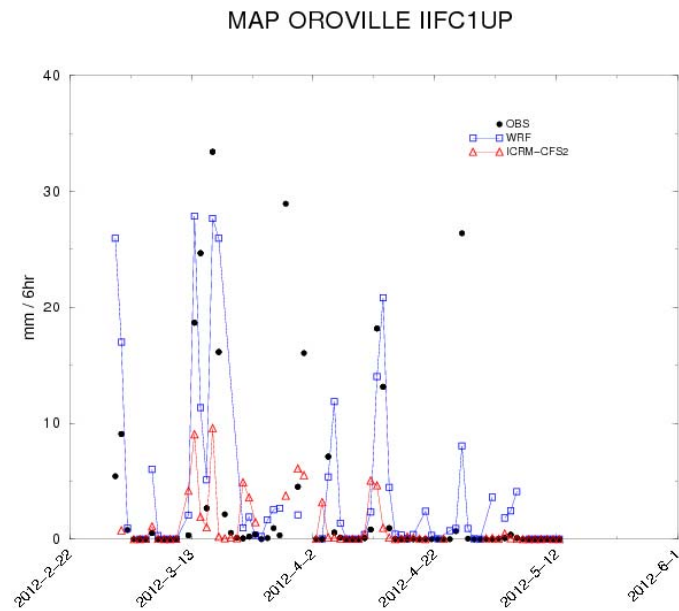


Figure 4.18: MAP Median Forecasts and Observations for Upper IIFC1 Subcatchment



Thus, the late peak production and underestimation of the ICRM-driven mean forecasts is most likely because the amount of forecast rain of the first pulse was inadequate to fill the soil water deficit immediately to produce surface runoff and from that river flow, but it was filled by the second pulse of rainfall and had a more gradual saturation path than the model receiving the WRF-generated MAP which filled the soil water deficit quickly with the first pulse. In that model case, the second pulse produced large surface runoff and river flow rates that reproduce better the observed timing and magnitude of inflow. Thus the timing, character and magnitude of forecast rainfall is very significant in the production of runoff and flow events, and errors in any one of these have significant influence for the reproduction of the timing and magnitude of severe inflow events. In addition, the temperature forecasts can also a significant influence. If the forecast temperatures below freezing, the precipitation would have fallen as snow and the forecast of the models for the warming surface air temperature would also have determined the rate and timing of the reservoir inflow event.

4.1.4.2 Probabilistic Performance of Reservoir Inflows

The Brier Skill Score (BSS) has been computed for both models providing MAP and MAT forecasts to the hydrologic model (GFS-WRF and CFS2-ICRM), for all watersheds and for both seasons NDJF (only for GFS-WRF) and MAM. It is here noted too that the ensemble reservoir inflow forecasts driven by the CFS2-ICRM model for the MAM season there is a very limited number of inflow events considered in the analysis (only those in 2012). As such (and as noted above for the MAP ensemble forecasts), the reliability diagrams and BSS carry substantial uncertainty. For this reason, such forecasts are not discussed here although shown for completeness in the plots.

Figure 4.19 shows the BSS values for multi-lead reservoir inflow forecasts for the NDJF season from the GFS-WRF model. Moderate skill is exhibited in the range from 0.2 (lowest for the Trinity reservoir) to 0.6 (Folsom reservoir), with BSS values maintained at about the 0.5 level out to lead times of about 7 days. Folsom inflows exhibit the largest skill fluctuations with lead time for this season. Analogous results for the MAM season are shown in Figure 4.20. Focusing on the GFS-WRF, skill is low for all watershed inflows except Trinity and Folsom for which it is moderate (0.2 to more than 0.5) for lead times out to 5 days or so. Folsom inflow forecasts have positive skill for short lead times, while Yuba and Oroville inflow forecasts show no skill for this season. It is likely that the BSS values are low because the number of events available for the validation is low. The BSS score is sensitive to the number of events used to compute the score (for GFS-WRF, just two seasons of events used to compute the reliability diagrams and the BSS performance index).

The AROC (area below the relative operating characteristic curve) values for the NDJF and MAM season are shown in Figures 4.21 and 4.22, respectively, for all reservoir inflows. Significant skill is shown for AROC throughout the range of lead times for GFS-WRF driven inflow forecasts and for the NDJF season (values above 0.8 for all cases). Lower skills are exhibited for the MAM season but with good performance for Folsom, Trinity and Shasta inflows for all lead times out to 16 days, and for Yuba (New Bullards Bar) and Oroville inflow forecasts for lead times out to at least 4 days. Greater differences among watersheds exist in the

MAM season than in the NDJF season, presumably because of the presence of snow in the upper regions of watersheds and dependence of inflow forecasts on both MAP and MAT forecasts in those regions. The CFS2-ICRM has AROC greater than 0.5 only for short lead times for all reservoir inflow forecasts but for those of the Trinity reservoir exhibiting skill out to more than 20 days.

Figure 4.19: BSS for Reservoir Inflows and for the NDJF Season

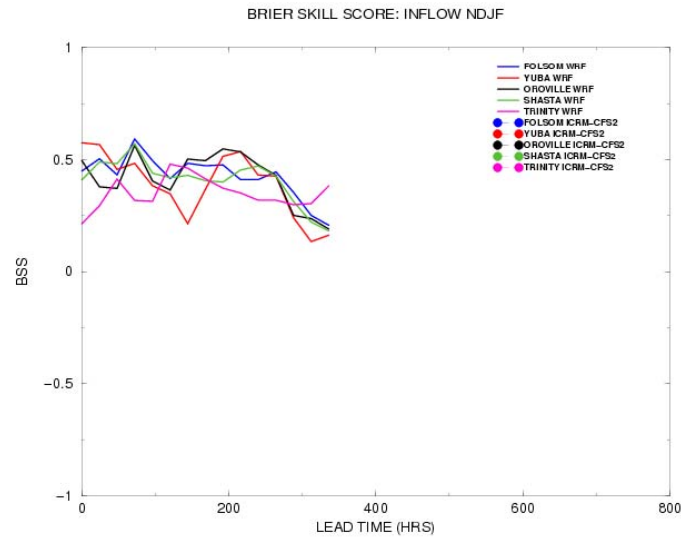


Figure 4.20: BSS for Reservoir Inflows and for the MAM Season

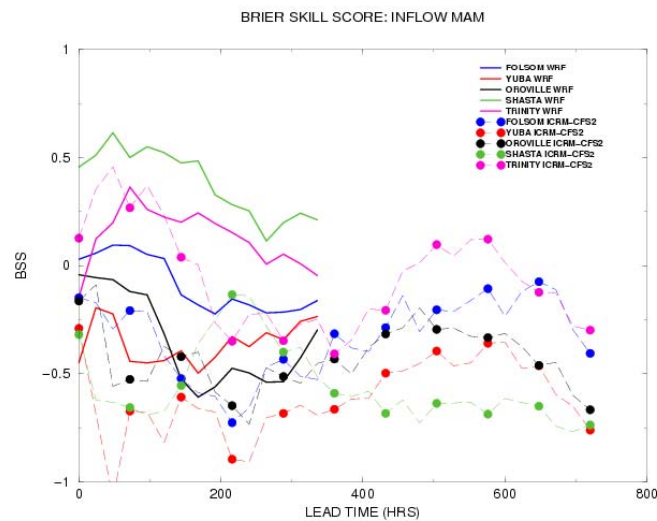


Figure 4.21: AROC for Reservoir Inflows and for the NDJF Season

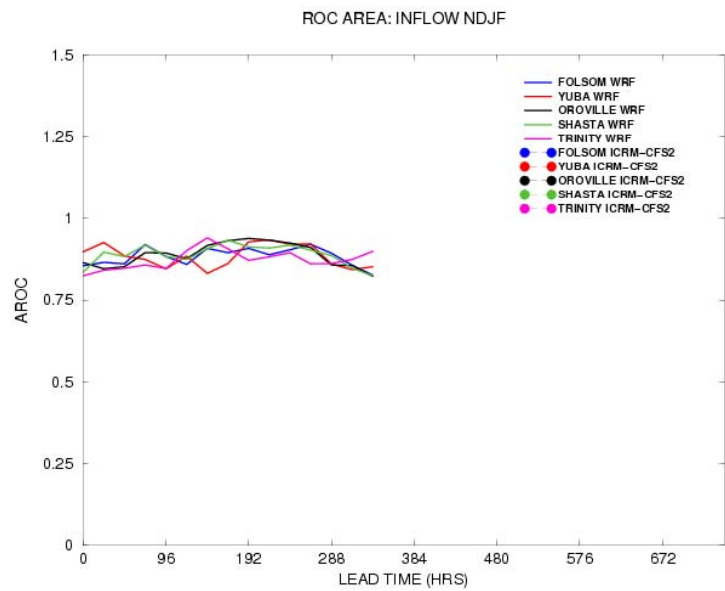
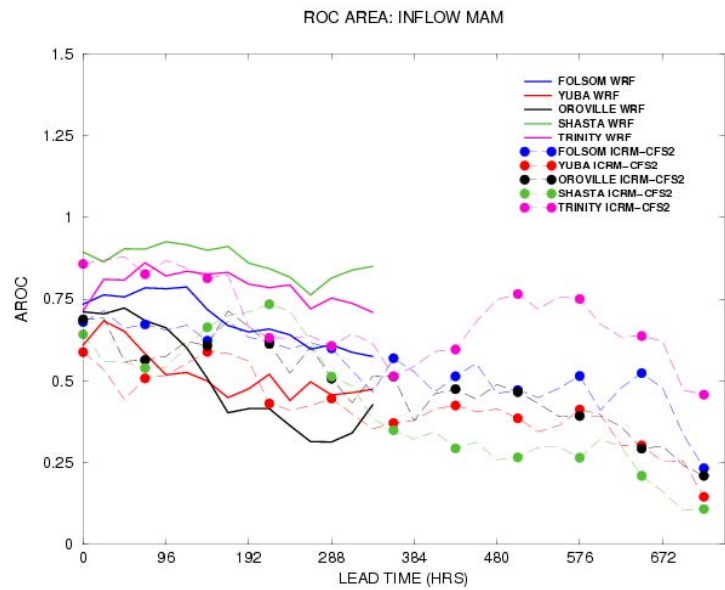


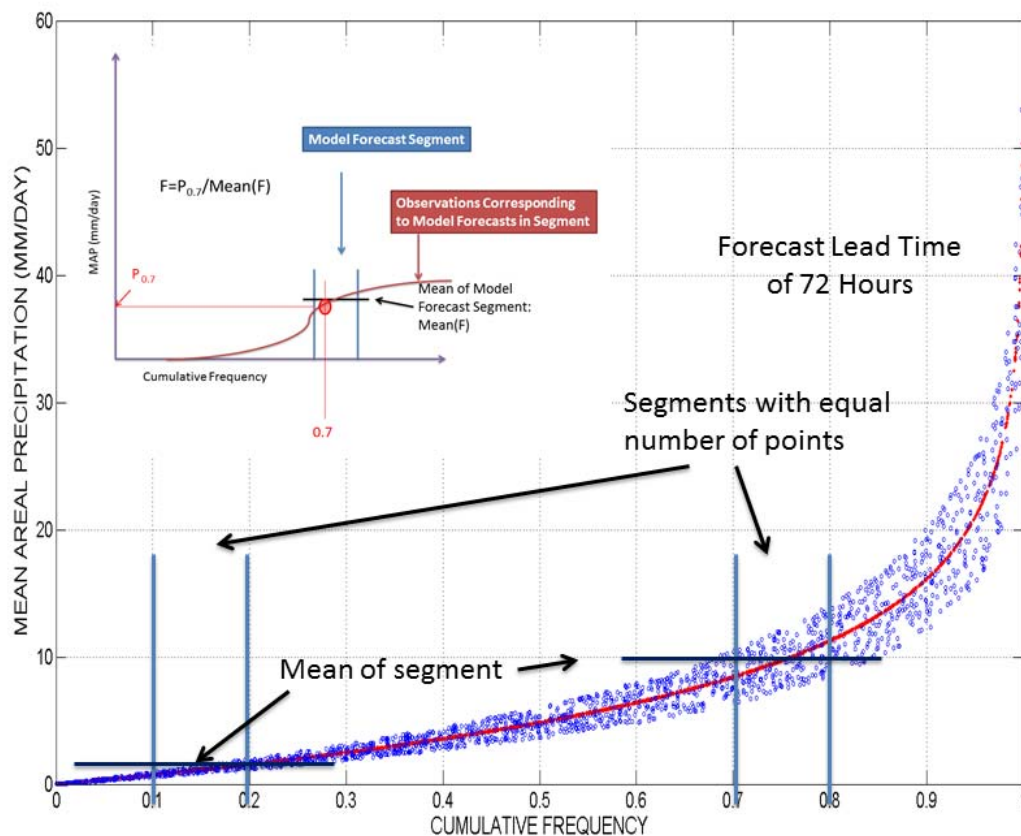
Figure 4.22: AROC for Reservoir Inflows and for the MAM Season



4.1.5 MAP and MAT Bias Adjustment and Impacts

Adjustment of the mean areal precipitation (MAP) and mean areal temperature (MAT) ensemble forecasts to correct for bias was done for each subcatchment, model (GFS-WRF and CFS2-ICRM) and each season (NDJF and MAM). The finding (see section 4.1.3) that the bias in MAP and MAT varies little with lead time in most cases allows focus on a particular lead time for the estimation of the bias factor and then application to all lead times. A probabilistic approach was formulated to account for the ensemble uncertainty and for the distribution of model forecast errors. The methodology is exemplified in Figure 4.23.

Figure 4.23: Schematic for Bias Factor Estimation Using a Probabilistic Approach



Consider the cumulative frequency plot of the ensemble daily mean areal precipitation produced by a given model (either GFS-WRF or CFS2-ICRM) for a given season and subcatchment, and for a particular lead time (shown is the forecast with lead time of 72 hours). The cumulative frequency plot may be divided into deciles (each decile then contains the same number of ensemble forecasts). The mean forecast (denoted in the Figure by Mean(F)) may then be estimated for each decile. Corresponding to the forecasts of each decile there are observations of mean areal precipitation estimated by CNRFC. These observations span a range

and form their own cumulative distribution function as depicted schematically in the inset of Figure 4.23 (the better the model forecasts the narrower the range of observations near the forecast decile). Selecting a statistic of the distribution of observations (in the schematic we selected the 70th percentile as an example, $P_{0.7}$), one may define the bias factor for each decile as the ratio: $P_{0.7}/\text{Mean}(F)$. Multiplication of the model values in the decile with the computed factor then provides for adjustment of the model ensemble forecasts to reduce their bias with respect to observations. In the present implementation of INFORM the deciles that are less than the cumulative frequency of 0.3 use $P_{0.3}$, those between 0.3 and 0.7 use the mean, and those greater than 0.7 use $P_{0.7}$ in the computation of the bias factor.

The procedure used is designed to reduce systematic bias in the forecast data while retaining some of the forecast uncertainty. The procedures used for MAP and MAT are slightly different, and it is important to keep in mind the following attributes for the two forecast systems:

- 1) The WRF-GFS system nominally runs twice per day (00, 12 GMT) out to a lead time of 384 hours (16 days) with output available at 6-hr increments. Each “run” consists of 20 ensemble members (NENS=20).
- 2) The ICRM-CFS2 system nominally runs four times per day (00, 06, 12, 18 GMT) out to a lead time of 996 hours (41.5 days) with output available at 6-hr increments. Each “run” consists of 4 ensemble members (NENS=4).
- 3) Observed MAP and MAT are available at 00, 06, 12, 18 GMT.
- 4) For WRF-GFS, the calibration period covered November 2011 to June 2012, so there are two nominally near-complete years of data available for each season (NDJF or MAM)
- 5) For ICRM-CFS2, the calibration period included only MAM of 2012.

Data preparation procedures were essentially identical for MAP and MAT and are summarized below.

- 1) Collate observed and simulated 6-hourly MAP (or MAT). This was done combining all validation times into single data sets (00 and 12 GMT for WRF; 00, 06, 12, and 18 GMT for ICRM-CFS2). This was done only for 66-hour lead forecasts. In the nomenclature used in the text and figures, a “N-hour lead forecast” validates N+6 hours after the initial time of the forecast (e.g., what is termed a “66-hour lead forecast” verifies 72-hours after the initial forecast time).
- 2) Identify all collated cases for which the nominal number of simulation ensemble members are present, discard other cases.
- 3) Separate collated data sets were created for NDJF and MAM.

- 4) Each collated observation / simulation pair then consists of a single 6-hour average observation and NENS 6-hourly 66-hour forecasts, where NENS is the number of ensemble members.

Derivation of MAP Calibration Factors

- For each season NDJF and MAM
 - a) Sort the model ensemble 6-hourly 66-hour forecasts from the available cases into 10 quantiles, keeping each forecast value paired with its corresponding validating observation. Note that each observed value will occur NENS times. Use only cases where simulated ensemble values are $> 1 \text{ mm } 6\text{-hr}^{-1}$.
 - b) For each quantile, calculate the mean (F_M) of the forecast values.
 - c) For each quantile, calculate the average, and 30th and 70th percentile values of the observed values (O_M , O_{30} , O_{70}) paired with the forecast values in that quantile.
 - d) For quantiles 3-8, the calibration factor (C_{MAP}) is defined as O_M / F_M .
 - e) For quantiles 1 and 2, C_{MAP} is defined as O_{30} / F_M .
 - f) For quantiles 9 and 10, C_{MAP} is defined as O_{70} / F_M .
- For June-October – set C_{MAP} to 1.0.

Derivation of MAT Calibration Factors

- For each season NDJF and MAM
 - a) Sort the model ensemble 6-hourly 66-hour forecasts from the available cases into 10 quantiles, keeping each simulated value paired with its corresponding validating observation. Note that each observed value will occur NENS times.
 - b) For each quantile, calculate the mean (F_M) of the forecast values.
 - c) For each quantile, calculate the mean of the observed values (O_M) paired with the simulated values in that quantile.
 - d) The calibration factor (C_{MAT}) is defined as $O_M - F_M$.
- For June-October – C_{MAT} set to 0.0.

Use of Calibration Bias Factors

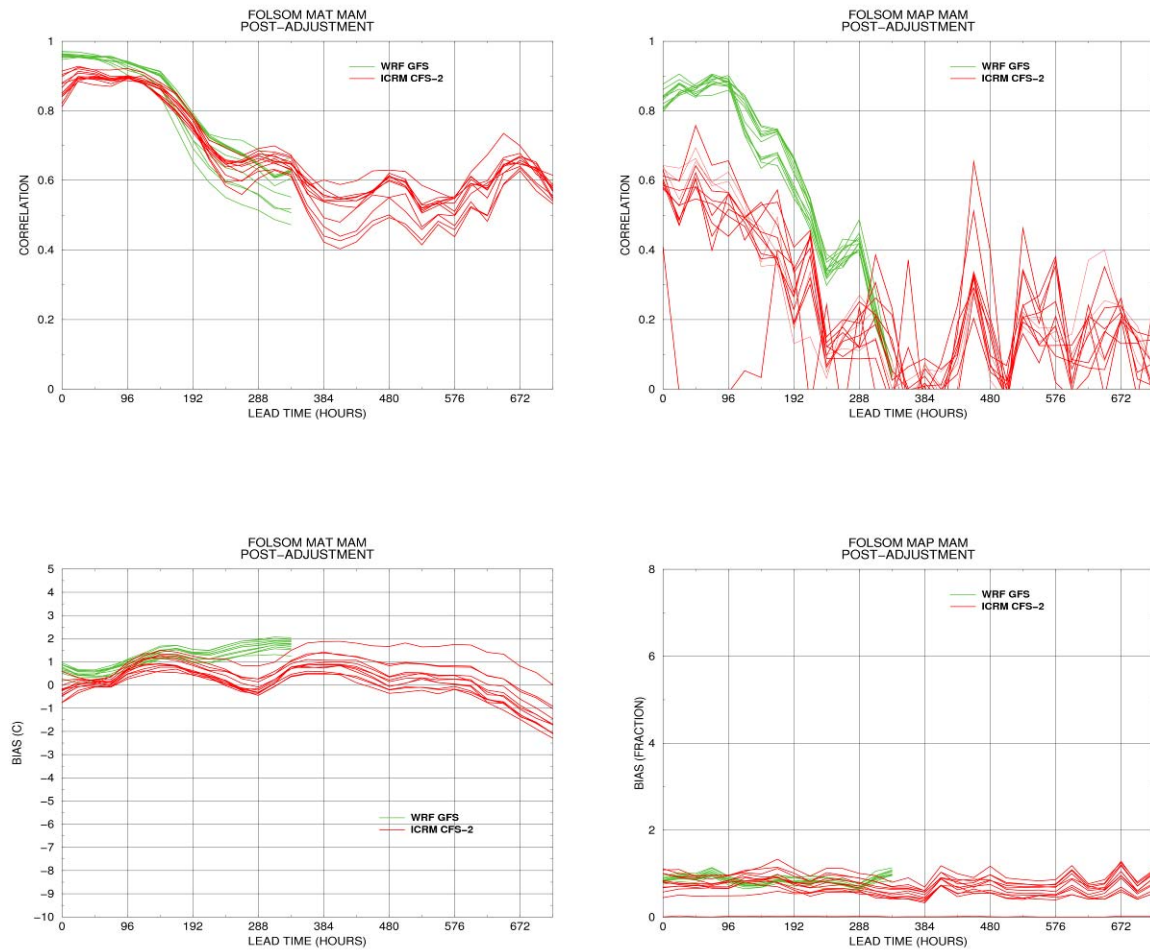
- Make separate files of C_{MAP} and C_{MAT} for each month of the year by replicating the seasonal values for each constituent month.
- Apply C_{MAP} as a multiplicative adjustment (“scale”) to the simulated forecast MAP values for the appropriate month and sub-catchment.

- Apply C_{MAT} as an additive adjustment (“offset”) to the simulated forecast MAT values for the appropriate month and sub-catchment.

Demonstration Results

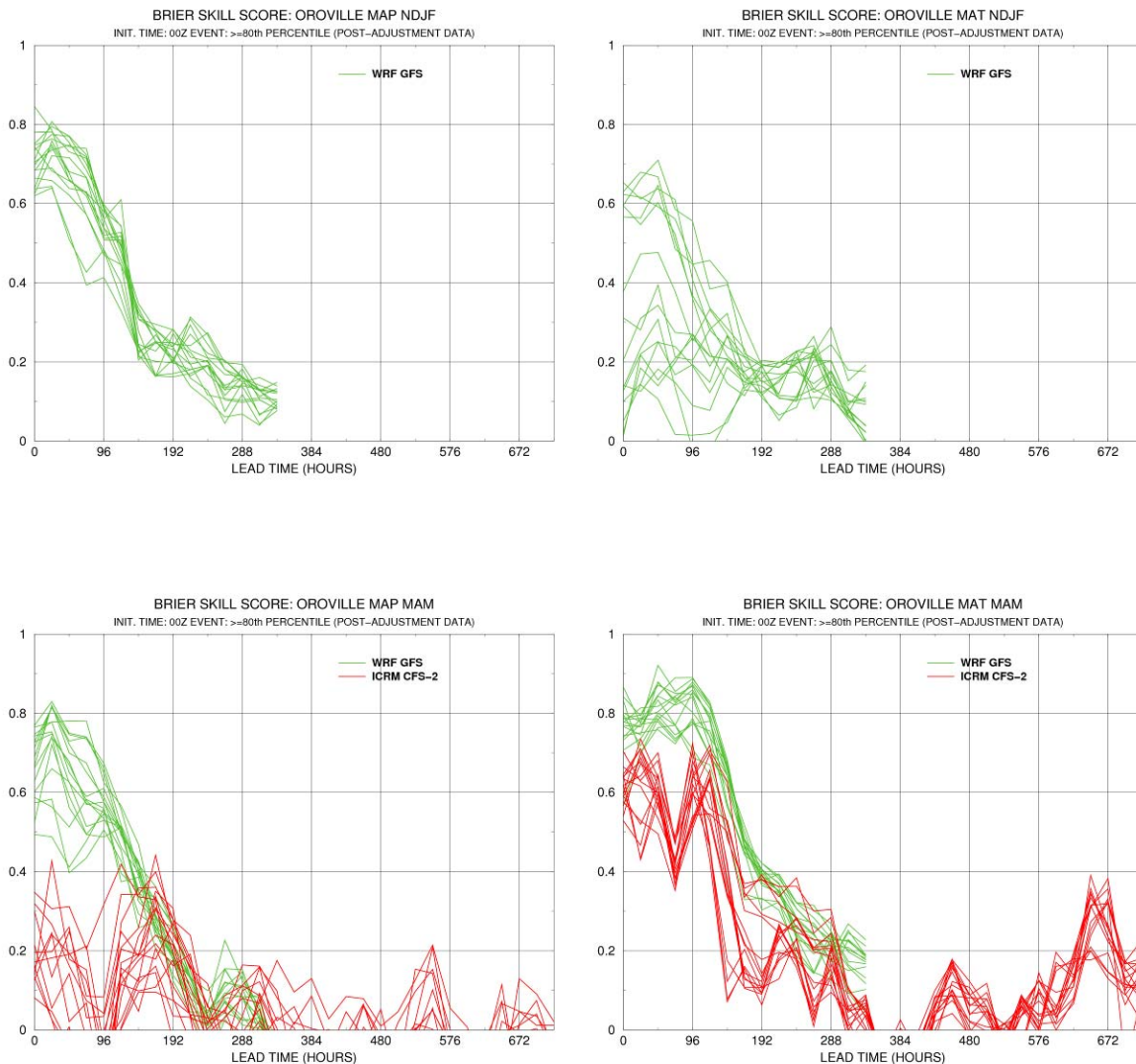
Application of the adjustment methodology described to the GFS-WRF and CFS2-ICRM model output was done as described in the previous section using the real-time information in INFORM. The results for the correlation and bias performance indices are exemplified in Figure 4.24 for the two models, the MAM melting season and for the Folsom Reservoir contributing subcatchments. In all cases the post-adjustment results show substantially lower bias than the original results (Figure 4.6) and even correlations have been improved in several cases or stayed the same in all but for one subcatchment for MAP and for shorter lead times. Detailed results are included in Appendix F for all the cases and are analogous to those discussed above (compare with corresponding original results in Appendix E).

Figure 4.24: Bias and Correlations of INFORM II Forecasts with Respect to Observations for MAT and MAP in Folsom Subcatchments – Post Bias Adjustment



Results pertaining to reliability for the post bias-adjusted results have also been obtained for all cases available in order to examine the impact of the bias adjustment methodology. An example is shown in Figure 4.25 for the Brier Skill Score (BSS) for the MAT and MAP and all of the subcatchments in the Oroville watershed. No significant changes were observed with respect to the original results (without bias adjustment as shown in Figure 4.11). Appendix F presents the detailed results for all the cases examined and support this assessment.

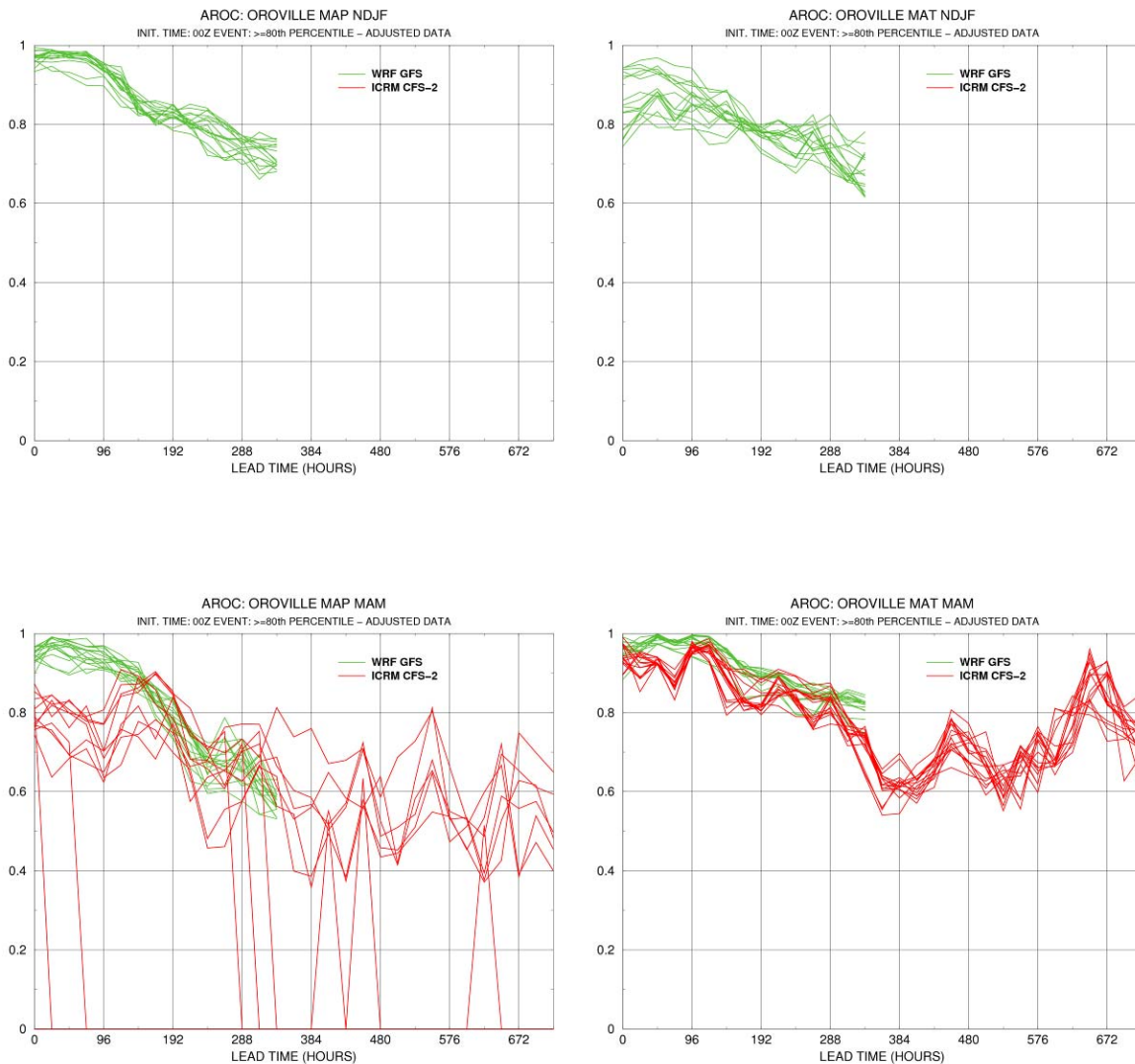
Figure 4.25: Brier Skill Score for MAT and MAP in Oroville Watershed – Post Bias Adjustment



The Oroville watershed area under the Relative Operating Characteristic (AROC) was also examined for the post bias adjustment results. Figure 4.26 exemplifies the results for the Oroville watershed. In this case too there is very little change in the AROC results for all cases apart from those in the low lying subcatchments and for the CFS2-ICRM where the orographic

component produces very few cases exceeding the event threshold (80th percentile), thus making the dataset inappropriate for AROC analysis. Appendix F provides the detailed information and ROC curves for each subcatchment and the reader can see the pathological situations for CFS2-ICRM for which the ROC aligns with the 45-degree axis.

Figure 4.26: AROC Values of MAP and MAT Ensemble Forecasts for the Oroville Watershed Subcatchments – Post Bias Adjustment

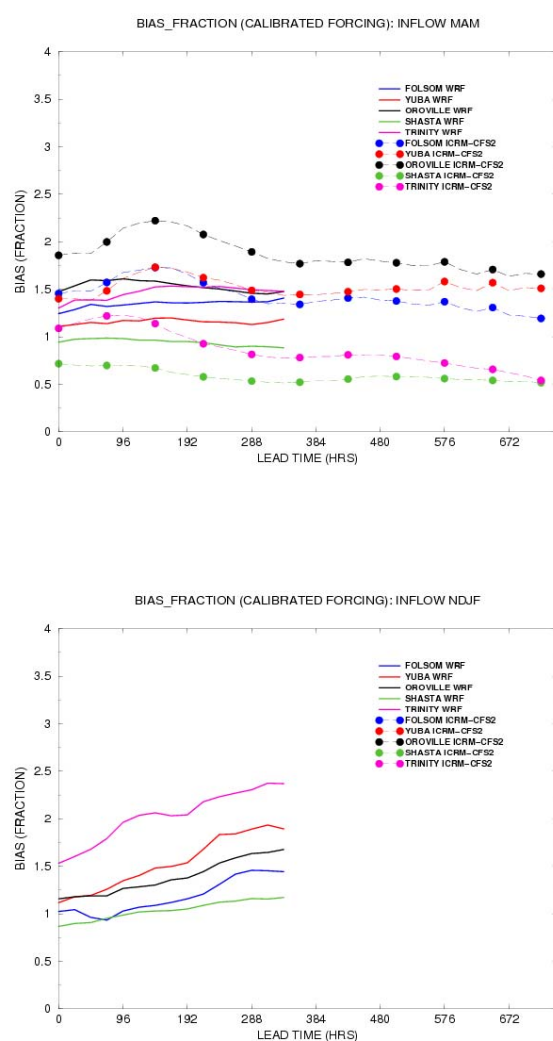


The overall conclusion for the validation of the MAT and MAP bias adjustment procedure is that the probabilistic methodology used provides useful results as it corrects the bias well for most lead times and leaves unaffected the performance of the models with respect to cross-correlations and probabilistic measures (in some cases even improves these results as well). The question is whether such bias adjustments are useful for the reservoir inflow forecasts. Note

that these inflow forecasts depend on both mean areal precipitation and temperature, and that adjustments to those will change the behavior of the snow accumulation and melt that feeds reservoir inflows in the spring time.

Figures 4.27 and 4.28 present the reservoir inflow performance metrics of bias fraction and cross-correlation with observations for all reservoirs, all seasons and both cases of hydrologic-model forcing (GFS-WRF and CFS2-ICRM). The bias results indicate substantial correction with respect to the original reservoir inflow metrics of Figures 4.13 and 4.14 for most basins (the Trinity inflow still maintains high bias for NDJF and for the GFS-WRF for all lead times).

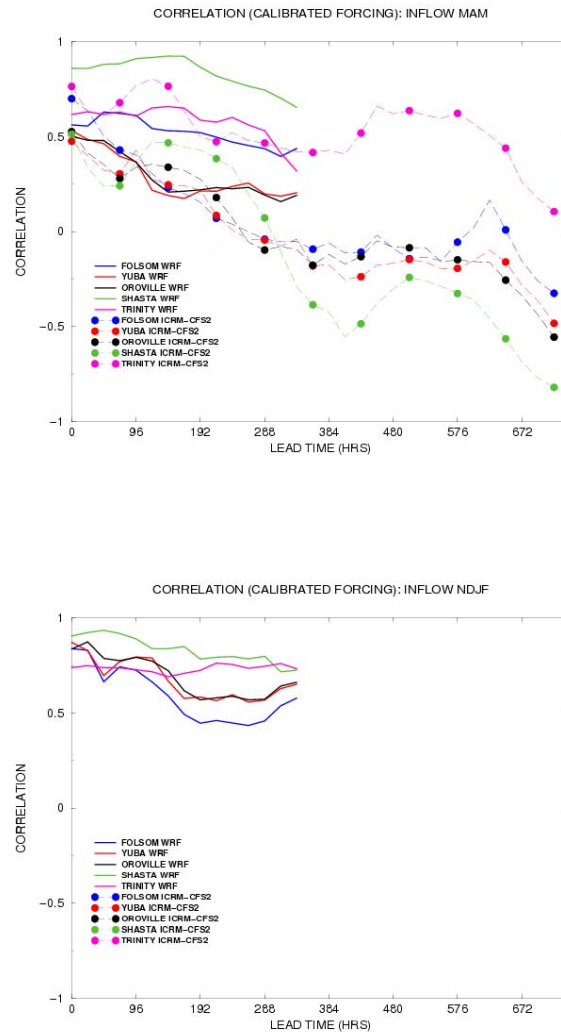
Figure 4.27: Bias Fraction of Reservoir Inflows for the MAM and NDJF Seasons – Post Bias Adjustment



The cross-correlations in Figure 4.28 show slightly modified results than those originally obtained (without bias adjustment in Figures 4.15 and 4.16) except from the CFS2-ICRM forced

hydrologic model forecasts for MAM that have improved (higher correlation values) substantially. The short lead time forecast of the GFS-WRF forced hydrologic model after bias adjustment of MAP and MAT exhibit lower cross-correlations with the observations. This points to the sensitive nature of the dependence of the reservoir inflow forecasts on simultaneous changes on the MAP and MAT forcing.

Figure 4.28: Correlations of Reservoir Inflows for the MAM and NDJF Seasons – Post Bias Adjustment



Probabilistic assessments were made for the reservoir inflow forecast ensembles after bias adjustment of the MAP and MAT as well. Figures 4.29 and 4.30 show the AROC and BSS reservoir-inflow results, respectively, for all cases available. The results indicate moderate improvements with respect to the original results shown in Figures 4.19 through 4.22, particularly for the CFS2-ICRM forcing for the AROC MAM and the GFS-WRF forcing for the

BSS NDJF. Thus, the most important impact of adjusting the MAP and MAT ensemble forecasts for bias is the improvement in the bias of the ensemble reservoir inflow forecasts.

Figure 4.29: AROC for Reservoir Inflows for the MAM and NDJF Seasons – Post Bias Adjustment

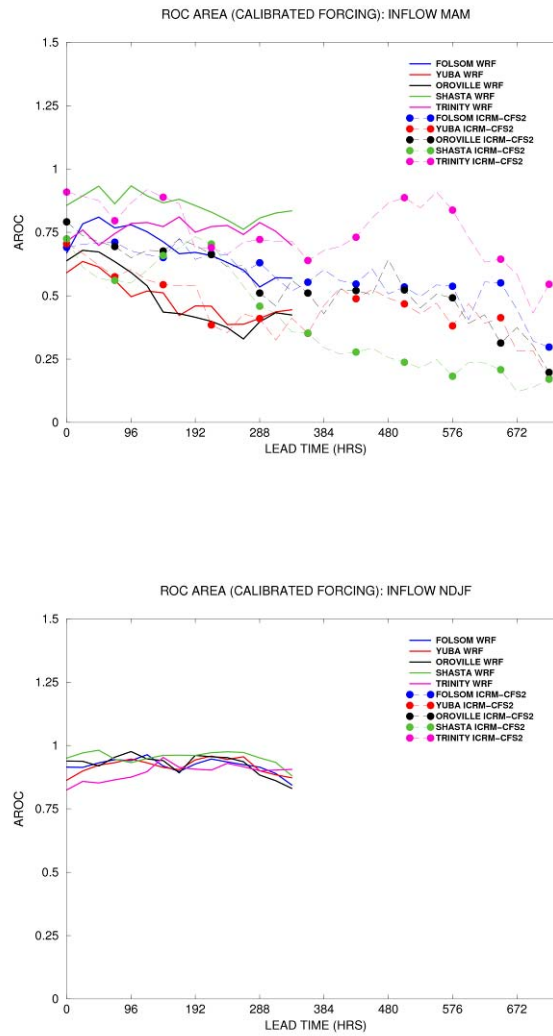
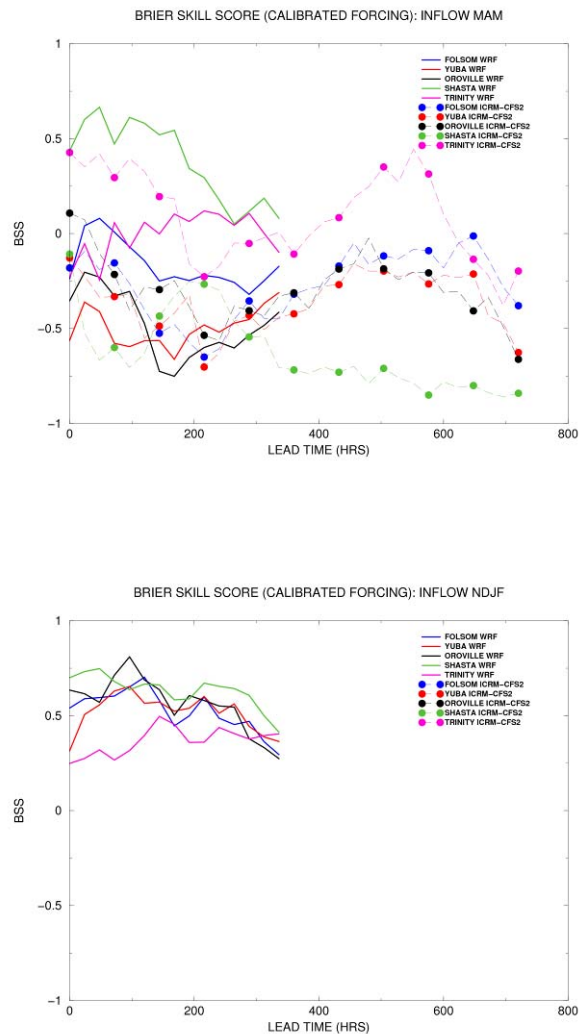


Figure 4.30: BSS for Reservoir Inflows for the MAM and NDJF Seasons – Post Bias Adjustment



4.2 Integrated Forecast-Decision Assessments

Integrated assessments were carried out for 2012. These are presented in the following sections and include long range planning for water quantity and quality objectives, and short range reservoir management for flood control.

4.2.1 Long Range Assessments for 2012 Forecasts

The INFORM long range management model is designed to assess seasonal and interannual tradeoffs that factor into the development of planning strategies aiming to balance this year's water deliveries, carry over storage for the following year, energy generation, river temperature requirements, and Bay Delta environmental conditions. These tradeoffs are generated for consideration by DWR, USBR, USACE, and other relevant stakeholders as they engage in their routine decision processes. After these deliberations, key decisions are made

regarding monthly water delivery contracts, reservoir releases, energy generation, and reservoir coordination strategies.

The long range management model uses monthly inflow forecasts. The forecasts are integrated with the decision models through data exchange. The forecasted inflows are saved in a pre-formatted Excel file. The DSS provides easy tools to read the data in the Excel file and save it into the database. The DSS also provides tools to plot and validate the forecasting results.

Results of integrated forecast-decision applications using the ensemble inflow forecasts for 2012 are presented below.

The application utilizes the following input data:

- Forecasted inflows starting from March 1st, 2012. The forecasts consist of 140 traces, have a nine-month forecast horizon (until the end of November), and are generated for the following five locations: Clair Engle Lake, Shasta, Oroville, Folsom, and Yuba;
- Historical monthly average values are used for locations where forecasted inflows are not available (Table 4.2.1);
- Monthly reservoir parameters and constraints (max, min, and target storages; and evaporation rates; Table 4.2.2);
- Minimum river flow requirements (Table 4.2.3);
- Base monthly demands at all locations (Table 4.2.4);
- Reservoir initial storages on March 1st, 2012, are set equal to their actual values.

4.2.1.1 Inflow Forecasts

The forecasted monthly inflow ensembles are shown in Figure 4.2.1. A comparison between the forecasted inflow mean and the corresponding historical means for the four major reservoirs are plotted in Figures 4.2.2 through 4.2.5. As shown, the forecasted inflow means at all four locations are lower than their historical means. Figure 4.2.6 shows the forecasted basin total inflow means for 2006 to 2012, excluding 2011 for which the forecasting system was being revised. The figure shows that the 2012 basin inflow forecasts are the lowest among the previous five years. Overall, the 2012 average forecasts indicate that 2012 will be approximately 23 percent drier than the average year. Figure 4.2.7 shows the initial reservoir storages on March 1st for the six years in this study. These values indicate a good recovery of the system storage during 2011, with the March 1st storages being close to their 2007 levels.

Figures 4.2.8 and 4.2.9 present the forecasts issued on December 1, 2011, January 1, 2012, February 1, 2012, and March 1, 2012. It is notable that the Trinity inflow forecasts are consistently shifted earlier relative to the historical inflows by one month. Also, the Folsom forecasts exhibit a significant increase from December to March.

4.2.1.2 Water Deliveries and Energy Generation

Using the forecasted inflows, the INFORM DSS generates planning tradeoffs by varying the base demands (water delivery commitments) at all locations from 60 percent to 110 percent. The

tradeoffs between the total reservoir carryover storage (i.e., the combined storage in Trinity, Shasta, Oroville, and Folsom at the end of the forecast horizon) versus the water deliveries and the system energy versus the water deliveries are depicted in Figures 4.2.10 and 4.2.11. As water deliveries increase, the system carryover storage decreases, but energy generation increases due to higher reservoir releases. The results show that the system can meet water deliveries up to 4,753 TAF. Meeting demands beyond this level would result in significant reservoir drawdown (especially at Shasta and Oroville) and diminished carryover storage.

Figure 4.2.12 compares the water deliveries over the 2006-2012 period (except 2011) assuming the actual initial storages and approximately the same system carryover storage of 7,500 TAF. As shown, the expected water deliveries are reduced by 23 percent compared to 2006 and 14 percent compared to 2007, but increased by 130 percent compared to 2008, 155 percent to 2009, and 27 percent to 2010. Similarly, average system energy generation for 2012 is shown in Figure 4.2.13 showing a decrease of 30 percent relative to 2006 and 20 percent relative to 2007, but an increase of 37 percent relative to 2008, 46 percent relative to 2009, and 22 percent relative to 2010. In summary, the forecast for 2012 portends a wetter year than the three previous years 2008, 2009, 2010, but a drier year than 2006, 2007, and the historical average year.

Selected reservoir elevation, release, and energy generation sequences corresponding to the 3rd tradeoff point in the middle of the tradeoff range (and to 3,541 TAF total water deliveries) are shown in Figures 4.2.14, 4.2.15, and 4.2.16.

4.2.1.3 Delta X2 Location and Delta Outflow

The X2 location sequences for the 3rd tradeoff point are shown in Figure 4.2.17, indicating all traces below 80 km, the maximum constraint set in the study. The X2 location meets this requirement for this and all other tradeoff points. The Delta outflow sequences are plotted in Figure 4.2.18.

Figure 4.2.1: Long Range Inflow Forecasts

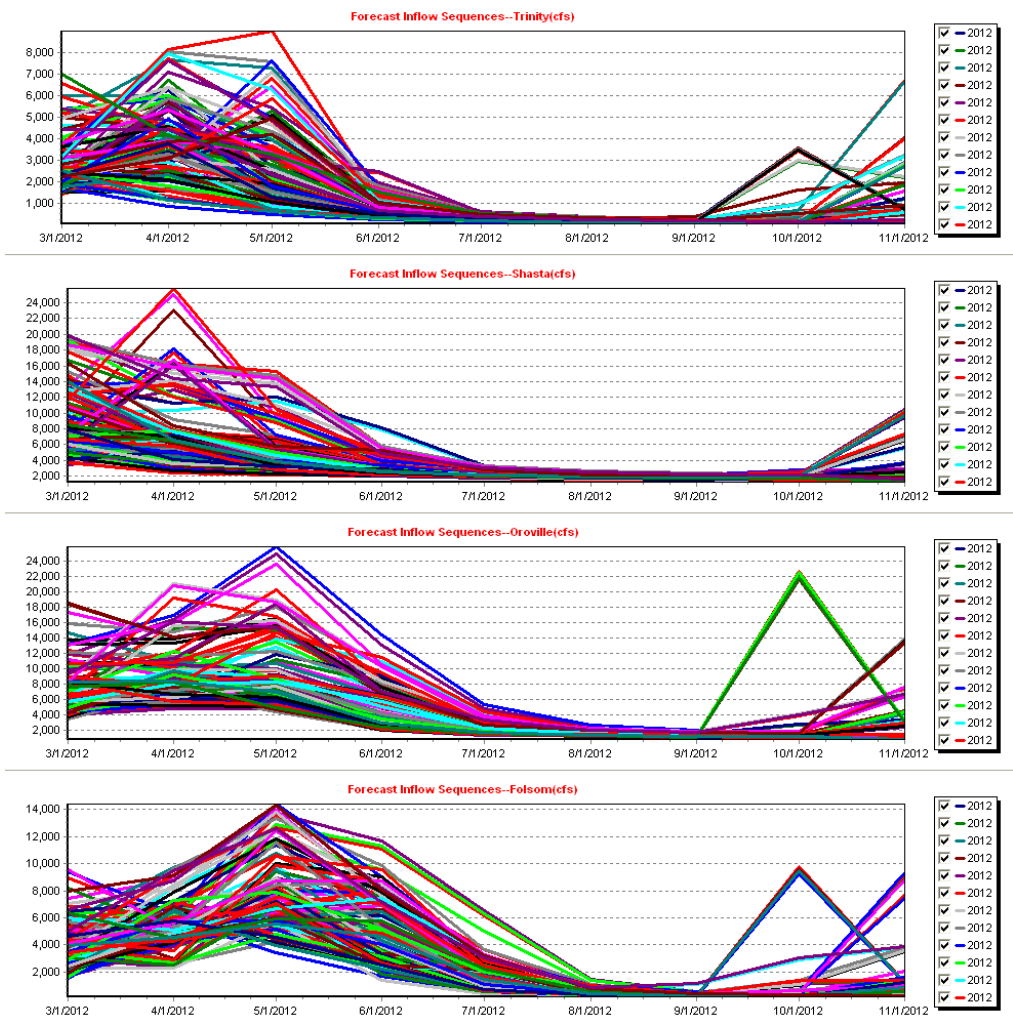


Figure 4.2.2: Inflow Forecast Comparison, Forecast vs. Historical Mean; Trinity

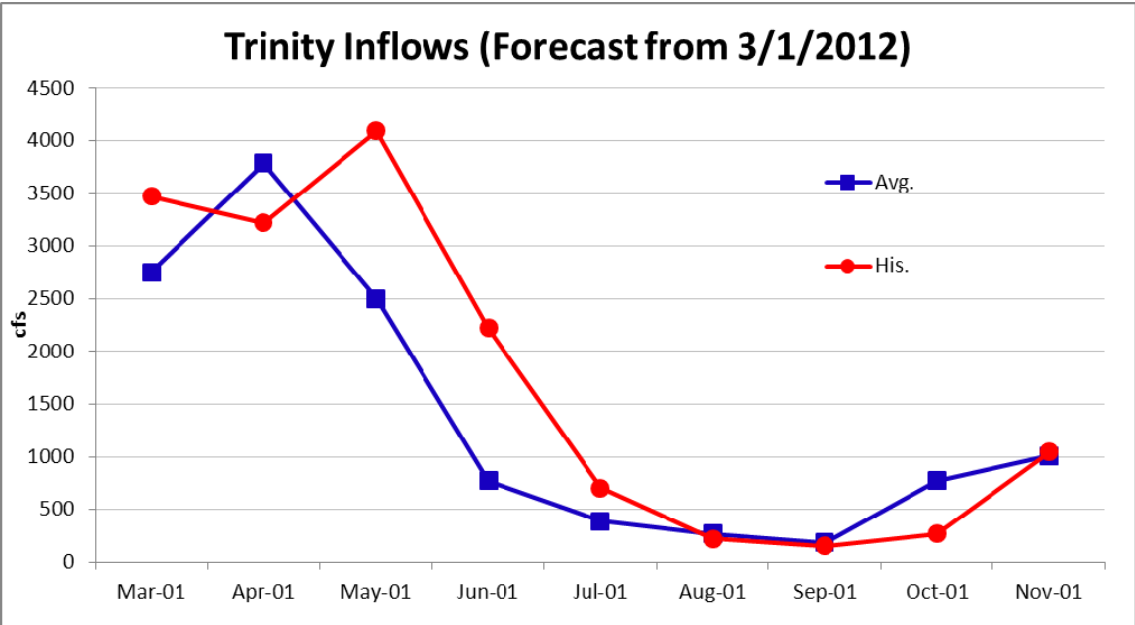


Figure 4.2.3: Inflow Forecast Comparison, Forecast vs. Historical Mean; Shasta

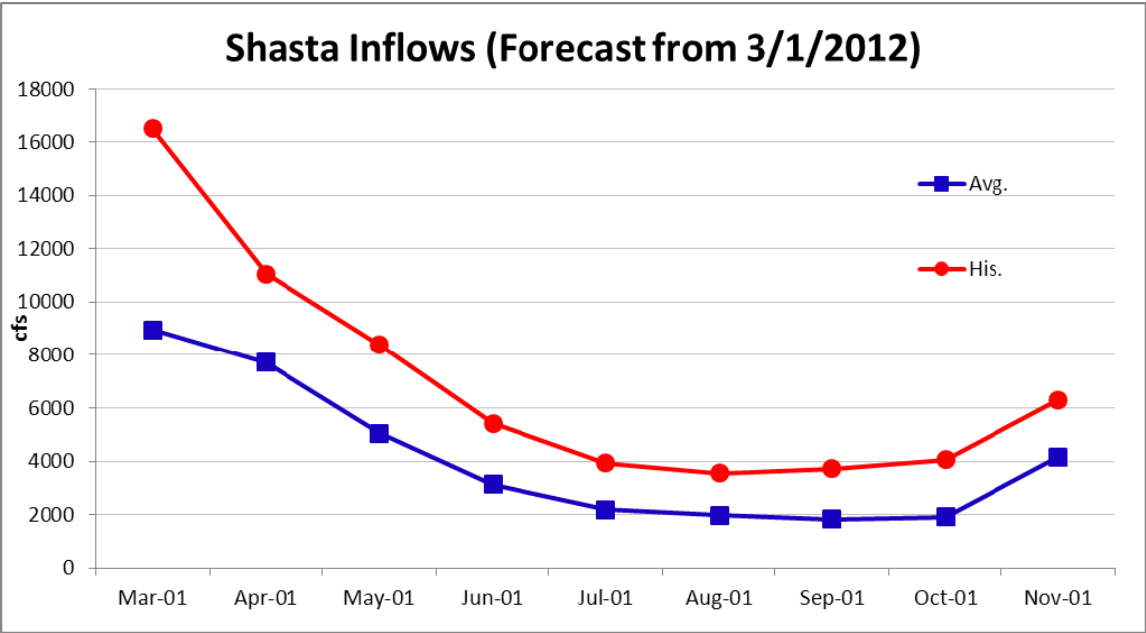


Figure 4.2.4: Inflow Forecast Comparison, Forecast vs. Historical Mean; Oroville

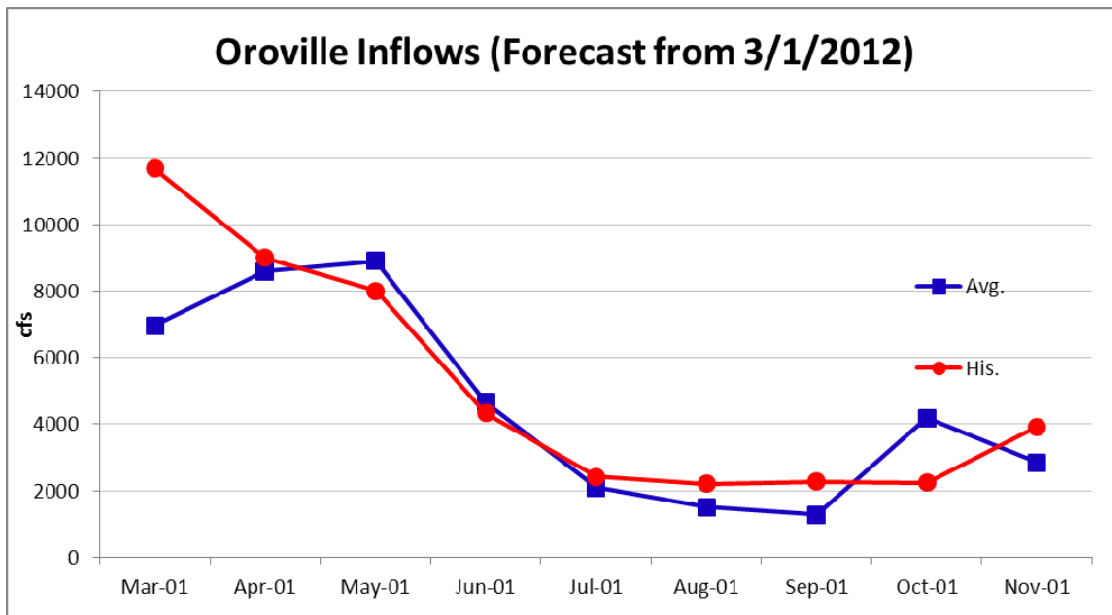


Figure 4.2.5: Inflow Forecast Comparison, Forecast vs. Historical Mean; Folsom

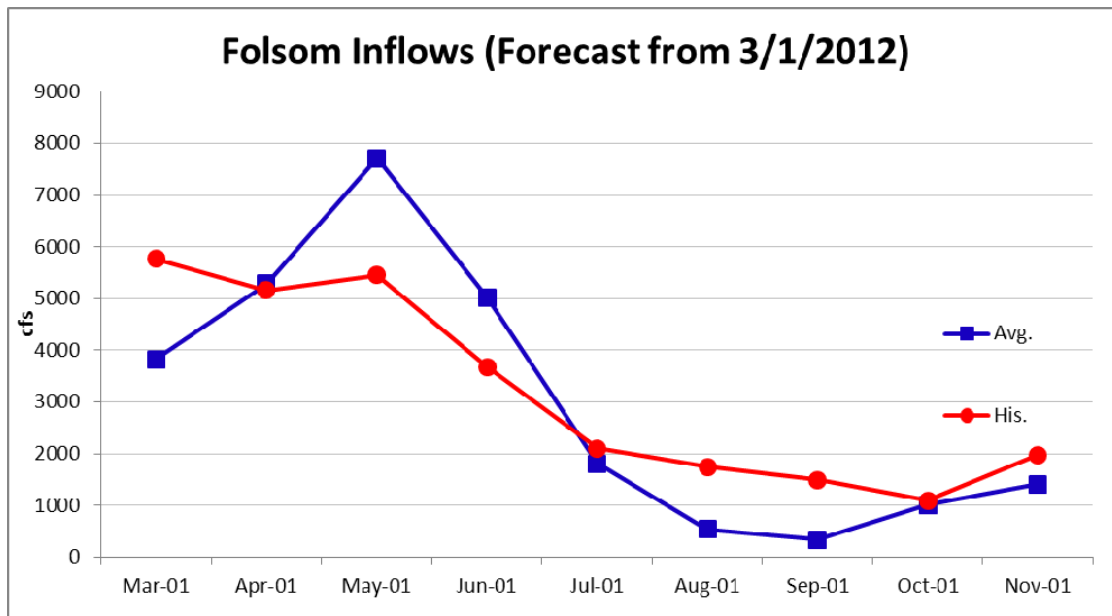


Figure 4.2.6: Average Basin Inflow Comparisons

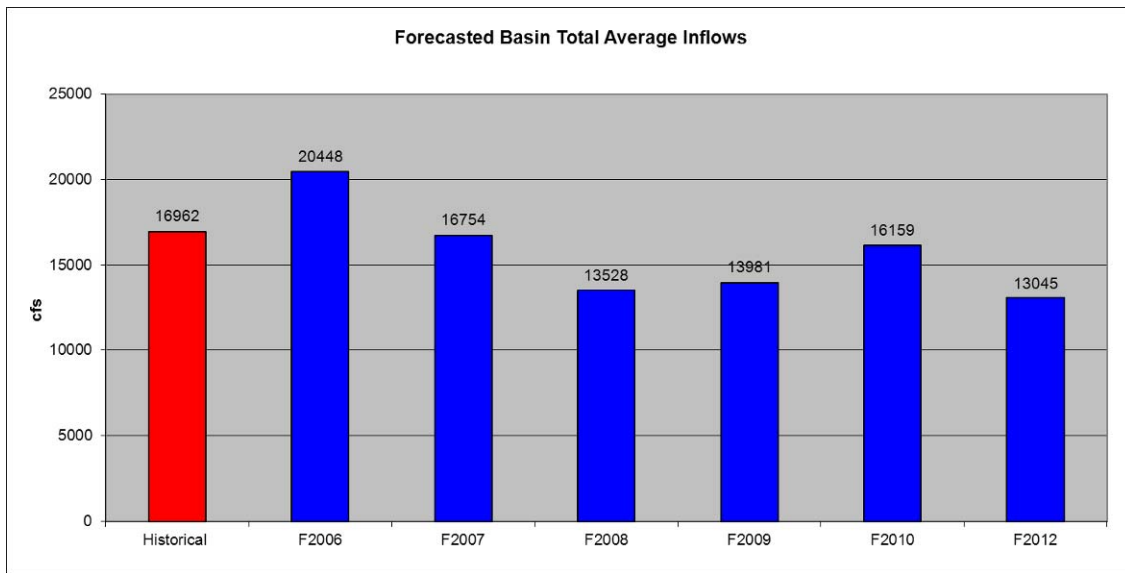


Figure 4.2.7: Reservoir Storages on March 1st

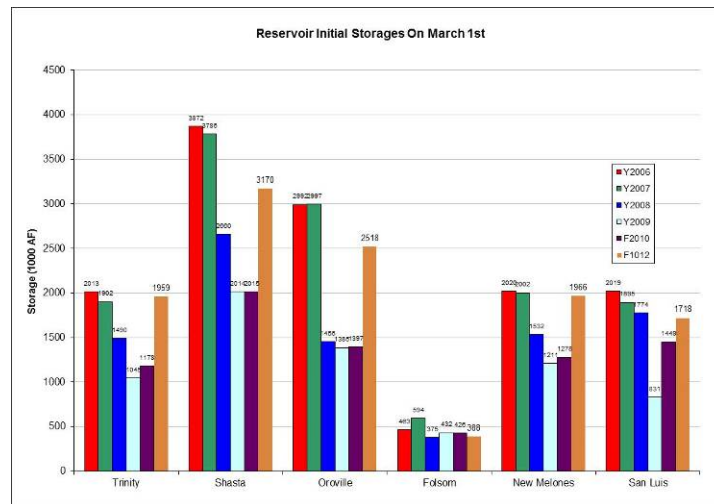


Figure 4.2.8: Monthly Forecast Updates; Trinity and Shasta

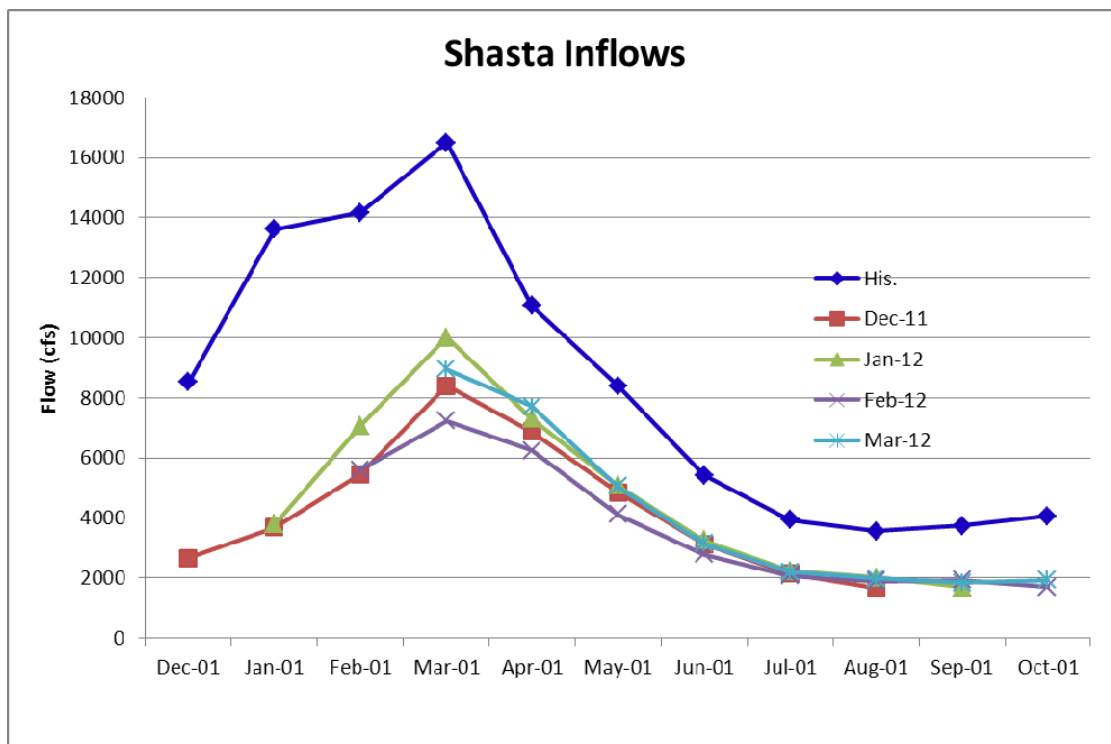
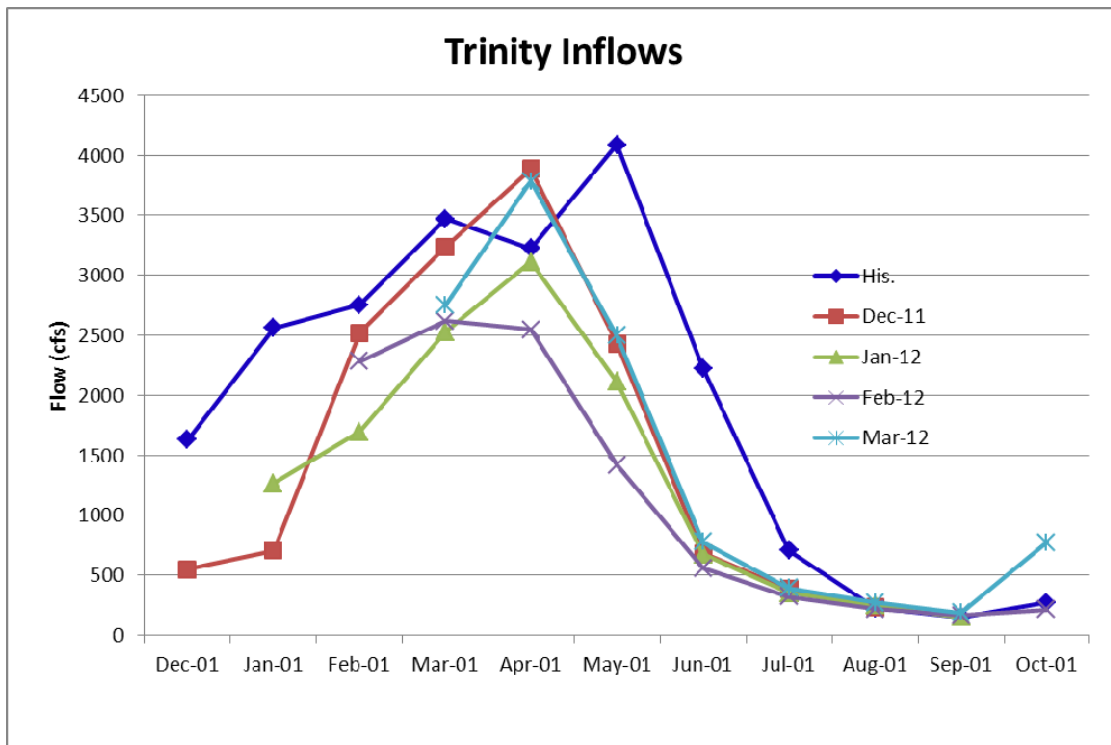


Figure 4.2.9: Monthly Forecast Updates; Oroville and Folsom

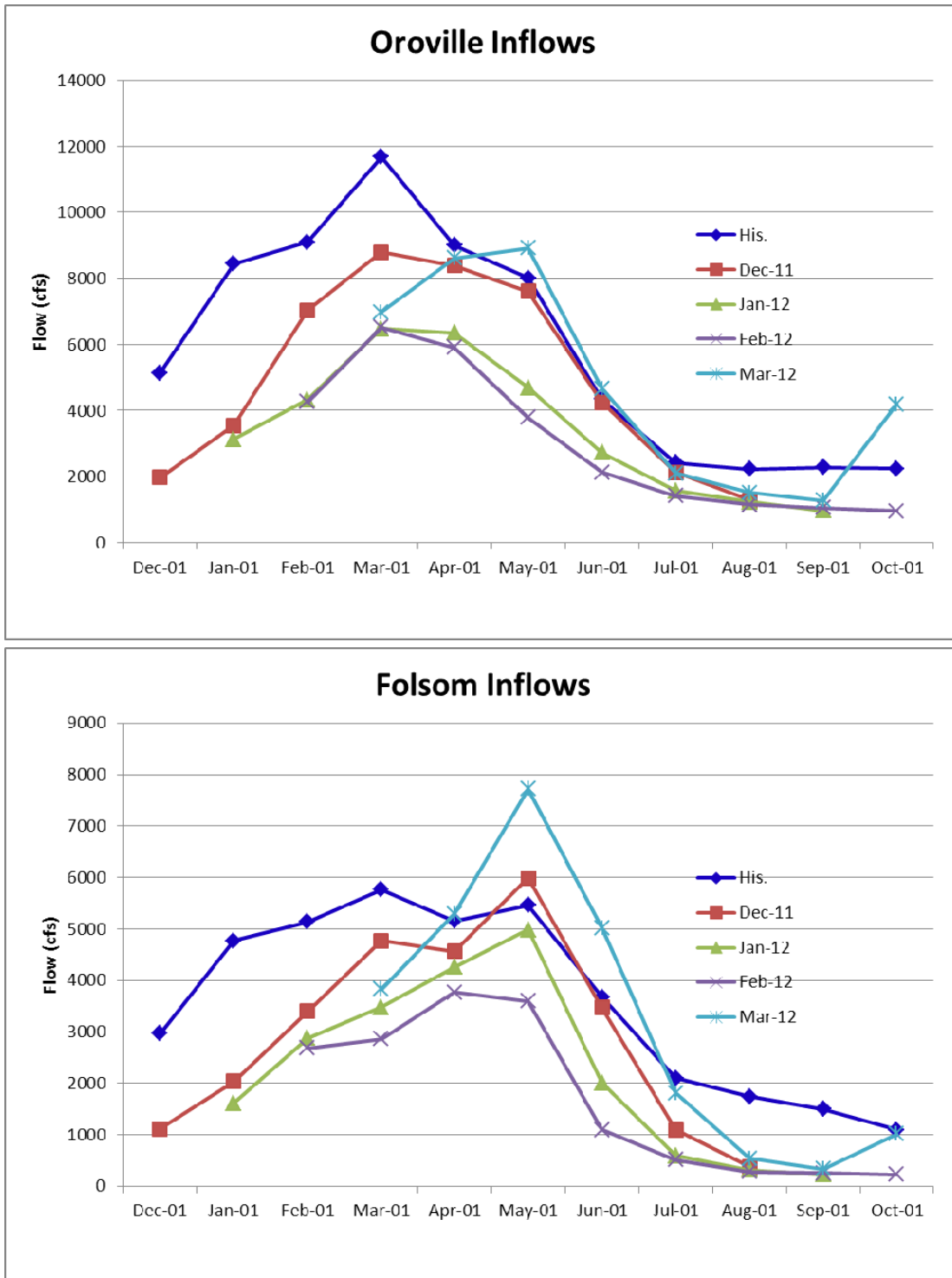


Figure 4.2.10: Water Deliveries vs. Carryover Storage Tradeoff

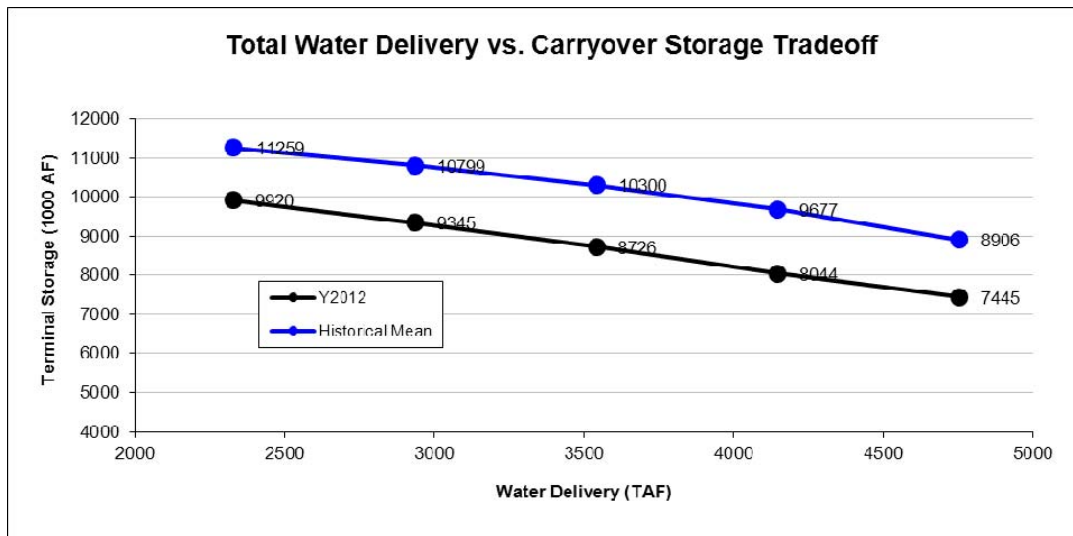


Figure 4.2.11: Water Deliveries vs. Energy Generation Tradeoff

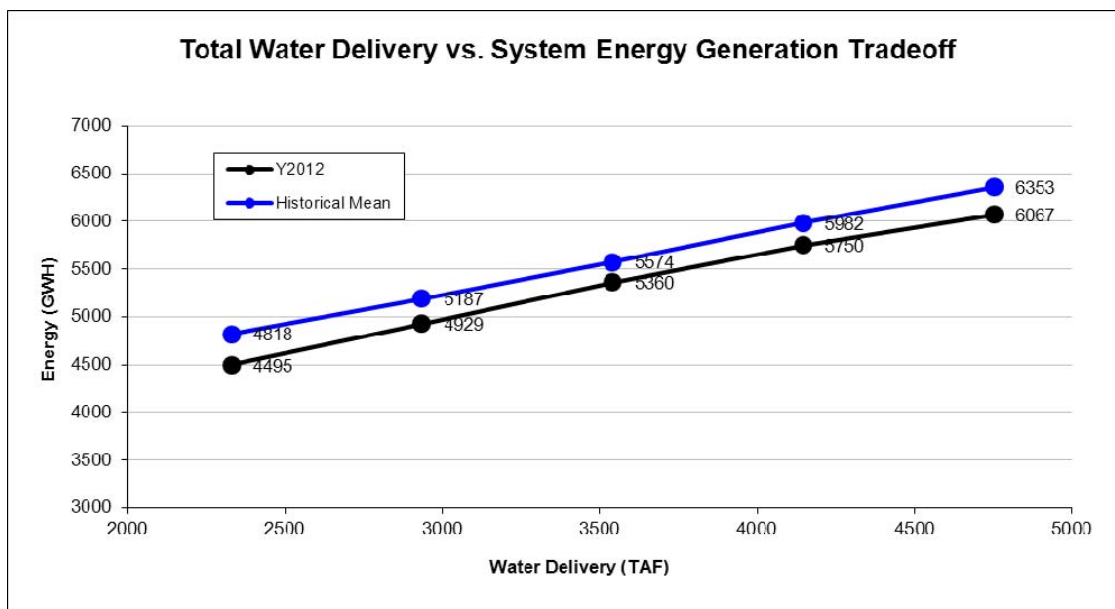


Figure 4.2.12: Mean Water Delivery Comparison

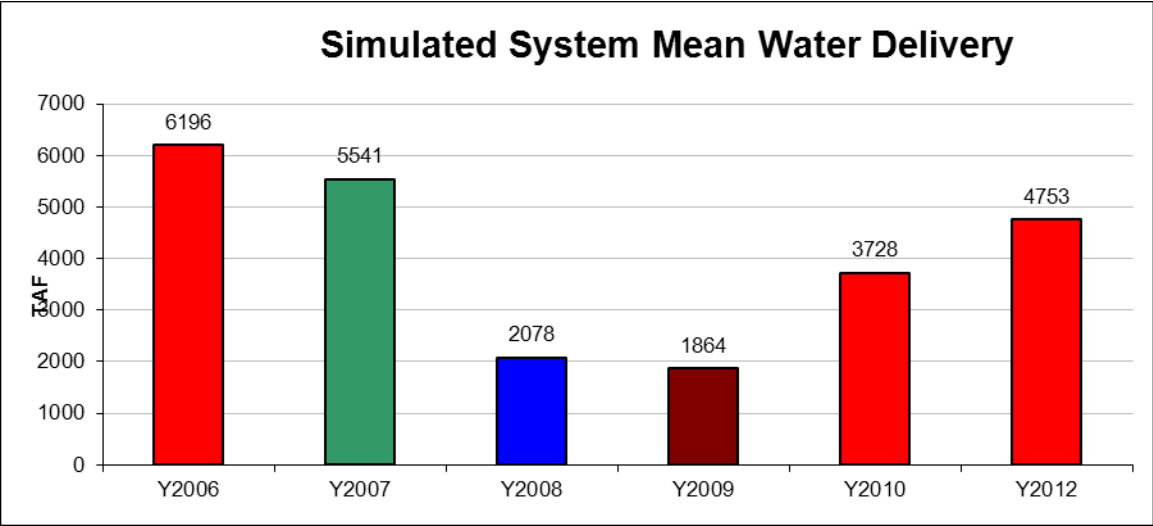


Figure 4.2.13: Mean Energy Generation Comparison

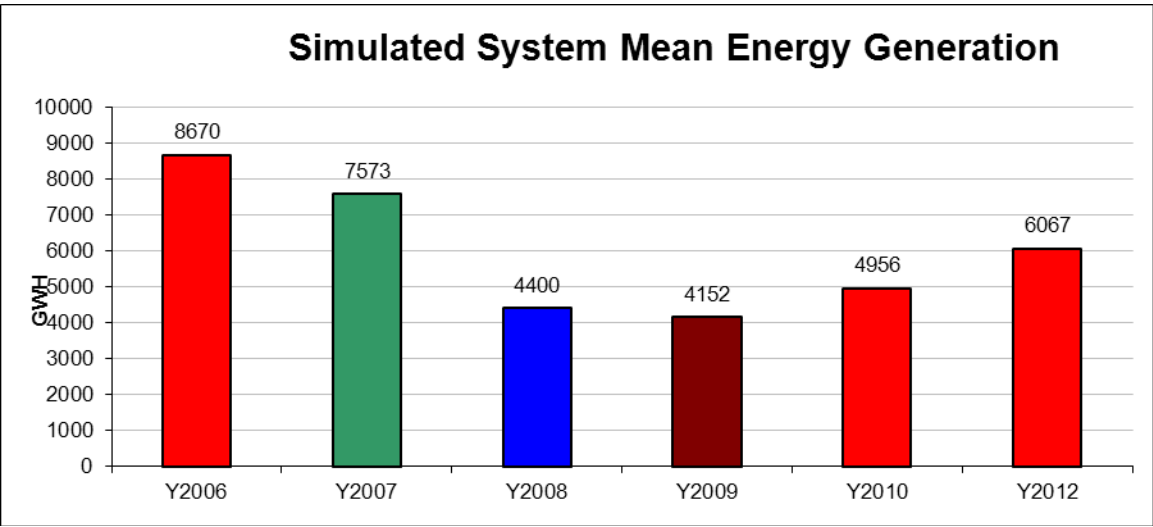


Figure 4.2.14: Reservoir Elevation Sequences for the 3rd Tradeoff Point

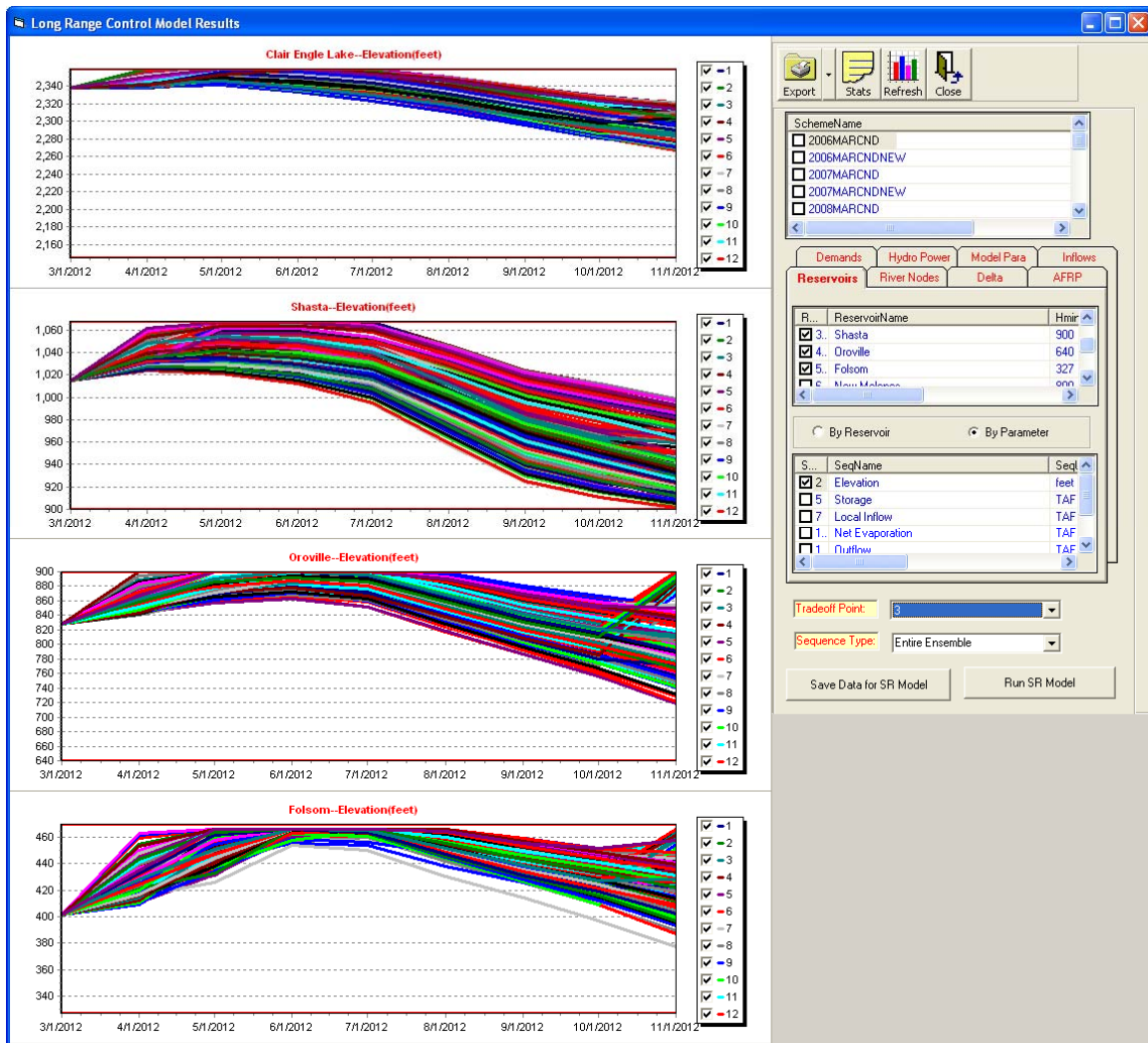


Figure 4.2.15: Reservoir Release Sequences for the 3rd Tradeoff Point

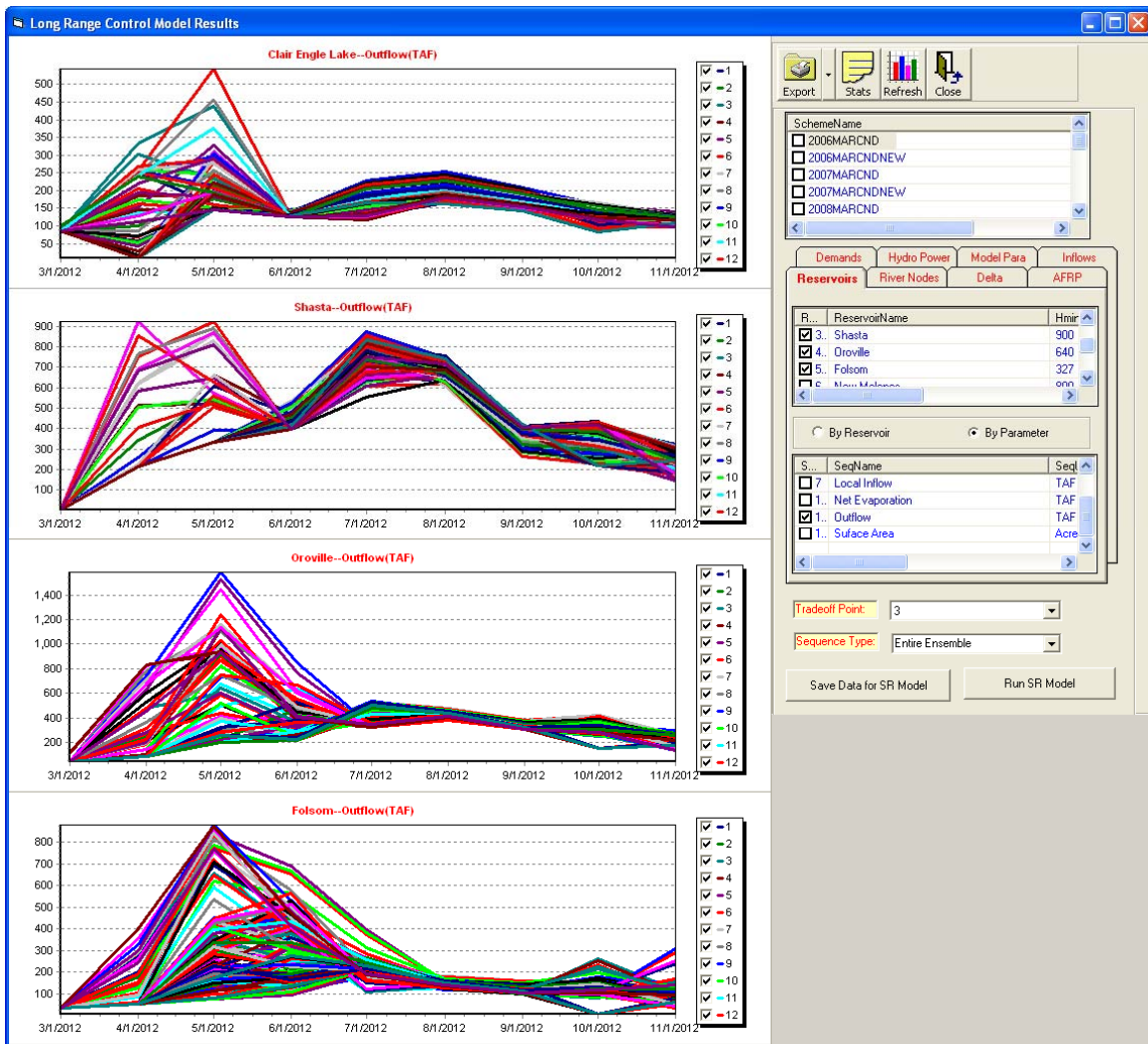


Figure 4.2.16: Reservoir Energy Generation Sequences for the 3rd Tradeoff Point

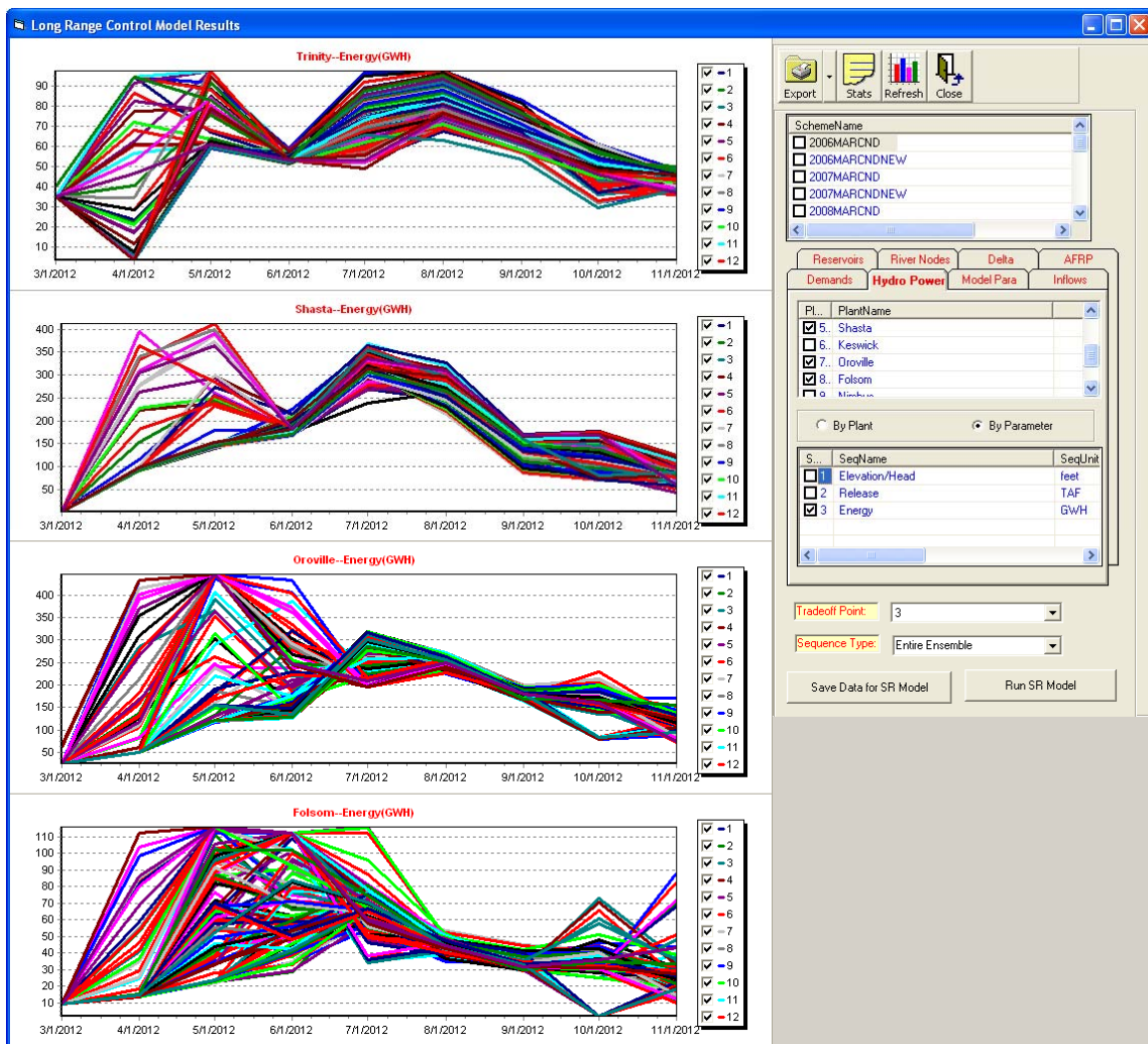


Figure 4.2.17: Delta X2 Location Sequences for the 3rd Tradeoff Point

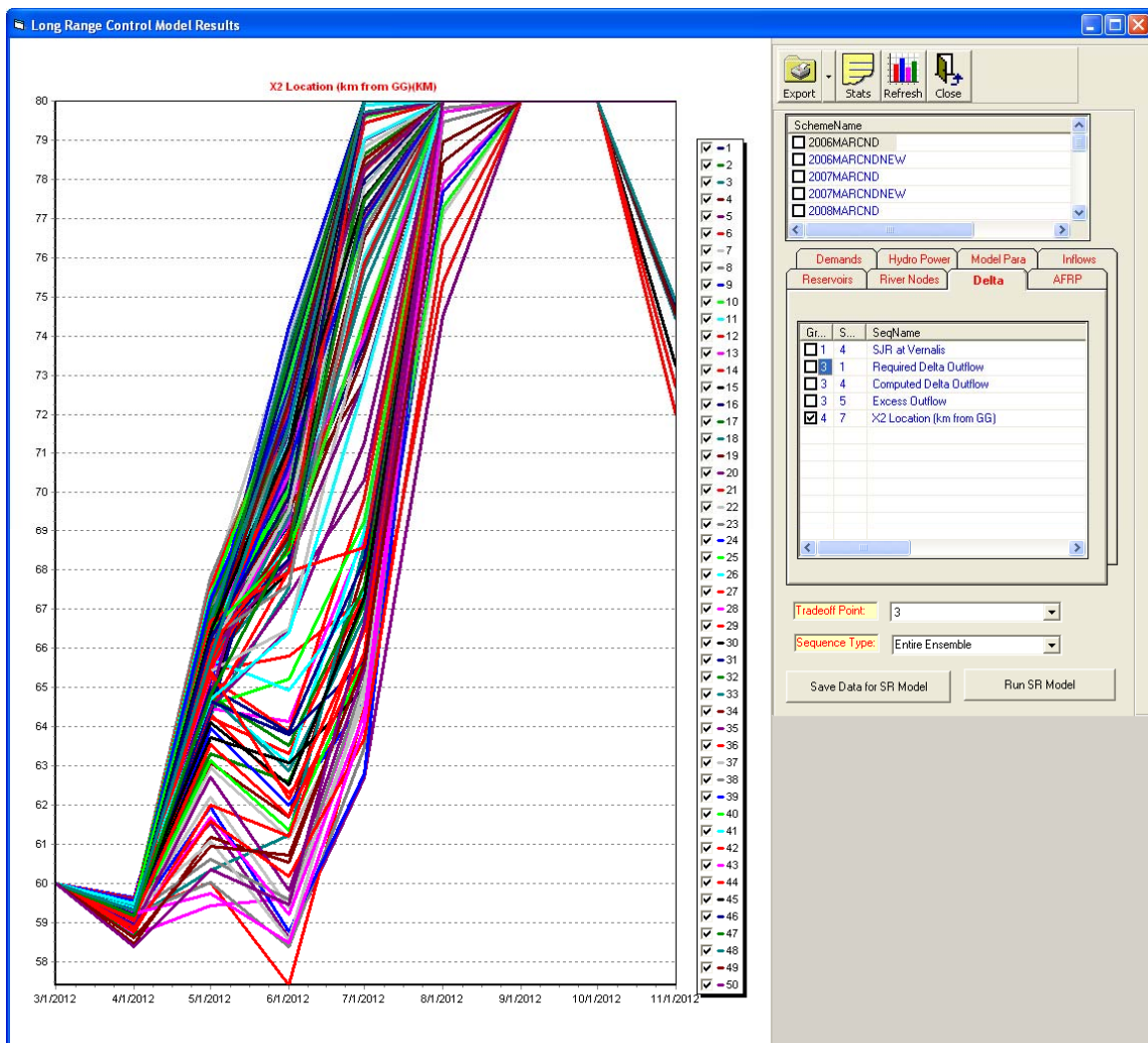


Figure 4.2.18: Delta Outflow Sequences for the 3rd Tradeoff Point

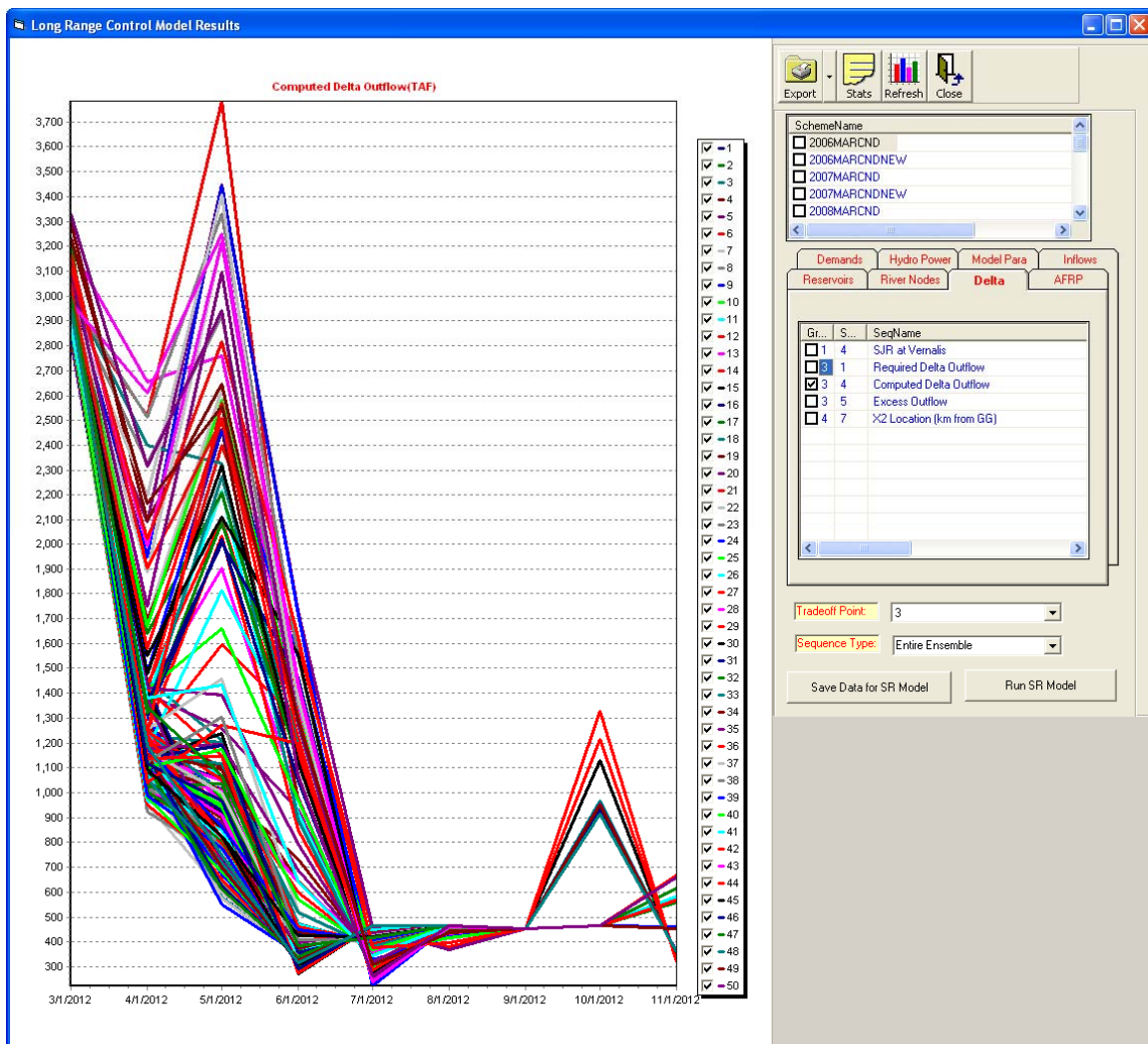


Table 4.2.1: Monthly Average Inflows for Selected Locations (TAF)

Month	Whisktown	Keswick-Wilkens	Sacrament Misc	Eastside Streams	Delta Misc Creeks	New Melones	SJR
Jan	8.	-211.27	-100.	80.67	25.5	76.	133.
Feb	4.	-299.69	-220.	60.44	25.5	43.	31.
Mar	2.	-370.28	-330.	20.72	29.	34.	33.
Apr	1.	-267.47	-175.	21.89	19.	33.	28.
May	1.	-117.56	45.	28.71	11.1	31.	33.
Jun	2.	-125.	-15.	33.2	0.8	30.	71.
Jul	2.	-31.24	121.	30.74	0.9	30.	62.
Aug	4.	564.46	981.	21.52	1.2	30.	63.
Sep	8.	841.7	1465.	21.52	1.8	30.	78.
Oct	12.	1767.58	2482.	40.03	32.3	40.	94.
Nov	45.	1021.	1763.	67.33	17.4	70.	103.
Dec	16.	74.65	328.	146.34	15.4	110.	126.

Table 4.2.2: Monthly Reservoir Parameters

Name	Month	Smax (TAF)	Smin (TAF)	Starget (TAF)	Evap Rate (feet)
Clair Engle	Jan	2287.00	312.63	2287.00	0.17
Clair Engle	Feb	2287.00	312.63	2287.00	0.13
Clair Engle	Mar	2287.00	312.63	2287.00	0.20
Clair Engle	Apr	2287.00	312.63	2287.00	0.39
Clair Engle	May	2287.00	312.63	2287.00	0.51
Clair Engle	Jun	2287.00	312.63	2287.00	0.58
Clair Engle	Jul	2287.00	312.63	2287.00	0.76
Clair Engle	Aug	2287.00	312.63	2287.00	0.71
Clair Engle	Sep	2287.00	312.63	2287.00	0.60
Clair Engle	Oct	2287.00	312.63	2287.00	0.30
Clair Engle	Nov	2287.00	312.63	2287.00	0.15
Clair Engle	Dec	2287.00	312.63	2287.00	0.09
WhiskeyTown	Jan	237.90	200.00	205.70	0.17
WhiskeyTown	Feb	237.90	200.00	205.70	0.13
WhiskeyTown	Mar	237.90	200.00	205.70	0.20
WhiskeyTown	Apr	237.90	200.00	237.90	0.39
WhiskeyTown	May	237.90	200.00	237.90	0.51
WhiskeyTown	Jun	237.90	200.00	237.90	0.58
WhiskeyTown	Jul	237.90	200.00	237.90	0.76
WhiskeyTown	Aug	237.90	200.00	237.90	0.71
WhiskeyTown	Sep	237.90	200.00	238.00	0.60
WhiskeyTown	Oct	237.90	200.00	230.00	0.30
WhiskeyTown	Nov	237.90	200.00	205.70	0.15
WhiskeyTown	Dec	237.90	200.00	205.70	0.09

Name	Month	Smax (TAF)	Smin (TAF)	Starget (TAF)	Evap Rate (feet)
Shasta	Jan	4552	1168	4552	0.17
Shasta	Feb	4552	1168	4552	0.13
Shasta	Mar	4552	1168	4552	0.20
Shasta	Apr	4552	1168	4552	0.39
Shasta	May	4552	1168	4552	0.51
Shasta	Jun	4552	1168	4552	0.58
Shasta	Jul	4552	1168	3882	0.76
Shasta	Aug	4552	1168	3252	0.71
Shasta	Sep	4552	1168	3252	0.60
Shasta	Oct	4552	1168	3872	0.30
Shasta	Nov	4552	1168	4252	0.15
Shasta	Dec	4552	1168	4552	0.09
Oroville	Jan	3538	855	3458	0.17
Oroville	Feb	3538	855	3538	0.13
Oroville	Mar	3538	855	3538	0.20
Oroville	Apr	3538	855	3538	0.39
Oroville	May	3538	855	3538	0.51
Oroville	Jun	3538	855	3343	0.58
Oroville	Jul	3538	855	3163	0.76
Oroville	Aug	3538	855	3163	0.71
Oroville	Sep	3538	855	3163	0.60
Oroville	Oct	3538	855	3163	0.30
Oroville	Nov	3538	855	3163	0.15
Oroville	Dec	3538	855	3163	0.09
Folsom	Jan	975	83	805	0.17

Name	Month	Smax (TAF)	Smin (TAF)	Starget (TAF)	Evap Rate (feet)
Folsom	Feb	975	83	975	0.13
Folsom	Mar	975	83	975	0.20
Folsom	Apr	975	83	975	0.39
Folsom	May	975	83	975	0.51
Folsom	Jun	975	83	975	0.58
Folsom	Jul	975	83	700	0.76
Folsom	Aug	975	83	575	0.71
Folsom	Sep	975	83	575	0.60
Folsom	Oct	975	83	575	0.30
Folsom	Nov	975	83	575	0.15
Folsom	Dec	975	83	675	0.09
New Melones	Jan	2420	273	2230	0.17
New Melones	Feb	2420	273	2420	0.13
New Melones	Mar	2420	273	2420	0.20
New Melones	Apr	2420	273	2420	0.39
New Melones	May	2420	273	2420	0.51
New Melones	Jun	2420	273	2270	0.58
New Melones	Jul	2420	273	1970	0.76
New Melones	Aug	2420	273	1970	0.71
New Melones	Sep	2420	273	1970	0.60
New Melones	Oct	2420	273	1970	0.30
New Melones	Nov	2420	273	1970	0.15
New Melones	Dec	2420	273	2040	0.09
Tulloch	Jan	67	57	57	0.00
Tulloch	Feb	67	57	57	0.00

Name	Month	Smax (TAF)	Smin (TAF)	Starget (TAF)	Evap Rate (feet)
Tulloch	Mar	67	57	58	0.00
Tulloch	Apr	67	57	60	0.00
Tulloch	May	67	57	67	0.00
Tulloch	Jun	67	57	67	0.00
Tulloch	Jul	67	57	67	0.00
Tulloch	Aug	67	57	67	0.00
Tulloch	Sep	67	57	62	0.00
Tulloch	Oct	67	57	57	0.00
Tulloch	Nov	67	57	57	0.00
Tulloch	Dec	67	57	57	0.00
San Luis	Jan	2027	450.00	1000.00	0.17
San Luis	Feb	2027	631.60	1464.02	0.13
San Luis	Mar	2027	748.10	1806.84	0.20
San Luis	Apr	2027	835.60	1975.02	0.39
San Luis	May	2027	879.92	1976.43	0.51
San Luis	Jun	2027	694.72	1546.00	0.58
San Luis	Jul	2027	442.12	1062.95	0.76
San Luis	Aug	2027	181.12	642.62	0.71
San Luis	Sep	2027	9.72	352.64	0.60
San Luis	Oct	2027	8.32	312.90	0.30
San Luis	Nov	2027	115.02	354.13	0.15
San Luis	Dec	2027	286.72	514.21	0.09

Table 4.2.3: Monthly Minimum and Target River Flows

Name	Month	Rmin (cfs)	Rtarget (cfs)
Lewiston	Jan	300	300
Lewiston	Feb	300	300
Lewiston	Mar	300	300
Lewiston	Apr	300	300
Lewiston	May	3939	300
Lewiston	Jun	2507	783
Lewiston	Jul	1102	450
Lewiston	Aug	450	450
Lewiston	Sep	450	450
Lewiston	Oct	373	0
Lewiston	Nov	300	300
Lewiston	Dec	300	300
Clear Creek	Jan	150	150
Clear Creek	Feb	200	200
Clear Creek	Mar	200	200
Clear Creek	Apr	200	200
Clear Creek	May	200	200
Clear Creek	Jun	200	200
Clear Creek	Jul	200	200
Clear Creek	Aug	200	200
Clear Creek	Sep	200	200
Clear Creek	Oct	200	200
Clear Creek	Nov	90	90
Clear Creek	Dec	90	90

Name	Month	Rmin (cfs)	Rtarget (cfs)
Spring Creek	Jan	325	325
Spring Creek	Feb	306	306
Spring Creek	Mar	2749	2749
Spring Creek	Apr	252	252
Spring Creek	May	813	813
Spring Creek	Jun	1681	1681
Spring Creek	Jul	2602	2602
Spring Creek	Aug	2114	2114
Spring Creek	Sep	2017	2017
Spring Creek	Oct	1138	1138
Spring Creek	Nov	504	504
Spring Creek	Dec	244	244
Keswick	Jan	3250	3250
Keswick	Feb	3250	3250
Keswick	Mar	3250	3250
Keswick	Apr	8000	8000
Keswick	May	9600	9600
Keswick	Jun	11000	11000
Keswick	Jul	14500	14500
Keswick	Aug	12000	12000
Keswick	Sep	5500	5500
Keswick	Oct	7200	7200
Keswick	Nov	5700	5700
Keswick	Dec	3250	3250
Wilkins	Jan	0	0

Name	Month	Rmin (cfs)	Rtarget (cfs)
Wilkins	Feb	0	0
Wilkins	Mar	0	0
Wilkins	Apr	5000	5000
Wilkins	May	5000	5000
Wilkins	Jun	5000	5000
Wilkins	Jul	5000	5000
Wilkins	Aug	5000	5000
Wilkins	Sep	5000	5000
Wilkins	Oct	5000	5000
Wilkins	Nov	0	0
Wilkins	Dec	0	0
FeatherBelowThermalito	Jan	1250	0
FeatherBelowThermalito	Feb	1250	0
FeatherBelowThermalito	Mar	1250	0
FeatherBelowThermalito	Apr	1250	0
FeatherBelowThermalito	May	2030	0
FeatherBelowThermalito	Jun	0	2706
FeatherBelowThermalito	Jul	0	5692
FeatherBelowThermalito	Aug	5040	5156
FeatherBelowThermalito	Sep	0	4386
FeatherBelowThermalito	Oct	1980	2683
FeatherBelowThermalito	Nov	1750	1815
FeatherBelowThermalito	Dec	1250	0
AmericanRiverbelowNimbus	Jan	800	0
AmericanRiverbelowNimbus	Feb	800	0

Name	Month	Rmin (cfs)	Rtarget (cfs)
AmericanRiverbelowNimbus	Mar	1000	0
AmericanRiverbelowNimbus	Apr	1500	0
AmericanRiverbelowNimbus	May	2300	0
AmericanRiverbelowNimbus	Jun	1800	0
AmericanRiverbelowNimbus	Jul	0	0
AmericanRiverbelowNimbus	Aug	0	0
AmericanRiverbelowNimbus	Sep	0	0
AmericanRiverbelowNimbus	Oct	0	0
AmericanRiverbelowNimbus	Nov	1000	0
AmericanRiverbelowNimbus	Dec	800	0
Goodwin	Jan	175	175
Goodwin	Feb	150	150
Goodwin	Mar	268	268
Goodwin	Apr	760	760
Goodwin	May	800	800
Goodwin	Jun	561	561
Goodwin	Jul	396	396
Goodwin	Aug	352	352
Goodwin	Sep	240	240
Goodwin	Oct	200	200
Goodwin	Nov	200	200
Goodwin	Dec	200	200
DeltaExit	Jan	6001	6001
DeltaExit	Feb	11398	11398
DeltaExit	Mar	11401	11401

Name	Month	Rmin (cfs)	Rtarget (cfs)
DeltaExit	Apr	7848	7848
DeltaExit	May	9319	9319
DeltaExit	Jun	7092	7092
DeltaExit	Jul	6505	6505
DeltaExit	Aug	4261	4261
DeltaExit	Sep	3008	3008
DeltaExit	Oct	4001	4001
DeltaExit	Nov	4655	4655
DeltaExit	Dec	4505	4505

Table 4.2.4: Monthly Water Delivery Targets

Month	Jan	Feb	Mar	Apr	May	Jun	Jul	Aug	Sep	Oct	Nov	Dec
Thermolito	35	0	11	67	189	178	200	178	78	95	104	71
Folsom Pumping	4	4	4	7	8	12	13	12	10	7	5	4
Folsom South Canal	1	1	1	1	2	3	4	4	3	2	1	1
OID/SSJID	0	0	14	60	90	90	95	95	74	14	0	0
CVP Contractors	0	0	0	0	0	0	0	0	0	0	0	0
CCWD	14	17	18	18	14	14	13	13	13	10	11	13
Barker Slough	2	2	1	2	4	5	7	7	6	5	3	3
Federal Tracy PP	258	233	258	250	135	169	270	268	260	258	250	258
Federal Banks On-Peak	0	0	0	0	0	0	28	28	28	0	0	0
State Banks PP	390	355	241	68	108	125	271	278	238	175	193	390
State Tracy PP	0	0	0	0	0	0	0	0	0	0	0	0
Delta Mendota Canal	30	60	100	120	190	220	270	240	180	110	40	30
Federal Dos Amigos	40	50	60	70	110	180	238	178	68	30	30	30
Federal O'Neil to Dos Amigos	0	1	1	1	1	2	2	1	0	0	0	0
San Felipe	6	6	10	15	19	20	21	20	13	11	8	8
South Bay/San Jose	2	2	2	5	5	7	7	8	7	12	8	6
State Dos Amigos	105	127	158	105	348	348	423	388	269	229	196	61
Delta Consumptive Use	-56	-37	-10	63	121	191	268	252	174	118	55	2
Freeport Treatment Plant	14	13	14	12	12	12	12	13	12	12	12	13

Table 4.2.5: Initial Reservoir Storages on March 1, 2012

Reservoirs	Max. Storage	Min. Storage	Initial Storage	Ini Act. Sto. Fraction (%)
Clair Engle Lake	2287	312.63	1958.8	83.38
Whiskeytown	237.9	200	205.56	14.67
Shasta	4552	1168	3170	59.16
Oroville	3538	855	2518.2	61.99
Folsom	975	83	387.6	34.15
New Melones	2420	273	1965.6	78.84
Tulloch	67	57	57	0.00
San Luis	2027	0	1717.5	84.73

4.2.2 Water Temperature Assessments for 2012 Forecasts

The 2012 forecasts and tradeoff points produced by the INFORM Long Range Planning model were used to generate water temperature forecasts. Specifically, the following input data was used:

- Monthly Long Range forecasted inflows starting from March 01, 2012 (50 traces, 9 month horizon, and two locations: Clair Engle Lake (Trinity) and Shasta).
- Forecasted inflows for all locations downstream of Clair Engle Lake and Shasta (1 sequence representing the average of 10 traces selected from the historical record through a historical analog forecasting scheme based on prior month inflows to Clair Engle Lake and Shasta).
- Meteorological conditions (equilibrium temperature, exchange rate, solar radiation, and wind) corresponding to the historical year 1924.
- Historical averages (1924-2003) of Upper Sacramento River diversions.
- Reservoir initial storages are set to their actual values on March 1, 2012.
- Reservoir initial temperature profiles set to their actual values measured in late February or early March 2012.
- Shasta release temperature targets set at 60.8 F from March 1 until April 6, 53.6 F from April 7 until May 9, 48.2 F from May 10 until September 14, and 41 F from September 15 until November 31.

For each of the above datasets, the release sequences computed by the INFORM Long Range Planning model corresponding to three different carryover storage tradeoff points (1, 3 and 5) were used to generate three different sets of water temperature ensemble forecasts.

4.2.2.1 INFORM Forecasts

The forecasted river flow and water temperature ensembles are shown in Figures 4.2.19 through 4.2.30. Three different locations are depicted: immediately downstream of Shasta, the Sacramento River at Balls Ferry, the Sacramento River at Jellys Ferry, and the Sacramento River at Bend Bridge. The approximate location of each of these potential control points is shown in Figure 3.3.2. For reference purposes, a line depicting a constant temperature of 56 F has also been provided. Furthermore, the amount of cold water stored in Shasta (the cold water pool is

defined as water below 52 F) is also shown. Comparisons between the flow rates, temperatures and remaining cold water storage resulting from the policies suggested for each tradeoff point are shown in Figures 4.2.31 through 4.2.34, where only the ensemble averages are plotted to facilitate comparisons.

The results reveal that under each of the three tradeoff policies a 56 F water temperature target at the most downstream control point (Bend Bridge) would not be met for the entire forecasting horizon. Given these forecasts, it seems likely that the managers will have to agree to meet temperature targets at control points that are further upstream of Bend Bridge, i.e., Jellys Ferry or even Balls Ferry. A comparison between the trajectories associated with each tradeoff point reveals the management problem with which system operators are faced. While the higher releases associated with tradeoff point #5 provide the coolest temperatures during the summer months, this policy struggles to provide any sort of temperature control during the month of September since the cold water storage in the reservoir has by then been depleted. Additionally, tradeoff point #5 is left with the smallest total carryover storage, which makes the entire system more vulnerable should the following year be abnormally dry. Tradeoff points #3 and #1 are better equipped to meet temperature requirements in September since lower releases from Shasta throughout the summer months conserve more cold water storage. However, this comes at the expense of more frequent temperature target violations in June and July.

The release policies associated with all three tradeoff points are nearly identical in the early months (March through May). There are a few violations at both Bend Bridge and the further upstream locations of Jellys Ferry and Balls Ferry in April and May, especially during days that are unusually hot and during times when the Clear Creek and Spring Creek Tunnel inflows are at elevated temperatures. These targets could be met by either increasing Shasta outflows or using the TCD to withdraw colder water (the temperature targets for April and early May were initially set to be higher than those for May through September).

By the end of October, the temperature targets are expected to be met at all locations due to the lower air temperatures despite the cold water storage having been depleted.

Additional simulations with altered releases and temperature targets could be made to identify policies that strike the best balance between meeting temperature targets at different times of the year. Further simulations were performed by using the release strategy identified by tradeoff point #3. This point presents a balance that provides increased reservoir releases while at the same time reserving sufficient carryover storage. Different simulation scenarios were derived by adjusting the Shasta reservoir release temperature target so that the TCD releases water in different temperatures ranges. Analysis of the July through August water temperatures at all control points reveals that the release temperature could actually be increased during those months. On the other hand, the frequent and sometimes significant temperature violations expected to occur in April and May were mitigated by setting colder release temperature targets during those months. Figures 4.2.35 through 4.2.38 depict results from another scenario based on altering the temperature targets as discussed above. The average temperatures at Balls Ferry are almost all forecasted to be below the 56 F threshold, while a few violations remain at Jellys Ferry and Bend Bridge, particularly due to hot days and warmer

inflows coming from the Trinity system. However, all of the water temperatures are more favorable under the new scenario.

Further management policies could be explored by identifying other temperature target sequences. Additionally, river temperatures could be altered by changing the magnitudes and timing of the releases of Shasta reservoir, as well as Whiskeytown and Spring Creek Tunnel. However, since such changes can affect a variety of other water management objectives, a large number of different strategies may have to be evaluated. To that end, a model that fully integrates water temperature criteria into the existing INFORM system-wide optimization framework through the procedure described in Section 3.3.4 would be useful to help screen and refine the large set of possible management strategies.

4.2.2.2 Actual 2012 Water Temperature Measurements

Actual water temperature measurements taken during the 2012 season at Balls Ferry, Jellys Ferry, and Bend Bridge are shown in Figure 4.2.39 through 4.2.41. The plots show more short term variation than the forecast plots since the measurements were taken at 1 hour intervals while the forecasts are issued at a daily time resolution. As a result, it is more meaningful to view the actual measurements on an average daily basis to facilitate comparison with the forecasts.

Figure 4.2.39 shows that the average water temperature at Balls Ferry was below 56 F for the majority of the season. These temperature conditions match up with those displayed in the forecasts, where a temperature target of 56 F was expected to be met at the Balls Ferry location. Figure 4.2.40 and Figure 4.2.41 shows that the measured temperatures at Jellys Ferry and Bend Bridge were quite similar. There were more exceedences of the 56 F temperature target than at Balls Ferry, though when viewed as daily averages the target was met the majority of the time. The water temperature forecasts for the most downstream location, Bend Bridge, were therefore somewhat pessimistic compared to the actual measurements. A possible reason for the differences between the actual measurements and the forecasts might be the fact that the Shasta reservoir inflow forecasts upon which the temperature forecasts were based were lower than the actual inflows that occurred in 2012, as shown in Figure 4.2.42. In particular, the March and April inflows turned out to be higher, primarily due to two large flood events, as shown in Figure 4.2.43. As a result, larger releases could be made to help maintain acceptable water temperatures in the upper Sacramento River while at the same time ensuring adequate carryover storage. The process of generating water temperature forecasts is therefore recommended to follow the same general framework as those used by the INFORM Long Range Planning model to generate forecasts of other management objectives: once new information about the actual inflows becomes available (i.e., each month or few weeks), the temperature forecasts should be updated to reflect the latest actual conditions and most recent inflow forecasts.

Figure 4.2.19: Shasta Tradeoff Point #1: Ensemble Forecasts of Release Magnitude/Temperature and the Amount of Reservoir Storage Below 52 F.

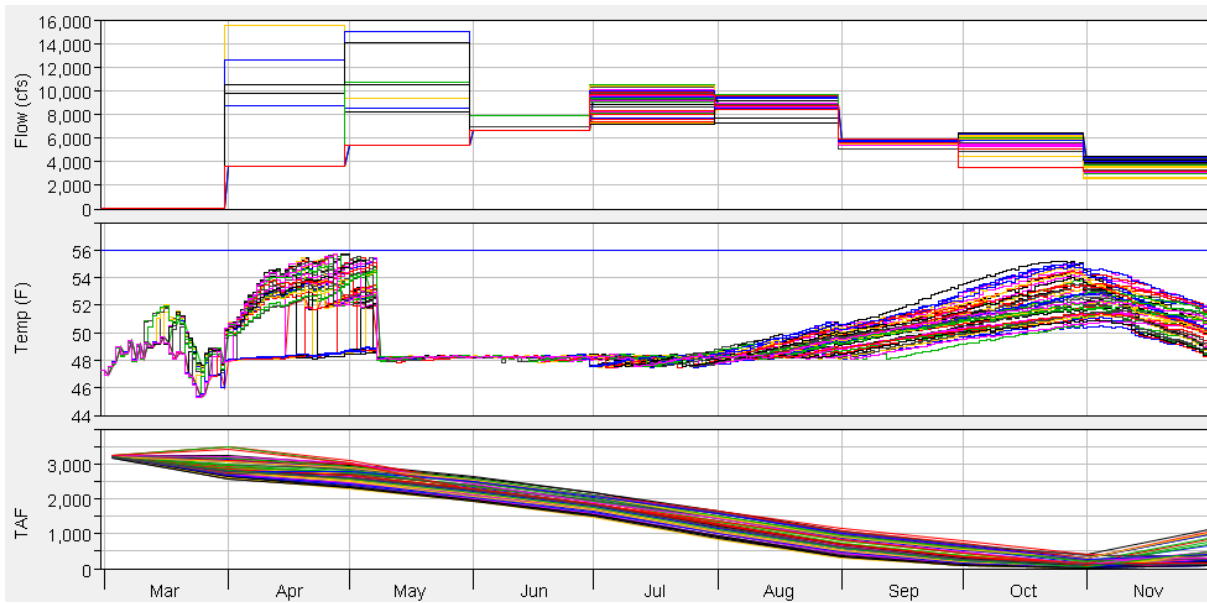


Figure 4.2.20: Balls Ferry Tradeoff Point #1: Ensemble Forecasts of Release Magnitude/Temperature.

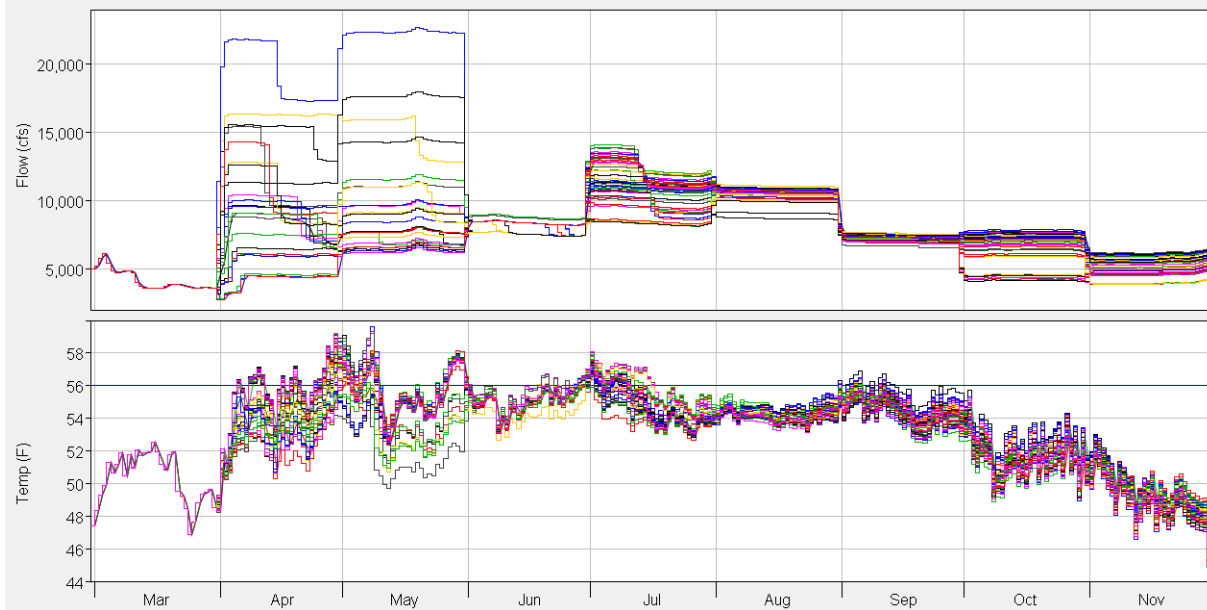


Figure 4.2.21: Jellys Ferry Tradeoff Point #1: Ensemble Forecasts of Release Magnitude/Temperature.

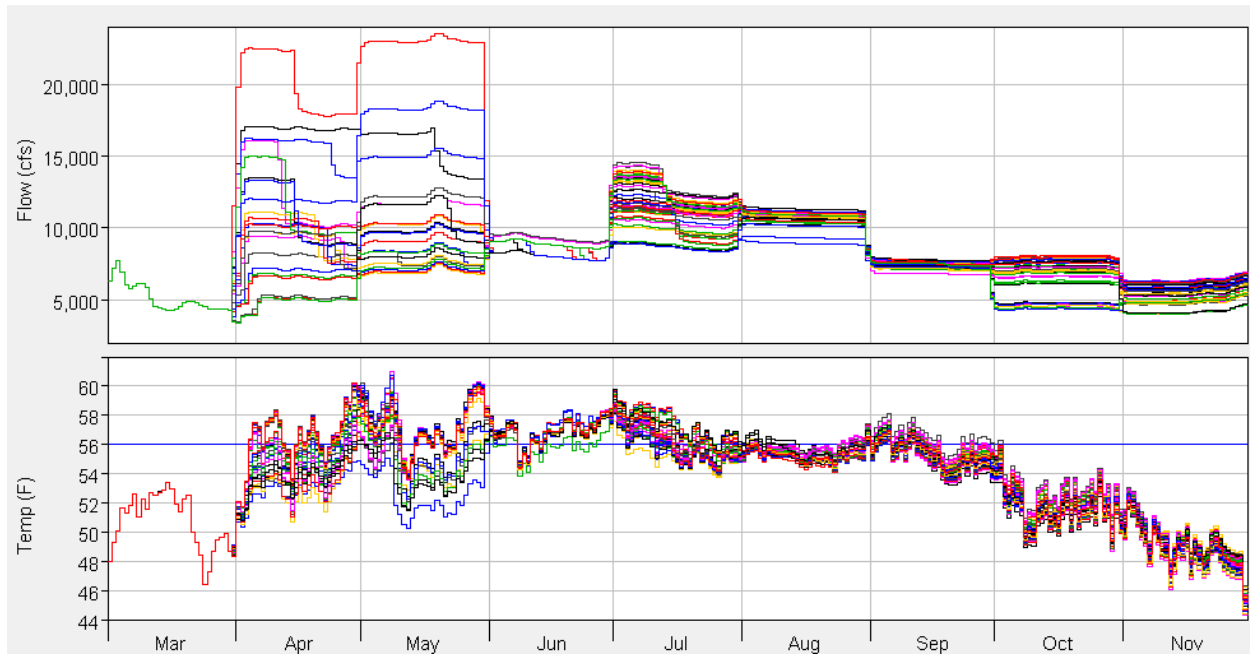


Figure 4.2.22: Bend Bridge Tradeoff Point #1: Ensemble Forecasts of Release Magnitude/Temperature.

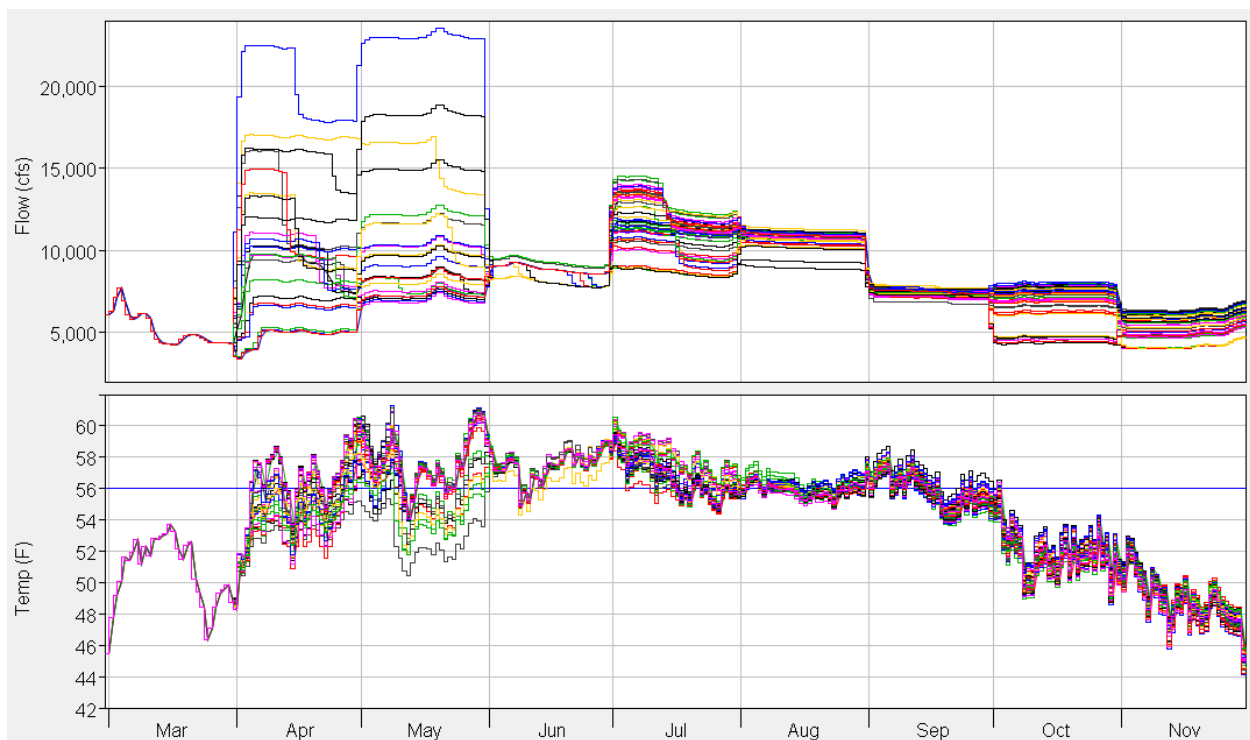


Figure 4.2.23: Shasta Tradeoff Point #3: Ensemble Forecasts of Release Magnitude/Temperature and the Amount of Reservoir Storage Below 52 F.

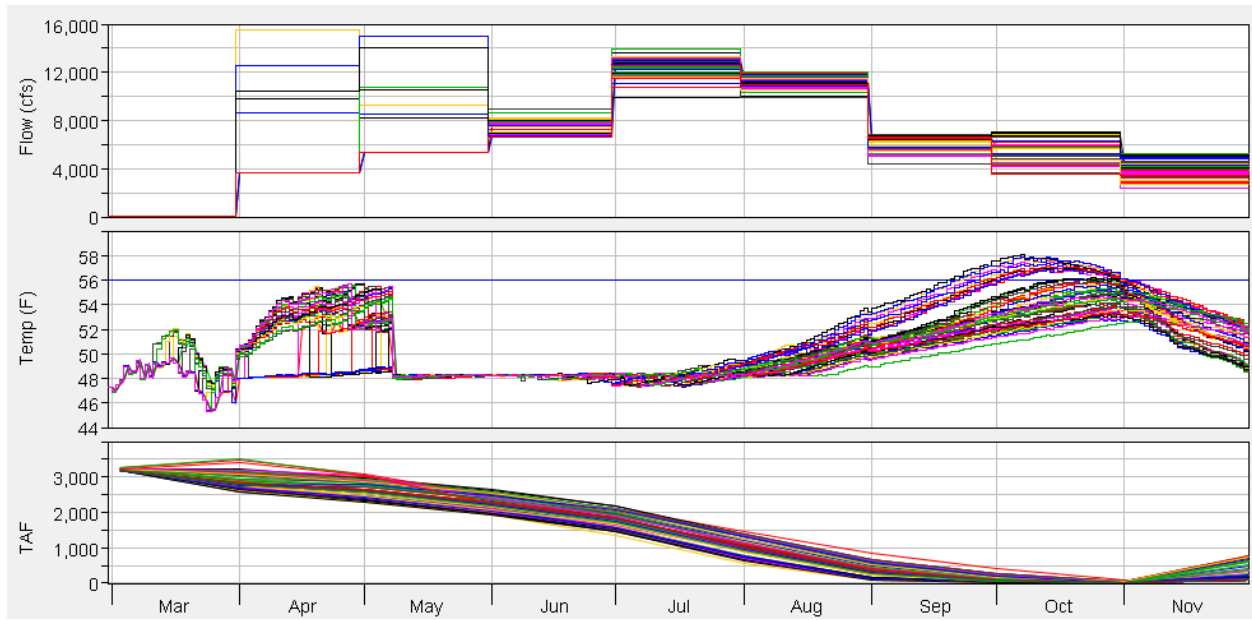


Figure 4.2.24: Balls Ferry Tradeoff Point #3: Ensemble Forecasts of Release Magnitude/Temperature.

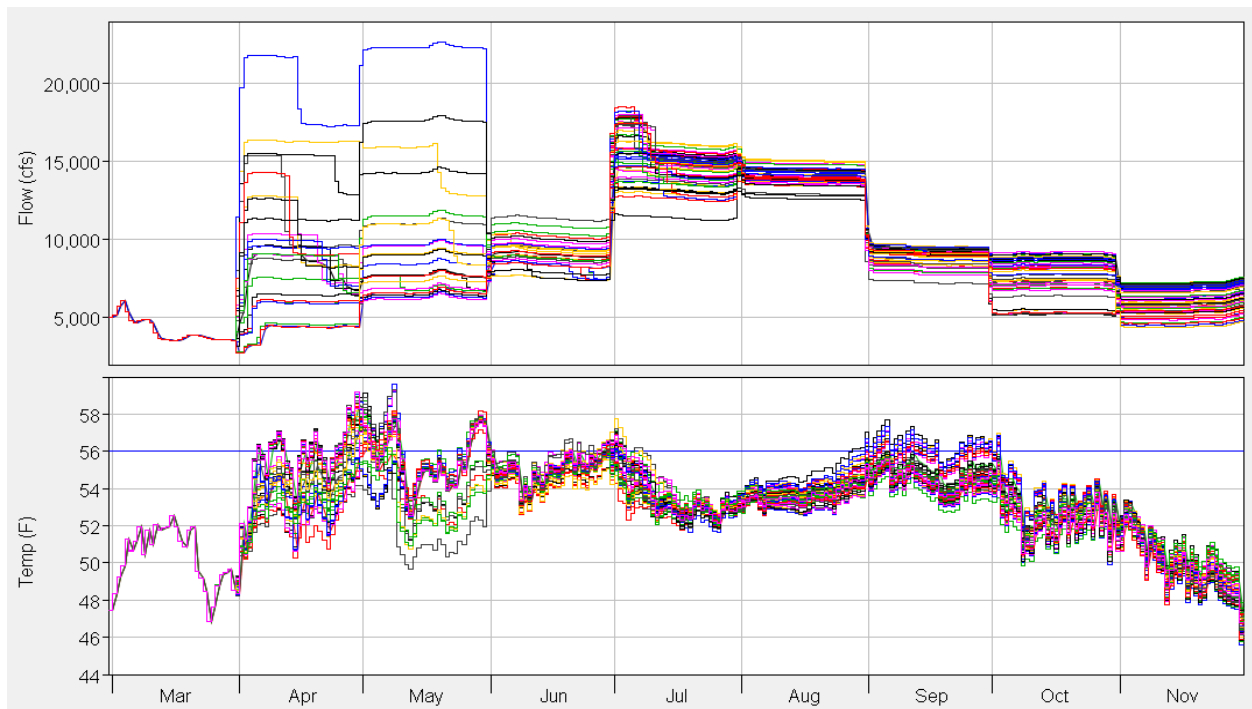


Figure 4.2.25: Jellys Ferry Tradeoff Point #3: Ensemble Forecasts of Release Magnitude/Temperature.

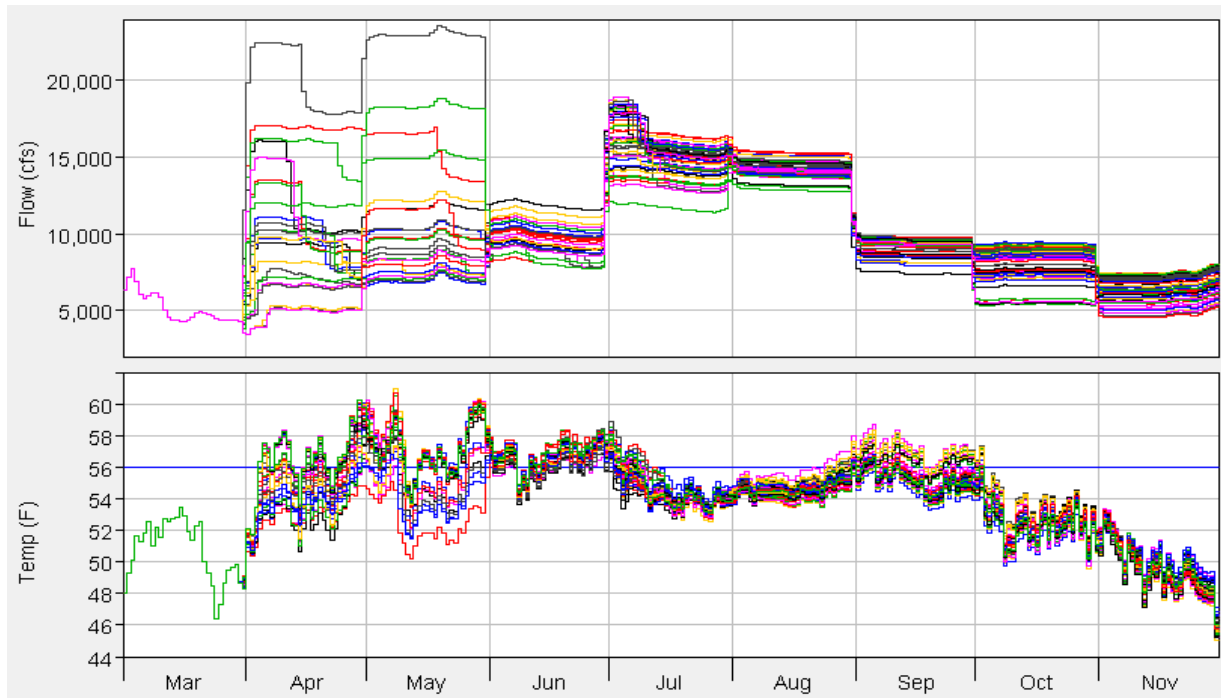


Figure 4.2.26: Bend Bridge Tradeoff Point #3: Ensemble Forecasts of Release Magnitude/Temperature.

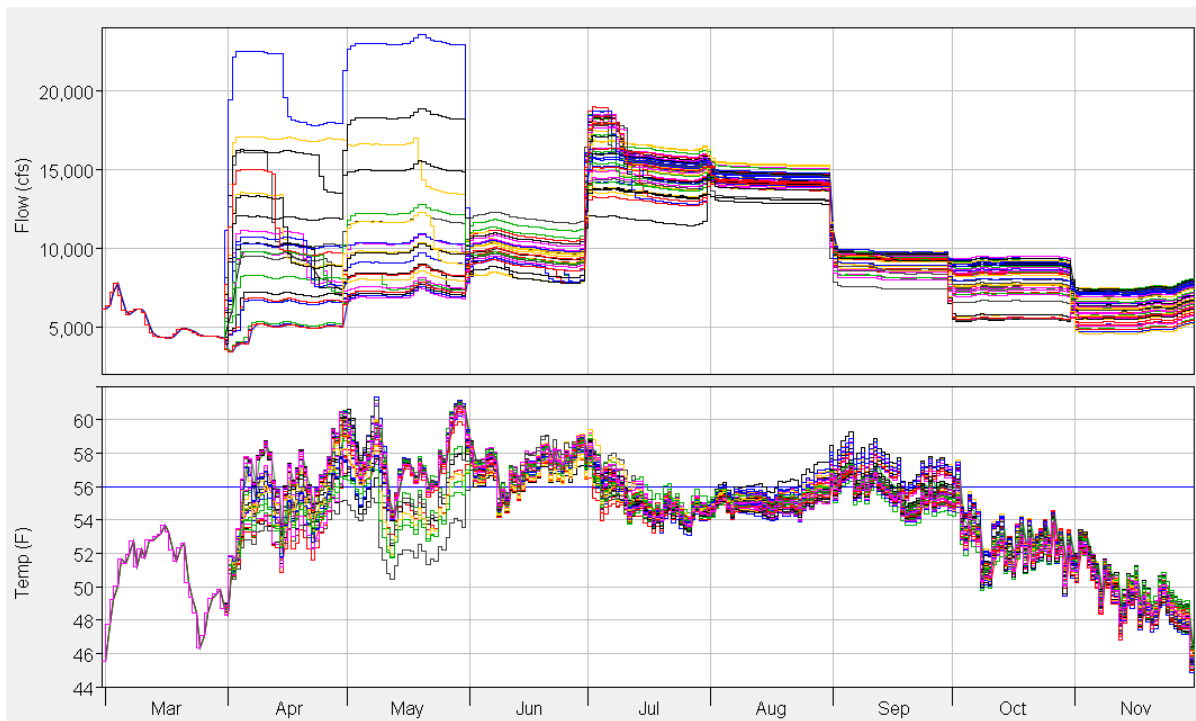


Figure 4.2.27: Shasta Tradeoff point #5: Ensemble Forecasts of Release Magnitude/Temperature and the Amount of Reservoir Storage below 52 F.

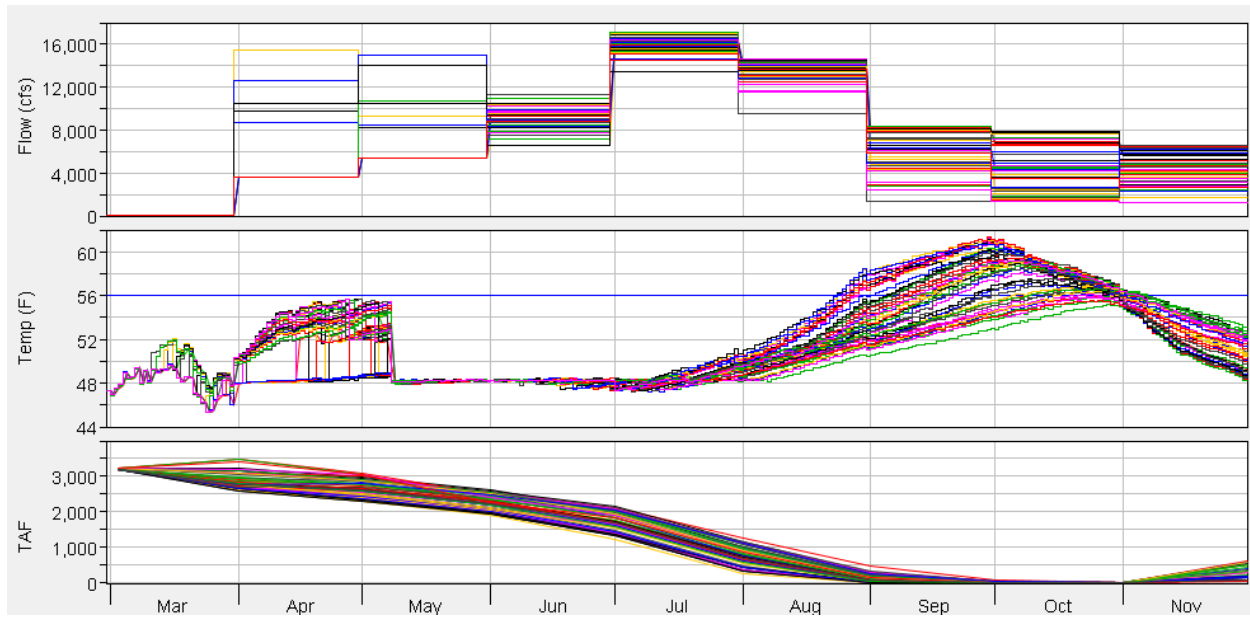


Figure 4.2.28: Balls Ferry Tradeoff Point #5: Ensemble Forecasts of Release Magnitude/Temperature.

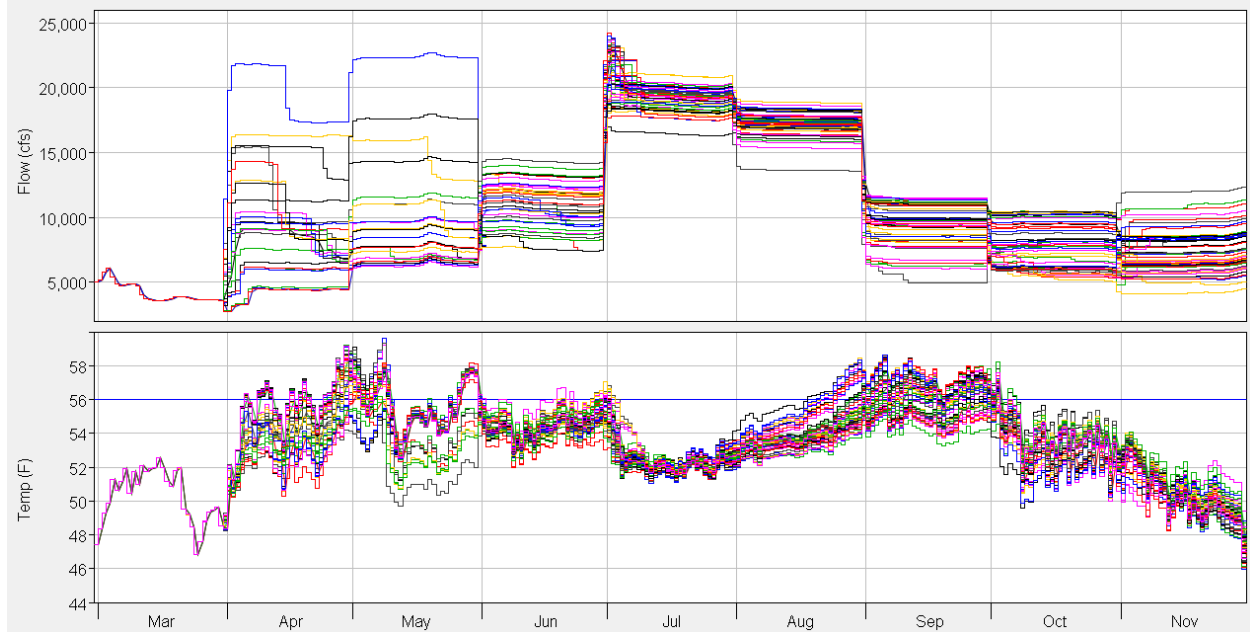


Figure 4.2.29: Jellys Ferry Tradeoff Point #5: Ensemble Forecasts of Release Magnitude/Temperature.

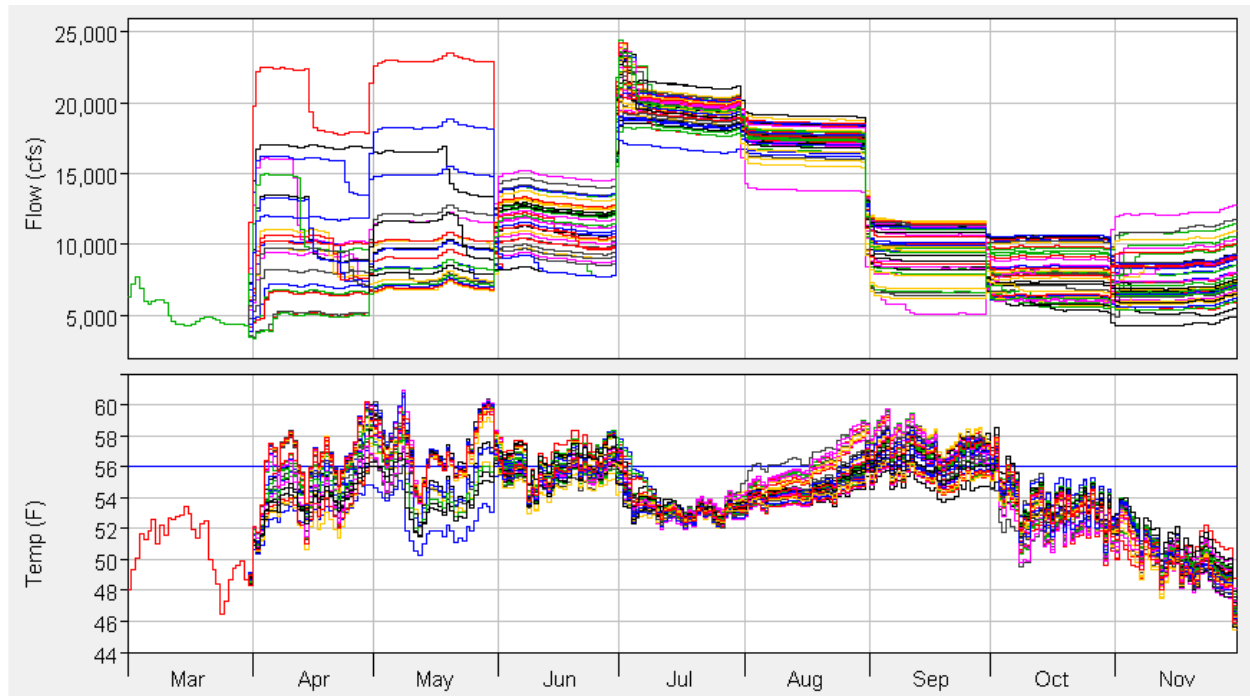


Figure 4.2.30: Bend Bridge Tradeoff Point #5: Ensemble Forecasts of Release Magnitude/Temperature.

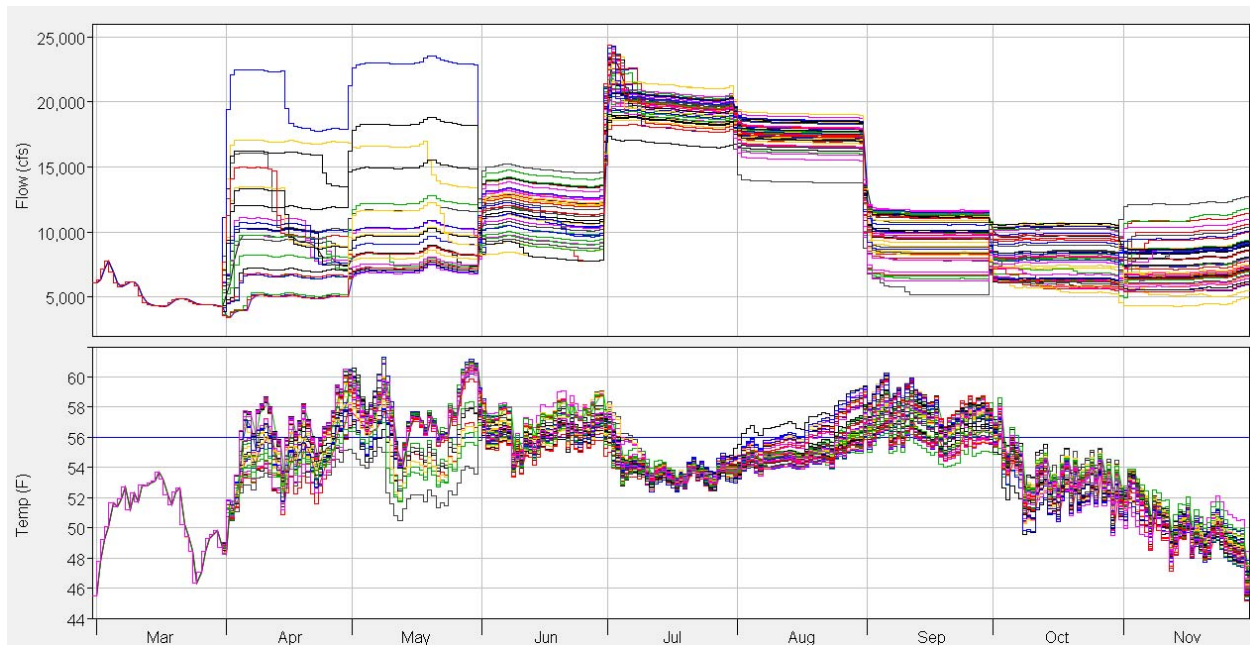


Figure 4.2.31: Shasta: Forecast Averages of Release Magnitude/Temperature and the Amount of Reservoir Storage below 52 F for Tradeoff Points #1 (Blue), #3 (Red) and #5 (Green).

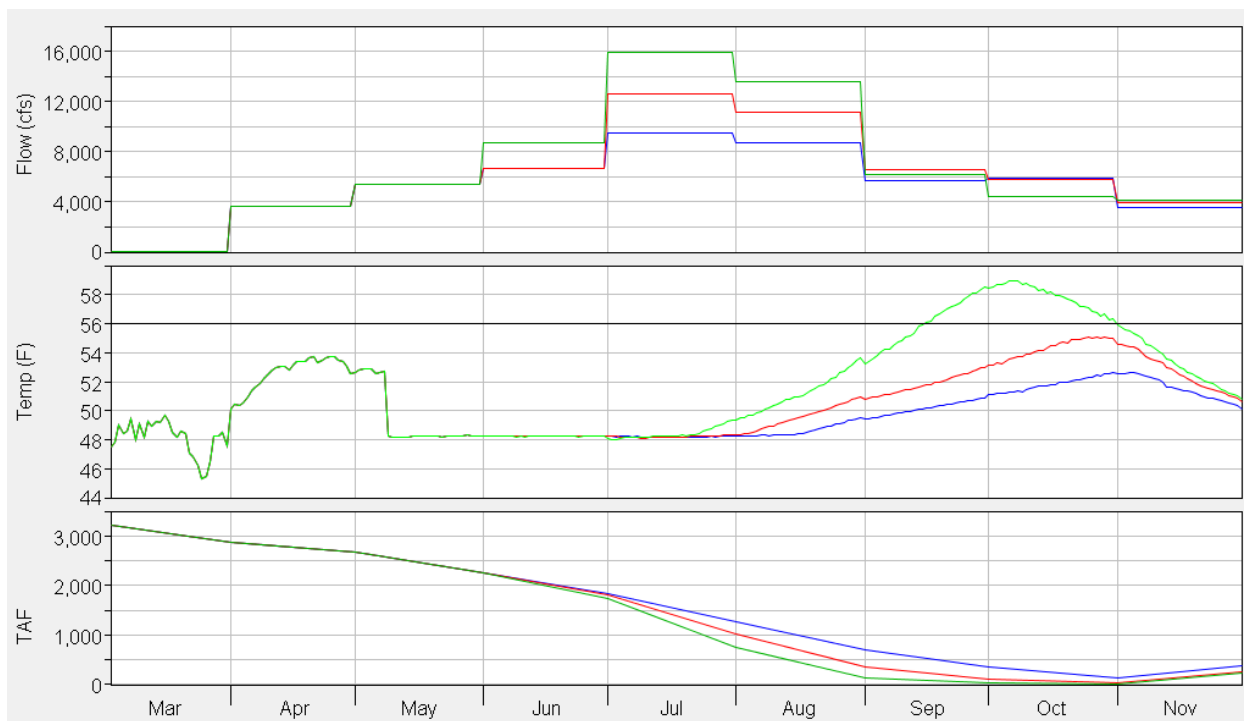


Figure 4.2.32: Balls Ferry: Forecast Averages of Release Magnitude/Temperature for Tradeoff Points #1 (Blue), #3 (Red) and #5 (Green).



Figure 4.2.33: Jellys Ferry: Forecast Averages of Release Magnitude/Temperature for Tradeoff Points #1 (Blue), #3 (Red) and #5 (Green).

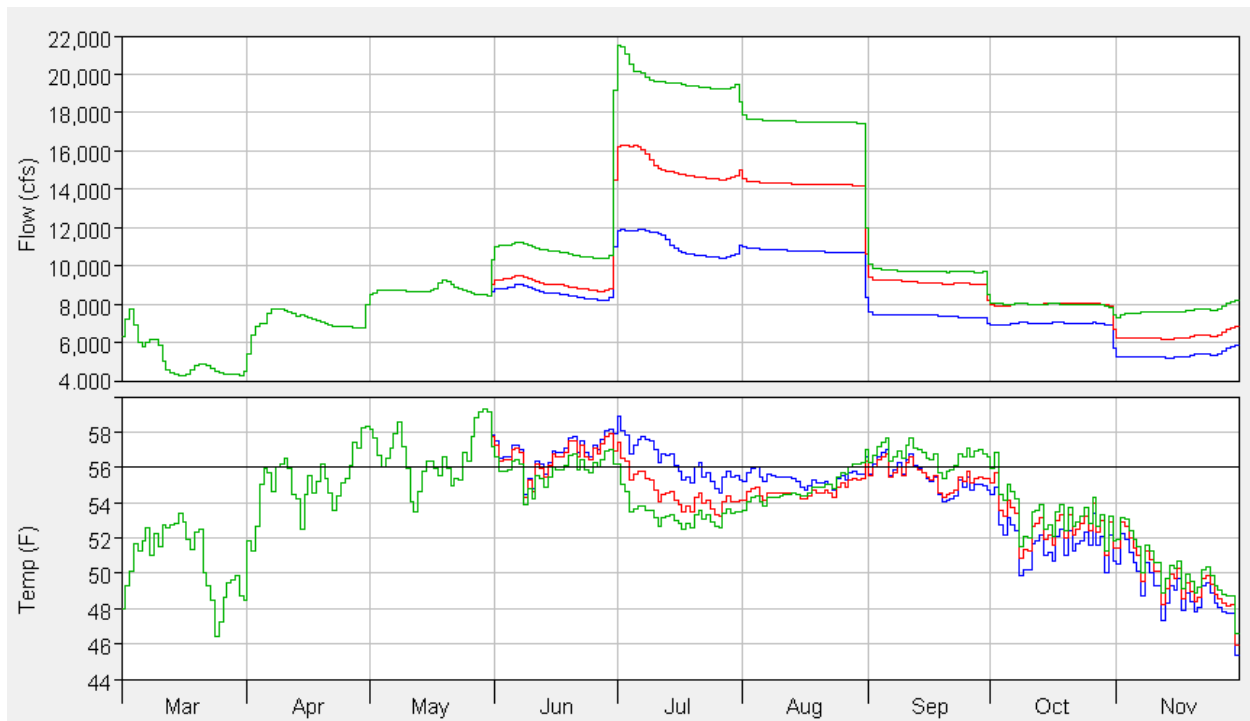


Figure 4.2.34: Bend Bridge: Forecast Averages of Release Magnitude/Temperature for Tradeoff Points #1 (Blue), #3 (Red) and #5 (Green).

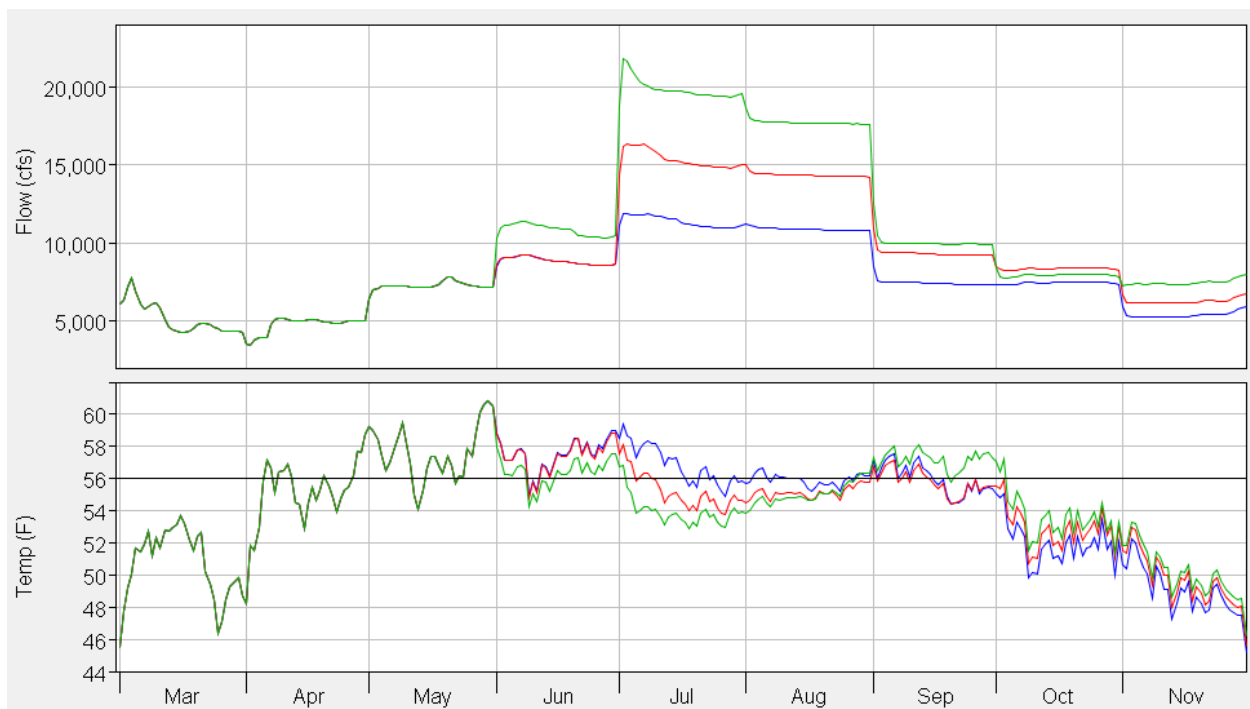


Figure 4.2.35: Shasta Tradeoff Point #3: Comparison of the Forecast Averages of Release Magnitude/Temperature between Two Scenarios. The Blue Scenario is Based on the Original Temperature Targets while the Red Scenario is Based on Adjusted Targets.

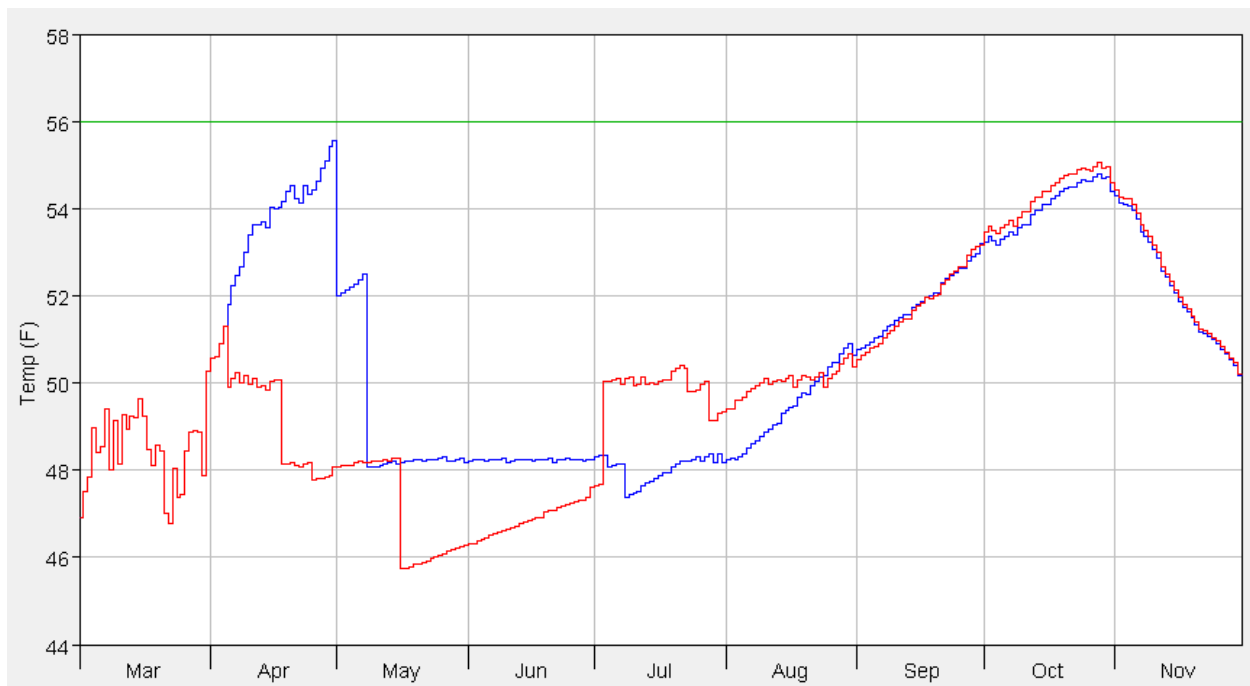


Figure 4.2.36: Balls Ferry Tradeoff Point #3: Comparison of the Forecast Averages of Release Magnitude/Temperature between Two Scenarios. The Blue Scenario is Based on the Original Temperature Targets while the Red Scenario is Based on Adjusted Targets.

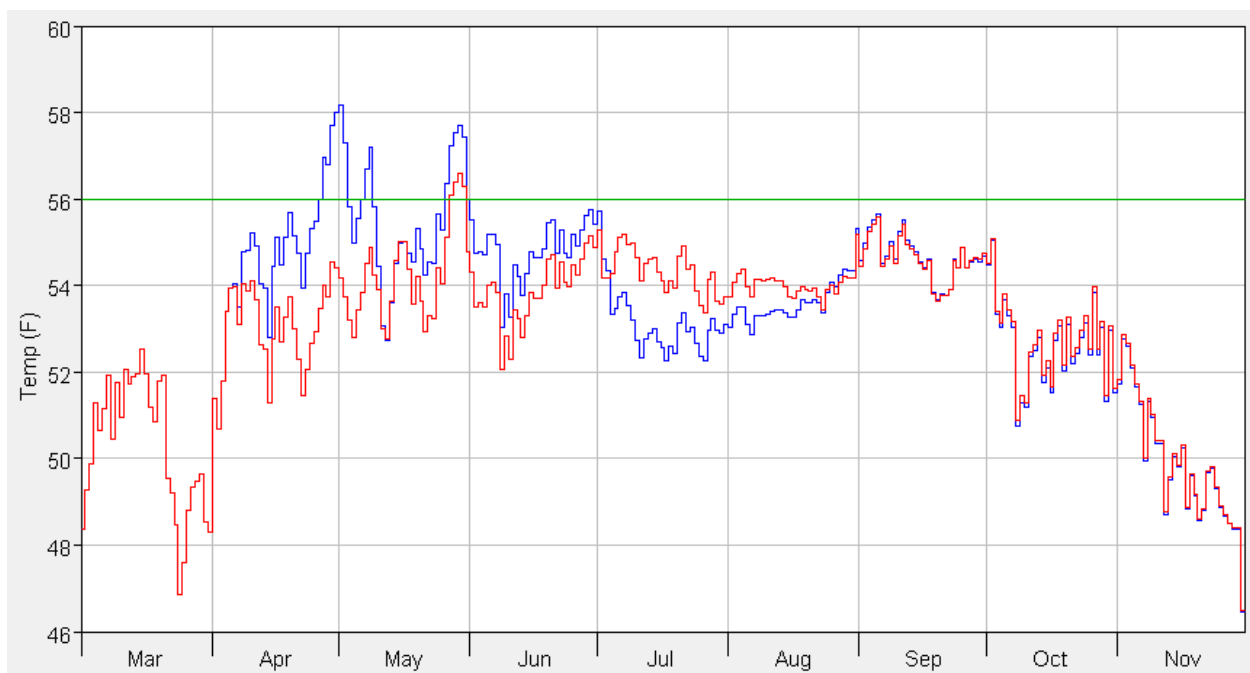


Figure 4.2.37: Jellys Ferry Tradeoff Point #3: Comparison of the Forecast Averages of Release Magnitude/Temperature between Two Scenarios. The Blue Scenario is Based on the Original Temperature Targets while the Red Scenario is Based on Adjusted Targets.

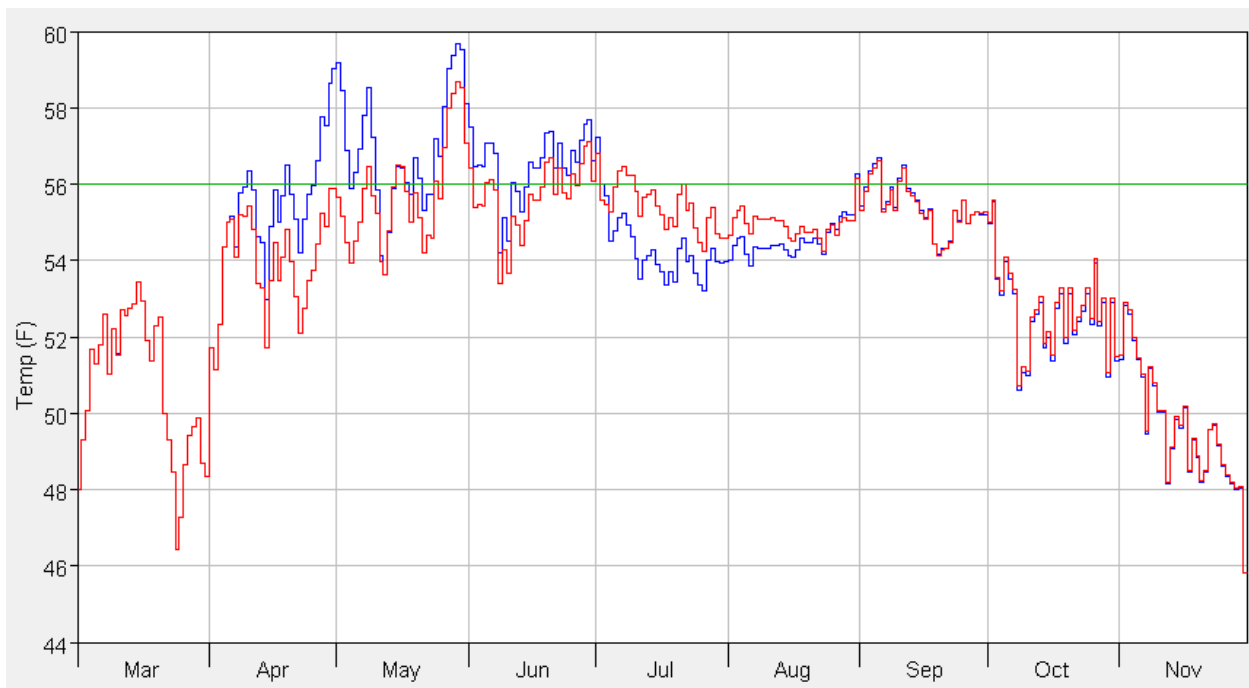


Figure 4.2.38: Bend Bridge Tradeoff Point #3: Comparison of the Forecast Averages of Release Magnitude/Temperature between Two Scenarios. The Blue Scenario is Based on the Original Temperature Targets while the Red Scenario is Based on Adjusted Targets.

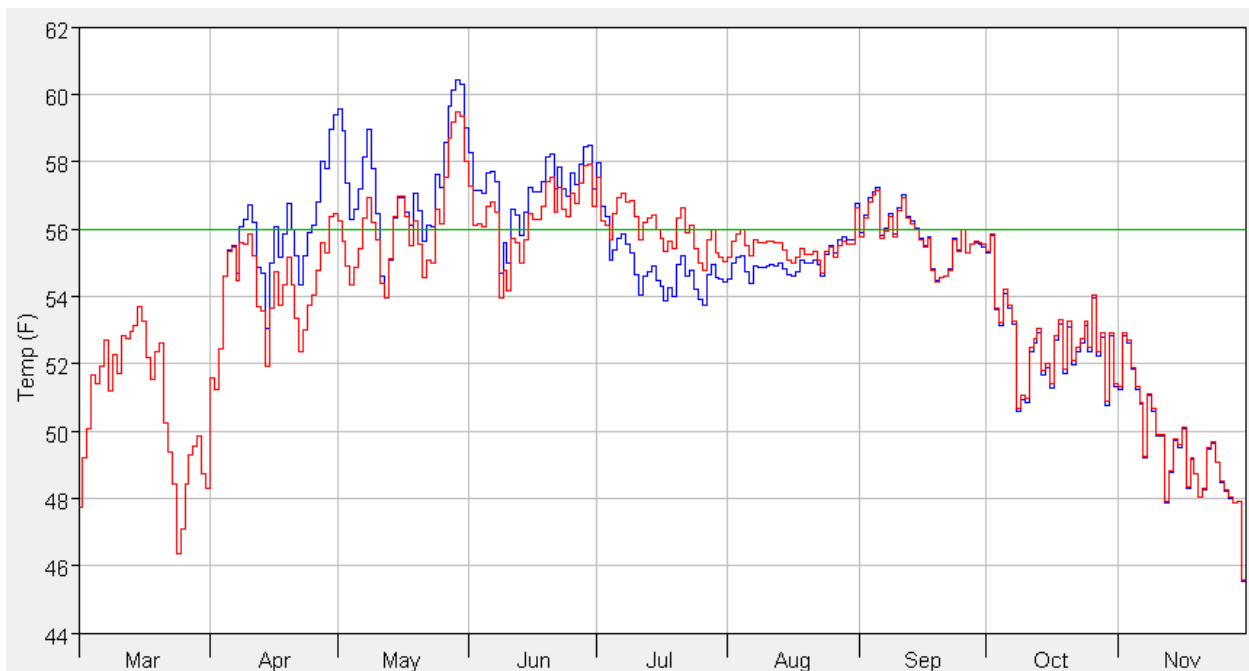


Figure 4.2.39: Measured Water Temperatures at Bend Bridge from February 2012 to February 2013.

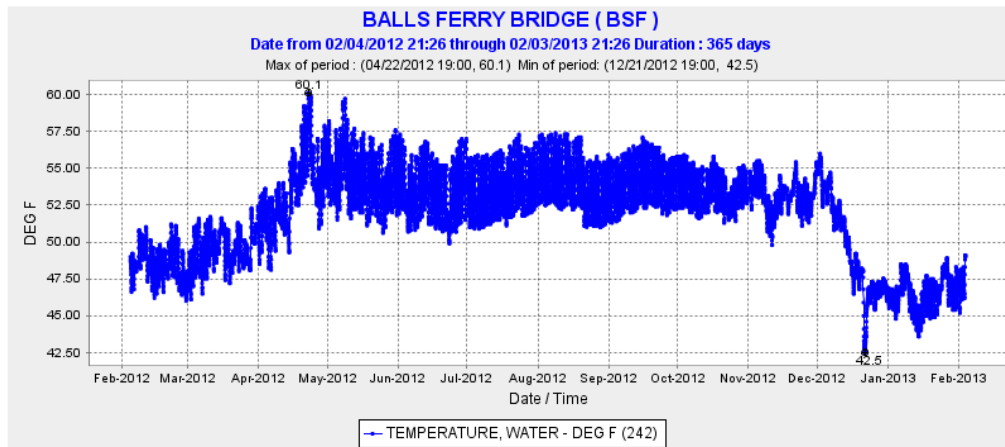


Figure 4.2.40: Measured Water Temperatures at Jellys Ferry from February 2012 to February 2013

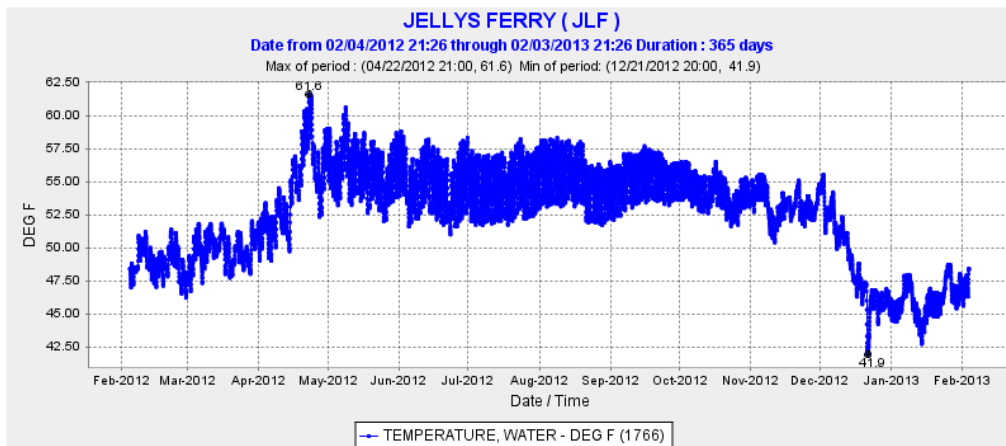


Figure 4.2.41: Measured Water Temperatures at Balls Ferry from February 2012 to February 2013.

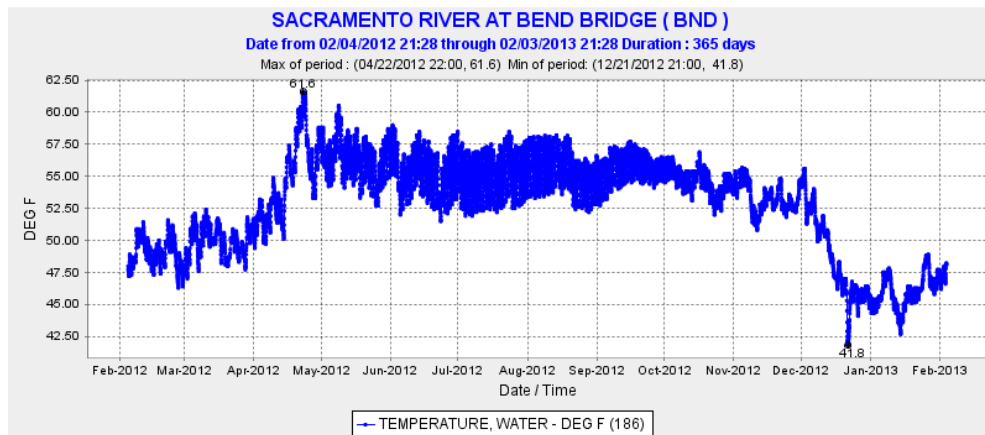


Figure 4.2.42: Comparison between Average Monthly Forecasted Inflows and Measured Inflows to Shasta Reservoir in 2012.

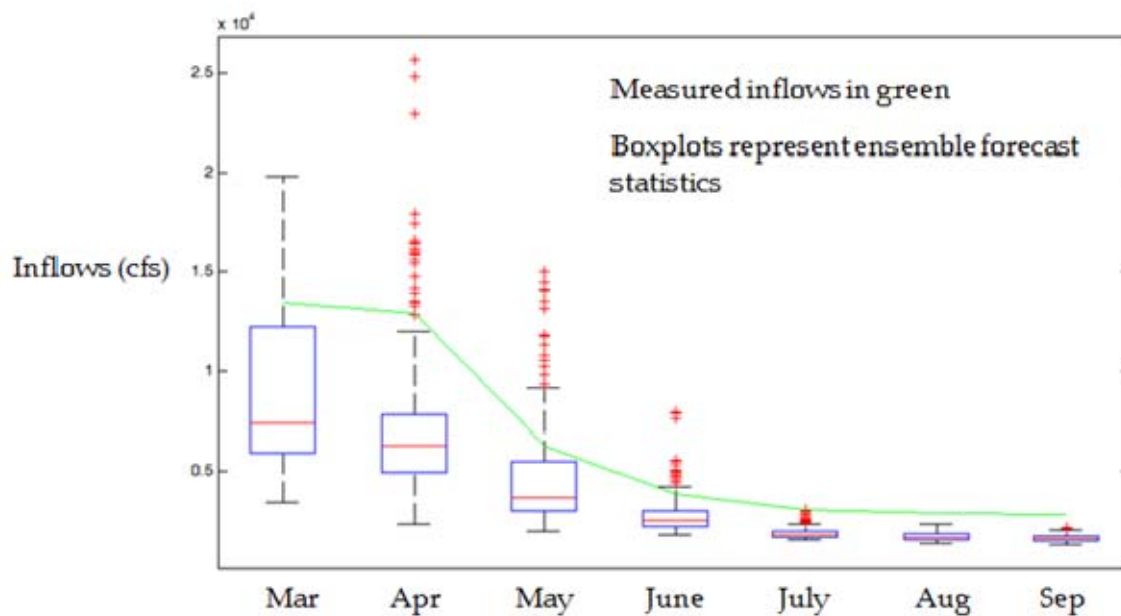
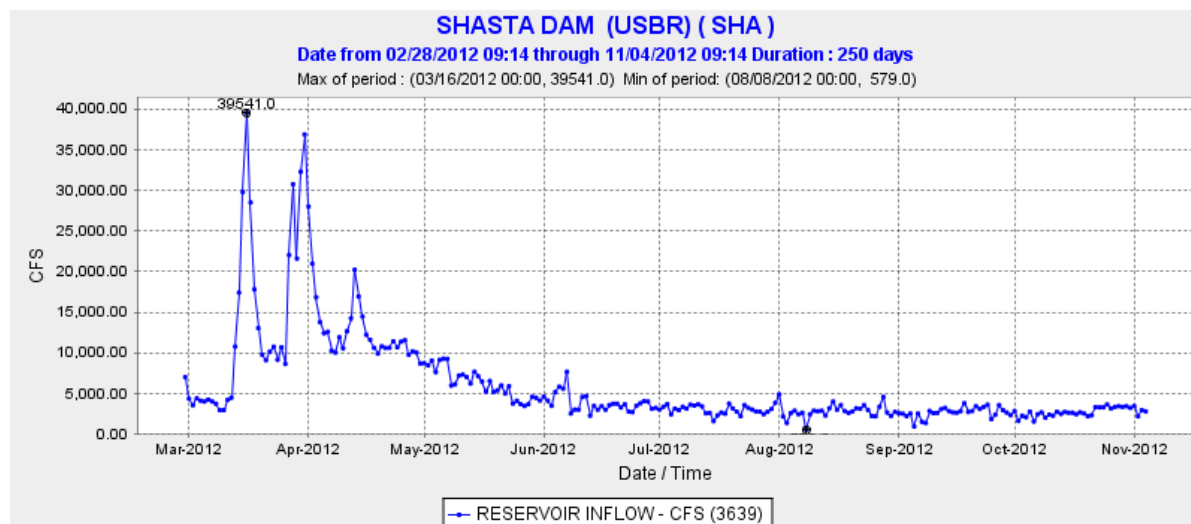


Figure 4.2.43: Daily Measured Inflow to Shasta Reservoir in 2012.



4.2.3 Flood Control Application

The INFORM short range management model addresses system operation at daily time resolution. The objectives of this decision layer include flood management, water supply, and power scheduling. This model uses hydrologic forecasts with a daily resolution and can assess various tradeoffs including upstream versus downstream flood risks, energy generation versus flood control, and other applicable tradeoffs. Such information is again intended for the management agencies (the operational departments) and other stakeholders to use it within their decision processes to select the most preferable operational policy.

This section presents a case study on the Upper Feather River aiming to demonstrate the potential of managing flood risks through the INFORM integrated forecast-decision approach. The schematic of the river network is shown in Figure 3.4.3. Four river nodes, GRIC1, FLVC1, YUBC1, and FBLC1, located downstream of Oroville reservoir are included. As indicated in Section 3.4, the flows at these nodes are the result of releases from Oroville and local watershed contributions. That section also describes the calibrated routing models from Oroville to these nodes.

Daily inflow forecasts to the Oroville reservoir are the model inputs. A 20-trace forecast ensemble (shown in Figure 4.2.44) beginning from April 1, 2012, with forecasting horizon of 16 days is used. The local inflows from YUBC1 during the same period are negligible. Forecasts of local flows from MRYC1 are not available, and the observed values for the same period (shown in Figure 4.2.45) are used in the routing and stage computations. The initial reservoir elevation on April 1st, 2012, was 861.26 feet.

To assess the impact of Oroville releases on the stages at the downstream nodes, three runs of the short range decision model were carried out.

The first run corresponds to the base case in which the target elevation for Oroville is set to 860 feet at the end of the 16-day forecast horizon. The reservoir target elevations were increased by 2 and 4 feet in the other two runs respectively. The initial reservoir elevation is the same for all runs and equal to the observed value of 861.26 feet.

Figure 4.2.46 and 4.2.47 show the Oroville elevation and release forecast ensembles of the first run. The mean trace is also plotted in the same figure (thick red line). To keep the reservoir elevation close to the ending target level of 860 feet, the reservoir has to release at high rates through most of the 16 day period. The average release is approximately 12,300 cfs. The maximum and mean reservoir elevations across the forecast traces are 872.23 feet and 862.3 feet, respectively. The maximum and mean daily energy generations are 15.68 GWH and 13.09 GWH.

Subsequently, the reservoir release sequences are routed through the downstream river reach using the routing model of Section 3.4. The flows and stage heights are computed and shown in Figures 4.2.48 to 4.2.56. The statistics are summarized in Table 4.2.6. The maximum predicted stage is 79.22 feet at GRIC1, 59.36 feet at FLVC1, 46.85 feet at YUBC1, and 38.13 feet at FBLC1.

The stage at YUBC1 is affected by backwater effects from MRYC1. As shown in Figure 4.2.45, the MRYC1 peak flow during this period occurs on April 14, 2012. This peak causes the stage at YUBC1 to rise on the same day (Figure 4.2.57).

Generally, the river stages computed in this case study are much lower than the flood stage levels identified for these locations by CNRFC. This is the case for all of the 2012 forecasts. It is thus not possible to explore a realistic flood control situation for 2012. Instead, this case study explores the tradeoff between Oroville ending storage and river stage at the downstream locations.

The 2nd and 3rd runs aim to reduce the river stage at the downstream locations by reducing the Oroville releases. This is done by increasing the reservoir target elevation at the end of the forecast horizon.

The results from the 2nd and 3rd runs are shown in Figures 4.2.58 to 4.2.77, and selected statistics are summarized in Tables 4.2.7 and 4.2.8.

The comparison of mean stage height sequences for the three runs are shown in Figures 4.2.78 to 4.2.84.

These runs show that using about 2 feet of Oroville flood storage reduces the downstream river stages by approximately 0.6 feet at GRIC1, FLVC1, and YUBC1, and by 0.8 feet at FBLC1.

At the same time, the reservoir energy generation is also reduced during this period as releases are reduced. Thus, the mean energy generation for these three runs is 13.09, 12.09, and 11.00 GWH/day respectively.

Although the simulated stage levels at the downstream locations are far below the real flood damage levels, the case study demonstrates the potential of the integrated INFORM approach

(which combines inflow forecasting, reservoir management, and downstream river routing) to quantify and potentially mitigate downstream flood risks.

Figure 4.2.44: Oroville Inflow Forecasting Ensemble

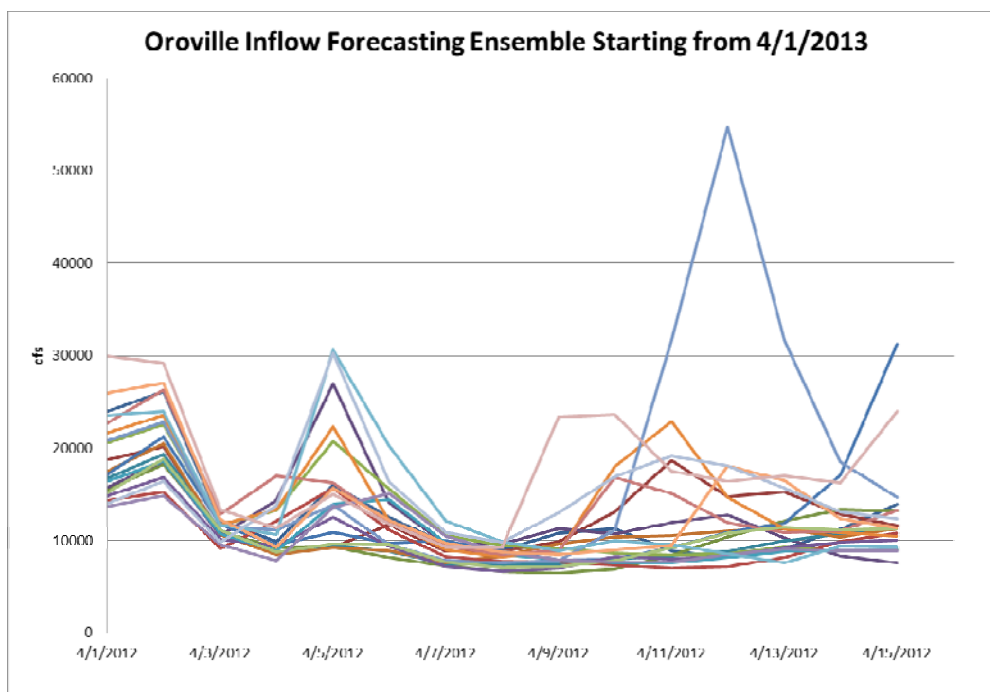
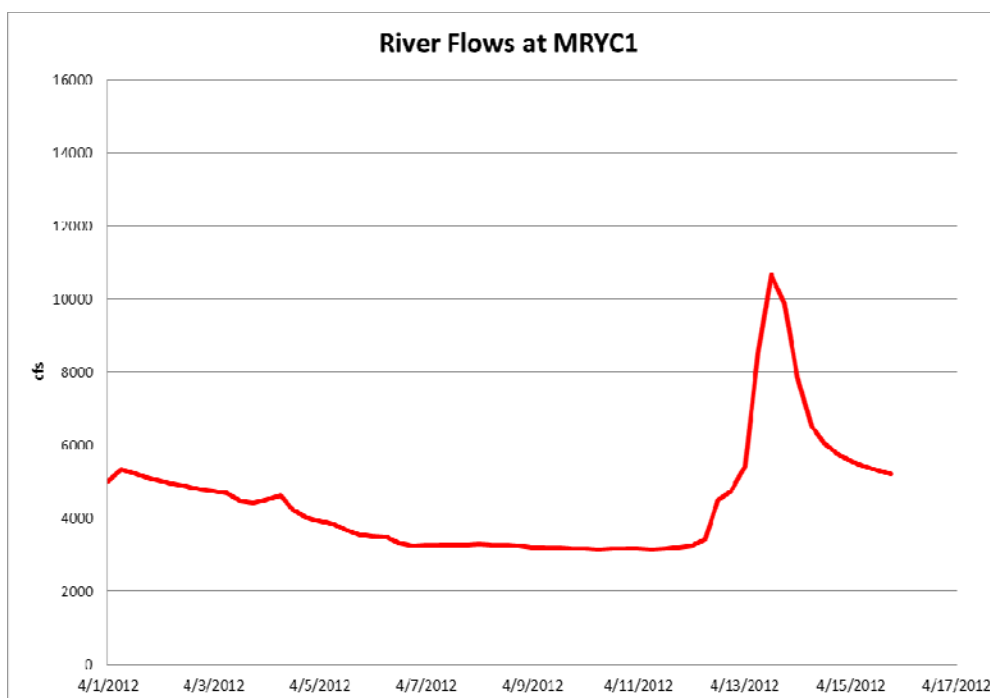


Figure 4.2.45: River Flow at MRYC1



Figure

4.2.46:

Oroville Elevation Sequences; Oroville Target Elevation 860 feet.

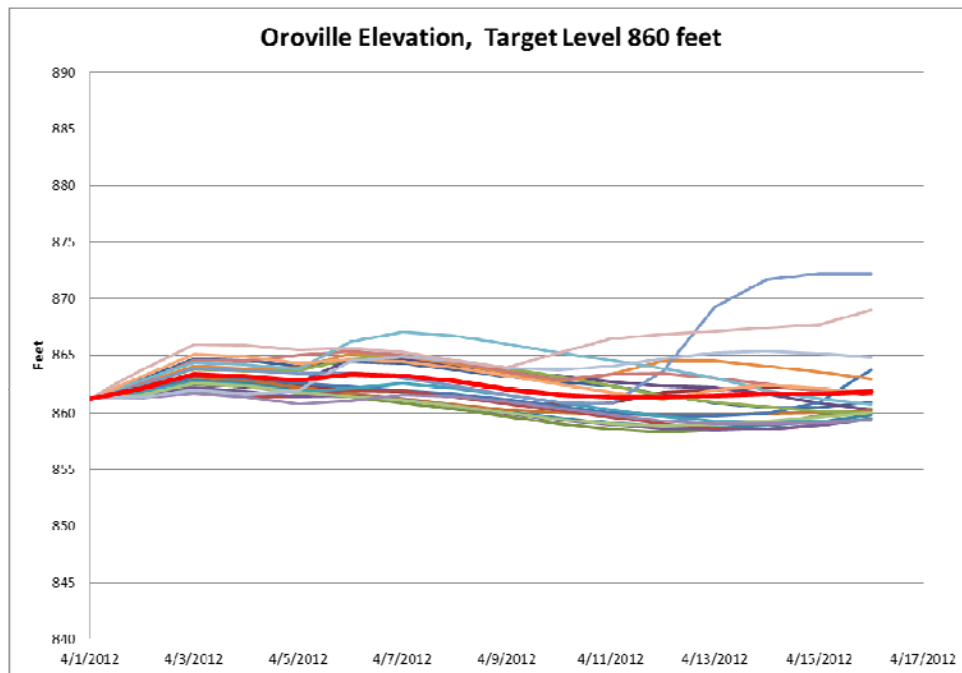


Figure 4.2.47: Oroville Release Sequences; Oroville Target Elevation 860 feet.

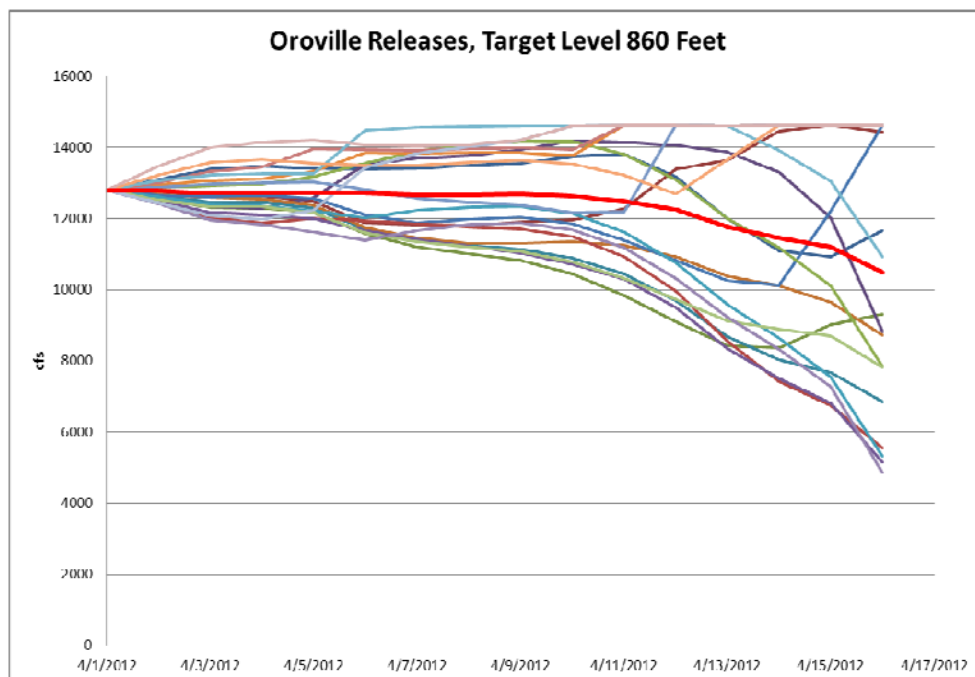


Figure 4.2.48: River Flow at GRIC1; Oroville Target Elevation 860 feet.

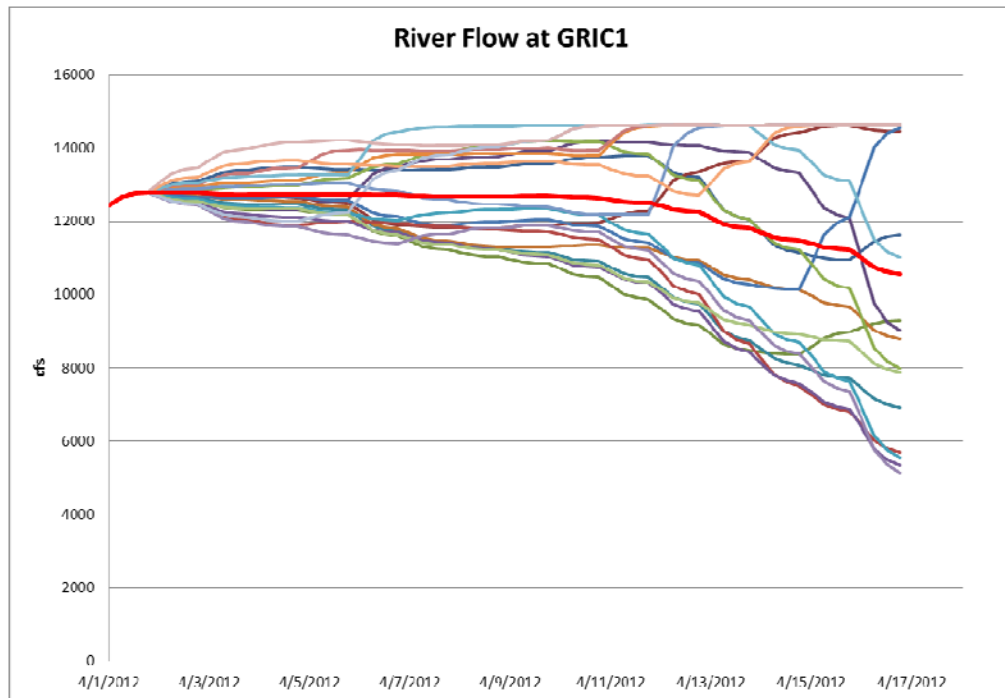


Figure 4.2.49: Stage Height at GRIC1; Oroville Target Elevation 860 feet.

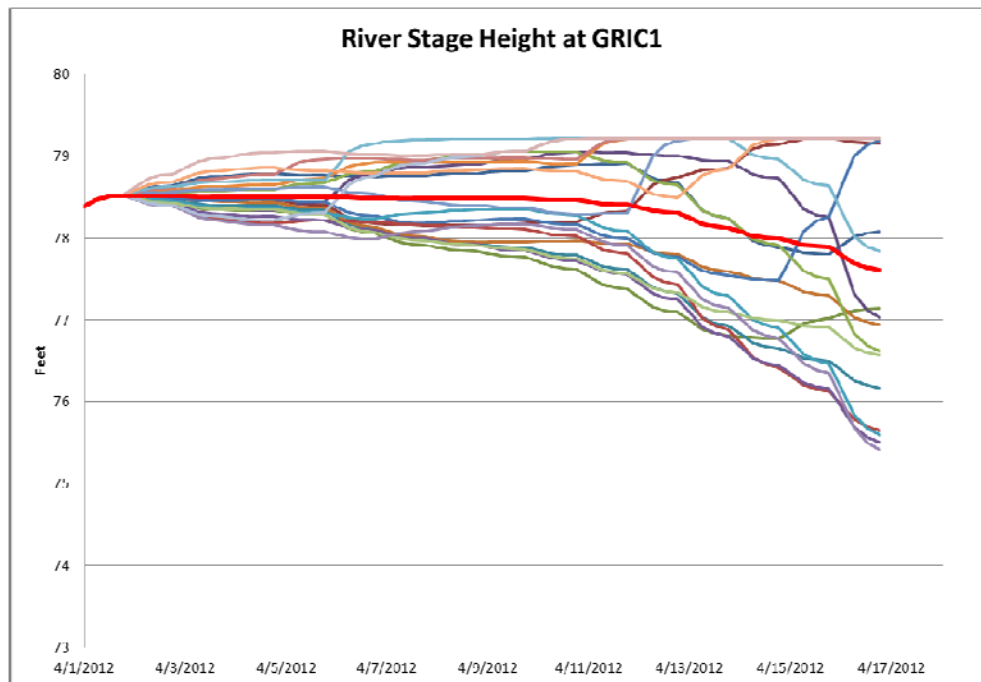


Figure 4.2.50: River Flow at FLVC1; Oroville Target Elevation 860 feet.

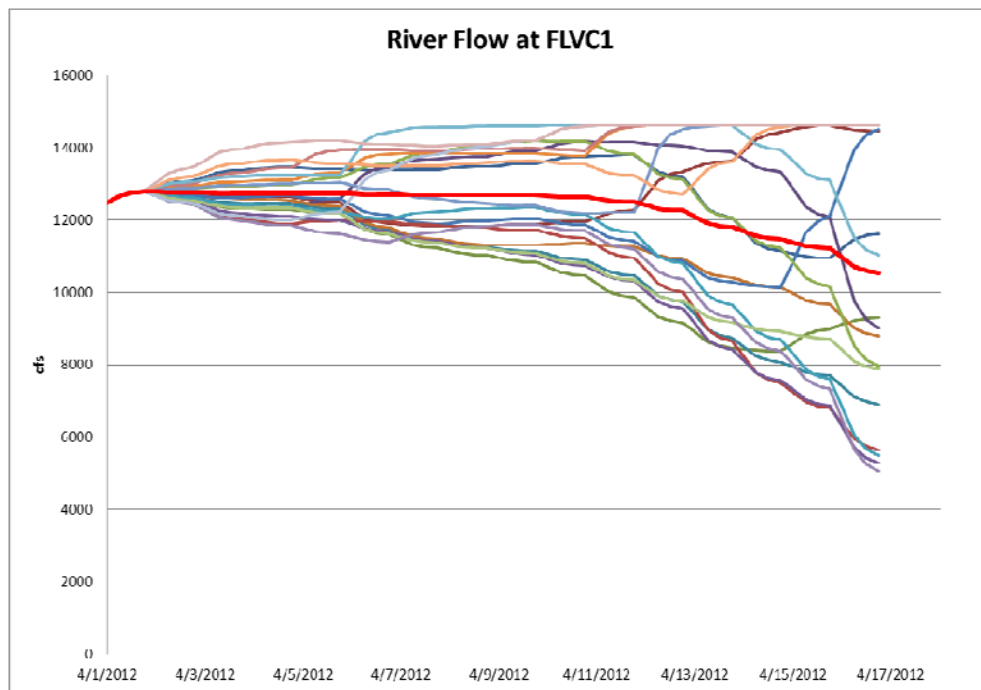


Figure 4.2.51: Stage Height at FLVC1; Oroville Target Elevation 860 feet.

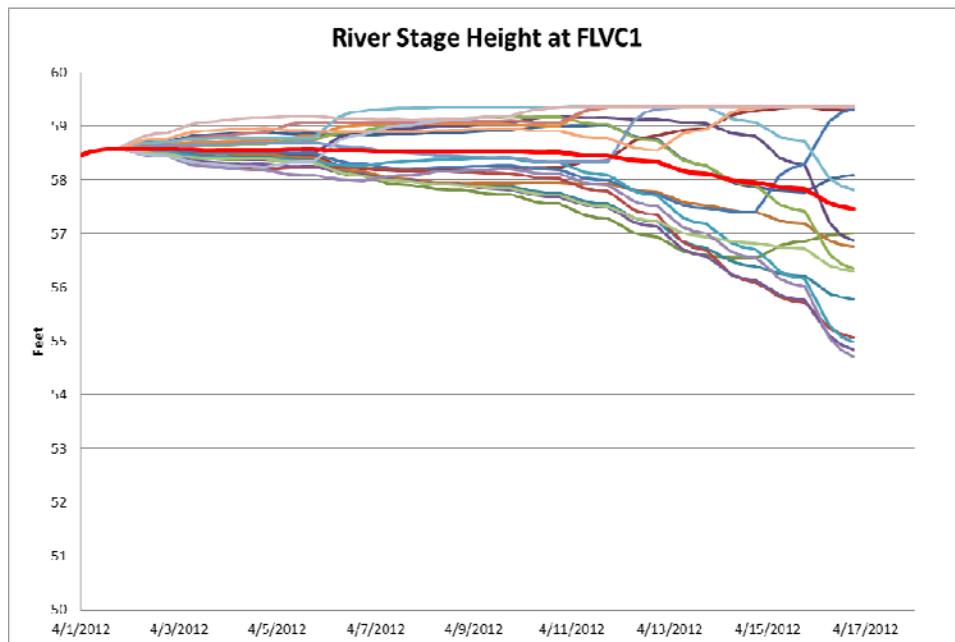


Figure 4.2.52: River Flow at YUBC1; Oroville Target Elevation 860 feet.

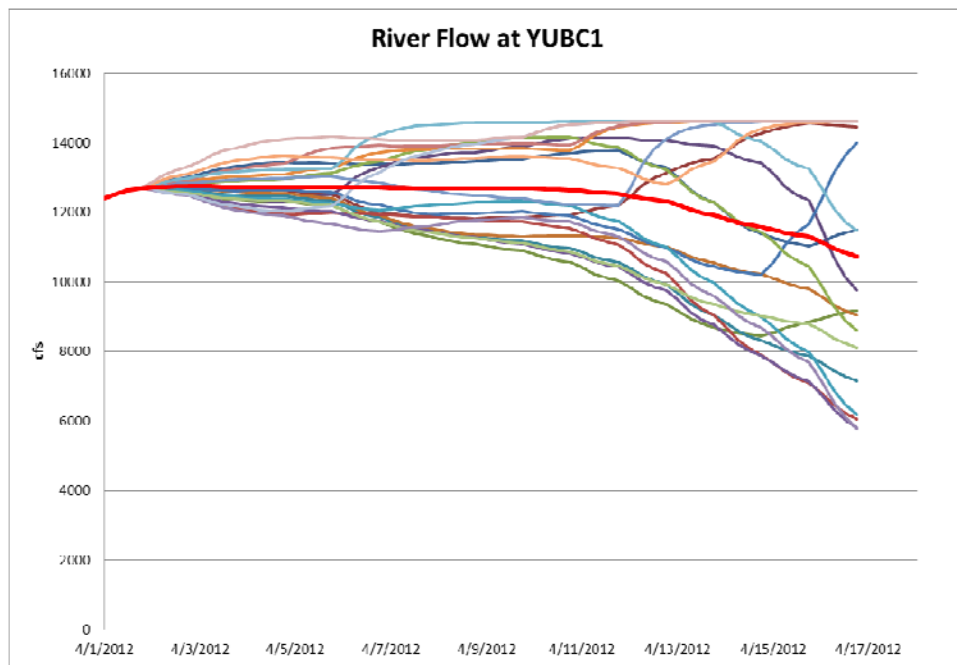


Figure 4.2.53: River Flow at Down Stream MRYC1

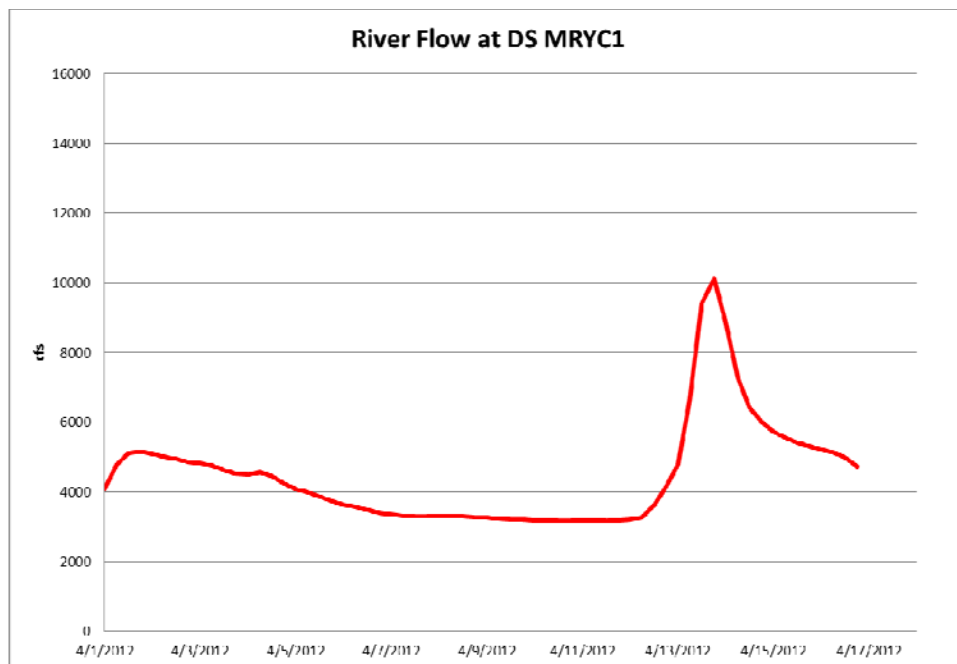


Figure 4.2.54: Stage Height at YUBC1; Oroville Target Elevation 860 feet.

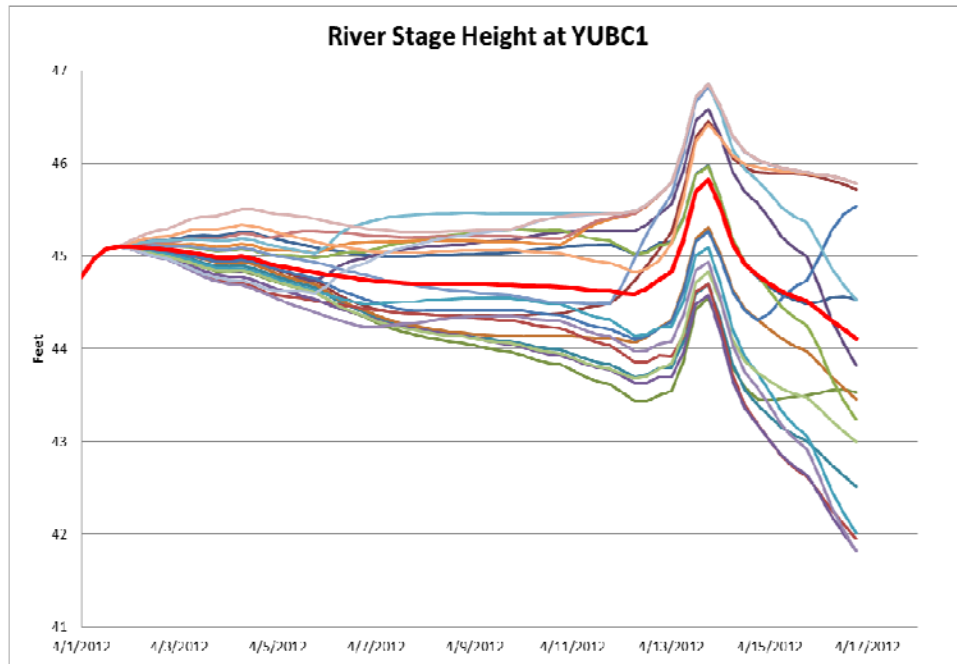


Figure 4.2.55: River Flow at FBLC1; Oroville Target Elevation 860 feet

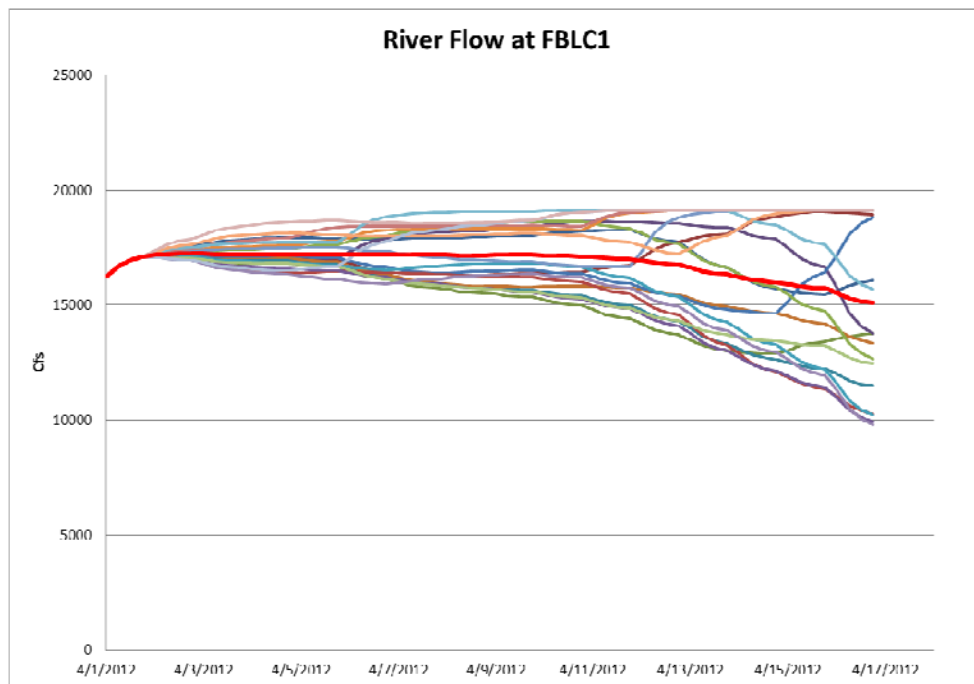


Figure 4.2.56: Stage Height at FBLC1; Oroville Target Elevation 860 feet.

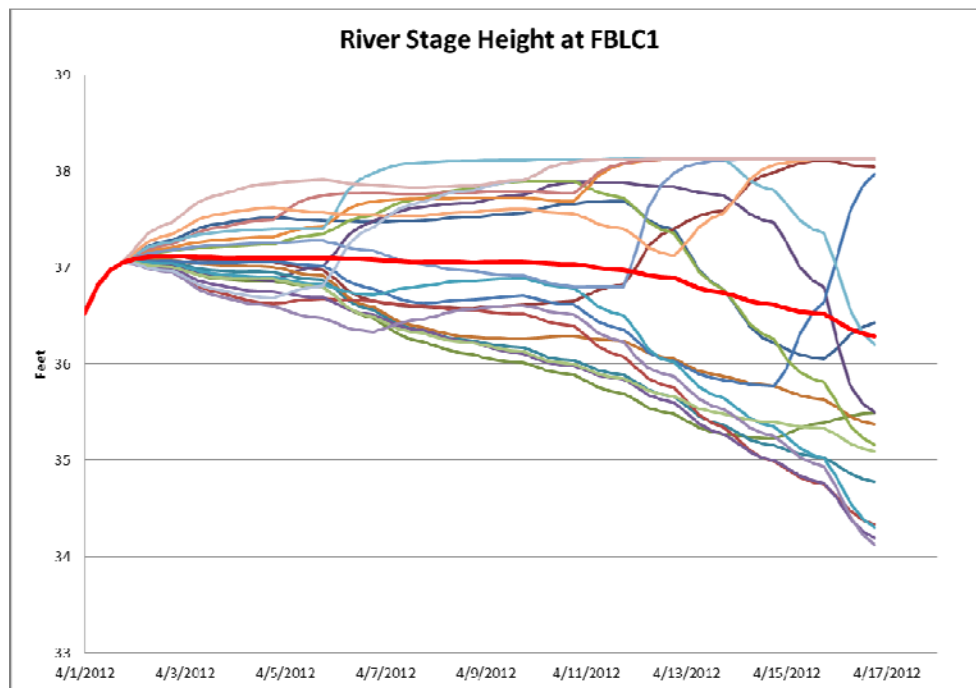


Figure 4.2.57: Oroville Release; Oroville Target Elevation 862 feet.

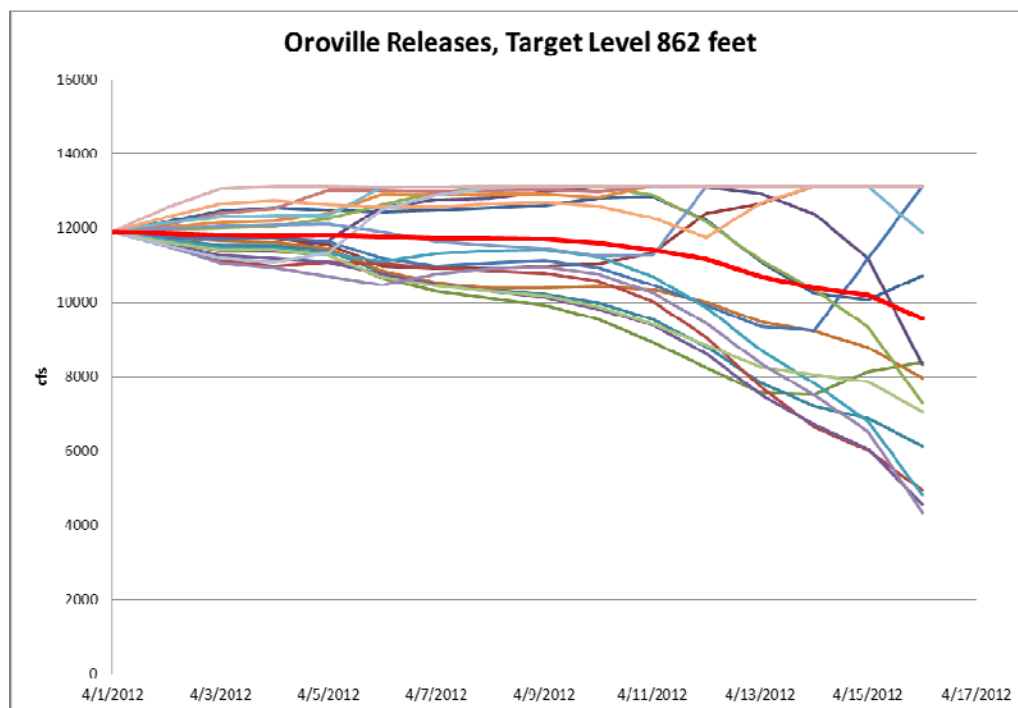


Figure 4.2.58: Oroville Elevations; Oroville Target Elevation 862 feet.

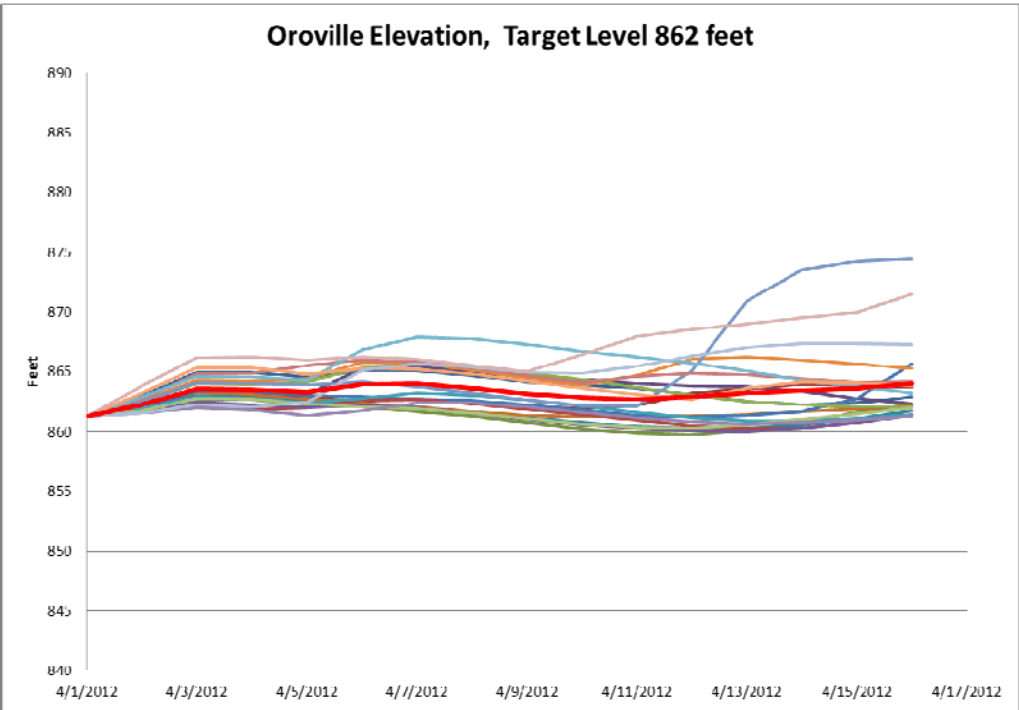


Figure 4.2.59: River Flow at FBLC1; Oroville Target Elevation 862 feet.

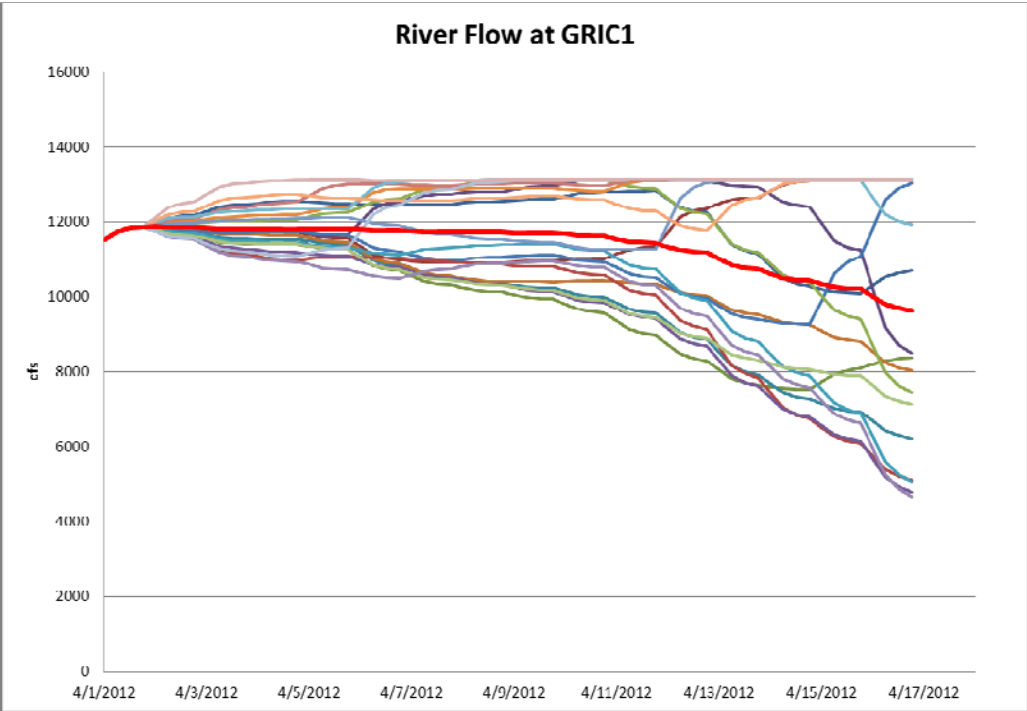


Figure 4.2.60: Stage Height at GRIC1; Oroville Target Elevation 862 feet.

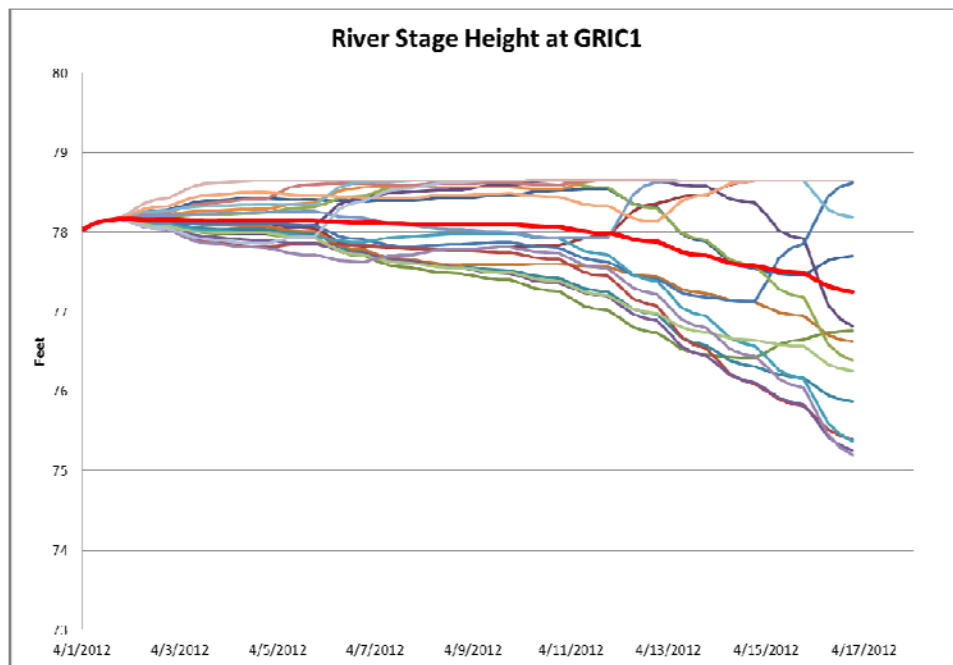


Figure 4.2.61: River Flow at FLVC1; Oroville Target Elevation 862 feet.

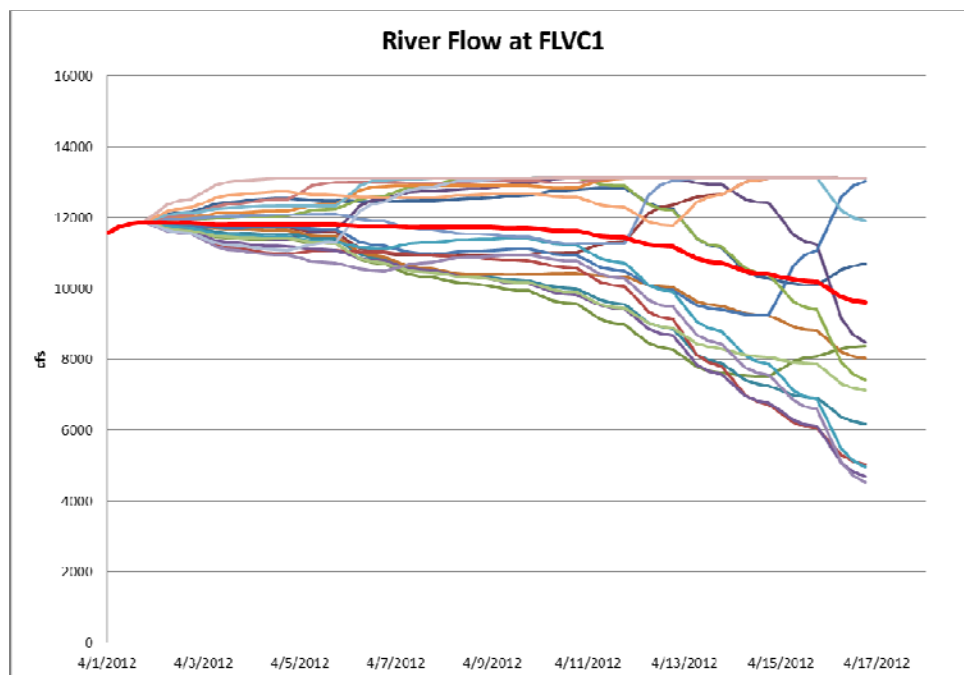


Figure 4.2.62: Stage Height at FLVC1; Oroville Target Elevation 862 feet.

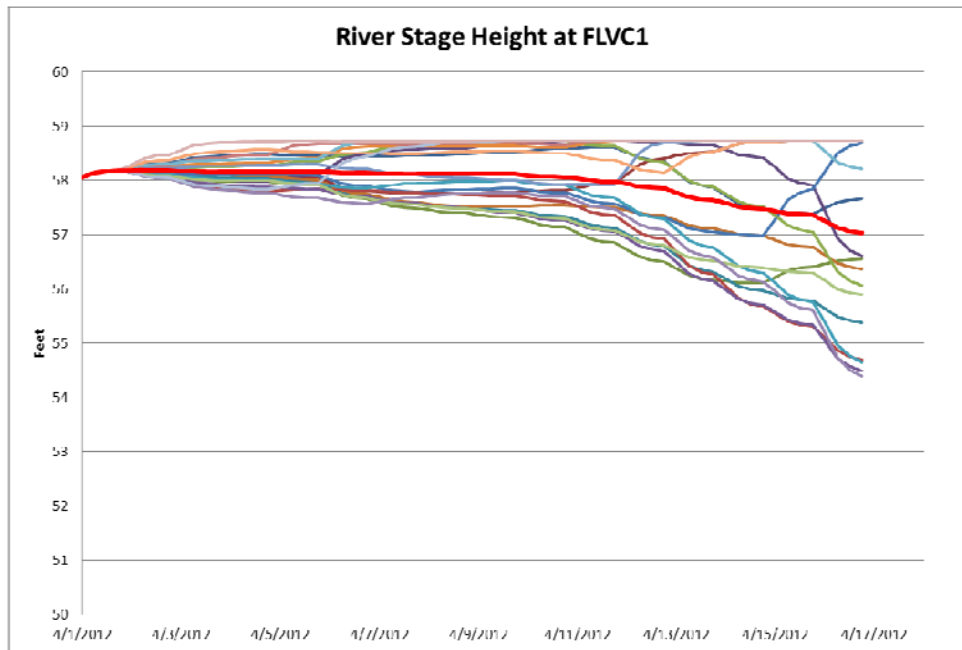


Figure 4.2.63: River Flow at YUBC1; Oroville Target Elevation 862 feet.

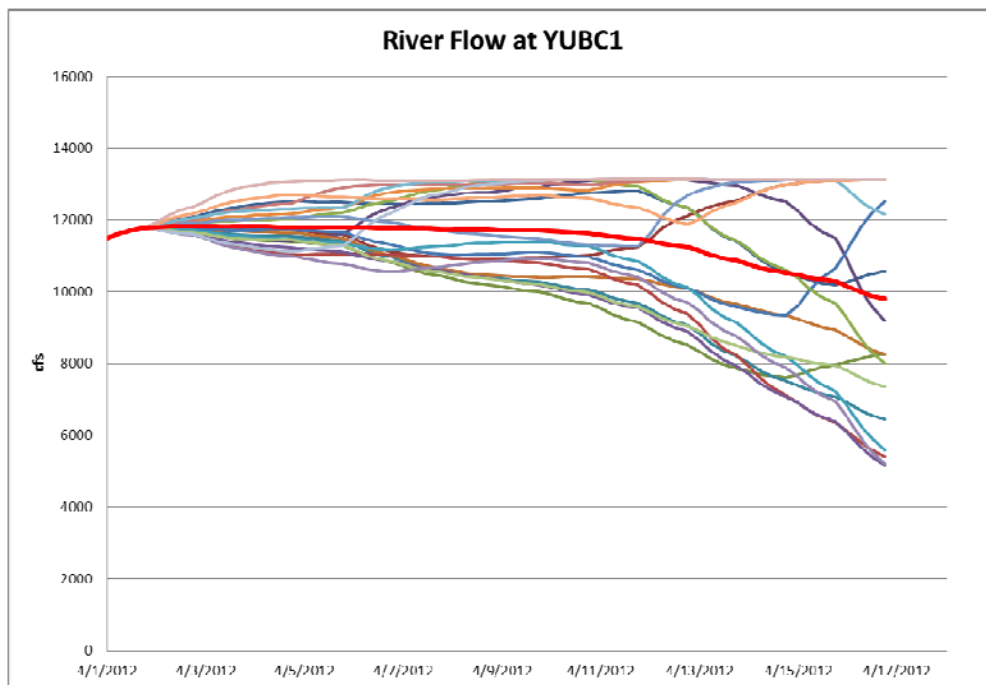


Figure 4.2.64: Stage Height at YUBC1; Oroville Target Elevation 862 feet.

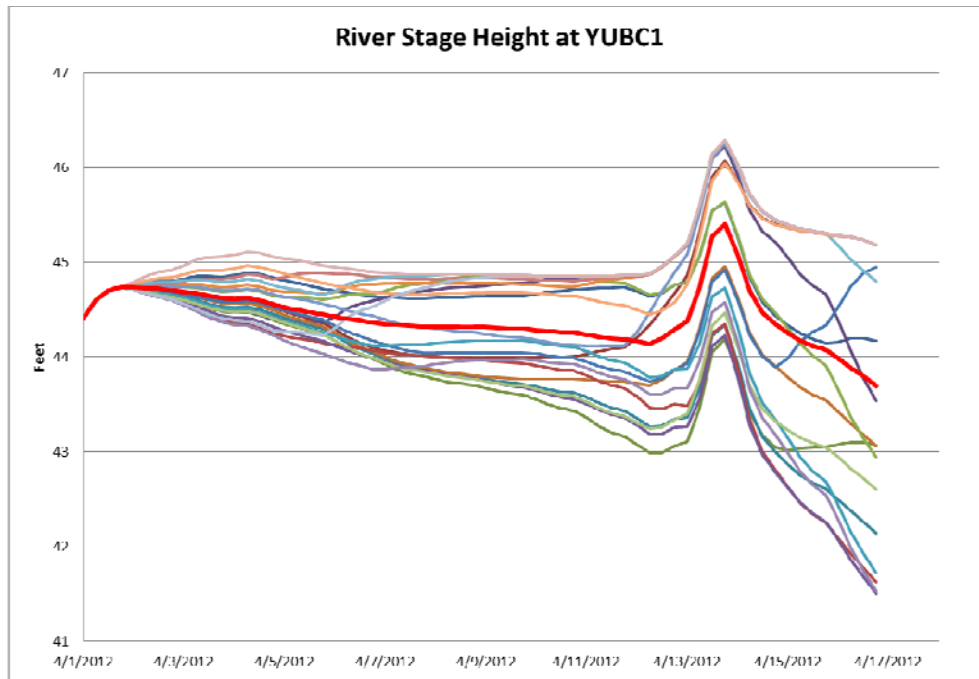


Figure 4.2.65: River Flow at FBLC1; Oroville Target Elevation 862 feet.

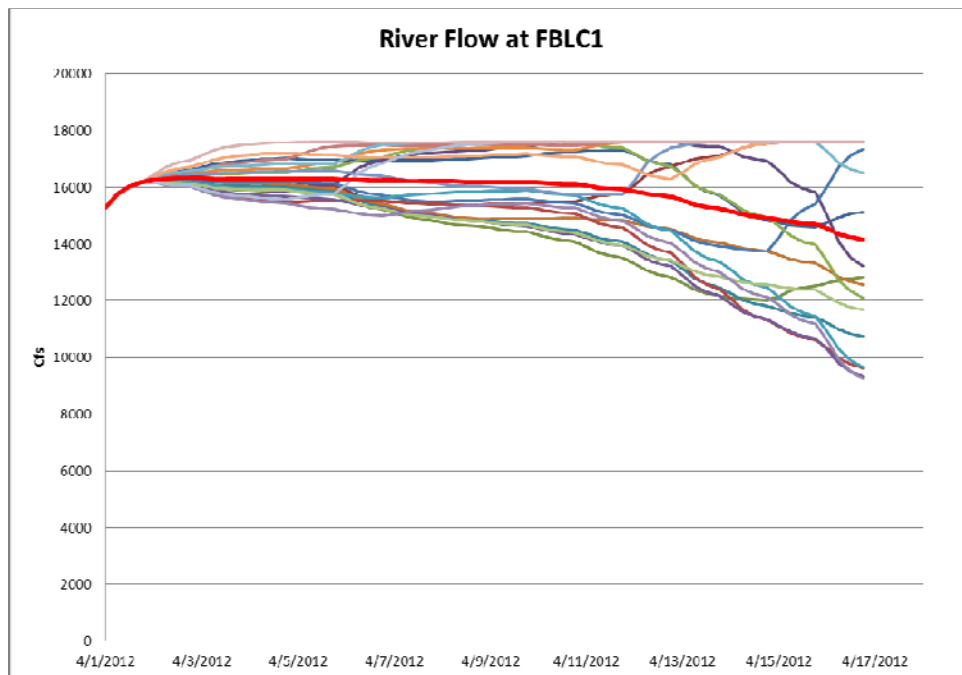


Figure 4.2.66: Stage Height at FBLC1; Oroville Target Elevation 862 feet.

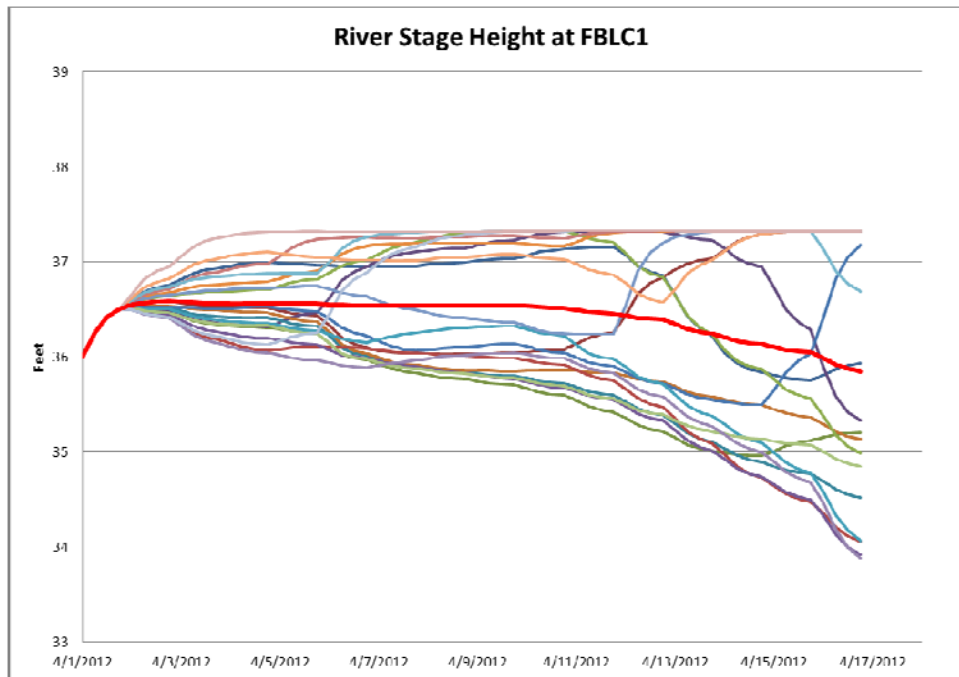


Figure 4.2.67: Oroville Elevation; Oroville Target Elevation 864 feet.

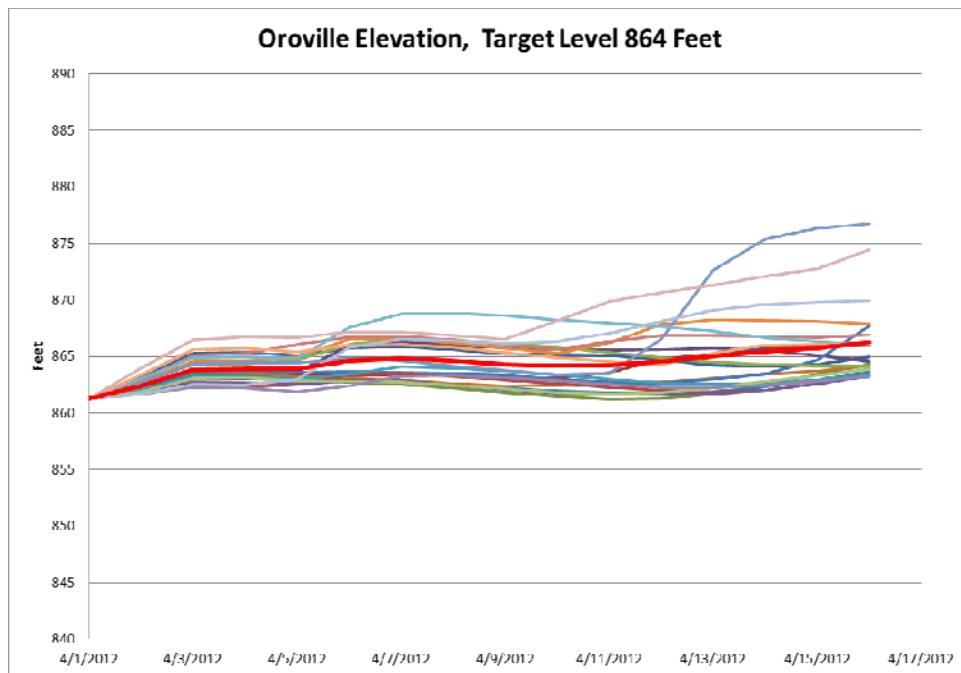


Figure 4.2.68: Oroville Release; Oroville Target Elevation 864 feet.

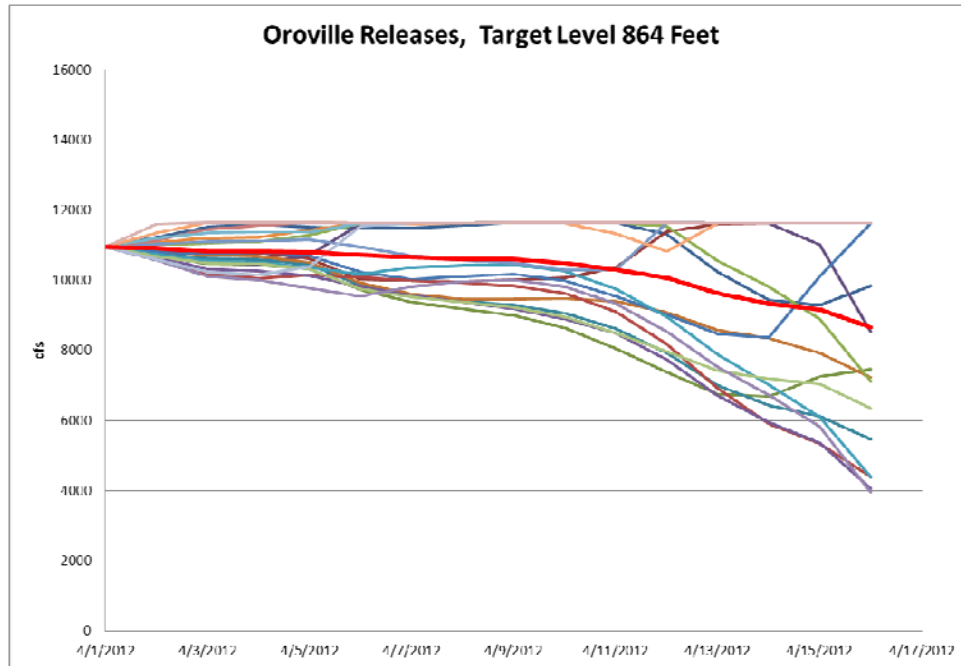


Figure 4.2.69: River Flow at GRIC1; Oroville Target Elevation 864 feet.

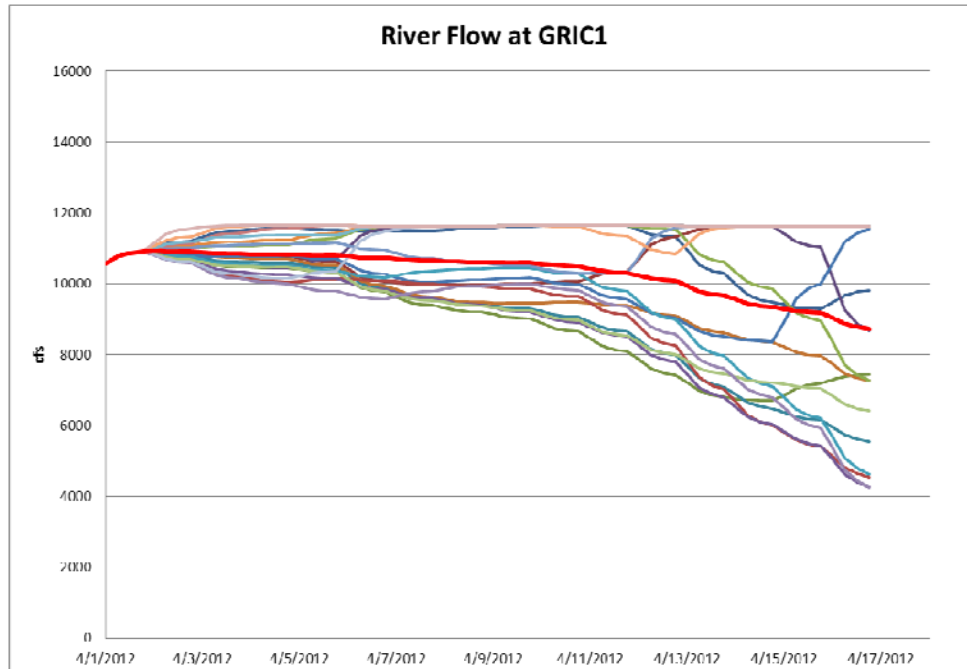


Figure 4.2.70: Stage Height at GRIC1; Oroville Target Elevation 864 feet.

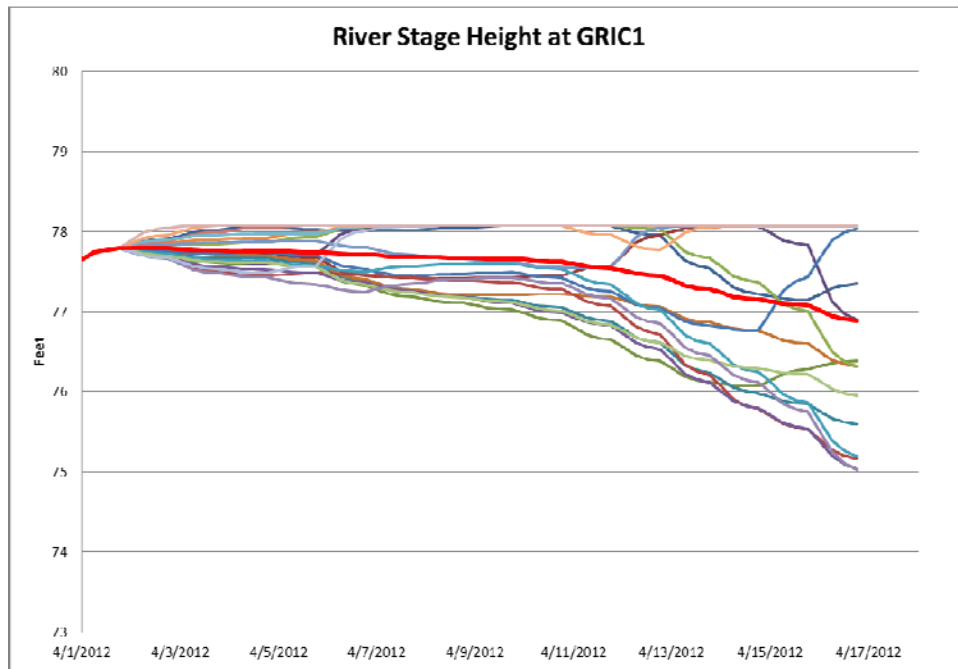


Figure 4.2.71: River Flow at FLVC1; Oroville Target Elevation 864 feet.

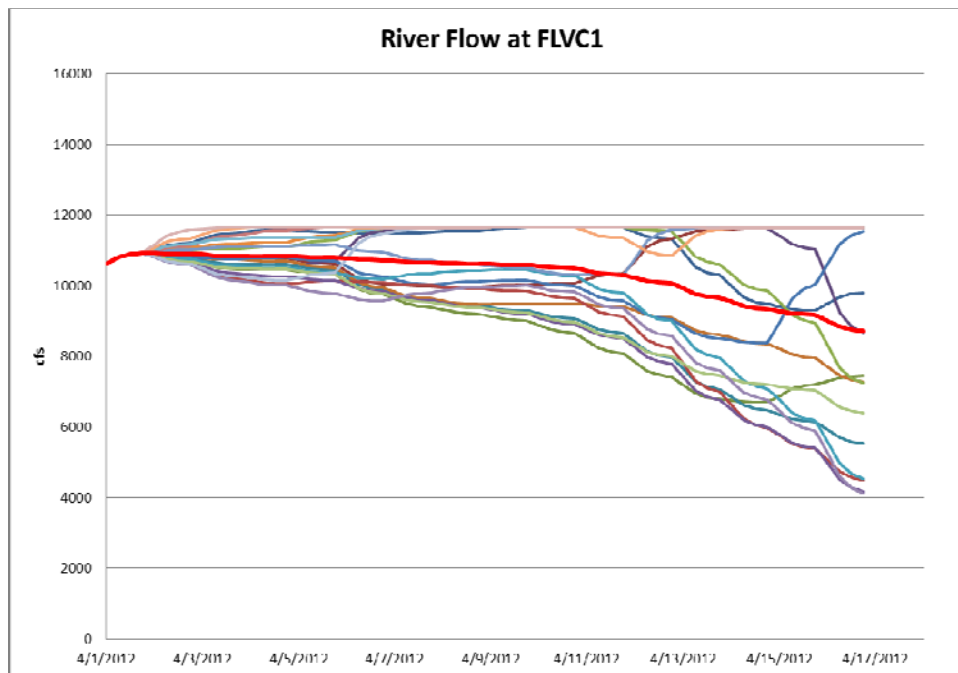


Figure 4.2.72: Stage Height at FLVC1; Oroville Target Elevation 864 feet.

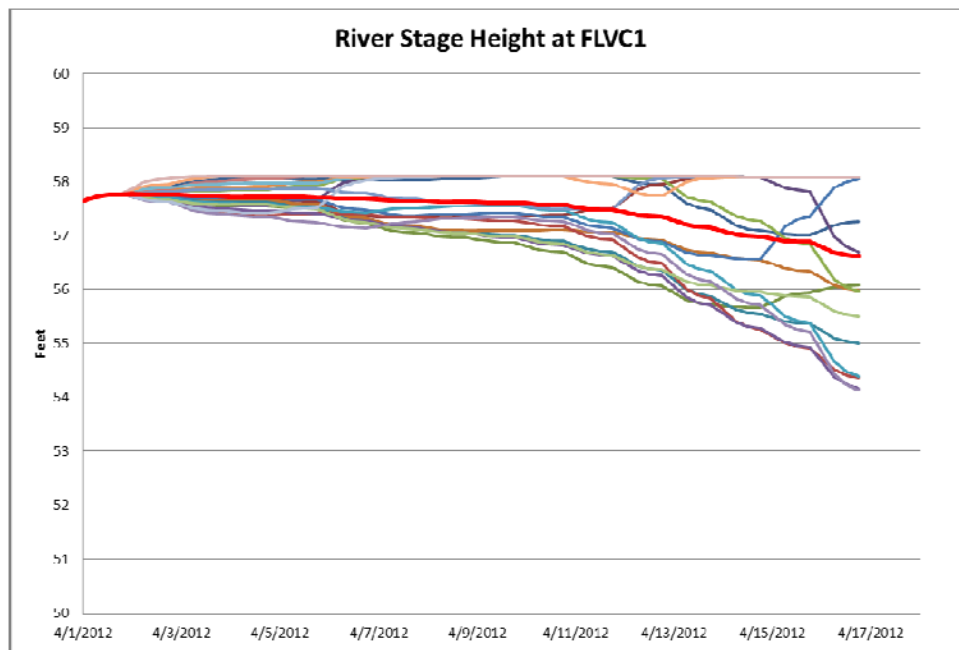


Figure 4.2.73: River Flow at YUBC1; Oroville Target Elevation 864 feet.

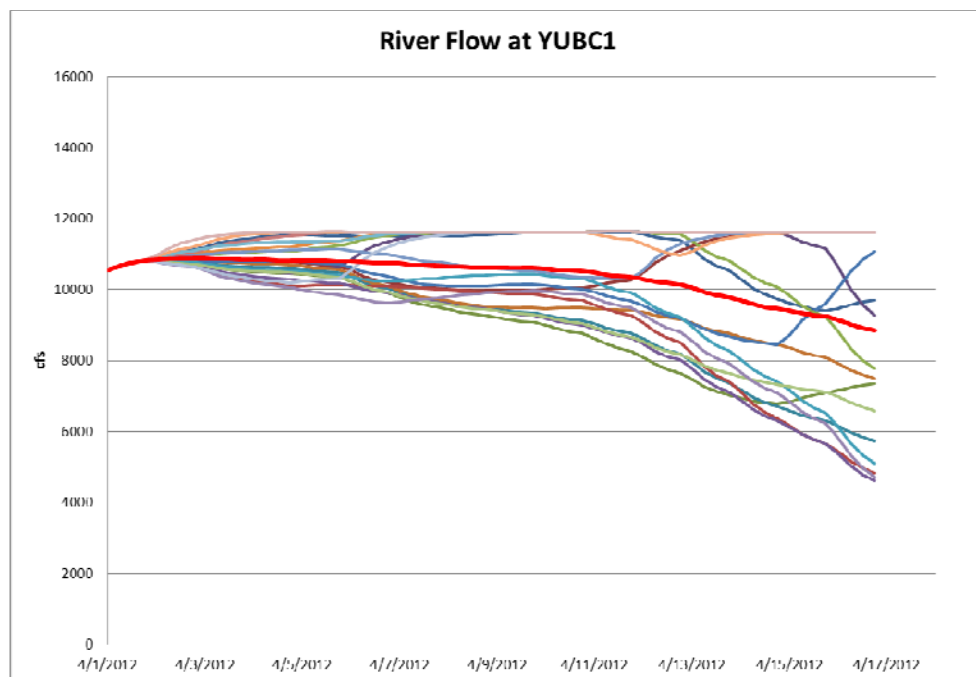


Figure 4.2.74: Stage Height at YUC1; Oroville Target Elevation 864 feet.

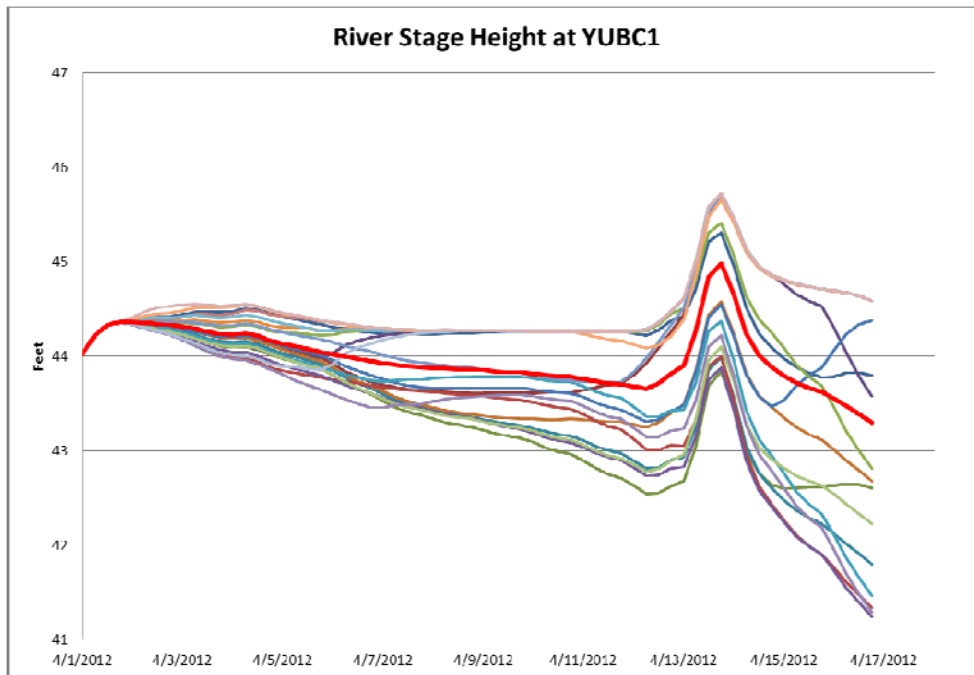


Figure 4.2.75: River Flow at FBLC1; Oroville Target Elevation 864 feet.

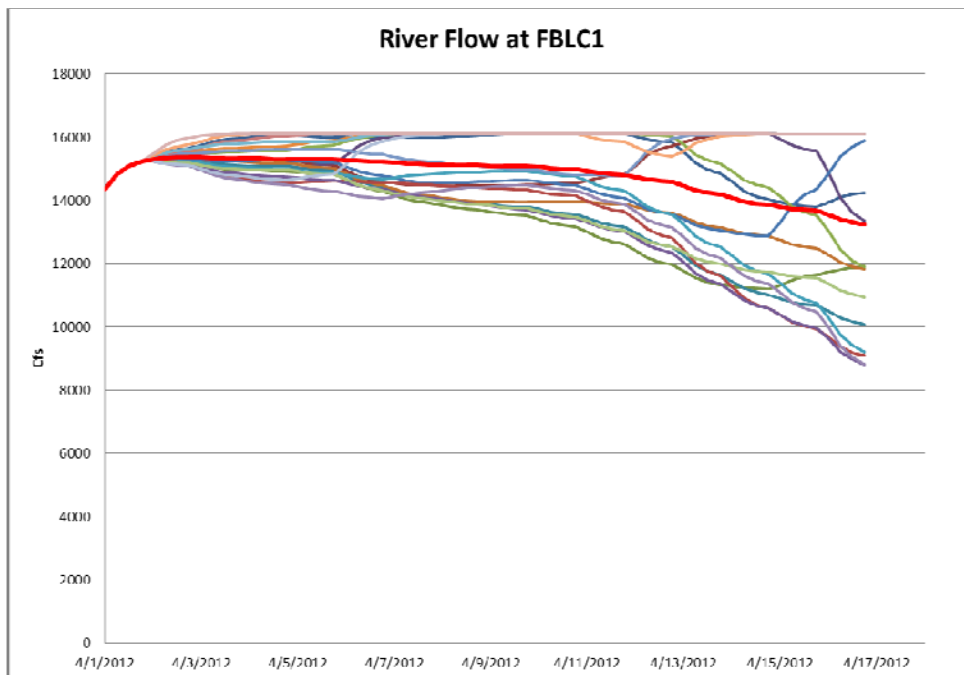


Figure 4.2.76: Stage Height at FBLC1; Oroville Target Elevation 864 feet.

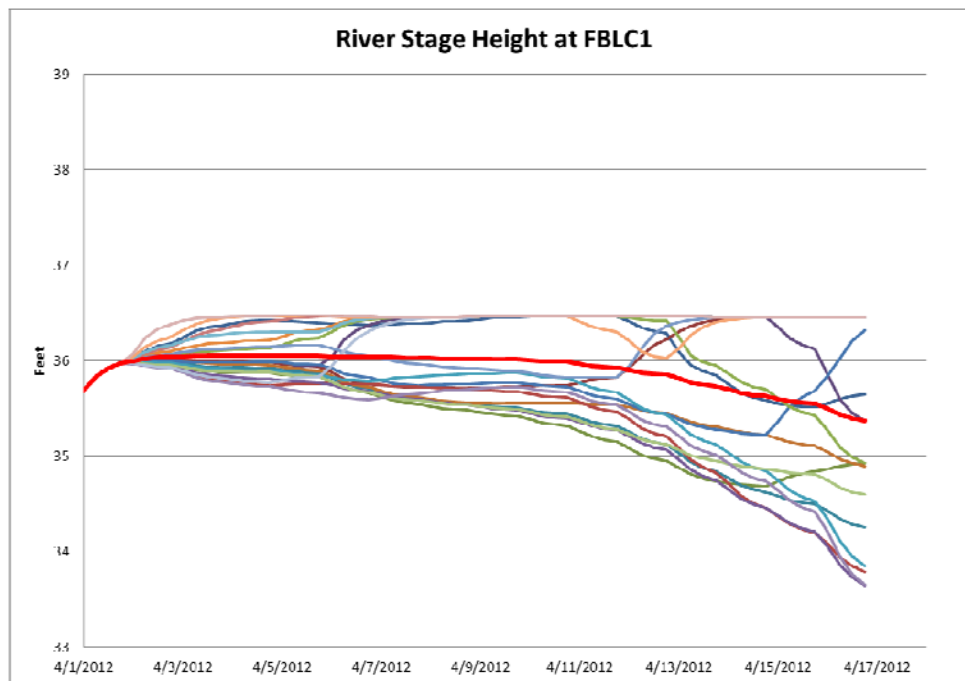


Figure 4.2.77: Oroville Mean Elevation Comparisons

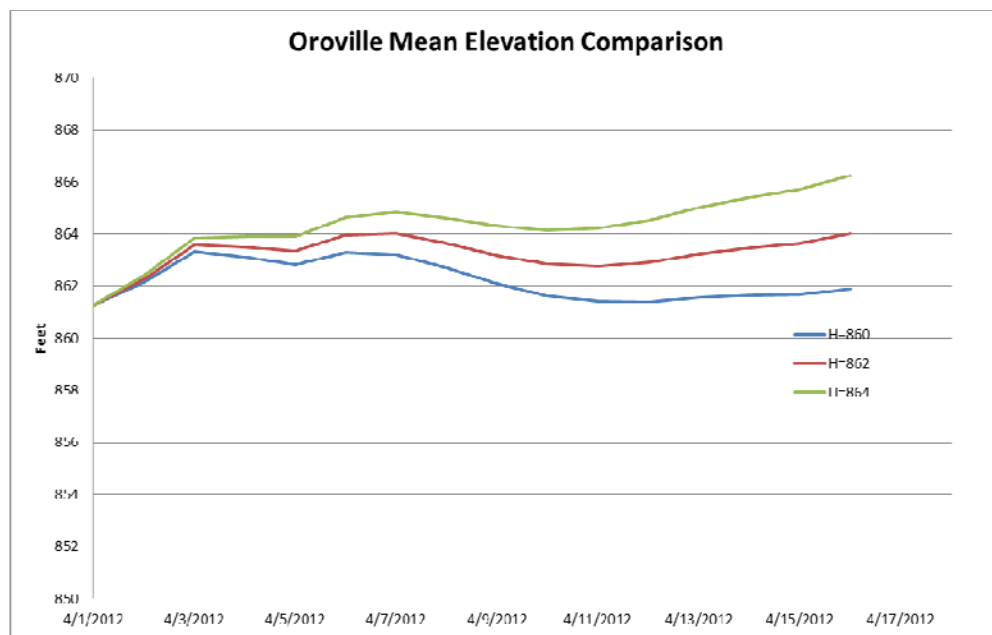


Figure 4.2.78: Oroville Mean Release Comparisons

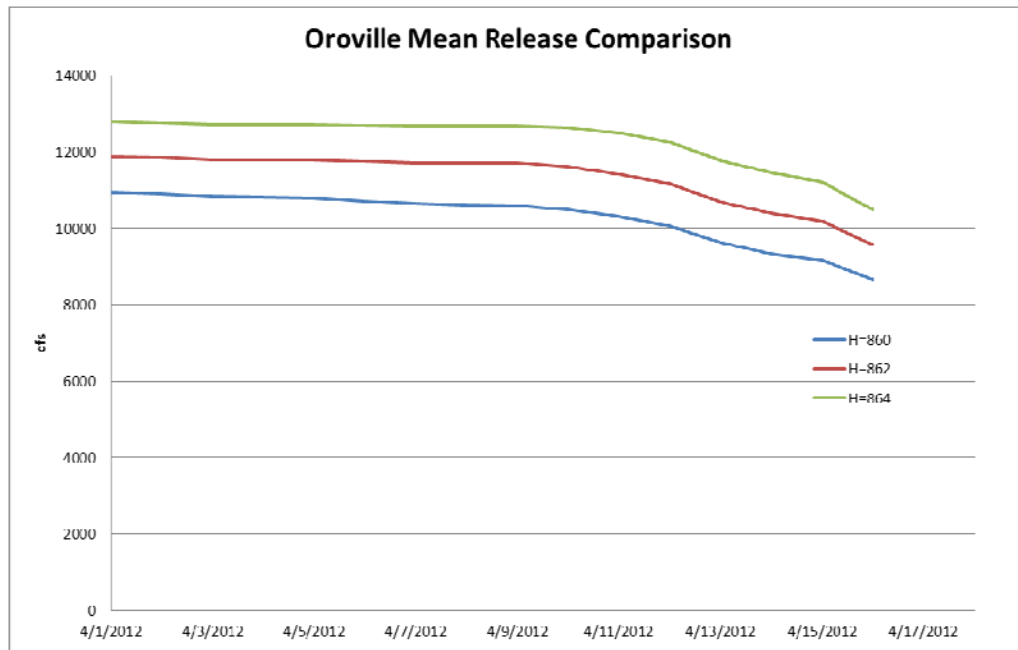


Figure 4.2.79: Stage Height Comparison at GRIC1

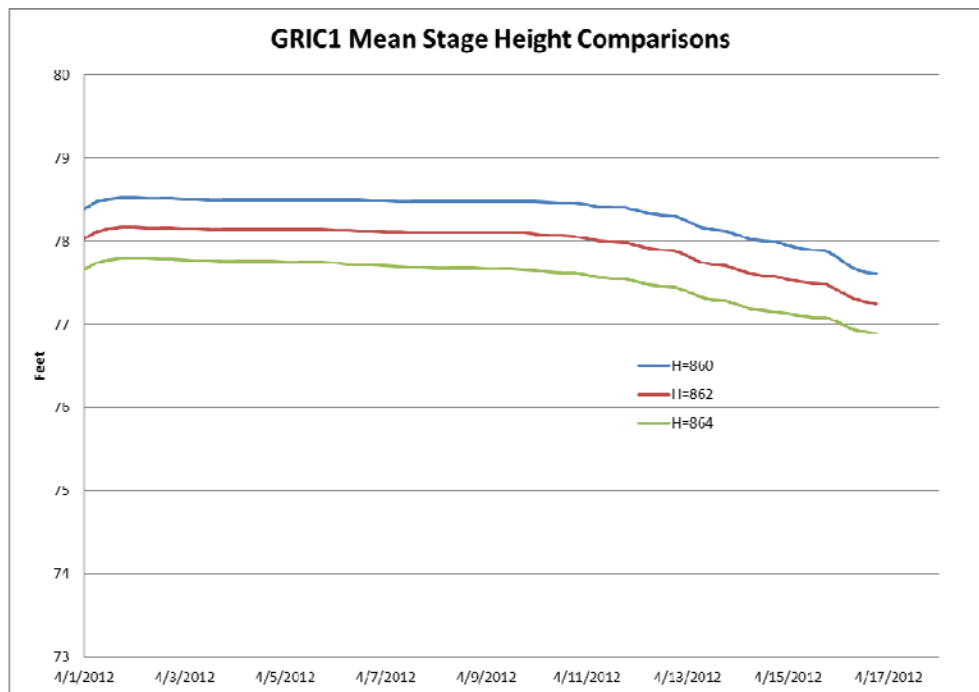


Figure 4.2.80: Stage Height Comparison at FLVC1

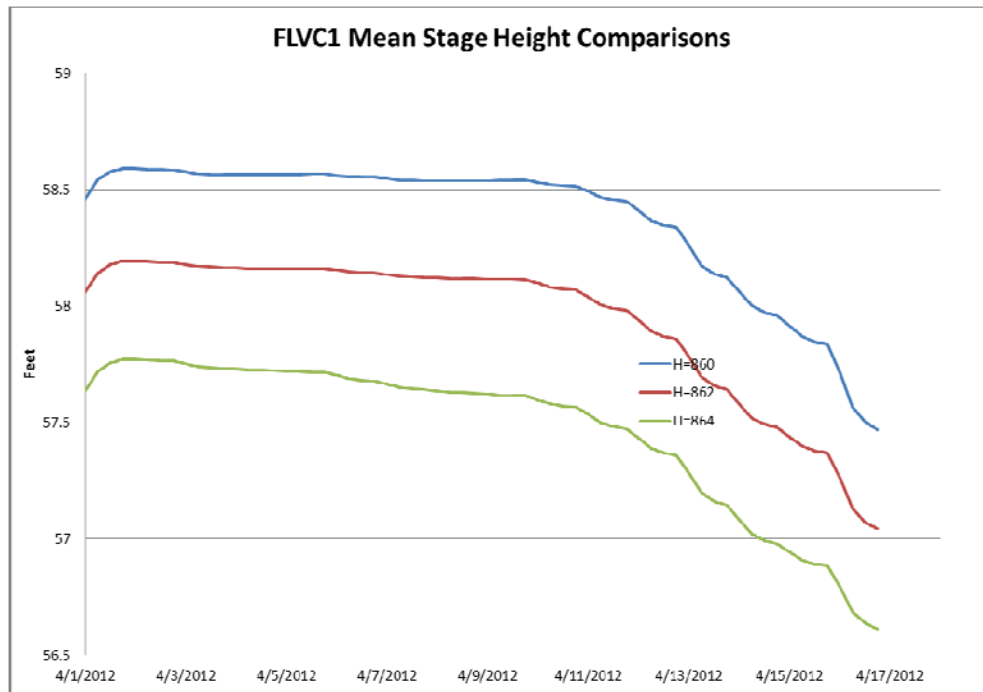


Figure 4.2.81: Stage Height Comparison at YUBC1

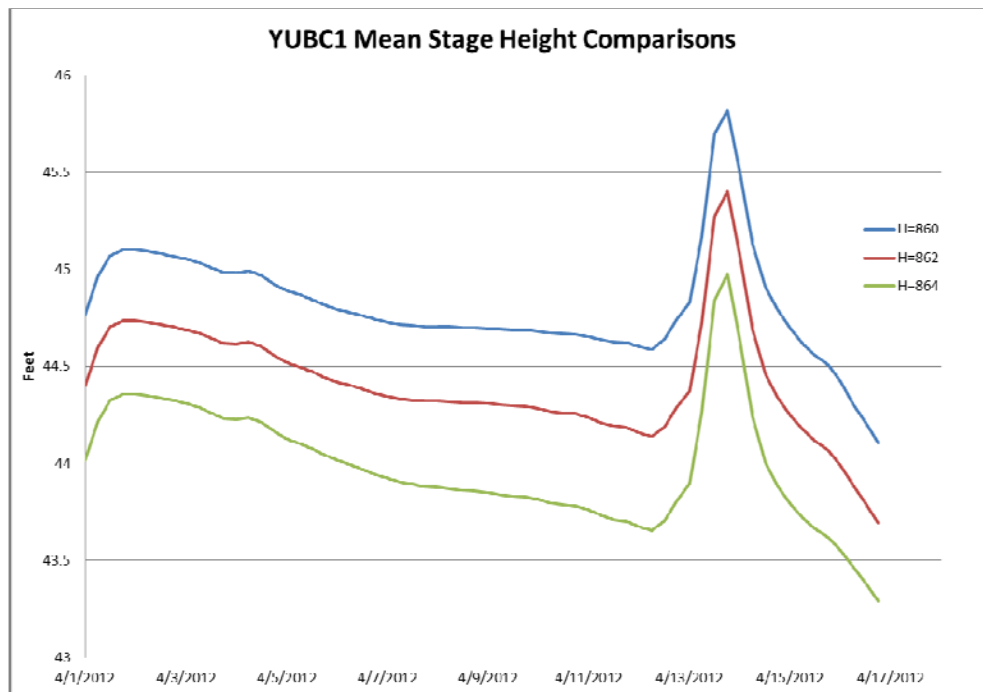


Figure 4.2.82: Stage Height Comparison at FBLC1

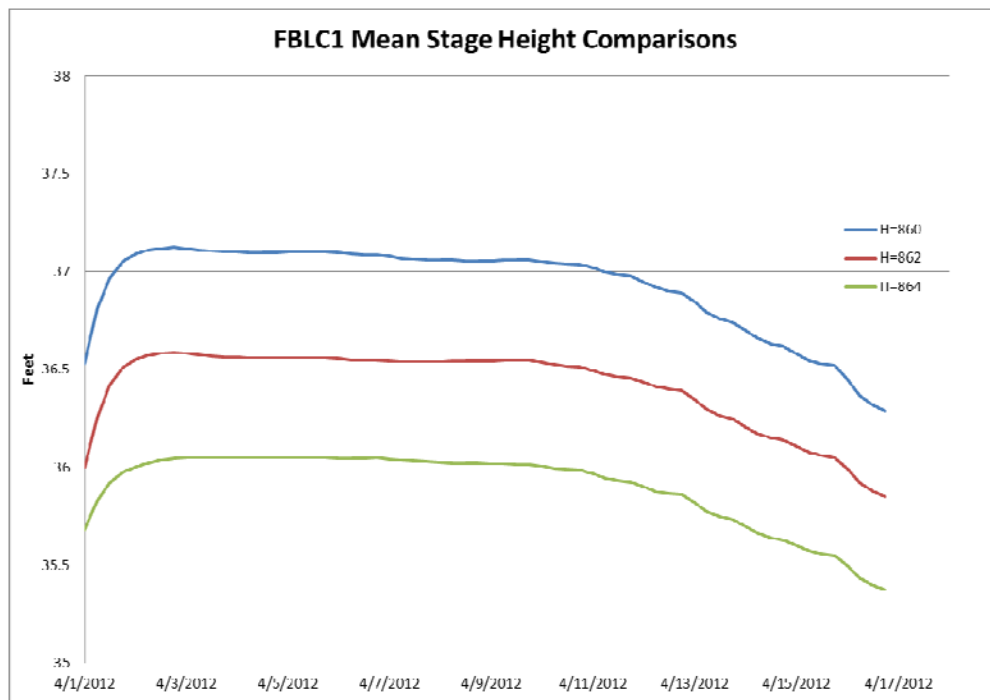


Figure 4.2.83: Oroville Mean Energy Comparison

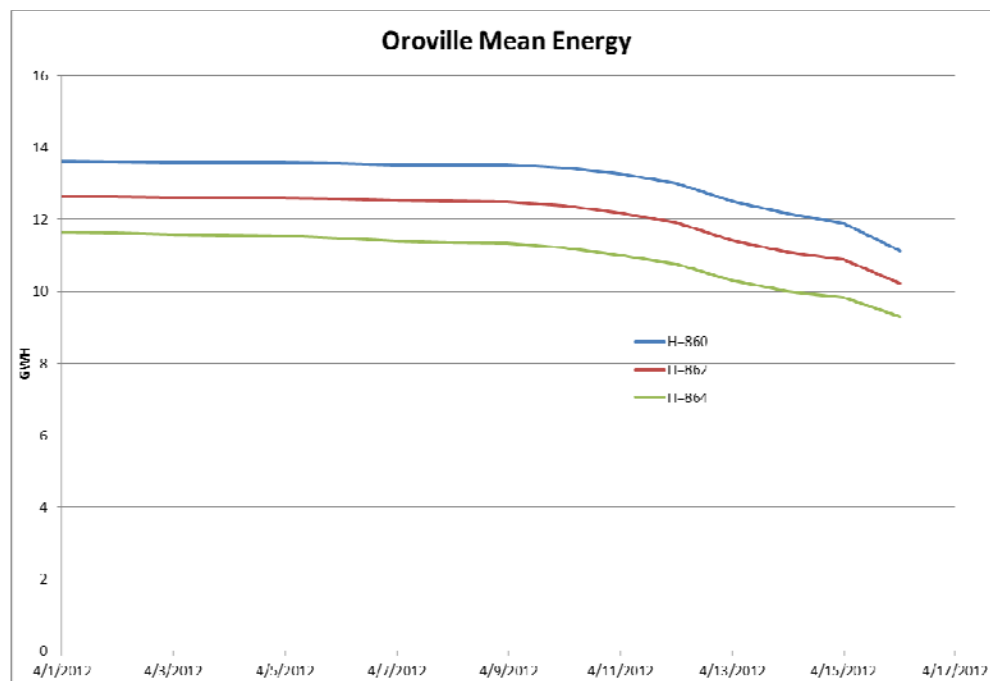


Table 4.2.6: Flow and Stage Height Statistics of River Nodes

	Stats	GRIC1	FLVC1	YUBC1	FBLC1
H=860	Max Flow (cfs)	14621	14621	14621	19101
	Mean Flow (cfs)	12336	12335	12378	16805
	Max Stage (feet)	79.22	59.36	46.85	38.13
	Mean Stage (feet)	78.34	58.37	44.82	36.93
H=862	Max Flow (cfs)	13126	13126	13126	17606
	Mean Flow (cfs)	11357	11355	11399	15825
	Max Stage (feet)	78.65	58.74	46.29	37.33
	Mean Stage (feet)	77.96	57.94	44.42	36.41
H=864	Max Flow (cfs)	11645	11645	11642	16124
	Mean Flow (cfs)	10322	10319	10363	14789
	Max Stage (feet)	78.08	58.09	45.72	36.47
	Mean Stage (feet)	77.55	57.47	43.99	35.90

Table 4.2.7: Oroville Statistics

	Stats	Value
H=860	Max Release (cfs)	14621
	Mean Release (cfs)	12300
	Max Elevation (feet)	872.23
	Mean Elevation (feet)	862.20
	Max Energy (GWH/d)	15.68
	Mean Energy (GWH/d)	13.09
H=862	Max Release (cfs)	13126
	Mean Release (cfs)	11320
	Max Elevation (feet)	874.48
	Mean Elevation (feet)	863.22
	Max Energy (GWH/d)	14.25
	Mean Energy (GWH/d)	12.09
H=864	Max Release (cfs)	11645
	Mean Release (cfs)	10285
	Max Elevation (feet)	876.76
	Mean Elevation (feet)	864.31
	Max Energy (GWH/d)	12.67
	Mean Energy (GWH/d)	11.00

CHAPTER 5:

Conclusions and Recommendations

5.1 Introduction

The second phase of the INFORM demonstration project implemented enhancements in the real-time weather forecast models, aligned the subcatchments used for hydrologic modeling to those of the operational CNRFC models, developed and tested a new optimization framework addressing management of system uncertainty, incorporated a reservoir and river water temperature modeling system for fisheries management, and developed new river routing models for downstream flood risk mitigation. The INFORM data ingest and forecast modeling system is now running in real time with forecasts presented through a secure web site for the collaborating agencies. This system provides information to the INFORM decision component for the development of risk-based trade-offs among objectives of water supply (for municipal, industrial, and agricultural users), hydroelectric energy generation, flood control, and fisheries management. Evaluation of the real-time performance of the INFORM forecast system was done as part of the second phase demonstration together with integrated assessments of forecast-management strategies. These developments and evaluations were presented in earlier chapters of this report and in the Appendices following this chapter.

5.2 Conclusions

The main conclusions from these analyses are mentioned below separately for the forecast and decision component of INFORM:

Forecast Component

- (1) Impressive skill for the CFS2-ICRM and especially the GFS-WRF ensemble forecasts was found for MAP and MAT in the subcatchments of the INFORM domain in Northern California. Clearly these models can be used to provide useful information for the INFORM subcatchments in real time out to two weeks both for the accumulation and the melt period.
- (2) Good forecast skill was found for reservoir ensemble full natural inflows generated by the GFS-WRF forcing and the hydrologic models of INFORM with lead times out to several days (4-6 days).
- (3) Low inter-catchment scatter in biases and steady values throughout the range of lead times provide clear evidence that bias corrections for the GFS-WRF model for MAP and MAT will be effective and provide improved flow forecasts.
- (4) There is evidence that indicates long-lead skill for CFS2-ICRM for large events in some cases.

Decision Component

- (1) A new uncertainty management framework was implemented and shown to be able to allocate the system forecast uncertainty selectively and effectively across the system storage and release variables. Putting this new capability to practice however requires that system planners and managers gain experience with the new framework and assess its value as part of the current decision processes.
- (2) The need and potential to support water temperature management to meet fisheries requirements together with other system objectives were clearly demonstrated. The management of water temperature imposes additional requirements on reservoir storage and release, and adds an important dimension to the system planning and management tradeoffs. A hybrid simulation-optimization methodology for water temperature management was implemented successfully. A full optimization approach seamlessly integrated with the INFORM DSS was also conceptualized and shown to have good potential for additional operational improvements.
- (3) A new state-space river routing model was developed and demonstrated for the Upper Feather and Sacramento Rivers. This routing model has the advantage of being compatible with the INFORM management framework while exhibiting accuracy comparable to the existing operational routing schemes. Using this model in connection with the INFORM forecast-decision system gave promising results as a means to manage downstream flooding risks. However, voluminous data requirements and acquisition delays prevented the development of the model for the lower river network reaches.

5.3 Recommendations

The following significant recommendations have emerged as part of INFORM II.

The first is to extend the demonstration period of the second-phase final INFORM system configuration in the following three wet seasons to provide additional opportunities for system evaluation and know-how transfer for agency personnel, managers, and planners.

In addition, work is needed to (i) fine tune the water temperature modeling system within the INFORM decision framework and (ii) allow for more extensive modeling of the numerous river network features to support flood management operations. Given the importance of large precipitation producing events and the need for longer lead time to manage them it is also recommended to couple the CFS2 with WRF and evaluate performance for lead times out to one month. For watersheds with significant upstream regulation effects, it is recommended that appropriate forecast adjustments be implemented based on a recent approach developed by the authors in collaboration with the NOAA River Forecast Centers. INFORM may also be used as a screening model for planning studies pertaining to the value of additional data, forecasts, long-

range predictions and management strategies in the integrated forecast and reservoir management of Northern California water resources.

INFORM may also be used as a screening model for planning studies pertaining to the value of additional data, forecasts, long-range predictions, re-operation strategies towards more integrated assessment and planning of the Northern California water resources.

REFERENCES

- Allen, R.G., Walter, I.A., Elliott, R., Howell, T., Itenfisu, D., and Jensen, M., (editors) 2005: *The ASCE Standardized Reference Evapotranspiration Equation*. American Society of Civil Engineers, Reston, VA, 59 pp + 6 Appendices.
- Becker, A. and Z. Kundzewicz, 1987: Nonlinear Flood Routing With Multilinear Models. *Water Resour. Res.* 23(6): 1043-1048.
- Camacho, L. A. and M. J. Lees, 1999: Multilinear discrete lag-cascade model for channel routing. *Journal of Hydrology* 226(1-2): 30-47.
- Carpenter, T. M., and K. P. Georgakakos, 2001: Assessment of Folsom Lake Response to Historical and Potential Future Climate Scenarios: 1. Forecasting. *J. of Hydrology*, **249**, 148-175.
- Castelletti, A., S. Galelli, M. Restelli, R. Soncini-Sessa, 2012: Data-driven dynamic emulation modeling for the optimal management of environmental systems. *Environmental Modeling & Software*. 34, pp. 30-43.
- Cunge, J. A. (1969). "On the subject of a flood propagation computation method (Muskingum method)." *J. Hydraulic Res.* 7(2): 205-230.
- Dooge, J. C. I. (1973). Linear theory of hydrologic systems. *USDA Tech. Bull.*. Washington, D.C., U.S. Department of Agriculture. **1468**.
- Dudhia, J., 1993: A nonhydrostatic version of the Penn State/NCAR mesoscale model: Validation tests and simulation of an Atlantic cyclone and cloud front. *Mon. Wea. Rev.*, **121**, 1493-1513.
- Elmore, K.L., 2005: Alternatives to the chi-square test for evaluating rank histograms from ensemble forecasts. *Weather and Forecasting*, **20**:789–795.
- Fischer, H.B., List, E.J., Koh, R.C, Imberger, J., Brooks, N.H., 1979: *Mixing in Inland and Coastal waters*. Academic Press.
- Fread, D. L. (1978). National Weather Service operational dynamics wave model. Silver Spring, Md., NOAA. **W23**.
- Garbrecht, J. and G. Brunner (1991). "Hydrologic Channel-Flow Routing for Compound Sections." *Journal of Hydraulic Engineering* **117**(5): 629-642.
- Georgakakos, A. (1989). "Extended Linear Quadratic Gaussian Control: Further Extensions." *Water Resour. Res.* **25**(2): 191-201.
- Georgakakos, A., K. Georgakakos and E. Baltas (1990). "A State-Space Model for Hydrologic River Routing " *Water Resour. Res.* **26**(5): 827-838.
- Georgakakos, A.P., 1989: Extended linear quadratic Gaussian control: Further extensions. *Water Resources Research*, **25**(2), 191–201.

Georgakakos, K. P., Graham, N. E., Carpenter, T. M., Georgakakos, A. P., and H. Yao, 2005: Integrating climate-hydrology forecasts and multi-objective reservoir management for Northern California. *EOS*, **86**(12), 122-127.

Georgakakos, K. P., Graham, N. E., Carpenter, T. M., Shamir E., Wang J., Sperfslage, J. A., Taylor, S. V., Georgakakos, A. P., Yao, H., and Kistenmacher, M., 2006: Integrated Forecast and Reservoir Management (INFORM) for Northern California: System Development and Initial Demonstration. *HRC TR No. 5*, Hydrologic Research Center, San Diego, CA, 268 pp. + 9 Appendices. Also on line at: http://www.hrc-lab.org/projects/dsp_projectSubPage.php?subpage=inform

Georgakakos, K., and R. Bras (1982). "Real-Time, Statistically Linearized, Adaptive Flood Routing." *Water Resour. Res.* **18**(3): 513-524.

Georgakakos, K.P., Carpenter, T.M., Graham, N.E., Georgakakos, A.P., Yao, H., and M. Kistenmacher, 2010: Operational Multisite Forecast and Reservoir Management in Northern California. *HRC Limited Distribution Report No. 34*. Hydrologic Research Center, San Diego, CA, (26 September 2010), 104pp.

Georgakakos, K.P., Taylor, S.V., and N.E. Graham, 2008: Implications of dynamic downscaling of Climate Forecast System (CFS) information for ensemble streamflow predictions in Northern California. *HRC Technical Note 42*. Hydrologic Research Center, San Diego, CA, (15 January 2010) 19pp.

Hoos, A., A. Koussis and G. Beale (1989). "A Channel Dynamics Model for Real-Time Flood Forecasting." *Water Resour. Res.* **25**(4): 691-705.

HRC-GWRI, 2007: Integrated Forecast and Reservoir Management (INFORM) for Northern California: System Development and Initial Demonstration. California Energy Commission, PIER Energy-Related Environmental Research. CEC-500- 2006-109, 244 pp. + 9 Appendices.

Hsu, W.R. and A. H. Murphy, 1986: The attributes diagram: a geometrical framework for assessing the quality of probability forecasts, *Int. J. Forecasting* **2**, 285-293.

Jolliffe, L. T., 2002: *Principal Component Analysis*. (Second Edition) Springer-Verlag, New York p. 167-195, 487pp. + illustrations.

Kalinin, G. P. and P. I. Milyukov (1957). On the computation of unsteady flow in open channels. Leningrad, USSR, *Meteorologiya Gidrologiya Zhurnal* **10**: 10-18.

Kalman, R. E. (1960). "A new approach to linear filtering and prediction problems." *J. Basic Eng.* **82D**: 35-45.

Karbowski, A., 1996: Methods of Determination of the Optimal Control Policies for Multireservoir Systems with Expected Value-variance Criteria in Bolza Problems. *Acta Geophys. Pol.*, **44**(3):287–300.

Kharin, V. and F. Zweirs, 2003: On the ROC Score of probability forecasts, *J. Climate* **16**, 4145-4150.

- Kim, D., and A.P. Georgakakos (2013), "A New Nonlinear Hydrologic River Routing Model", in review.
- Kistenmacher, M., 2012: Reservoir System Management under Uncertainty. Doctoral Dissertation. Georgia Institute of Technology, August 2012.
- Kistenmacher, M., and A. Georgakakos, 2013: Uncertainty management for multi-objective and multi-dimensional reservoir systems, in review.
- Kundzewicz, Z. W. (1984). "Multilinear flood routing." Acta, Geophys. Pol. **32**: 419-445.
- Leitch, M., 2010: ISO 31000:2009 The New International Standard on Risk Management. Risk Analysis, 30(6):887–892.
- Lewis, F. L. and V. L. Syrmos (1995). Optimal control. New York, J. Wiley.
- Liou, K.N., 2002: *An Introduction to Atmospheric Radiation (Second Edition)*. Academic Press, New York, 583pp.
- Liston, 1995: "Local advection of momentum, heat, and moisture during the melt of patchy snow covers." *Journal of Applied Meteorology* **34**, 1705-1715.
- Mason, S. J. and N. E. Graham, 2002: Areas beneath the Relative Operating Characteristics (ROC) and Levels (ROL) curves: Statistical significance and interpretation, *Quart. J. Royal Met. Soc.* **128**, 2145-1266.
- Muzik, I. (1974). "State variable model of overland flow." Journal of Hydrology **22**(3-4): 347-364.
- Nash, J. E. (1960). "A unit hydrograph study with particular reference to British catchments." Proc. Inst. Civ. Eng. **17**: 249-282.
- National Marine Fisheries Service, Southwest Region, 2009: Biological opinion and conference opinion on the long-term operations of the Central Valley Project and State Water Project. June 2009.
- O'Connor, K. M. (1976). "A discrete linear cascade model for hydrology." Journal of Hydrology **29**: 203-242.
- Perumal, M. (1992). "Multilinear muskingum flood routing method." Journal of Hydrology **133**(3-4): 259-272.
- Perumal, M. (1994). "Multilinear discrete cascade model for channel routing." Journal of Hydrology **158**(1-2): 135-150.
- Pielke, R.A., 1984: *Mesoscale Meteorological Modeling*. Academic Press, San Diego, CA, 612pp.
- Price, A. G., and T. Dunne, 1976: "Energy balance computations of snowmelt in a subarctic area." *Water Resources Research*, **12**, 686-694.

Resource Management Associates, Inc., 1998: User Manual: Simulation of Flood Control and Conservation Systems, Appendix on Water Quality Analysis. Report prepared for United States Army Corps of Engineers by Resource Management Associates, Inc. August 1998.

Resource Management Associates, Inc., 2003: Upper Sacramento River Water Quality Modeling with HEC-5Q: Model Calibration and Validation. Report prepared for US Bureau of Reclamation by Resource Management Associates, Inc. December 2003.

Rockel, B., and E. Raschke, 1994: "Inclusion of radiation in mesoscale models." *Mesoscale Modeling of the Atmosphere*, AMS Meteorological Monograph No. 47, R.A. Pielke and R.P. Pearce editors, American Meteorological Society, Boston, MA, 39-45.

Rowell, J. H., 1979: Mathematical Model Investigations: Trinity Dam Multilevel Outlet Evaluation, Trinity River Temperature Prediction Study. U.S. Bureau of Reclamation, Sacramento, CA.

Rowell, J. H., 1993 (revised 1997): Stanislaus River Basin Temperature Model. U.S. Bureau of Reclamation, Sacramento, CA, draft report.

Rowell, J.H., 1990: USBR Monthly Temperature Model-Sacramento River Basin. U.S. Bureau of Reclamation, Sacramento, CA.

Shamir, E., T.M. Carpenter, P. Fickenscher, and K.P. Georgakakos, 2006: Evaluation of the NWS Operational Hydrologic Model for the American River Basin. *ASCE J. Hydrologic Engineering*, **11**(5), 392-407.

Skamarock, W. C., J. B. Klemp, J. Dudhia, D. O. Gill, D. M. Barker, M. G. Duha, X. Huang, W. Wang, and J. G. Powers, 2008: A description of the Advanced Research WRF Version 3. *NCAR Tech. Note 475 STR*, 113 pp.

Smith, L.A., 2000: Disentangling uncertainty and error: On the predictability of nonlinear systems. *Nonlinear Dynamics and Statistics*, pages 31-64.

Sniedovich, M., 1980: A Variance-Constrained Reservoir Control Problem. *Water Resources Research*, **16**(2):271-274.

Stauffer, D.R. and N.L. Seaman, 1990: Use of four-dimensional data assimilation in a limited-area mesoscale model. Part I: Experiments with synoptic-scale data. *Mon. Wea. Rev.*, **118**, 1250-1277.

Stephens, G. L., 1978: "Radiation profiles in extended water clouds. II: Parameterization schemes." *J. Atmos. Sci.* **35**, 2123-2132.

Wasimi, S. and P. Kitanidis (1983). "Real-Time Forecasting and Daily Operation of a Multireservoir System During Floods by Linear Quadratic Gaussian Control." Water Resour. Res. **19**(6): 1511-1522.

Watkins, D. W., and D. C. McKinney, 1997: Finding Robust Solutions to Water Resources Problems. *Journal of Water Resources Planning and Management*, **123**(1):49-58.

Weinmann, P. E. and E. M. Laurenson (1979). "Approximate flood routing methods: A review." Journal of Hydraulic Engineering **105**(12): 1521-1536.

Wilks, D.S., 2004: The minimum spanning tree histogram as a verification tool for multidimensional ensemble forecasts. *Monthly Weather Review*, **132**, 1329–1340.

Wilks, D.S., 2006: *Statistical Methods in the Atmospheric Sciences*. Elsevier, Amsterdam.

Yao, H., and A. P. Georgakakos, 2001: Assessment of Folsom lake response to historical and potential future climate scenarios 2: reservoir management. *Journal of Hydrology*, **249**, 176–196.

APPENDIX A:

Computational Upgrades for INFORM II Forecast Component

INFORM II Hardware

The INFORM II project phase included the acquisition by HRC of a complete computational system upgrade. This section provides an overview of the hardware and software that hosts the INFORM II system. Upgrading of the hardware platform was considered necessary to provide expedient processing of ensemble forecasts in near real time (see design diagram in Figure 2.1 of Chapter 2).

The INFORM II computational system is hosted on a High Performance Computing (HPC) Linux cluster comprised of a total of 24 processing cores on 6 CPUs hosted across three backend nodes attached privately via gigabit Ethernet to a dedicated frontend node (Figure A.1). The specific hardware profile of the INFORM cluster involves three identical backend nodes whose role focuses on the computational processing while the frontend involves a unique hardware profile that is used to primarily provide data acquisition, data storage resources, data processing and management, processing control and product export for the web interface (images and text). Table A.1 outlines the hardware specifications for the various computer servers in the INFORM II cluster and Table A.2 identifies the general supporting hardware for installation and interconnectivity.

Figure A.1: INFORM Phase II HPC Linux Cluster Hardware - Frontend and Backend Servers

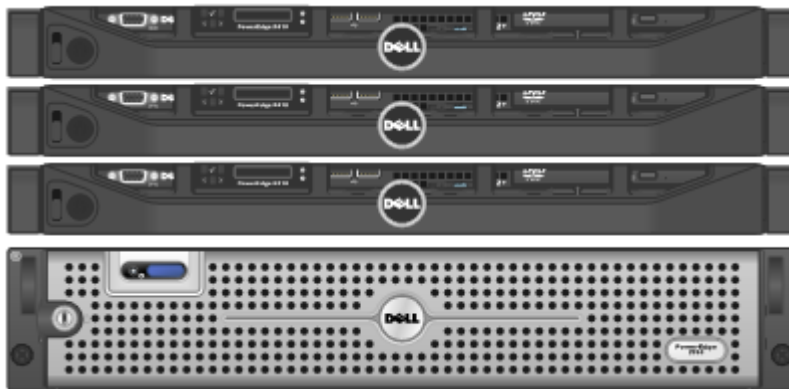


Table A.1: INFORM Phase II Cluster Computer Server Specifications – 6-CPU/24-Core Computational Backend

Specification Type	Frontend Node x 1	Backend Node x 3
Manufacturer	Dell	Dell
Model	PowerEdge 2950 III Rackmount Server	PowerEdge R410 Rackmount Server
Operating System	CentOS v5.9, 64-bit	CentOS v5.9, 64-bit
CPU Spec	Intel Xeon X5450 3.0GHz, 2x6MB L2Cache, 1333MHz FSB	Intel Xeon X5560 2.8GHz, 1MB L2 Cache, 8MB L3 Cache, 1333MHz FSB
CPUs Per Node	2	2
Cores Per CPU	4	4
RAM	16GB 667MHz, Dual Ranked DIMMs	8GB 1066MHz, Dual Ranked UDIMMS
RAID Controller	Add-in PERC 6i SATA/SAS	Integrated PERC 6/i SATA/SAS
Storage	2x250GB SATA HD in RAID1, 2x1TB SATA HD in RAID1	2x250GB SATA HD in RAID1
Optical Drive	DVD-ROM	DVD-ROM
Gigabit NIC Ports	4	2
Compiler	Intel Cluster Toolkit 3.2 Linux Edition	(only runtime support is required)

Table A.2: INFORM Phase II Cluster Supporting Hardware

Component	Description
Cluster Interconnectivity	D-Link 5-port Gigabit Ethernet Switch
Uninterruptable Power Supply	Dell 3000VA 120V 2U Rackmount UPS
Installation Rack	APC AR3100 42U 600mmx1070mm Rack

The INFORM II project included budget and effort to procure all new cluster hardware and migrate the INFORM system from its former Linux cluster procured under Phase I of the project in 2002. The previous cluster involved four computational nodes hosting a total of 8 single-core CPUs and a dedicated frontend server. The backend nodes were comprised of four distinct dual-processor motherboards contained within a single floor-standing tower chassis manufactured by *Rocketcalc* that were attached privately via gigabit Ethernet to an independent frontend server. For comparison, the corresponding specifications of the former cluster are provided in Table A.3.

The INFORM cluster uses a CentOS (Community Enterprise Operating System) v.5.9 64-bit operating system. CentOS is a no-cost, open-source upstream-vendor (Red Hat Inc.) redistribution of enterprise Linux available under the GPL license model. The primary motivation for selecting CentOS over its upstream source OS is that it has no subscription fees for ongoing access to updated software packages, security updates and errata patches. The CentOS distribution also supports a few key third-party software components that are utilized by the primary operational processing functionality of the HRC-developed INFORM forecast system. In some cases, the CentOS support is in terms of known compatibility while in other cases the OS distribution itself provides the necessary component. Among these key software components is the WRF (Weather Research and Forecasting Model) v3.2 developed by the National Center for Atmospheric Research (NCAR) which is operated by the University Corporation for Atmospheric Research (UCAR). The WRF software is in the public domain and provided "as-is" for download from www.mmm.ucar.edu. Another key contributing software component is the PostgreSQL v8.4 object-relational database management system (often referred to as simply as "Postgres"). The Postgres v8.4 database server is used by the INFORM system and comes included with the CentOS v5.9 enterprise Linux distribution as an optional upgrade to PostgreSQL v8.1 that is the standard release for CentOS v5. PostgreSQL is available at no cost as open-source software with its own licensing model. Additional third-party components that require independent acquisition, either through their providing agencies or by

using the pre-built packages of the Fedora EPEL (Extra Packages for Enterprise Linux) distribution channels, are the NetCDF and the related NCL (NCAR Command Language) packages. These provide specific data formatting, conversion and graphics rendering capabilities and are available at no cost under various open-source licensing models. See Table 2.4 for a summary listing of these software components.

Table A.3: INFORM Phase I Cluster Computer Specifications - 8 CPU/8-Core Computational Backend

Specification Type	Frontend Node x 1 (Independent Server Chassis)	Backend Node x 4 (Single Tower Chassis for All)
Manufacturer	Rocketcalc	Rocketcalc
Model	Titan T4-200	Custom
Operating System	Red Hat Linux 8.0 Professional (32-bit)	MOTOR Linux (32-bit)
CPU Spec	Intel Pentium IV 2.4GHz, 512KB L2 Cache, 533MHz FSB	Intel Xeon 2.0GHz, 512KB L2 Cache, 400MHz FSB
CPUs Per Node	1	2
Cores Per CPU	1	1
RAM	512MB PC2100 (266MHz) ECC DDR SDRAM	1GB PC2100 (at 200MHz) ECC DDR SDRAM
RAID Controller	none	none
Storage	1x120GB ATA HD, 1x300GB ATA HD	128MB Flash Drive
Optical Drive	CD-RW	none
Gigabit NIC Ports	4	2
Compiler	Portland Group Inc. Cluster Development Kit for Linux	(only runtime support is required)

Table A.4: INFORM Phase II Primary Software Components

Name	Description	Developer	Source of Acquisition	License
CentOS	Community Enterprise Operating System (Linux)	CentOS Project	www.centos.org	GNU Public License (GPL)
INFORM	Integrated Forecast and Reservoir Management System	HRC	HRC	HRC End-User License Agreement (EULA)
WRF v3.2	Weather Research and Forecasting Model	NCAR/UCAR	www.mmm.ucar.edu	Public Domain
PostgreS QL v.8.4	Object-Relational Database Management System	PostgreSQL Global Development Group	Included with CentOS v5.9	PostgreSQL
NetCDF	Network Common Data Form	NCAR/UCAR	Fedora EPEL repositories	UCAR (MIT-Style NetCDF C Library License)
NCL	NCAR Command Language	NCAR/UCAR	Fedora EPEL repositories	NCL Binary License

Implementation of Updated INFORM System Backbone

Overview of Goals

INFORM II development efforts included the implementation of the INFORM II System on the newly acquired hardware that was detailed in the previous section above. These efforts focused on (a) the migration of the relevant INFORM forecast components to the new hardware, (b) design and implementation of any necessary changes in the existing INFORM software to accommodate as many ensemble members as possible, and (c) testing the new operational hardware-software system with real-time input from Global Forecast System (GFS) and Climate Forecast System (CFS) ensemble forecasts from the National Centers of Environmental Prediction (NCEP).

Design goals of updated INFORM System Backbone

The primary design goals for the updated INFORM System “Backbone” software were to maintain modularity, flexibility and ease of expandability; they were motivated largely by the fact that the INFORM System performs real-time processing of numerous data sets produced at regular intervals throughout the day and derived from multiple ensemble members of the GFS and CFS. These data products require management and the potential for expansion relating to the number of ensemble members and input streams, each of which require analogous processing operations. As a consequence, the INFORM System data-management strategy has been developed to treat all data products as abstract, or generalized, data that can be applied across multiple, easily configurable, modularized processing components. To this end, all real-time input and processed data products undergo “standardization” and are stored within a defined and common data-management framework in the INFORM PostgreSQL Database. Once standardized, any data product may be processed as appropriate by any INFORM processing module according to a set of fully-configurable parameters that dictate the particulars of each standardized data product. Such fully-configurable parametric metadata are referred to as “Definitions” while processing tasks performed according to these definitions are referred to as “Operations.”

Consider as an example of this generalized processing according to configurable metadata the GFS input processing. The GFS provides forecasts with 20 ensemble members. Each of these 20 ensemble members, after WRF processing, provides a gridded precipitation and a gridded temperature product. These 20 gridded precipitation products and 20 gridded temperature products are standardized gridded data with definitions describing every aspect of their application within the system, including but not limited to: the grid domain and resolution, processing interval at which each is initialized, the maximum lead time for each forecast, file-repository in which each data file is stored, and more. With this information, “Operations” are configured for a Mean Areal Aggregation Module to transform each of these gridded data products into 20 independent mean areal precipitation (MAP) and 20 independent mean areal temperature (MAT) data products, each of which having analogous product description definitions. These description definitions are later applied as input to the Basin Hydrology and Routing Model Module according to the configured Operations for that module.

At any time in the future that new input data streams or new data products are added, a simple expansion of the INFORM configuration to include new or updated Definitions and/or Operations is all that will be required for inclusion of the new data. Additionally, as new or expanded data processing functionality becomes necessary in the INFORM System, modularized processing components can be added in order to apply the standardized data products as appropriate with no alteration to the existing data management framework. For example, upon the completion of the Bias-Adjustment Module (see Figure 2.1 in Chapter 2), the INFORM definitions and operations will be re-configured to perform Bias-Adjustment Operations on each of the independent reservoir inflow products, regardless of ensemble origin.

Update and Integration of Existing INFORM Components as Modules

In order to leverage the flexibility of the new system hardware and the updated backbone, the relevant existing processing components of the INFORM System were migrated and integrated into the newly developed framework. While several of the data-management and processing components included in the new INFORM framework represent new design and development, two processing components, in particular, required careful integration into the new framework: the simplified orographic model of the first phase of INFORM (called SIMOROP Model) and the Basin Hydrologic and Routing Models. Both of these models were migrated as component modules in the updated framework.

The SIMOROP Model, which processes the CFS sounding input data files and produces estimates of orographic precipitation in the form of gridded fields, has been expanded to include sounding input files for Eureka in addition to the existing Oakland sounding input files and updated to operate as a single modularized component of the Intermediate Complexity Regional Model (ICRM). The end result of this processing module is a standardized forecast MAP data product, which is ingested into the database for future application within the ICRM component and the Hydrologic Models. The processing capability of the SIMOROP Model has also been updated as part of the migration to account for scalability of the CFS ensemble size in preparation for the expansion of the CFS to 4 ensemble members 4 times daily as well as allow for the parallel processing of multiple SIMOROP operations in isolated working environments.

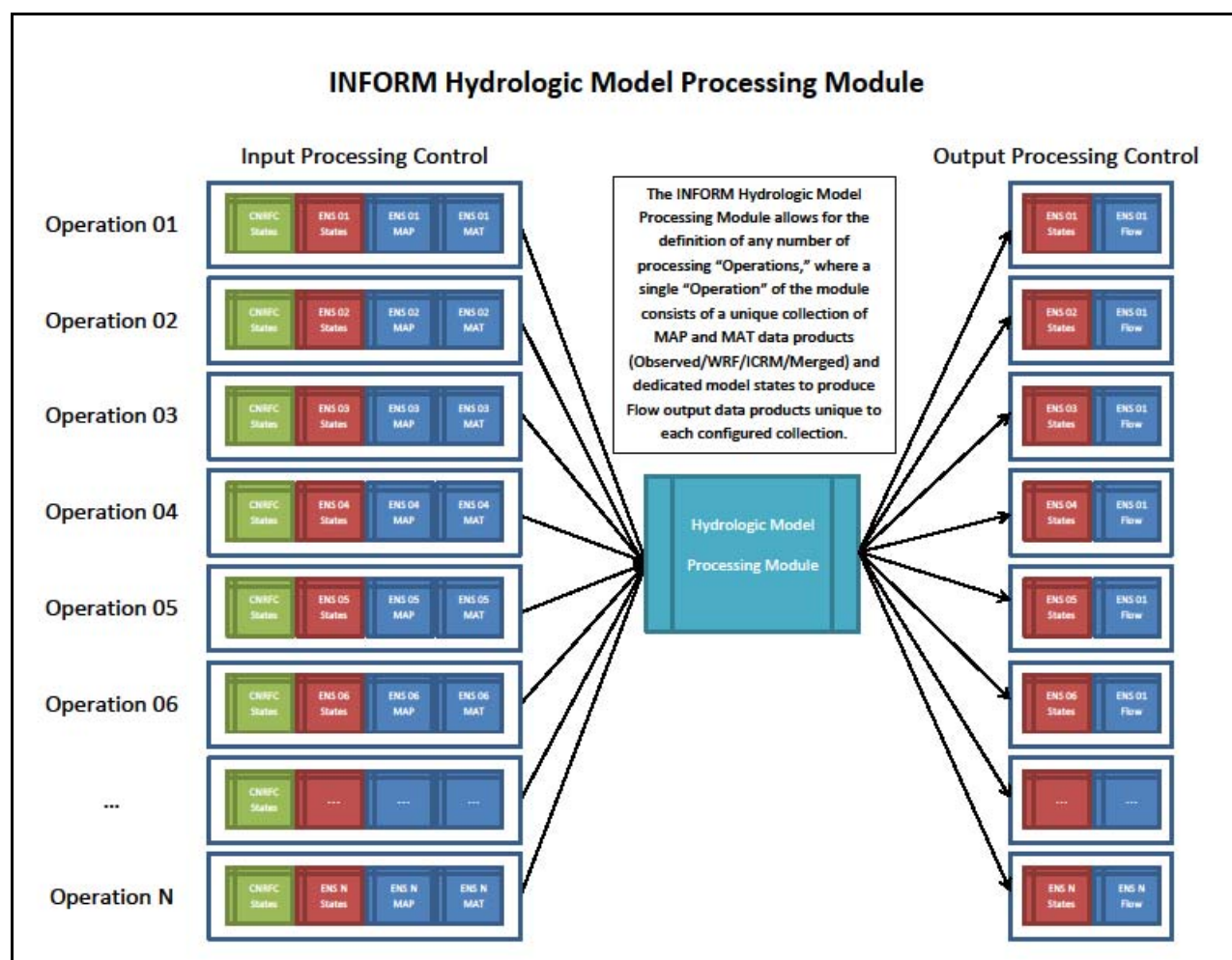
Similarly, the existing INFORM Hydrologic Models were updated to reflect the current CNRFC segment definitions and parameters refined. Once this update was complete, the hydrologic models for the drainage basins of Folsom, Oroville, Shasta, Trinity and New Bullards Bar/Englebright were integrated into the updated INFORM System Backbone for flexible processing orchestration. The framework for the Basin Hydrology and Routing models was designed to facilitate configuration of processing operations to be performed for any of the five reservoirs individually using any standardized MAP & MAT data product and defined model states as input while storing the data results (unimpaired or FNF reservoir inflow) and model states of any defined operation as standardized data sets. This flexible configuration allows for operations to be defined for any number of data-processing streams or, in this case, any number of standardized data products from any number of ensemble members or processing origins. As it is configured now, the INFORM System is capable to independently process the Basin Hydrology and Routing model with forcing data produced by the 20 GFS ensemble members as processed by WRF every 12 hours and the 4 CFS ensemble members as processed by the ICRM four times every day, with each of these defined processing operations storing its respective output (reservoir inflow and model states) separately. Additionally, each operation is configured such that, when available in the database, CNRFC-provided operational hydrologic (SAC SMA) and snow (SNOW17) forecast model states are applied as initial conditions. In the absence of CNRFC-provided model states, each operation is configured to apply the model states produced during the previous model initialization for that operation as initial conditions. See Figure A.2 for a schematic of the configuration of this module.

Overview of Processing Activities

Acquisition of CFS Forecast Input

The real-time CFS2 forecast input data product features four ensemble members valid from CFS initializations at 00:00, 06:00, 12:00 and 18:00 UTC, daily, and has a latency of approximately 12 hours from model initialization. The CFS data is downloaded from NCEP data servers four times per day, with acquisition execution scheduled at 1:00, 7:00, 13:00 and 19:00 UTC. The acquisition is scheduled to coincide with the anticipated initial availability of the latest CFS forecast and concludes processing after roughly 60 to 90 minutes, depending on factors such as bandwidth congestion and file size during retrieval from NCEP serves. Once successfully acquired, each of the four CFS ensemble members undergo pre-processing to prepare the sounding data sets that are applied throughout subsequent system processing. These soundings are then stored in the INFORM File Repository where they are accessible to all other INFORM processing modules. Figure A.3 presents an overview of the INFORM System processing module inter-dependencies and timing for the acquisition of CFS Forecast Input and for all additional INFORM modules. Figure A.4 shows the timeline of the scheduling and estimated completion of sequential INFORM processing activities by forecast model initialization time.

Figure A.2: Configuration of the INFORM Hydrologic Model Operations



Acquisition of GFS Forecast Input

The 20 GEFS ensemble perturbations are obtained in GRIB2 format from the NOAA Operational Model Archive and Distribution System (NOMADS). These forecasts are downloaded twice daily as soon as they become available online for the 00:00 UTC and 12:00 UTC forecast initializations. The full GEFS forecast, out to forecast hour 384 for each ensemble perturbation, is required for use for the WRF-ARW. See Figure A.3 for GFS processing information and Figure A.4 for execution time lines.

Figure A.3: INFORM Phase II Module Dependency and Processing Overview

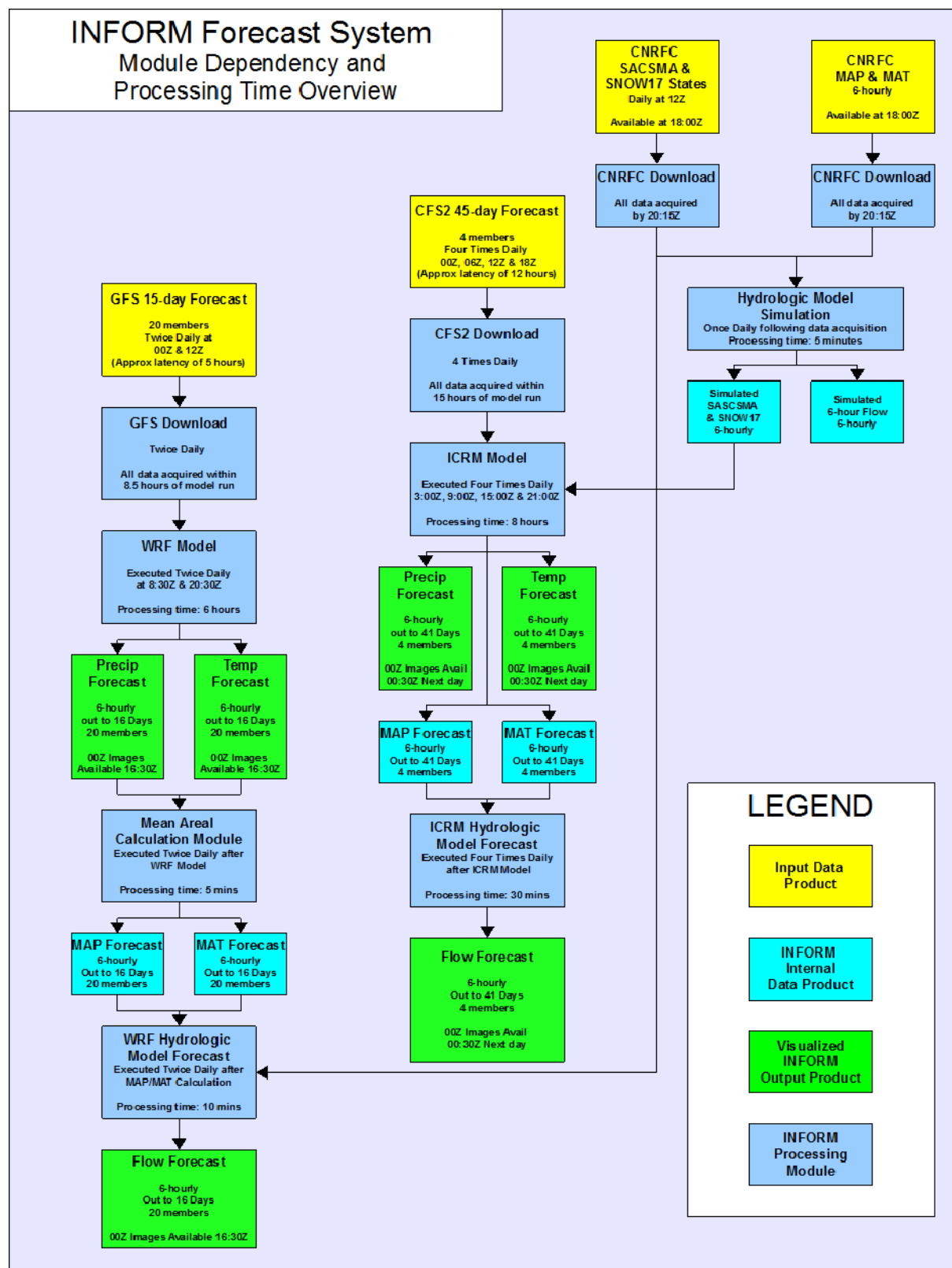
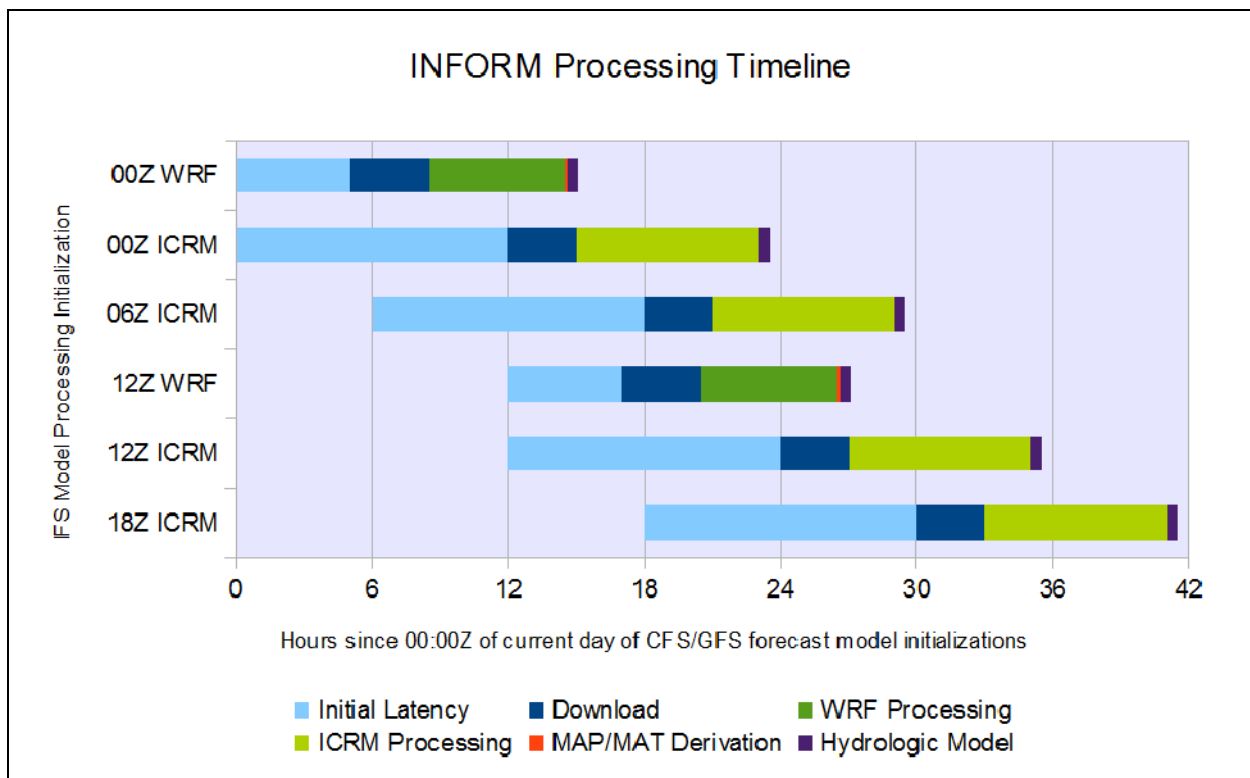


Figure A.3: INFORM Phase II Processing Timeline



Acquisition of CNRFC Observations & Model States

The California-Nevada River Forecast Center (CNRFC), part of the National Oceanic Atmospheric Administration (NOAA) / National Weather Service (NWS), provides once per day real-time estimates of mean areal precipitation (MAP) and mean areal temperature (MAT) over the hydrologic basins of the INFORM output domain. These estimates are based on point observations of precipitation and temperature. In addition to these real-time estimates the CNRFC provisions also include SAC-SMA and SNOW-17 model states, updated at the conclusion of each day's operational forecast run.

The CNRFC data is downloaded once per day at approximately 18:30 UTC. (See a summary of acquisition specifics in Table A.5.) The local pre-processing of the data for INFORM use involves extracting all the files of that day's NWSRFS fs5files directory contents contained in the downloaded "tar" archive file. In order to extract specific data product from resulting collection of fs5files contents, which are binary-formatted components of an NWSRFS-specific database file structure, specialized INFORM extraction utilities are invoked to directly access the various files, inventory the data sets within and extract all relevant observations and model states to separate files formatted as generic CSV (Comma Separated Values) files. Once observations and model states have been extracted, the many CSV files are then ingested to a stand-alone PostgreSQL database that serves as a localized repository that can be accessed directly to subsequently populate the operational INFORM database tables with selected data.

Table A.5: INFORM Real-Time Observations and Model States Provided by CNRFC - Acquisition Specifications

Data Provider	CNRFC (NOAA/NWS)
Transfer Protocol	FTP
Data Product(s)	MAP, MAT, SNOW-17 carryover states, SAC-SMA carryover states, SAC-SMA model parameters
Data Format	TAR archive of the NWSRFS "fs5files" directory contents
Files of interest	FCCARRY (Snow-17 and SAC-SMA carryover states), FCPARAM (Snow-17 and SAC-SMA model parameters), PRDTSn (MAP and MAT time series data), plus various support files for parsing reference
Spatial Resolution	Hydrologic basins
Data Production/Correspondence Time	12:00 UTC
Data interval	06 hours for MAP, MAT; daily for carryover states and parameters
Approximate download file size	4.8MB
Typical latency for availability	6.25 hours
Typical latency for download	1-2 minutes
Typical Pre-Processing Time	45 minutes

The design decision to keep the pre-processed CNRFC-extracted fs5files data in an independent database had two primary motivations: 1) to serve as a stand-alone database for access to historical fs5files data content through a standardized database interface (which, once

populated, eliminates the need for installing and configuring the NWSRFS software and its fs5files interfacing capabilities as well as eliminating the need for customized fs5files-direct extraction utilities) and 2) to provide an easily replaceable, non-integrated, black box data provision of the CNRFC NWSRFS-provided data. The non-integrated approach is strategic in that the fs5files-formatted data source will likely become unnecessary once CNRFC completes its operational migration to the new FEWS/CHPS platform and establishes the necessary FEWS-specific data provisions for INFORM's real-time data and model state needs. (FEWS data provisions will not involve any fs5files data formats).

As CNRFC continues in their migration from NWSRFS to FEWS, additional accommodations will be implemented into the INFORM data acquisition and delivery schema that are suitable to the capabilities and constraints of FEWS as well as the related operational environment and protocols of CNRFC.

Acquisition of NAM Input

The NAM (NCEP's North American Model) analysis is obtained in GRIB format from the NOAA Operational Model Archive and Distribution System (NOMADS). These analyses are downloaded twice daily as soon as they become available online for the 00:00 UTC and 12:00 UTC forecast initializations. The full NAM forecast is not downloaded because only the NAM analysis (initial conditions for the model) is required for use as the initial conditions for the WRF-ARW for "warm" start.

WRF Processing

Chapter 2 provides information pertaining to the integration of the WRF model within the INFORM processing system. Upon completion of processing for the 20 GFS ensemble members, the WRF component produces gridded accumulated precipitation and instantaneous temperature forecast products for each ensemble member at a 6-hourly temporal resolution out to 16 days (384 hours) from the GFS model initialization time. These gridded data products are then processed to derive the standardized WRF mean areal precipitation (MAP) and mean areal temperature (MAT) forecast data products for each processed ensemble member at the same 6-hourly temporal resolution out to 16 days, which are then stored in the INFORM database where they are available for application in subsequent processing components. Immediately following the successful conclusion of WRF MAP and MAT processing, the Basin Hydrology and Routing Model is executed with the derived MAP & MAT forecast time series applied as input for each GFS ensemble member.

ICRM Processing

Following the successful acquisition of the CFS forecast product and 3D-transformation pre-processing into Oakland and Eureka soundings, the Intermediate Complexity Regional Model (ICRM), which applies the CFS soundings as forcing input, begins processing to produce precipitation and temperature field forecasts out to 41 days from CFS model initialization. These fields are then applied to produce MAP and MAT forecast time series for each ensemble member. The models of the ICRM component are described in Chapter 2. The ICRM

component is scheduled to execute four times daily, at 03:00, 09:00, 15:00 and 21:00 UTC, immediately following the completion of the acquisition and pre-processing of the CFS input product for the corresponding CFS model initialization approximately 15 hours prior. At every execution, each CFS ensemble member is processed independently and in parallel with the appropriate CFS sounding input and ICRM carryover states for that ensemble member. Where available, the SACSMA and SNOW17 model states acquired from CNRFC are applied to update the ICRM carryover states at the time of ICRM model initialization. In the absence of CNRFC-provided model states, model states from the INFORM Basin Hydrologic Model and Routing component execution corresponding to the appropriate CFS ensemble member are applied to update the ICRM carryover. At the end of ICRM execution, the carryover states and gridded precipitation and temperature forecasts are deposited in the INFORM file repository while the derived MAP and MAT forecast results are standardized and ingested into the operational INFORM database. Following every execution of the ICRM Component, the resulting standardized forecasts MAP and MAT are immediately applied as input to the INFORM Basin Hydrologic Model and Routing Component. For additional information on the ICRM Processing Component, please refer to Chapter 2.

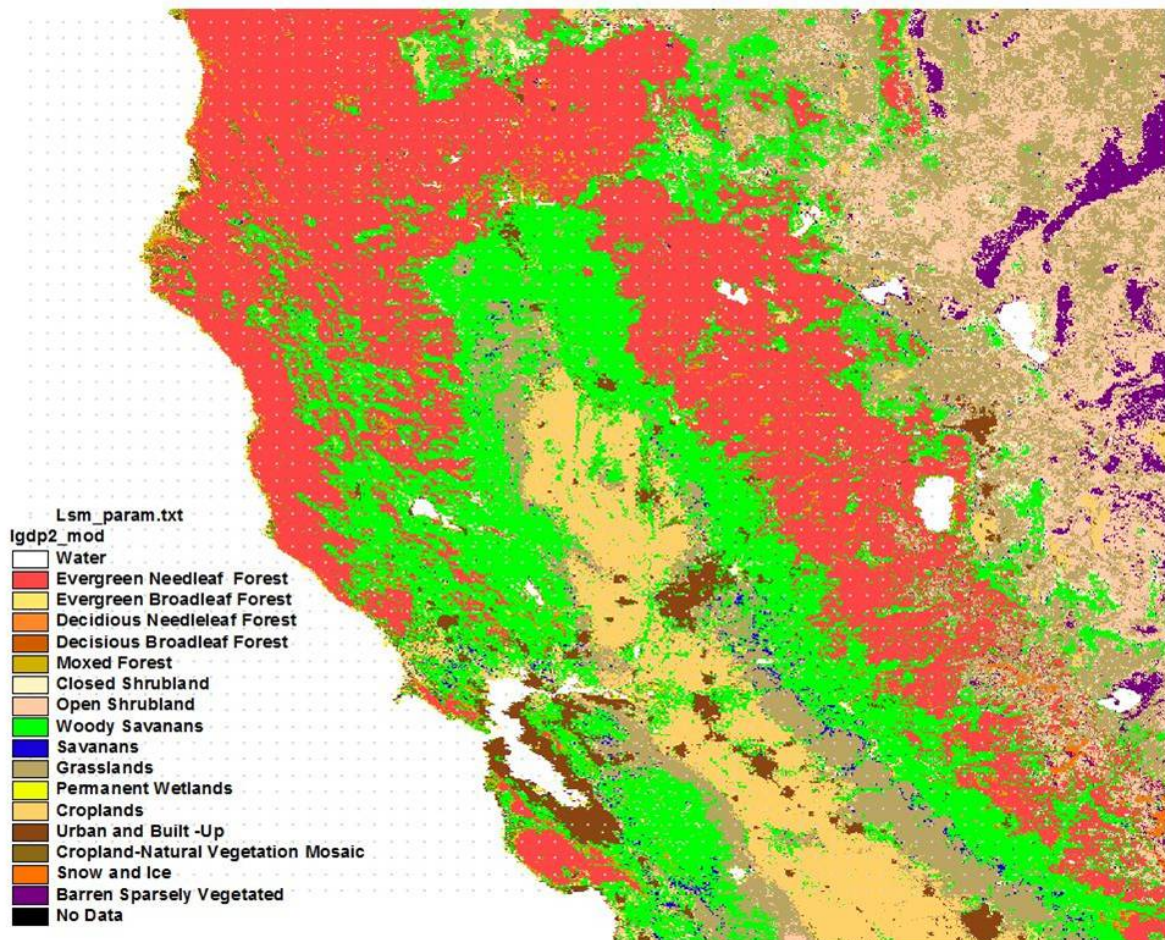
INFORM Basin Hydrologic Model and Routing

The final data-processing phase of the INFORM II System is the Basin Hydrology and Routing Model. Operating on standardized MAP and MAT forecast on input, this module produces forecasts of reservoir-inflow at a 6-hourly temporal resolution from the model initialization out to the maximum lead-time (for WRF 16 days, for ICRM 41 days). Chapter 2 describes the upgrades of the INFORM hydrologic models with respect to earlier INFORM implementation (INFORM Phase I) and shows simulation performance results. The Basin Hydrology and Routing Model is executed independently twice a day for each of the 20 ensemble members of WRF out to 16 days from each initialization and four times a day for each of the 4 ensemble members of ICRM out to 41 days from each initialization. At each scheduled execution of this model, the appropriate MAP and MAT forecast data and model states are acquired from the INFORM database. When available, CNRFC-provided SACSMA and SNOW17 model states are applied as initial conditions for each initialization of the Basin Hydrology and Routing Model. In the absence of CNRFC-provided model states, the carryover states from the most recent execution of the Basin Hydrology and Routing Model for the corresponding ensemble member are applied as initial conditions. At the conclusion of processing for each ensemble member, the resulting reservoir inflow forecasts and model states are posted to the INFORM database.

APPENDIX B: ICRM Surface Temperature Model Parameters

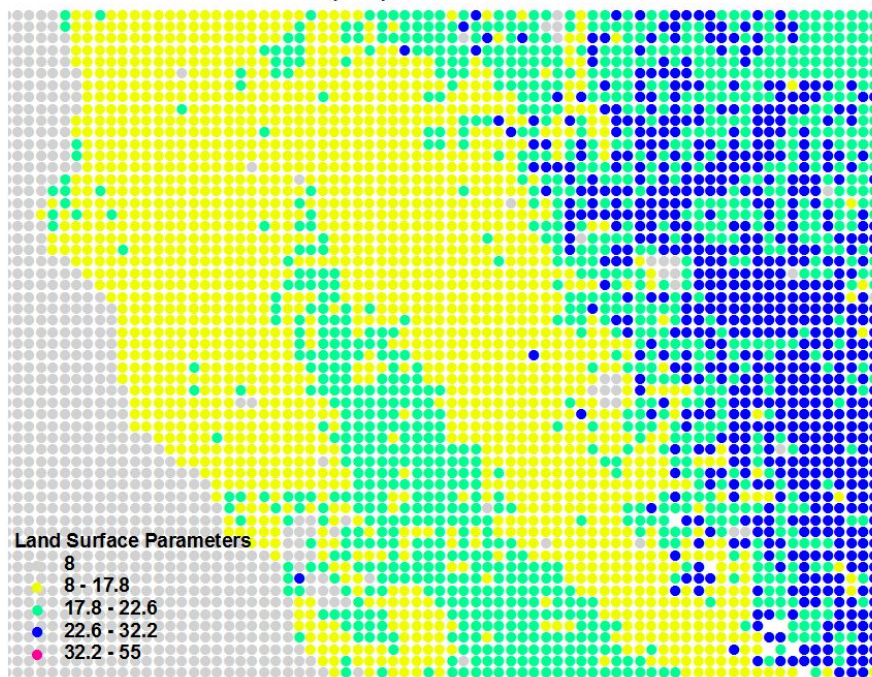
The parameter values are shown in a series of color figures and the legend identifies the values of the parameters for each color used.

Land Cover

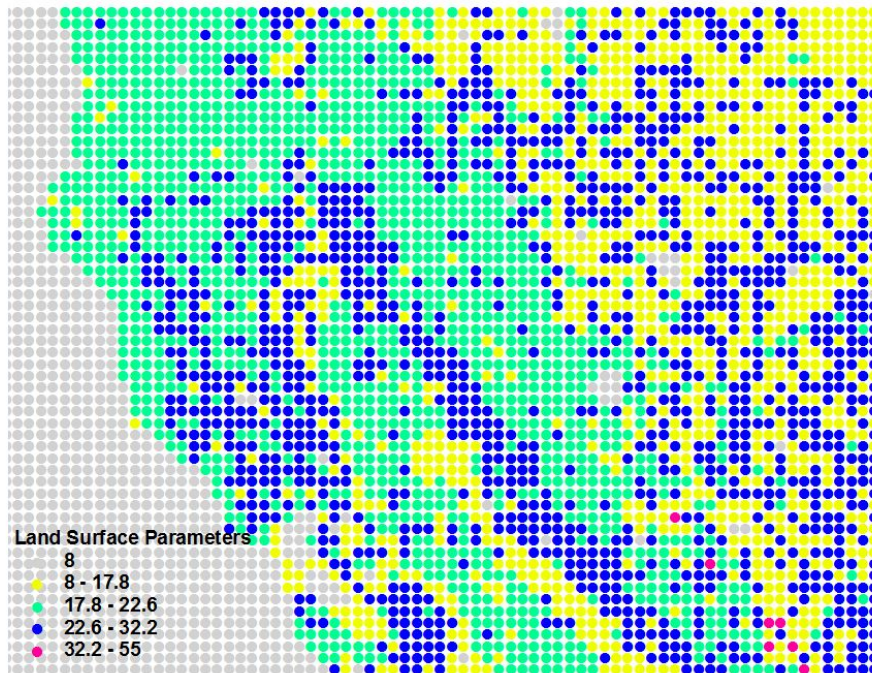


Shortwave Albedo

Winter Albedo (%)

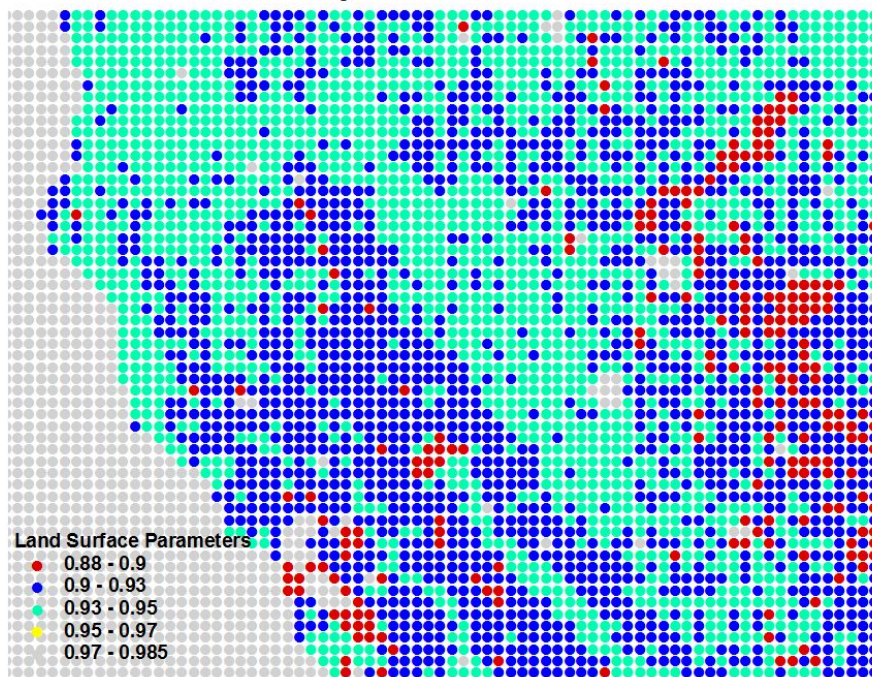


Summer Albedo (%)

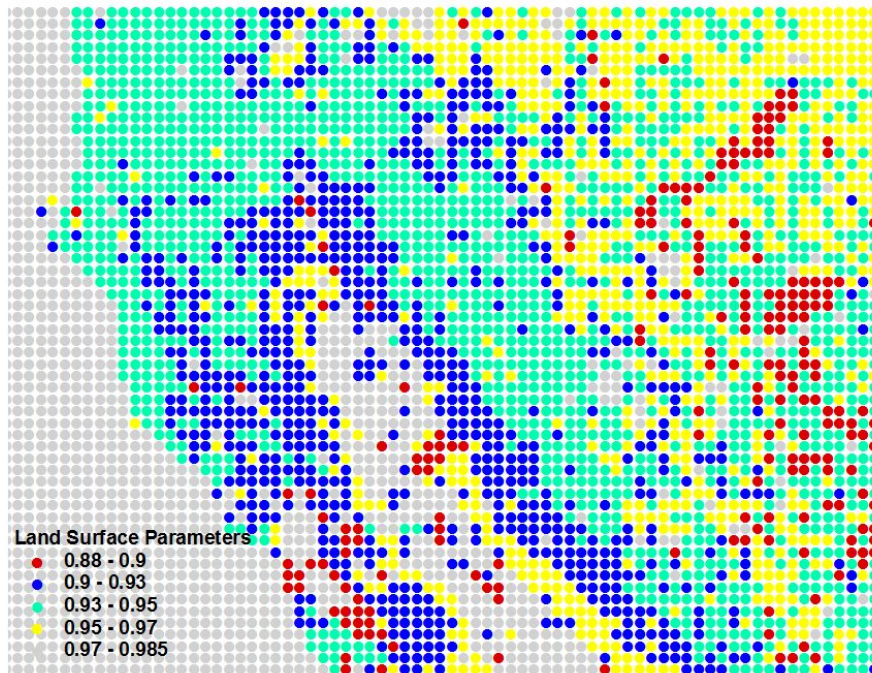


Emissivity

Winter Emissivity

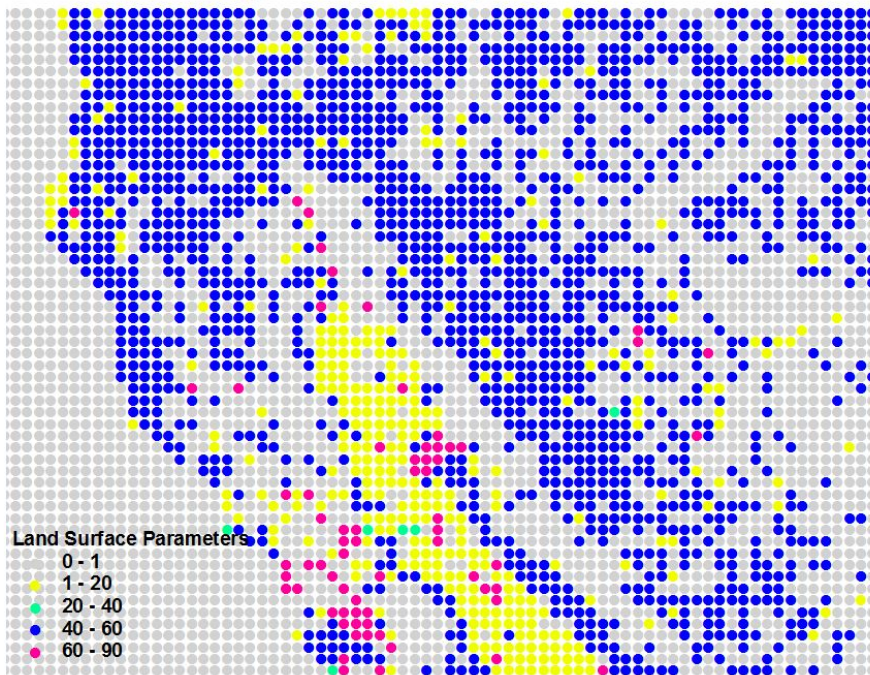


Summer Emissivity

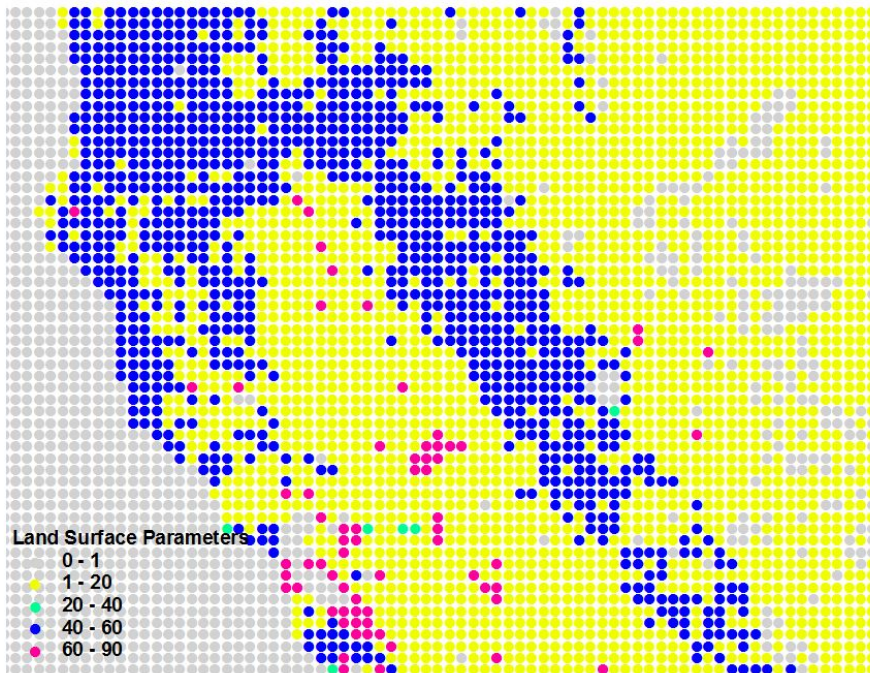


Surface Roughness

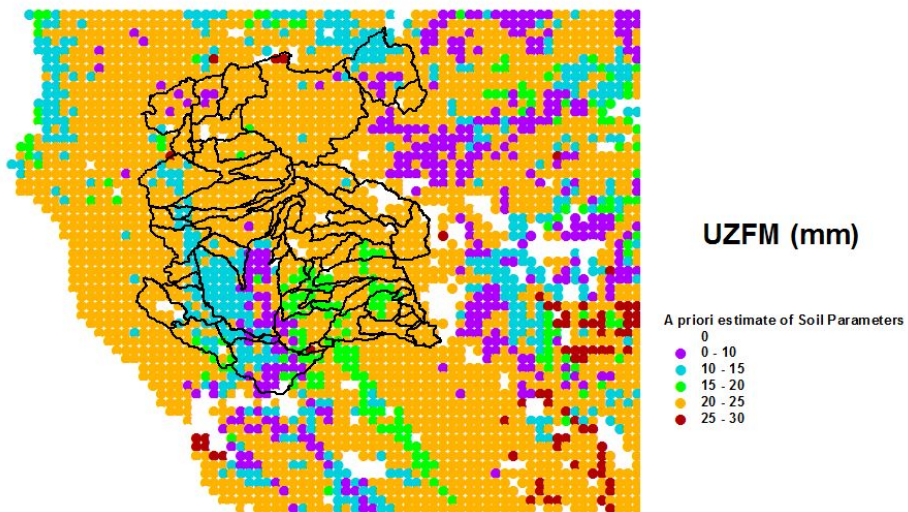
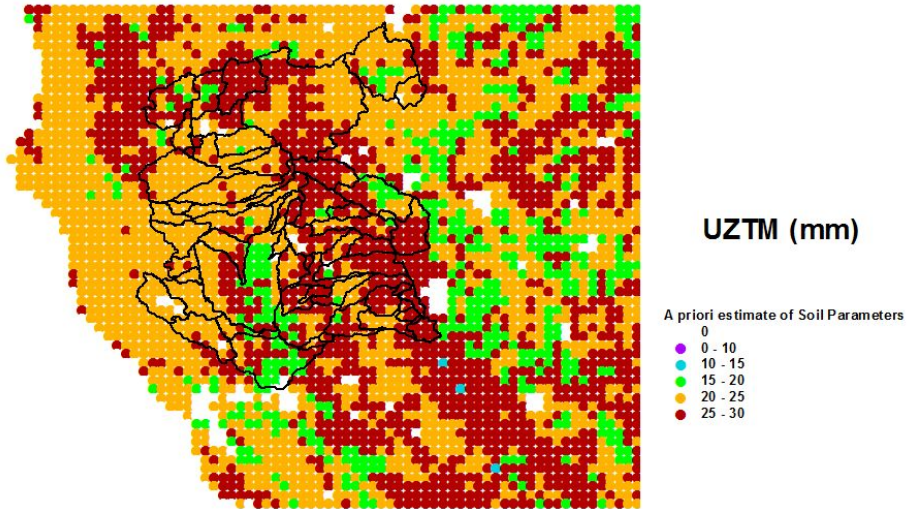
Winter Roughness (cm)

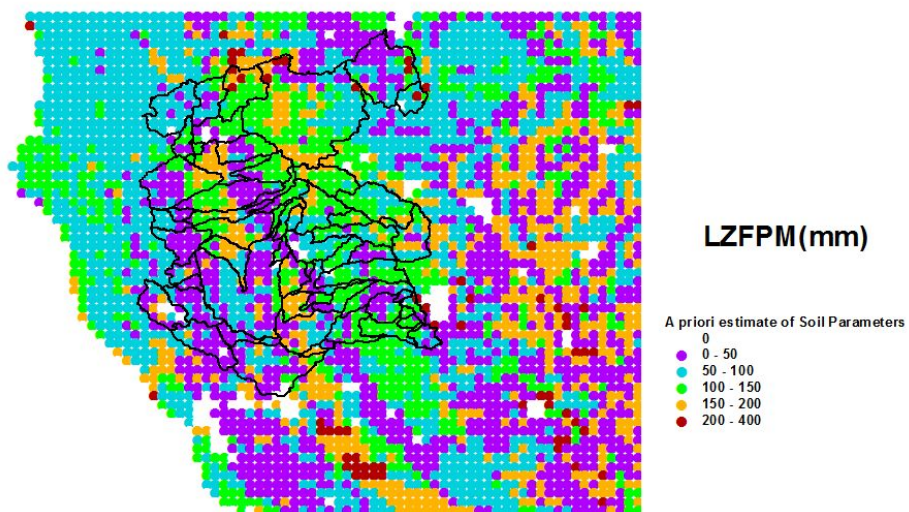
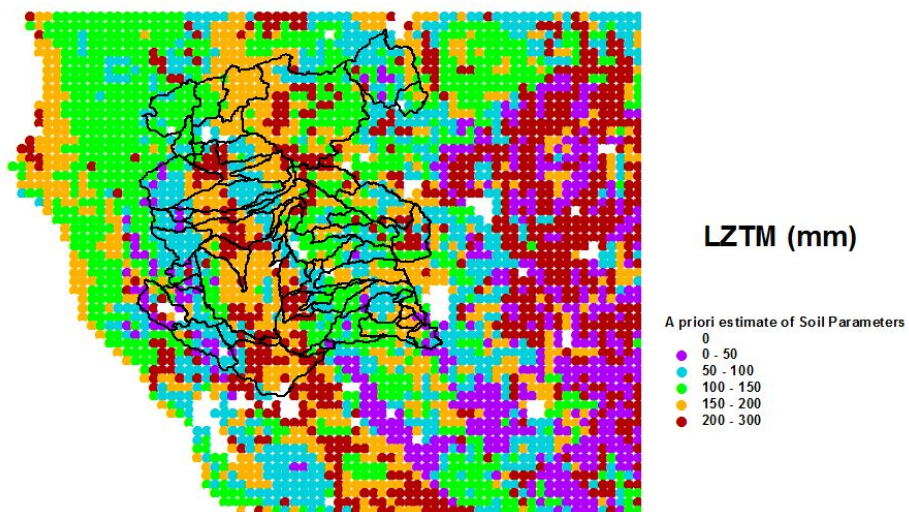


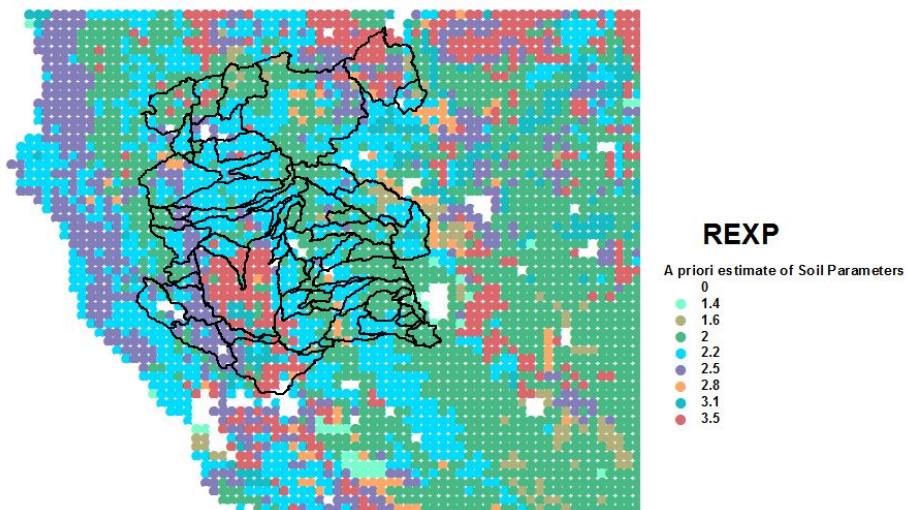
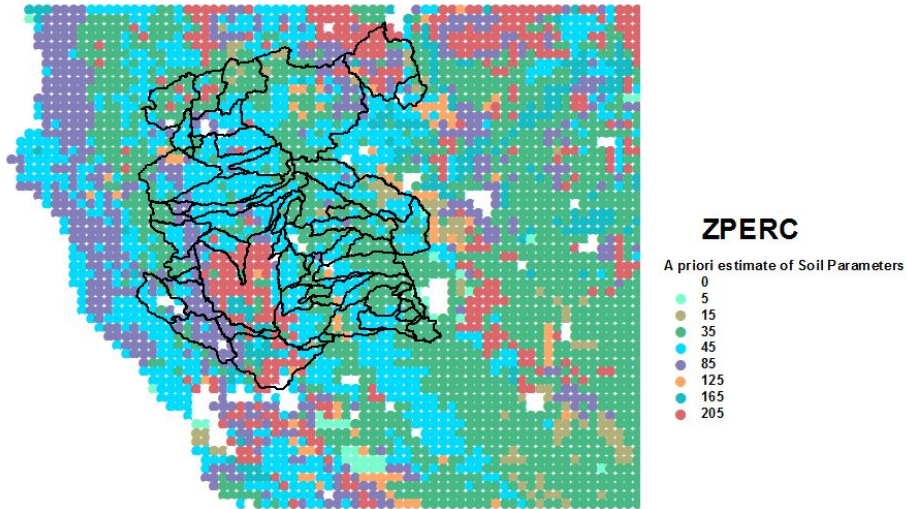
Summer Roughness (cm)



Gridded Major SACSMA Parameters







APPENDIX C:

Hydrologic Model Parameters and Simulations

Tables of Model Parameters

Table C.1: Model Parameters for Trinity Reservoir

SNOW PARAMETERS - TRINITY

%	CEGC1UP	CEGC1LW
	1.0000	1.0000
	0.7500	0.8500
	0.2000	0.4000
	0.1500	0.1500
	0.0200	0.0200
	0.2500	0.2500
	0.0000	0.0000
	0.0900	0.1000
	0.3000	0.3000
	1.5000	1.5000
	675.0000	300.0000
	18.2900	10.6700
	0.8000	0.8000
	0.3500	0.3500
	17.0700	9.4500
	1.5000	1.5000
	0.5500	0.5500
	1.1000	0.9800

SACRAMENTO MODEL PARAMETERS - TRINITY

%	CEGC1UP	CEGC1LW
	100.000	85.000
	50.000	50.000
	150.000	135.000
	150.000	150.000
	30.000	30.000
	0.300	0.300
	0.013	0.012
	0.110	0.100
	25.000	25.000
	1.700	1.700

0.300	0.300
0.000	0.000
0.005	0.015
0.020	0.020
1.000	1.000

KINEMATIC CHANNEL ROUTING MODEL PARAMETERS - TRINITY - 13 ROUTING SEGMENTS

1	2	5.0	245.7	1
2	2	1.0	173.5	2
3	2	5.0	272.0	1
4	2	2.0	57.6	2
5	2	5.0	191.3	2
6	2	9.0	95.9	1
7	2	5.0	66.2	2
8	2	8.0	123.4	1
9	2	2.0	167.7	2
10	2	8.0	105.0	1
11	2	6.0	34.6	2
12	2	3.0	121.4	2
13	2	3.0	137.2	2

SUB-CATCHMENT AREAS IN SQKM

%	CEGC1UP	CEGC1LW
	842.0	949.5

Table C.2: Model Parameters for Shasta Reservoir

SNOW PARAMETERS (SHASTA)											
%	CNBC1UP	CNBC1LW	PITC1UP	PITC1LW	DLTC1UP	DLTC1LW	MSSC1UP	MSSC1LW	PLYC1UP	PLYC1LW	SHDC1L
	1.0000	0.9000	0.9500	0.8500	1.5000	0.9000	1.3000	0.8000	1.1100	0.9000	1.0000
	0.7500	0.8000	0.8500	1.2000	1.1000	0.8500	0.9000	0.6500	0.4500	0.7000	0.9000
	0.0500	0.1000	0.1500	0.2000	0.0500	0.1500	0.0500	0.2500	0.0500	0.0500	0.1000
	0.1500	0.1500	0.1500	0.1500	0.1500	0.1500	0.1500	0.1500	0.1500	0.1500	0.1500
	0.0300	0.0300	0.0200	0.0200	0.0200	0.2500	0.0200	0.2500	0.0300	0.0300	0.0200
	0.2500	0.2500	0.2500	0.2500	0.2500	0.2500	0.2500	0.2500	0.2500	0.2500	0.2500
	0.0000	0.0000	0.0000	1.0000	0.0000	0.0000	0.0000	0.0000	0.0000	0.0000	0.0000
	0.1000	0.1000	0.1200	0.1700	0.1800	0.0700	0.1800	0.0700	0.1000	0.1000	0.1200
	0.3000	0.3000	0.3000	0.3000	0.3000	0.3000	0.3000	0.3000	0.3000	0.3000	0.3000
	0.8000	1.0000	1.3000	1.5000	1.7000	1.5000	0.9000	1.0000	2.5000	1.0000	0.5000
200.0000	75.0000	1500.0000	500.0000	2000.0000	350.0000	2000.0000	350.0000	200.0000	75.0000	500.0000	
18.9000	14.9600	17.9800	13.1100	17.9800	10.6700	17.9800	15.1900	21.5100	15.8500	5.7900	
0.0000	0.6000	0.0000	0.0000	0.0000	0.0000	0.0000	0.0000	0.6000	0.6000	0.0000	
0.0000	0.4500	0.0000	0.0000	0.0000	0.0000	0.0000	0.0000	0.4500	0.4500	0.0000	
0.0000	14.9400	0.0000	0.0000	0.0000	0.0000	0.0000	0.0000	18.9000	14.9400	0.0000	
1.0300	1.0300	1.0300	0.9000	1.1000	0.9400	1.0100	0.8800	1.0000	1.0000	1.1000	
SAC PARAMETERS - SHASTA											
%	CNBC1UP	CNBC1LW	PITC1UP	PITC1LW	DLTC1UP	DLTC1LW	MSSC1UP	MSSC1LW	PLYC1UP	PLYC1LW	SHDC1L
30.0000	102.0000	53.0000	104.0000	73.0000	75.0000	200.0000	60.0000	80.0000	102.0000	123.0000	
85.0000	40.0000	82.0000	36.0000	32.0000	63.0000	26.0000	38.0000	85.0000	40.0000	45.0000	
218.0000	319.0000	101.0000	113.0000	102.0000	100.0000	69.0000	52.0000	118.0000	319.0000	263.0000	
122.0000	46.0000	600.0000	1362.0000	1050.0000	179.0000	2900.0000	600.0000	322.0000	46.0000	129.0000	
33.0000	71.0000	116.0000	145.0000	104.0000	78.0000	117.0000	96.0000	93.0000	71.0000	76.0000	
0.1000	0.3600	0.4400	0.5000	0.2200	0.2300	0.2000	0.2000	0.1000	0.2600	0.8200	
0.0070	0.0010	0.0010	0.0010	0.0020	0.0050	0.0020	0.0050	0.0070	0.0010	0.0170	
0.1200	0.1800	0.0800	0.0870	0.1900	0.0500	0.1200	0.1200	0.0700	0.1800	0.1900	
15.0000	10.0000	100.0000	125.0000	78.0000	60.0000	9.4000	19.0000	115.0000	10.0000	70.0000	
1.1600	1.2000	1.3000	1.1800	1.2000	1.2200	1.1700	2.5000	1.1600	1.2000	1.0300	
0.1100	0.4000	0.3840	0.4000	0.1900	0.0000	0.2200	0.3000	0.1100	0.4000	0.3000	
0.2800	0.0300	0.0300	0.1400	0.0300	0.0400	0.0100	0.0500	0.4700	0.0500	0.2000	
0.0030	0.0100	0.0200	0.1400	0.1300	0.1800	0.0400	0.0650	0.0030	0.0500	0.0200	
0.0000	0.0000	0.0120	0.0120	0.0100	0.0100	0.0000	0.0100	0.0000	0.0000	0.0900	
1.0000	1.0000	1.0000	1.0000	1.0000	1.0000	1.0000	1.0000	1.0000	1.0000	1.0000	
KINEMATIC CHANNEL ROUTING MODEL PARAMETERS - SHASTA - 50 ROUTING SEGMENTS											
1	2	2.02	168.0	1	% CNBup-SouthF						
2	2	1.60	607.3	2	% CNBlo-SouthF						
3	2	2.00	184.0	1	% CNBup-NorthF						

4	2	1.60	607.3	2	% CNBlo-NorthF
5	2	2.02	148.8	1	% CNBup-BigSage
6	2	3.20	300.0	2	% CNBlo-BigSage
7	2	2.02	143.2	1	% CNBup
8	2	0.80	908.0	2	% CNBlo
9	2	1.85	530.1	4	% PITlo-Junct1
10	2	1.85	530.1	4	% PITlo-Scarface
11	2	1.50	339.9	3	% PITup-BigAsh
12	2	1.85	530.1	4	% PITlo-BigAsh
13	1	3.00	101.2	3	% PITup-Junct2
14	2	1.85	530.1	4	% PITlo-Junct2
15	2	1.50	340.4	3	% PITup-Horse
16	2	3.70	265.0	4	% PITlo-Horse
17	2	1.85	530.1	4	% PITlo-Junct3
18	1	2.00	330.2	3	% PITup-Bear1
19	2	2.00	530.1	4	% PITlo-Bear1
20	2	2.00	530.1	4	% PITlo-Bear2
21	2	2.00	530.1	4	% PITlo-Bear3
22	2	3.70	265.0	4	% PITlo-Beaver
23	2	3.70	265.0	4	% PITlo-Junct4
24	2	1.50	339.6	3	% PITup-HatCrk1
25	2	1.50	226.2	3	% PITup-HatCrk2
26	1	3.00	108.2	3	% PITup-HatCrk3
27	2	2.00	530.1	4	% PITlo-HatCrk
28	1	2.00	129.4	3	% PITup-Burney
29	2	2.00	530.1	4	% PITlo-Burney
30	2	1.85	530.1	4	% PITlo-Junct5
31	2	3.70	192.6	4	% PITlo-FoskCrk
32	2	2.14	505.4	9	% PLYup
33	2	3.70	193.0	4	% PITlo
34	2	3.70	192.6	4	% PITlo-Hatchet
35	3	7.73	243.9	11	% SHDlo-PitR
36	3	6.73	161.8	11	% SHDlo-Squaw
37	2	3.02	438.0	7	% MSSup-Up
38	2	4.12	200.3	8	% MSSlo-Junct1
39	2	4.12	175.3	8	% MSSlo-Angel
40	2	2.20	375.5	8	% MSSlo-Junct2
41	2	2.20	250.2	8	% MSSlo-SquawValley
42	2	6.59	125.1	8	% MSSlo-Junct3
43	3	7.73	243.9	11	% SHDlo-McCloudR
44	3	5.42	286.2	5	% DLTup-Jlup

45	3	3.80	305.6	6	% DLTlo-Junct1
46	3	3.80	305.4	6	% DLTlo-Junct2
47	3	3.80	203.6	6	% DLTlo-Lamoine
48	3	7.73	254.1	11	% SHDlo-Delta
49	3	9.00	235.9	11	% SHDlo-Local
50	2	8.06	134.3	10	% PLYlo

SUB-CATCHMENT AREAS IN SQKM

%	CNBC1UP	CNBC1LW	PITC1UP	PITC1LW	DLTC1UP	DLTC1LW	MSSC1UP	MSSC1LW	PLYC1UP	PLYC1LW	SHDC1L
	644.0	2422.6	1915.1	7204.3	286.2	814.6	438.0	1126.4	505.4	134.3	1139.6

Table C.3: Model Parameters for Oroville Reservoir

SNOW PARAMETERS - Oroville

%	PLLC1UP	PLLC1LW	IIFC1UP	IIFC1LW	PLGC1UP	PLGC1LW	MFTC1UP	MFTC1LW	MRMC1UP	MRMC1LW	ORDC1UP
	1.0800	1.0800	1.3700	1.0000	1.4700	0.8500	1.0000	1.0000	1.2600	1.0000	1.4000
	0.5500	0.6500	0.9000	1.3000	1.3500	1.3000	0.9000	1.1000	1.2000	1.0500	1.0000
	0.0100	0.0200	0.1000	0.1500	0.2500	0.2000	0.5500	0.5500	0.0500	0.1500	0.0500
	0.1500	0.1500	0.1500	0.1500	0.1500	0.1500	0.1500	0.1500	0.1500	0.1500	0.1500
	0.0500	0.0500	0.0200	0.2500	0.0200	0.0500	0.0200	0.2500	0.0200	0.0500	0.0200
	0.1000	0.1000	0.2500	0.2500	0.2500	0.2500	0.2500	0.2500	0.2500	0.2500	0.2500
	2.0000	0.0000	0.0000	0.0000	0.0000	0.0000	0.0000	0.0000	0.0000	0.0000	0.0000
	0.0000	0.0100	0.0900	0.0500	0.1800	0.1500	0.1600	0.0700	0.1600	0.1800	0.1600
	0.3000	0.3000	0.3000	0.3000	0.3000	0.3000	0.3000	0.3000	0.3000	0.3000	0.3000
	2.1000	1.1500	2.0000	1.5000	2.0000	1.5000	1.0000	1.5000	1.6000	1.5000	1.2000
	2000.0	1249.0	2000.0	1250.0	2000.0	500.00	2000.0	1250.0	2000.0	500.00	2000.0
	17.8800	14.1800	18.1000	12.0000	16.2300	10.9200	18.4900	15.2100	17.4500	13.4700	16.7600
	0.6000	0.6000	0.6000	0.6000	0.6000	0.6000	0.6800	0.6800	0.6000	0.6000	0.6000
	0.4500	0.4500	0.4500	0.4500	0.4500	0.4500	0.4800	0.4800	0.4500	0.4500	0.4500
	17.9800	10.3600	18.9000	10.3600	17.3700	12.8000	17.9800	14.0200	17.3700	10.3600	18.9000
	1.1000	1.1000	1.0700	1.0000	1.0200	1.0400	0.9000	0.9000	1.1500	1.0200	1.1500

SNOW PARAMETERS - Oroville (Continued)

%	ORDC1LW	SCBC1UP	SCBC1LW	WBGC1UP	WBGC1LW
	1.0000	1.3500	1.0000	1.3000	1.0000
	1.1000	0.8500	1.0000	0.9500	1.1000
	0.1500	0.1000	0.1500	0.1000	0.1500
	0.1500	0.1500	0.1500	0.1500	0.1500
	0.2500	0.0200	0.2500	0.0200	0.2500
	0.2500	0.2500	0.2500	0.2500	0.2500
	0.0000	0.0000	0.0000	0.0000	0.0000
	0.0700	0.0900	0.1400	0.1600	0.0700
	0.3000	0.3000	0.3000	0.3000	0.3000

1.5000	1.5000	1.0000	1.1000	1.5000
1250.0	2000.0	1250.0	2000.0	1250.0
8.1500	17.8100	12.8000	17.5000	10.6200
0.6000	0.6000	0.6000	0.6000	0.6000
0.4500	0.4500	0.4500	0.4500	0.4500
12.8000	17.9800	14.0200	17.3700	12.8000
0.9800	1.7500	1.0600	1.0200	0.9200

SAC PARAMETERS - Oroville

%	PLLC1UP	PLLC1LW	IIFC1UP	IIFC1LW	PLGC1UP	PLGC1LW	MFTC1UP	MFTC1LW	MRMC1UP	MRMC1LW	ORDC1UP
150.0000	50.0000	150.0000	85.0000	65.0000	65.0000	170.0000	100.0000	80.0000	50.0000	140.0000	
90.0000	90.0000	36.0000	48.0000	90.0000	34.0000	100.0000	80.0000	51.0000	30.0000	26.0000	
30.0000	40.0000	300.0000	230.0000	100.0000	228.0000	20.0000	20.0000	227.0000	100.0000	365.0000	
900.0000	800.0000	120.0000	160.0000	620.0000	155.0000	250.0000	150.0000	450.0000	115.0000	250.0000	
70.0000	80.0000	52.0000	50.0000	35.0000	105.0000	60.0000	50.0000	145.0000	85.0000	100.0000	
0.1000	0.1300	0.3000	0.3000	0.1700	0.4700	0.0800	0.0500	0.3100	0.5000	0.4100	
0.0020	0.0020	0.0140	0.0030	0.0050	0.0150	0.0050	0.0050	0.0020	0.0060	0.0040	
0.0300	0.0300	0.1400	0.0700	0.0150	0.1100	0.0300	0.0200	0.0700	0.1400	0.1400	
15.0000	35.0000	12.0000	17.0000	32.0000	47.0000	15.0000	15.0000	64.0000	50.0000	48.0000	
1.1000	1.1000	1.1500	1.2500	1.0900	1.0100	1.1000	1.1000	1.2700	1.2000	1.0100	
0.8000	0.8000	0.3500	0.6500	0.3400	0.3100	0.8000	0.5000	0.3600	0.3000	0.3400	
0.0000	0.0000	0.0000	0.0000	0.0500	0.2000	0.0000	0.0000	0.0600	0.0000	0.2000	
0.0700	0.0500	0.0000	0.1000	0.1000	0.1300	0.0700	0.0700	0.1100	0.2000	0.0150	
0.0150	0.2500	0.0020	0.0010	0.0100	0.0250	0.0100	0.0100	0.0050	0.0080	0.0030	
1.0000	1.0000	1.0000	1.0000	1.0000	1.0000	1.0000	1.0000	1.0000	1.0000	1.0000	

SAC PARAMETERS - Oroville (Continued)

%	ORDC1LW	SCBC1UP	SCBC1LW	WBGC1UP	WBGC1LW
165.0000	110.0000	110.0000	60.0000	145.0000	
30.0000	50.0000	40.0000	20.0000	28.0000	
290.0000	80.0000	150.0000	390.0000	360.0000	
200.0000	500.0000	90.0000	210.0000	210.0000	
165.0000	110.0000	95.0000	145.0000	65.0000	
0.8200	0.3000	0.8000	0.5000	0.5000	
0.0030	0.0010	0.0040	0.0090	0.0070	
0.1100	0.0800	0.1100	0.1400	0.1400	
42.0000	12.0000	15.0000	25.0000	25.0000	
1.0300	1.2000	1.2000	1.1000	1.1000	
0.3900	0.3000	0.3000	0.2500	0.2500	
0.1200	0.0000	0.0000	0.0000	0.0000	

0.0700	0.0500	0.1600	0.0500	0.0900
0.0800	0.0050	0.0050	0.0030	0.0800
1.0000	1.0000	1.0000	1.0000	1.0000

KINEMATIC CHANNEL ROUTING MODEL PARAMETERS - OROVILLE - 51 ROUTING SEGMENTS

1	2	1.50	267.6	1	% PLLup-NF & Warner
2	2	1.50	290.1	1	% PLLup-BBR
3	2	0.80	460.2	1	% PLLup-Robbers
4	4	5.73	253.8	2	% PLLlo-Almanor
5	2	0.80	314.4	3	% IIFup-RedClover
6	2	0.80	477.3	3	% IIFup-LastChance
7	2	1.00	329.7	3	% IIFup-Indian
8	2	2.00	181.0	3	% IIFup-Junct1
9	2	1.50	98.2	4	% IIFlo-Junct1
10	2	2.25	190.5	3	% IIFup-Lights
11	2	2.00	97.4	4	% IIFlo-Lights
12	2	1.00	182.1	4	% IIFlo-Wolf
13	2	4.00	43.4	4	% IIFlo-Junct2
14	2	4.00	122.0	5	% PLGup-ButtCrk
15	2	3.00	98.6	6	% PLGlo-ButtCrk
16	2	3.00	148.7	6	% PLGlo-Junct1
17	3	3.34	166.8	13	% PLGup-Greenhorn/SCBup
18	3	1.80	223.0	14	% PLGlo-Spanish1/SCBlo
19	3	2.20	86.8	14	% PLGlo-Spanish2/SCBlo
20	2	3.00	148.7	6	% PLGlo-Junct2
21	2	2.60	240.5	5	% PLGup-Yellow
22	2	3.00	57.7	6	% PLGlo-Yellow
23	2	4.00	209.9	5	% PLGup
24	2	3.60	369.9	6	% PLGlo
25	5	1.30	377.9	7	% FTCup-ColdStream/MFTup
26	5	1.80	238.8	7	% FTCup-Smithneck/MFTup
27	5	1.30	395.1	7	% FTCup-FrenchLake/MFTup
28	5	3.90	380.1	8	% FTClo-Junct1/MFTlo
29	5	3.00	128.4	7	% FTCup-BigGrizzley/MFTu
30	2	8.53	71.4	10	% FTClo-Junct2/MRMlo
31	2	4.27	213.3	10	% FTClo/MRMlo
32	2	3.80	113.1	9	% MRMup-Up1
33	2	4.27	28.8	10	% MRMlo-Junct1
34	2	3.80	197.3	9	% MRMup-Up2
35	2	4.27	60.4	10	% MRMlo-Junct2
36	2	3.80	174.0	9	% MRMup-Nelson

37	2	3.80	167.8	9	% MRMup-Up3							
38	2	2.13	93.4	10	% MRMlo-Junct3							
39	2	4.00	87.5	9	% MRMup-LittleNF							
40	2	8.53	25.8	10	% MRMlo-LittleNF							
41	2	8.50	120.7	11	% ORDup-FallR							
42	2	8.50	90.0	12	% ORDlo-FallR							
43	2	4.00	150.9	12	% ORDlo-MiddleF							
44	2	9.00	81.1	11	% ORDup-UpSouthF							
45	2	8.00	79.0	12	% ORDlo-UpSouthF							
46	2	8.00	96.9	12	% ORDlo-Lost							
47	2	2.76	205.1	12	% ORDlo-SouthF							
48	2	6.00	291.8	12	% ORDlo-NorthF							
49	2	3.66	114.2	15	% ORDup-WestBr/WBGup							
50	2	2.67	157.7	16	% ORDlo-WestBr/WBGlo							
51	2	5.50	145.8	12	% ORDlo-Local							
SUB-CATCHMENT AREAS IN SQKM												
%	PLLC1UP	PLLC1LW	IIFC1UP	IIFC1LW	PLGC1UP	PLGC1LW	MFTC1UP	MFTC1LW	MRMC1UP	MRMC1LW	ORDC1UP	
	1017.9	253.8	1492.9	421.1	572.4	823.6	1140.2	380.1	739.7	493.1	201.8	
%	ORDC1LW	SCBC1UP	SCBC1LW	WBG1UP	WBG1LW							
	1059.5	166.8	309.8	114.2	157.7							

Table C.4: Model Parameters for Yuba River

SNOW PARAMETERS - Yuba

%	NBBC1UP	NBBC1LW	HLEC1UP	HLEC1LW	GYRC1UP	GYRC1LW
	1.0000	1.0000	1.3000	1.0000	1.0000	1.0000
	0.7000	0.8500	0.9000	1.1000	0.7000	0.8000
	0.1000	0.1500	0.1000	0.1000	0.1000	0.2000
	0.1500	0.1500	0.1500	0.1500	0.1500	0.1500
	0.0200	0.2500	0.0200	0.2500	0.0200	0.2500
	0.2500	0.2500	0.2500	0.2500	0.2500	0.2500
	0.0000	0.0000	0.0000	0.0000	0.0000	0.0000
	0.0700	0.0600	0.1200	0.0700	0.0800	0.0800

0.3000	0.3000	0.3000	0.3000	0.3000	0.3000
1.7500	1.7500	1.7000	1.5000	1.7500	1.7500
300.0000	300.0000	2000.0000	1250.0000	1050.0000	500.0000
17.2700	10.6300	19.9300	9.1300	19.2000	12.8000
0.6000	0.6000	0.6000	0.6000	0.6000	0.6000
0.4500	0.4500	0.4500	0.4500	0.4500	0.4500
18.9000	10.3600	18.9000	10.3600	18.9000	10.3600
1.0000	1.0000	1.0500	0.8400	1.0000	1.0000

SAC PARAMETERS - Yuba

%	NBBC1UP	NBBC1LW	HLEC1UP	HLEC1LW	GYRC1UP	GYRC1LW
80.0000	70.0000	60.0000	155.0000	60.0000	55.0000	
25.0000	20.0000	30.0000	30.0000	60.0000	50.0000	
300.0000	275.0000	215.0000	225.0000	200.0000	175.0000	
270.0000	250.0000	90.0000	90.0000	280.0000	245.0000	
30.0000	25.0000	65.0000	40.0000	70.0000	40.0000	
0.3000	0.3000	0.2500	0.5000	0.5000	0.5000	
0.0160	0.0160	0.0090	0.0070	0.0150	0.0140	
0.1300	0.1200	0.1400	0.1800	0.1300	0.1200	
25.0000	25.0000	25.0000	25.0000	20.0000	20.0000	
1.1000	1.1000	1.1000	1.1000	1.1000	1.1000	
0.2500	0.2500	0.2500	0.2500	0.2500	0.2500	
0.0000	0.0000	0.0000	0.0000	0.0000	0.0000	
0.0050	0.0350	0.1000	0.1500	0.0010	0.0010	
0.0300	0.0150	0.0030	0.0350	0.0500	0.0300	
1.0000	1.0000	1.0000	1.0000	1.0000	1.0000	

KINEMATIC CHANNEL ROUTING MODEL PARAMETERS

1	2	3.83	79.5	1	%SLATE-UP
2	2	3.83	95.5	2	%SLATE-LO
3	2	3.83	86.1	1	%CANYON-UP
4	2	3.83	93.3	2	%CANYON-LO
5	3	4.22	191.9	5	%PAULEY-UP
6	3	4.22	258.7	5	%NF_HAYPRESS-UP
7	3	4.22	189.4	6	%NF_J1-LO
8	2	6.50	98.2	2	%NF-LO
9	2	3.83	166.4	2	%NBB-LO
10	2	3.30	209.6	3	%MF-UP
11	2	3.30	217.1	4	%MF-LO
12	2	3.30	108.5	4	%OREGON-LO

13	2	3.30	515.8	3	%SF-UP
14	2	3.30	236.3	4	%SF-LO
15	2	3.30	324.7	4	%HLE-LO

SUB-CATCHMENT AREAS IN SQKM

%	NBBC1UP	NBBC1LW	HLEC1UP	HLEC1LW	GYRC1UP	GYRC1LW
	165.6	453.4	725.4	886.6	450.6	189.4

Table C.5: Model Parameters for Folsom Reservoir

SNOW PARAMETERS		American										
%	NFDC1UP	NFDC1LW	MFAC1UP	MFAC1LW	CBDC1UP	CBDC1LW	FOLC1L	FMDC1	HLLC1	RRGC1	UNVC1	AKYC1
	1.2000	1.1000	1.2800	1.1000	1.2000	1.1000	1.1000	1.1500	1.0900	1.1600	1.2500	1.2500
	0.9000	0.9500	0.9500	1.0000	0.9000	0.9500	0.9000	1.0500	0.9000	1.0000	1.1000	1.2000
	0.0700	0.3000	0.0500	0.0500	0.0500	0.0500	0.0500	0.0300	0.0300	0.0300	0.0500	0.0600
	0.1500	0.1500	0.1500	0.1500	0.1500	0.1500	0.1500	0.1500	0.1500	0.1500	0.1500	0.1500
	0.0200	0.0200	0.0800	0.0400	0.0800	0.0400	0.0400	0.0800	0.0800	0.0300	0.0200	0.0100
	0.2500	0.2500	0.2500	0.2500	0.2500	0.2500	0.2500	0.1000	0.1000	0.2500	0.2500	0.2500
	0.0000	0.0000	0.0000	0.0000	0.0000	0.0000	0.0000	0.0000	0.0000	0.0000	2.0000	2.0000
	0.1200	0.0800	0.0800	0.0800	0.0800	0.0800	0.0400	0.0400	0.0400	0.0800	0.0600	0.0200
	0.3000	0.3000	0.3000	0.3000	0.3000	0.3000	0.1000	0.1500	0.1500	0.3000	0.3000	0.3000
	1.9000	1.5000	1.9000	1.5000	1.8000	1.5000	1.5000	1.4000	0.5000	1.5000	1.5000	1.0000
	1600.00	409.00	1600.00	409.00	1600.00	409.00	200.00	1600.0	1600.0	1600.0	1600.0	1600.0
	19.0000	11.0000	19.0000	11.6000	19.5000	10.4000	6.2500	19.200	20.700	19.000	19.400	21.750
	0.6000	0.6000	0.6000	0.6000	0.6000	0.6000	0.6000	0.6000	0.6000	0.6000	0.6000	0.6000
	0.4500	0.4500	0.4500	0.4500	0.4500	0.4500	0.4500	0.4500	0.4500	0.4500	0.4500	0.4500
	19.8100	10.6700	19.8100	10.6700	19.8100	10.6700	4.8800	19.810	19.810	19.810	19.8100	19.8100
	1.2500	1.0200	0.9500	0.9500	1.2000	0.9500	0.9600	1.000	1.000	1.000	1.1400	1.0300
SAC PARAMETERS		American										
%	NFDC1UP	NFDC1LW	MFAC1UP	MFAC1LW	CBDC1UP	CBDC1LW	FOLC1L	FMDC1	HLLC1	RRGC1	UNVC1	AKYC1
	145.000	155.000	155.000	155.000	155.000	155.000	155.000	115.000	95.000	115.000	120.000	115.000
	50.000	50.000	50.000	40.000	40.000	40.000	30.000	40.000	30.000	40.000	40.000	30.000
	250.000	310.000	300.000	310.000	350.000	380.000	140.000	150.000	150.000	90.000	170.000	150.000
	210.000	70.000	110.000	180.000	60.000	140.000	180.000	50.000	70.000	20.000	70.000	60.000
	130.000	90.000	60.000	120.000	110.000	120.000	45.000	80.000	70.000	80.000	100.000	170.000
	0.2500	0.1500	0.2000	0.2500	0.2000	0.2500	0.4500	0.2000	0.4000	0.2500	0.2500	0.5000
	0.0020	0.0040	0.0020	0.0020	0.0020	0.0050	0.0030	0.0020	0.0020	0.0020	0.0020	0.0020
	0.0800	0.1000	0.0600	0.1000	0.0600	0.1000	0.0900	0.0600	0.0600	0.0600	0.0600	0.0600
	12.000	9.000	14.000	16.000	10.000	16.000	12.000	15.000	14.000	12.000	12.000	15.000
	1.050	1.100	1.200	1.100	1.200	1.100	1.300	1.300	1.200	1.200	1.200	1.200
	0.300	0.200	0.200	0.200	0.200	0.200	0.300	0.200	0.150	0.060	0.300	0.300
	0.000	0.000	0.000	0.000	0.000	0.000	0.000	0.000	0.000	0.000	0.000	0.000
	0.250	0.000	0.000	0.000	0.000	0.000	0.100	0.100	0.040	0.150	0.130	0.120
	0.005	0.008	0.005	0.008	0.005	0.008	0.040	0.005	0.005	0.020	0.005	0.005
	1.000	1.000	1.000	1.000	1.000	1.000	1.000	1.000	1.000	1.000	1.000	1.000
KINEMATIC CHANNEL ROUTING MODEL PARAMETERS												
1	2	5.40	327.6	1	%NF-UP							
2	2	0.85	557.8	2	%NF-LO							
3	2	8.80	277.6	3	%MF-UP							
4	2	0.95	538.9	4	%MF-LO							

5	2	8.01	191.1	5	%SF-UP
6	2	1.80	639.9	6	%SF-LO
7	2	4.40	293.7	7	%J1-LO
8	2	2.95	146.8	7	%LOCAL-NF+MF
9	2	2.95	587.3	7	%LOCAL-SF
10	2	8.80	148.9	8	%FMDC1 (ALL UP)
11	2	8.80	295.1	9	%HLLC1 (ALL UP)
12	2	8.80	123.3	10	%RRGC1 (ALL UP)
13	2	4.40	217.5	11	%UNVC1 (ALL UP)
14	2	4.40	499.7	12	%AKYC1 (ALL UP)

SUB-CATCHMENT AREAS IN SQKM

%	NFDC1UP	NFDC1LW	MFAC1UP	MFAC1LW	CBDC1UP	CBDC1LW	FOLC1L	FMDC1	HLLC1	RRGC1	UNVC1	AKYC1
	327.6	557.8	277.6	538.9	191.1	639.9	1027.8	148.9	295.1	123.3	217.5	499.7

Table C.6: Model Parameters for Sacramento River Downstream

SNOW PARAMETERS		Downstream Basins - SACRAMENTO RIVER									
%	WHSC1	RDGC1L	CWCC1UP	CWCC1LW	CTWC1UP	CTWC1LW	COTC1UP	COTC1LW	BDBC1L	EDCC1UP	EDCC1LW
	1.0000	1.1500	1.5000	1.1500	1.3500	0.9500	1.2000	1.0000	1.1500	1.1000	0.8500
	0.7500	1.1000	0.9000	1.1000	1.0000	1.1000	0.5500	0.9000	1.1000	1.0000	0.8500
	0.1500	0.3000	0.2000	0.3000	0.4500	0.3000	0.0500	0.0300	0.3000	0.3000	0.4000
	0.1500	0.1500	0.1500	0.1500	0.1500	0.1500	0.1500	0.1500	0.1500	0.1500	0.1500
	0.2500	0.0200	0.0200	0.0200	0.0200	0.0200	0.0200	0.0100	0.0200	0.0500	0.1000
	0.2500	0.2000	0.1000	0.2000	0.2500	0.2000	0.0500	0.2000	0.2000	0.0500	0.2500
	0.0000	0.0000	0.0000	0.0000	0.0000	0.0000	0.0000	0.0000	0.0000	1.0000	1.5000
	0.0700	0.0700	0.1200	0.0700	0.1200	0.0700	0.0500	0.0700	0.0700	0.1200	0.1200
	0.3000	0.3000	0.3000	0.3000	0.3000	0.3000	0.3000	0.3000	0.3000	0.3000	0.3000
	1.5000	2.5000	2.0000	2.5000	2.0000	2.5000	1.0000	2.5000	2.5000	1.0000	1.0000
	500.000	500.000	1500.000	500.000	800.000	500.000	1500.000	500.000	500.000	700.000	500.000
	8.7900	2.4300	16.7600	4.8000	16.7600	4.8000	17.9000	9.7300	2.4300	16.7000	6.7700
	0.8000	0.7000	0.7000	0.7000	0.7000	0.7000	0.7000	0.7000	0.7000	0.6000	0.6000
	0.5500	0.5500	0.4500	0.4500	0.4500	0.4500	0.5500	0.5500	0.5500	0.4500	0.4500
	10.6700	4.2700	17.0700	4.2700	17.0700	4.2700	17.0700	9.7500	4.2700	17.0700	10.0600
	1.0000	0.9300	1.1900	1.0700	1.1700	1.0800	0.8700	0.9500	1.3500	1.0000	1.0800
SNOW PARAMETERS		Downstream Basins - SACRAMENTO RIVER (Continued)									
%	MLMC1UP	MLMC1LW	TCRC1UP	TCRC1LW	DCVC1UP	DCVC1LW	TEHC1UP	TEHC1LW	VWBC1L	HKCC1	BKCC1UP
	1.2500	1.0500	1.1000	0.8500	1.1500	0.9500	1.2000	1.2000	1.2000	0.9500	1.2500
	0.9000	0.9000	1.0000	0.8500	0.9500	0.9000	0.8000	0.9000	0.9000	0.9000	0.9500
	0.1000	0.3000	0.3000	0.4000	0.1000	0.3000	0.2000	0.3000	0.3000	0.3000	0.1000
	0.2000	0.1500	0.1500	0.1500	0.2000	0.1500	0.2000	0.1500	0.1500	0.1500	0.2000
	0.0400	0.0400	0.0500	0.1000	0.0400	0.0400	0.0400	0.0400	0.0400	0.0400	0.0400
	0.2500	0.2500	0.0500	0.2500	0.2500	0.2500	0.2500	0.2500	0.2500	0.2500	0.2500
	1.0000	0.7000	1.0000	1.5000	1.0000	0.7000	1.0000	0.7000	0.7000	0.7000	1.0000
	0.1500	0.0700	0.1200	0.1200	0.1500	0.0700	0.1500	0.0700	0.0700	0.0700	0.1500
	0.3000	0.1000	0.3000	0.3000	0.3000	0.3000	0.3000	0.3000	0.3000	0.3000	0.3000
	1.5000	1.8000	1.0000	1.0000	1.5000	1.8000	1.5000	1.8000	1.8000	1.8000	1.5000
	1500.000	500.000	700.000	500.000	900.000	500.000	1500.000	500.000	500.000	500.000	900.000
	17.220	7.9200	17.2300	11.1200	16.8000	8.1900	17.2200	3.4700	2.7400	9.5000	16.8000
	0.7000	0.7000	0.7000	0.7000	0.7000	0.7000	0.7000	0.7000	0.7000	0.7000	0.7000
	0.5500	0.5500	0.5500	0.5500	0.5500	0.5500	0.5500	0.5500	0.5500	0.5500	0.5500
	17.0700	10.0700	17.0700	10.0600	17.0700	10.0700	17.0700	3.0500	3.0500	10.0600	17.0700
	1.0500	0.8300	0.8500	1.0300	1.0500	0.7000	0.9800	0.8000	0.9000	0.9000	1.0000
SNOW PARAMETERS		Downstream Basins - SACRAMENTO RIVER (Continued)									
%	BKCC1LW	EPRC1	SGEC1UP	SGEC1LW	BLBC1UP	BLBC1LW	ORFC1L	MRYC1L	HCTC1	YUBC1L	CFWC1UP
	0.9500	1.2000	1.1000	1.0000	1.1000	1.0000	1.0000	1.0000	1.5000	1.0000	1.1000

0.9000	1.3000	0.9000	1.1000	0.9000	1.1000	0.9000	0.8000	1.1000	0.8000	0.9000
0.3000	0.5000	0.1000	0.2000	0.1000	0.4000	0.3000	0.2500	0.5500	0.2500	0.4000
0.1500	0.1500	0.1500	0.1500	0.1500	0.1500	0.1500	0.1500	0.1500	0.1500	0.1500
0.0400	0.3000	0.3000	0.3000	0.3000	0.1000	0.0400	0.0400	0.0400	0.0400	0.1200
0.2500	0.2500	0.2500	0.2500	0.2500	0.2500	0.2500	0.2500	0.2500	0.2500	0.0500
0.7000	0.0000	0.0000	0.0000	0.0000	0.0000	0.7000	1.0000	1.0000	1.0000	0.0000
0.0700	0.1000	0.2000	0.1500	0.2000	0.1000	0.0700	0.0400	0.0700	0.0400	0.0700
0.3000	0.3000	0.3000	0.3000	0.3000	0.3000	0.3000	0.1000	0.1000	0.1000	0.3000
1.8000	2.5000	2.5000	2.5000	2.5000	2.5000	1.8000	2.0000	2.0000	2.0000	1.5000
500.000	1600.000	1600.000	1600.000	1600.000	1600.000	500.000	200.000	1250.000	200.000	500.000
8.1900	8.5000	16.8100	5.4100	16.8500	5.9000	1.0700	5.2200	5.1400	0.5900	11.5000
0.7000	0.7000	0.7000	0.7000	0.8000	0.8000	0.7000	0.8000	0.6000	0.7000	0.6000
0.5500	0.5500	0.5500	0.5500	0.3500	0.3500	0.7500	0.3500	0.4000	0.4500	0.4500
10.0600	5.4900	17.0700	5.4900	17.0700	5.4900	3.0500	10.3600	9.1400	9.1400	9.1400
0.8600	1.1500	1.3000	1.1300	1.0500	0.9700	0.8800	0.9000	0.8900	0.9800	1.0200

SNOW PARAMETERS Downstream Basins - SACRAMENTO RIVER (Continued)

%	CFWC1LW	DCWC1	RCVC1	FMWC1L	SAMC1L	SACC1L
1.0000	1.0000	1.0000	1.0000	1.0000	1.0000	1.0000
1.0000	0.8000	0.9000	0.8000	0.9000	0.9000	0.9000
0.6700	0.2500	0.3000	0.2500	0.2500	0.5000	0.5000
0.1500	0.1500	0.1500	0.1500	0.1500	0.1500	0.1500
0.0200	0.0400	0.0400	0.0400	0.0400	0.0200	0.0200
0.2500	0.2500	0.2500	0.2500	0.2500	0.2500	0.2500
0.0000	1.0000	0.7000	1.0000	1.0000	0.0000	0.0000
0.0700	0.0400	0.0700	0.0400	0.0400	0.0700	0.0700
0.3000	0.1000	0.3000	0.1000	0.1000	0.3000	0.3000
2.0000	2.0000	1.8000	2.0000	2.0000	1.5000	1.5000
357.000	200.000	500.000	200.000	200.000	500.000	500.000
5.5000	2.2200	1.0500	0.5900	0.5900	0.5900	0.5900
0.6000	0.8000	0.7000	0.7000	0.7000	0.7000	0.7000
0.4500	0.3500	0.5500	0.4500	0.4500	0.4500	0.4500
9.1400	5.2200	3.0500	9.1400	9.1400	9.1400	9.1400
0.9500	0.8600	0.9300	0.9800	0.9900	0.9900	0.9900

SAC PARAMETERS Downstream Basins - SACRAMENTO RIVER

%	WHSC1	RDGC1L	CWCC1UP	CWCC1LW	CTWC1UP	CTWC1LW	COTC1UP	COTC1LW	BDBC1L	EDCC1UP	EDCC1LW
125.0000	124.0000	80.0000	84.0000	116.0000	120.0000	50.0000	128.0000	140.0000	100.0000	112.0000	112.0000
85.0000	35.0000	29.0000	47.0000	58.0000	20.0000	69.0000	46.0000	58.0000	35.0000	35.0000	35.0000
900.0000	148.0000	295.0000	138.0000	115.0000	80.0000	280.0000	133.0000	156.0000	137.0000	150.0000	150.0000
325.0000	131.0000	247.0000	285.0000	91.0000	208.0000	1500.0000	773.0000	131.0000	152.0000	112.0000	112.0000

25.0000	50.0000	65.0000	128.0000	30.0000	61.0000	90.0000	100.0000	100.0000	70.0000	88.0000
0.2500	0.8000	0.7000	0.7200	0.2300	0.3200	0.1000	0.1800	0.5300	0.2500	0.4000
0.0110	0.0200	0.0100	0.0100	0.0010	0.0040	0.0010	0.0020	0.0200	0.0030	0.0070
0.0700	0.2460	0.2700	0.3100	0.1600	0.1660	0.0900	0.0330	0.1030	0.1100	0.1000
30.0000	29.5000	15.0000	4.7000	8.3000	7.8000	36.0000	30.0000	19.0000	68.0000	44.0000
1.2000	1.2300	1.1200	1.0200	1.1400	1.2900	1.5000	1.3500	1.2600	1.0400	1.0000
0.0150	0.3800	0.1800	0.1220	0.2200	0.3100	0.3800	0.2700	0.3900	0.2500	0.1500
0.0000	0.0000	0.0500	0.1400	0.0060	0.0500	0.0200	0.0100	0.0000	0.1200	0.2500
0.0250	0.0000	0.1300	0.1100	0.0230	0.0920	0.0200	0.1100	0.0300	0.2200	0.2200
0.0100	0.0150	0.0040	0.0040	0.0040	0.0040	0.0030	0.0050	0.0150	0.0050	0.0080
1.0000	1.0000	1.0000	1.0000	1.0000	1.0000	1.0000	1.0000	1.0000	1.0000	1.0000

SAC PARAMETERS Downstream Basins - SACRAMENTO RIVER (Continue)

%	MLMC1UP	MLMC1LW	TCRC1UP	TCRC1LW	DCVC1UP	DCVC1LW	TEHC1UP	TEHC1LW	VWBC1L	HKCC1	BKCC1UP
120.0000	138.0000	100.0000	112.0000	100.0000	124.0000	70.0000	78.0000	118.0000	141.0000	100.0000	
33.0000	21.0000	35.0000	35.0000	25.0000	34.0000	23.0000	41.0000	26.0000	60.0000	25.0000	
157.0000	56.0000	117.0000	250.0000	247.0000	157.0000	75.0000	75.0000	56.0000	225.0000	247.0000	
850.0000	100.0000	152.0000	112.0000	581.0000	190.0000	150.0000	79.0000	60.0000	236.0000	581.0000	
83.0000	31.0000	70.0000	88.0000	132.0000	62.0000	28.0000	24.0000	22.0000	32.0000	132.0000	
0.2000	0.7600	0.2500	0.4000	0.2100	0.4700	0.5500	0.6700	0.4500	0.3800	0.2100	
0.0030	0.0100	0.0030	0.0070	0.0050	0.0020	0.0050	0.0080	0.0100	0.0030	0.0050	
0.1700	0.1930	0.1400	0.1000	0.1800	0.1400	0.1200	0.1000	0.1930	0.1600	0.1800	
21.0000	21.0000	68.0000	44.0000	11.0000	14.0000	15.0000	38.0000	35.0000	43.4000	11.0000	
1.1600	1.0300	1.0400	1.0000	1.1100	1.1500	1.1000	1.4000	1.0300	1.0800	1.1100	
0.2000	0.2900	0.2500	0.1500	0.3600	0.3900	0.1200	0.1900	0.2900	0.3100	0.3600	
0.0800	0.0500	0.1200	0.2500	0.0100	0.0900	0.0000	0.0500	0.0500	0.0500	0.0100	
0.0030	0.0030	0.0900	0.2200	0.0040	0.1550	0.0050	0.2800	0.4500	0.0800	0.0040	
0.0030	0.0050	0.0050	0.0080	0.0030	0.0150	0.0030	0.0150	0.1200	0.0050	0.0030	
1.0000	1.0000	1.0000	1.0000	1.0000	1.0000	1.0000	1.0000	1.0000	1.0000	1.0000	

SAC PARAMETERS Downstream Basins - SACRAMENTO RIVER (Continue)

%	BKCC1LW	EPRC1	SGEC1UP	SGEC1LW	BLBC1UP	BLBC1LW	ORFC1L	MRYC1L	HCTC1	YUBC1L	CFWC1UP
176.0000	30.0000	62.0000	74.0000	50.0000	75.0000	118.0000	75.0000	130.0000	70.0000	62.0000	
80.0000	36.0000	64.0000	29.0000	27.0000	26.0000	36.0000	30.0000	10.0000	25.0000	37.0000	
300.0000	55.0000	61.0000	123.0000	120.0000	150.0000	120.0000	320.0000	90.0000	85.0000	275.0000	
250.0000	63.0000	93.0000	104.0000	90.0000	141.0000	60.0000	50.0000	50.0000	36.0000	420.0000	
93.0000	61.0000	73.0000	44.0000	40.0000	59.0000	22.0000	120.0000	80.0000	28.0000	65.0000	
0.2600	0.3700	0.4000	0.5800	0.3800	0.3800	0.4500	0.7000	0.3000	0.3500	0.2700	
0.0030	0.0200	0.0080	0.0020	0.0080	0.0020	0.0100	0.0120	0.0100	0.0070	0.0060	
0.1040	0.1700	0.0830	0.0850	0.1000	0.0610	0.1500	0.2200	0.1000	0.0700	0.0500	
29.3000	73.0000	84.0000	74.0000	65.0000	27.0000	35.0000	20.0000	1.0000	30.0000	95.0000	
1.1600	1.0000	1.0700	1.0100	1.2000	1.2100	1.0300	1.5000	0.5000	2.2000	1.3000	
0.2700	0.2400	0.0500	0.0500	0.1000	0.0500	0.2900	0.3000	0.1000	0.1500	0.1500	

0.0300	0.2900	0.0000	0.0000	0.0000	0.0000	0.0500	0.0000	0.0000	0.0000	0.0000
0.1900	0.1900	0.0800	0.1900	0.1500	0.2100	0.4500	0.0000	0.0500	0.2400	0.0000
0.0050	0.0050	0.0050	0.0150	0.0050	0.0150	0.0200	0.0250	0.0800	0.0050	0.0000
1.0000	1.0000	1.0000	1.0000	1.0000	1.0000	1.0000	1.0000	1.0000	1.0000	1.0000

SAC PARAMETERS Downstream Basins - SACRAMENTO RIVER (Continue)

%	CFWC1LW	DCWC1	RCVC1	FMWC1L	SAMC1L	SACC1L
130.0000	83.0000	81.0000	70.0000	70.0000	70.0000	
44.0000	33.0000	26.0000	25.0000	25.0000	25.0000	
125.0000	71.0000	70.0000	85.0000	85.0000	85.0000	
360.0000	117.0000	25.0000	36.0000	156.0000	36.0000	
70.0000	33.0000	29.0000	28.0000	48.0000	28.0000	
0.2700	0.2100	0.8200	0.3500	0.8500	0.3500	
0.0040	0.0030	0.0190	0.0070	0.0070	0.0070	
0.0300	0.0720	0.1900	0.0700	0.1100	0.1100	
53.0000	7.8000	51.0000	30.0000	12.0000	30.0000	
1.5000	1.0800	1.1400	2.2000	1.2000	2.2000	
0.1500	0.1600	0.2500	0.1500	0.1500	0.1500	
0.0000	0.0500	0.0900	0.0000	0.3000	0.0000	
0.0900	0.4100	0.3100	0.2400	0.3000	0.2000	
0.0050	0.0050	0.0200	0.0050	0.5000	0.0250	
1.0000	1.0000	1.0000	1.0000	1.0000	1.0000	

KINEMATIC CHANNEL ROUTING MODEL PARAMETERS

1	6	3.50	517.8	1	%WHSC1
2	6	2.40	72.5	2	%RDGC1
3	1	0.81	88.0	3	%CWC-UP
4	3	0.81	1012.3	4	%CWC-LO
5	1	0.65	168.0	5	%CTW-UP
6	5	0.65	2231.9	6	%CTW-LO
7	1	0.85	305.0	7	%COT-UP
8	3	0.85	619.2	8	%COT-LO
9	0	1.00	1281.5	9	%BDB-LOCAL
10	1	1.40	35.9	10	%EDC-UP
11	4	1.40	203.3	11	%EDC-LO
12	2	1.30	115.3	12	%MLM-UP
13	4	1.30	223.8	13	%MLM-LO
14	2	1.30	178.7	14	%TCR-UP
15	4	1.30	346.8	15	%TCR-LO
16	1	0.98	183.1	16	%DCV-UP
17	3	0.98	355.4	17	%DCV-LO
18	1	0.95	38.9	18	%TEH-UP
19	0	1.00	1905.3	19	%TEH-LO

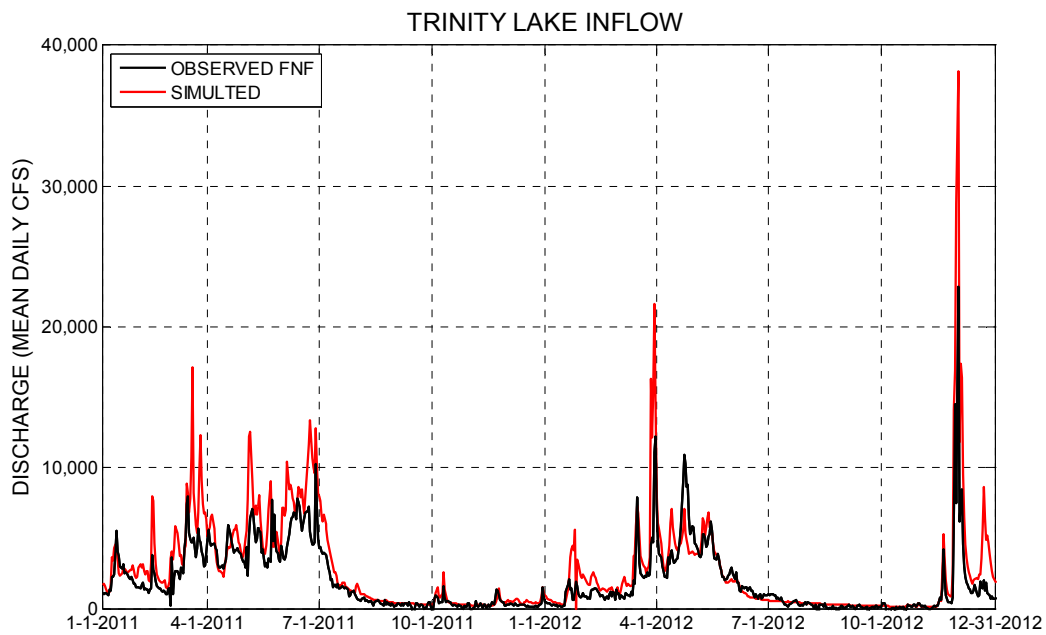
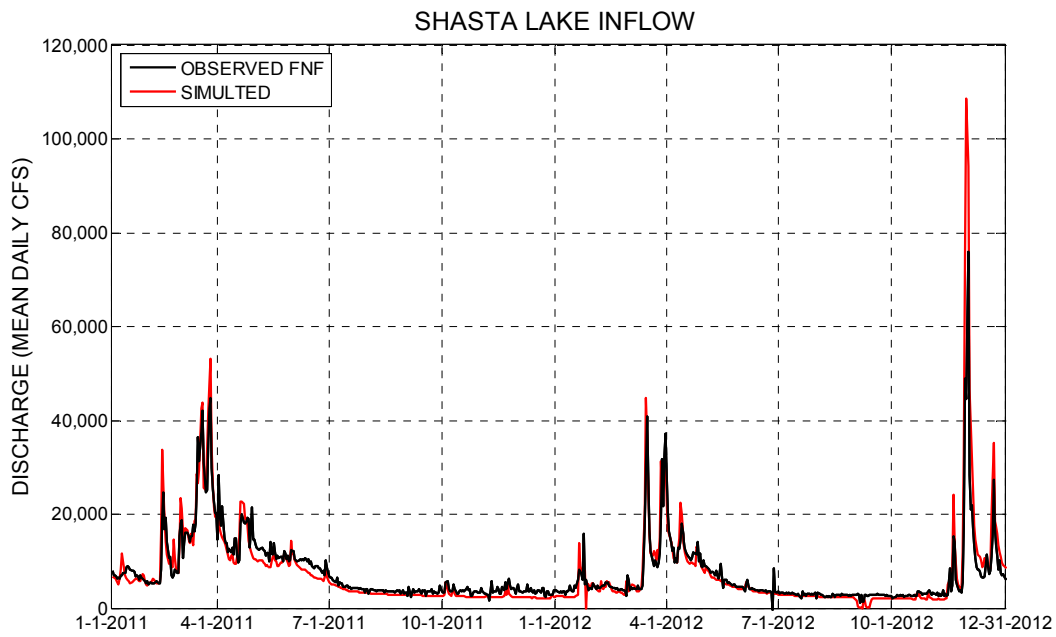
20	0	1.00	719.5	20	% VWB-LOCAL
21	4	0.67	168.4	21	% HKC
22	1	1.13	106.6	22	% BKC-UP
23	3	1.13	274.0	23	% BKC-LO
24	2	2.11	253.7	24	% EPRC1
25	1	1.58	63.0	25	% SGE-UP
26	2	1.58	462.5	26	% SGE-LO
27	1	2.32	79.7	27	% BLB-UP
28	2	2.32	1059.4	28	% BLB-LO
29	0	1.00	1579.2	29	% ORF-LOCAL
30	0	1.00	598.0	30	% MRY-LOCAL
31	2	0.90	79.2	31	% HCTC1
32	0	1.00	894.1	32	% YUB-LOCAL
33	1	1.11	145.0	33	% CFW-UP
34	2	1.11	579.9	34	% CFW-LO
35	6	4.10	258.9	35	% DCWC1
36	5	0.86	207.1	36	% RVC1
37	0	1.00	6409.3	37	% FMW-LOCAL
38	0	1.00	1826.2	39	% SAM-LOCAL
39	0	1.00	1826.2	39	% SAC-LOCAL

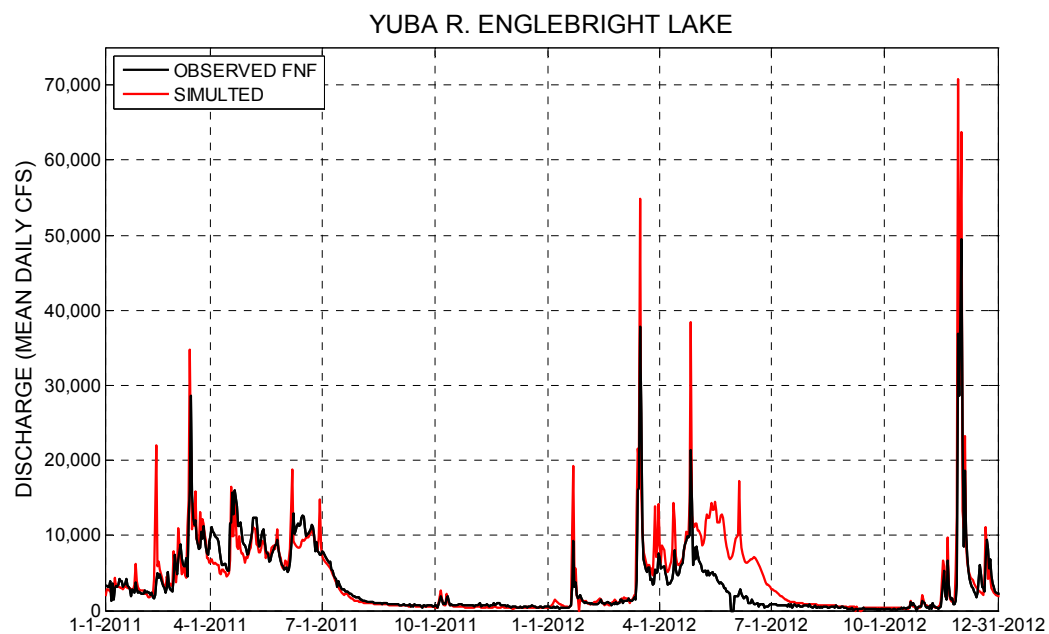
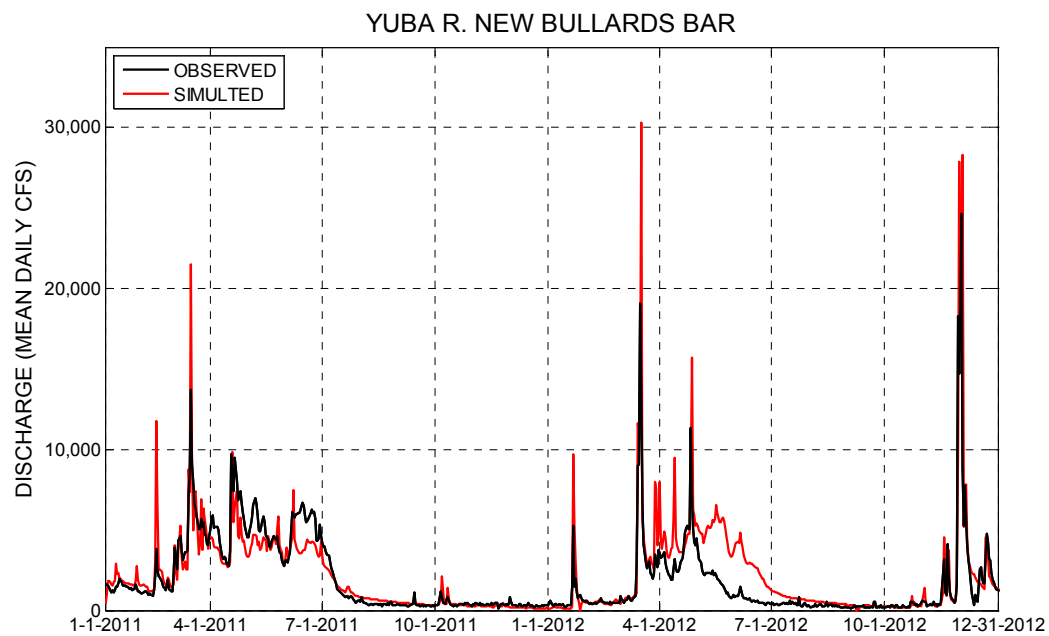
SUB-CATCHMENT AREAS IN SQKM

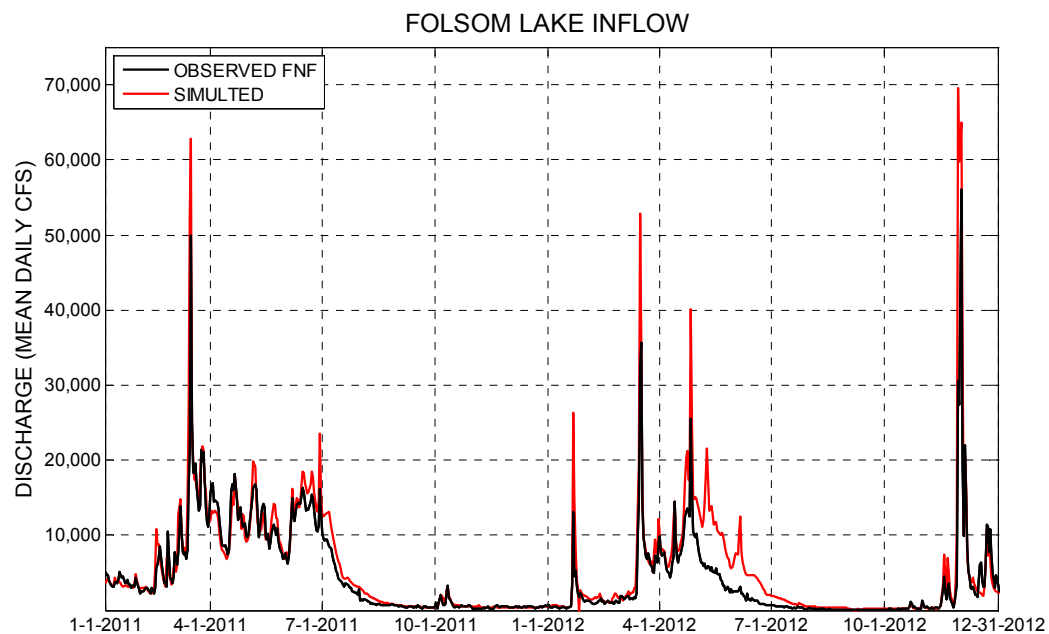
%	WHSC1	RDGC1L	CWCC1UP	CWCC1LW	CTWC1UP	CTWC1LW	COTC1UP	COTC1LW	BDBC1L	EDCC1UP	EDCC1LW
%	MLMC1UP	MLMC1LW	TCRC1UP	TCRC1LW	DCVC1UP	DCVC1LW	TEHC1UP	TEHC1LW	VWBC1L	HKCC1	BKCC1UP
%	BKCC1LW	EPRC1	SGEC1UP	SGEC1LW	BLBC1UP	BLBC1LW	ORFC1L	MRYC1L	HCTC1	YUBC1L	CFWC1UP
%	CFWC1LW	DCWC1	RCVC1	FMWC1L	SAMC1L	SACC1L					
	517.8	72.5	88.0	1012.3	168.0	2231.9	305.0	619.2	1281.5	35.9	203.3
	115.3	223.8	178.7	346.8	183.1	355.4	38.9	1905.3	719.5	186.4	106.6
	274.0	253.7	63.0	462.5	79.7	1059.4	1579.2	598.0	79.2	894.1	145.0
	579.9	258.9	207.1	6409.3	274.5	1826.2					

FNF Simulations versus Observations (2011-2012)

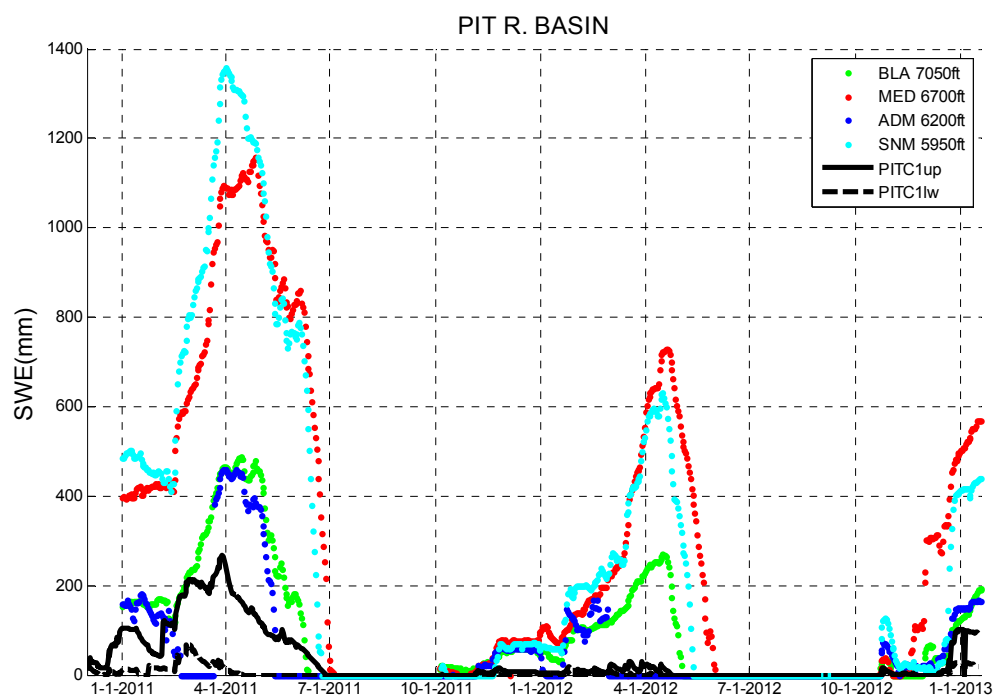
\

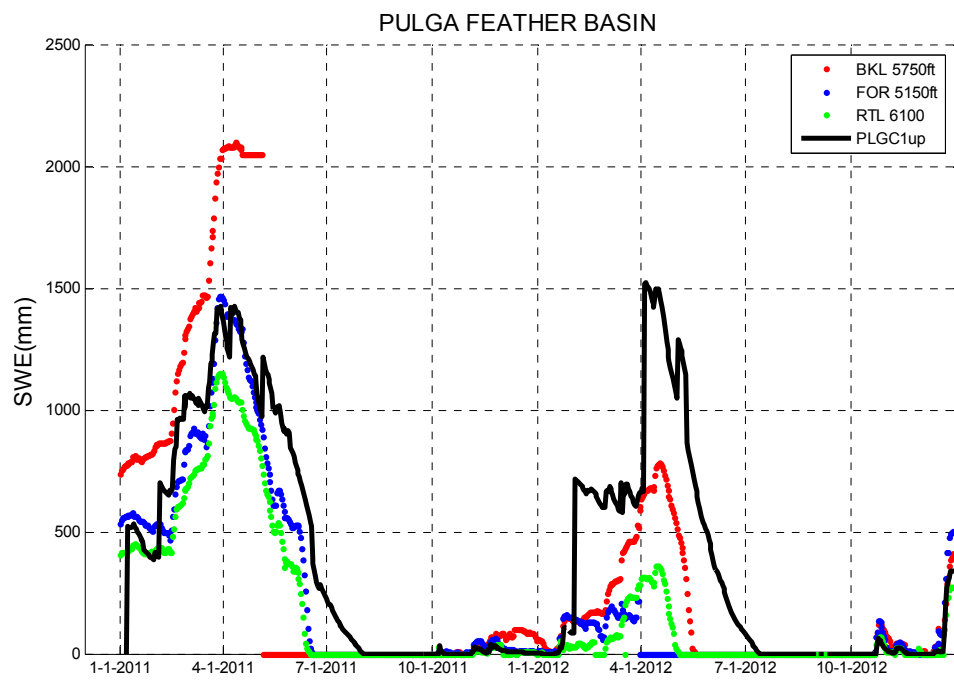
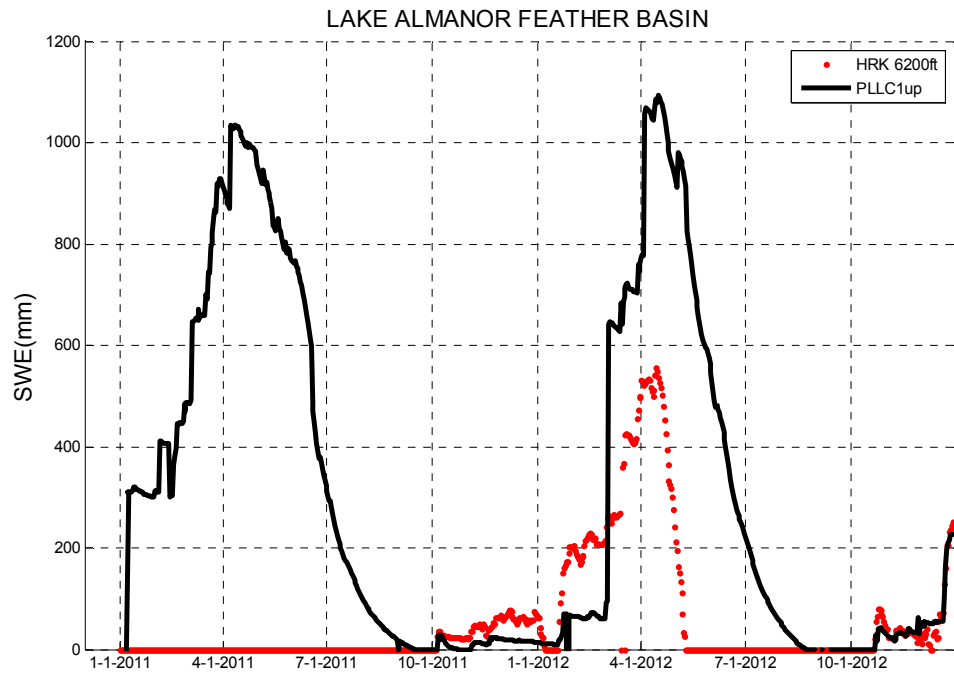


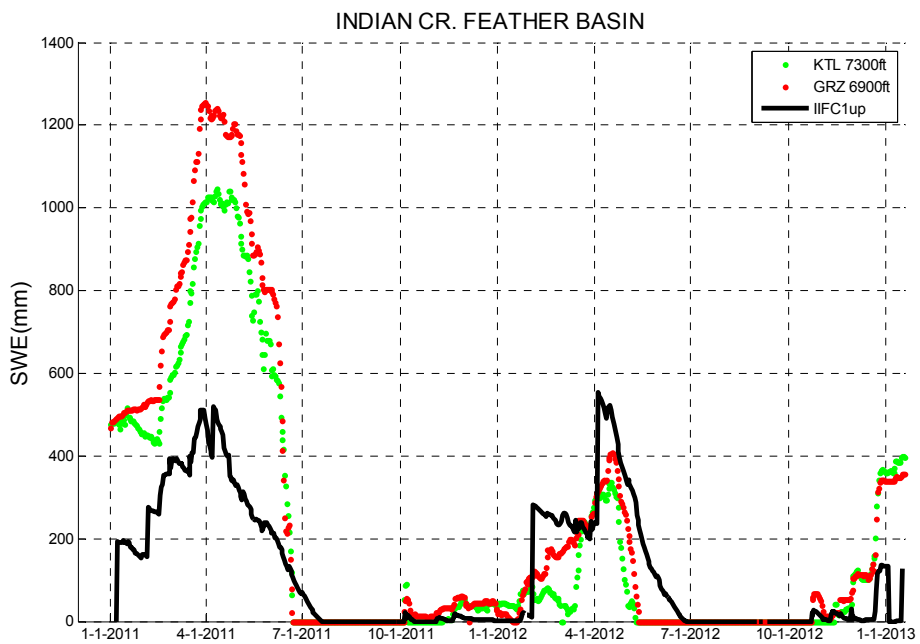
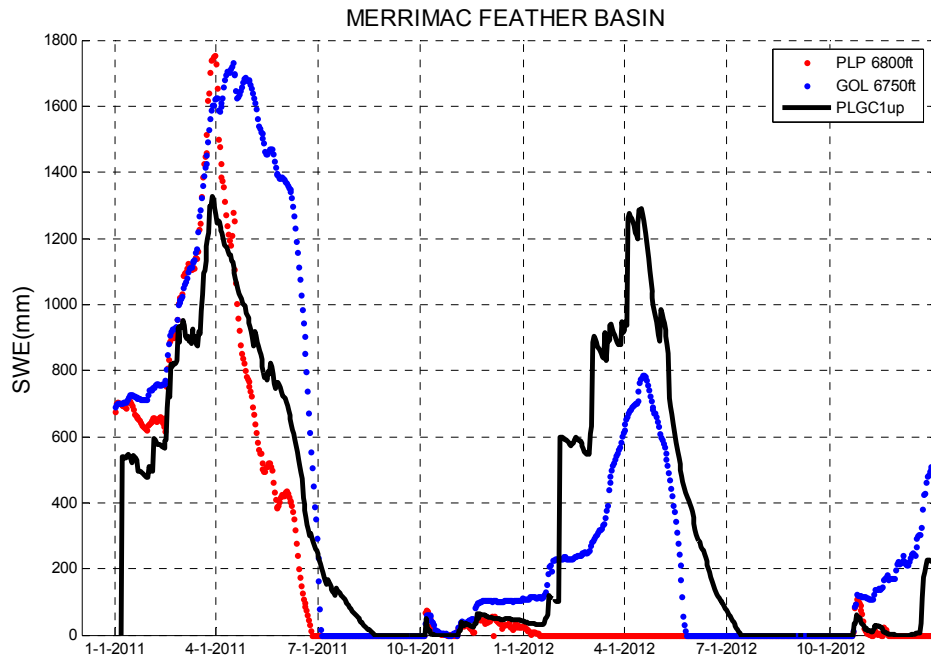


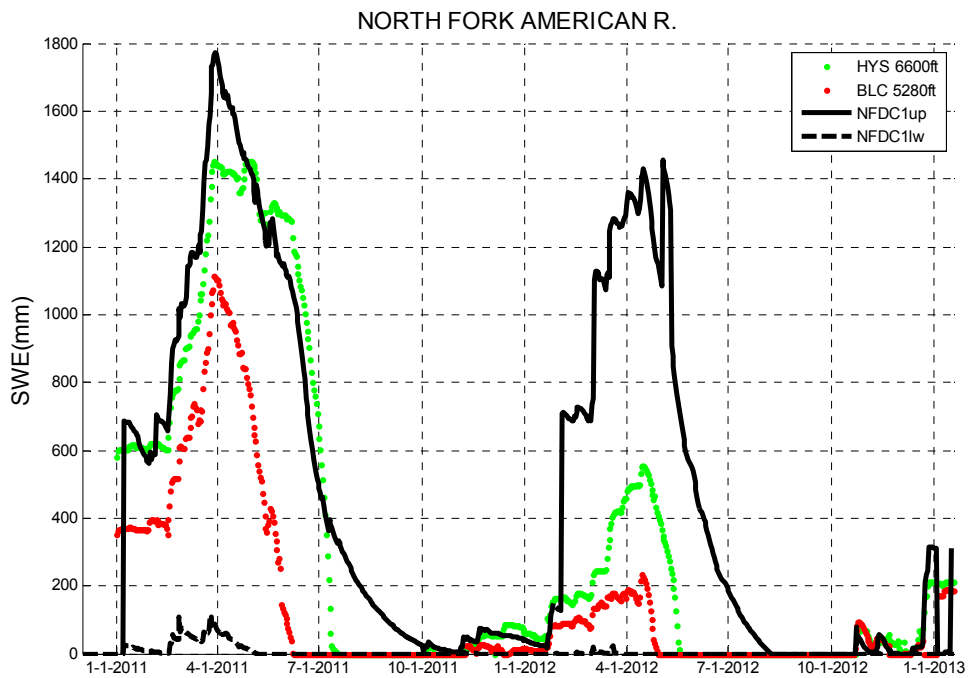
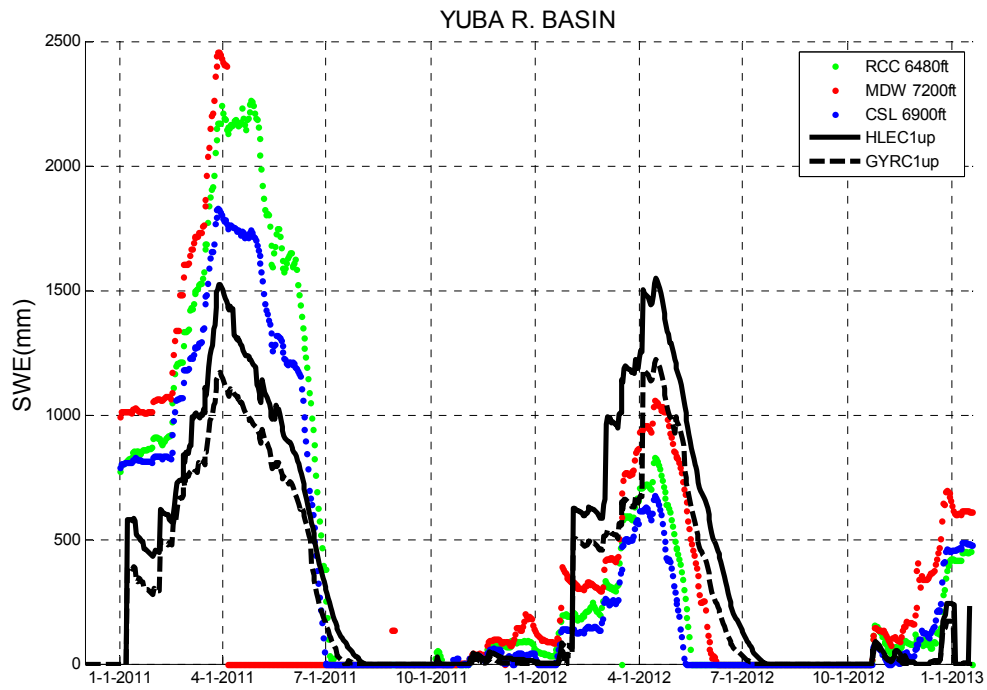


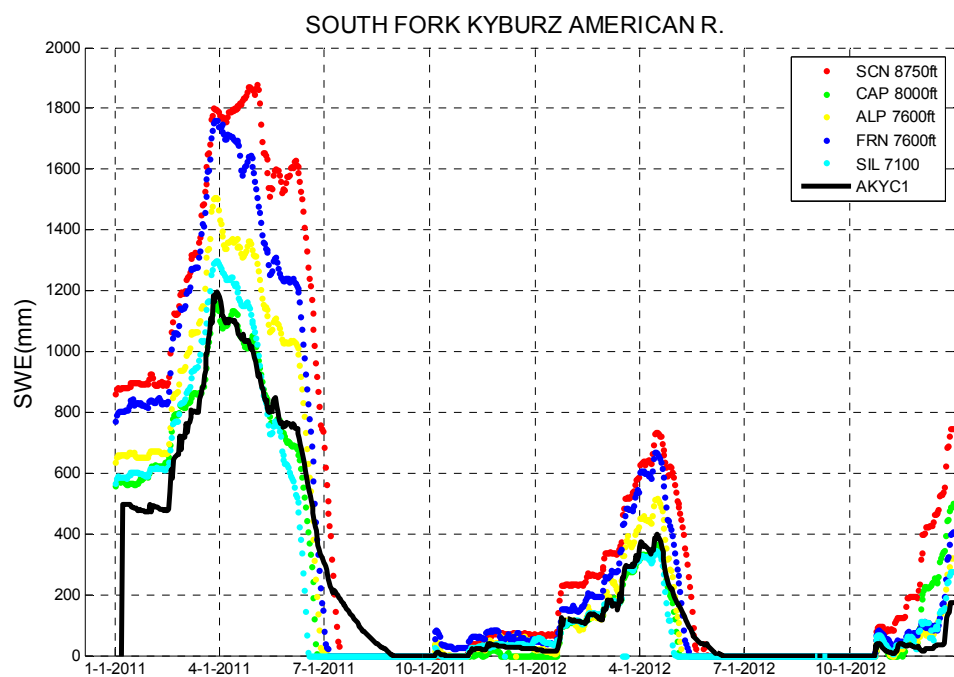
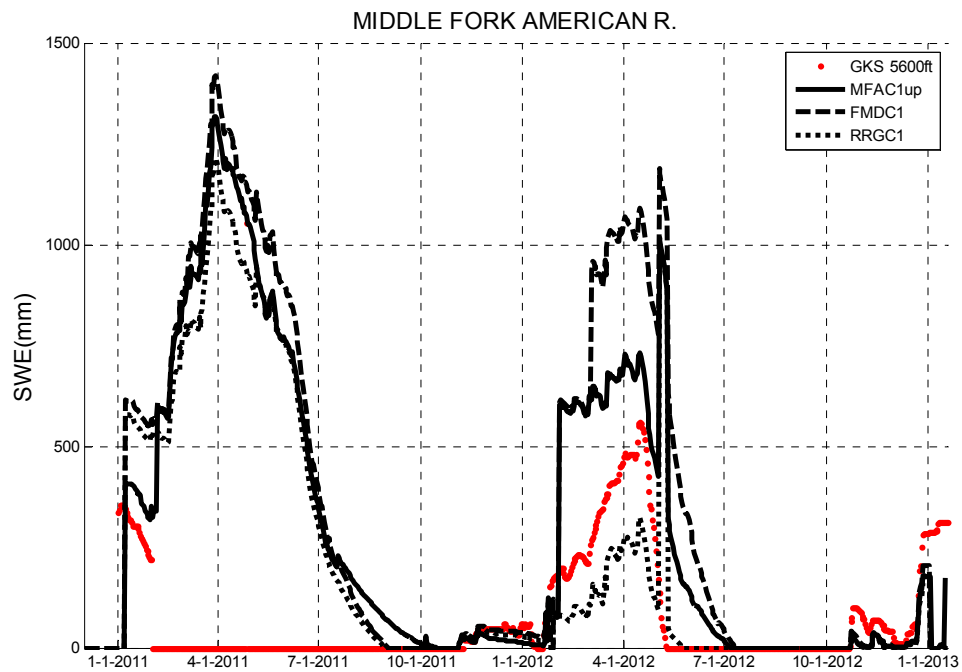
SWE Simulations versus Observations (2011-2012)

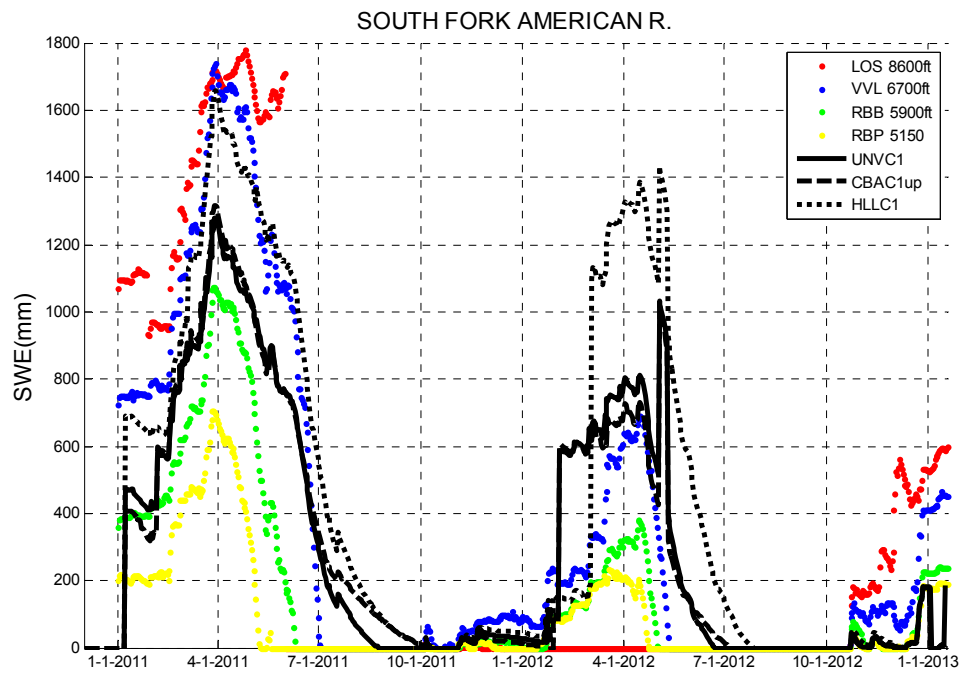




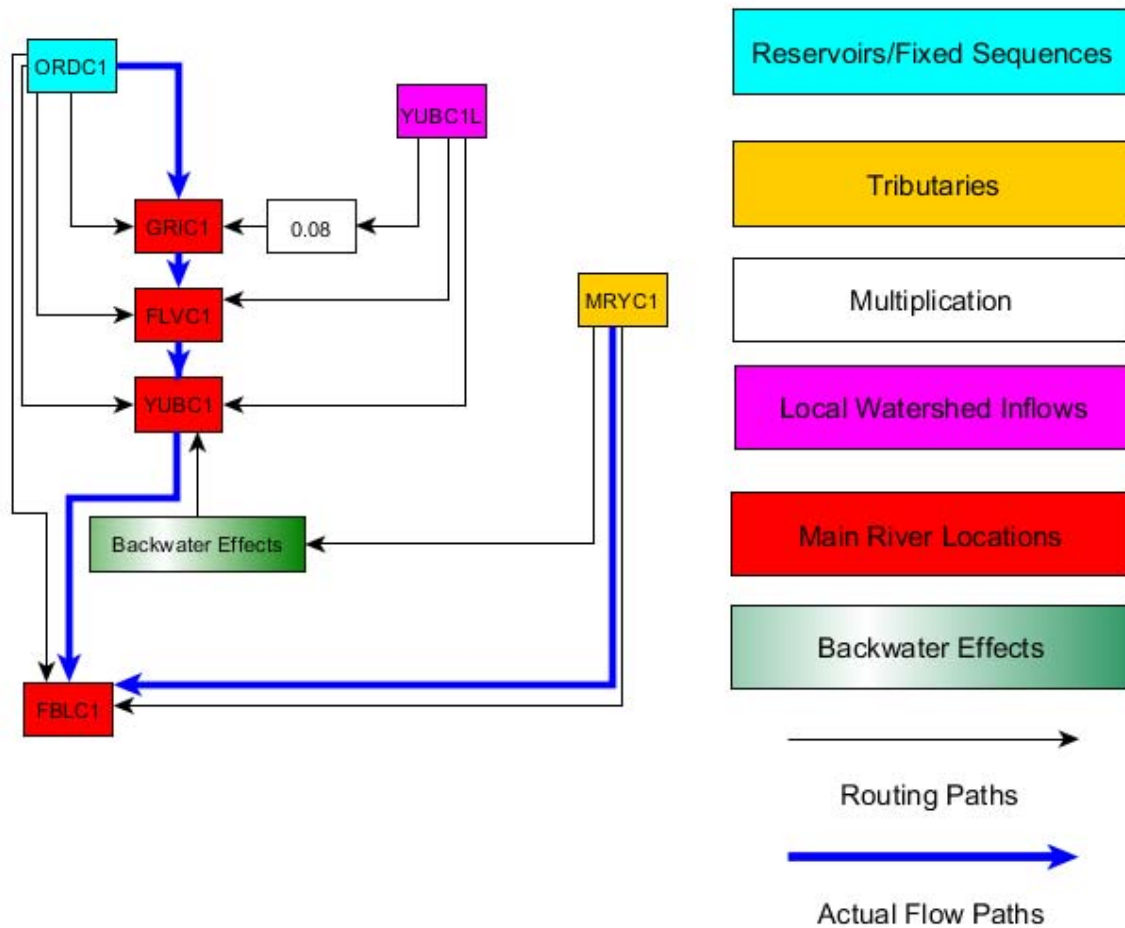








APPENDIX D: Feather River Routing Models



D.1 Reach 1: ORDC1 to GRIC1

D.1.1 Routing Model

$$S_1(k+1) = S_1(k) + \text{Units} * [I_1(k) + w_1(k) - LS_1(k) - u_1(k)] .$$

The terms in the above equation are defined as follows:

k : Time index corresponding to 6-hour intervals.

$S_1(k)$: Reach storage in billion cubic feet at the beginning of time interval k .

Units: Unit factor to convert reach fluxes from million cubic feet to billion cubic feet,
Units = 1/1000.

$I_1(k)$: Upstream inflow in mcf/6-hrs.

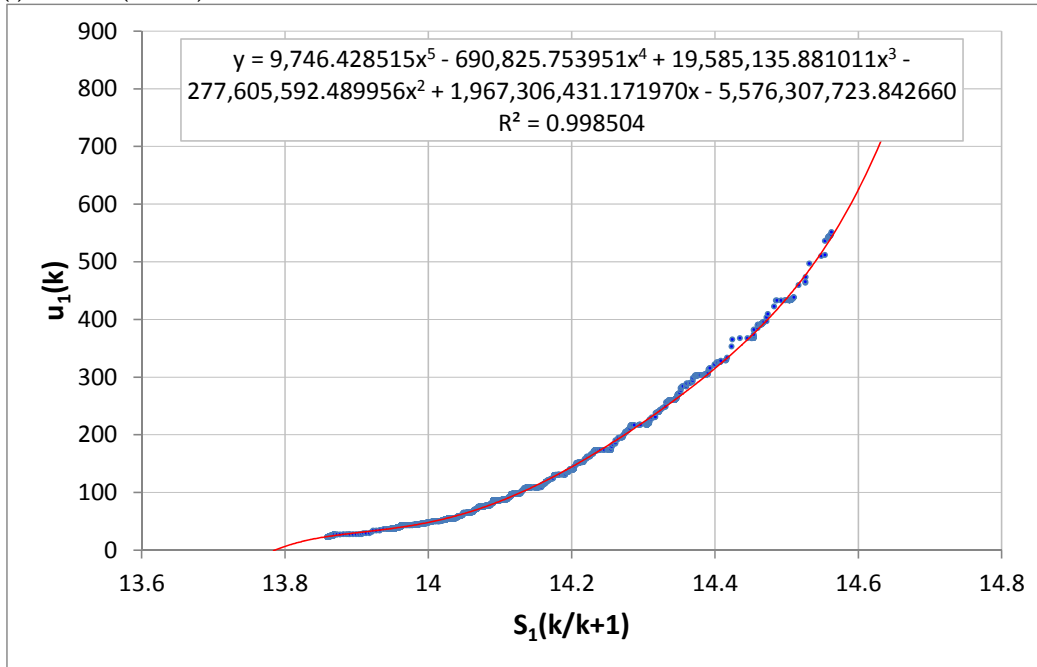
$w_1(k)$: Local reach inflow in mcf/6-hrs.

$LS_1(k)$: Reach losses in mcf/6-hrs. The losses in this reach are negligible.

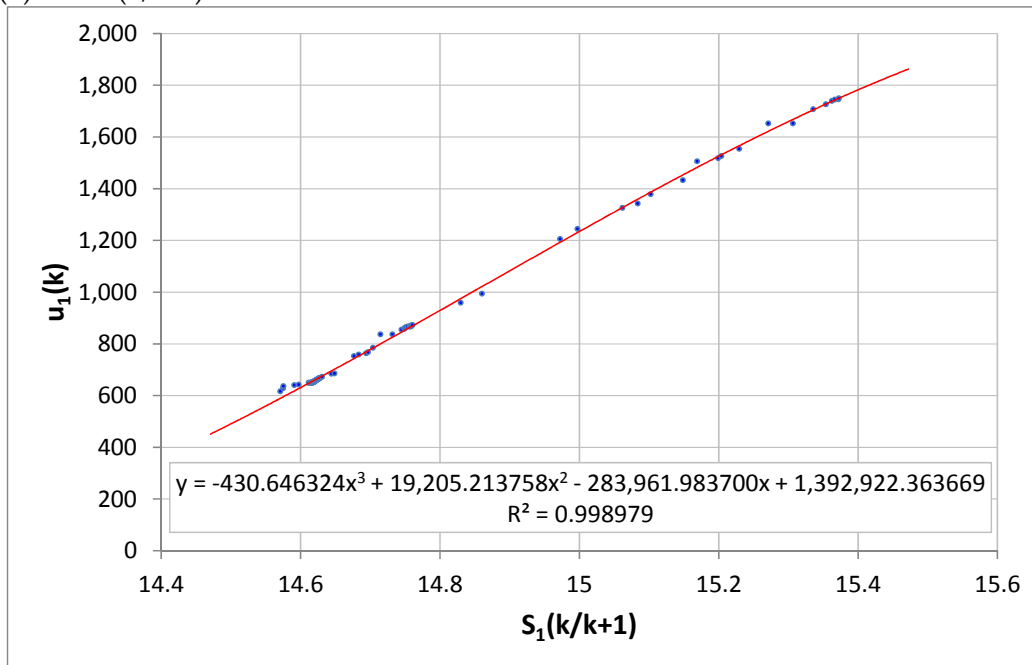
$u_1(k)$: Reach release to the downstream system as a function of the reach storage, $S_1(k/k+1)$,
where $S_1(k/k+1) = x_1 * S_1(k) + (1-x_1) * S_1(k+1)$, with $x_1=0.4$.

The $u_1(k)$ vs. $S_1(k/k+1)$ function is given by the following relationships:

(i) $S_1(k/k+1) \leq 14.56$ bcf:



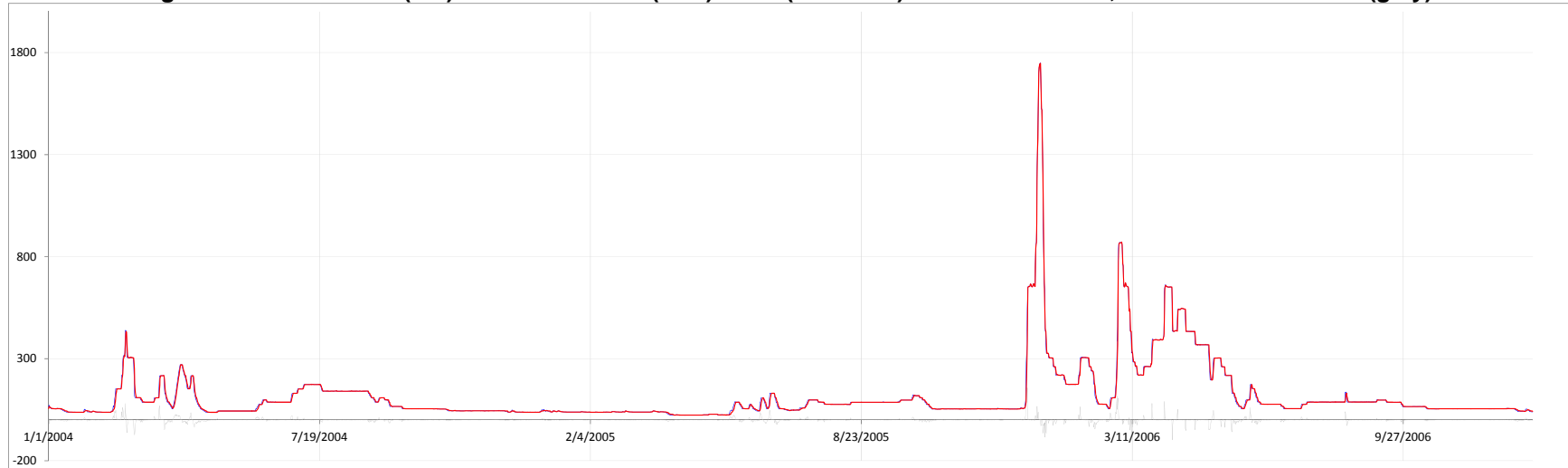
(ii) $S_1(k/k+1) > 14.56$ bcf:



D.1.2 Model Calibration and Validation Statistics:

D.1.2.1 Model Calibration Period: 1/1/2004 – 12/31/2006

Figure D.1.1: Simulated (red) versus observed (blue) flows (mcf/6-hrs) at the reach outlet, and associated errors (grey).



$$\text{Average Error} = 0.000 \text{ mcf/6-hrs} ; \quad \frac{1}{N} \sum_{k=1}^N \{Error(k)\}; \quad Error(k) = Obs.Flow(k) - Sim.Flow(k);$$

$$\text{Abs. Avg. Error} = 2.927 \text{ mcf/6-hrs} ; \quad \frac{1}{N} \sum_{k=1}^N |Error(k)|;$$

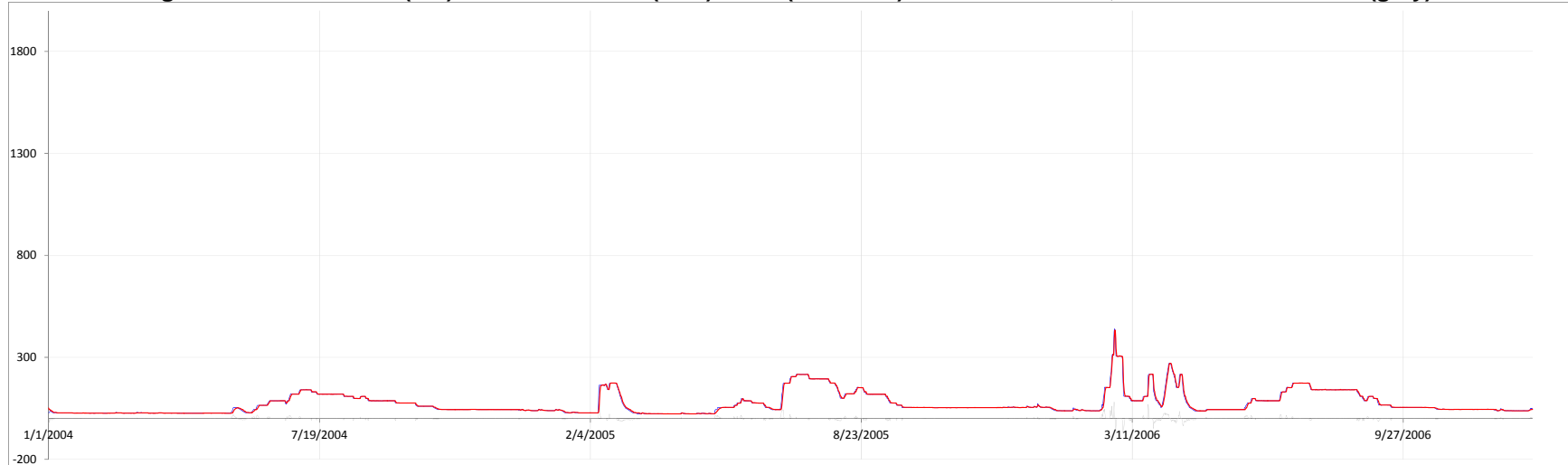
$$\% \text{ Abs. Avg. Error} = 2.626 \% ; \quad \frac{1}{N} \sum_{k=1}^N \left| \frac{Error(k)}{Obs.Flow(k)} 100 \right|;$$

$$\text{Mean Square Error} = 9.921 \text{ mcf/6-hrs} ; \quad \sqrt{\frac{1}{N} \sum_{k=1}^N Error(k)^2} ;$$

$$\% \text{ Mean Sq. Error} = 6.210 \% ; \quad \sqrt{\frac{1}{N} \sum_{k=1}^N \left(\frac{Error(k)}{Obs.Flow(k)} 100 \right)^2} .$$

D.1.2.2 Model Validation Period: 1/1/2002 – 12/31/2004

Figure D.1.2: Simulated (red) versus observed (blue) flows (mcf/6-hrs) at the reach outlet, and associated errors (grey).



$$\text{Average Error} = 0.018 \text{ mcf/6-hrs}; \quad \frac{1}{N} \sum_{k=1}^N \{Error(k)\}; \quad Error(k) = Obs.Flow(k) - Sim.Flow(k);$$

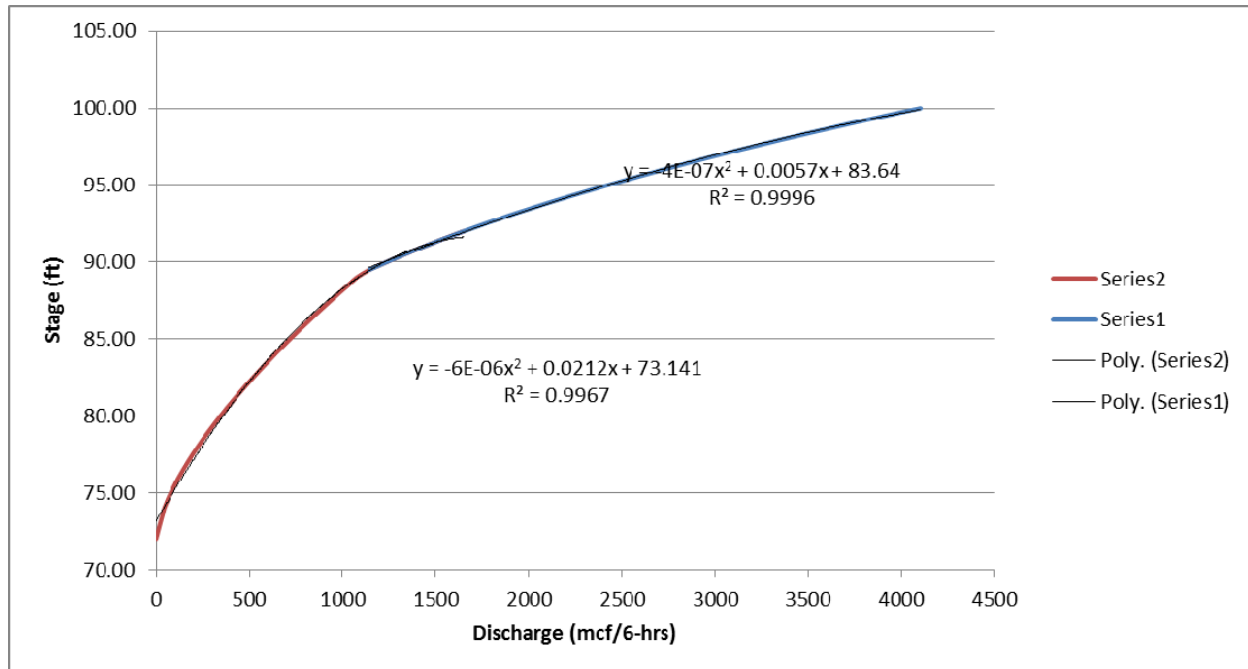
$$\text{Abs. Avg. Error} = 1.817 \text{ mcf/6-hrs}; \quad \frac{1}{N} \sum_{k=1}^N |Error(k)|;$$

$$\% \text{ Abs. Avg. Error} = 2.471 \%; \quad \frac{1}{N} \sum_{k=1}^N \left| \frac{Error(k)}{Obs.Flow(k)} 100 \right|;$$

$$\text{Mean Square Error} = 6.085 \text{ mcf/6-hrs}; \quad \sqrt{\frac{1}{N} \sum_{k=1}^N Error(k)^2};$$

$$\% \text{ Mean Sq. Error} = 6.089 \%; \quad \sqrt{\frac{1}{N} \sum_{k=1}^N \left(\frac{Error(k)}{Obs.Flow(k)} 100 \right)^2}.$$

D.1.3 Rating Curve:



(i) Discharge ≤ 1236.55

$$\text{Stage} = \text{Max} \{ 72, -6.03401E-06 * (\text{Discharge})^2 + 0.021152317 * (\text{Discharge}) + 73.1405108 \}$$

(ii) $1236.55 < \text{Discharge} \leq 6600$

$$\text{Stage} = -4.31175E-07 * (\text{Discharge})^2 + 0.005733343 * (\text{Discharge}) + 83.63980353$$

(iii) Discharge > 6600

$$\text{Stage} = 102.70$$

Units: stage (ft), discharge (mcf/6-hrs)

D.2 Reach 2: ORDC1 to FLVC1

D.2.1 Routing Model:

$$S_1(k+1) = S_1(k) + \text{Units} * [I_1(k) + w_1(k) - LS_1(k) - u_1(k)] .$$

The terms in the above equation are defined as follows:

k : Time index corresponding to 6-hour intervals.

$S_1(k)$: Reach storage in billion cubic feet at the beginning of time interval k .

Units: Unit factor to convert reach fluxes from million cubic feet to billion cubic feet,
Units = 1/1000.

$I_1(k)$: Upstream inflow in mcf/6-hrs.

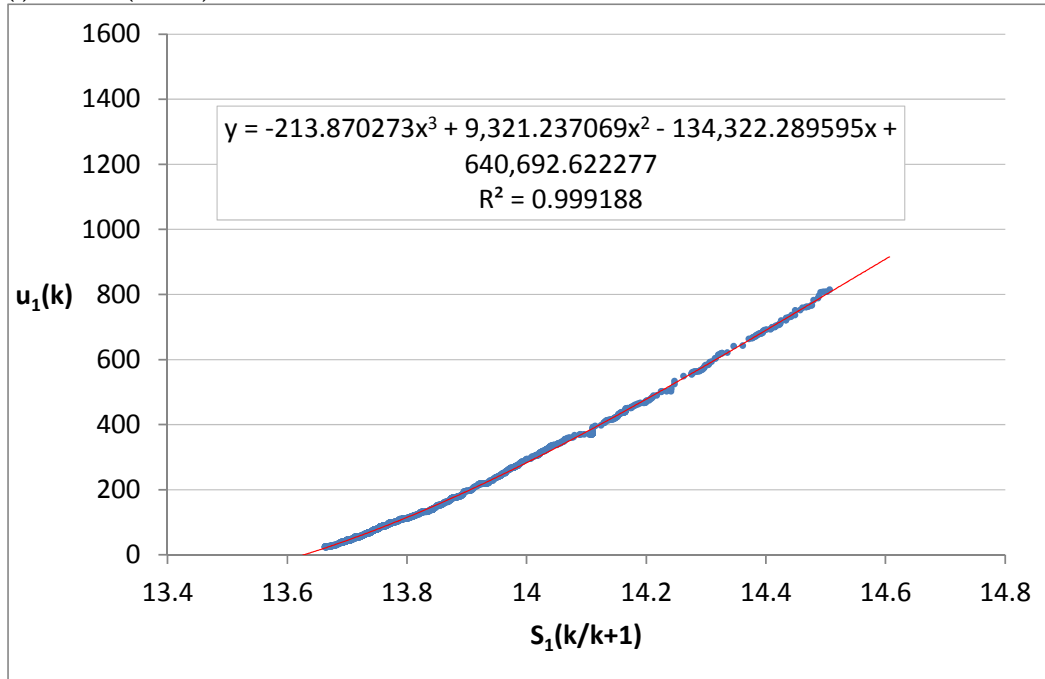
$w_1(k)$: Local reach inflow in mcf/6-hrs.

$LS_1(k)$: Reach losses in mcf/6-hrs. The losses in this reach are negligible.

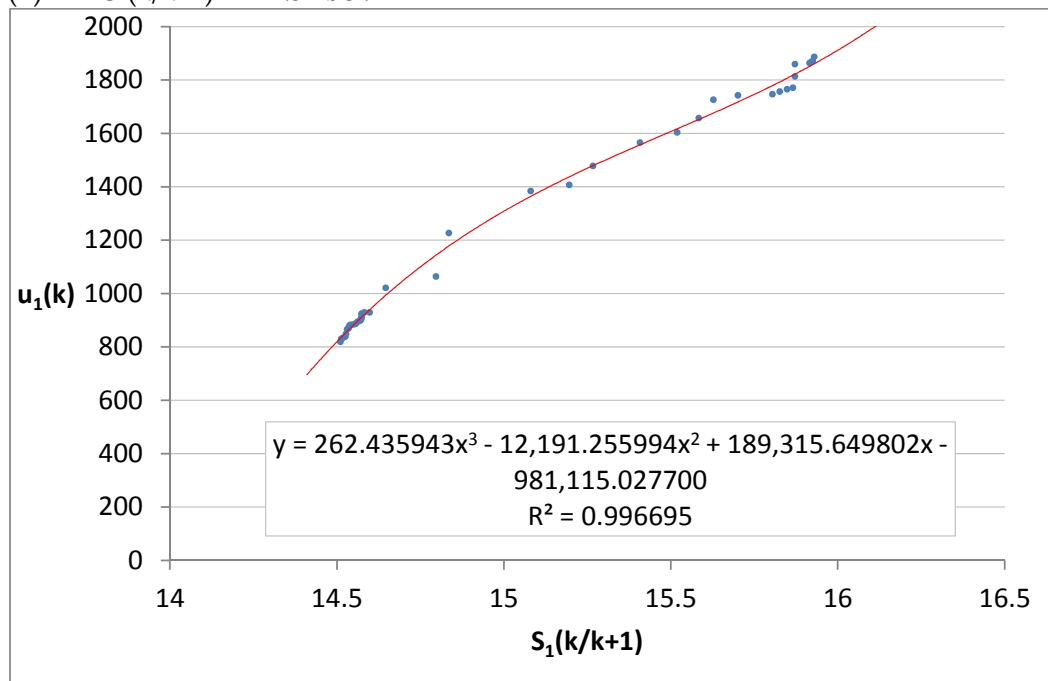
$u_1(k)$: Reach release to the downstream system as a function of the reach storage, $S_1(k/k+1)$,
where $S_1(k/k+1) = x_1 * S_1(k) + (1-x_1) * S_1(k+1)$, with $x_1=0.4$.

The $u_1(k)$ vs. $S_1(k/k+1)$ function is given by the following relationships:

(i) $S_1(k/k+1) \leq 14.51$ bcf:



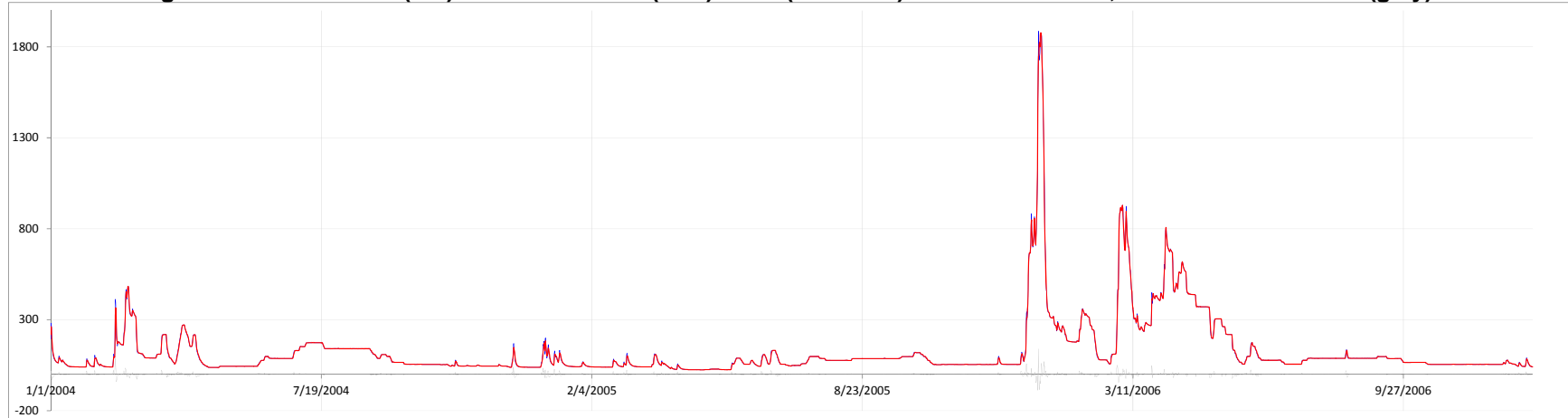
(ii) $S_1(k/k+1) > 14.51$ bcf:



D.2.2 Model Calibration and Validation Statistics:

D.2.2.1 Model Calibration Period: 1/1/2004 – 12/31/2006

Figure D.2.1: Simulated (red) versus observed (blue) flows (mcf/6-hrs) at the reach outlet, and associated errors (grey).



$$\text{Average Error} = -0.036 \text{ mcf/6-hrs}; \quad \frac{1}{N} \sum_{k=1}^N \{Error(k)\}; \quad Error(k) = Obs. Flow(k) - Sim. Flow(k);$$

$$\text{Abs. Avg. Error} = 1.977 \text{ mcf/6-hrs}; \quad \frac{1}{N} \sum_{k=1}^N |Error(k)|;$$

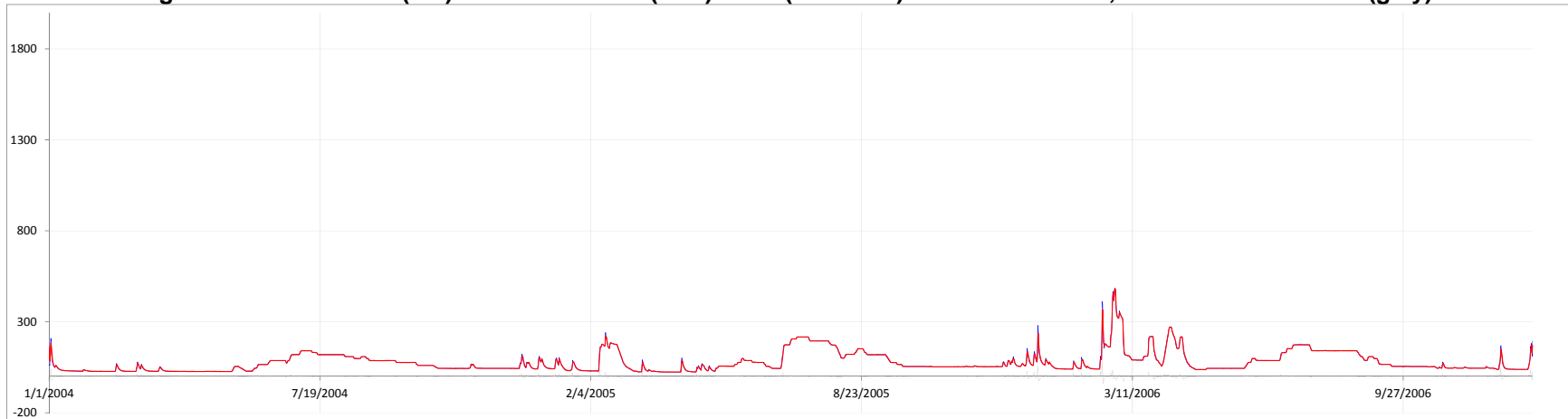
$$\% \text{ Abs. Avg. Error} = 1.630 \% ; \quad \frac{1}{N} \sum_{k=1}^N \left| \frac{Error(k)}{Obs. Flow(k)} 100 \right|;$$

$$\text{Mean Square Error} = 6.215 \text{ mcf/6-hrs}; \quad \sqrt{\frac{1}{N} \sum_{k=1}^N Error(k)^2};$$

$$\% \text{ Mean Sq. Error} = 3.553 \% ; \quad \sqrt{\frac{1}{N} \sum_{k=1}^N \left(\frac{Error(k)}{Obs. Flow(k)} 100 \right)^2}.$$

D.2.2.2 Model Validation Period: 1/1/2002 – 12/31/2004

Figure D.2.2: Simulated (red) versus observed (blue) flows (mcf/6-hrs) at the reach outlet, and associated errors (grey).



Average Error = 0.010 mcf/6-hrs ; $\frac{1}{N} \sum_{k=1}^N \{Error(k)\}; \quad Error(k) = Obs.Flow(k) - Sim.Flow(k);$

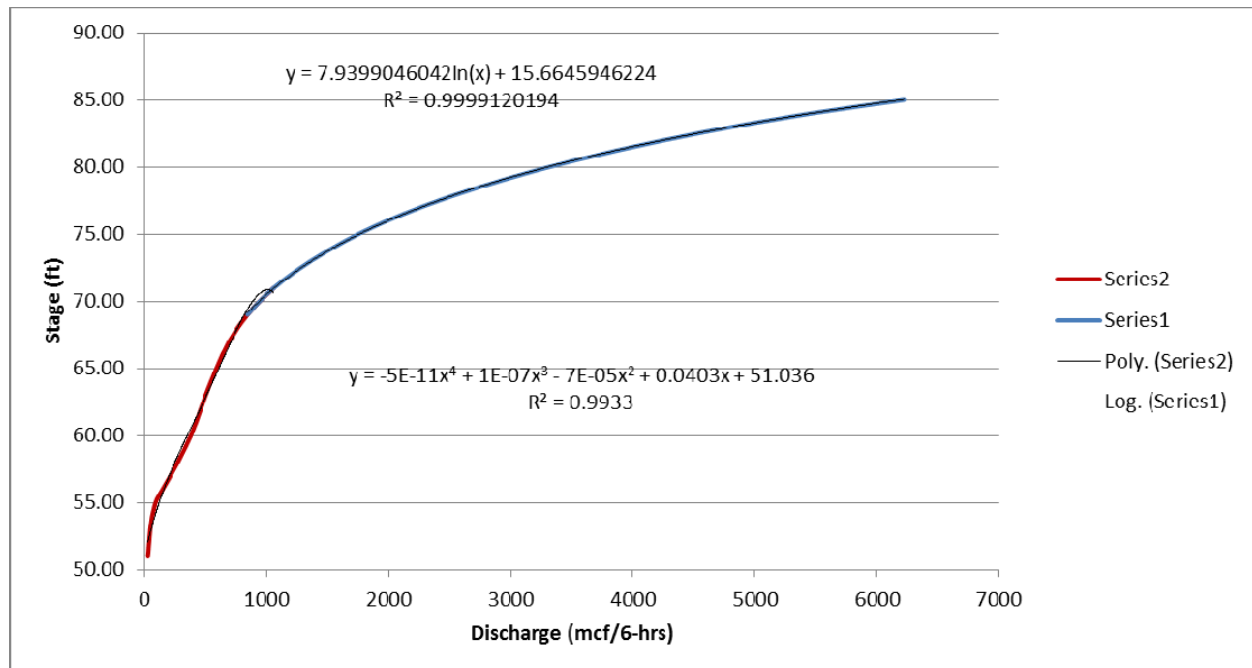
Abs. Avg. Error = 1.462 mcf/6-hrs ; $\frac{1}{N} \sum_{k=1}^N |Error(k)|;$

% Abs. Avg. Error = 1.876 % ; $\frac{1}{N} \sum_{k=1}^N \left| \frac{Error(k)}{Obs.Flow(k)} 100 \right|;$

Mean Square Error = 4.593 mcf/6-hrs ; $\sqrt{\frac{1}{N} \sum_{k=1}^N Error(k)^2} ;$

% Mean Sq. Error = 4.778 % ; $\sqrt{\frac{1}{N} \sum_{k=1}^N \left(\frac{Error(k)}{Obs.Flow(k)} 100 \right)^2} .$

D.2.3 Rating Curve:



(i) Discharge ≤ 803.68

$$\text{Stage} = \text{Max} \{ 51, -4.79217E-11 * (\text{Discharge})^4 + 9.75114E-08 * (\text{Discharge})^3 - 7.00671E-05 * (\text{Discharge})^2 + 0.040278807 * (\text{Discharge}) + 51.03573947 \}$$

(ii) Discharge > 803.68

$$\text{Stage} = 7.939904604 * \ln(\text{Discharge}) + 15.66459462$$

Units: stage (ft), discharge (mcf/6-hrs)

D.3 Reach 3: ORDC1 to YUBC1

D.3.1 Routing Model:

$$S_i(k+1) = S_i(k) + \text{Units} * [I_i(k) + w_i(k) - LS_i(k) - u_i(k)] .$$

The terms in the above equation are defined as follows:

k: Time index corresponding to 6-hour intervals.

$S_i(k)$: Reach storage in billion cubic feet at the beginning of time interval k.

Units: Unit factor to convert reach fluxes from million cubic feet to billion cubic feet,
Units = 1/1000.

$I_i(k)$: Upstream inflow in mcf/6-hrs.

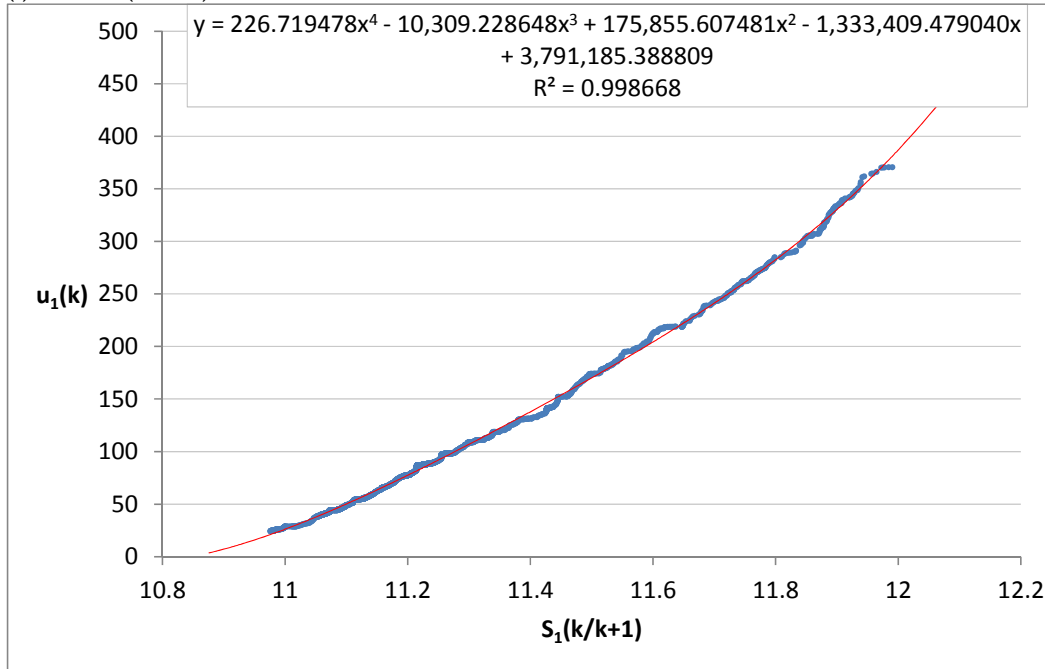
$w_i(k)$: Local reach inflow in mcf/6-hrs.

$LS_i(k)$: Reach losses in mcf/6-hrs. The losses in this reach are negligible.

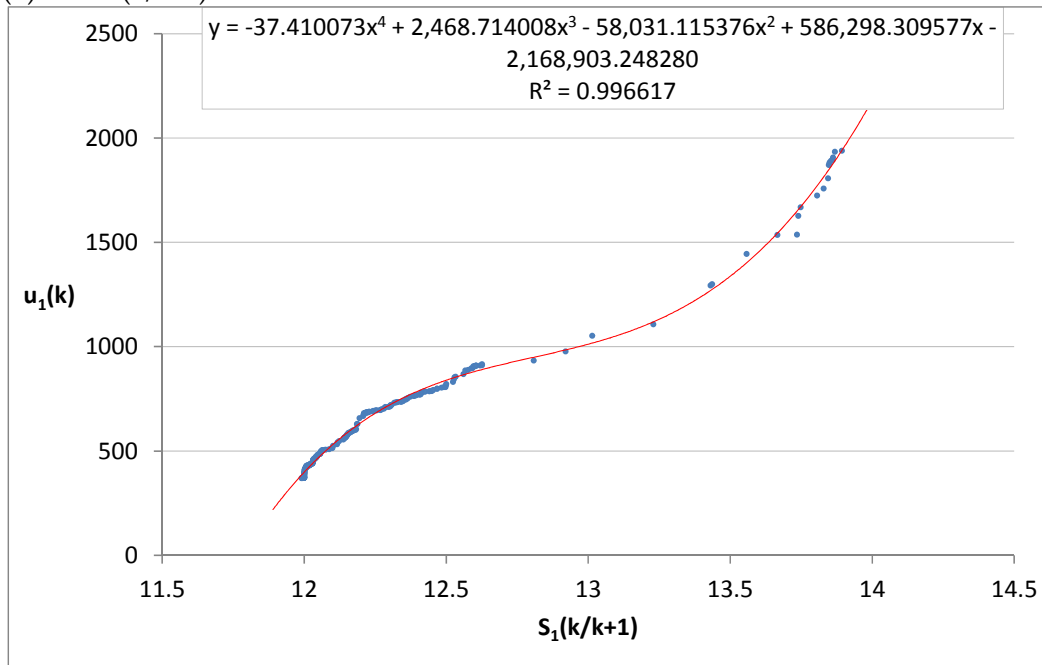
$u_i(k)$: Reach release to the downstream system as a function of the reach storage, $S_i(k/k+1)$, where $S_i(k/k+1) = x_1 * S_i(k) + (1-x_1) * S_i(k+1)$, with $x_1=0.4$.

The $u_i(k)$ vs. $S_i(k/k+1)$ function is given by the following relationships:

(i) $S_i(k/k+1) \leq 11.99$ bcf:



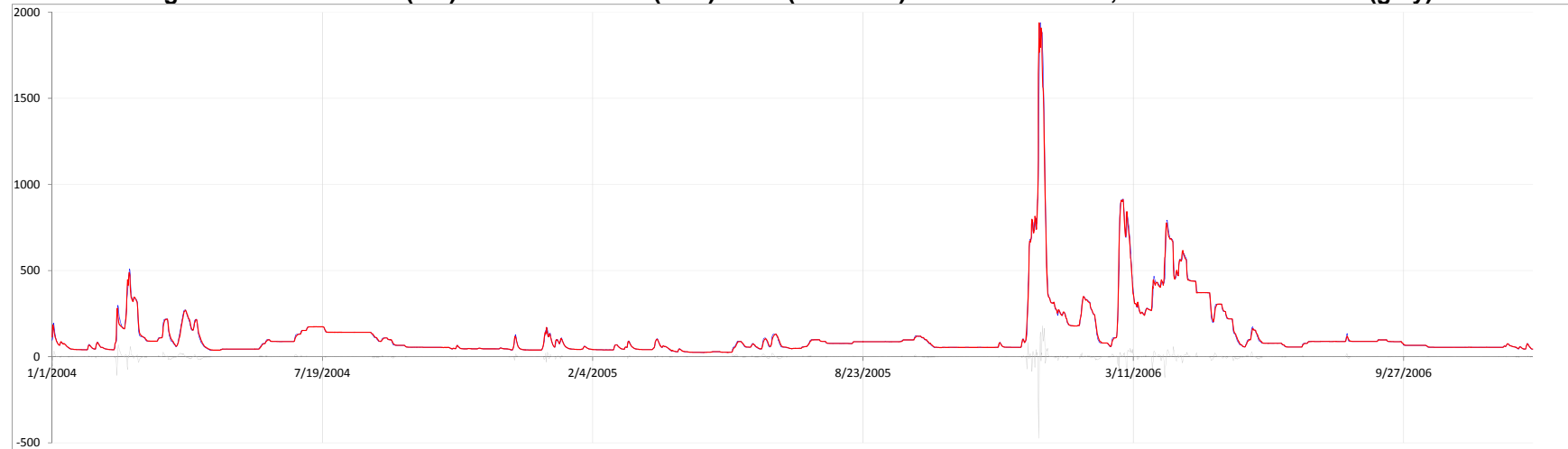
(ii) $S_1(k/k+1) > 11.99$ bcf:



D.3.2 Model Calibration and Validation Statistics:

D.3.2.1 Model Calibration Period: 1/1/2004 – 12/31/2006

Figure D.3.1: Simulated (red) versus observed (blue) flows (mcf/6-hrs) at the reach outlet, and associated errors (grey).



$$\text{Average Error} = 0.014 \text{ mcf/6-hrs} ; \quad \frac{1}{N} \sum_{k=1}^N \{Error(k)\}; \quad Error(k) = Obs.Flow(k) - Sim.Flow(k);$$

$$\text{Abs. Avg. Error} = 3.605 \text{ mcf/6-hrs} ; \quad \frac{1}{N} \sum_{k=1}^N |Error(k)|;$$

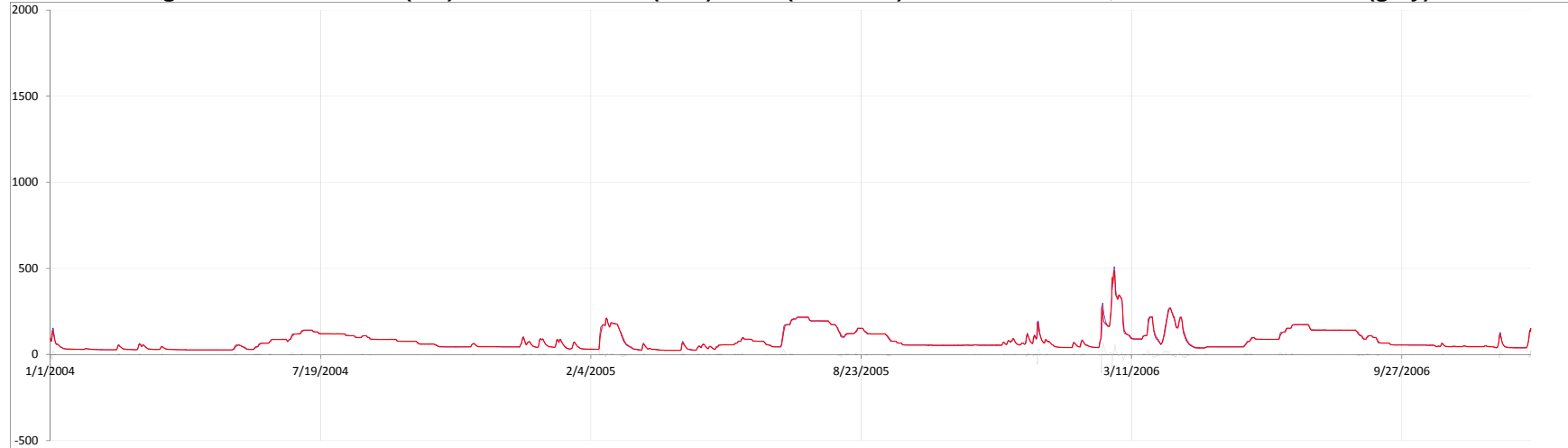
$$\% \text{ Abs. Avg. Error} = 2.159 \% ; \quad \frac{1}{N} \sum_{k=1}^N \left| \frac{Error(k)}{Obs.Flow(k)} 100 \right|;$$

$$\text{Mean Square Error} = 15.209 \text{ mcf/6-hrs} ; \quad \sqrt{\frac{1}{N} \sum_{k=1}^N Error(k)^2} ;$$

$$\% \text{ Mean Sq. Error} = 4.732 \% ; \quad \sqrt{\frac{1}{N} \sum_{k=1}^N \left(\frac{Error(k)}{Obs.Flow(k)} 100 \right)^2} .$$

D.3.2.2 Model Validation Period: 1/1/2002 – 12/31/2004

Figure D.3.2: Simulated (red) versus observed (blue) flows (mcf/6-hrs) at the reach outlet, and associated errors (grey).



$$\text{Average Error} = 0.019 \text{ mcf/6-hrs} ; \quad \frac{1}{N} \sum_{k=1}^N \{Error(k)\}; \quad Error(k) = Obs.Flow(k) - Sim.Flow(k);$$

$$\text{Abs. Avg. Error} = 1.746 \text{ mcf/6-hrs} ; \quad \frac{1}{N} \sum_{k=1}^N |Error(k)|;$$

$$\% \text{ Abs. Avg. Error} = 2.043 \% ; \quad \frac{1}{N} \sum_{k=1}^N \left| \frac{Error(k)}{Obs.Flow(k)} 100 \right|;$$

$$\text{Mean Square Error} = 5.456 \text{ mcf/6-hrs} ; \quad \sqrt{\frac{1}{N} \sum_{k=1}^N Error(k)^2} ;$$

$$\% \text{ Mean Sq. Error} = 4.416 \% ; \quad \sqrt{\frac{1}{N} \sum_{k=1}^N \left(\frac{Error(k)}{Obs.Flow(k)} 100 \right)^2} .$$

D.3.3 Rating Curve:

The rating curve for this location is influenced by backwater effects and is discussed in Section D.5.2.

D.4 Reach 4: MRYC1 to YUBC1-Downstream

D.4.1 Routing Model:

$$S_1(k+1) = S_1(k) + \text{Units} * [I_1(k) + w_1(k) - LS_1(k) - u_1(k)] .$$

The terms in the above equation are defined as follows:

k: Time index corresponding to 6-hour intervals.

$S_1(k)$: Reach storage in billion cubic feet at the beginning of time interval k.

Units: Unit factor to convert reach fluxes from million cubic feet to billion cubic feet,
Units = 1/1000.

$I_1(k)$: Upstream inflow in mcf/6-hrs.

$w_1(k)$: Local reach inflow in mcf/6-hrs.

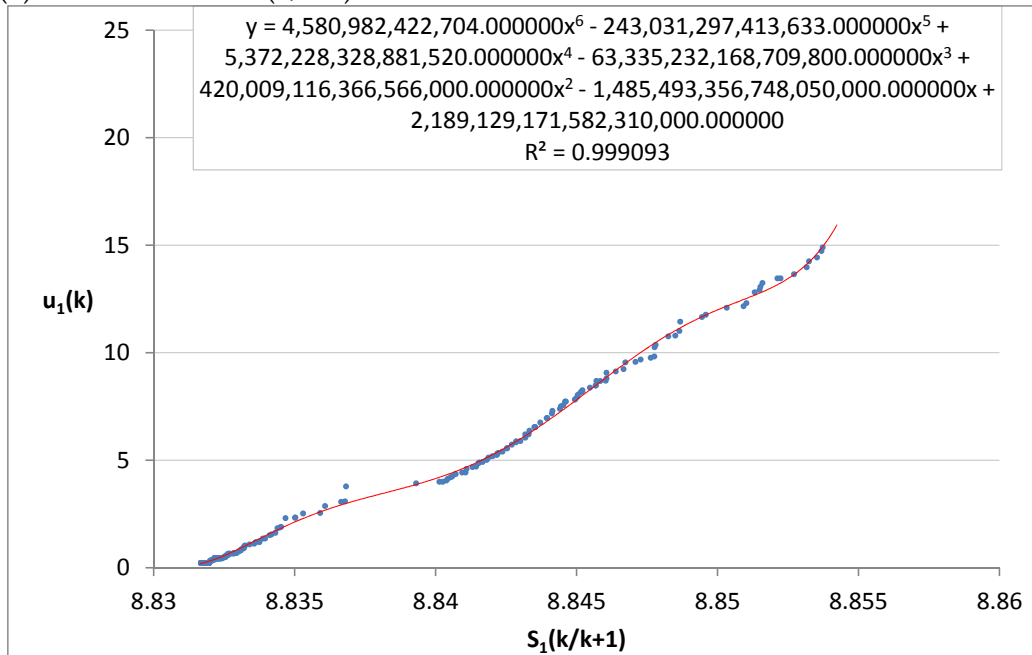
$LS_1(k)$: Reach losses in mcf/6-hrs. The losses in this reach are negligible.

$u_1(k)$: Reach release to the downstream system as a function of the reach storage, $S_1(k/k+1)$,
where $S_1(k/k+1) = x_1 * S_1(k) + (1-x_1) * S_1(k+1)$, with $x_1=0.4$.

The $u_1(k)$ vs. $S_1(k/k+1)$ function is given by the following relationships:

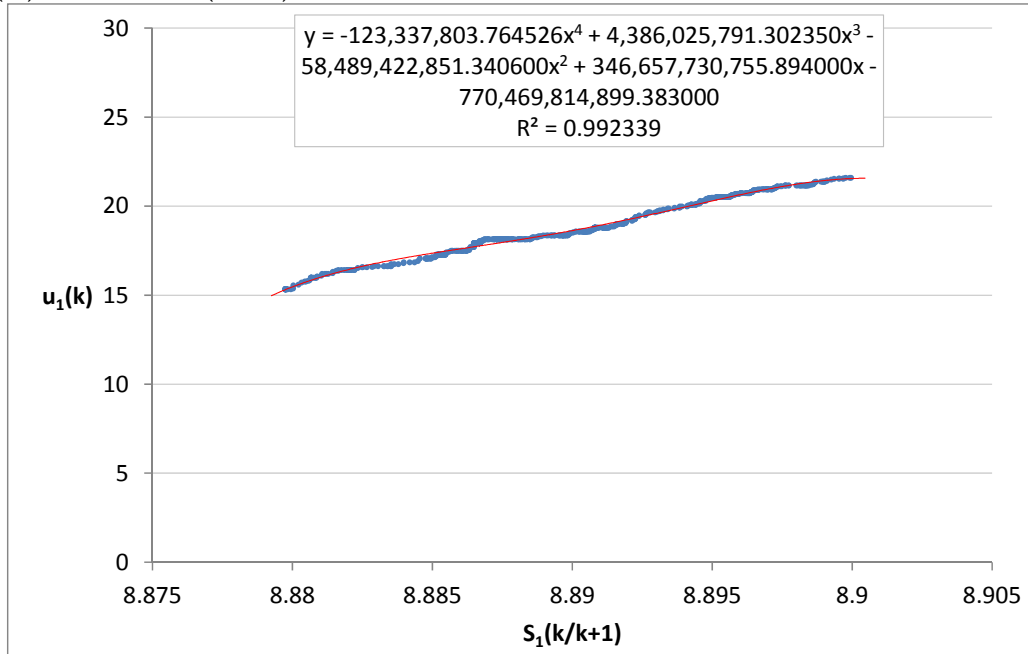
(i) $S_1(k/k+1) < 8.832$ bcf: $u_1(k) = 0$;

(ii) $8.832 \text{ bcf} \leq S_1(k/k+1) \leq 8.853 \text{ bcf}$:

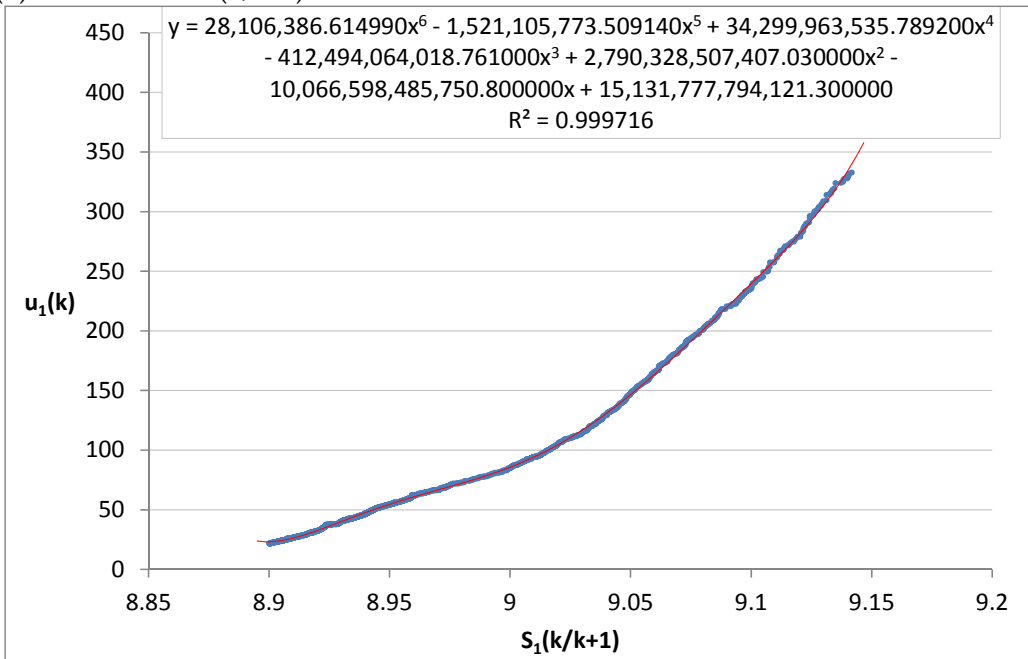


(iii) $8.853 \text{ bcf} \leq S_1(k/k+1) \leq 8.880 \text{ bcf}$: $u_1(k) = 15.3 \text{ mcf/6-hrs}$;

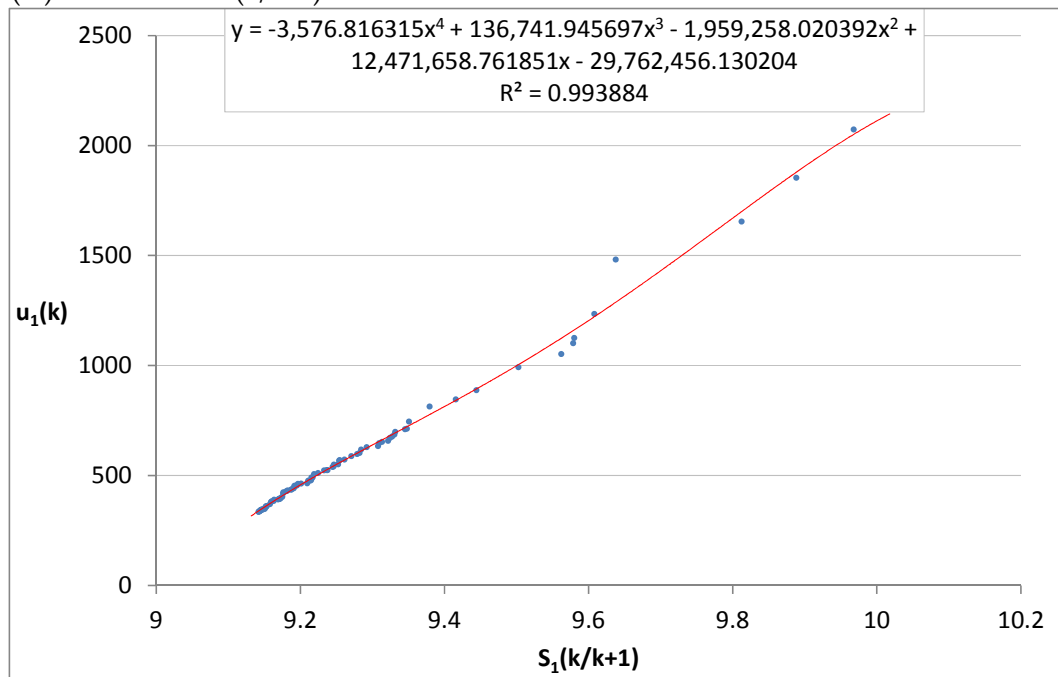
(iv) $8.880 < S_1(k/k+1) \leq 8.900 \text{ bcf}$:



(v) $8.900 < S_1(k/k+1) \leq 9.142 \text{ bcf}$:



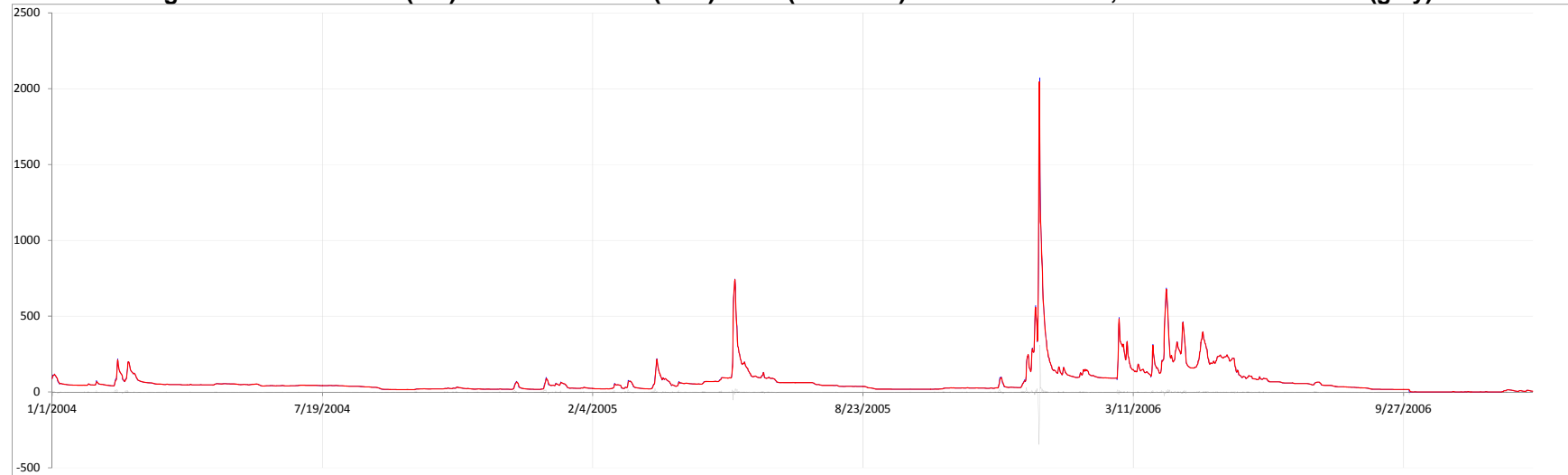
(vi) $9.142 < S_1(k/k+1)$ bcf:



D.4.2 Model Calibration and Validation Statistics:

D.4.2.1 Model Calibration Period: 1/1/2004 – 12/31/2006

Figure D.4.1: Simulated (red) versus observed (blue) flows (mcf/6-hrs) at the reach outlet, and associated errors (grey).



$$\text{Average Error} = -0.004 \text{ mcf/6-hrs} ; \quad \frac{1}{N} \sum_{k=1}^N \{ \text{Error}(k) \}; \quad \text{Error}(k) = \text{Obs. Flow}(k) - \text{Sim. Flow}(k);$$

$$\text{Abs. Avg. Error} = 1.227 \text{ mcf/6-hrs} ; \quad \frac{1}{N} \sum_{k=1}^N | \text{Error}(k) |;$$

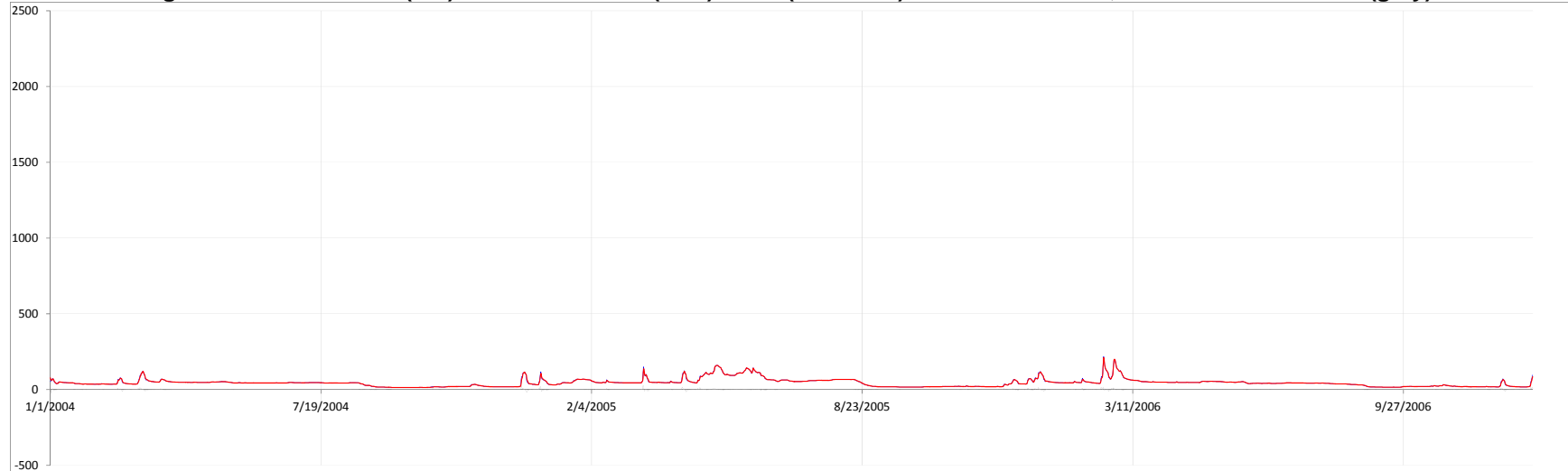
$$\% \text{ Abs. Avg. Error} = 4.185 \% ; \quad \frac{1}{N} \sum_{k=1}^N \left| \frac{\text{Error}(k)}{\text{Obs. Flow}(k)} 100 \right|;$$

$$\text{Mean Square Error} = 9.861 \text{ mcf/6-hrs} ; \quad \sqrt{\frac{1}{N} \sum_{k=1}^N \text{Error}(k)^2} ;$$

$$\% \text{ Mean Sq. Error} = 56.200 \% ; \quad \sqrt{\frac{1}{N} \sum_{k=1}^N \left(\frac{\text{Error}(k)}{\text{Obs. Flow}(k)} 100 \right)^2} .$$

D.4.2.2 Model Validation Period: 1/1/2002 – 12/31/2004

Figure D.4.2: Simulated (red) versus observed (blue) flows (mcf/6-hrs) at the reach outlet, and associated errors (grey).



$$\text{Average Error} = 0.017 \text{ mcf/6-hrs}; \quad \frac{1}{N} \sum_{k=1}^N \{Error(k)\}; \quad Error(k) = Obs.Flow(k) - Sim.Flow(k);$$

$$\text{Abs. Avg. Error} = 0.662 \text{ mcf/6-hrs}; \quad \frac{1}{N} \sum_{k=1}^N |Error(k)|;$$

$$\% \text{ Abs. Avg. Error} = 1.511 \%; \quad \frac{1}{N} \sum_{k=1}^N \left| \frac{Error(k)}{Obs.Flow(k)} 100 \right|;$$

$$\text{Mean Square Error} = 2.022 \text{ mcf/6-hrs}; \quad \sqrt{\frac{1}{N} \sum_{k=1}^N Error(k)^2};$$

$$\% \text{ Mean Sq. Error} = 3.464 \%; \quad \sqrt{\frac{1}{N} \sum_{k=1}^N \left(\frac{Error(k)}{Obs.Flow(k)} 100 \right)^2}.$$

D.4.3 Rating Curve:

The rating curve for this location is influenced by backwater effects and is discussed in Section D.5.2.

D.5 Reach 5: Computed final stage and flow rate at YUBC1 through a combination of Reaches 3 and 4

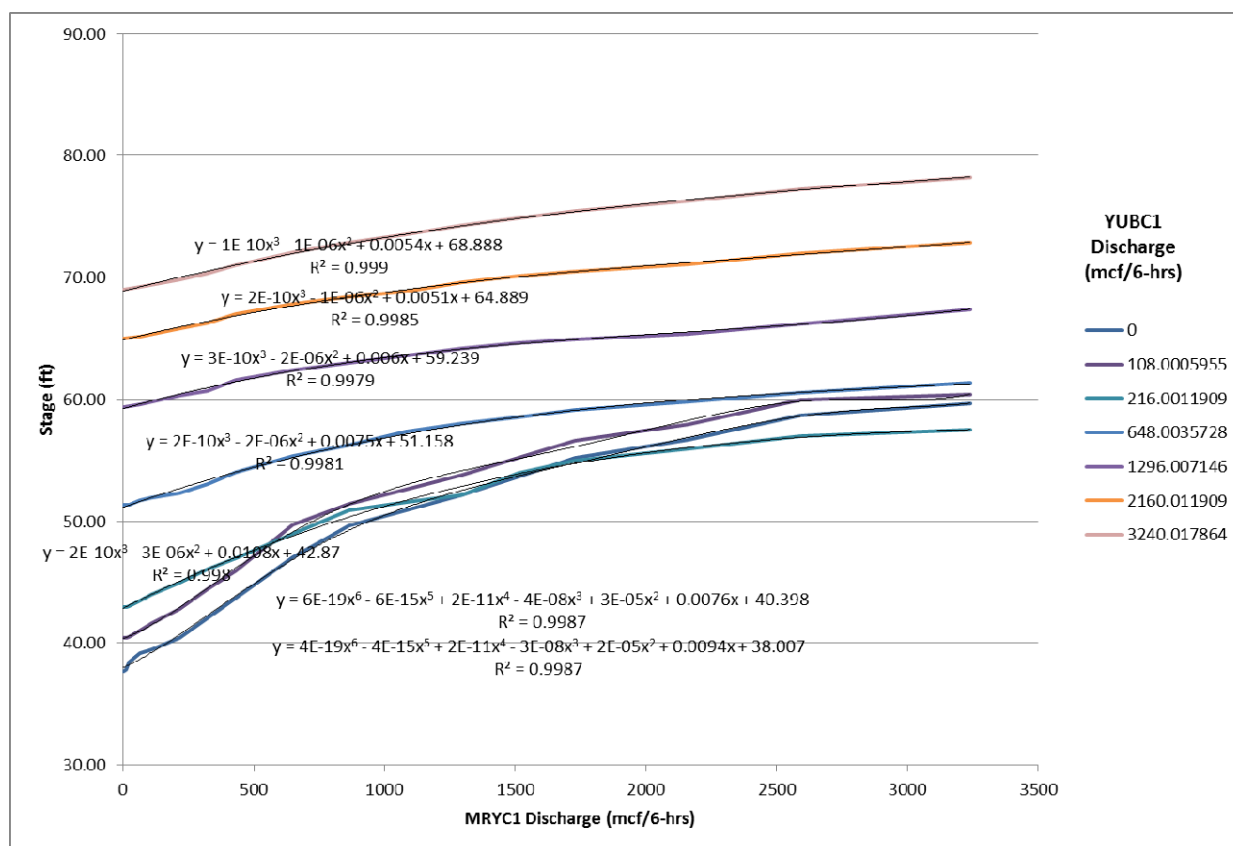
D.5.1 Routing Model:

The following steps are implemented to compute the final YUBC1 stage and flow rates:

- Use reach 3 model to compute flow rate at YUBC1.
- Use reach 4 model to compute flow rate downstream of YUBC1 due to MRYC1.
- Use multi-dimensional rating curve (section 5.2,1) to compute final stage as a function of reach 3 and reach 4 flow rates.
- Use one dimensional rating curve (section 5.2,2) to compute the final flow rate as a function of the final stage.

D.5.2 Rating Curves:

D.5.2.1 Multi-Dimensional Rating Curve using Reach 3 (YUBC1) and Reach 4 (MRYC1) Flow Rates



(i) Reach 3 discharge = 0

a. Reach 4 discharge ≤ 3240.018

$$\text{Stage} = \text{Max} \{ 37.67, 3.8345\text{E-}19 * (\text{Reach 4 discharge})^6 - 4.04308\text{E-}15 * (\text{Reach 4 discharge})^5 + 1.60067\text{E-}11 * (\text{Reach 4 discharge})^4 - 2.87168\text{E-}08 * (\text{Reach 4 discharge})^3 + 1.94195\text{E-}05 * (\text{Reach 4 discharge})^2 + 0.009439746 * (\text{Reach 4 discharge}) + 38.00686222 \}$$

b. Reach 4 discharge > 3240.018

$$\text{Stage} = 59.67$$

(ii) Reach 3 discharge = 108.00

a. Reach 4 discharge ≤ 3240.018

$$\text{Stage} = \text{Max} \{ 40.43, 6.34104\text{E-}19 * (\text{Reach 4 discharge})^6 - 6.38074\text{E-}15 * (\text{Reach 4 discharge})^5 + 2.40042\text{E-}11 * (\text{Reach 4 discharge})^4 - 4.08307\text{E-}08 * (\text{Reach 4 discharge})^3 + 2.70097\text{E-}05 * (\text{Reach 4 discharge})^2 + 0.007612476 * (\text{Reach 4 discharge}) + 40.3976498 \}$$

b. Reach 4 discharge > 3240.018

$$\text{Stage} = 60.43$$

(iii) Reach 3 discharge = 216.00

a. Reach 4 discharge ≤ 3240.018

$$\text{Stage} = \text{Max} \{ 42.98, 2.1678\text{E-}10 * (\text{Reach 4 discharge})^3 - 2.63034\text{E-}06 * (\text{Reach 4 discharge})^2 + 0.010766397 * (\text{Reach 4 discharge}) + 42.86952196 \}$$

b. Reach 4 discharge > 3240.018

$$\text{Stage} = 57.48$$

(iv) Reach 3 discharge = 648.00

a. Reach 4 discharge ≤ 3240.018

$$\text{Stage} = \text{Max} \{ 51.33, 2.20428\text{E-}10 * (\text{Reach 4 discharge})^3 - 2.06974\text{E-}06 * (\text{Reach 4 discharge})^2 + 0.007518479 * (\text{Reach 4 discharge}) + 51.15772779 \}$$

b. Reach 4 discharge > 3240.018

$$\text{Stage} = 61.33$$

(v) Reach 3 discharge = 1296.01

a. Reach 4 discharge \leq 3240.018

$$\text{Stage} = \text{Max} \{ 59.40, 3.2511\text{E-}10 * (\text{Reach 4 discharge})^3 - 2.11922\text{E-}06 * (\text{Reach 4 discharge})^2 + 0.005972852 * (\text{Reach 4 discharge}) + 59.23891818 \}$$

b. Reach 4 discharge $>$ 3240.018

$$\text{Stage} = 67.40$$

(vi) Reach 3 discharge = 2160.01

a. Reach 4 discharge \leq 3240.018

$$\text{Stage} = \text{Max} \{ 64.99, 1.82443\text{E-}10 * (\text{Reach 4 discharge})^3 - 1.40714\text{E-}06 * (\text{Reach 4 discharge})^2 + 0.005119074 * (\text{Reach 4 discharge}) + 64.88871154 \}$$

b. Reach 4 discharge $>$ 3240.018

$$\text{Stage} = 72.89$$

(vii) Reach 3 discharge = 3240.02

a. Reach 4 discharge \leq 3240.018

$$\text{Stage} = \text{Max} \{ 69.05, 1.14105\text{E-}10 * (\text{Reach 4 discharge})^3 - 1.15105\text{E-}06 * (\text{Reach 4 discharge})^2 + 0.005419774 * (\text{Reach 4 discharge}) + 68.88795446 \}$$

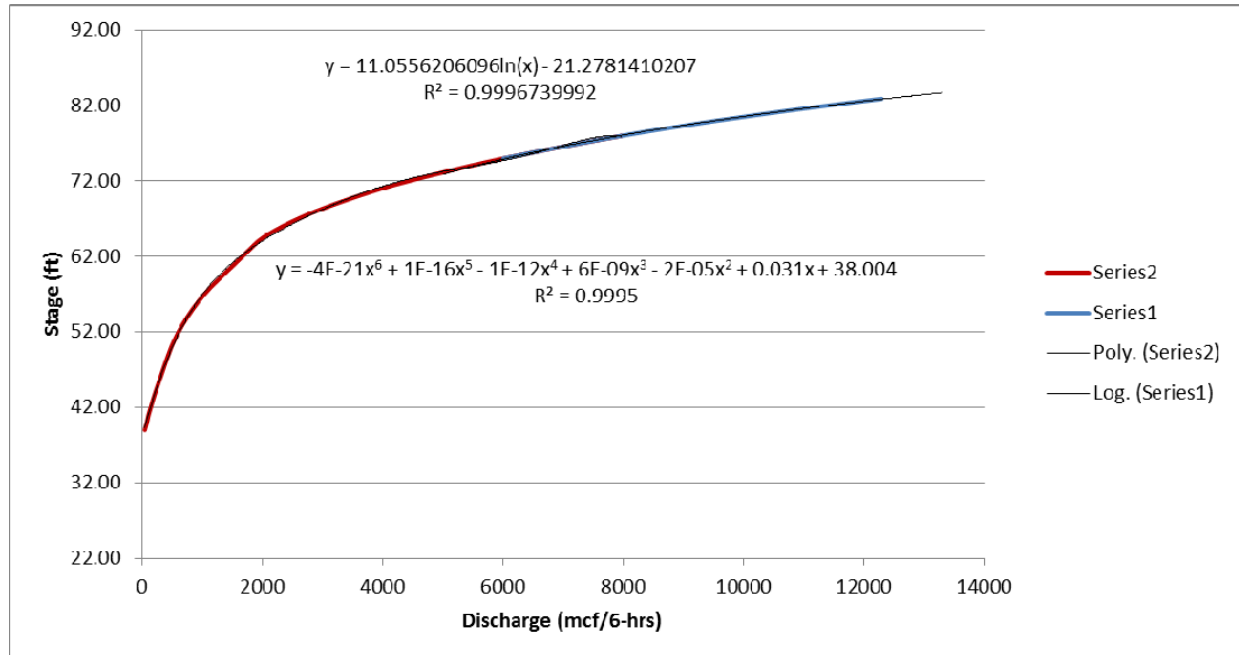
b. Reach 4 discharge $>$ 3240.018

$$\text{Stage} = 78.25$$

Units: stage (ft), discharge (mcf/6-hrs)

D.5.2.2 One-Dimensional Rating Curve to compute Final YUBC1 Flow Rates

D.5.2.2.1 Stage as a function of Discharge



(i) Discharge ≤ 5521.07

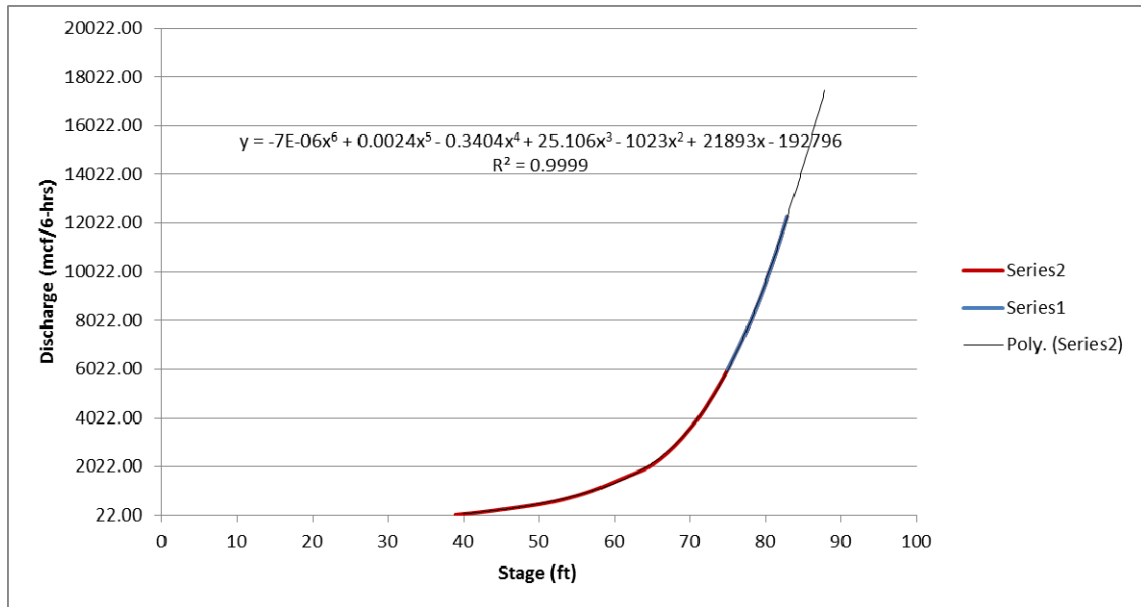
$$\text{Stage} = \text{Max} \{ 39, -3.74117\text{E-}21 * (\text{Discharge})^6 + 9.91836\text{E-}17 * (\text{Discharge})^5 - 1.0406\text{E-}12 * (\text{Discharge})^4 + 5.57458\text{E-}09 * (\text{Discharge})^3 - 1.67101\text{E-}05 * (\text{Discharge})^2 + 0.031009159 * (\text{Discharge}) + 38.00355108 \}$$

(ii) Discharge > 5521.07

$$\text{Stage} = 11.05562061 * \ln(\text{Discharge}) - 21.27814102$$

Units: stage (ft), discharge (mcf/6-hrs)

D.5.2.2.2 Discharge as a function of Stage



- (i) Stage ≤ 39.00
Discharge = 43.20
- (ii) $39.00 < \text{Stage} \leq 97.00$
Discharge = $-6.91262\text{E-}06 * (\text{Stage})^6 + 0.002410016 * (\text{Stage})^5 - 0.340363753 * (\text{Stage})^4 + 25.10618197 * (\text{Stage})^3 - 1022.998468 * (\text{Stage})^2 + 21893.39454 * (\text{Stage}) - 192795.7802$
- (iii) Stage > 97.00
Discharge = 24653.00

Units: stage (ft), discharge (mcf/6-hrs)

D.6 Reach 6: ORDC1 to FBLC1

D.6.1 Routing Model:

$$S_1(k+1) = S_1(k) + \text{Units} * [I_1(k) + w_1(k) - LS_1(k) - u_1(k)] .$$

The terms in the above equation are defined as follows:

k: Time index corresponding to 6-hour intervals.

$S_1(k)$: Reach storage in billion cubic feet at the beginning of time interval k.

Units: Unit factor to convert reach fluxes from million cubic feet to billion cubic feet,
Units = 1/1000.

$I_1(k)$: Upstream inflow in mcf/6-hrs.

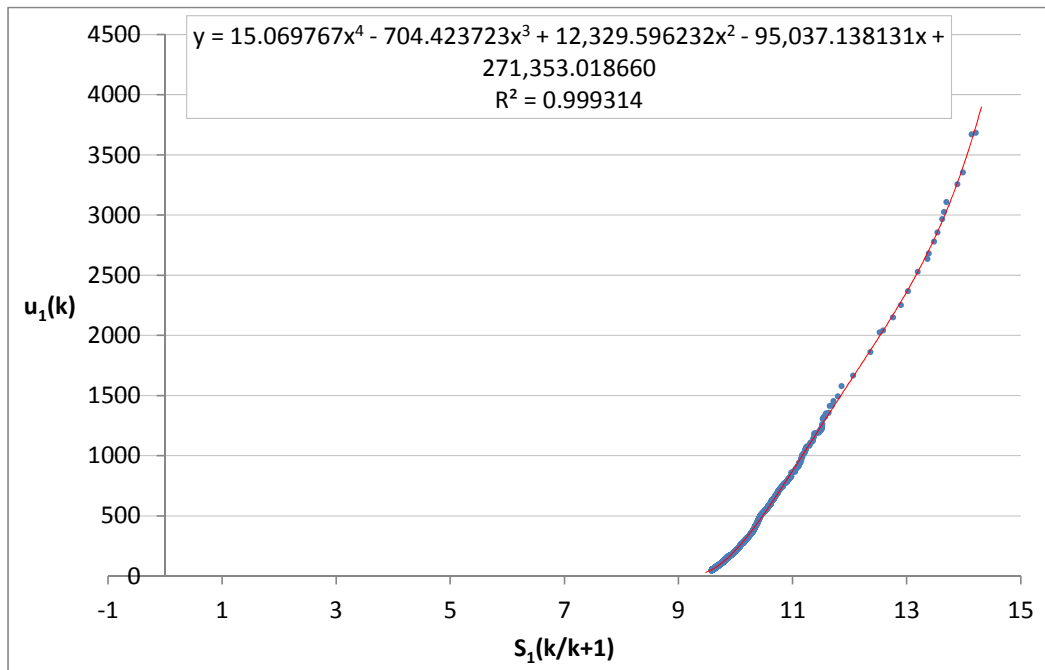
$w_1(k)$: Local reach inflow in mcf/6-hrs.

$LS_1(k)$: Reach losses in mcf/6-hrs. The losses in this reach are negligible.

$u_1(k)$: Reach release to the downstream system as a function of the reach storage, $S_1(k/k+1)$,
where $S_1(k/k+1) = x_1 * S_1(k) + (1-x_1) * S_1(k+1)$, with $x_1=0.4$.

The $u_1(k)$ vs. $S_1(k/k+1)$ function is given by the following relationship:

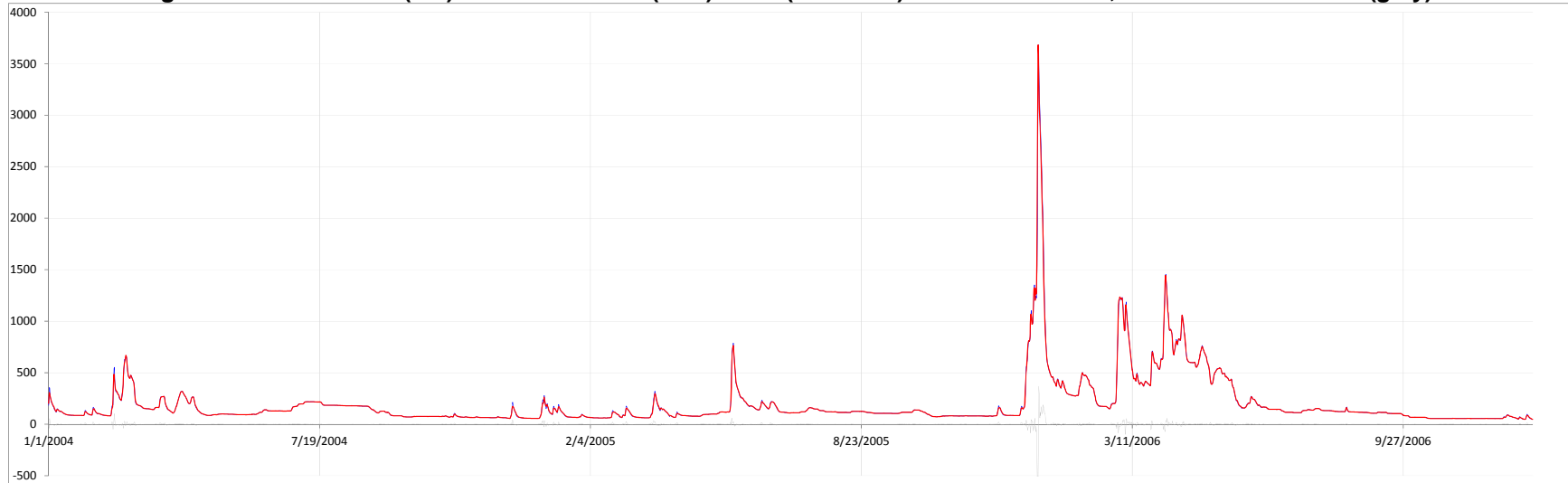
(i)



D.6.2 Model Calibration and Validation Statistics:

D.6.2.1 Model Calibration Period: 1/1/2004 – 12/31/2006

Figure D.6.1: Simulated (red) versus observed (blue) flows (mcf/6-hrs) at the reach outlet, and associated errors (grey).



$$\text{Average Error} = -0.004 \text{ mcf/6-hrs} ; \quad \frac{1}{N} \sum_{k=1}^N \{ \text{Error}(k) \}; \quad \text{Error}(k) = \text{Obs. Flow}(k) - \text{Sim. Flow}(k);$$

$$\text{Abs. Avg. Error} = 3.873 \text{ mcf/6-hrs} ; \quad \frac{1}{N} \sum_{k=1}^N | \text{Error}(k) |;$$

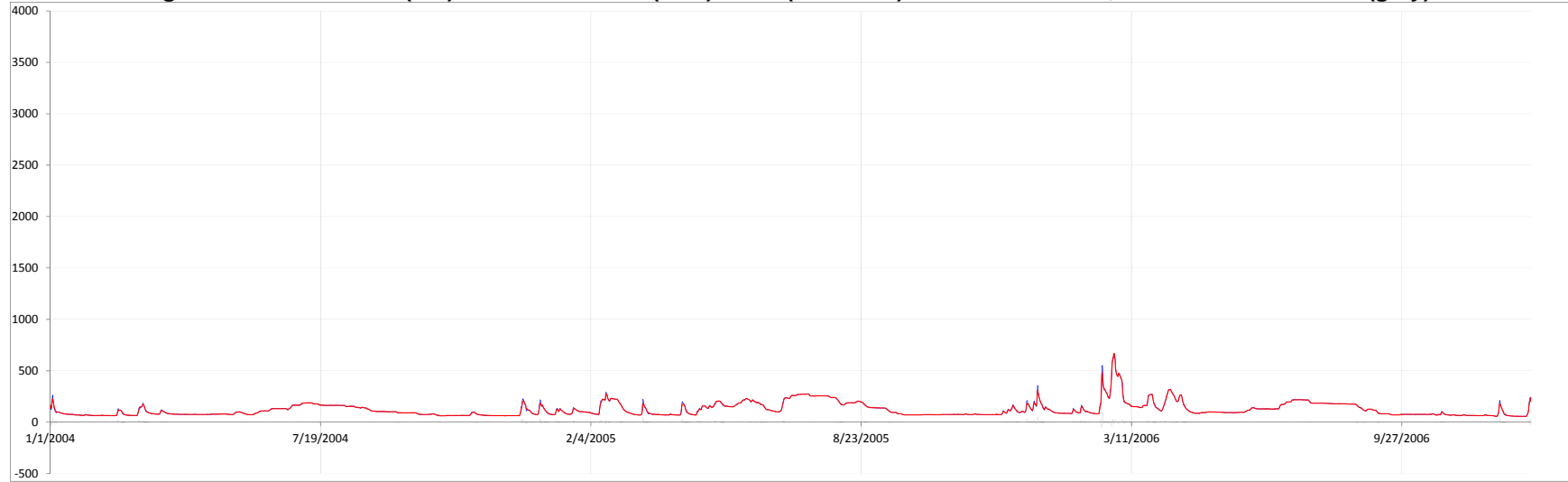
$$\% \text{ Abs. Avg. Error} = 1.316 \% ; \quad \frac{1}{N} \sum_{k=1}^N \left| \frac{\text{Error}(k)}{\text{Obs. Flow}(k)} 100 \right|;$$

$$\text{Mean Square Error} = 23.186 \text{ mcf/6-hrs} ; \quad \sqrt{\frac{1}{N} \sum_{k=1}^N \text{Error}(k)^2} ;$$

$$\% \text{ Mean Sq. Error} = 2.637 \% ; \quad \sqrt{\frac{1}{N} \sum_{k=1}^N \left(\frac{\text{Error}(k)}{\text{Obs. Flow}(k)} 100 \right)^2} .$$

D.6.2.2 Model Validation Period: 1/1/2002 – 12/31/2004

Figure D.6.2: Simulated (red) versus observed (blue) flows (mcf/6-hrs) at the reach outlet, and associated errors (grey).



$$\text{Average Error} = 0.021 \text{ mcf/6-hrs}; \quad \frac{1}{N} \sum_{k=1}^N \{Error(k)\}; \quad Error(k) = Obs.Flow(k) - Sim.Flow(k);$$

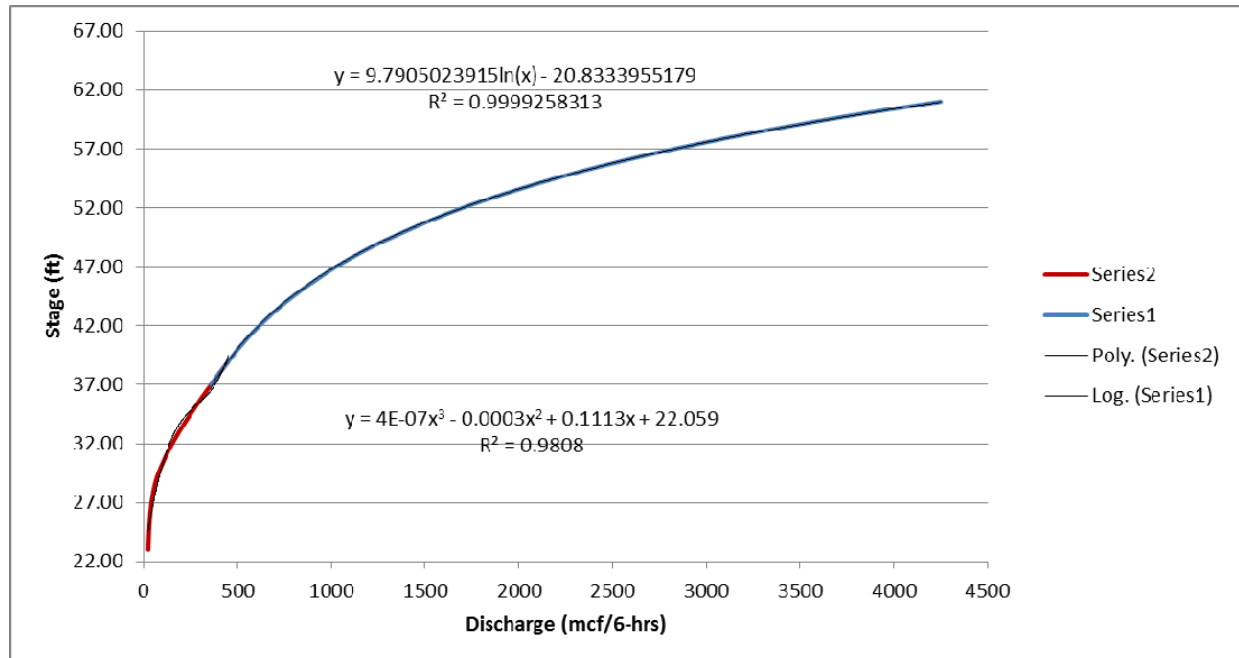
$$\text{Abs. Avg. Error} = 1.676 \text{ mcf/6-hrs}; \quad \frac{1}{N} \sum_{k=1}^N |Error(k)|;$$

$$\% \text{ Abs. Avg. Error} = 1.253 \%; \quad \frac{1}{N} \sum_{k=1}^N \left| \frac{Error(k)}{Obs.Flow(k)} 100 \right|;$$

$$\text{Mean Square Error} = 4.684 \text{ mcf/6-hrs}; \quad \sqrt{\frac{1}{N} \sum_{k=1}^N Error(k)^2};$$

$$\% \text{ Mean Sq. Error} = 2.566 \%; \quad \sqrt{\frac{1}{N} \sum_{k=1}^N \left(\frac{Error(k)}{Obs.Flow(k)} 100 \right)^2}.$$

D.6.3 Rating Curve:



(i) Discharge ≤ 333.62

$$\text{Stage} = \text{Max} \{ 23, 3.96617E-07 * (\text{Discharge})^3 - 0.000340222 * (\text{Discharge})^2 + 0.111296196 * (\text{Discharge}) + 22.05885668 \}$$

(ii) Discharge > 333.62

$$\text{Stage} = 9.790502391 * \ln(\text{Discharge}) - 20.83339552$$

Units: stage (ft), discharge (mcf/6-hrs)

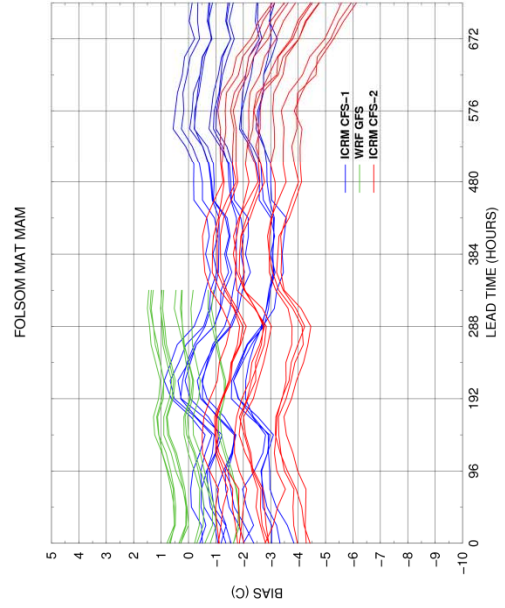
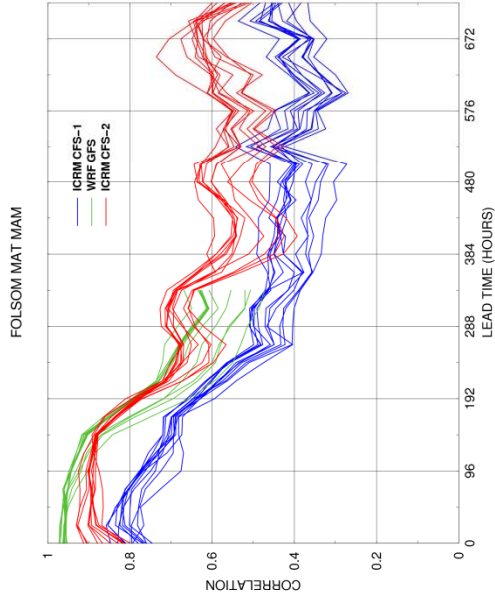
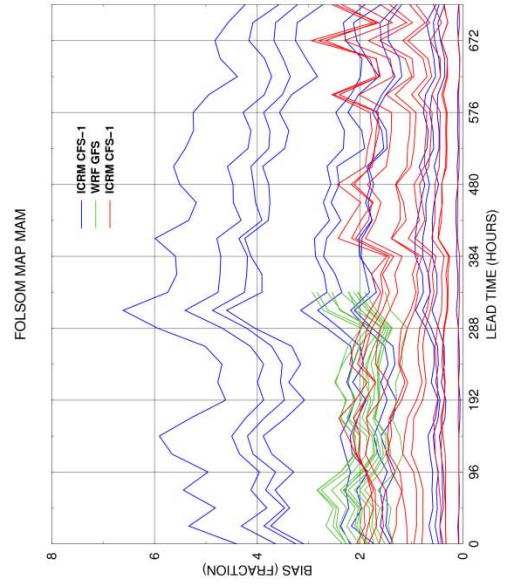
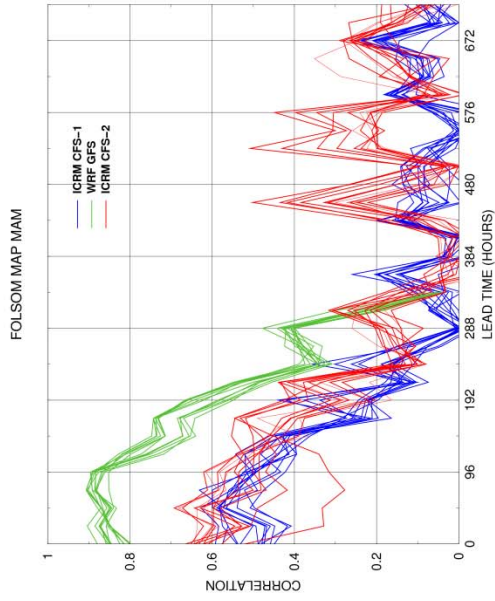
APPENDIX E:

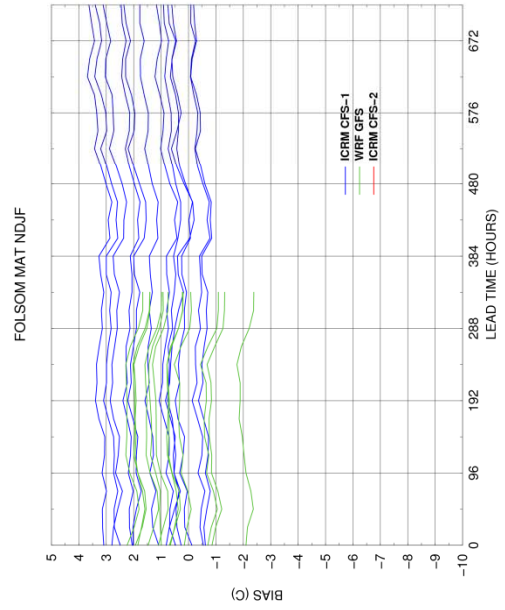
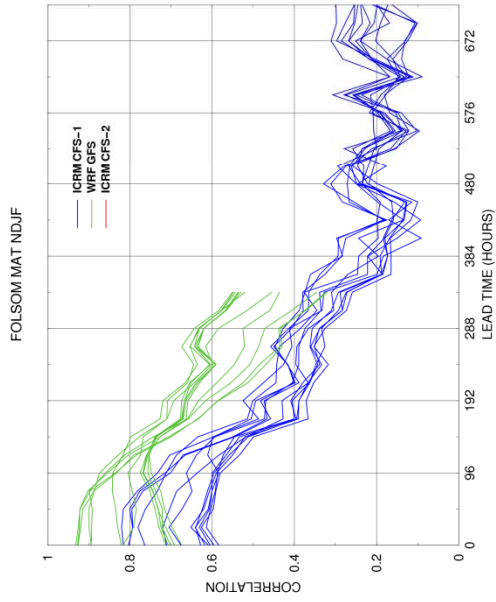
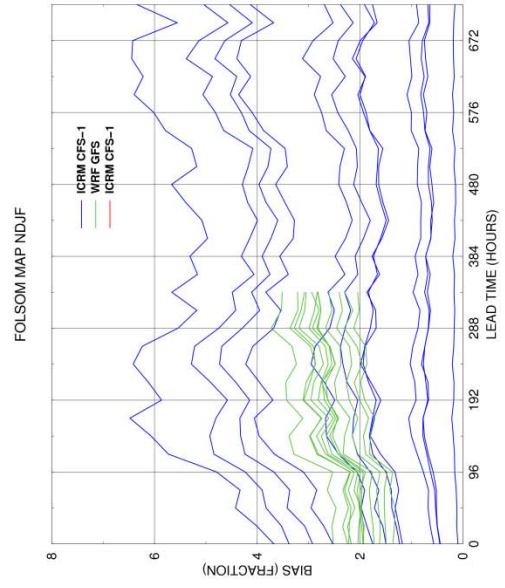
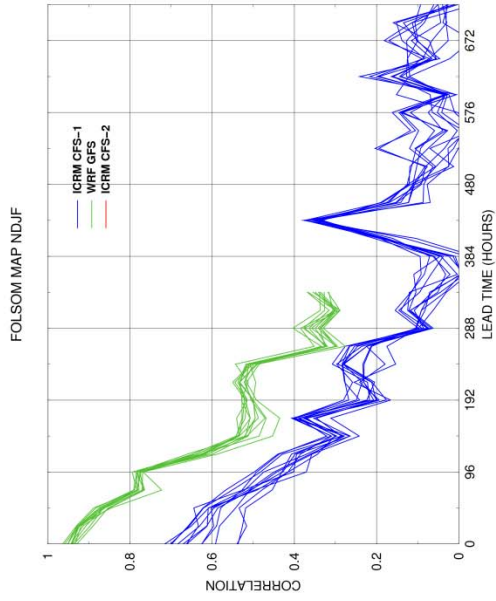
Comprehensive Statistical Performance Results

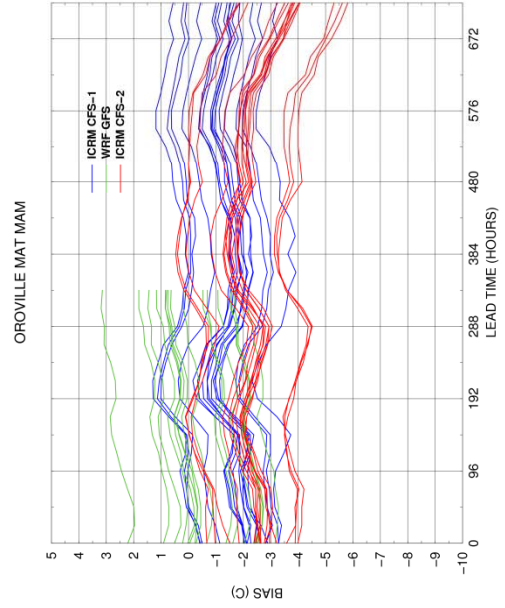
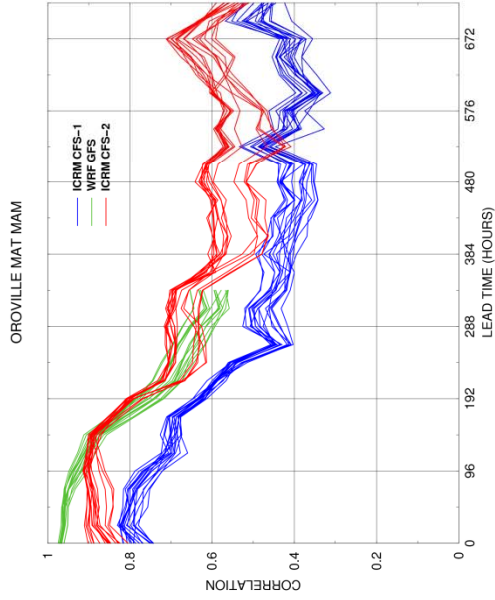
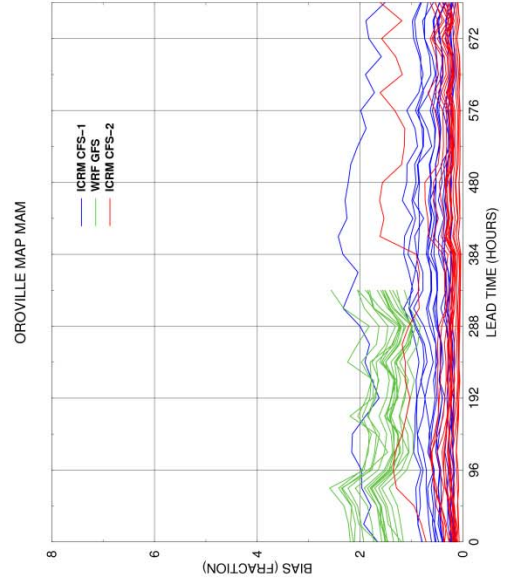
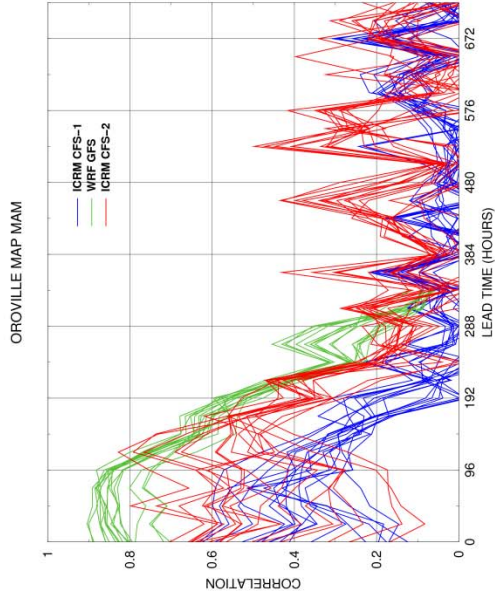
MAP and MAT Forecast Biases and Correlations with Observed

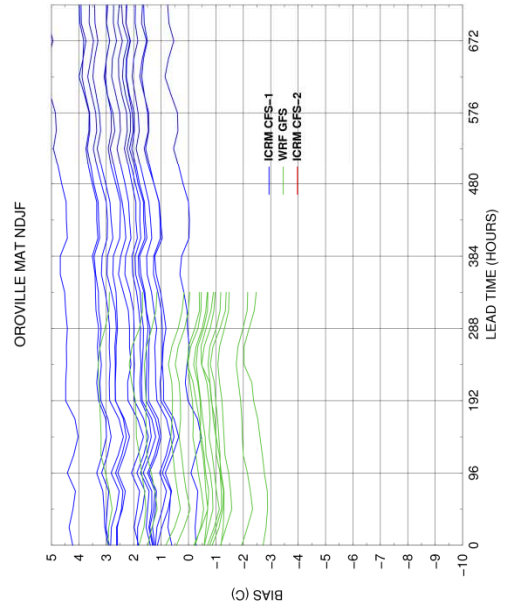
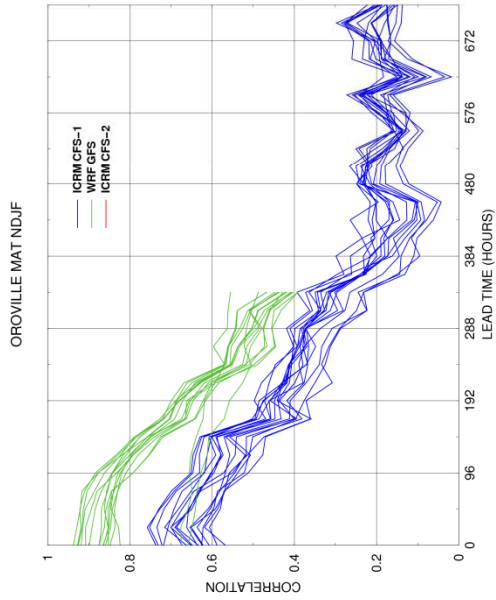
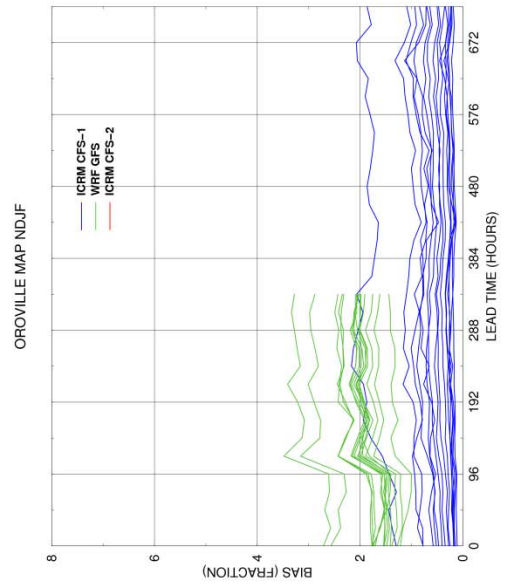
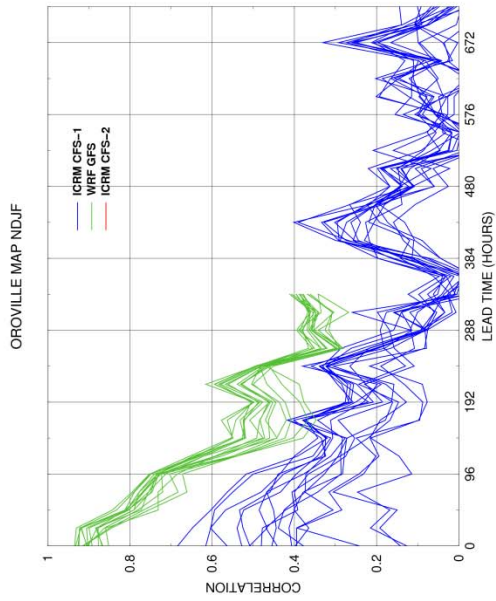
This section of Appendix E presents the results for the bias of the multi-lead forecasts for MAP and MAT as fraction for the MAP and difference for the MAT. It also presents the cross-correlation between the forecasts and observations for the lead times available. These results are presented as plots of bias (or correlation) as a function of lead time, and are for GFS-WRF, CFS1-ICRM, and CFS2-ICRM ensemble forecasts as described in Chapter 4. Green lines are for the GFS-WRF forecasts, blue lines are for the CFS1-ICRM forecasts and red lines are for the CFS2-ICRM forecasts. Each plot is for a different watershed (drainage of each of the five major reservoirs: Folsom, New Bullards Bar, Oroville, Shasta and Trinity). Multiple lines for each watershed are shown; one for each of the sub-catchments in the watershed (includes upper and lower areas delineated for the snow and soil model). Results for both the accumulation season (NDJF) and the melt season (MAM) are shown in the plots. The NDJF season does not contain any CFS2-ICRM forecasts as they started on 21 February 2012.

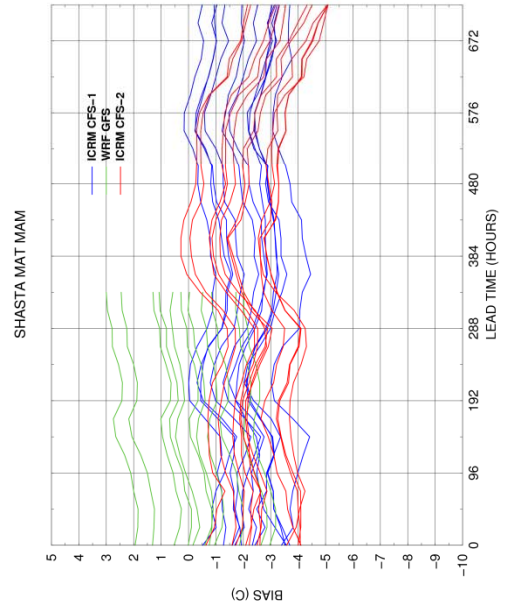
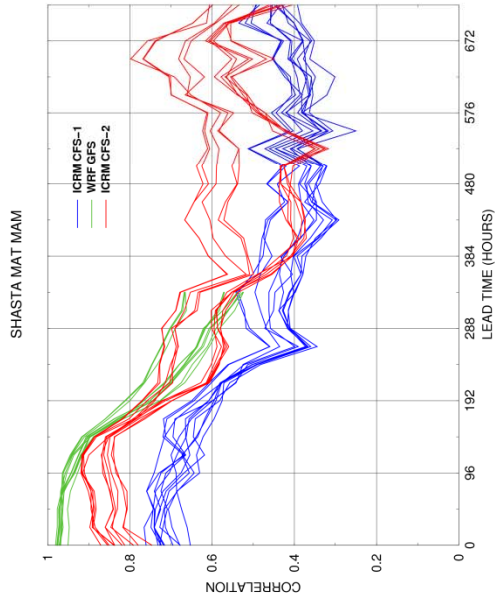
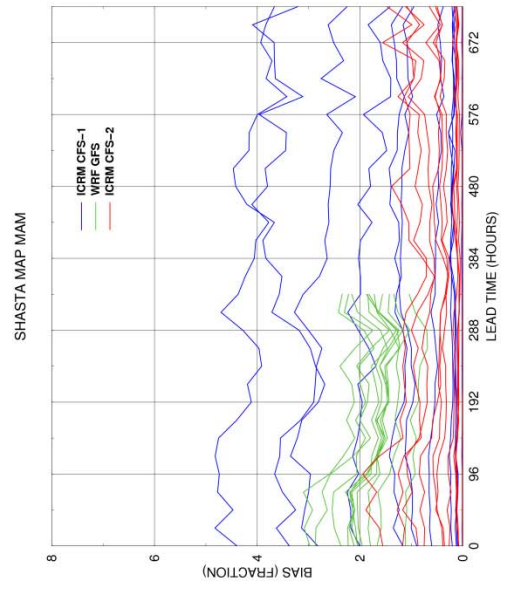
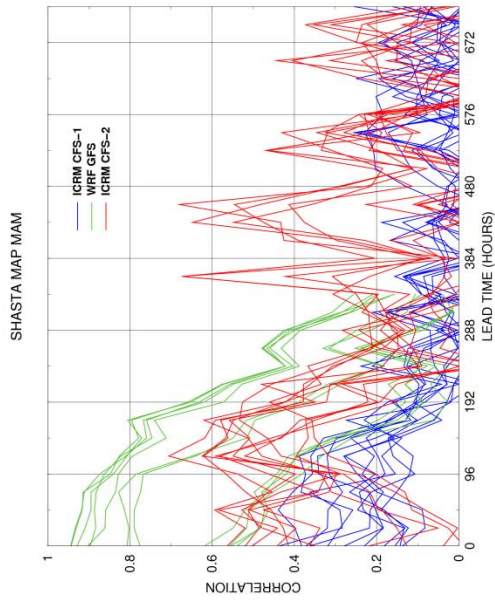
Following the multilead bias and correlation plots, this section of Appendix E also contains maps of the spatial distribution of the MAP and MAT bias and correlations for the forecast lead time of 48 hours by subcatchment. Each panel of four of these maps is for one of the three models (GFS-WRF, CFS1-ICRM, and CFS2-ICRM) and either MAP or MAT results, with the left-side maps depicting NDJF-season and the right-side maps depicting MAM-season results. The upper maps are for correlation results and the lower maps are for bias results (bias fraction for MAP and bias difference for MAT). It is noted that no results are shown for the case of CFS2-ICRM and for NDJF (the maps depict zero values both for MAP and MAT) due to the lack of forecasts in the season from the CFS2-ICRM model.

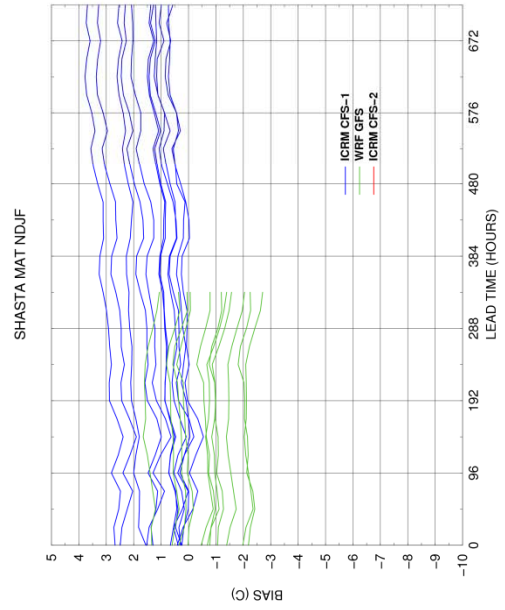
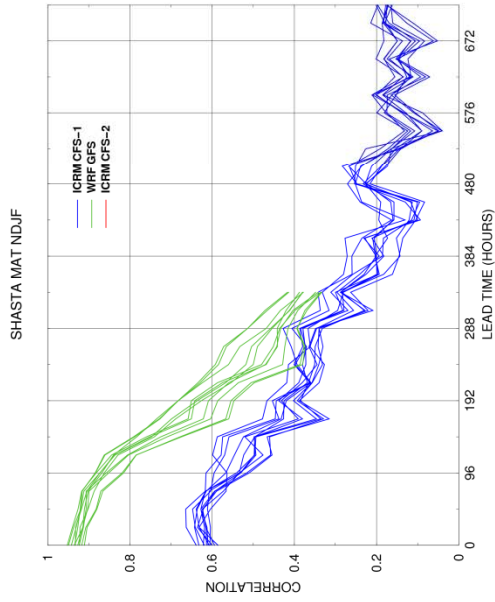
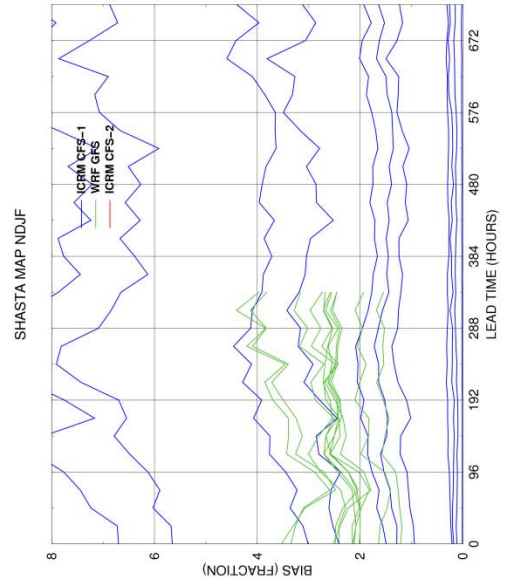
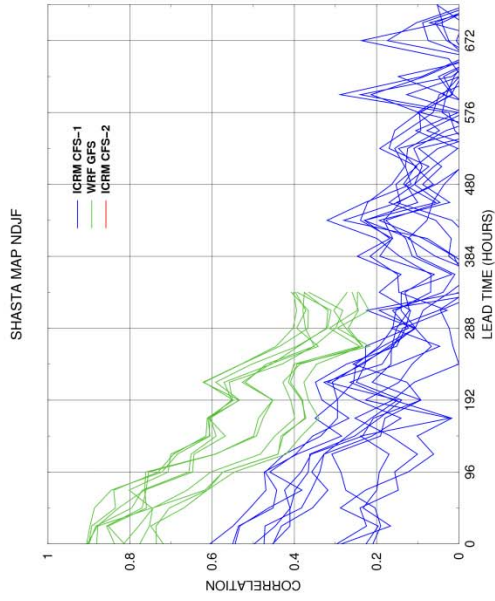


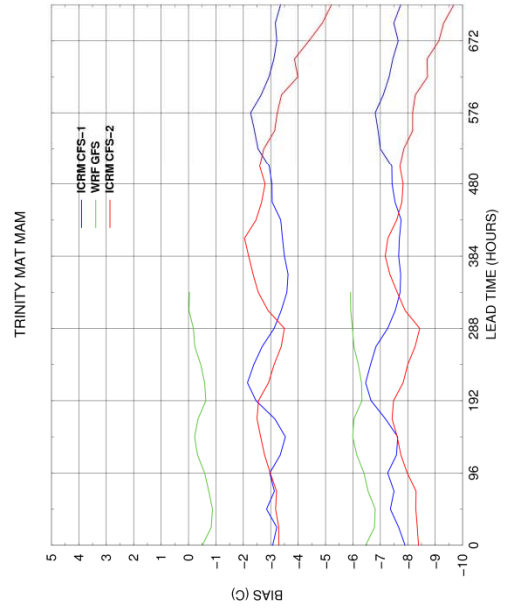
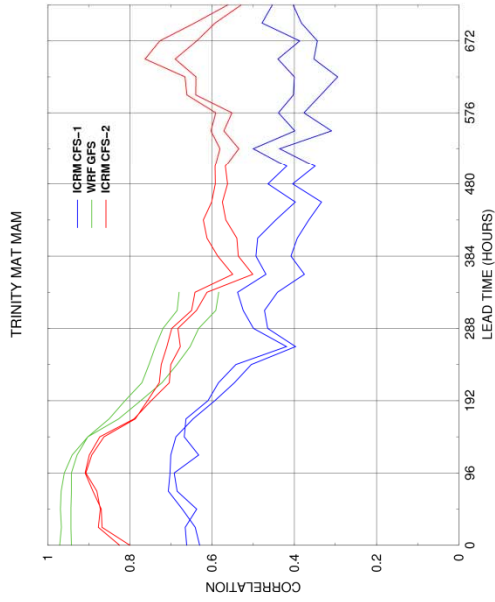
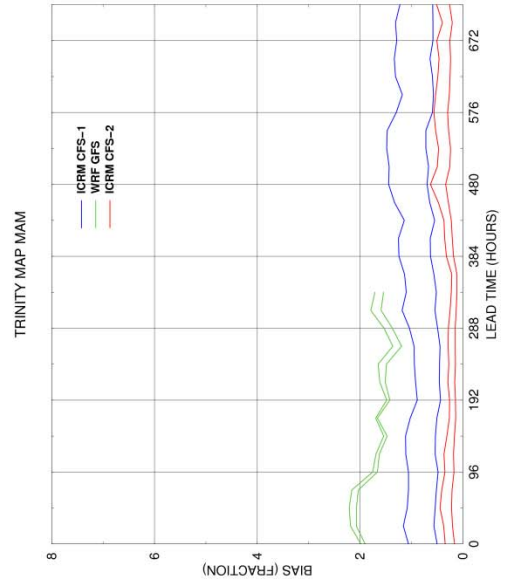
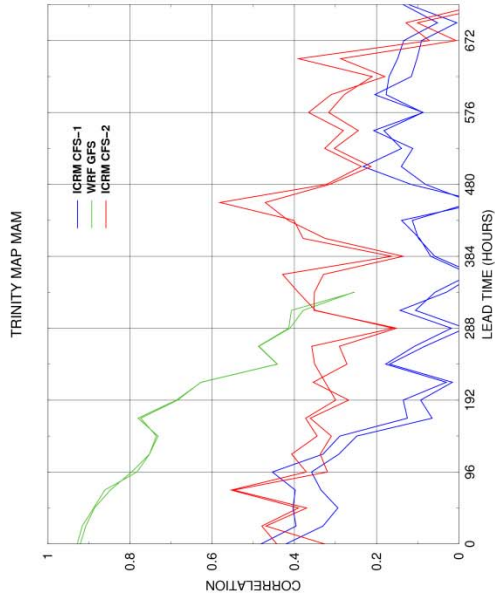


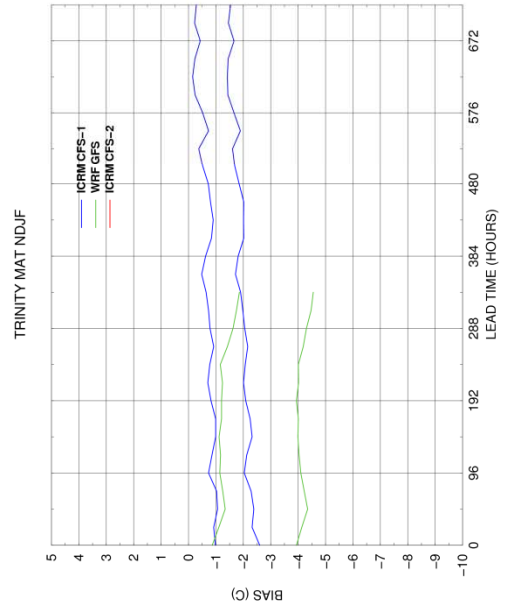
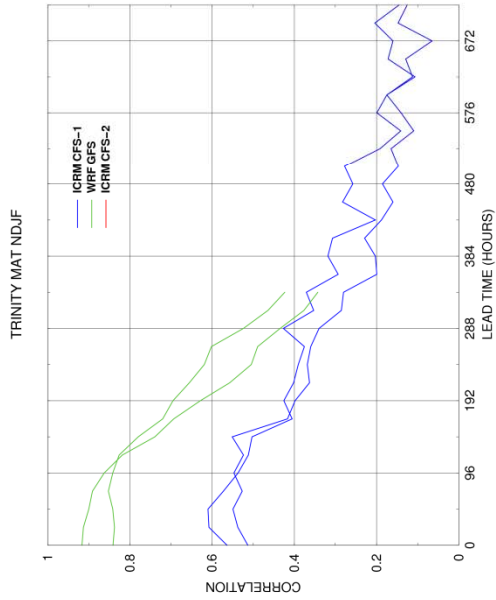
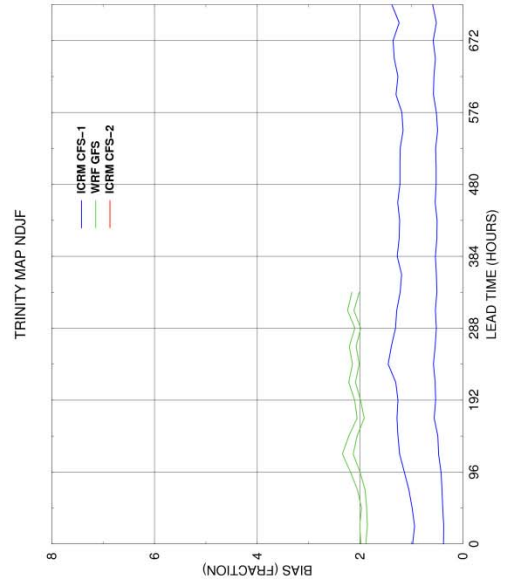
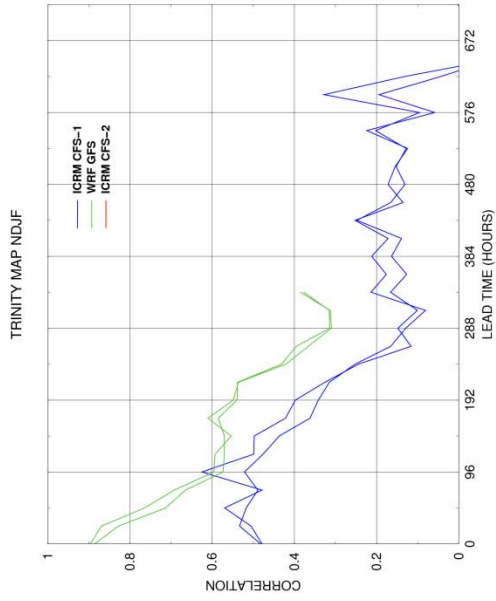


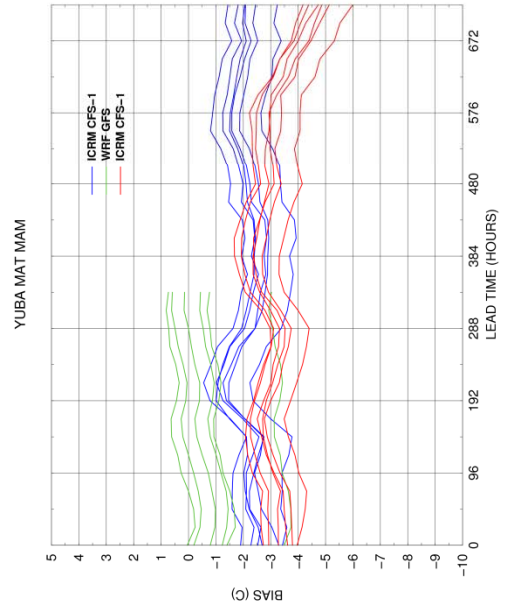
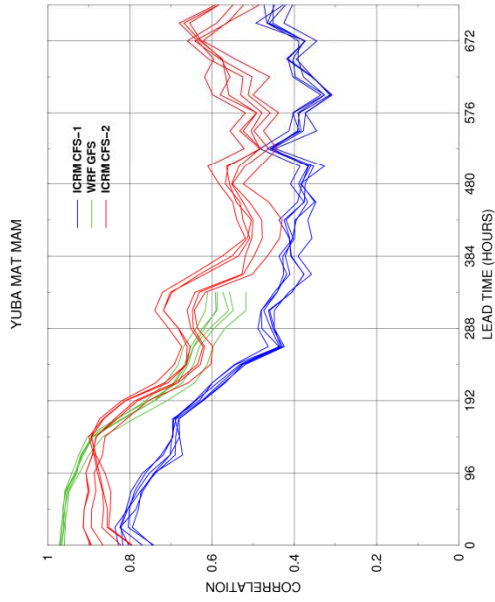
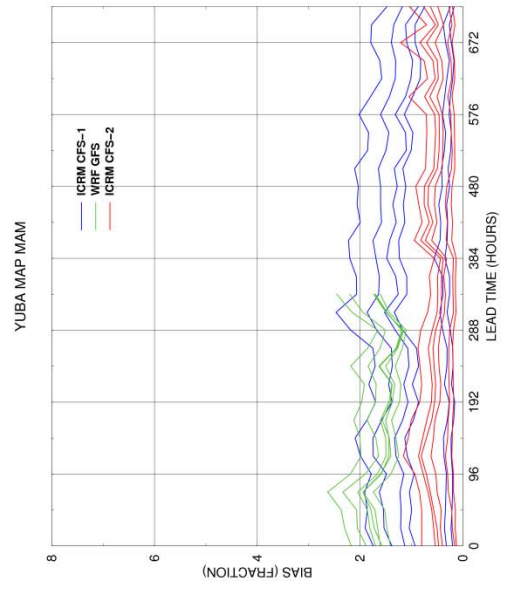
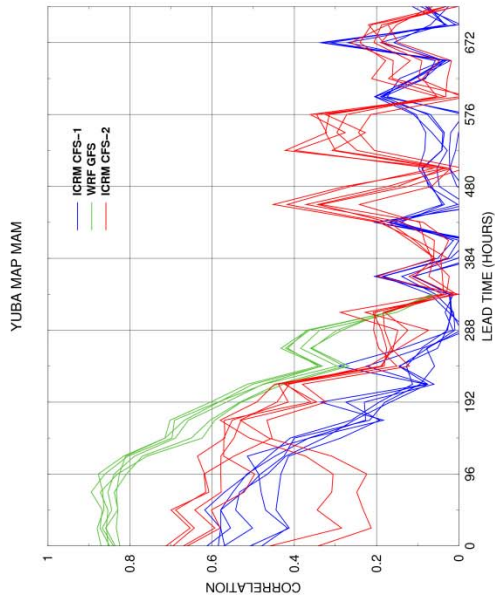


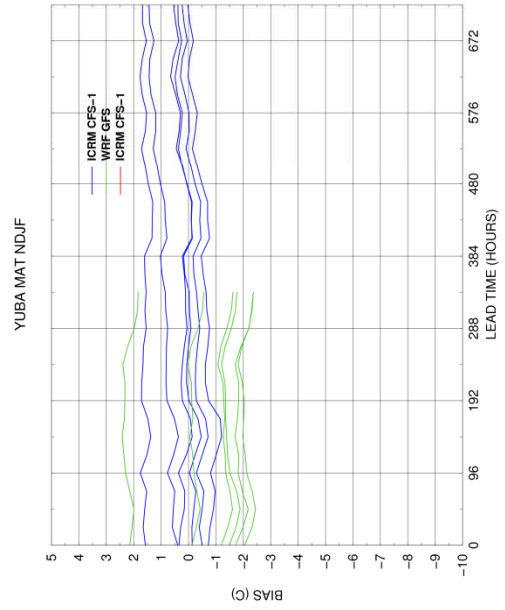
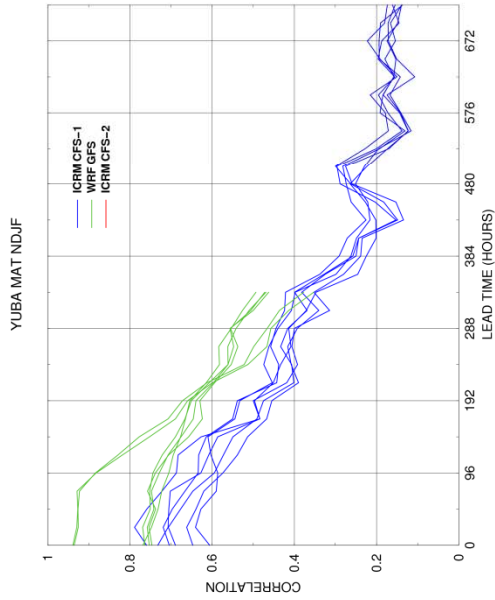
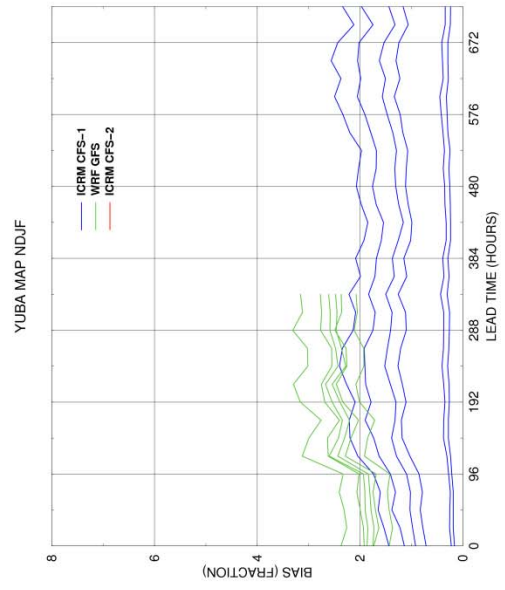
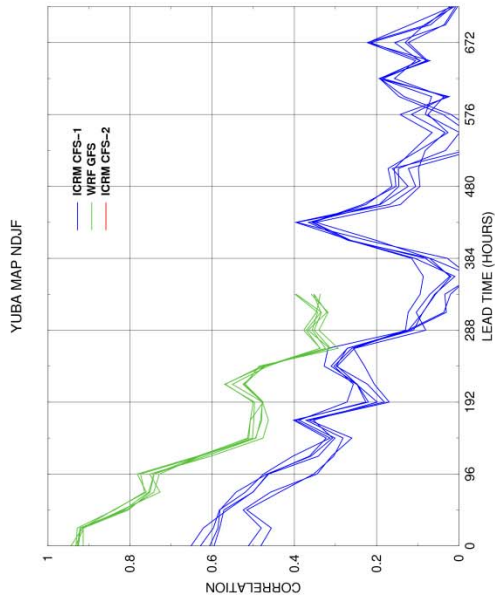


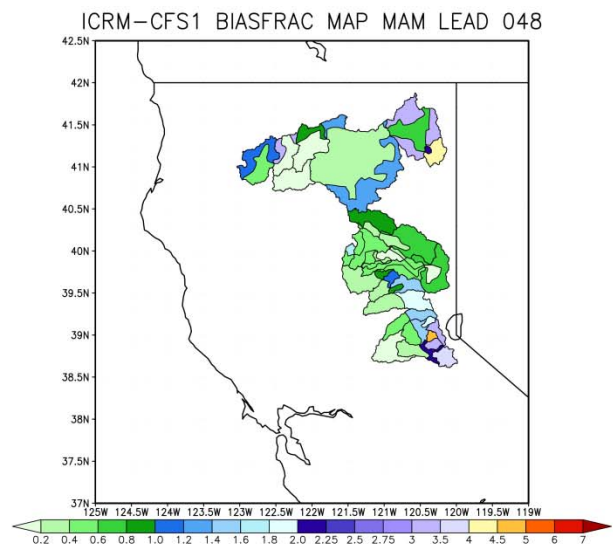
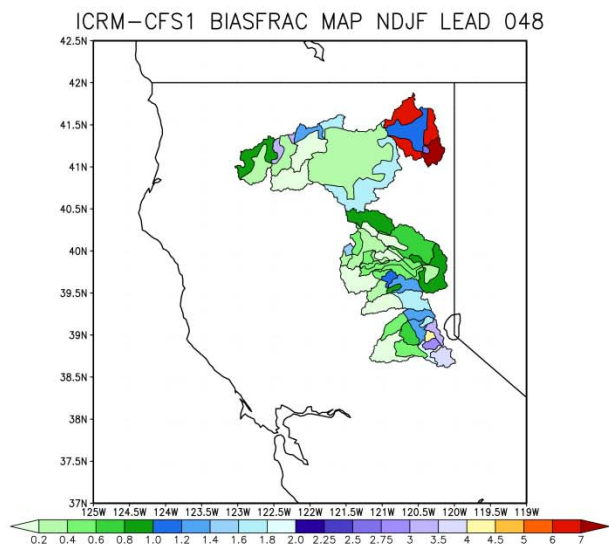
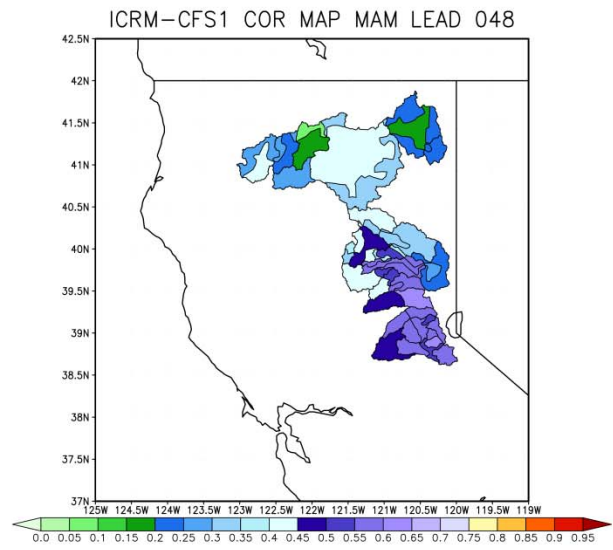
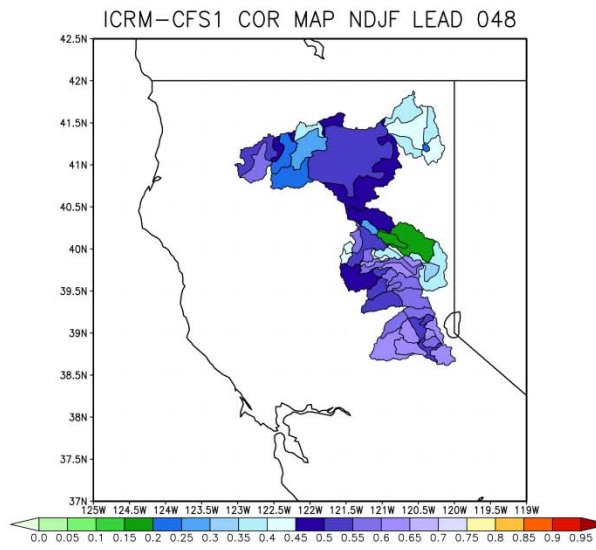


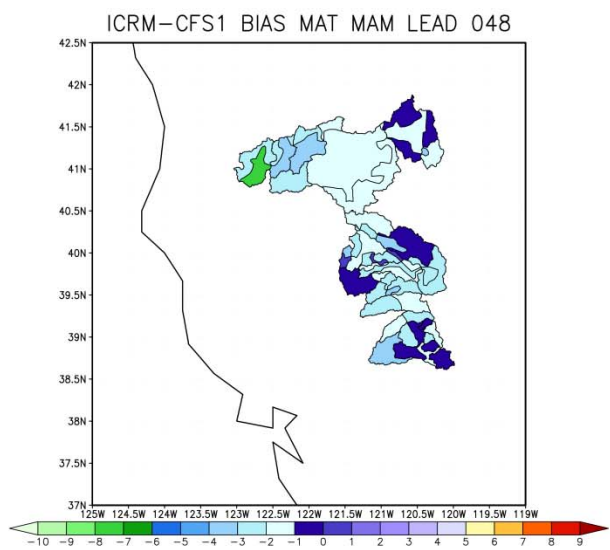
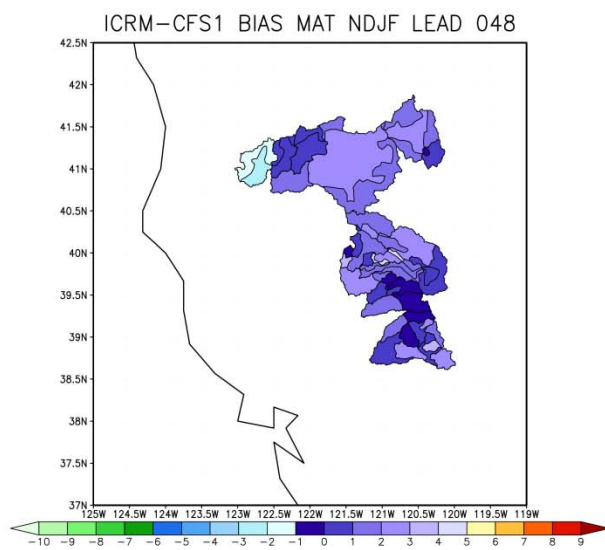
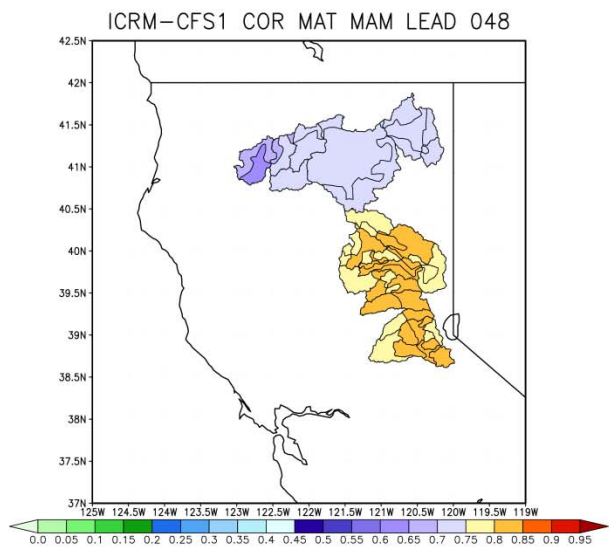
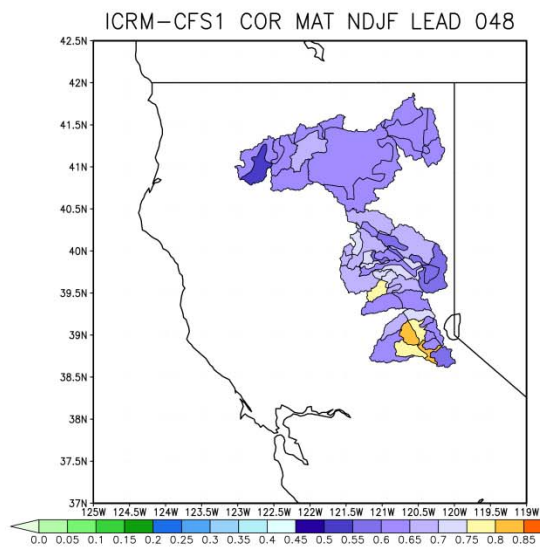


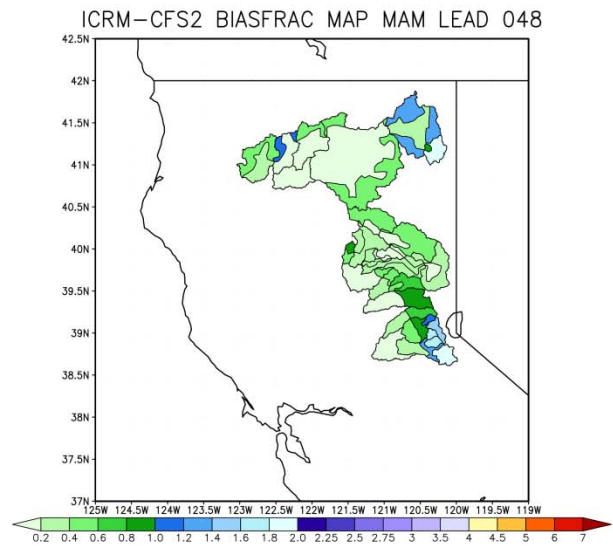
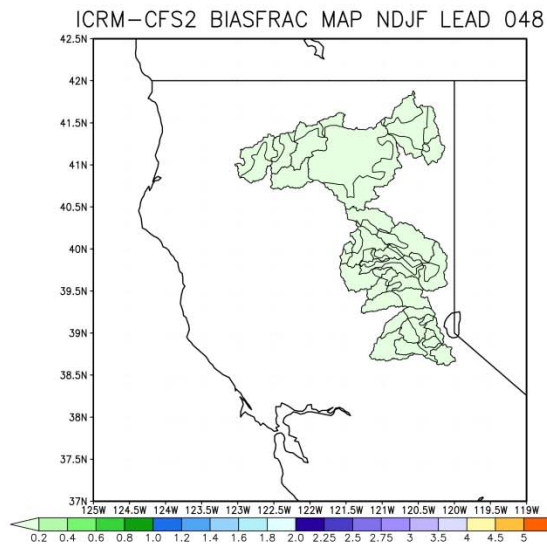
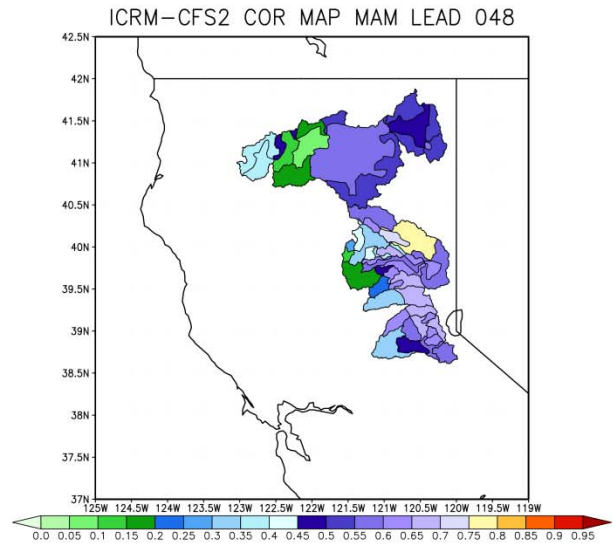
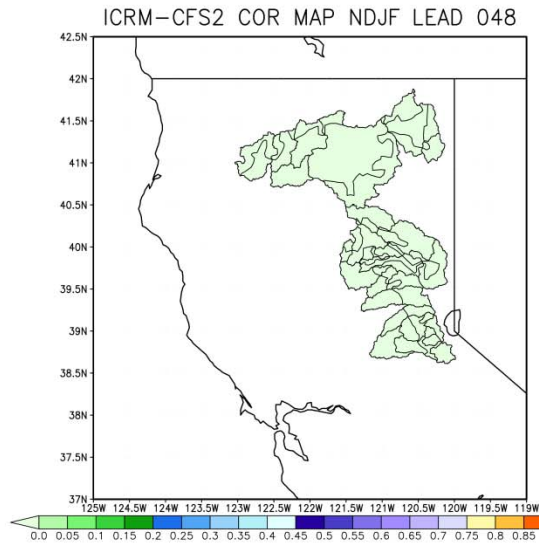


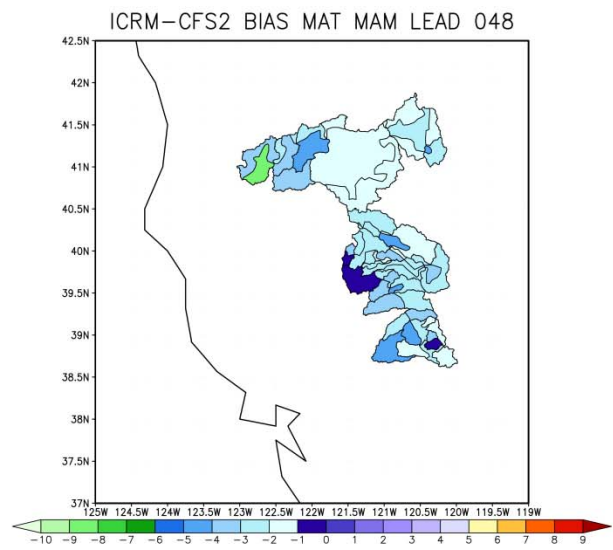
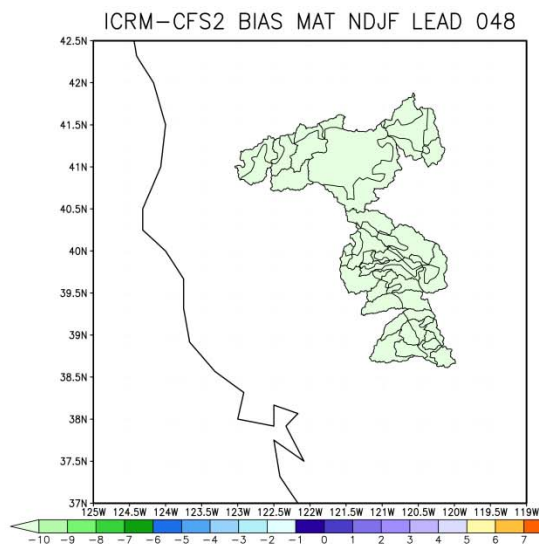
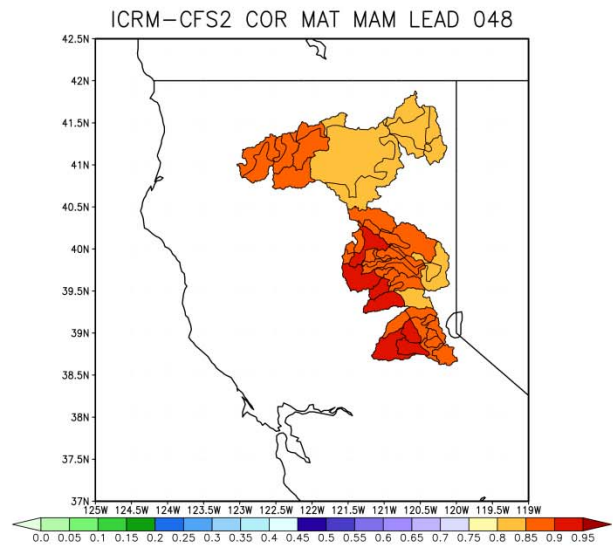
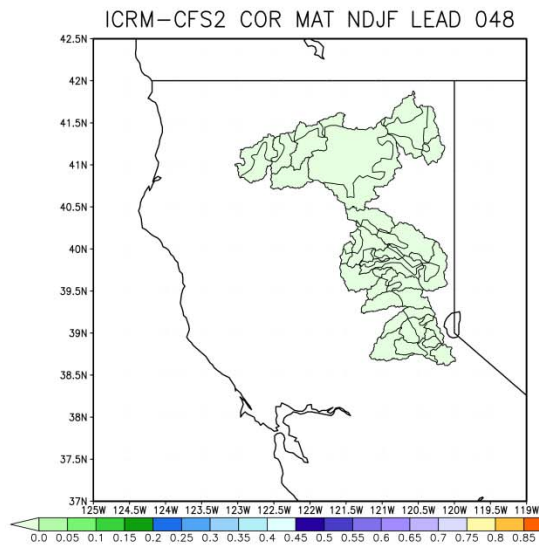


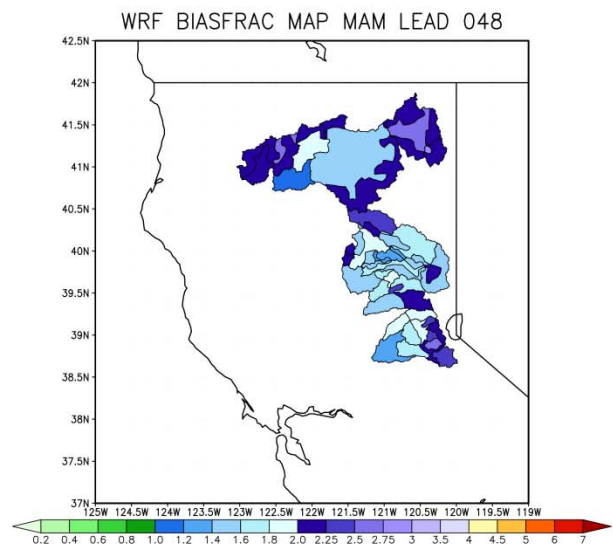
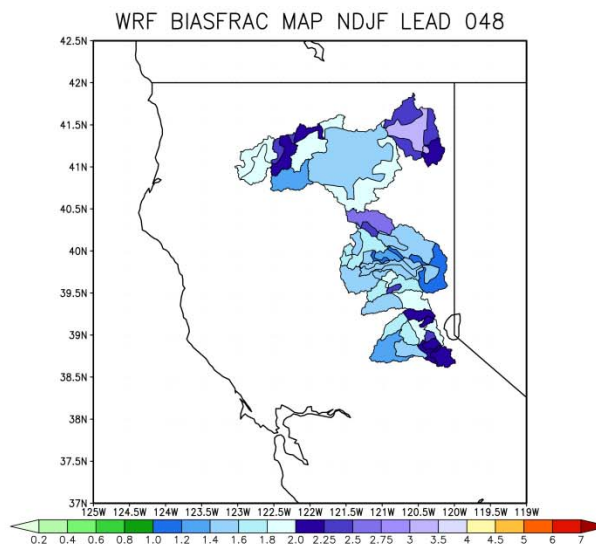
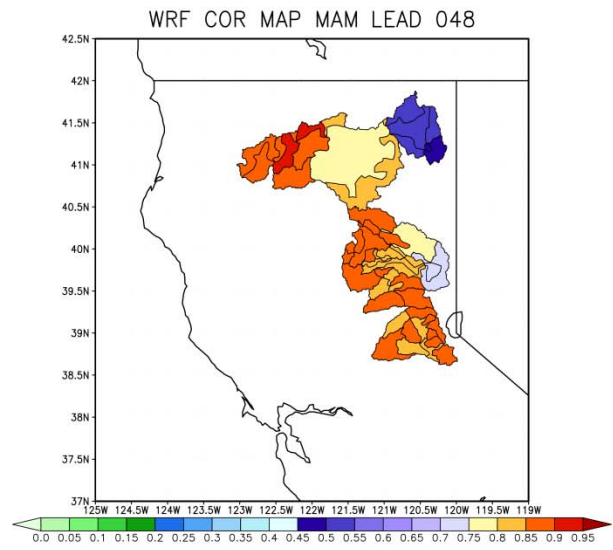
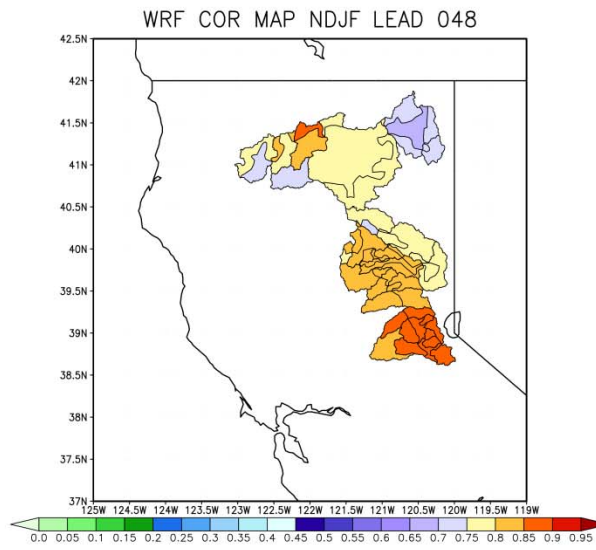


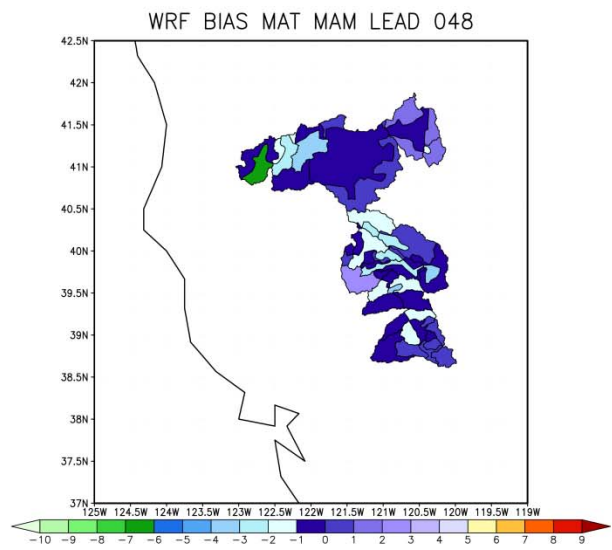
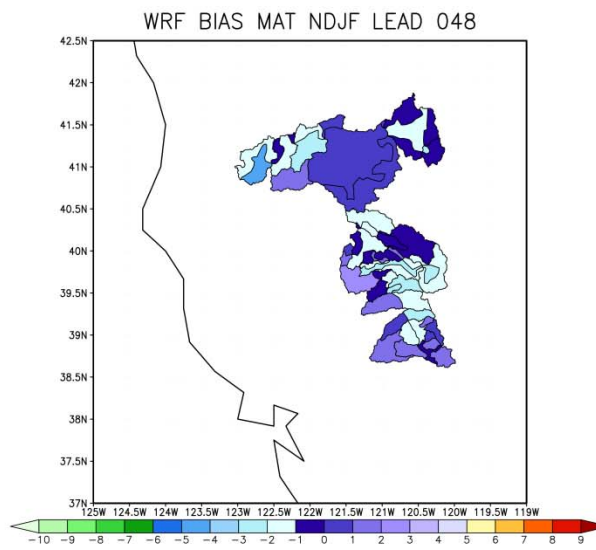
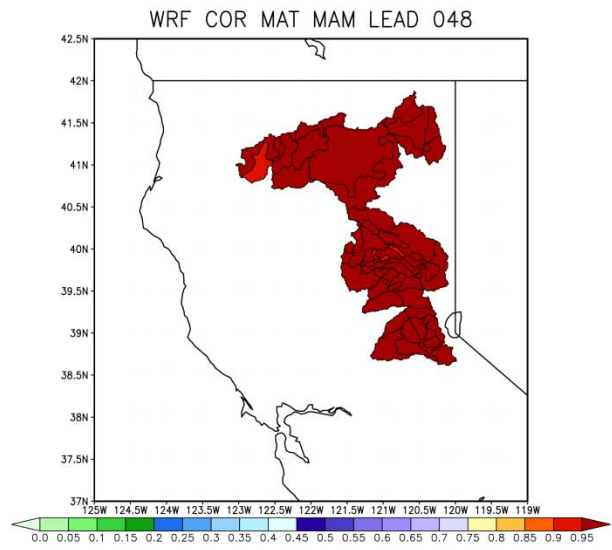
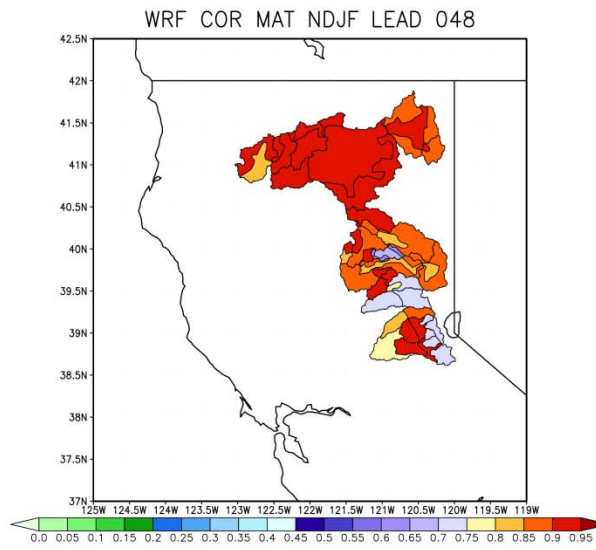






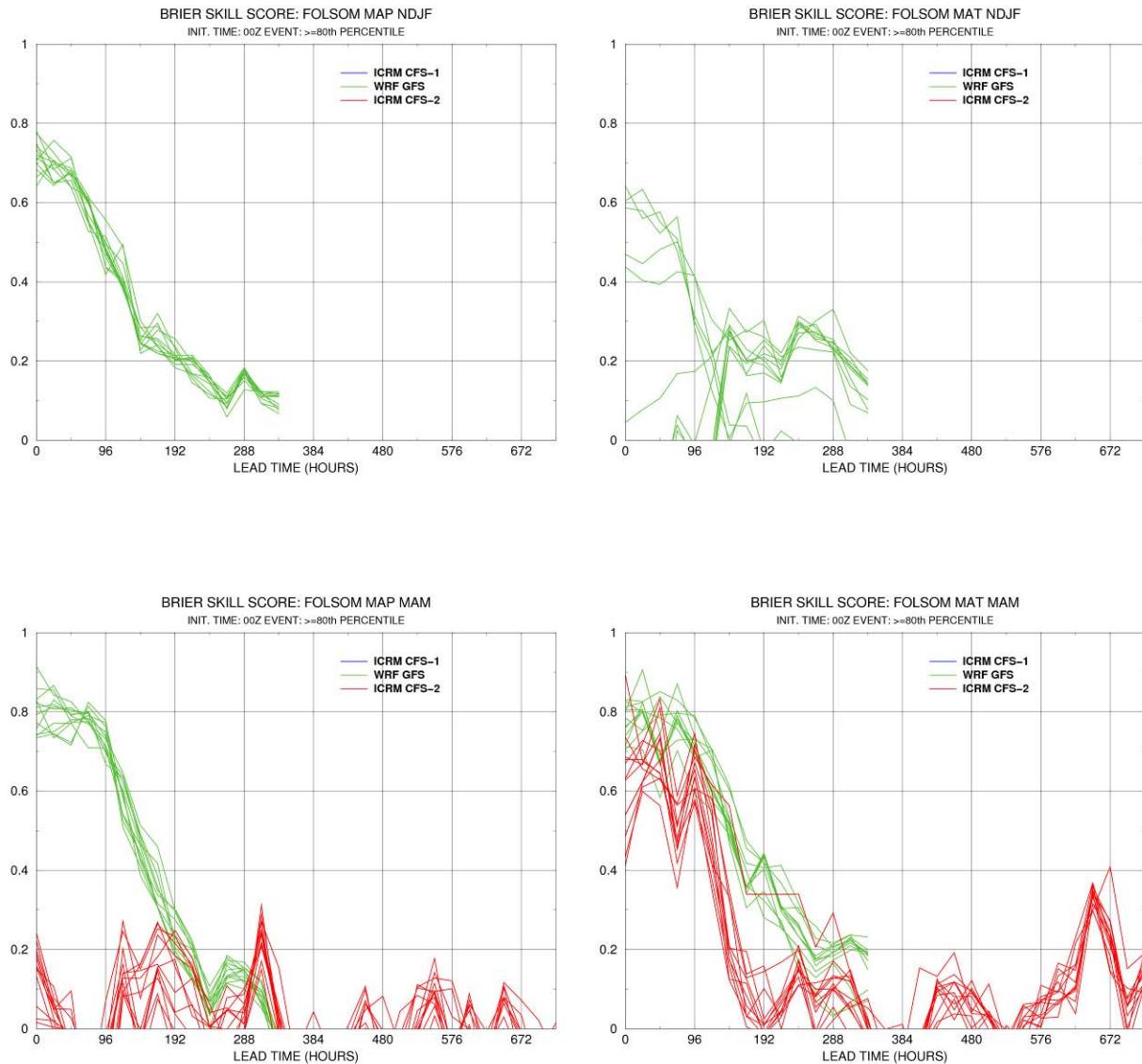


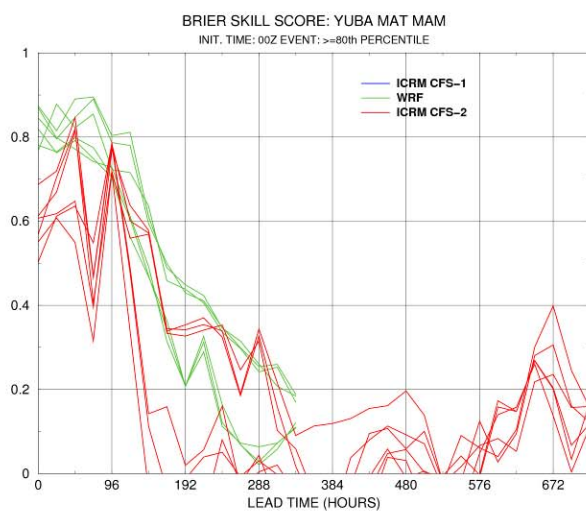
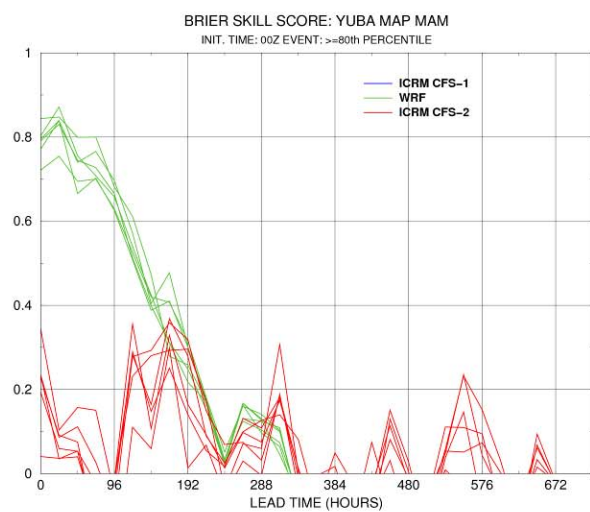
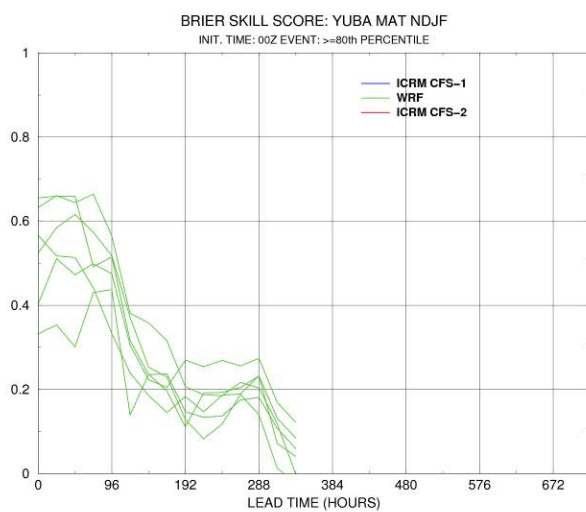
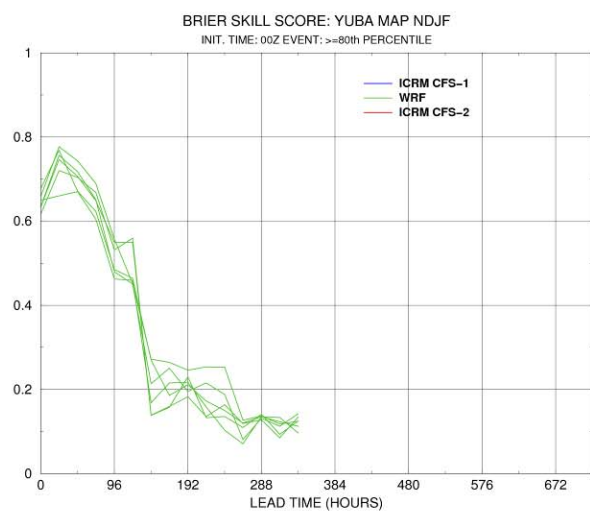


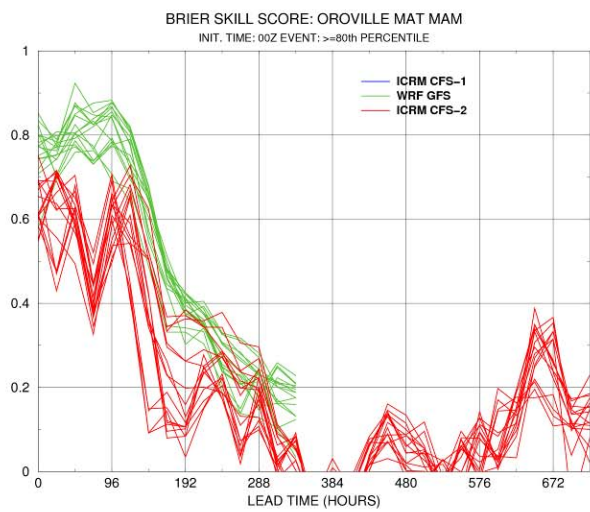
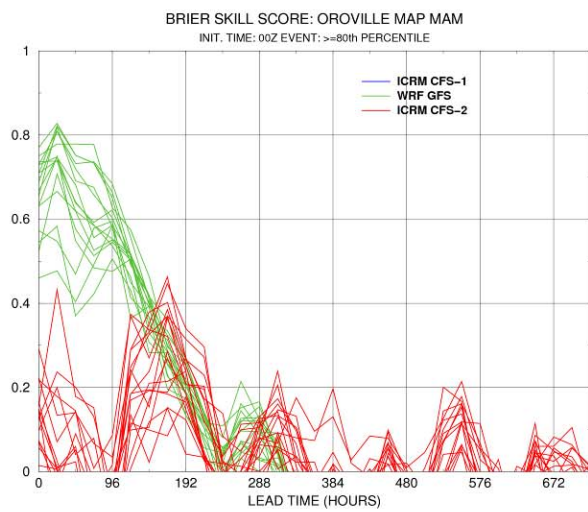
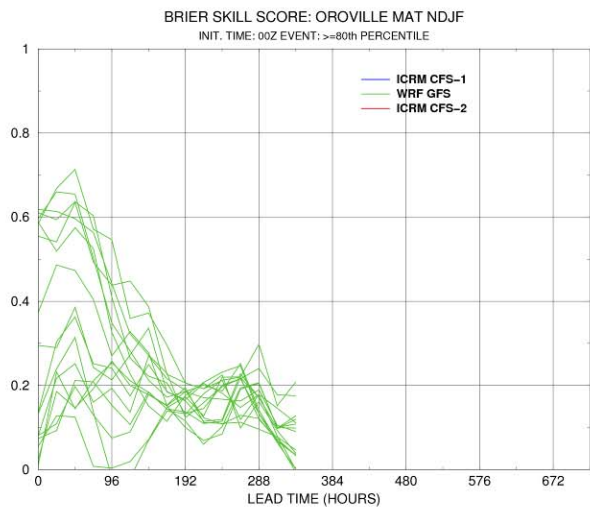
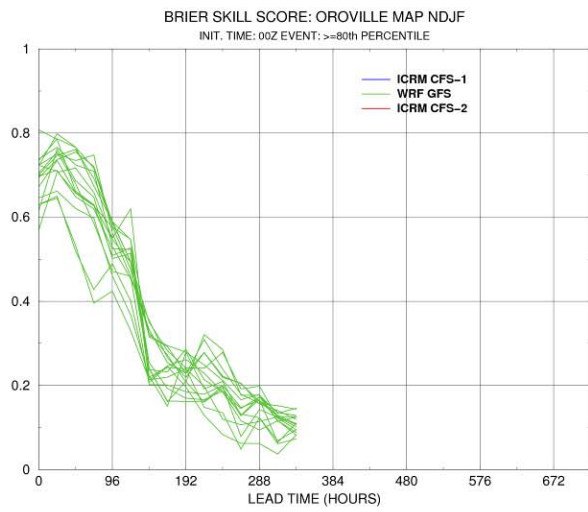


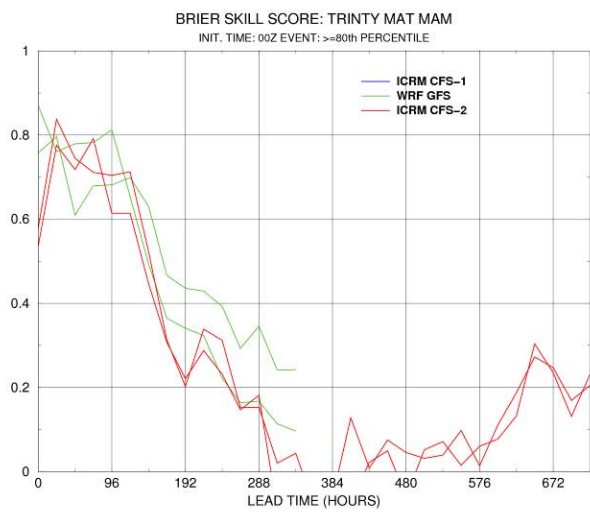
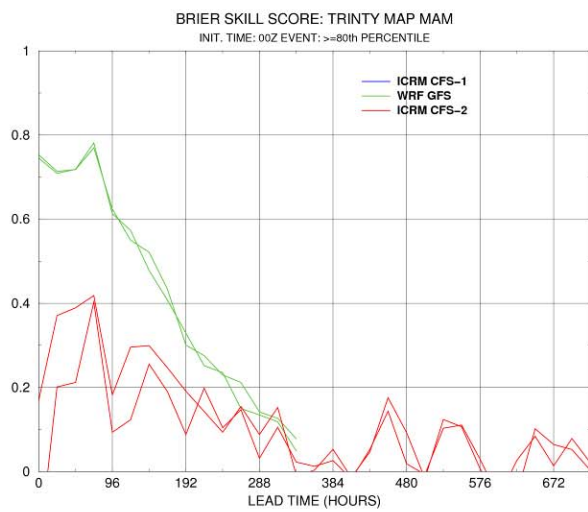
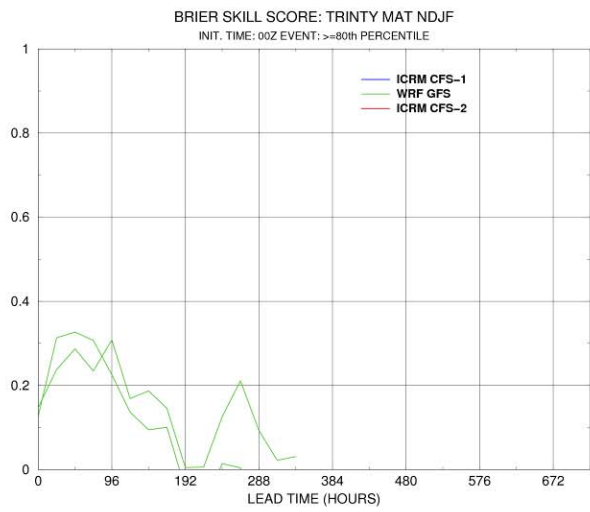
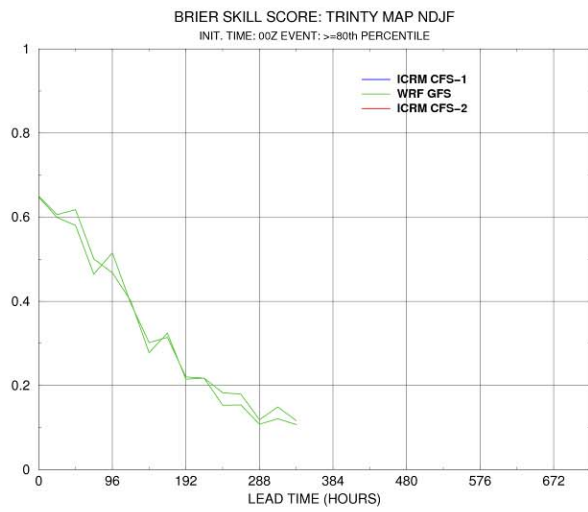
MAP and MAT Reliability Analysis

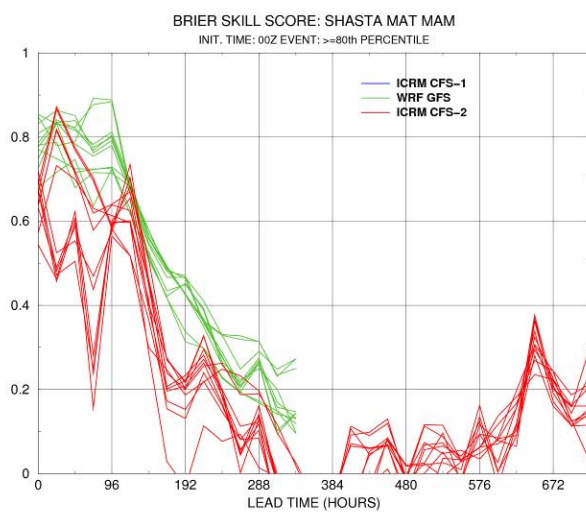
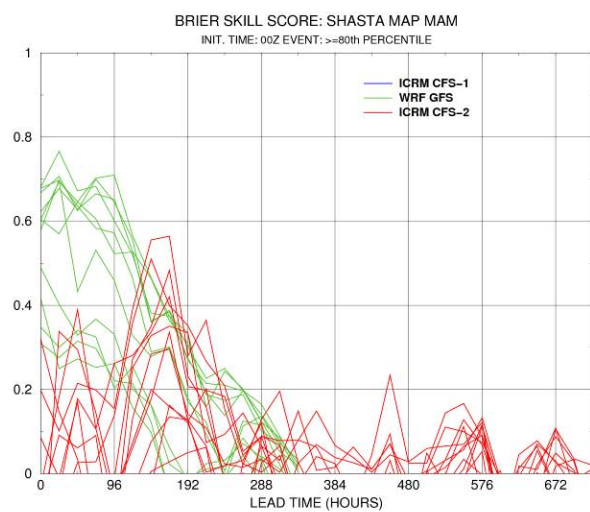
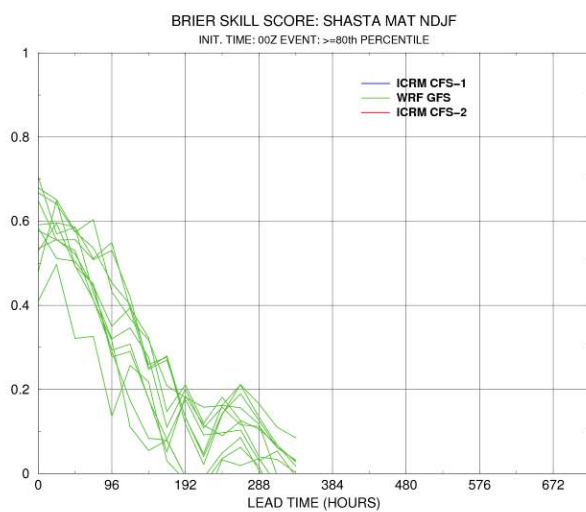
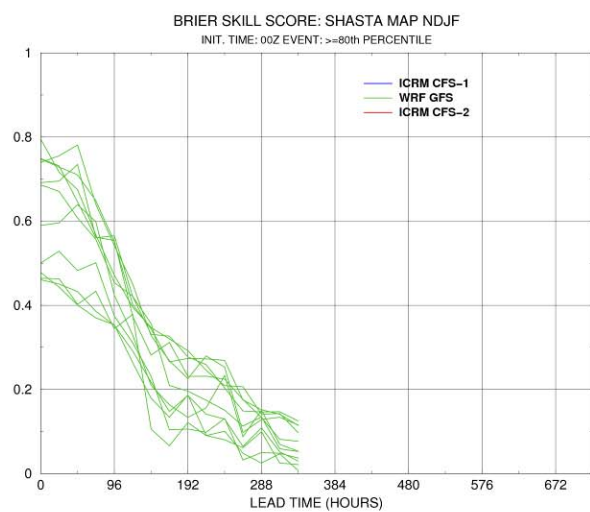
This section of Appendix E presents the Brier Skill Score (BSS) results for multi-lead MAP and MAT ensemble forecasts for all the subcatchments of the INFORM domain watersheds and for both seasons, NDJF and MAM. Following the BSS results, the reliability diagrams of the 48-hr MAP and MAT ensemble forecasts of the GFS-WRF model and for NDJF and MAM are shown for individual subcatchments of the INFORM watersheds.

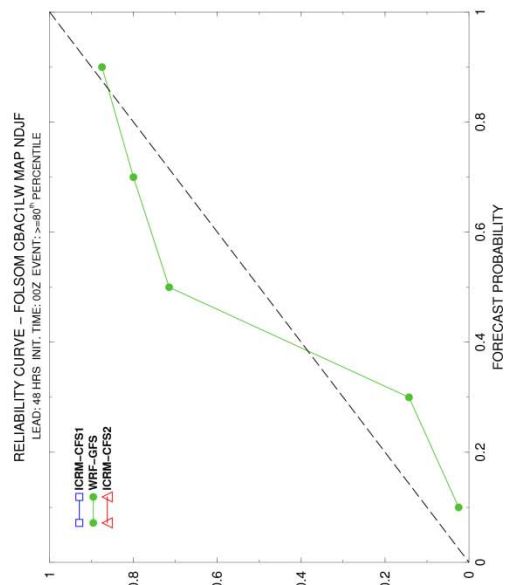
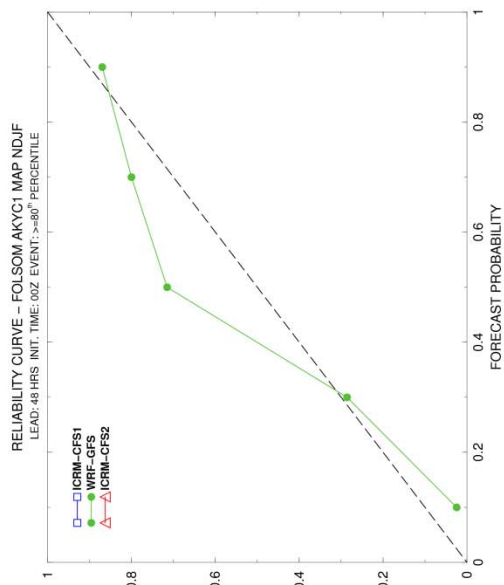
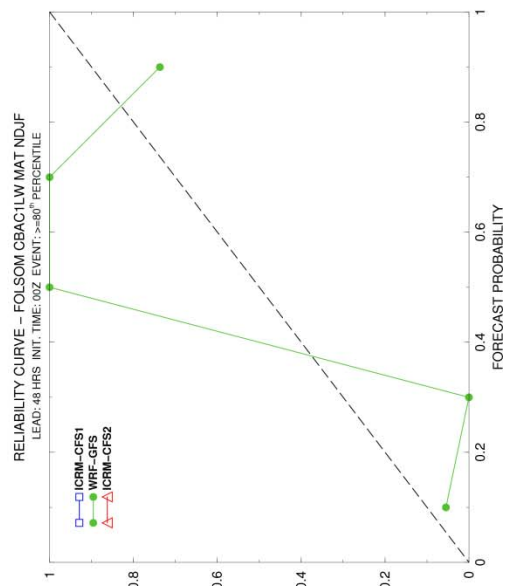
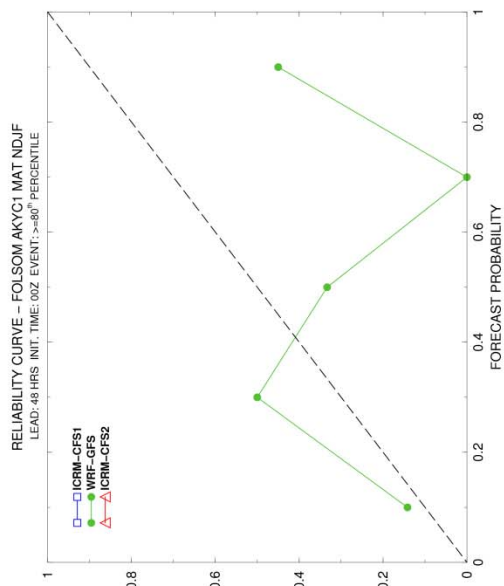


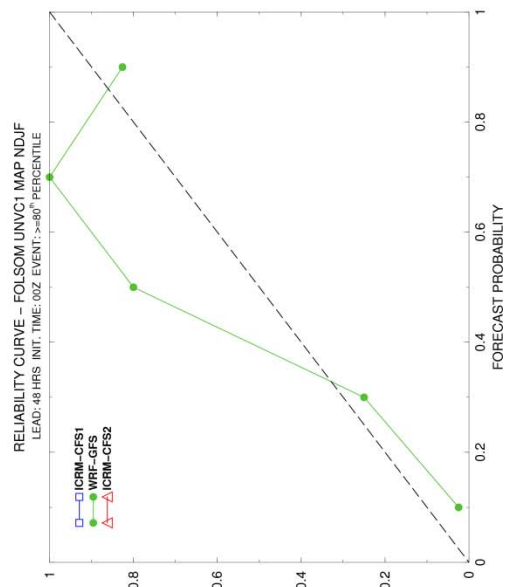
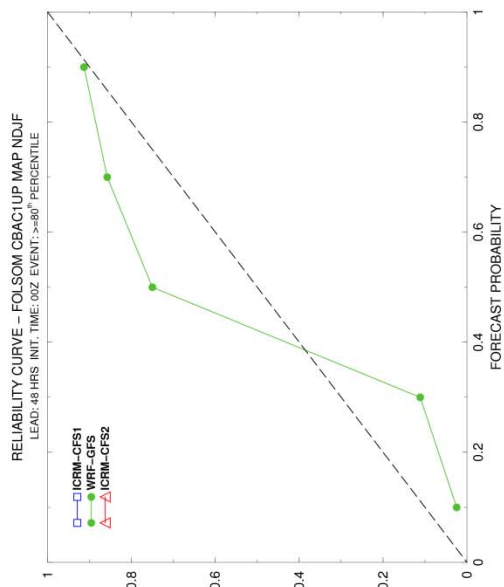
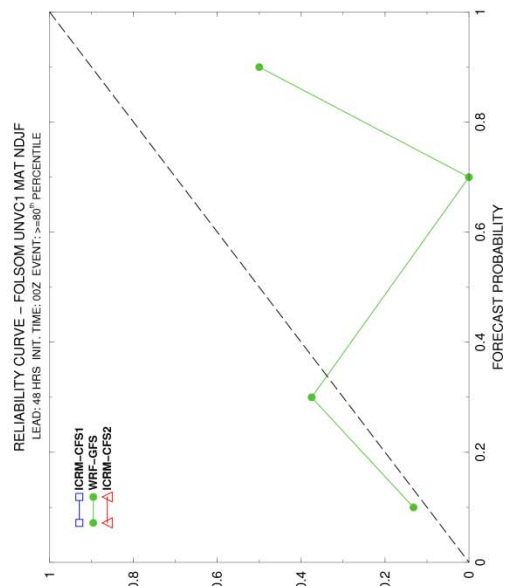
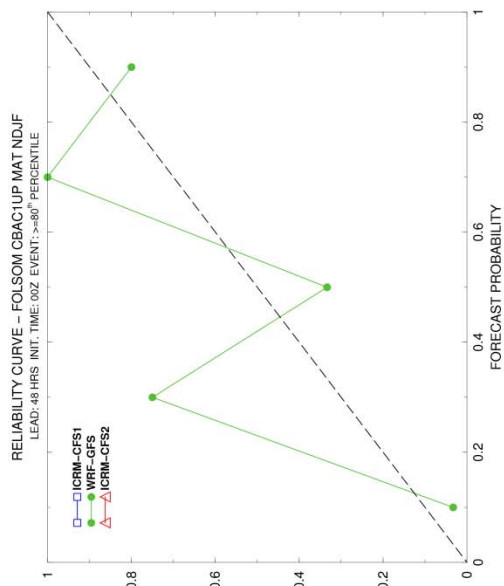


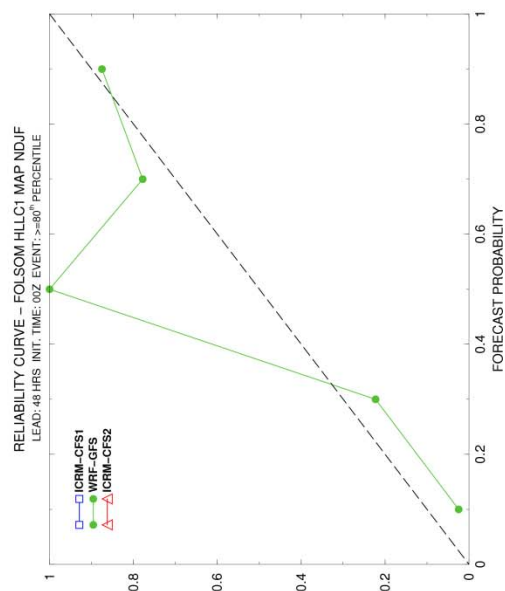
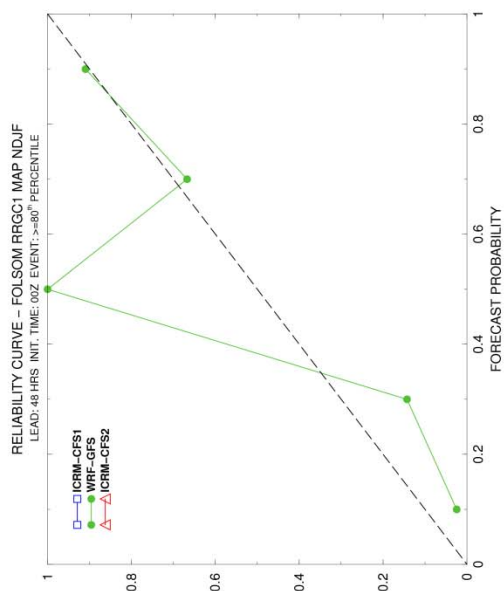
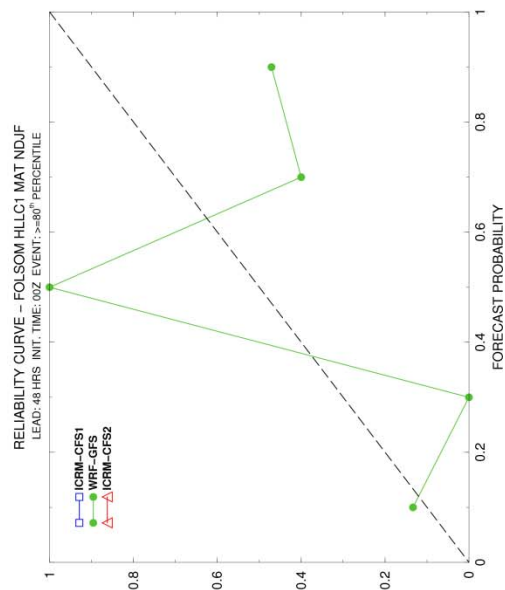
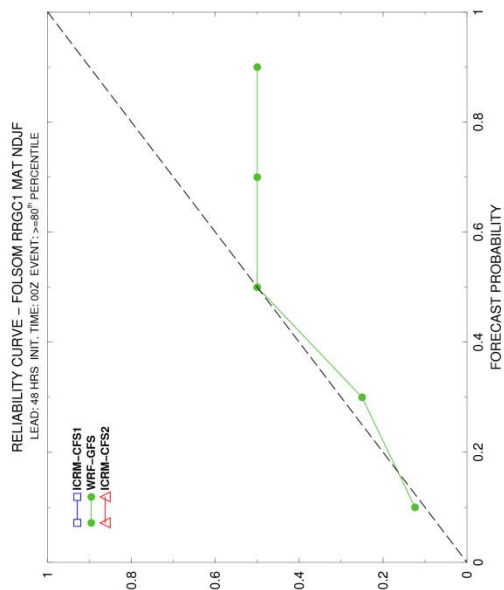


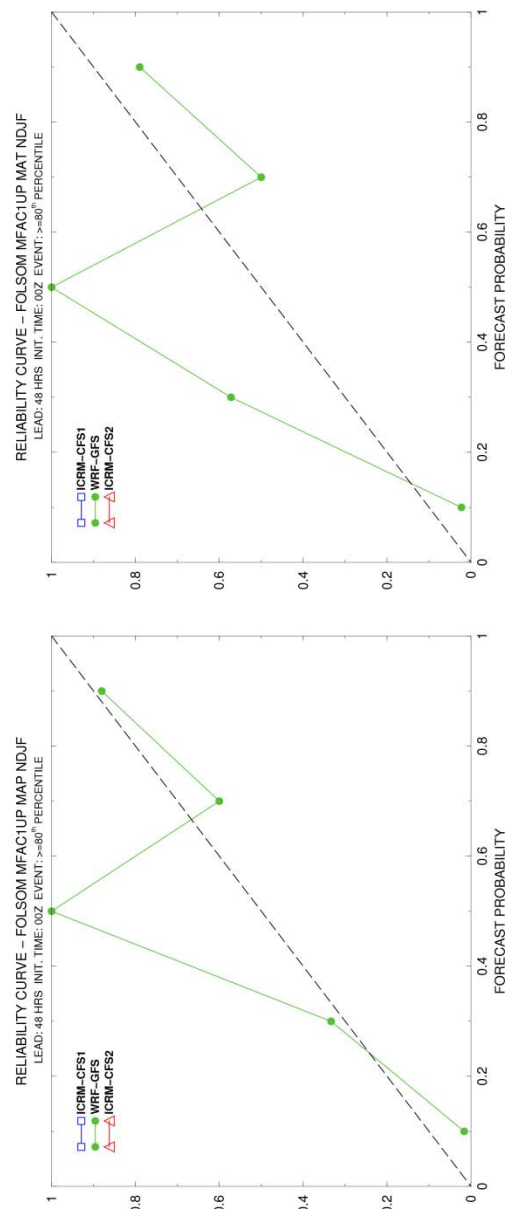
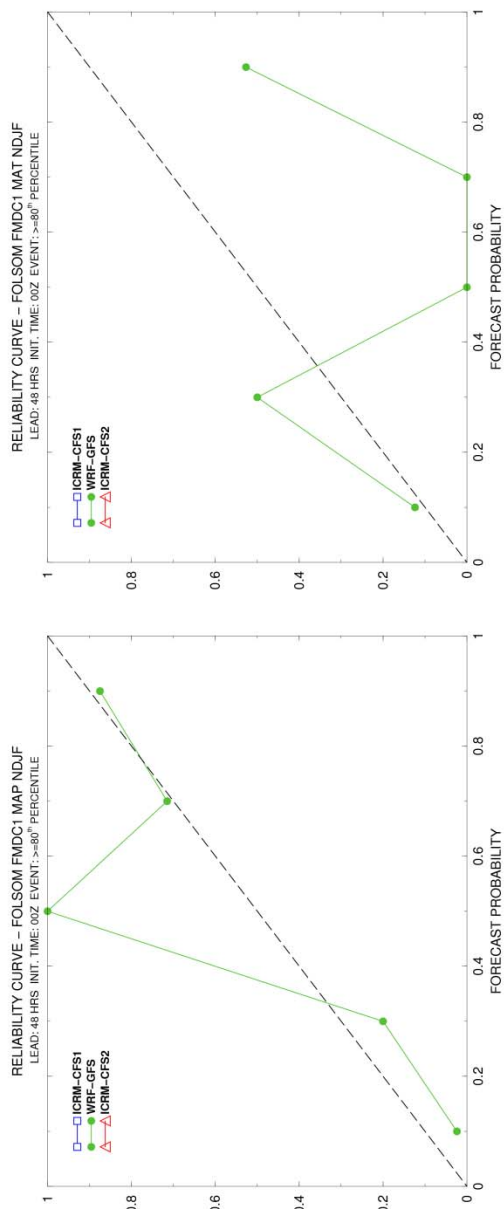


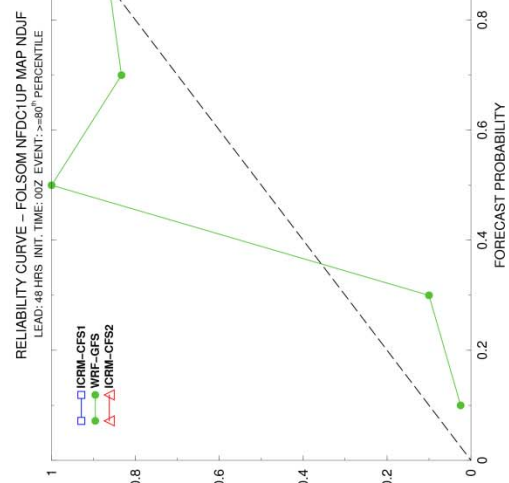
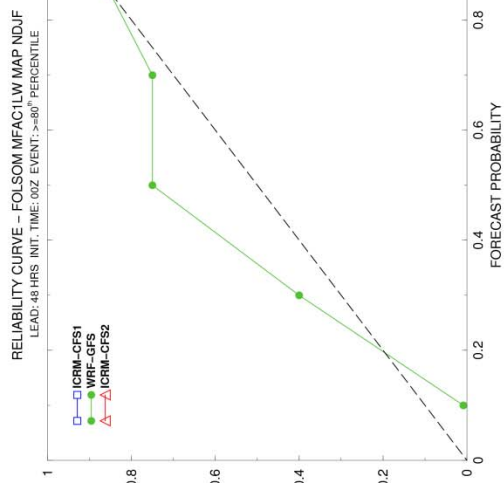
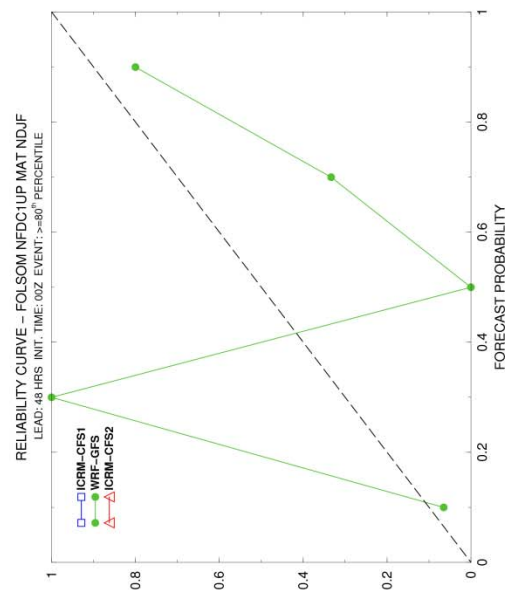
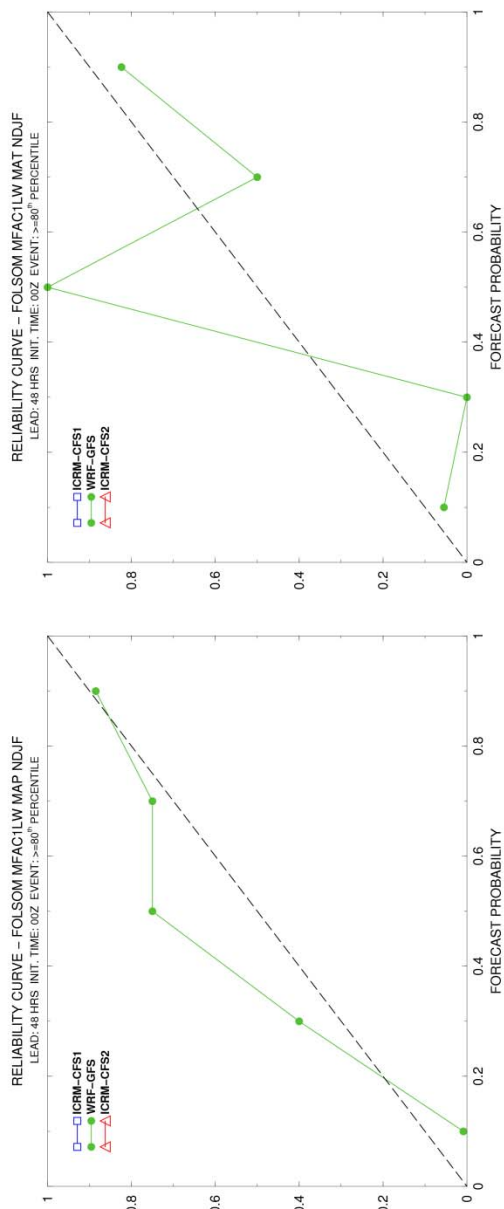


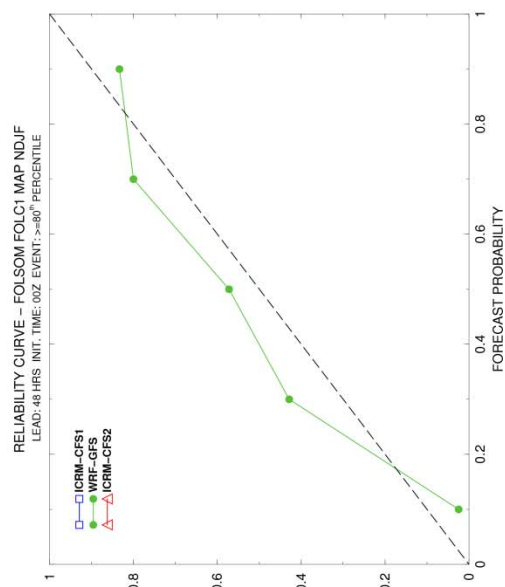
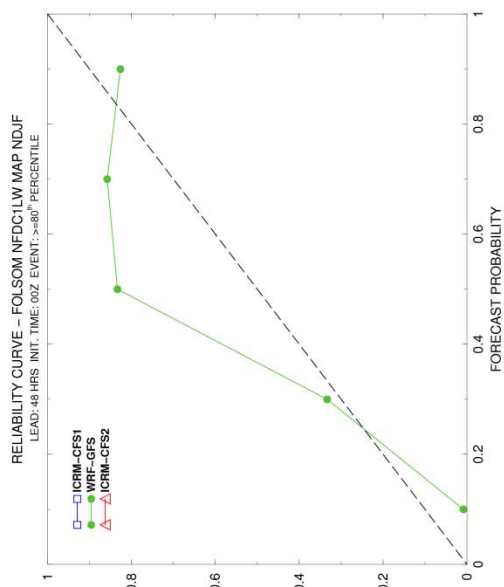
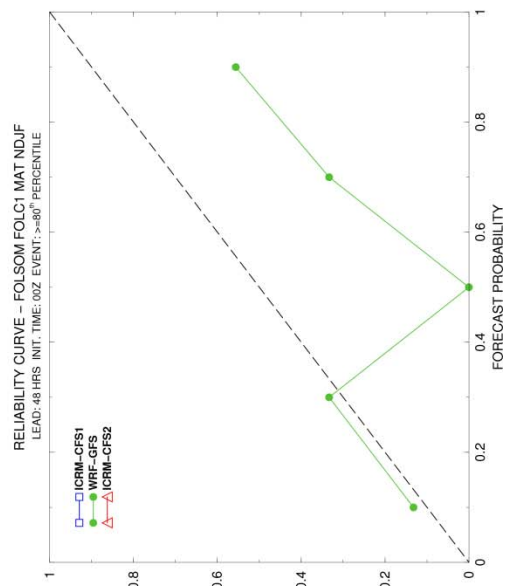
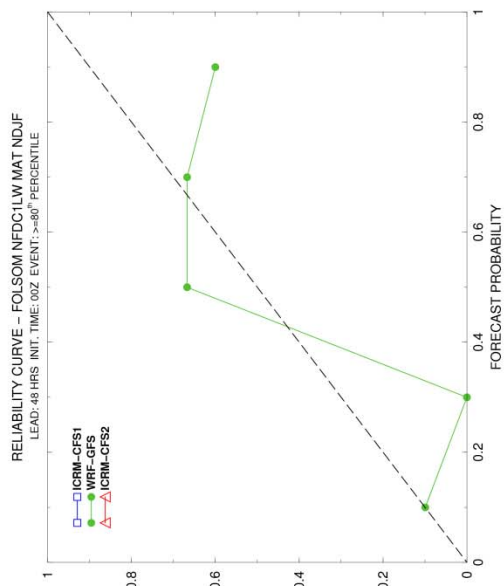


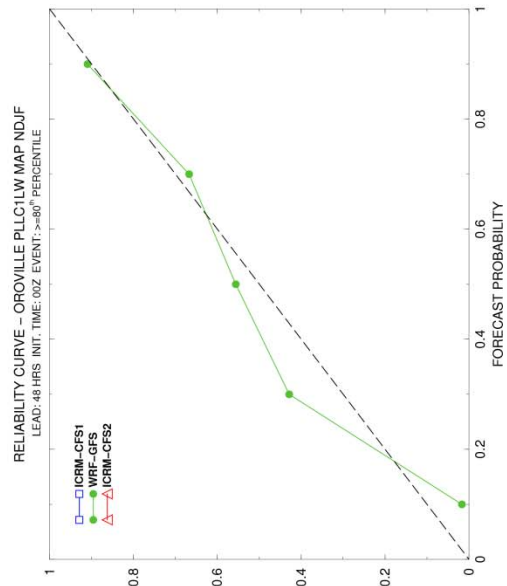
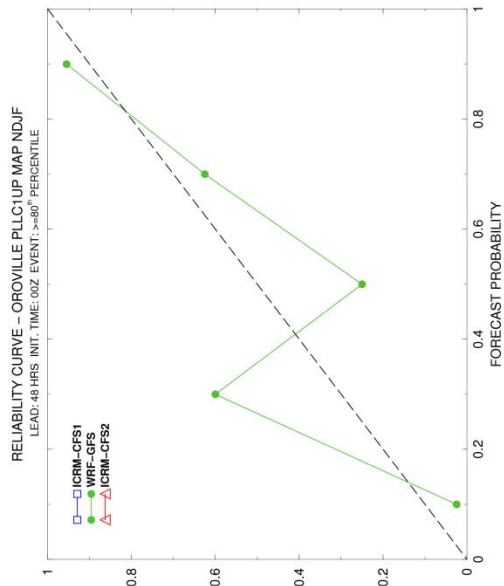
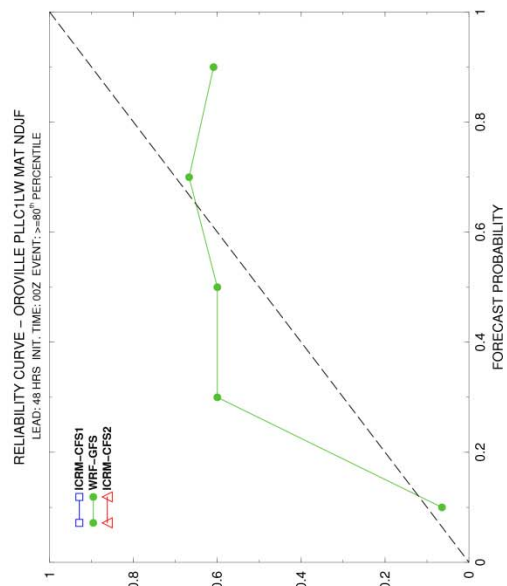
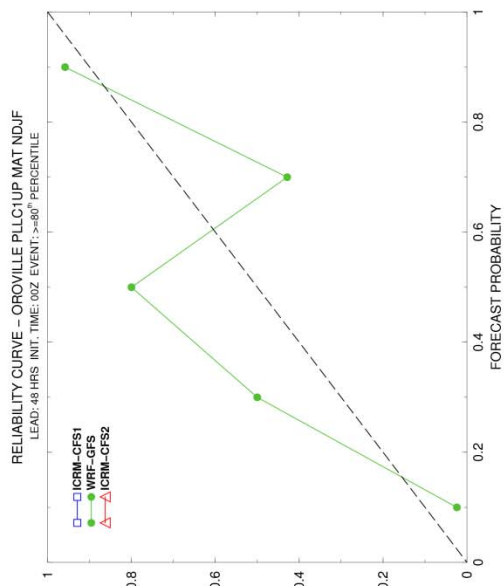


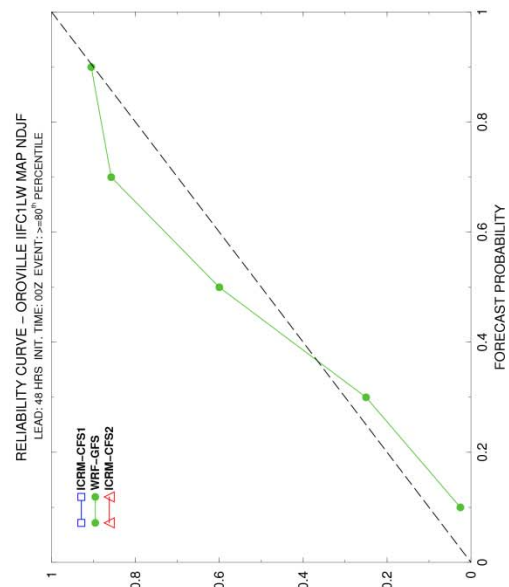
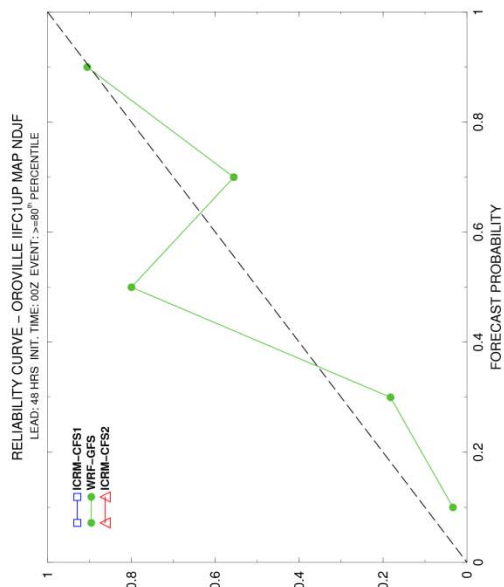
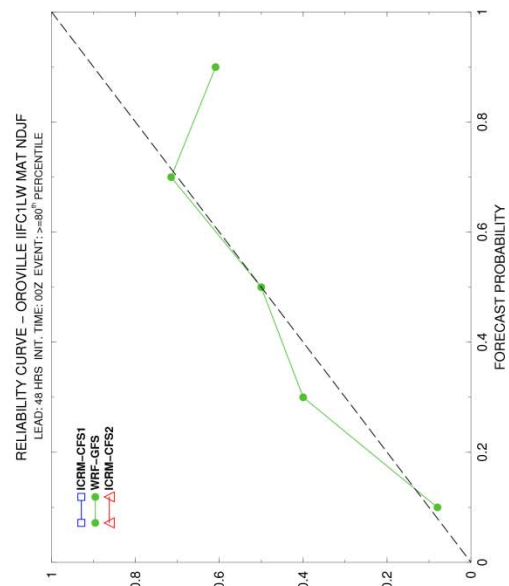
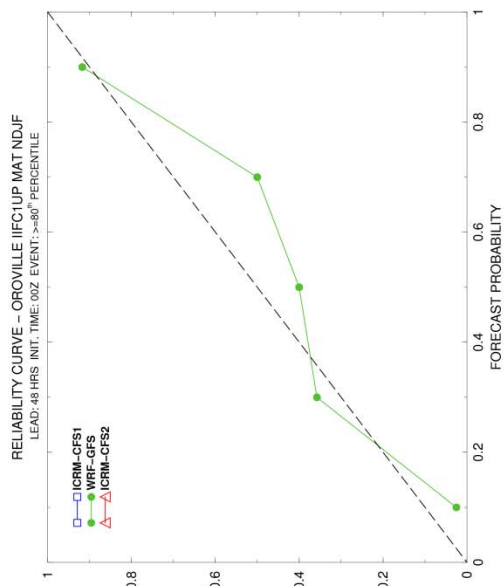


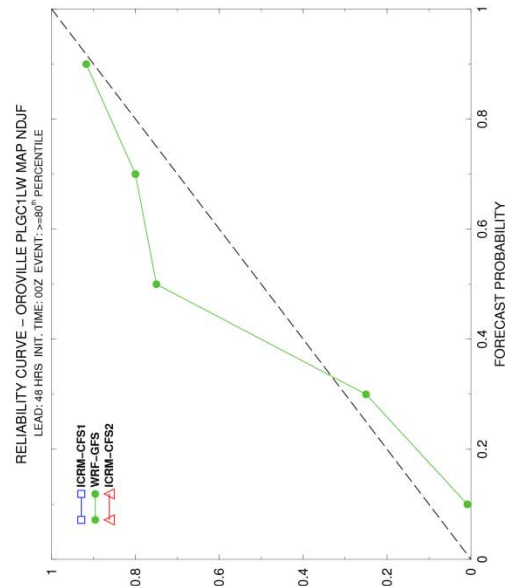
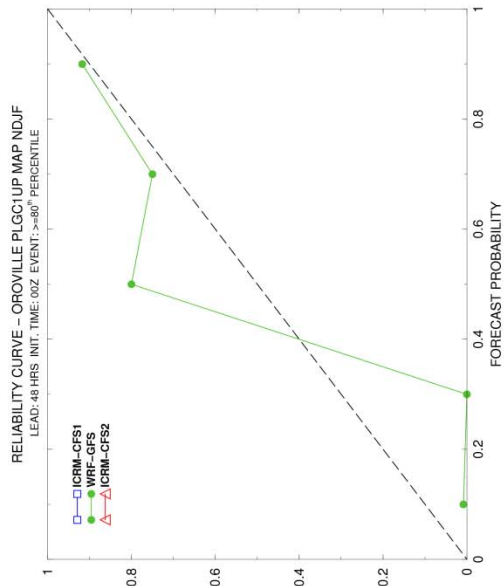
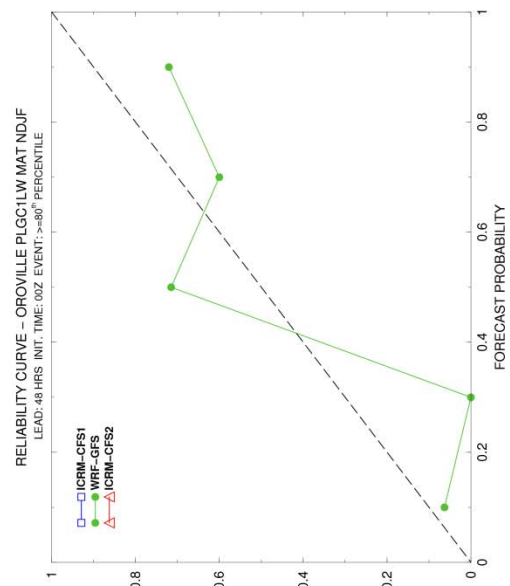
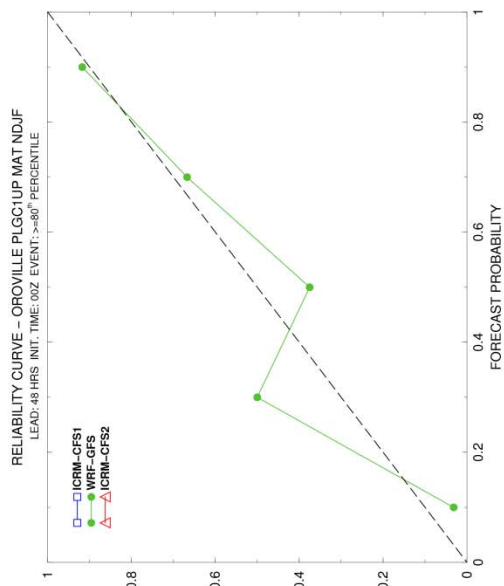


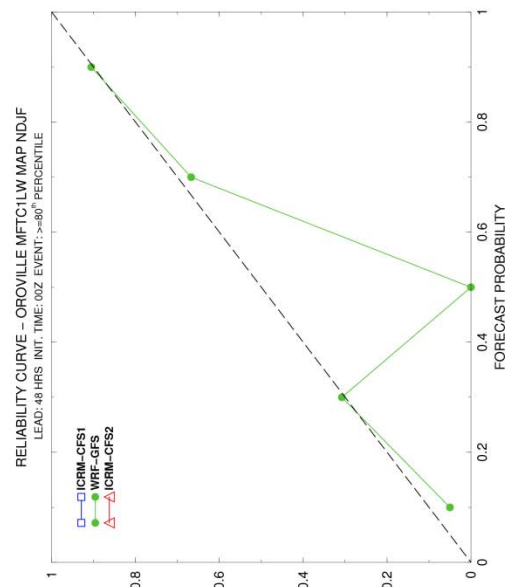
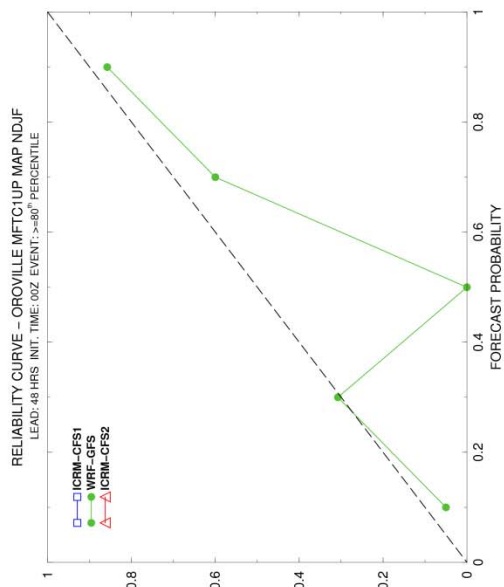
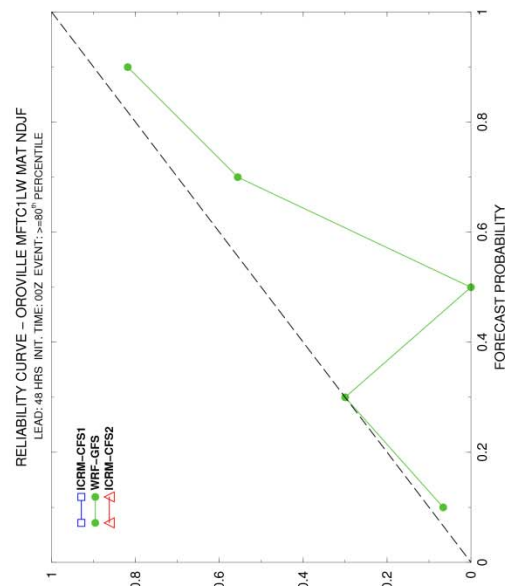
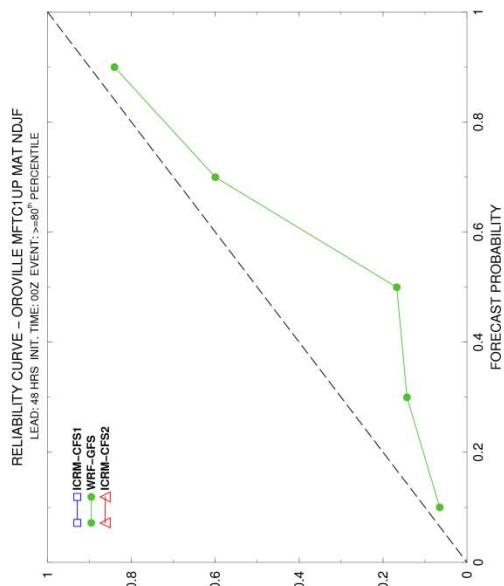


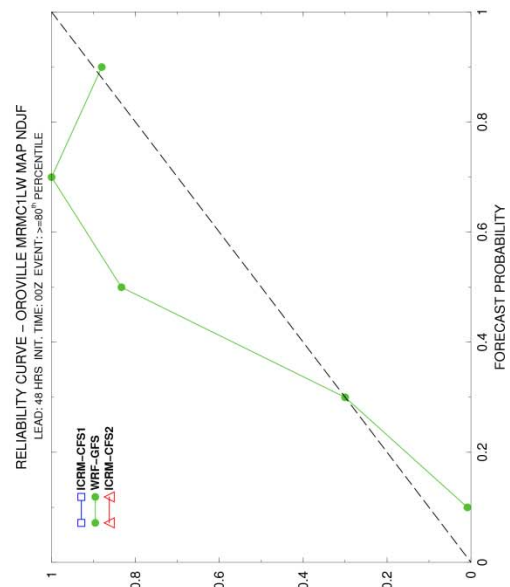
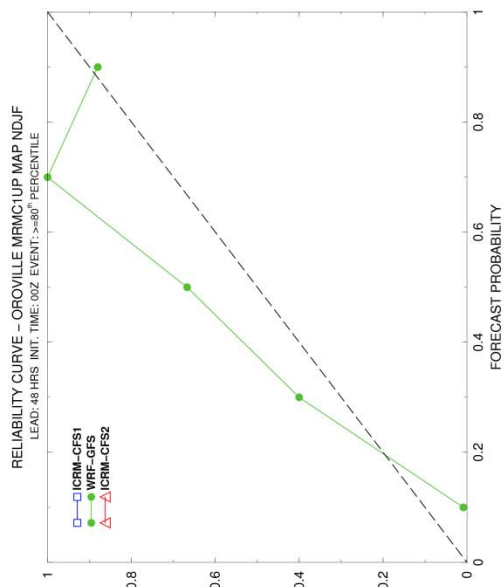
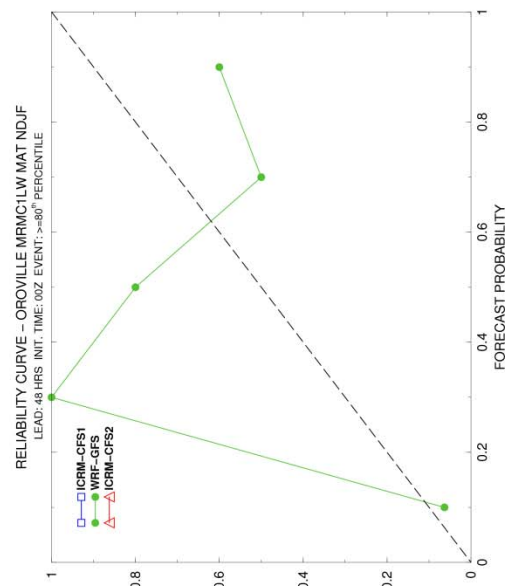
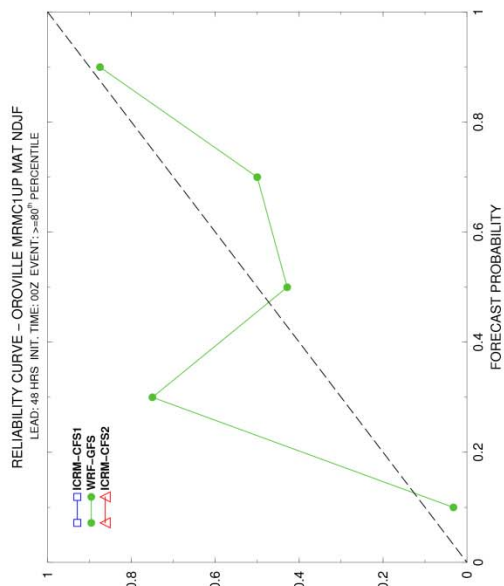


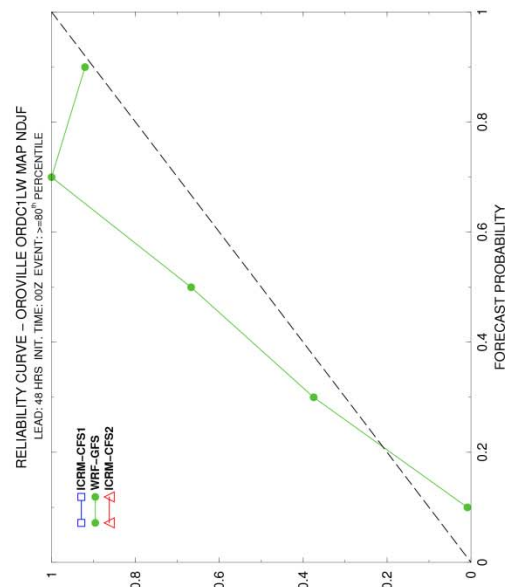
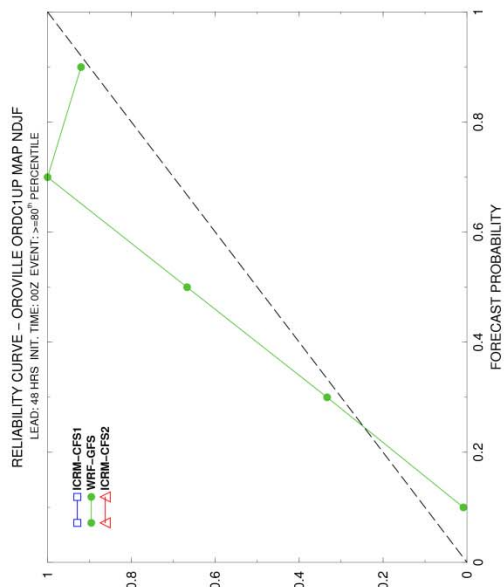
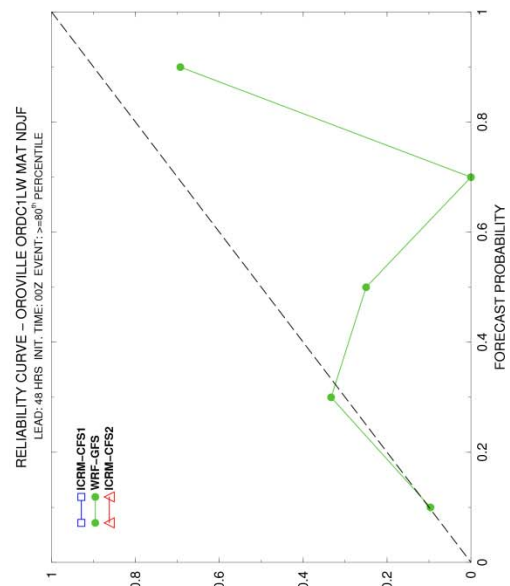
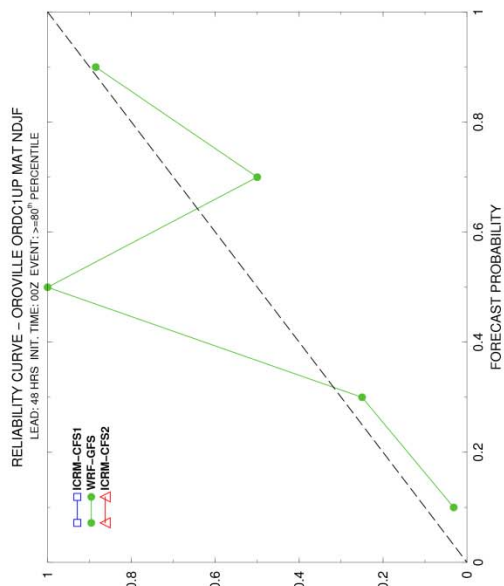


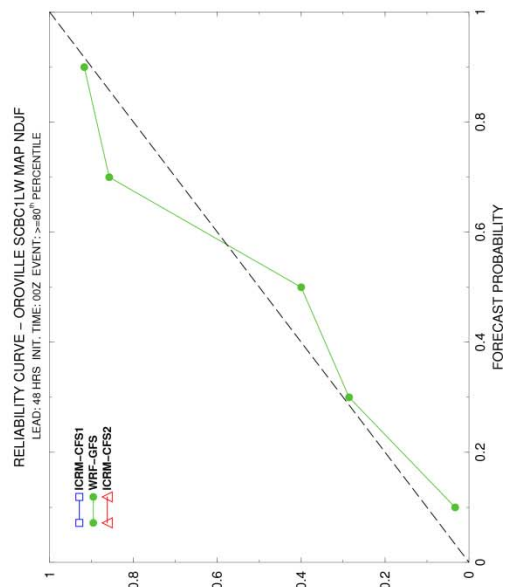
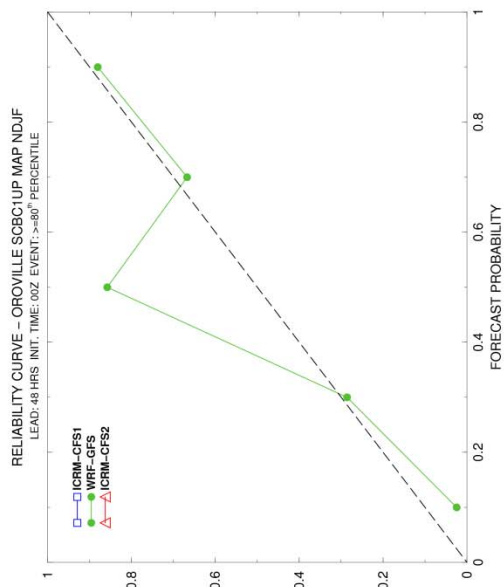
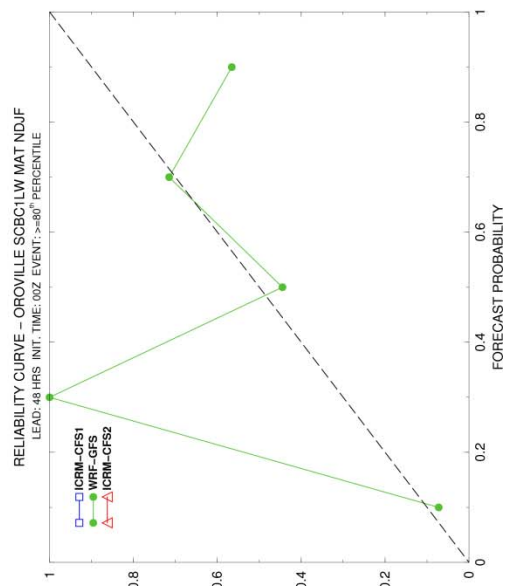
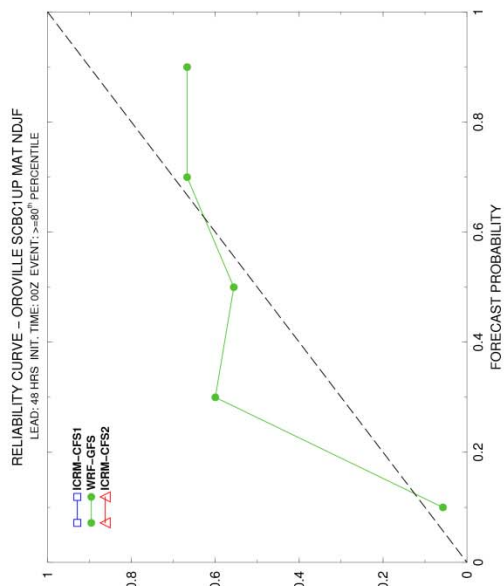


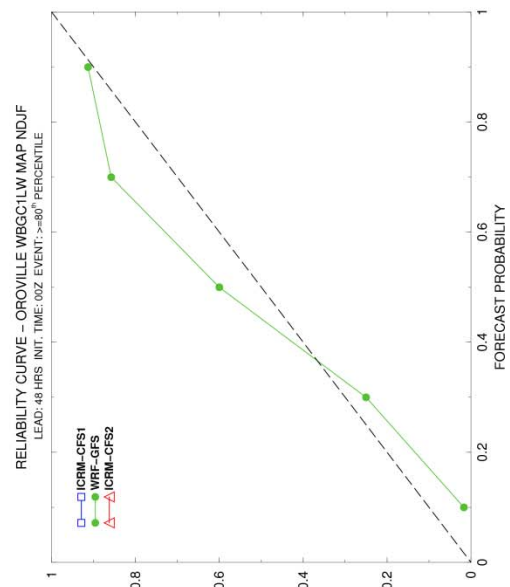
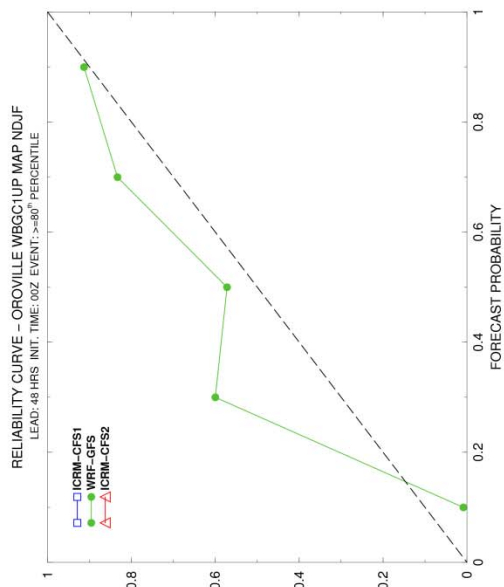
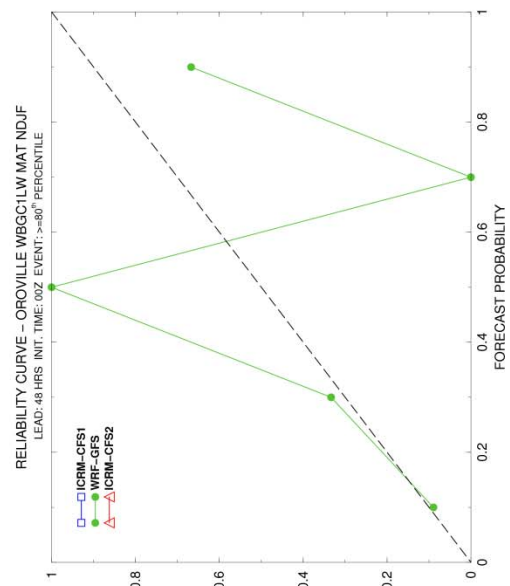
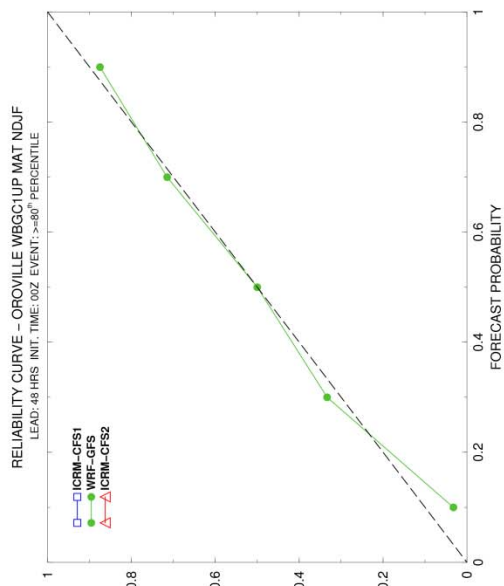


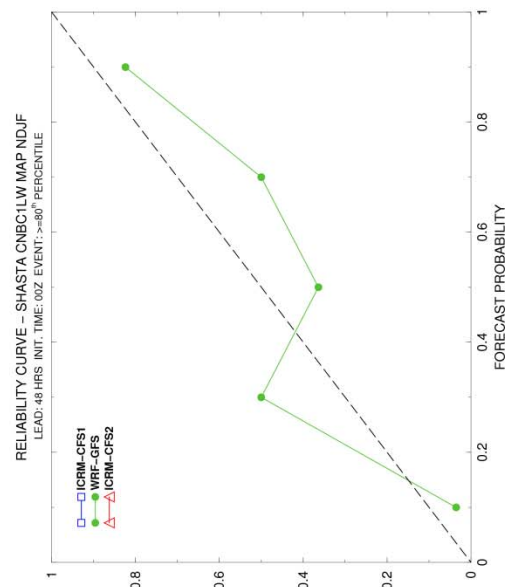
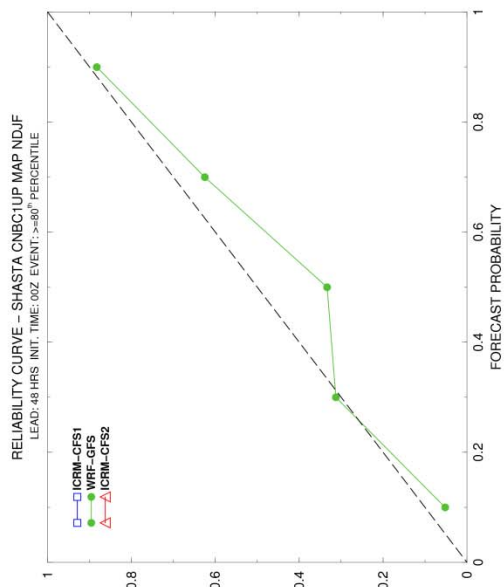
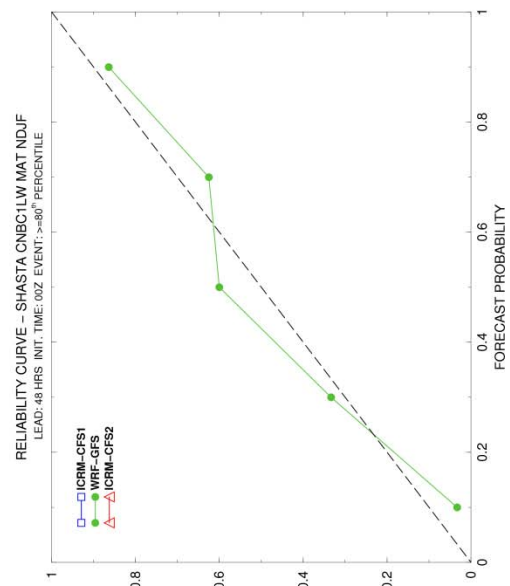
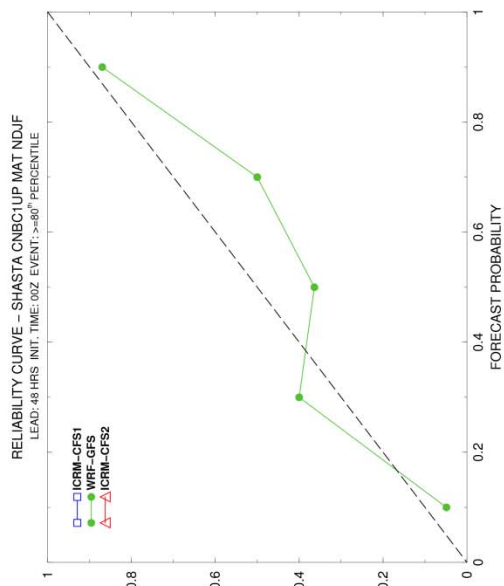


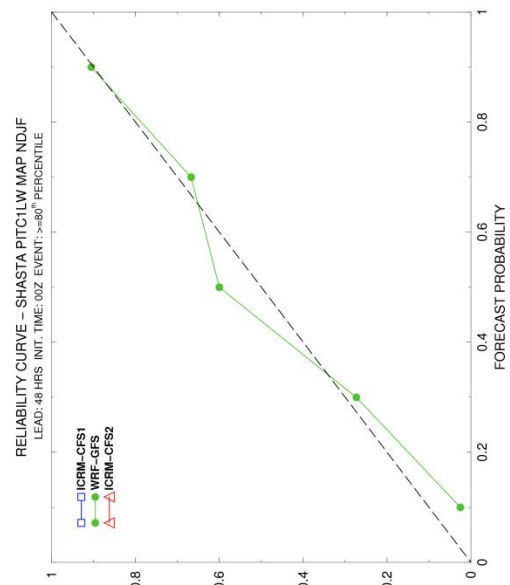
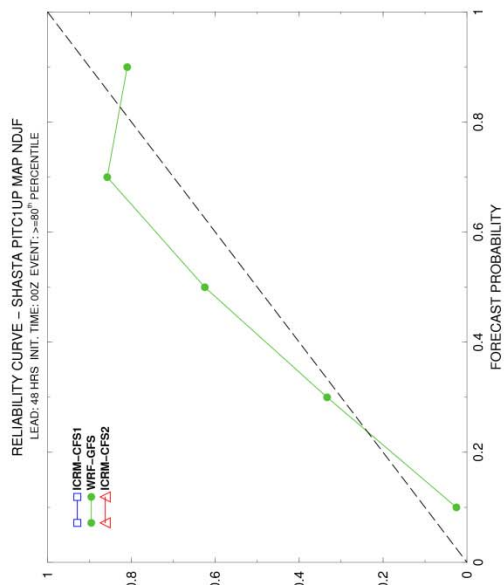
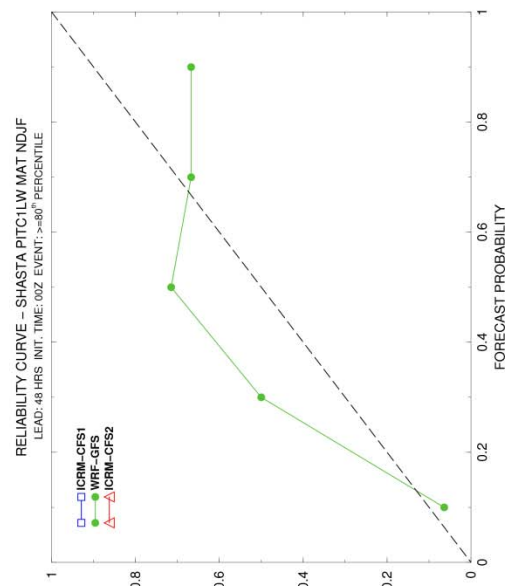
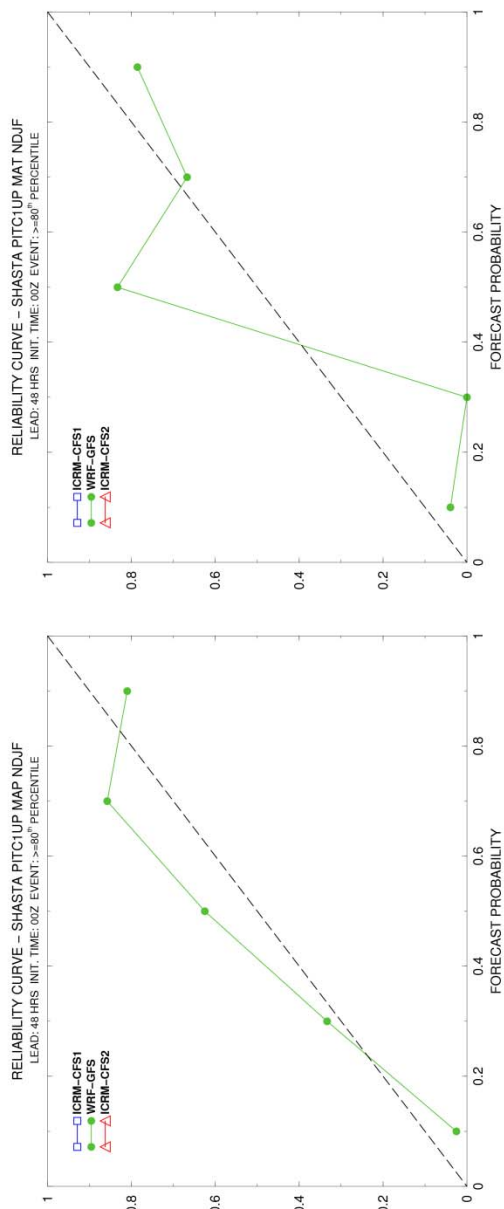


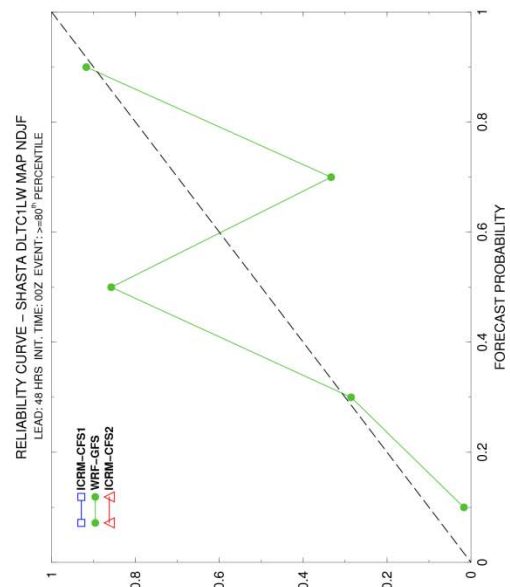
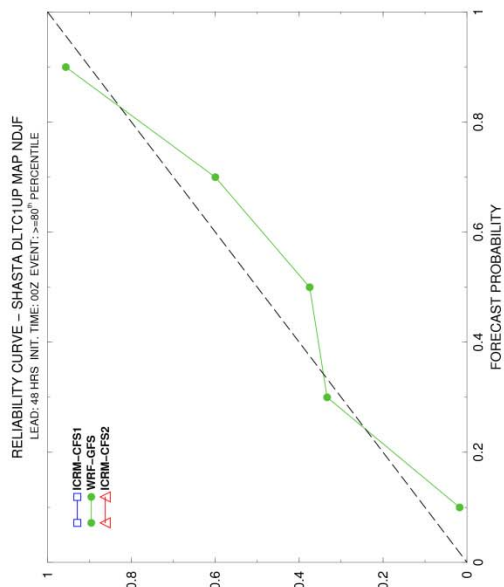
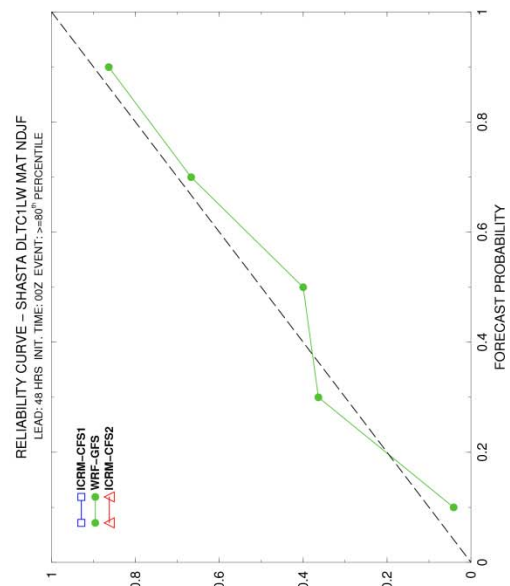
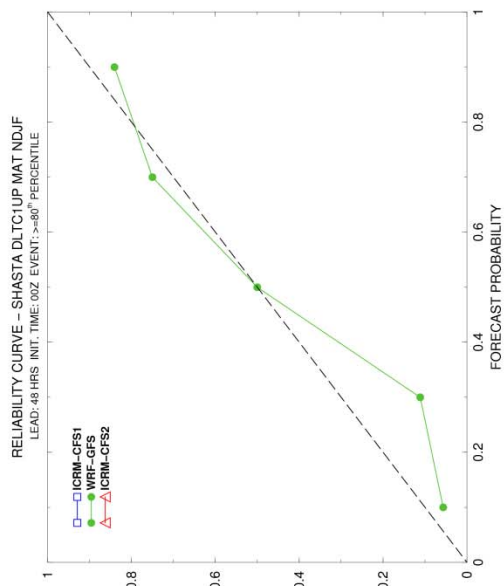


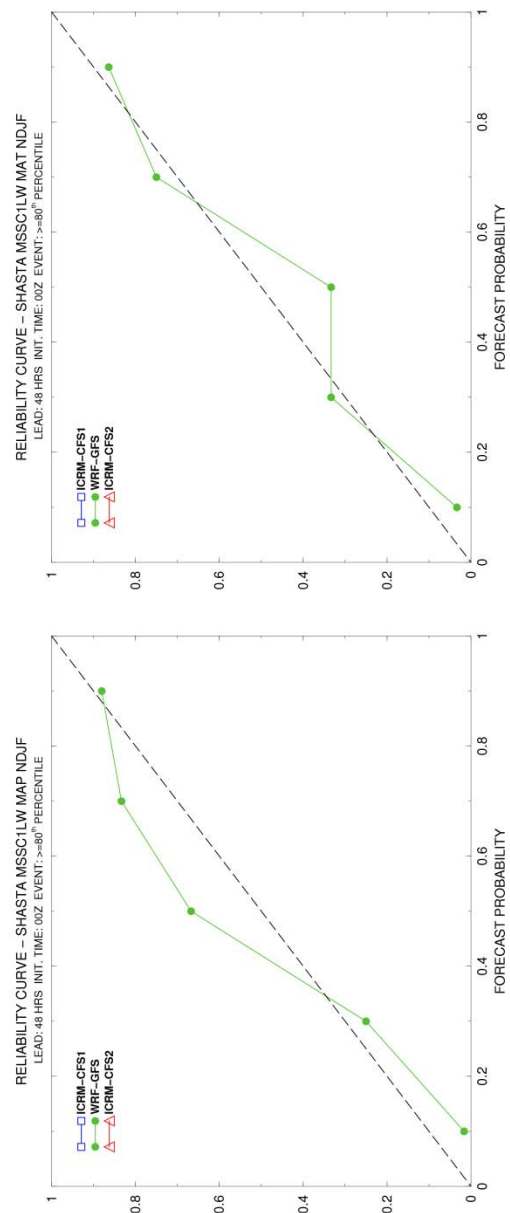
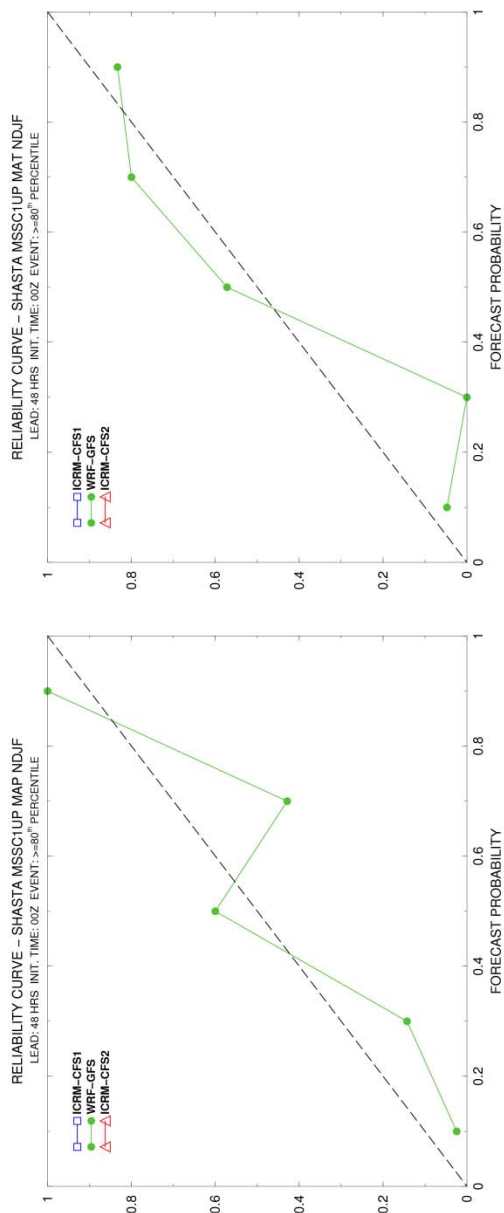


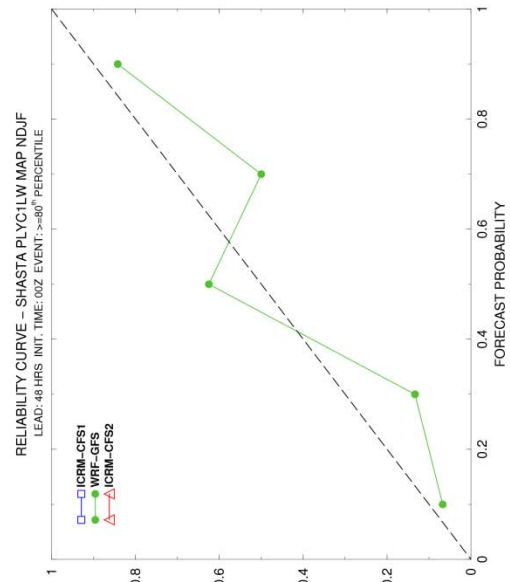
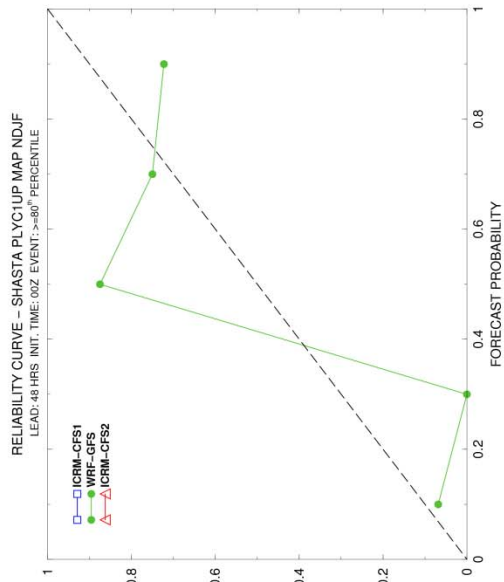
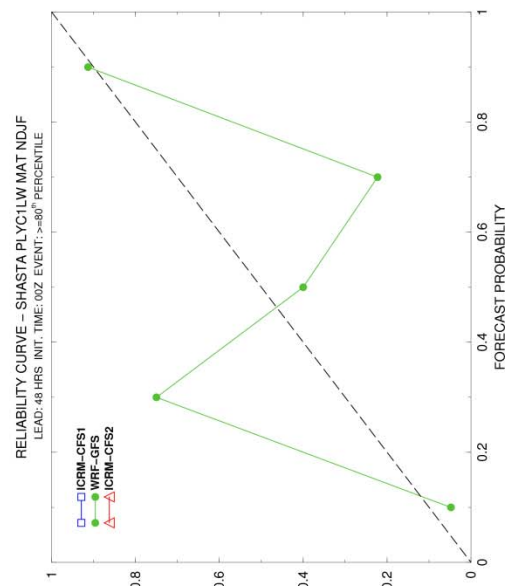
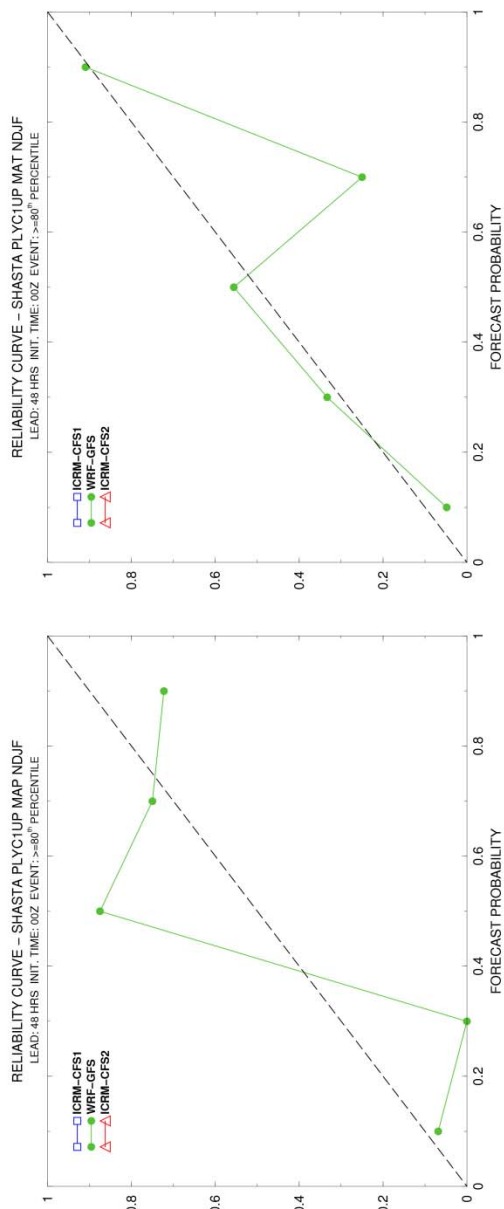


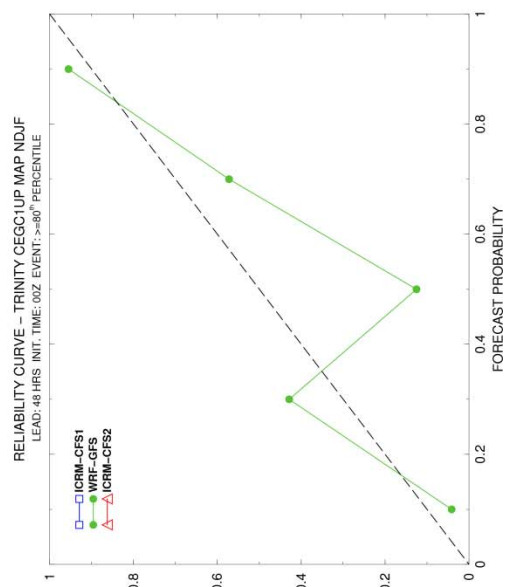
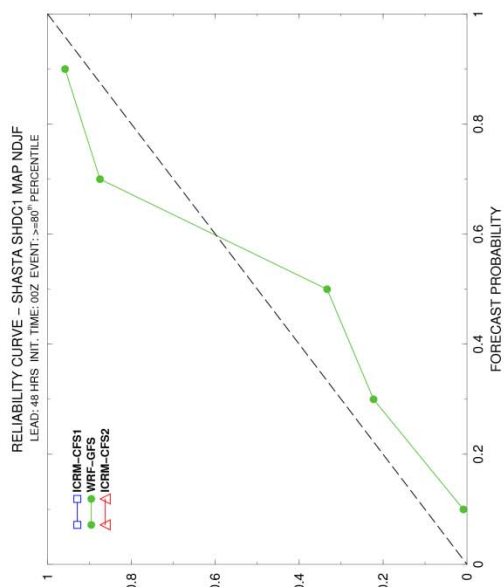
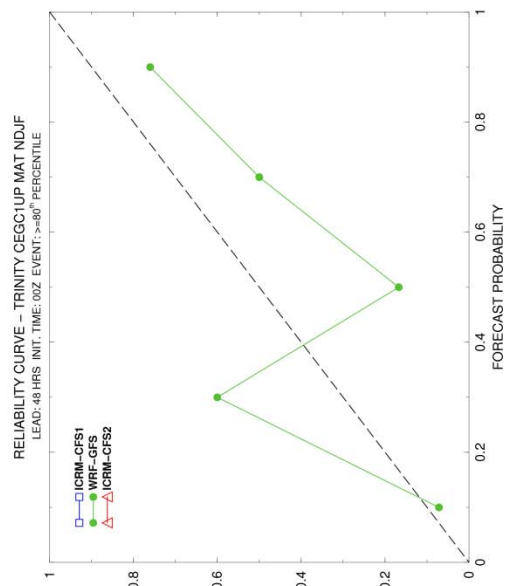
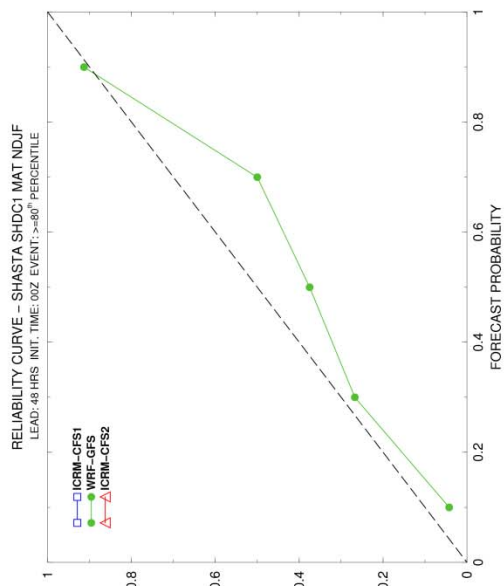


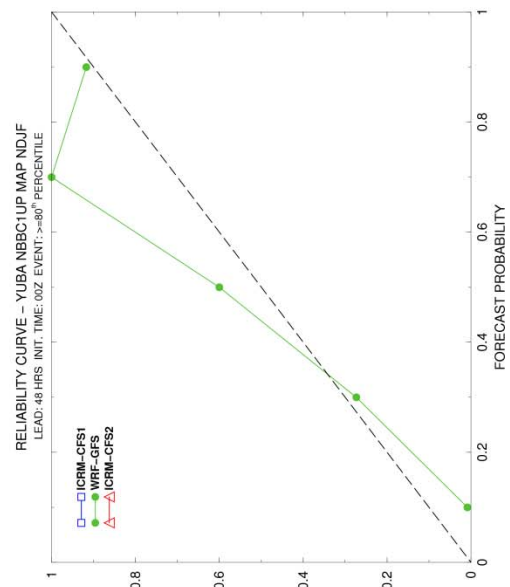
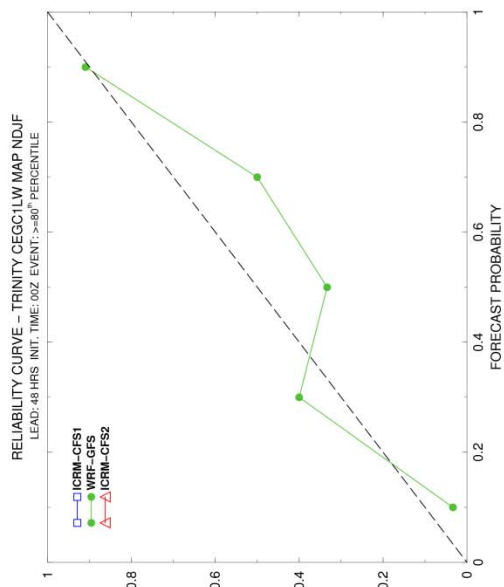
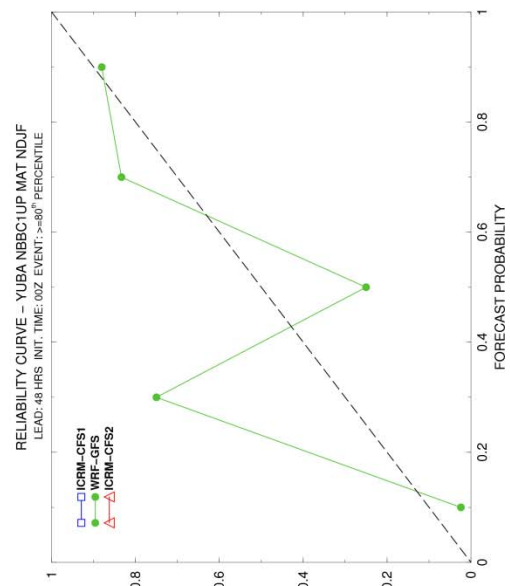
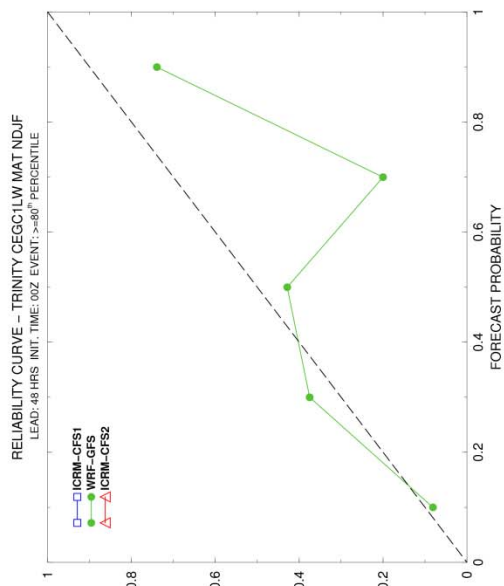


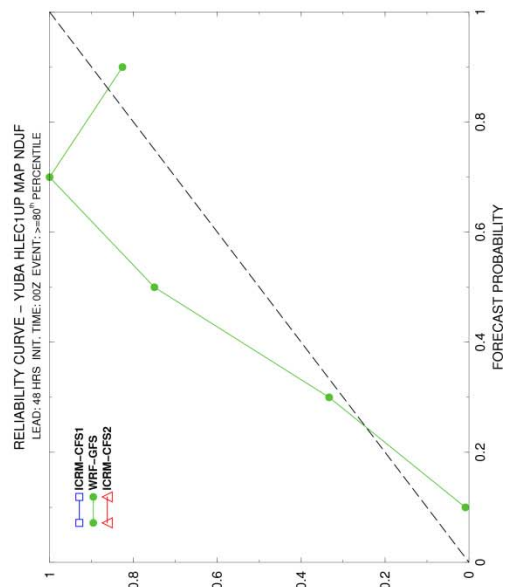
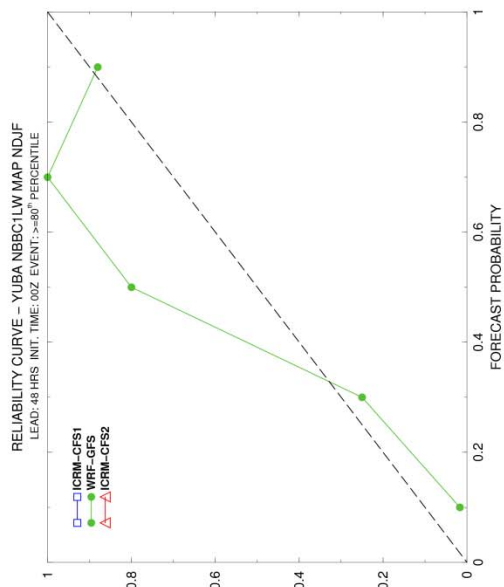
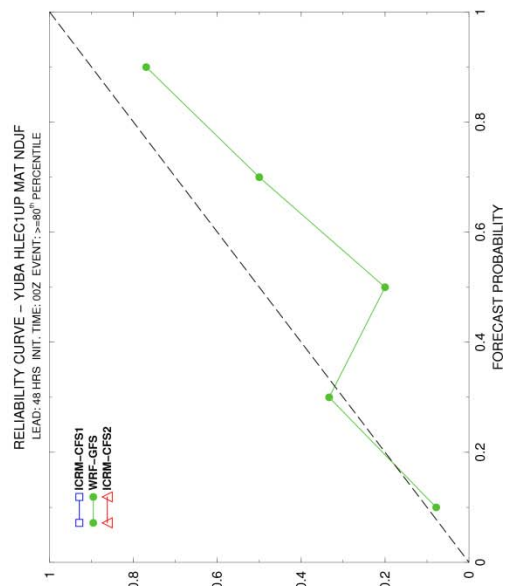
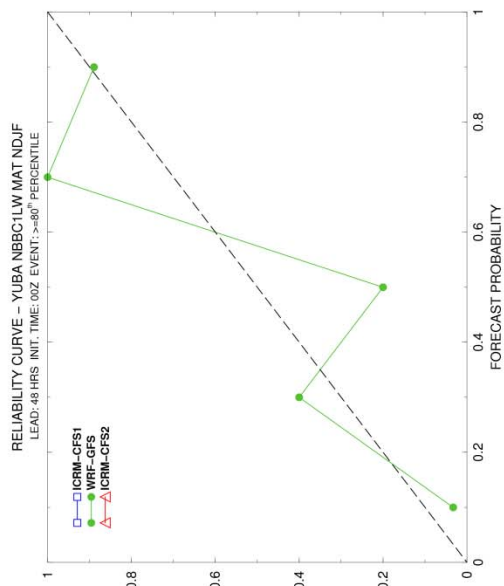


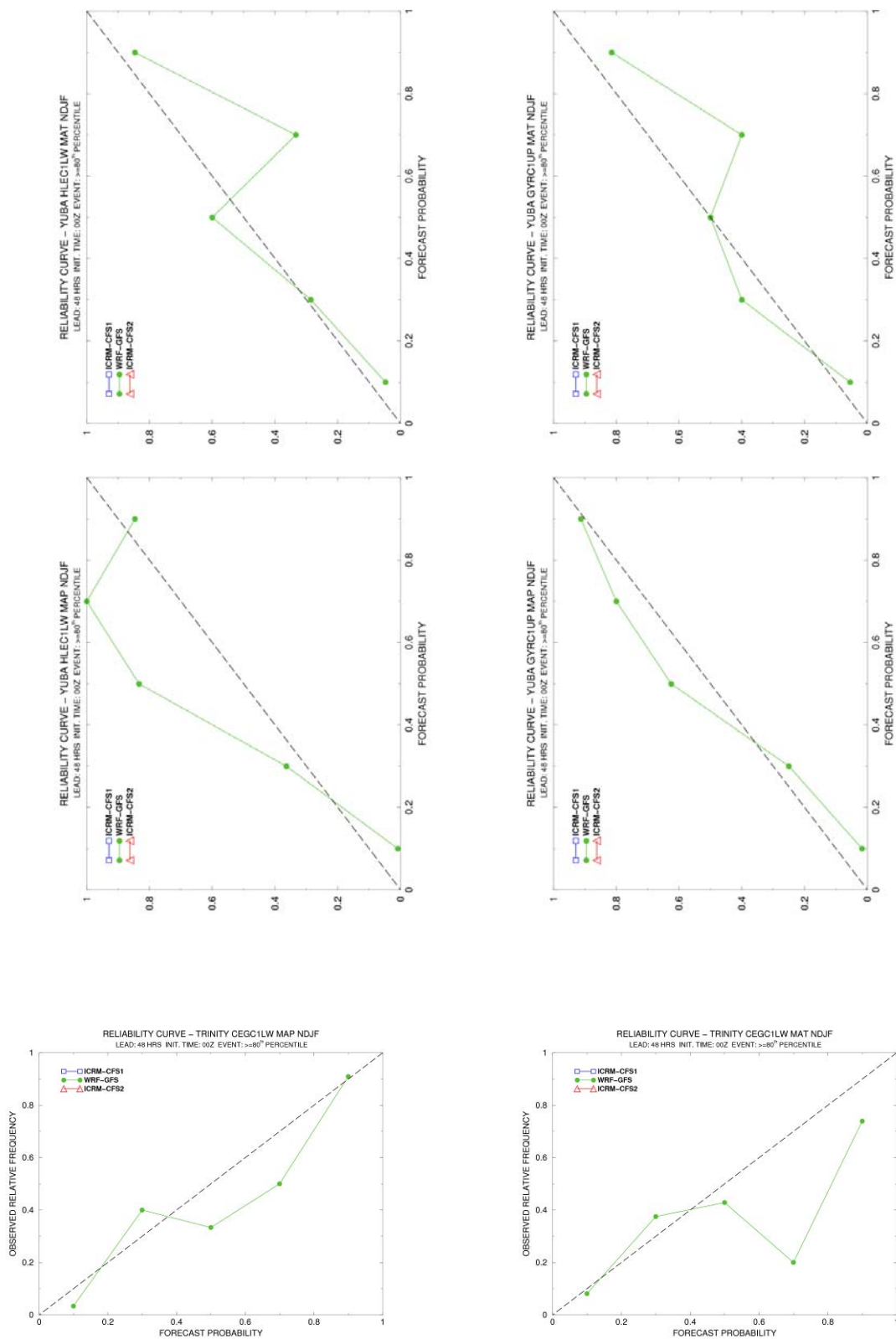






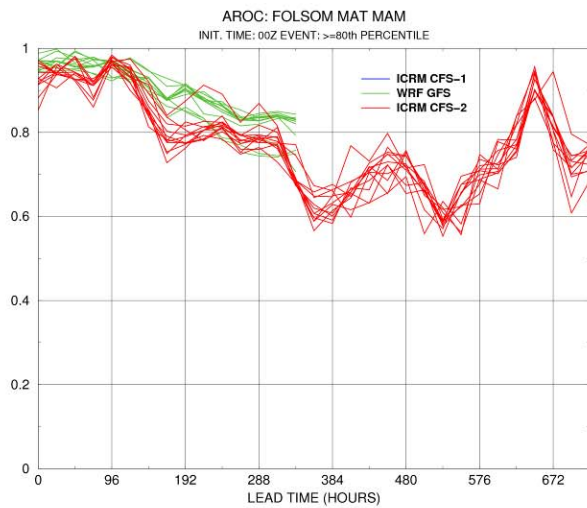
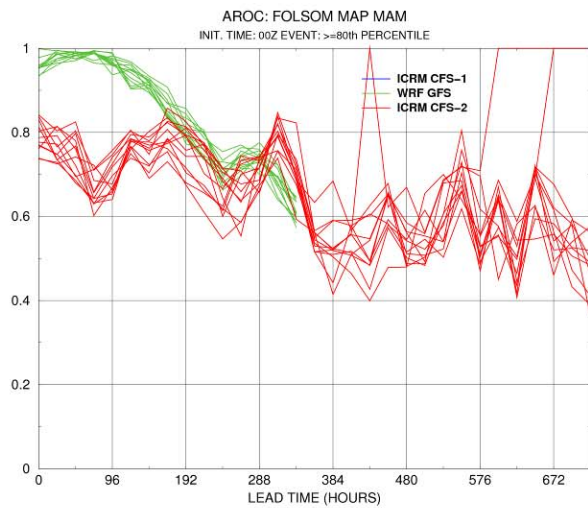
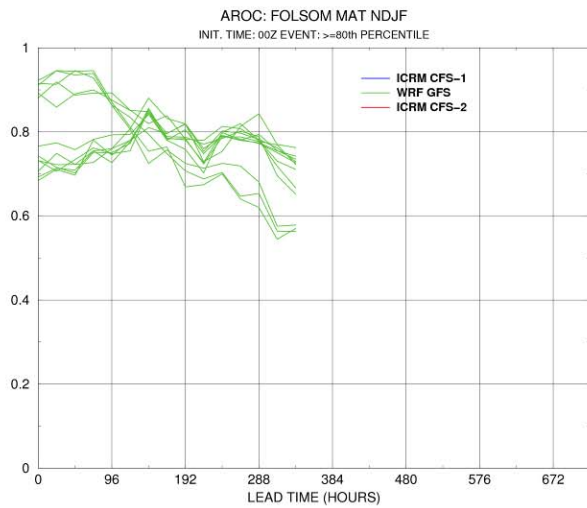
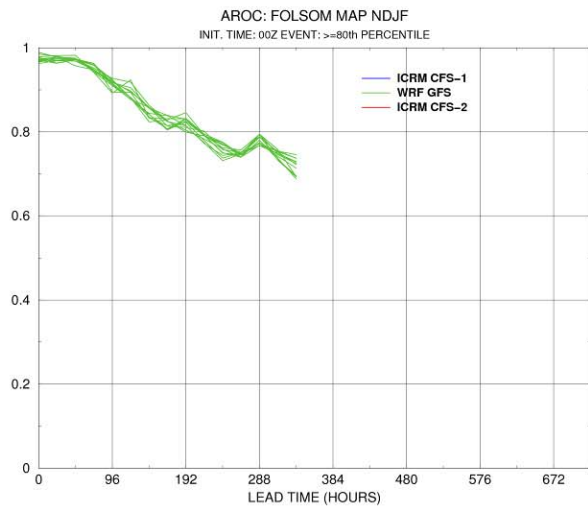


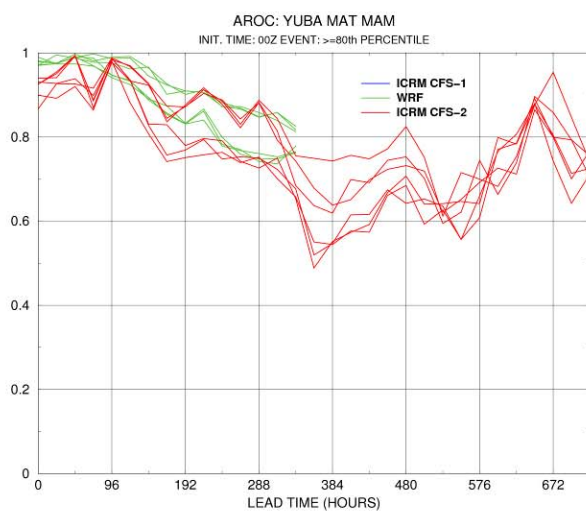
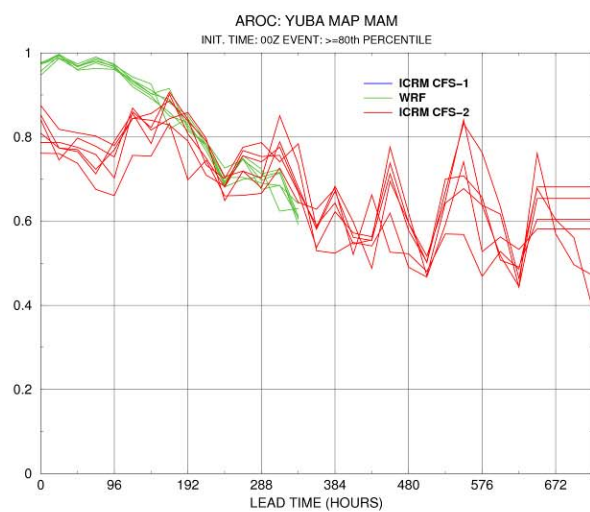
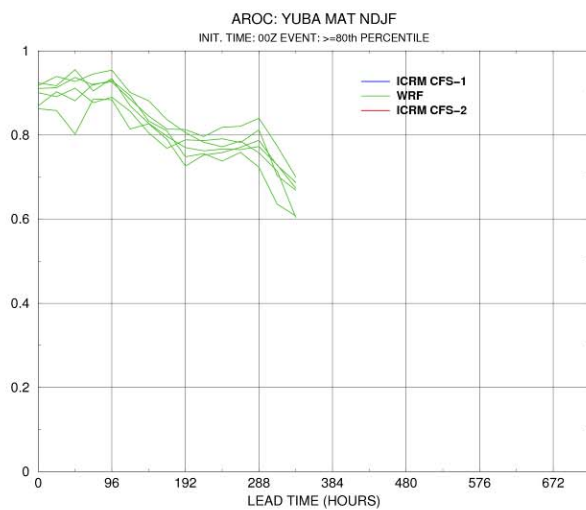
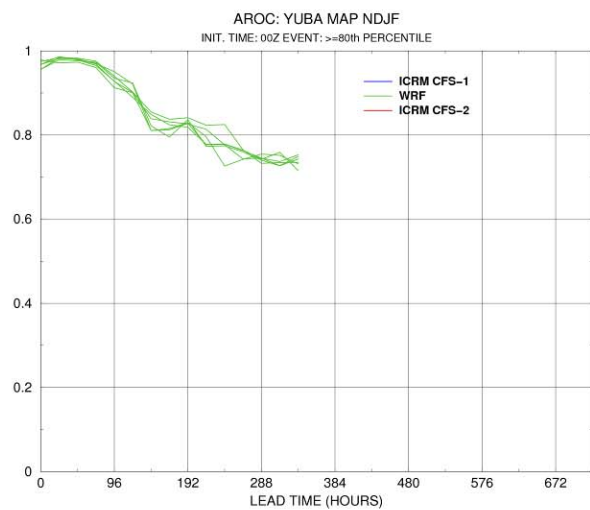


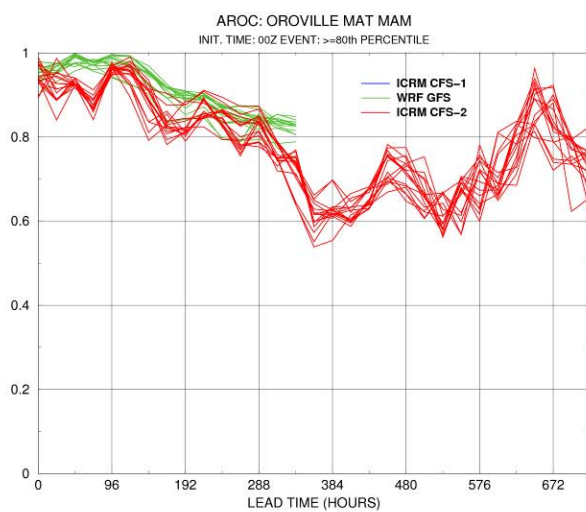
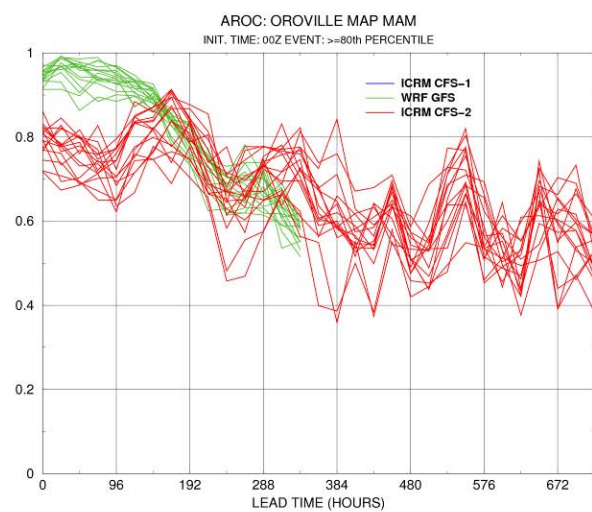
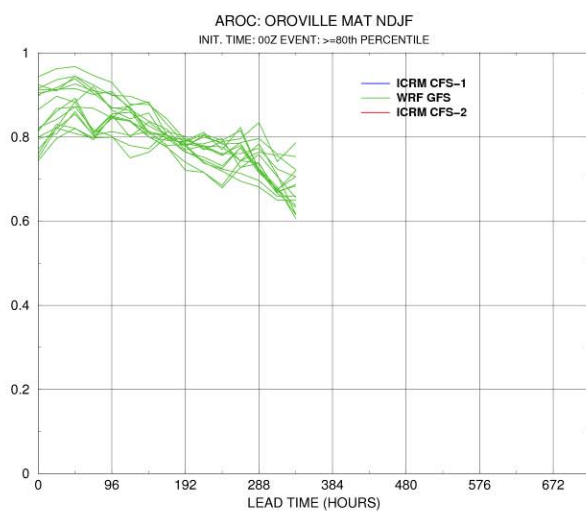
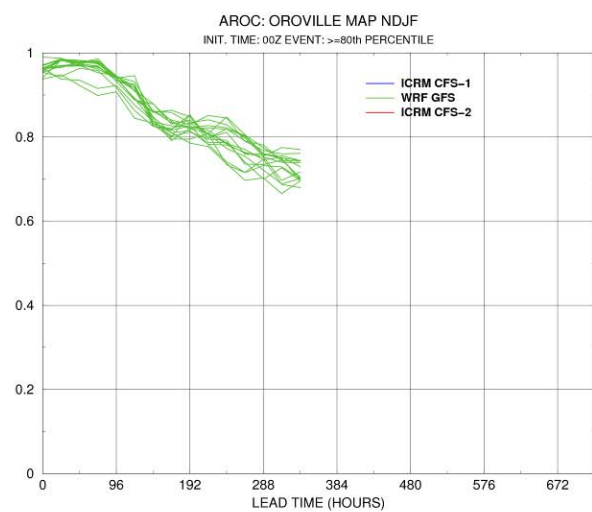


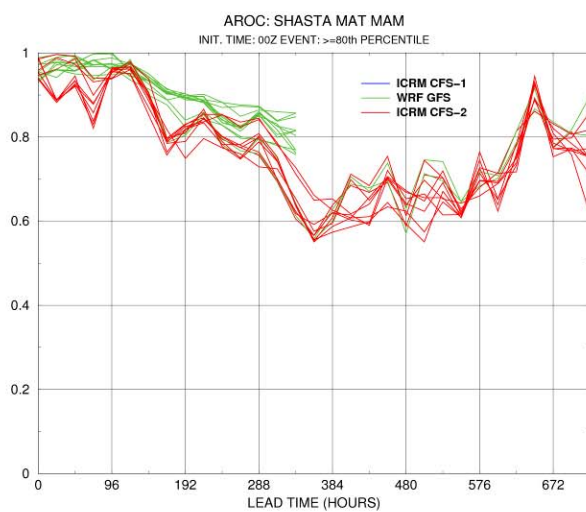
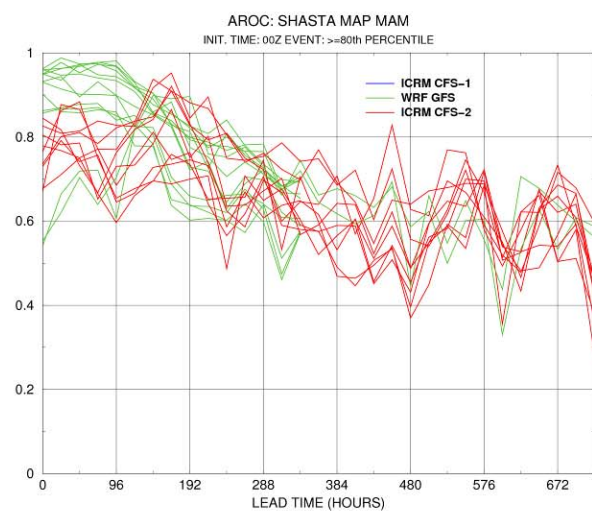
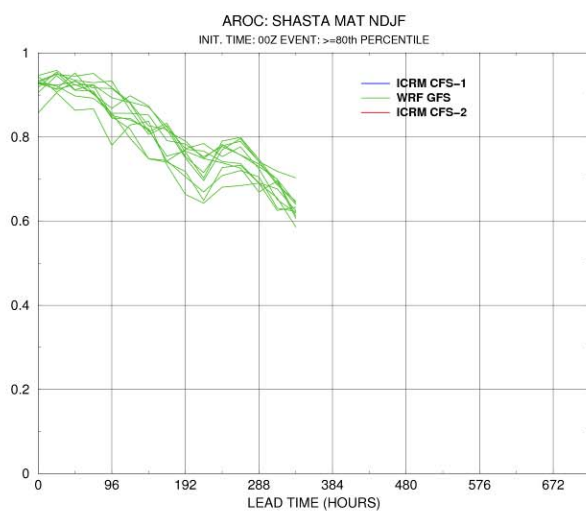
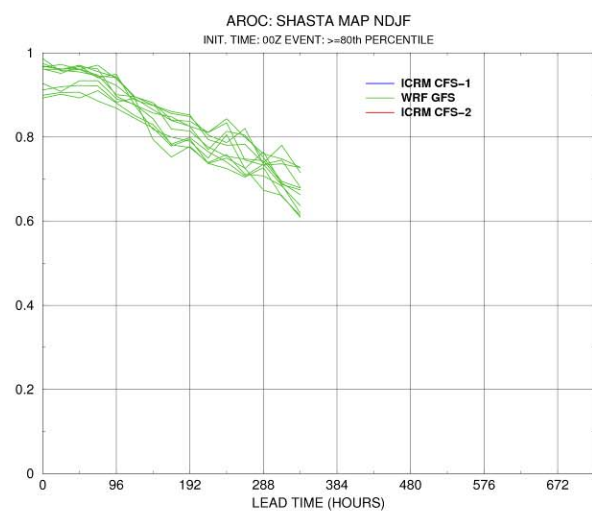
MAP and MAT Relative Operating Characteristic Analysis

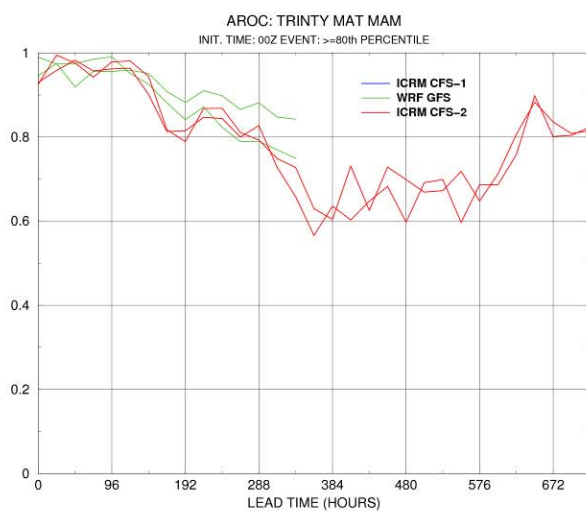
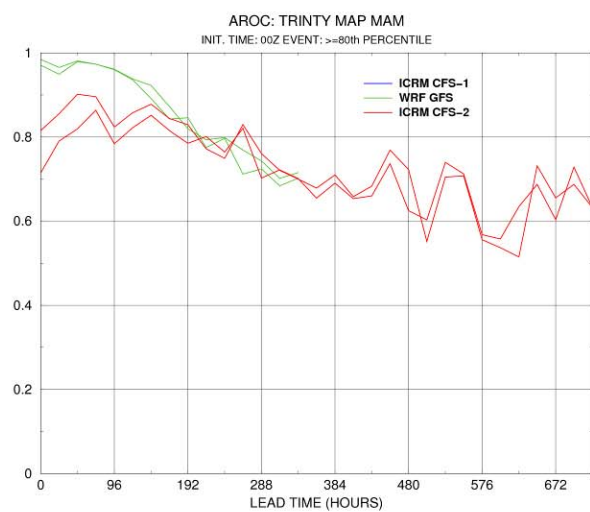
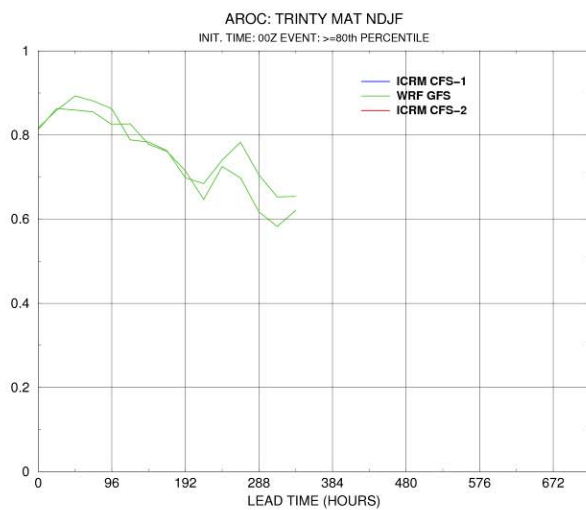
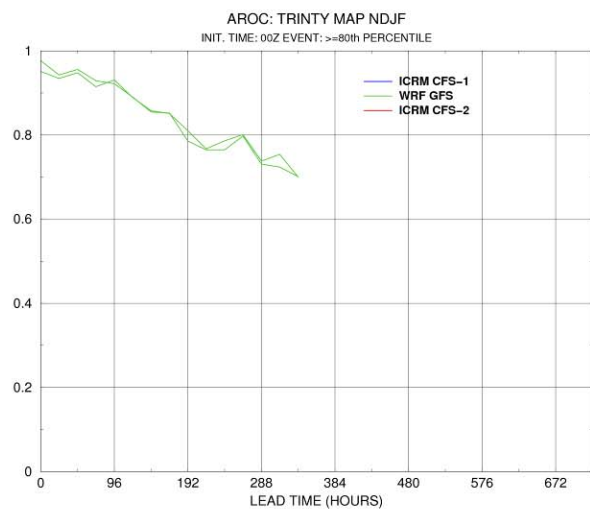
In this section, first the plots of the area under the ROC curve (AROC) are presented for all the INFORM domain watersheds, and, subsequently, the individual subcatchment plots showing the ROC curve are shown for all cases available and for both the GFS-WRF and CFS2-ICRM models.

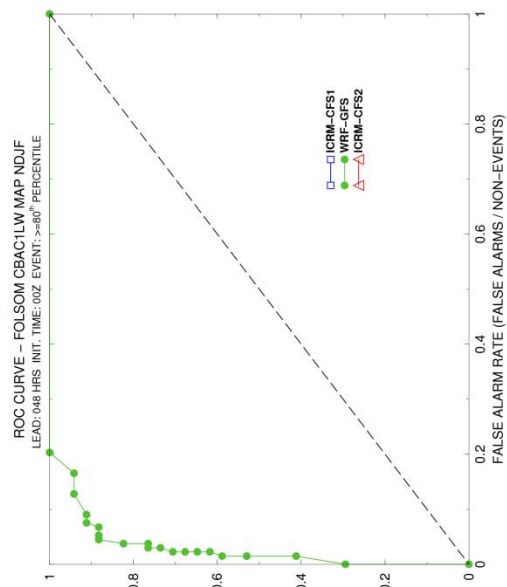
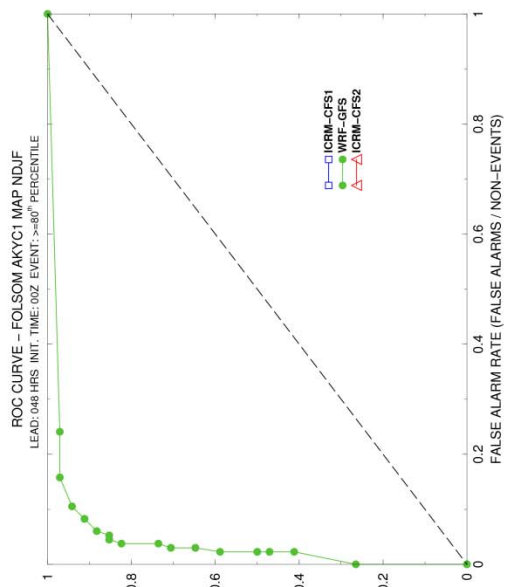
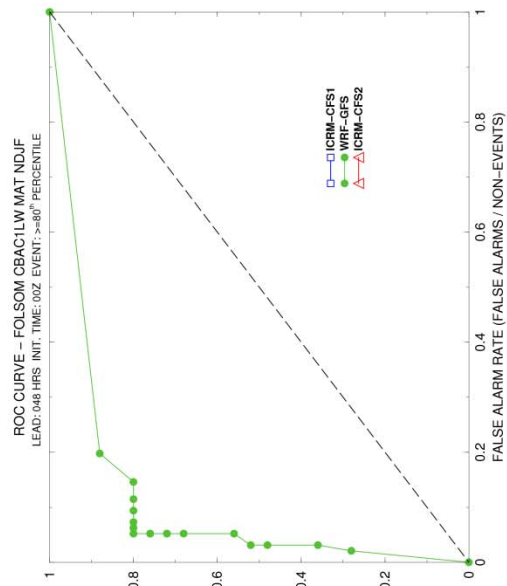
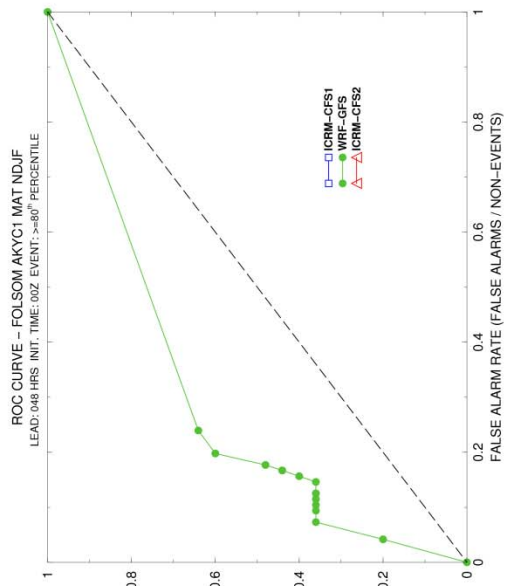


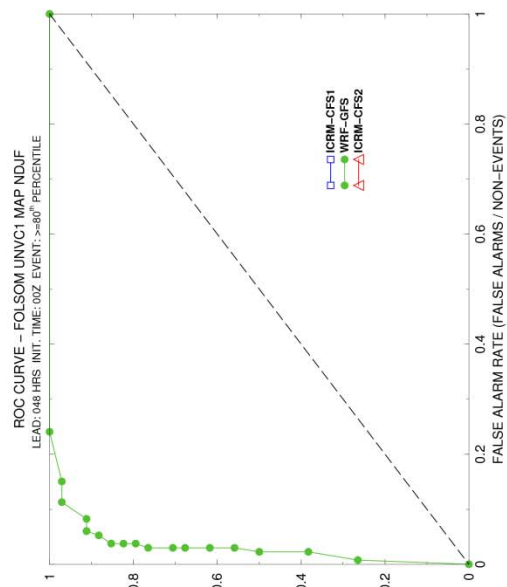
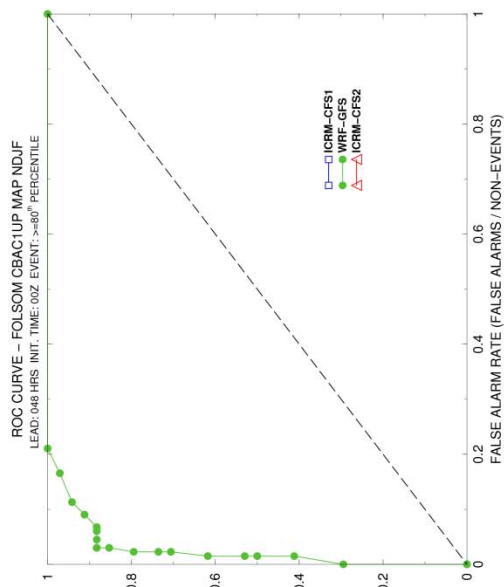
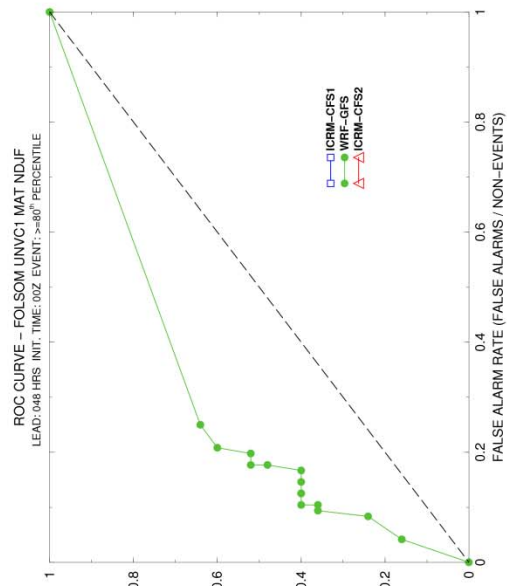
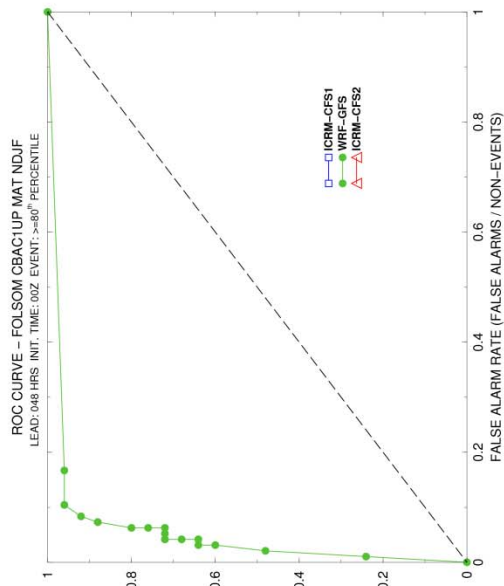


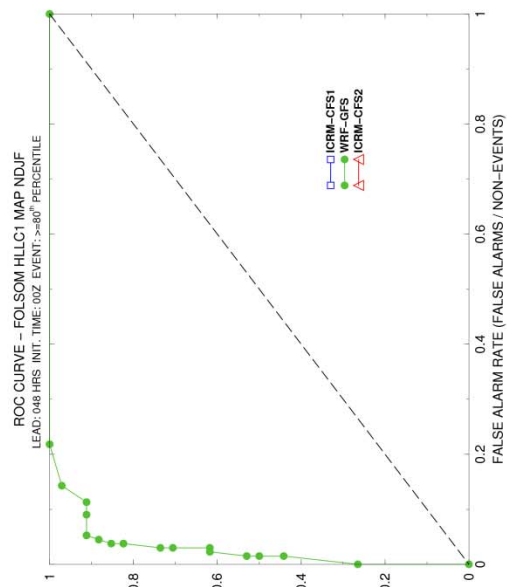
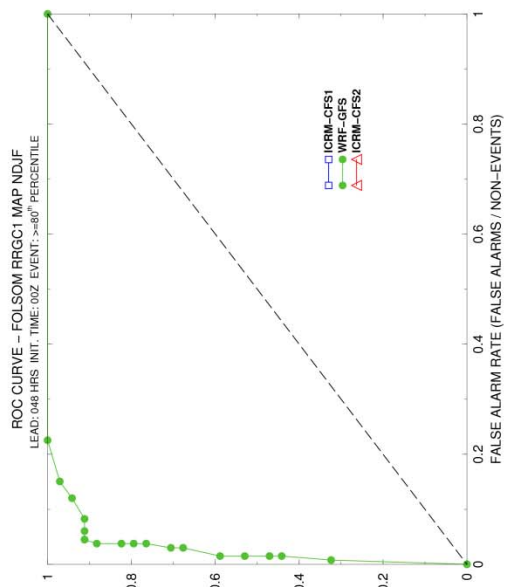
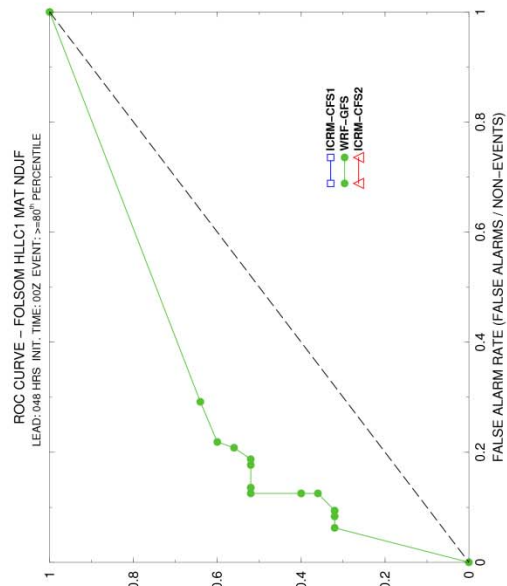
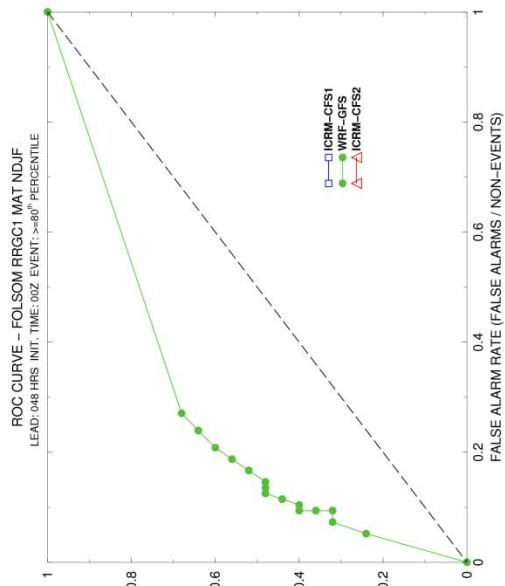


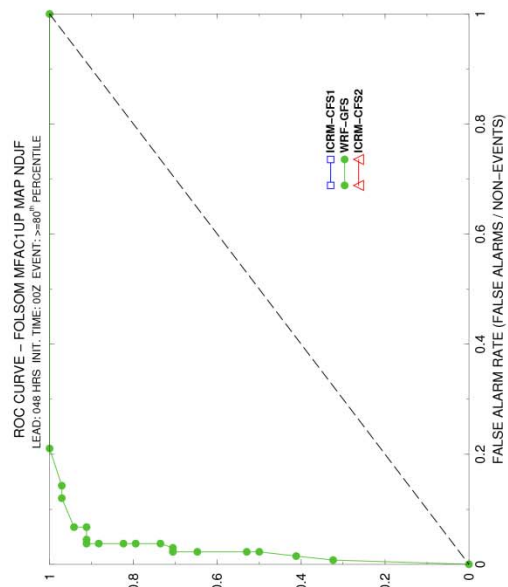
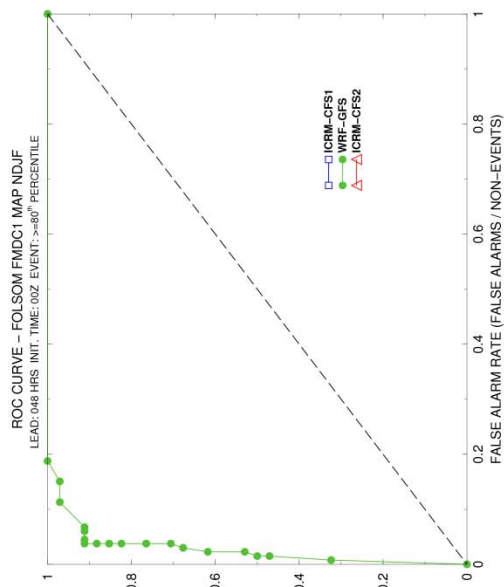
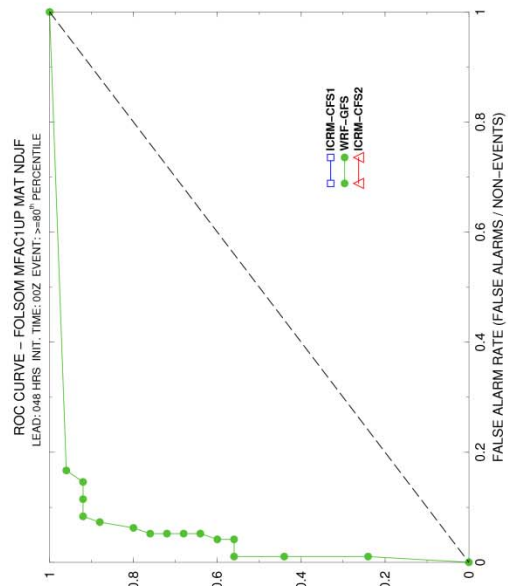
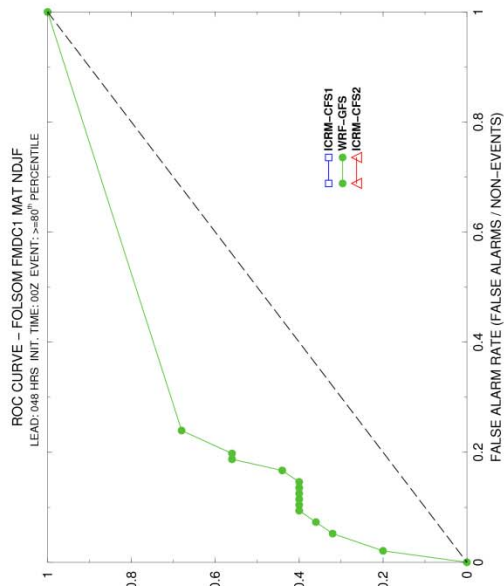


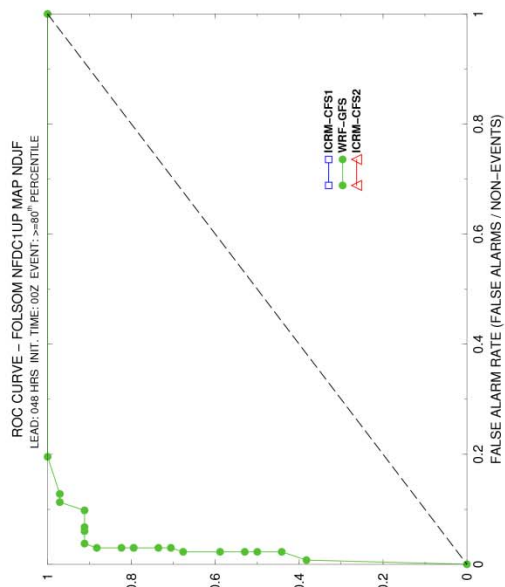
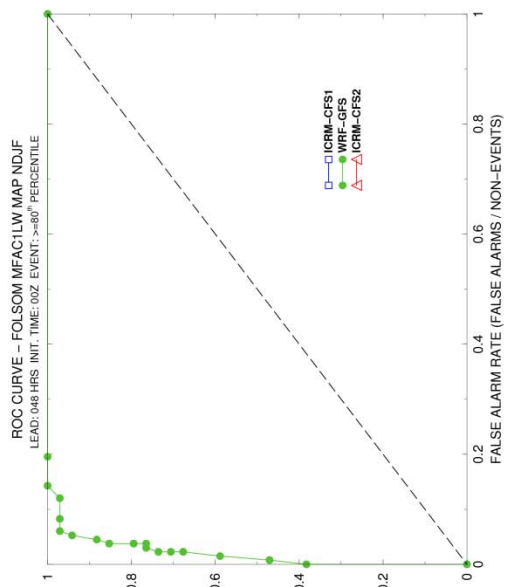
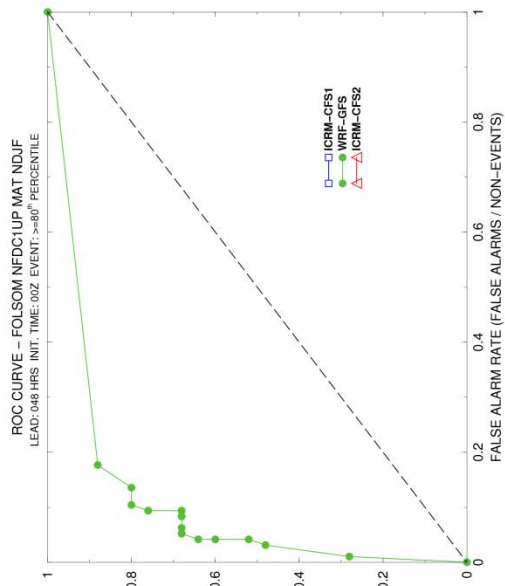
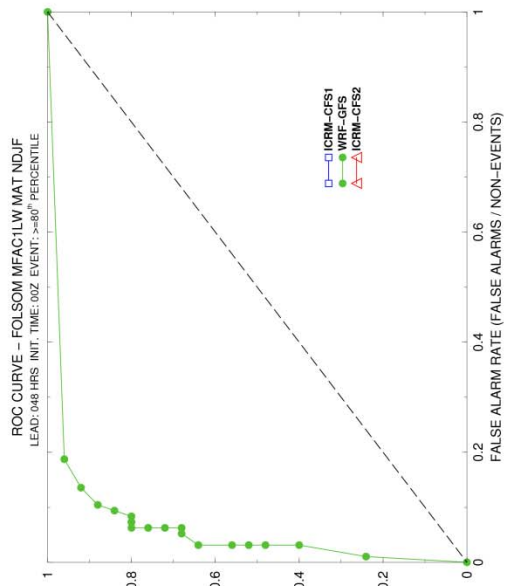


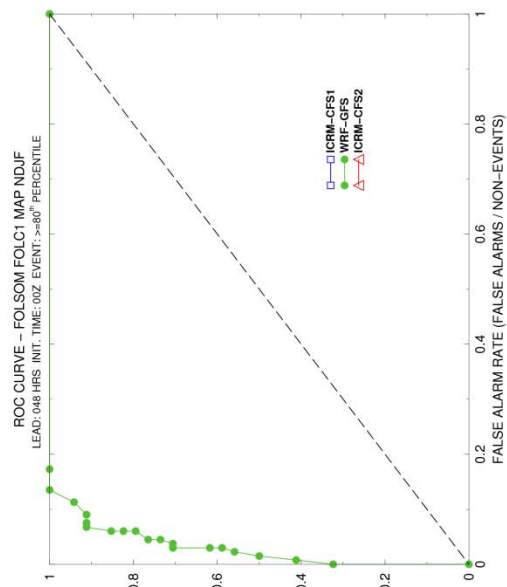
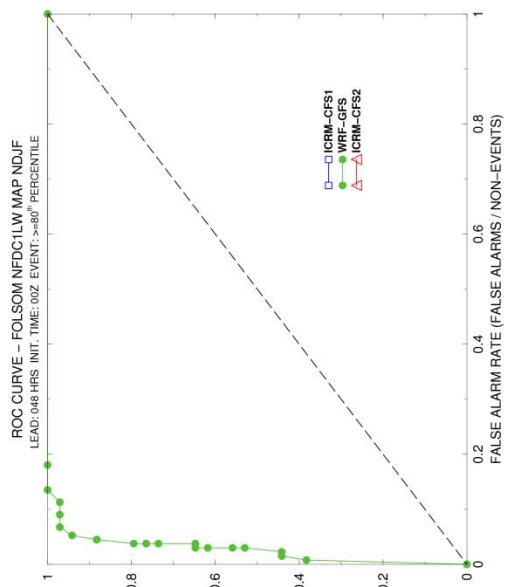
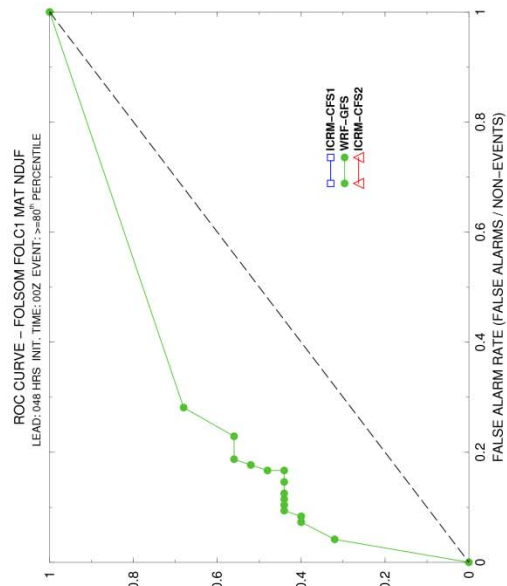
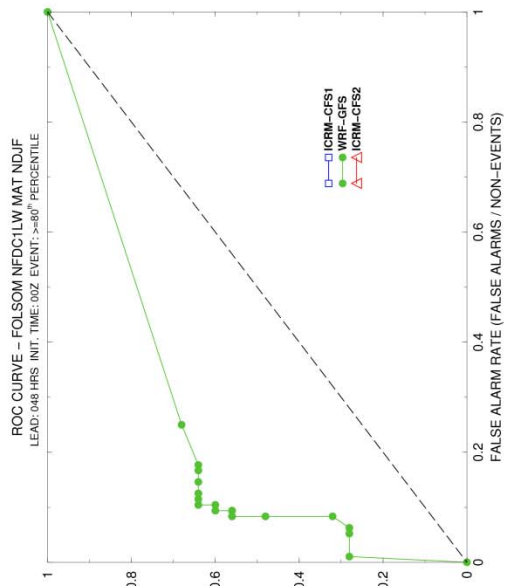


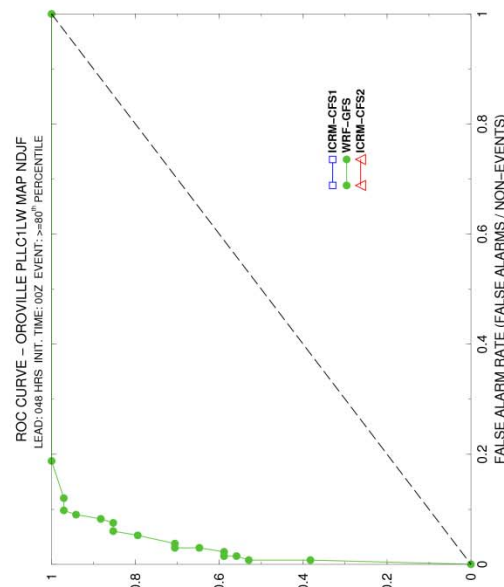
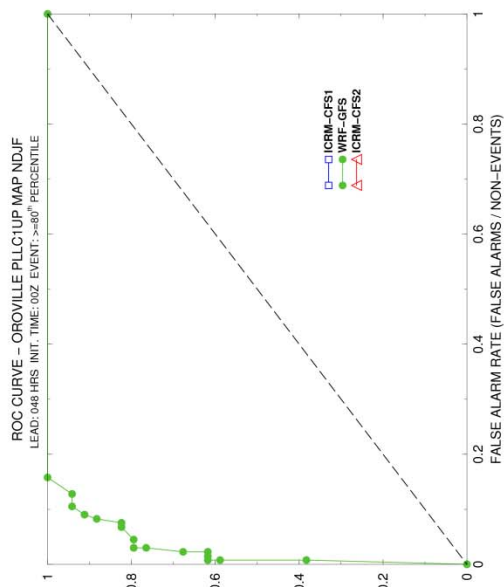
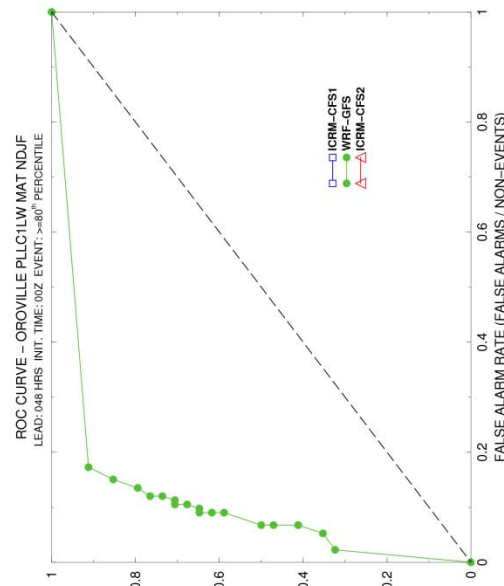
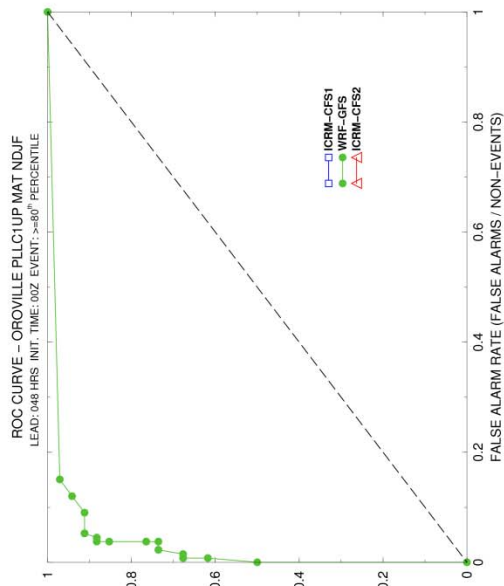


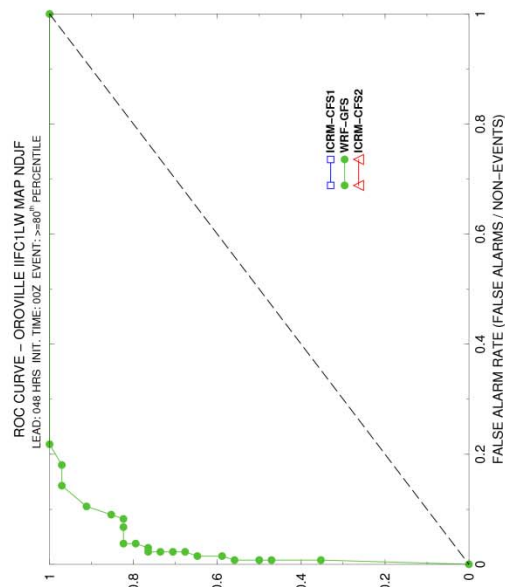
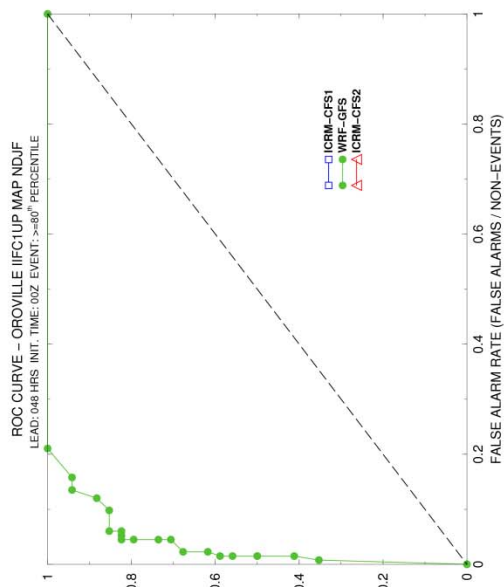
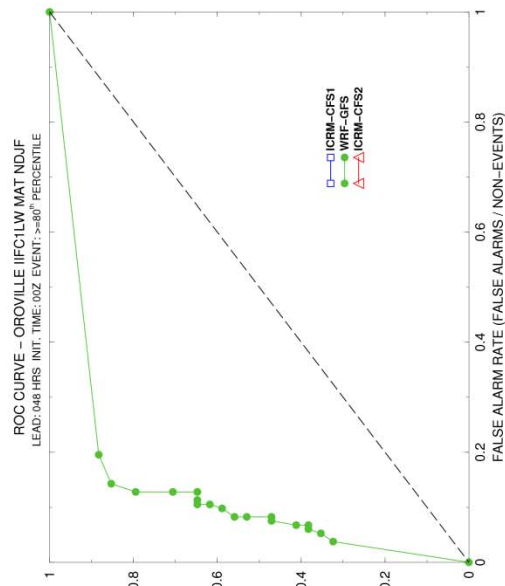
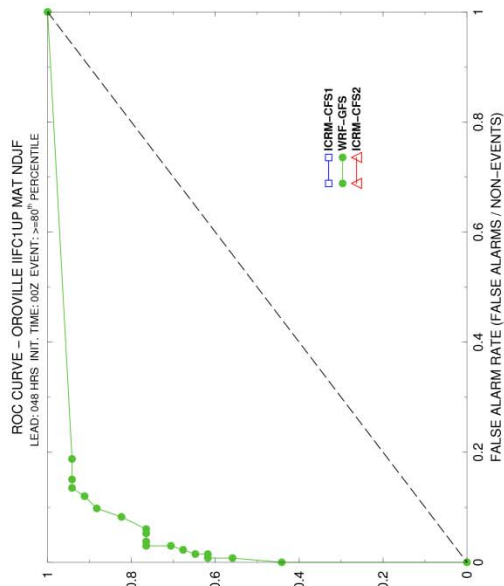


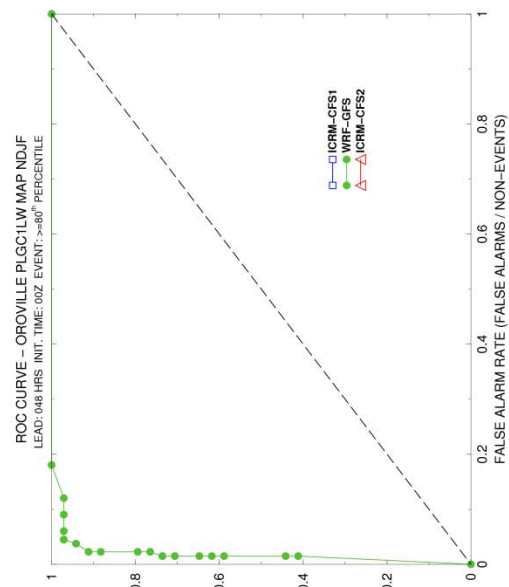
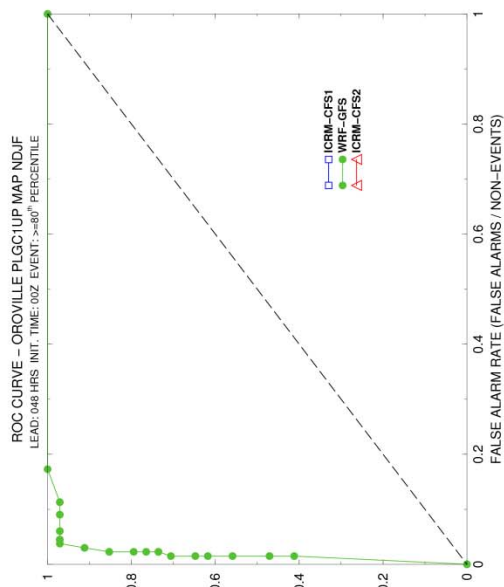
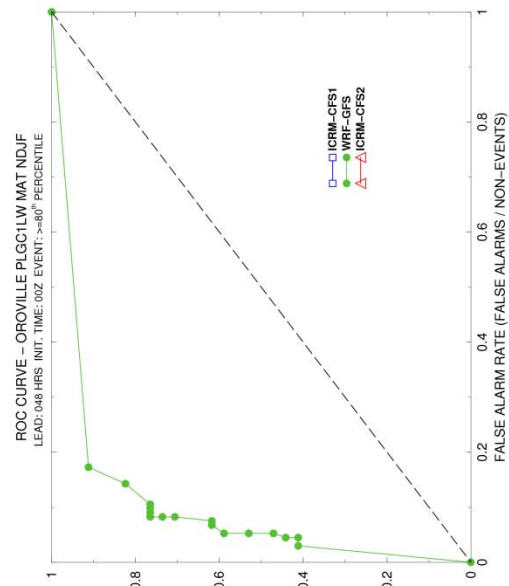
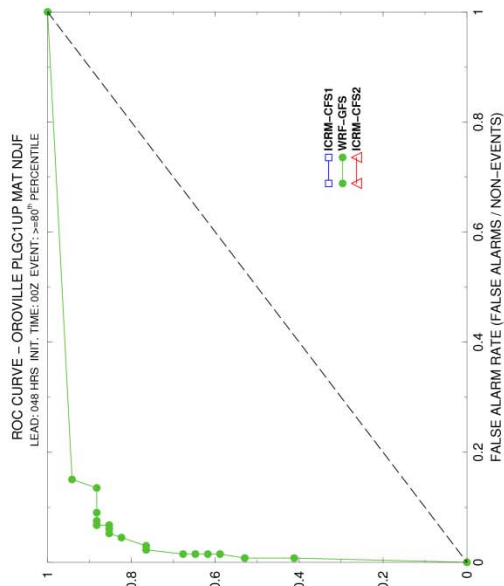


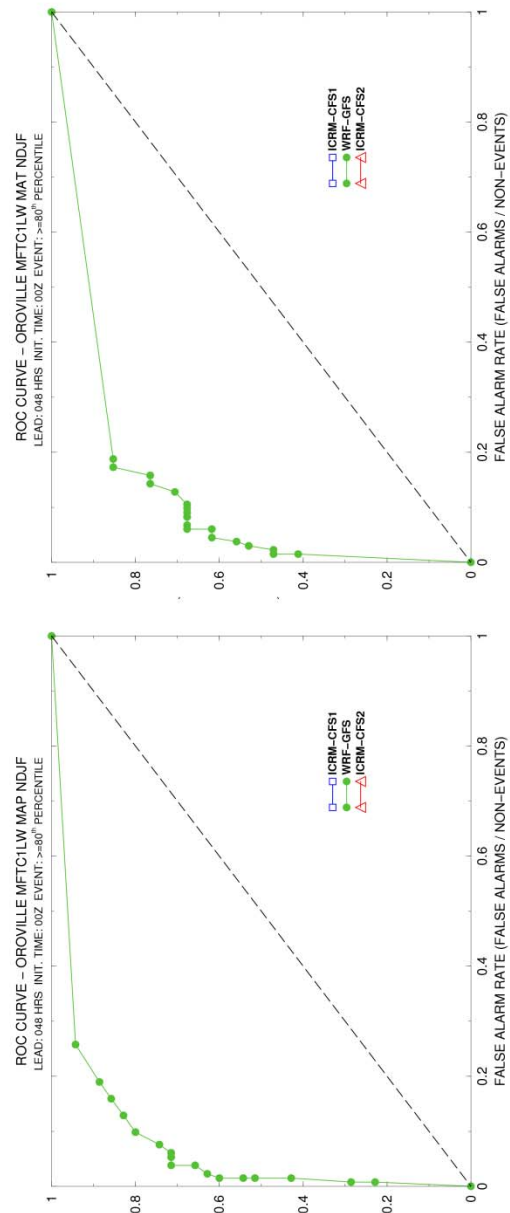
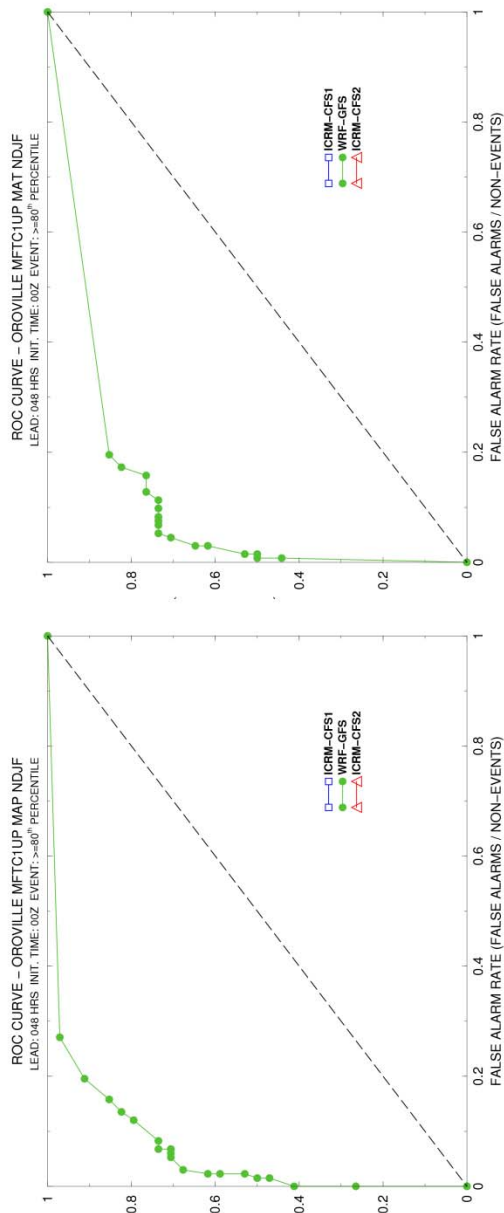


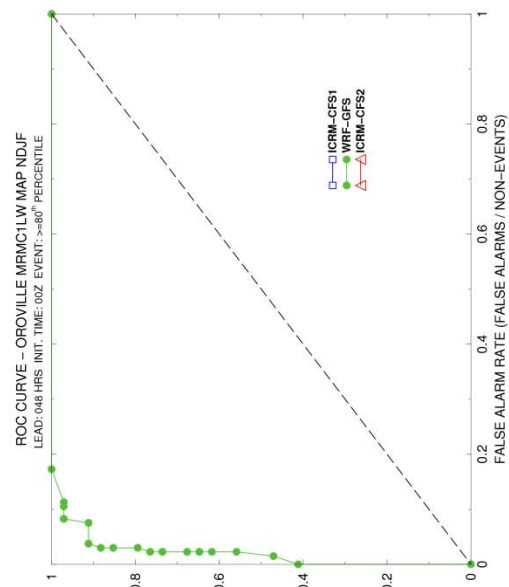
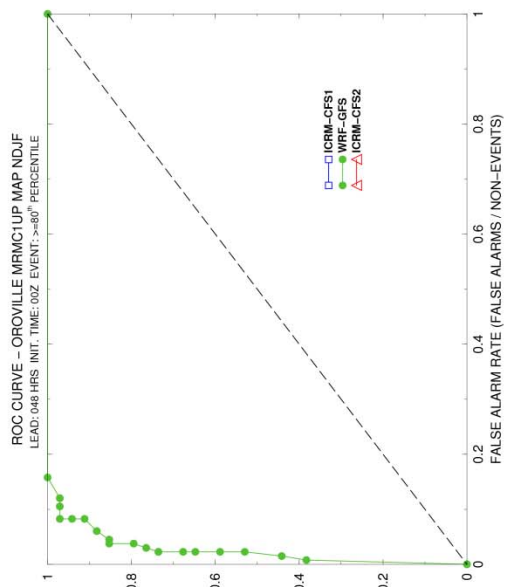
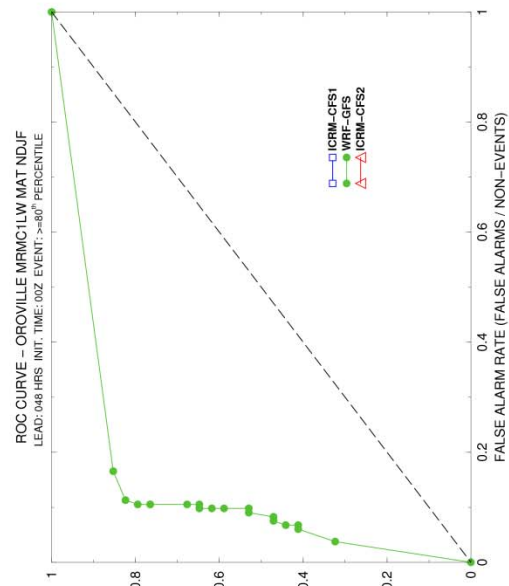
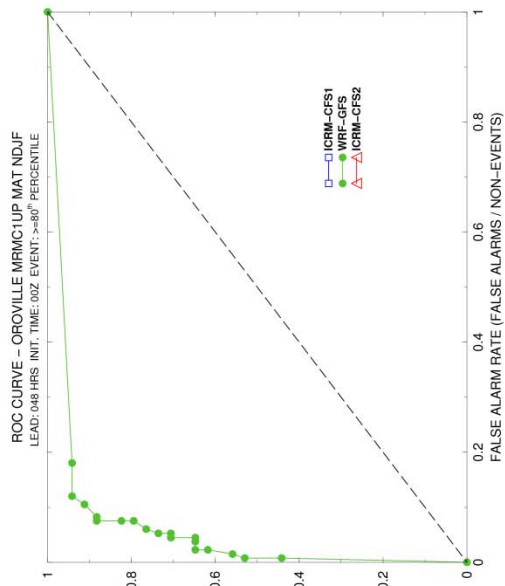


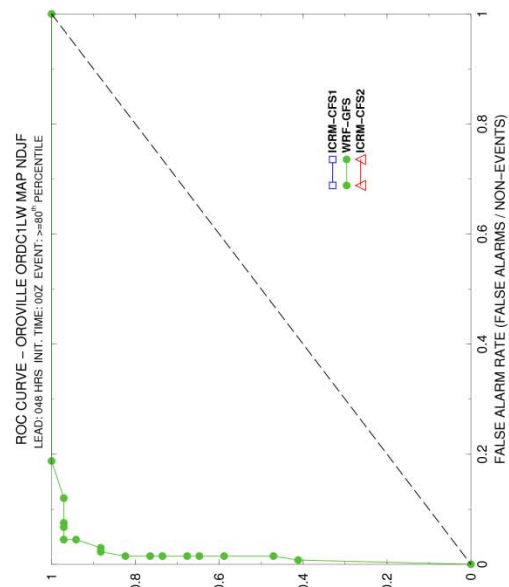
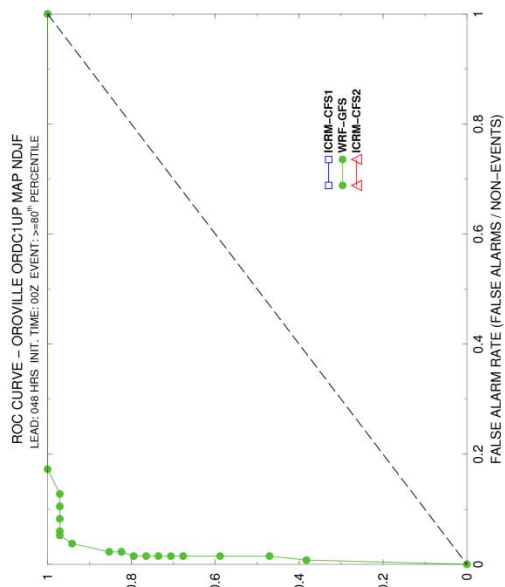
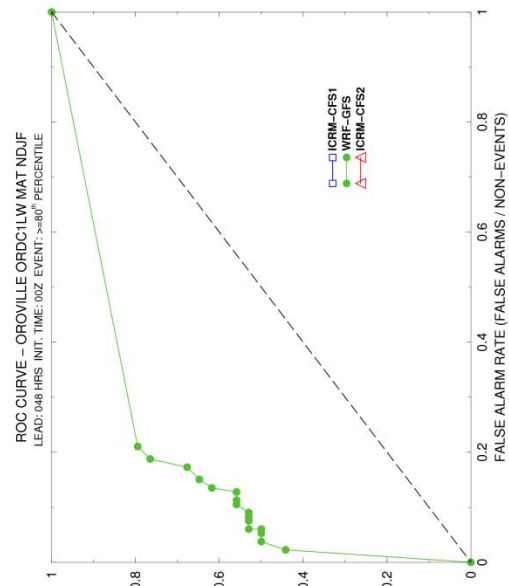
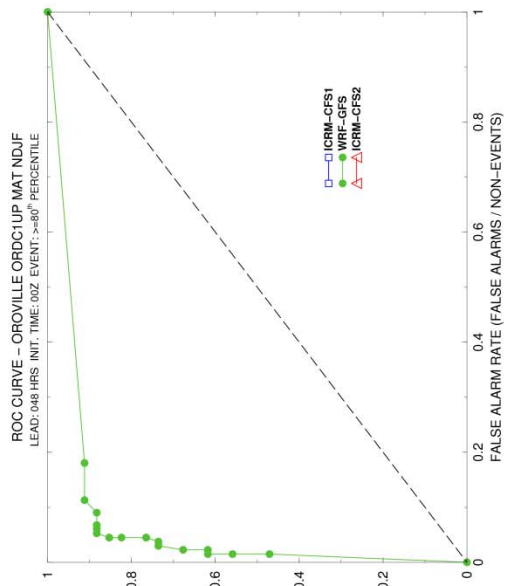


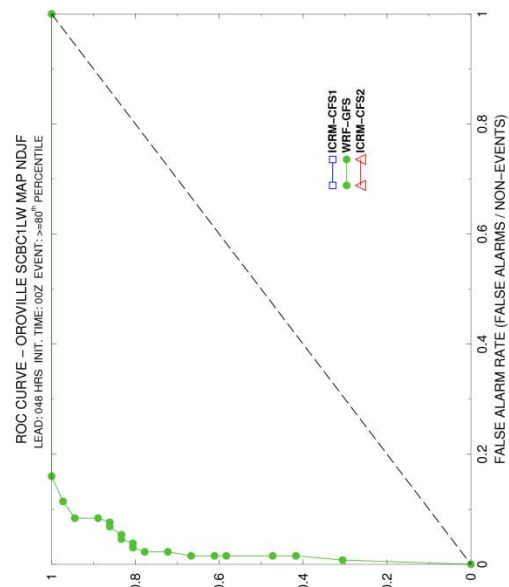
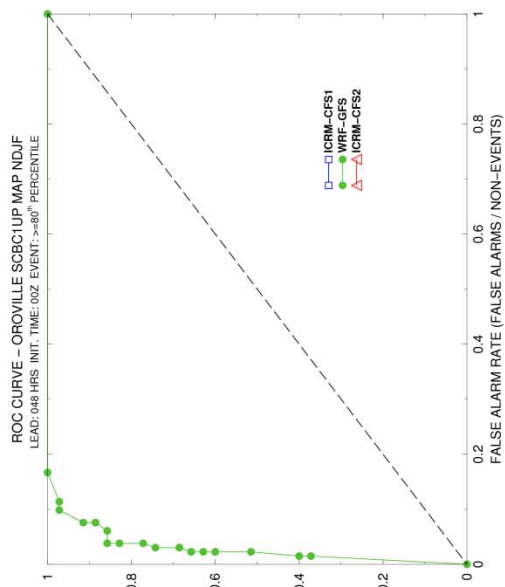
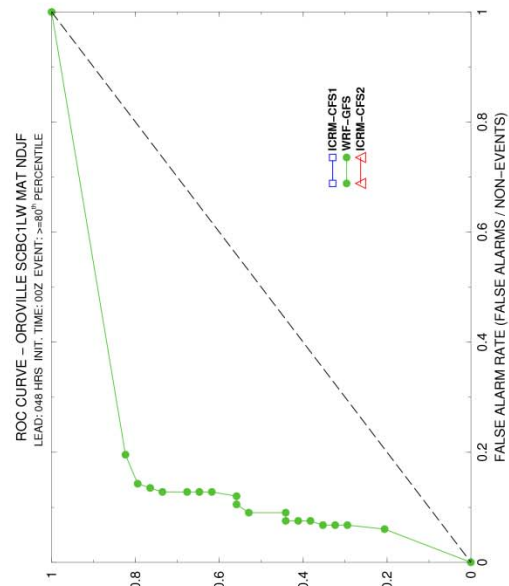
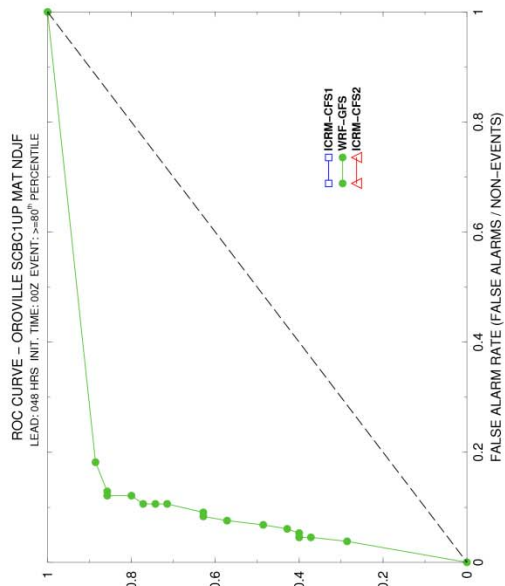


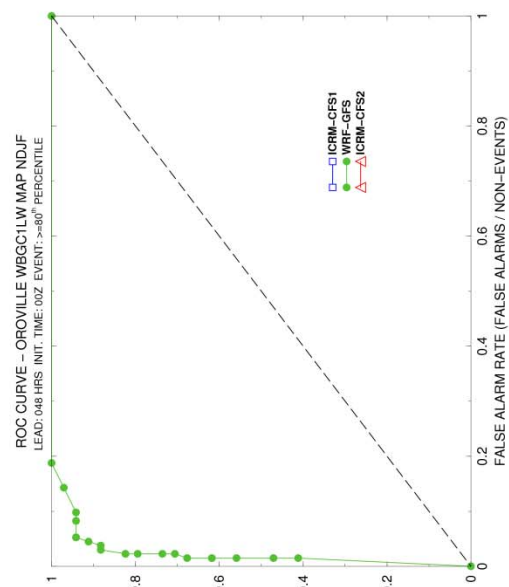
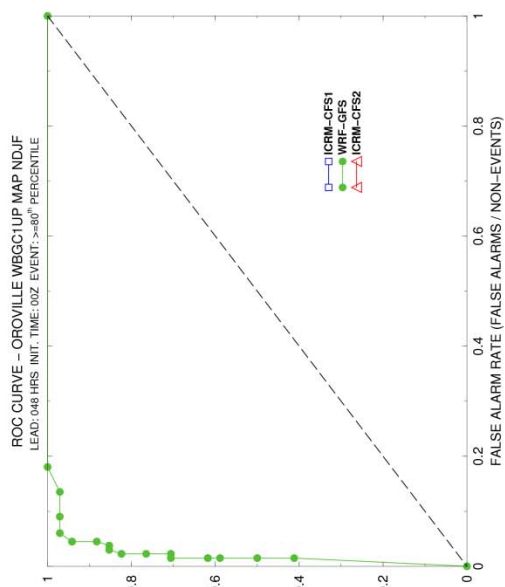
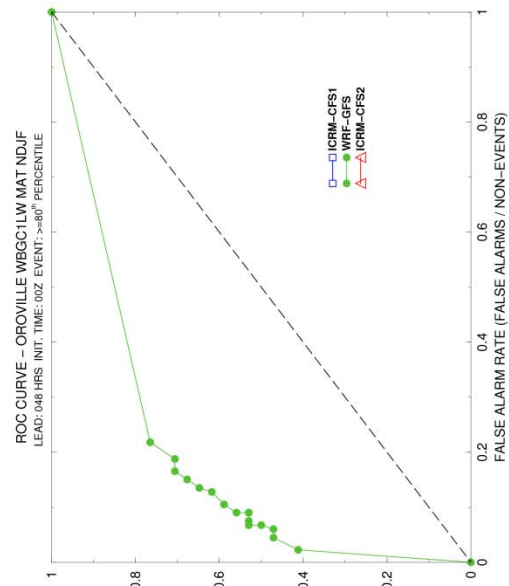
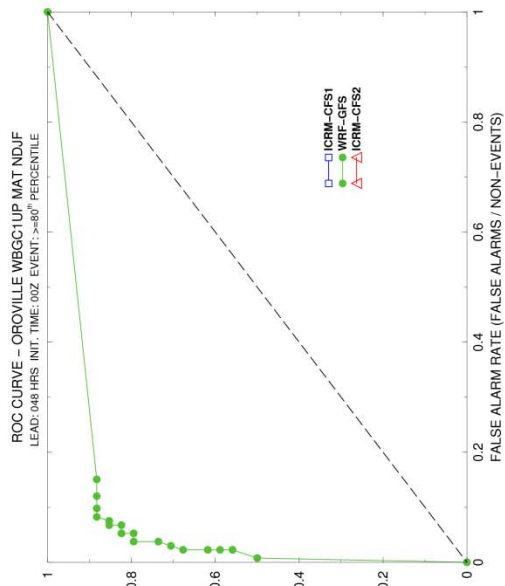


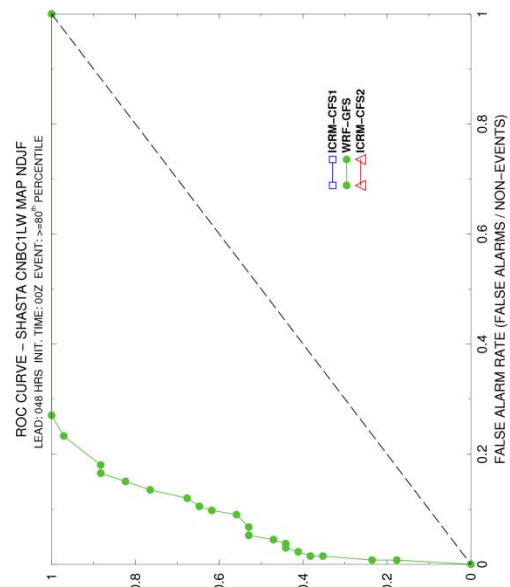
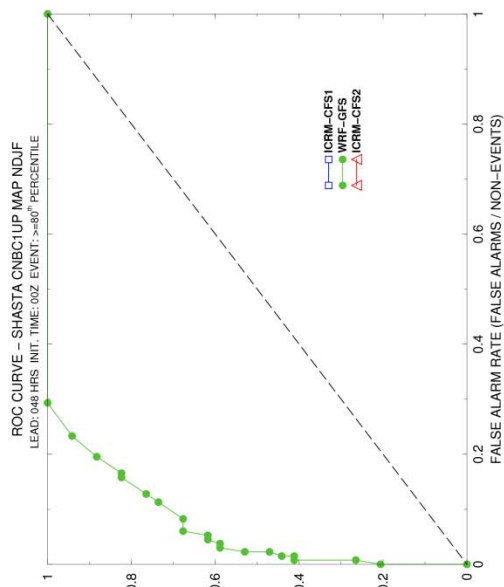
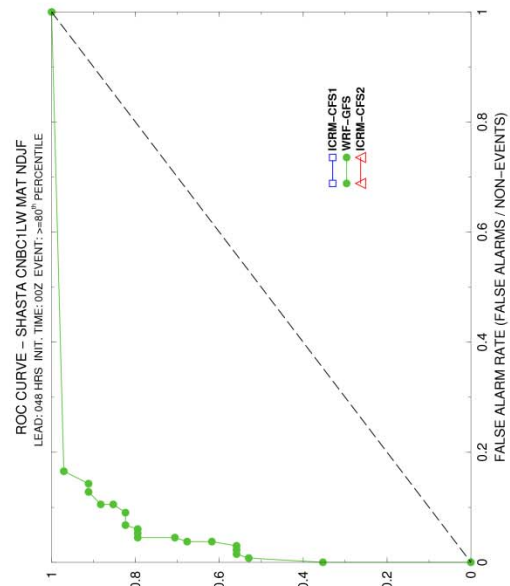
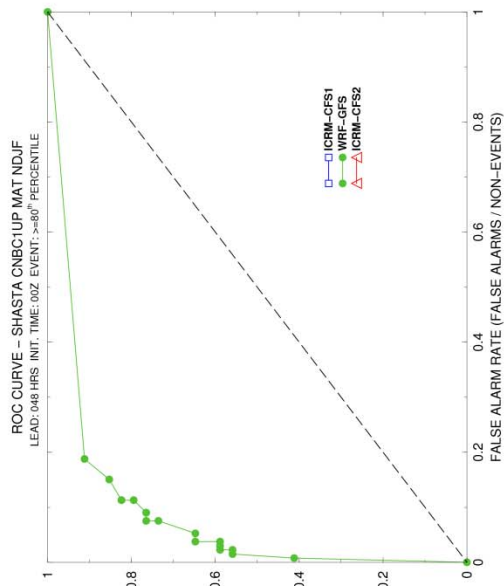


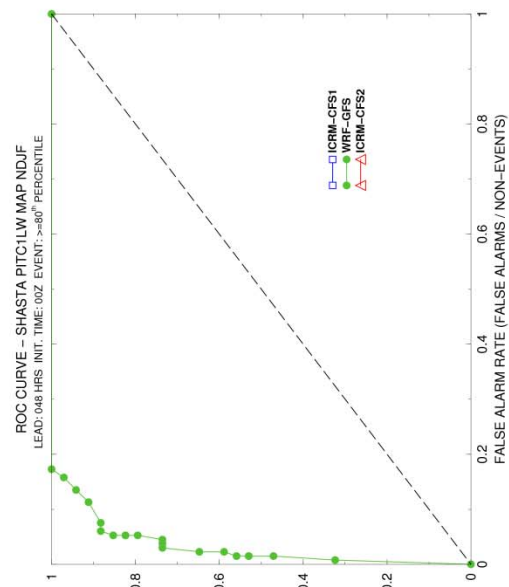
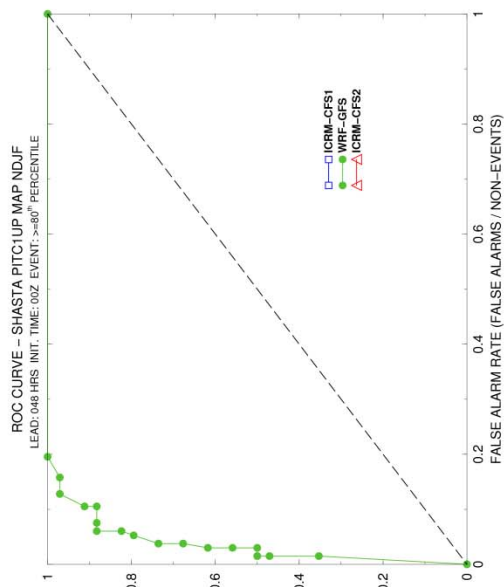
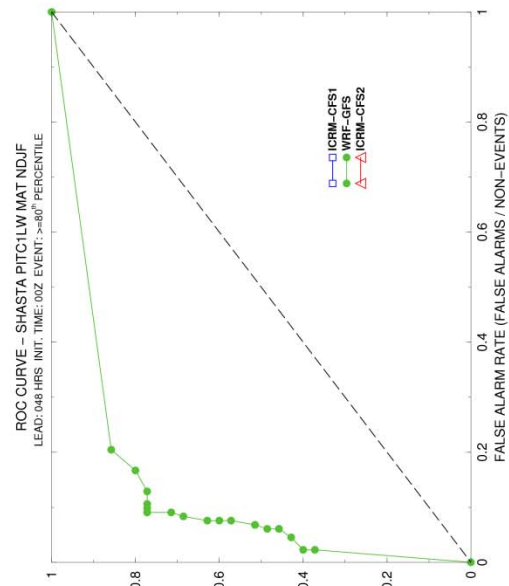
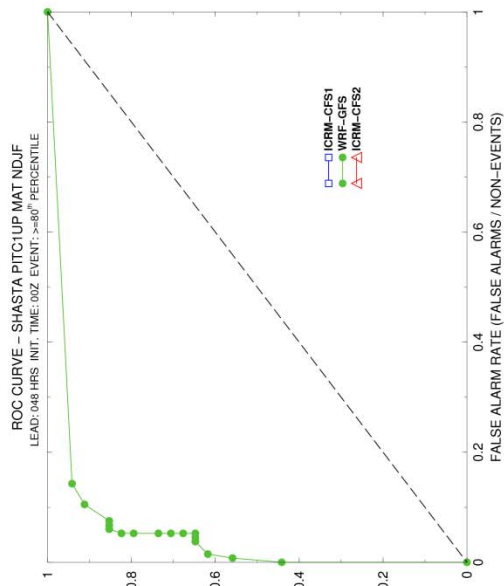


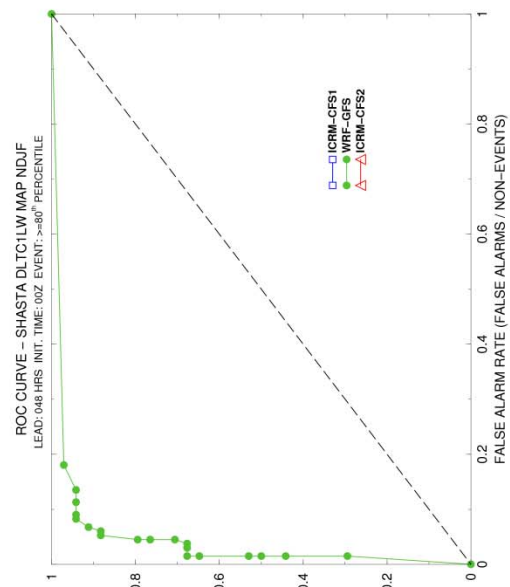
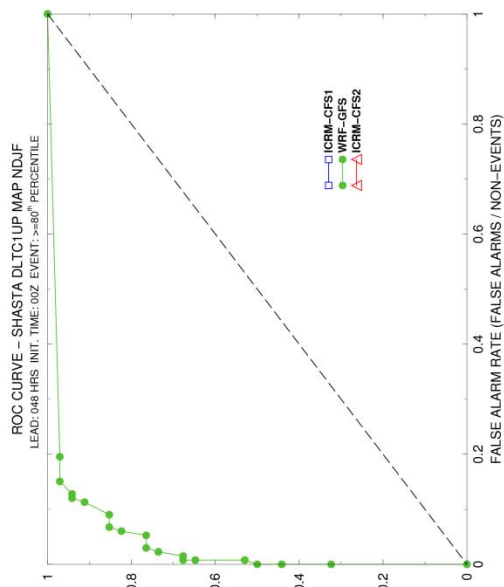
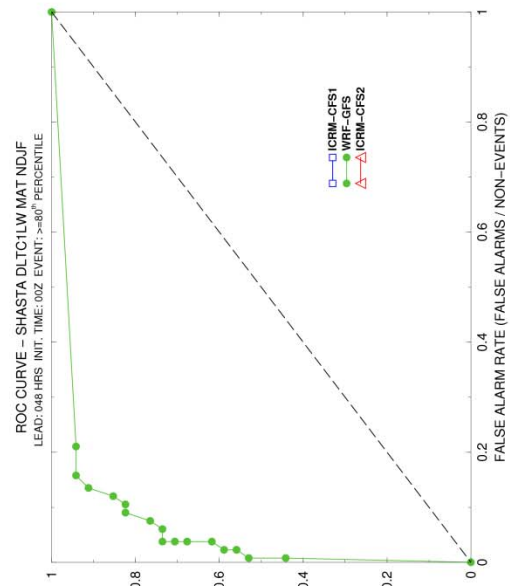
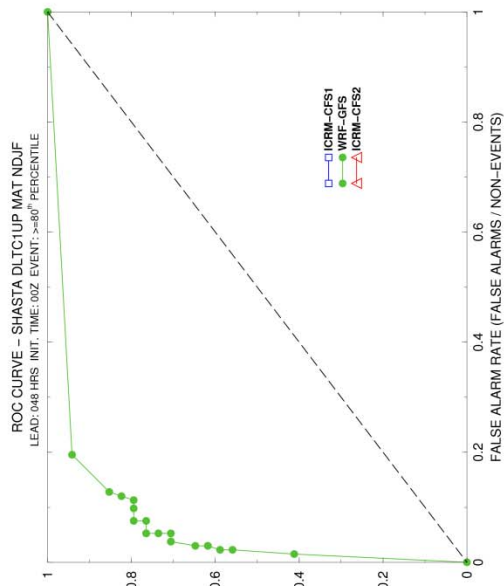


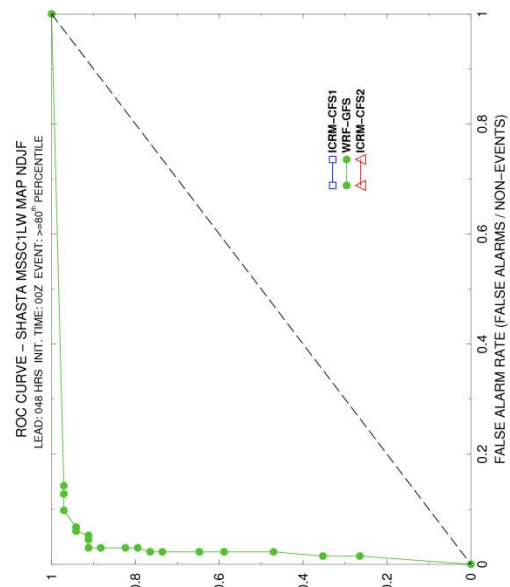
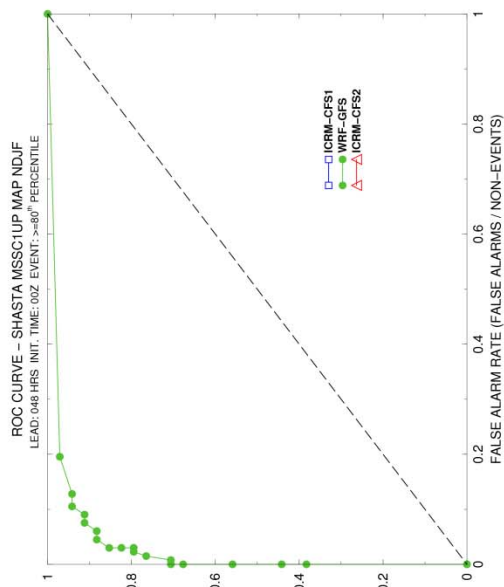
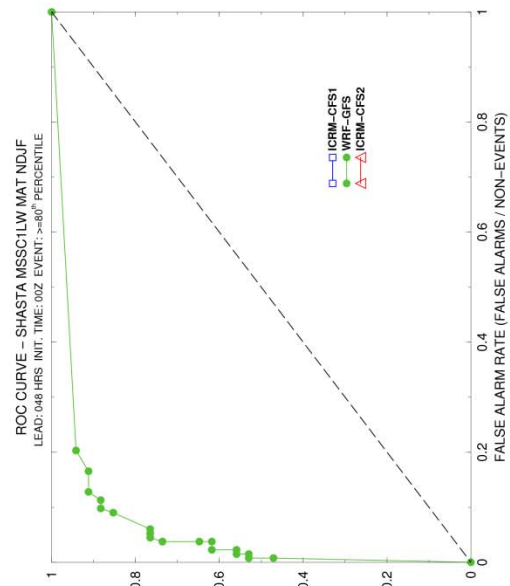
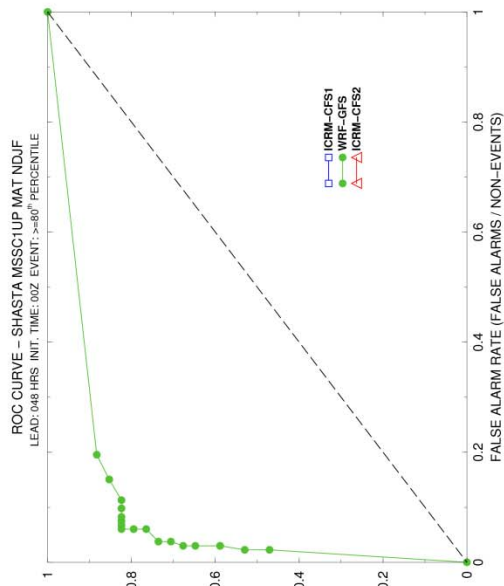


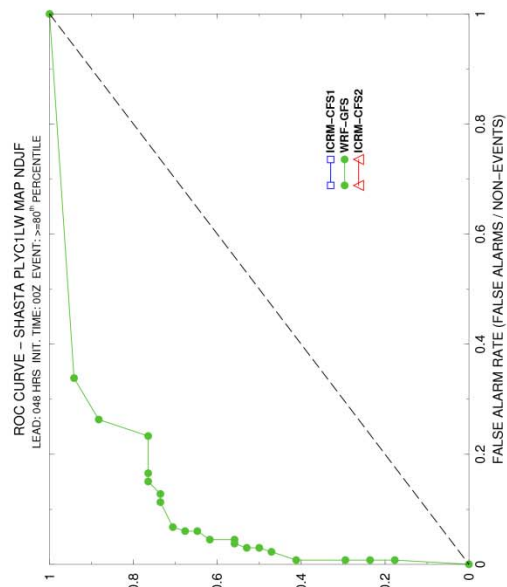
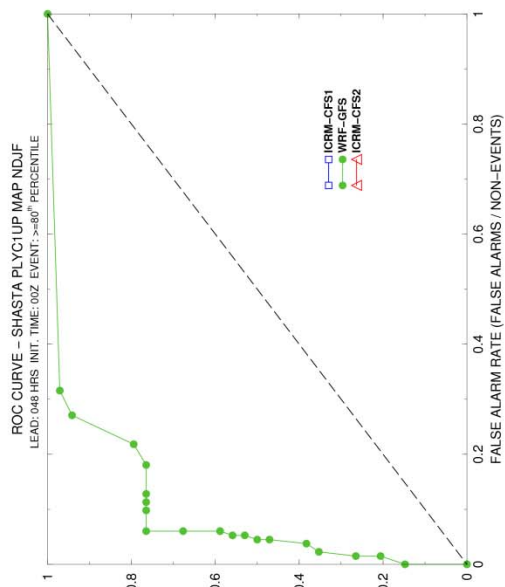
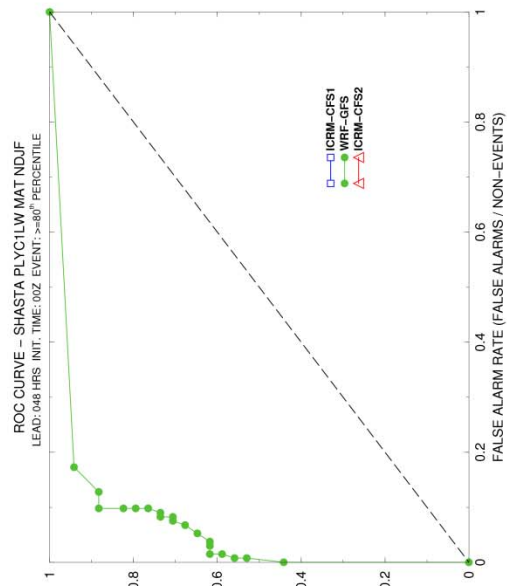
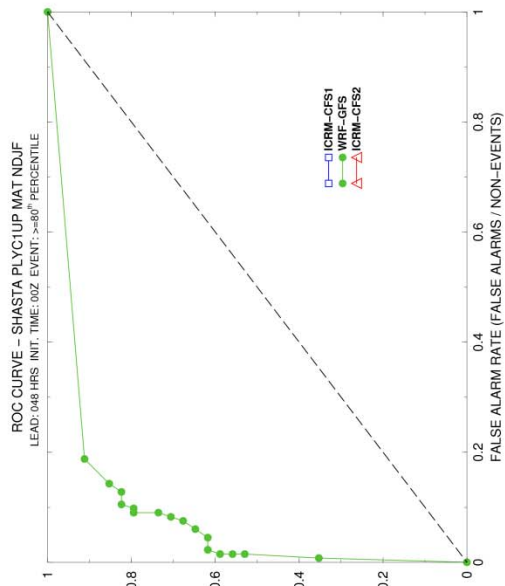


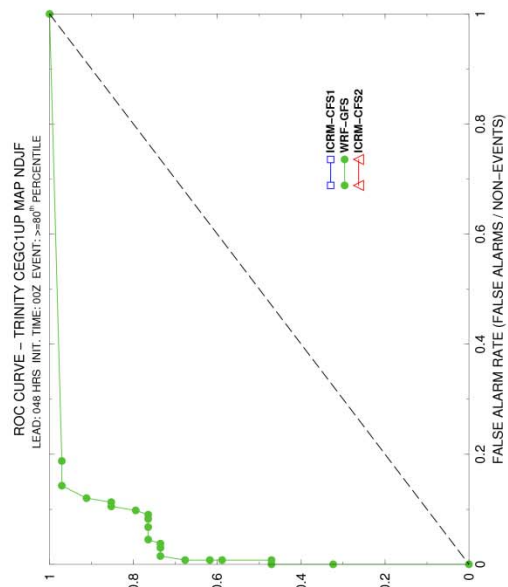
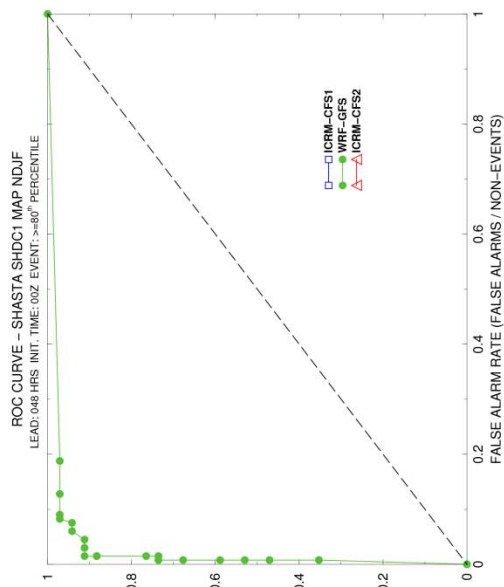
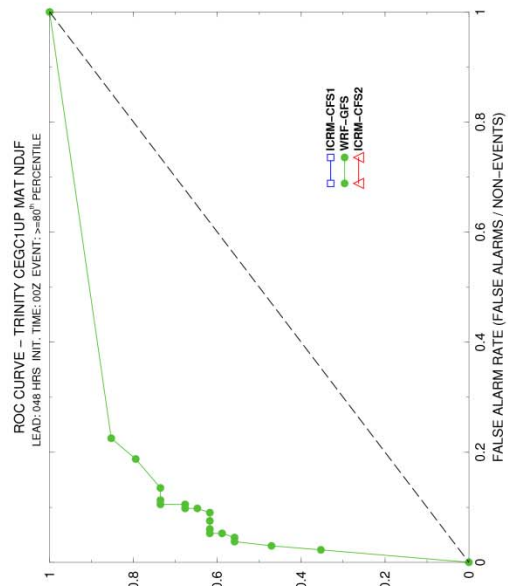
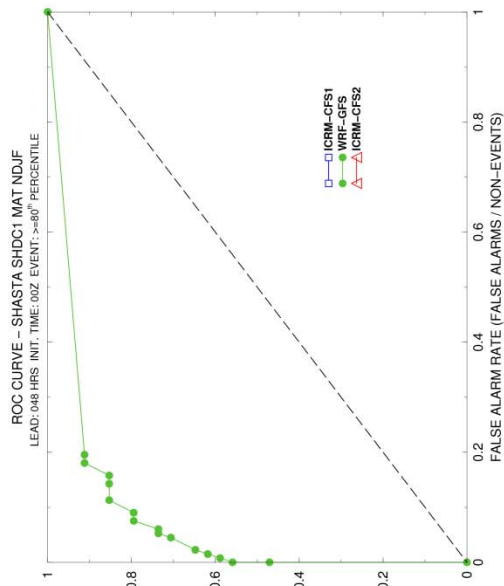


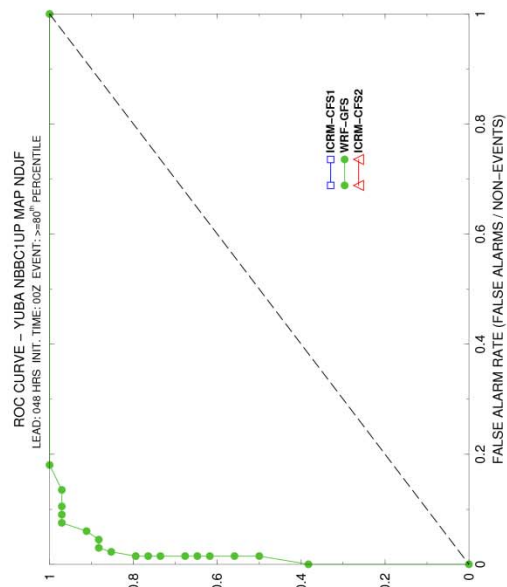
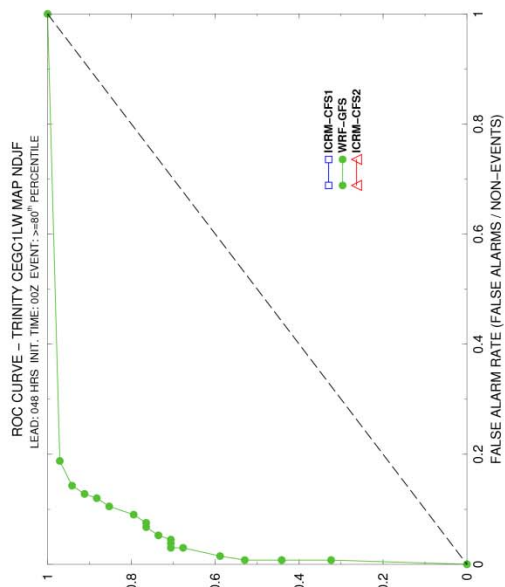
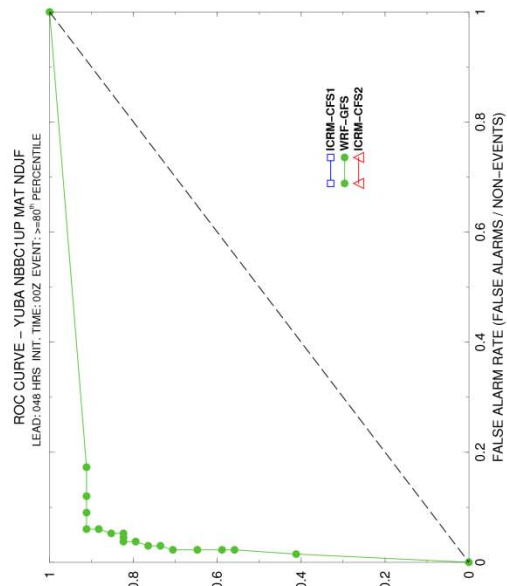
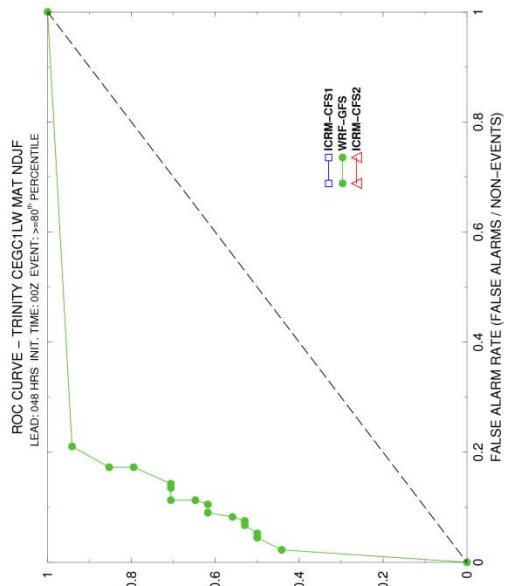


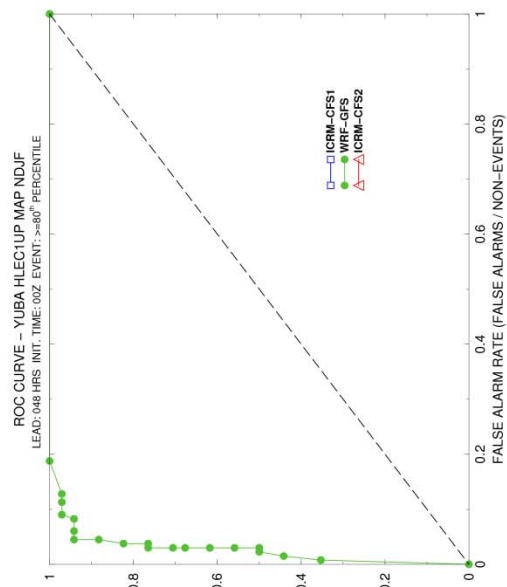
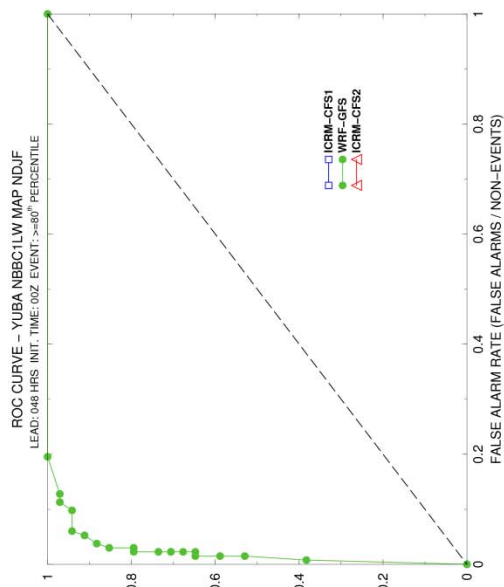
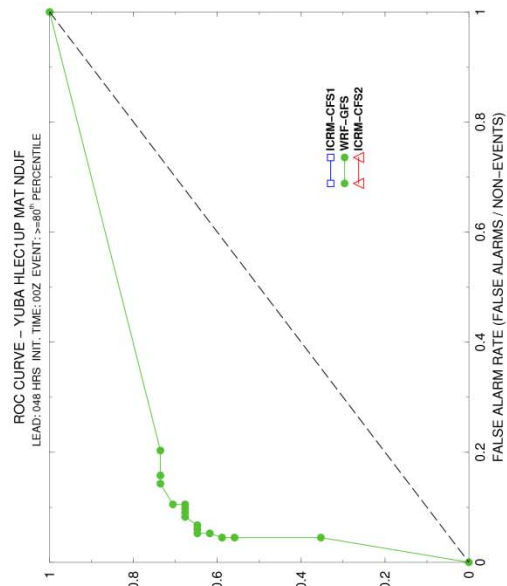
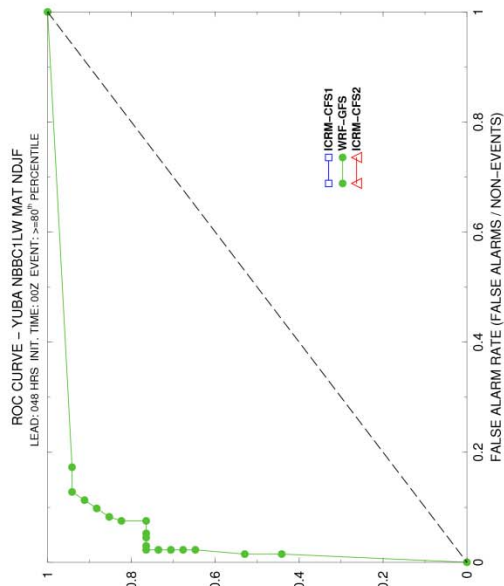


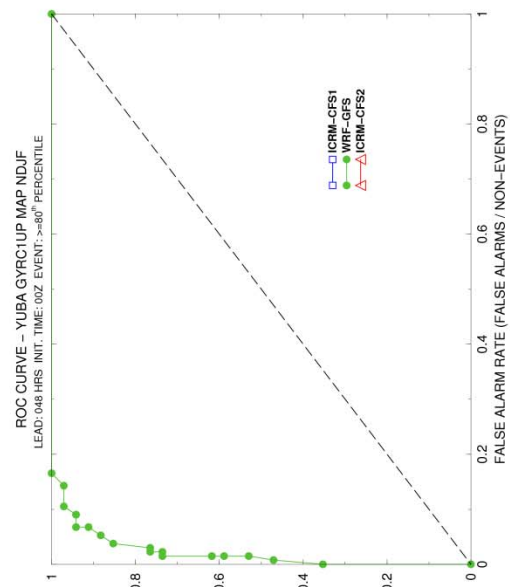
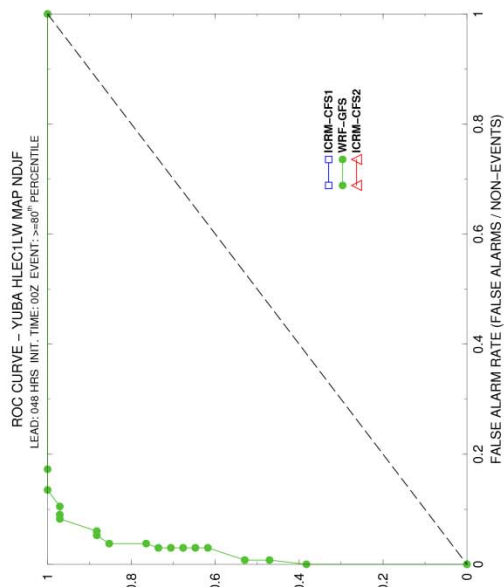
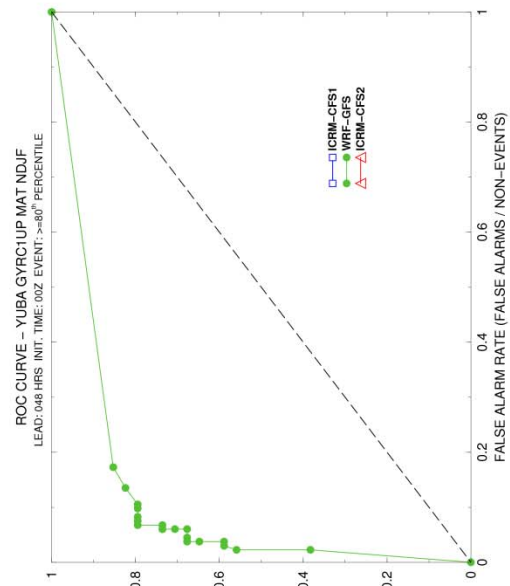
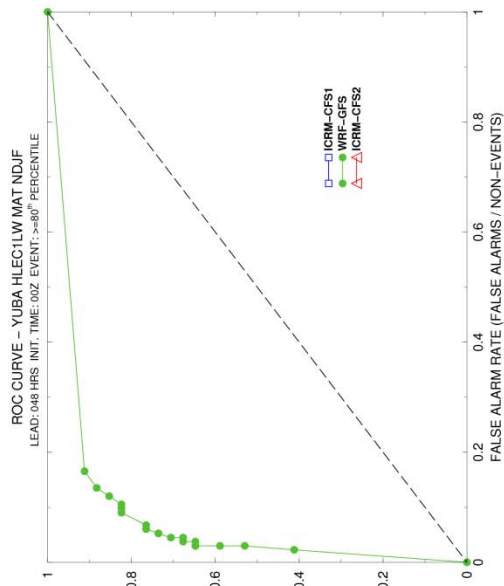


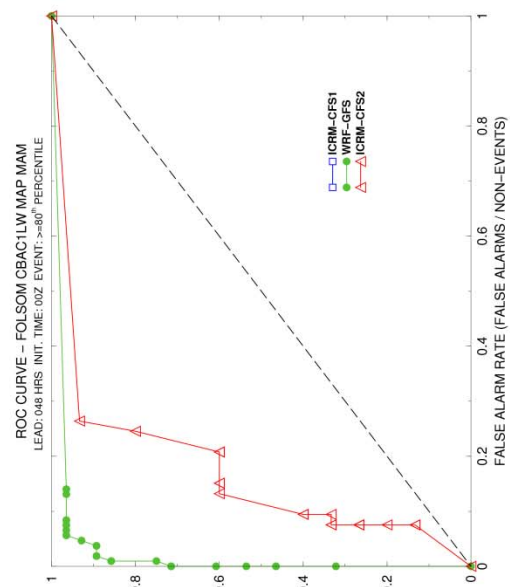
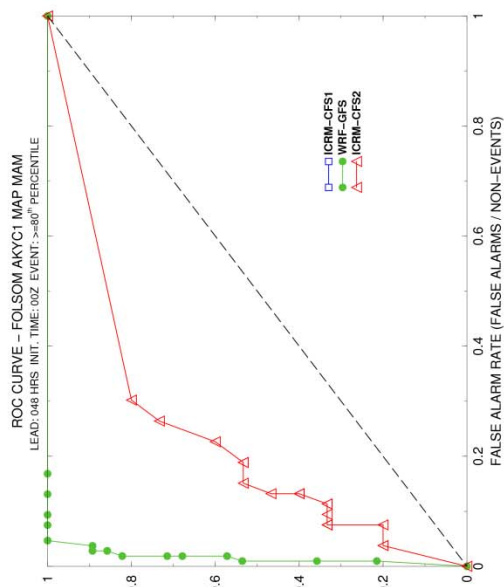
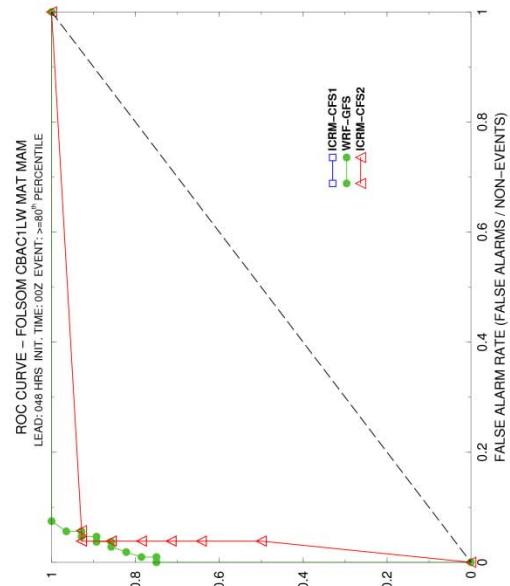
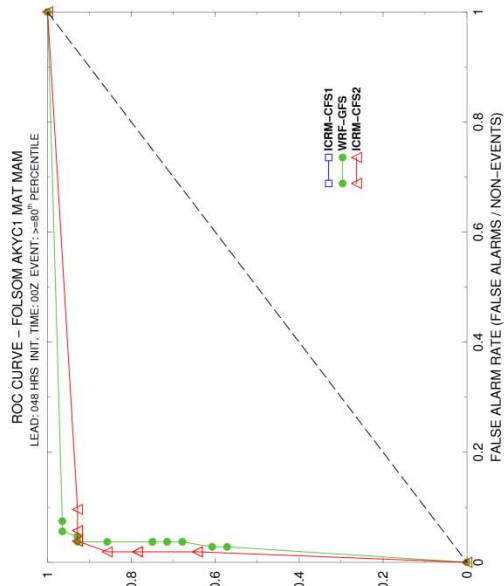


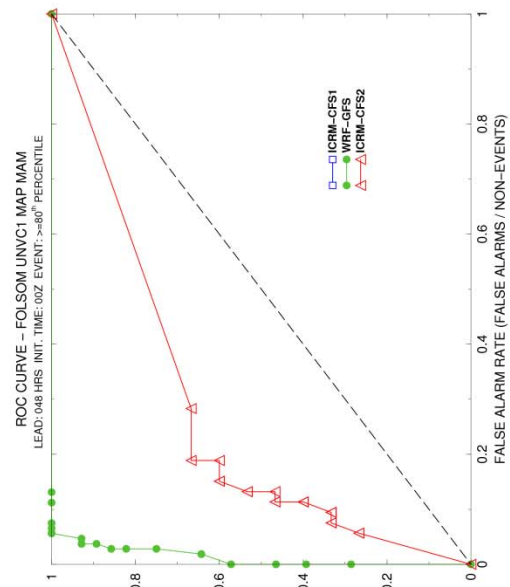
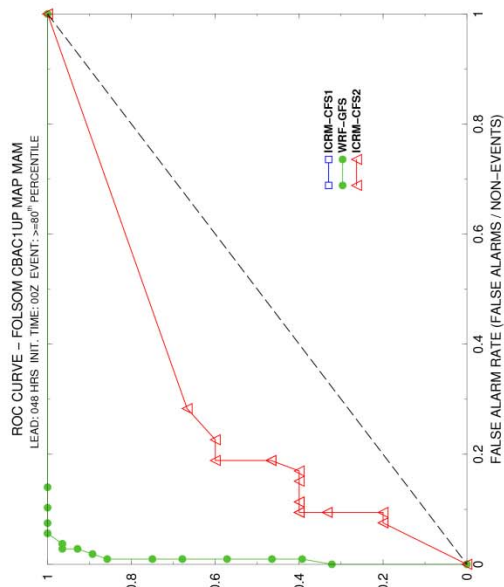
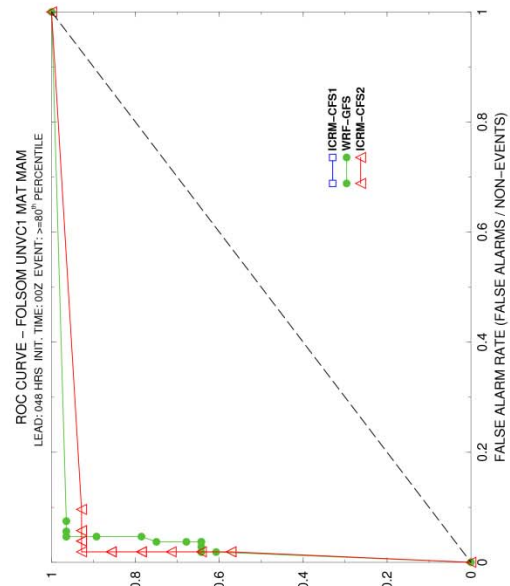
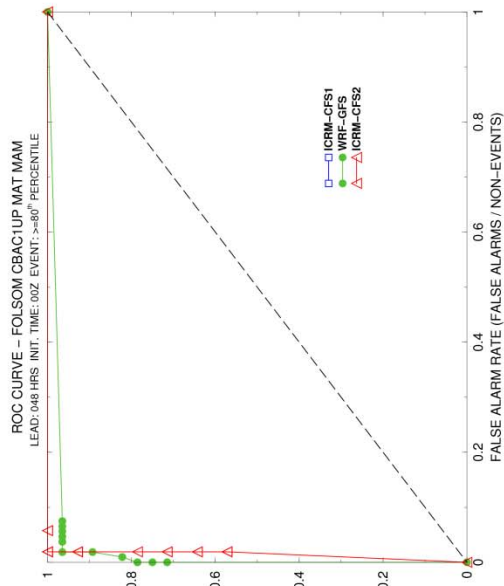


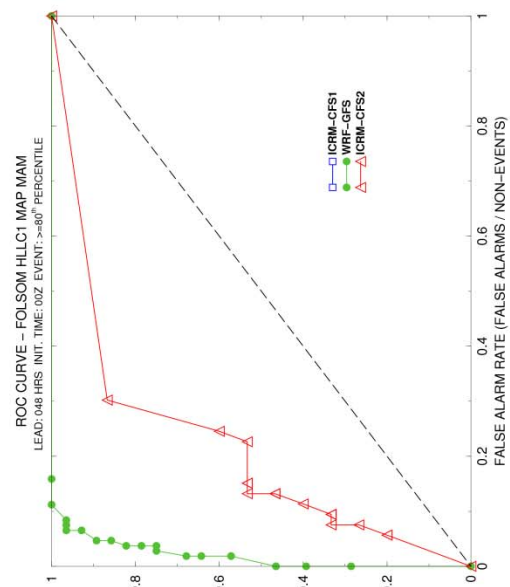
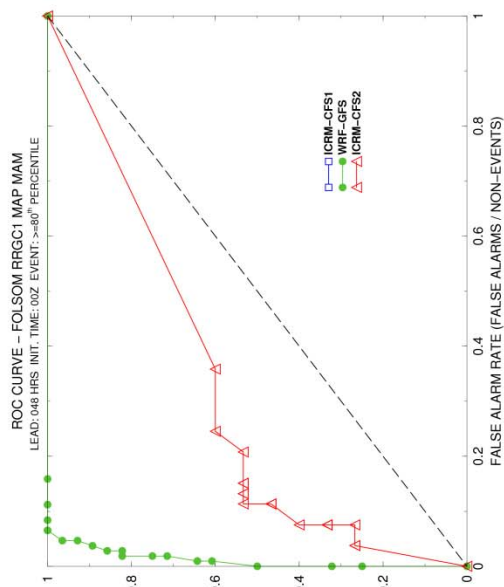
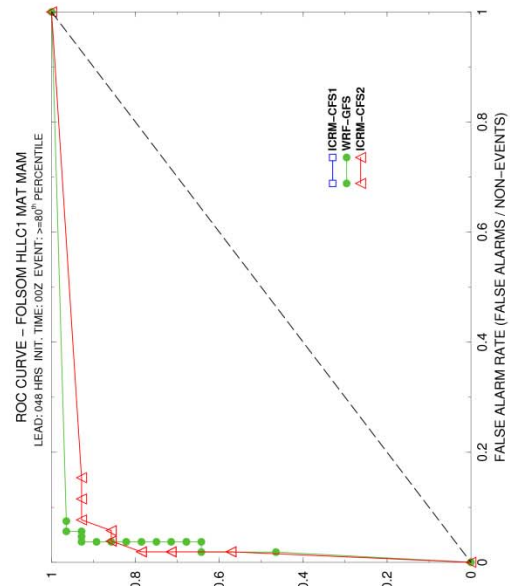
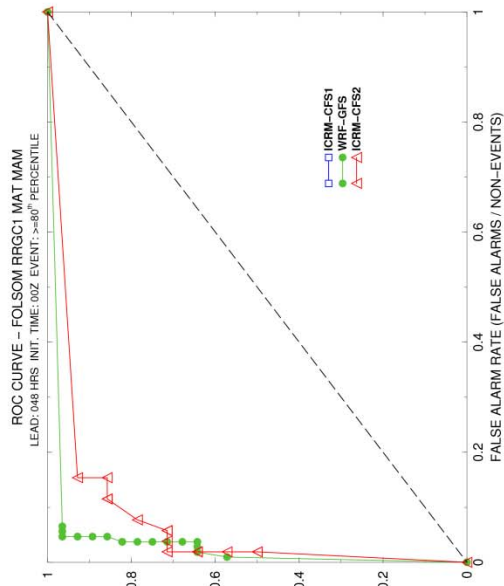


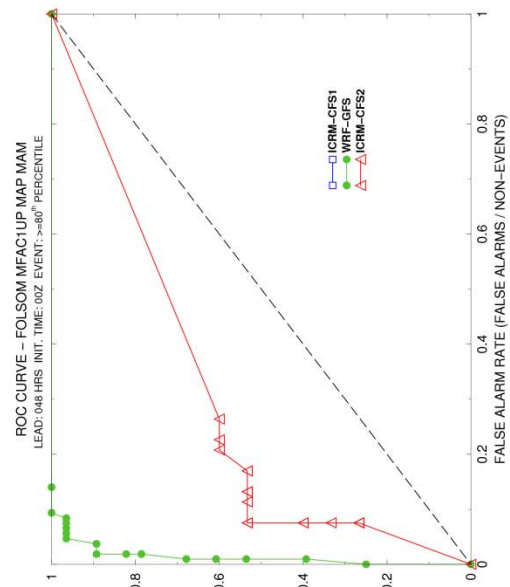
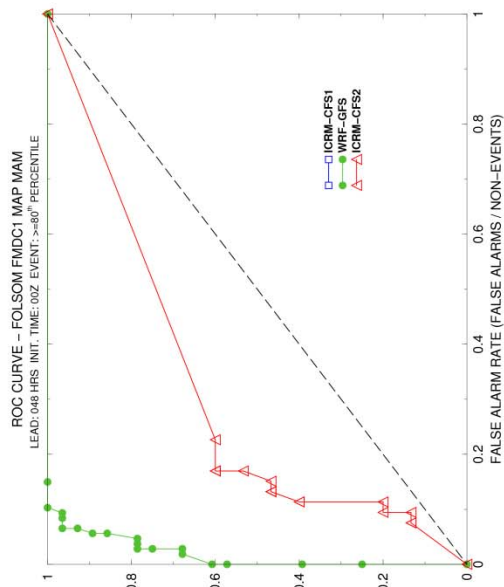
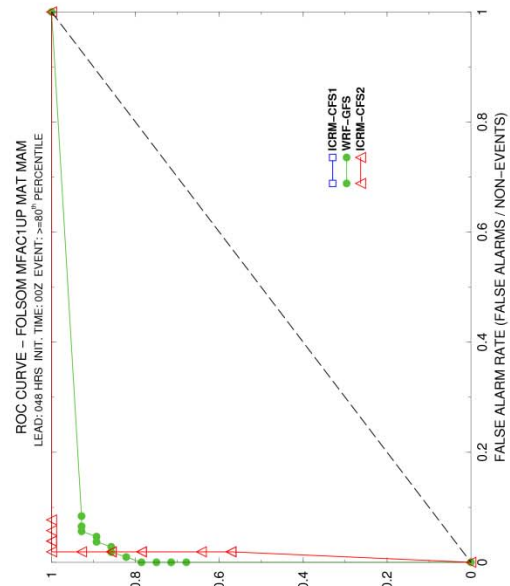
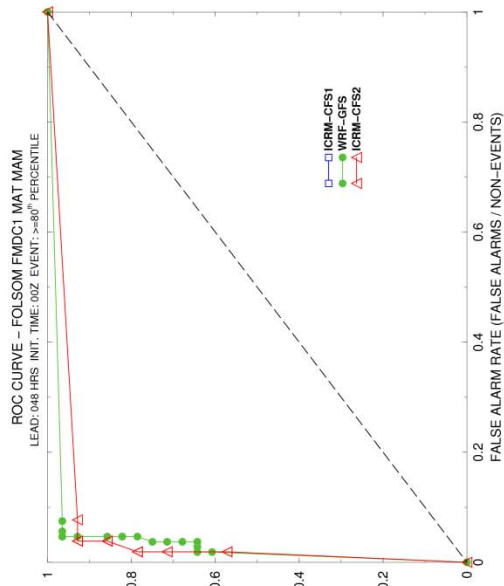


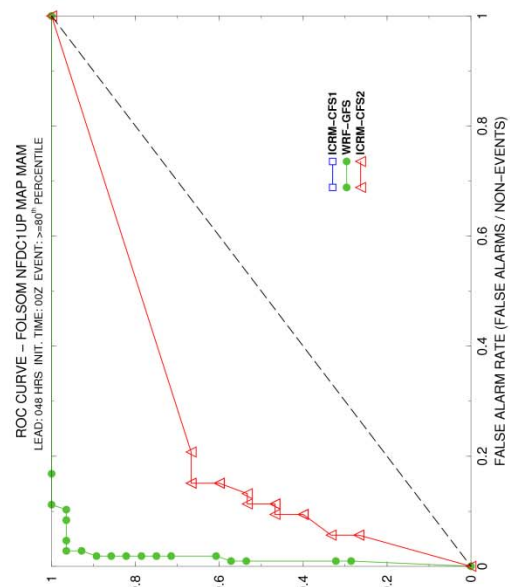
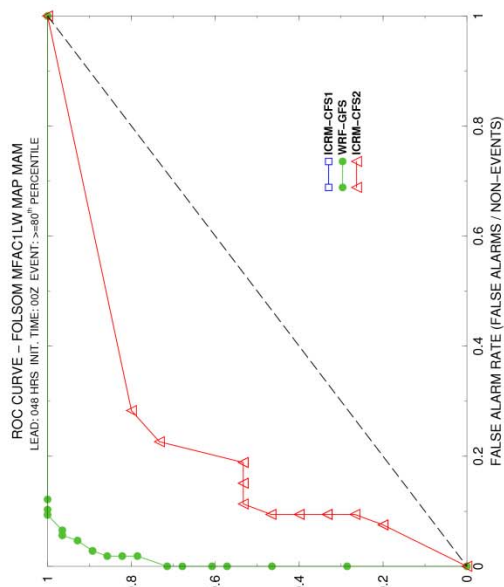
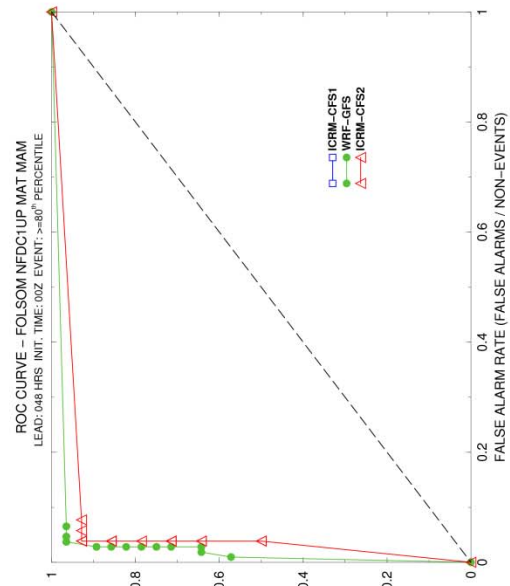
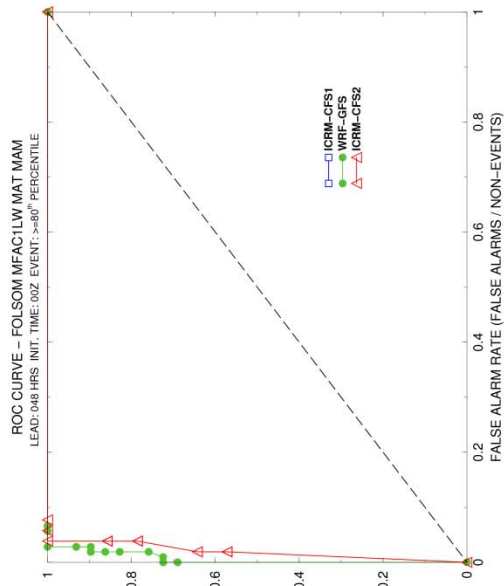


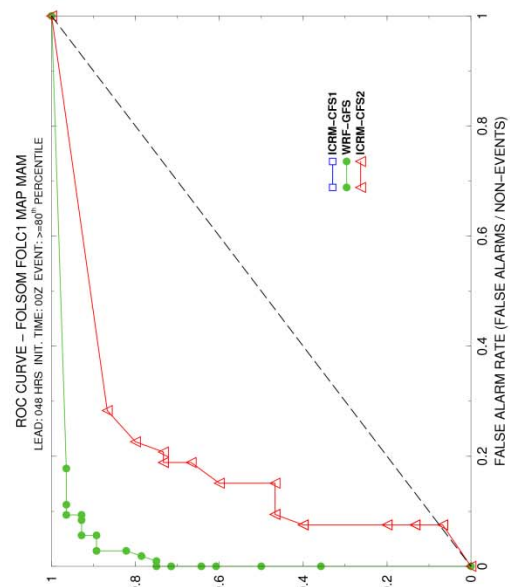
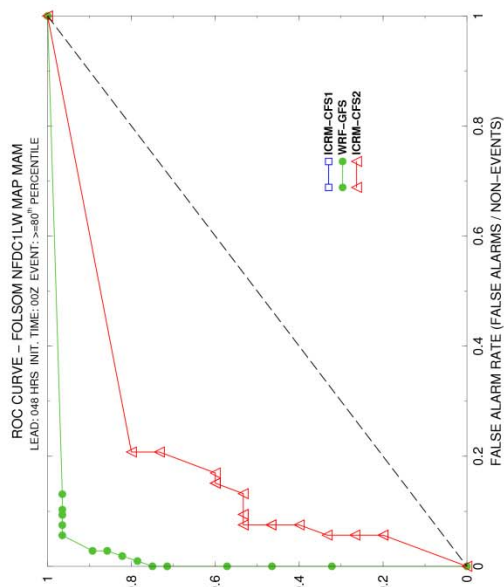
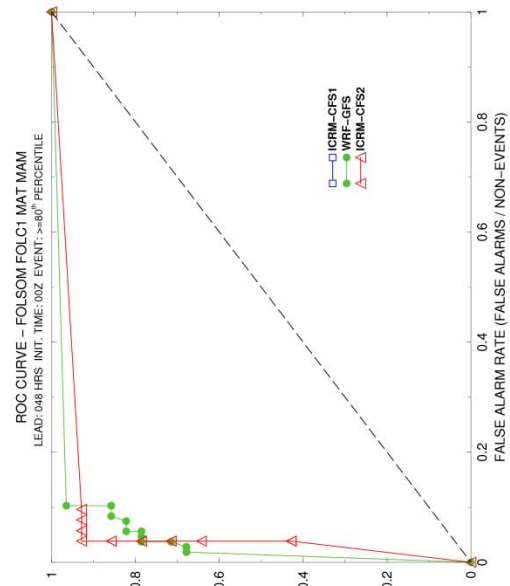
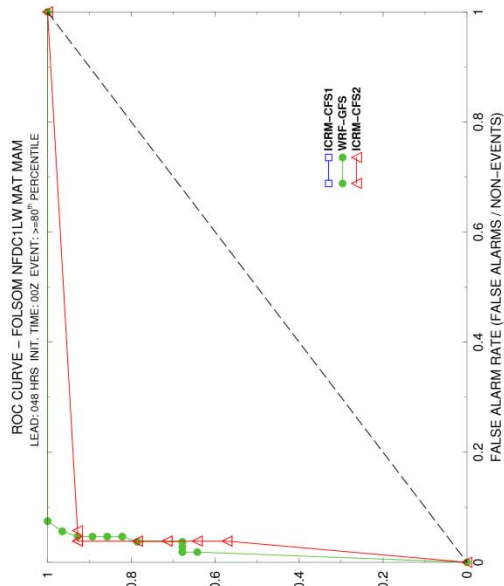


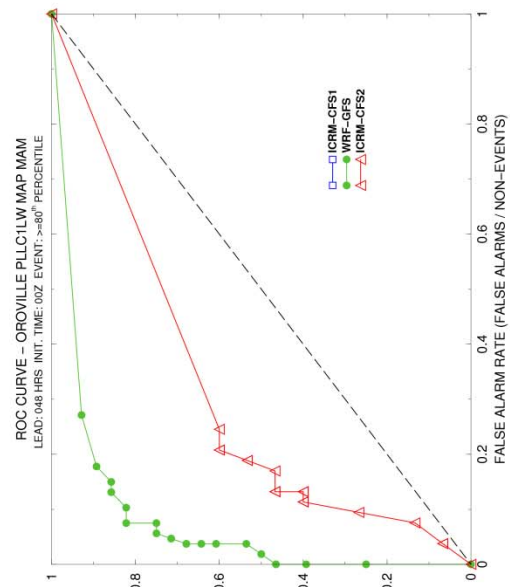
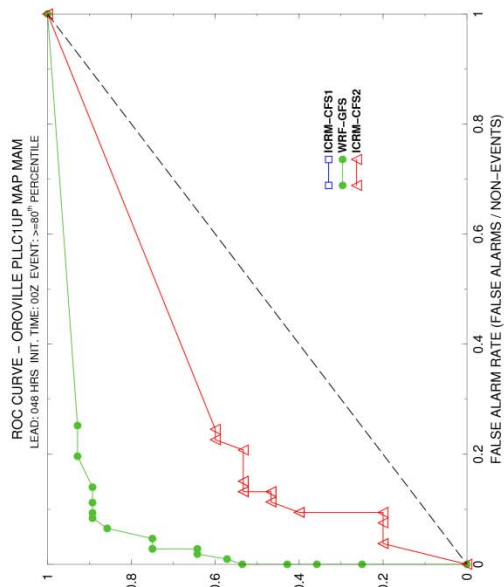
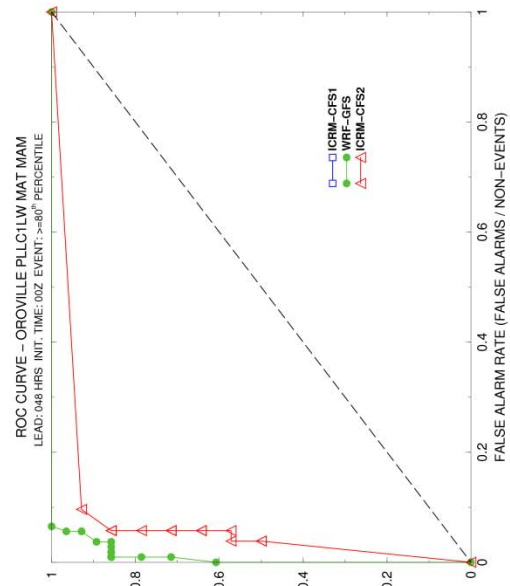
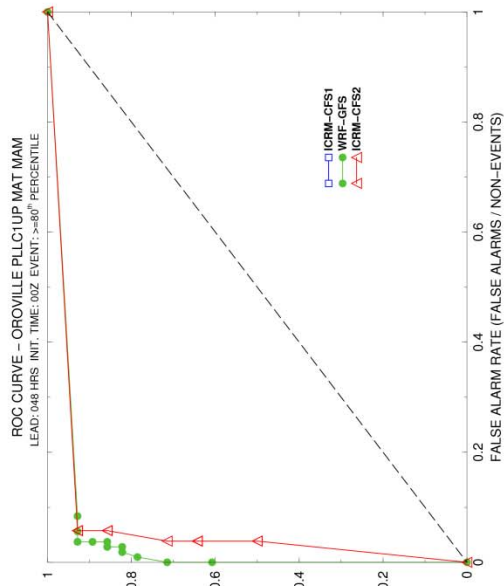


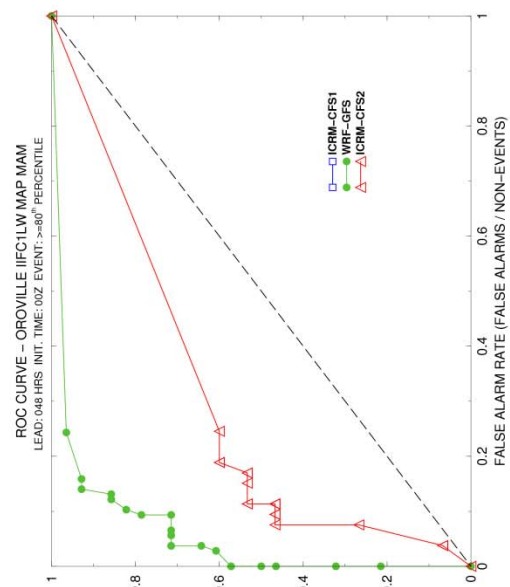
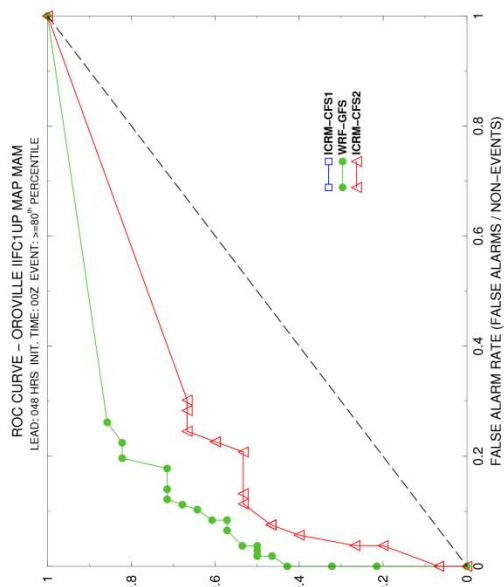
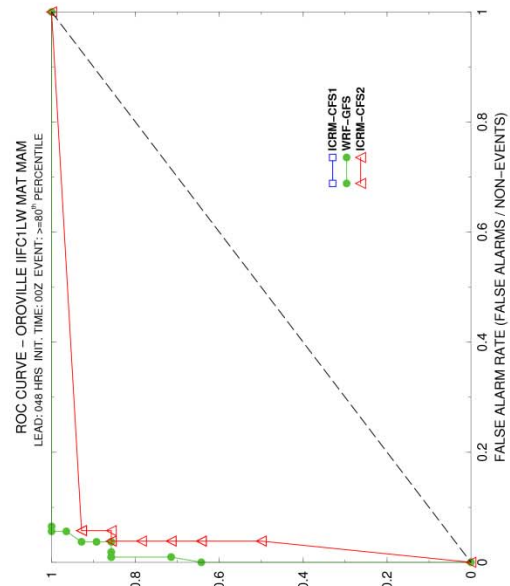
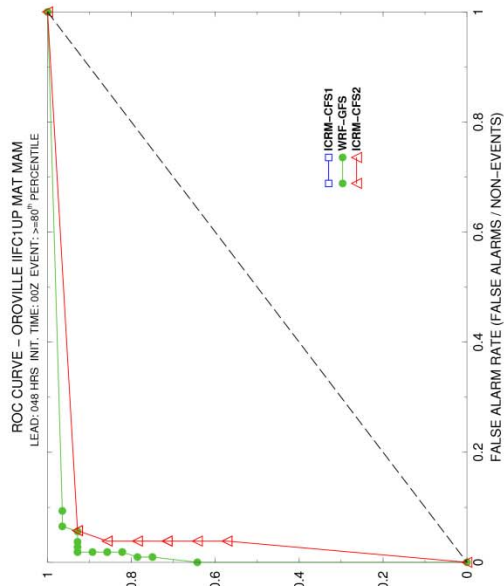


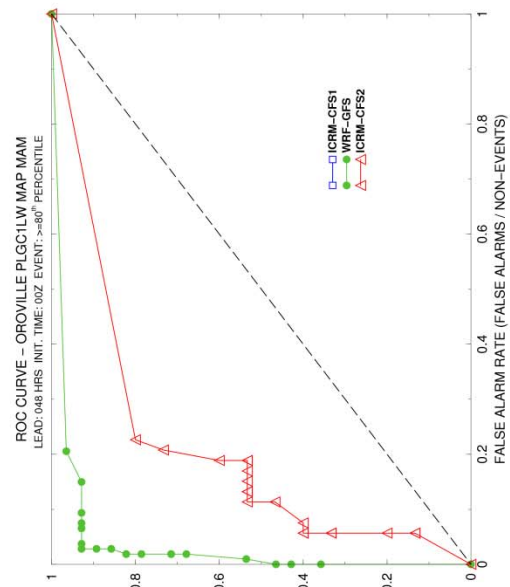
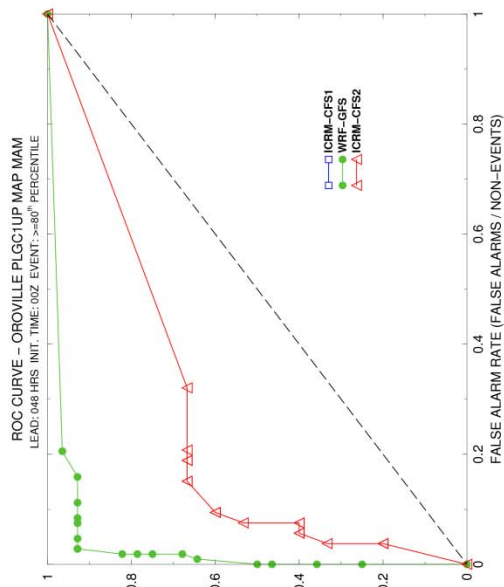
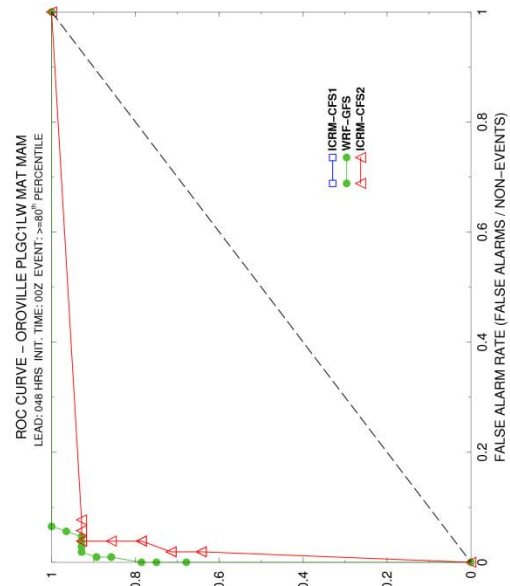
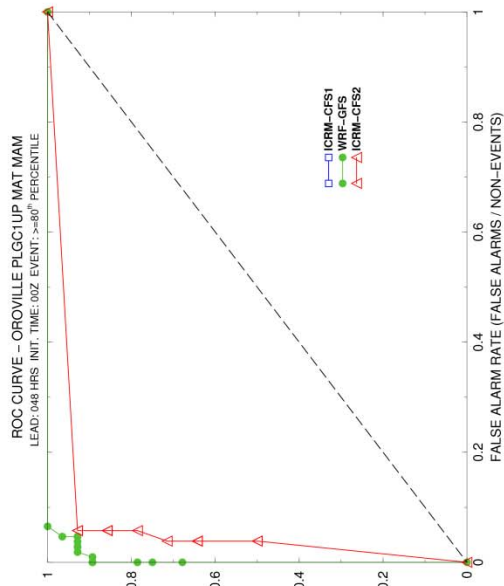


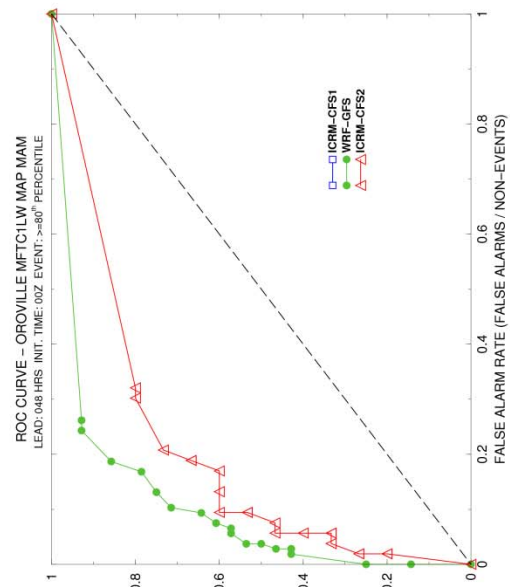
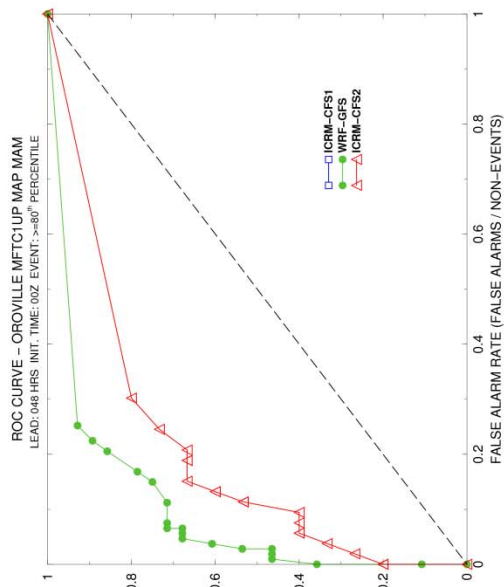
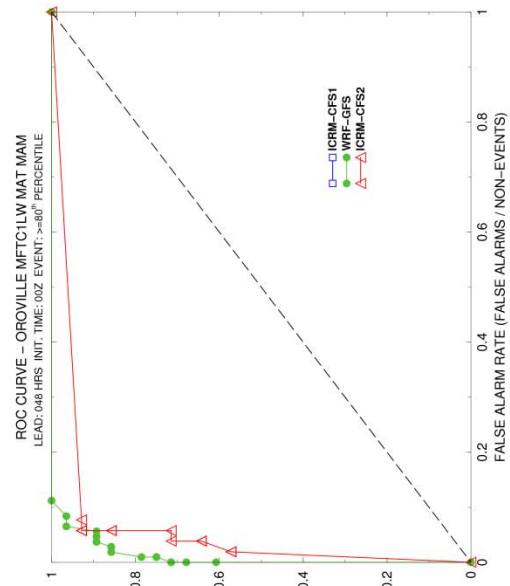
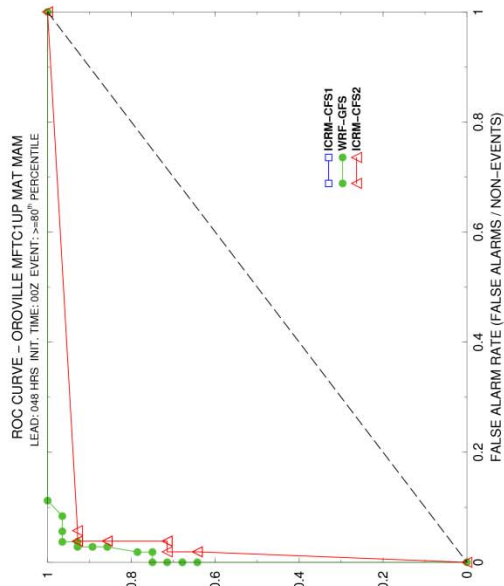


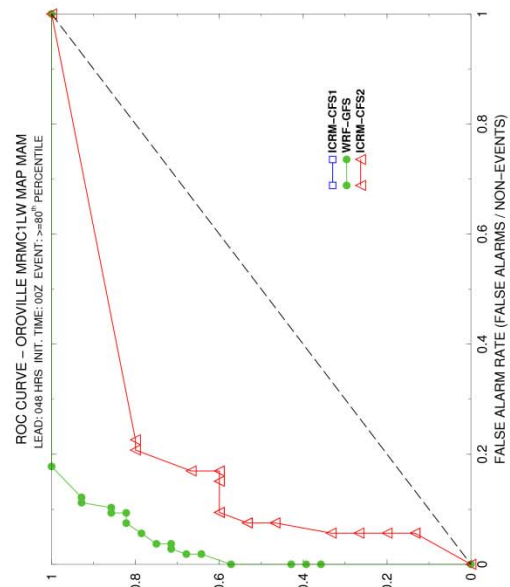
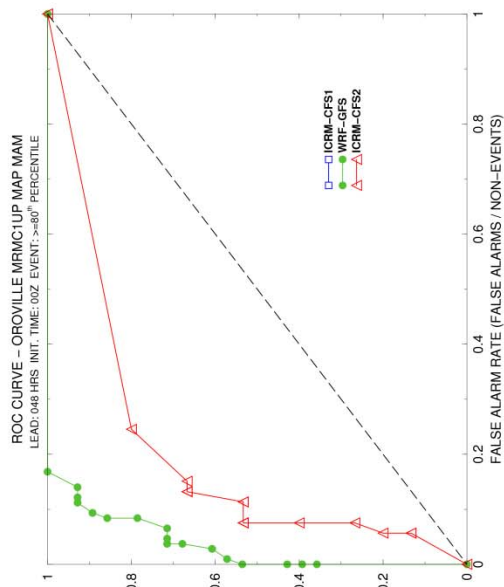
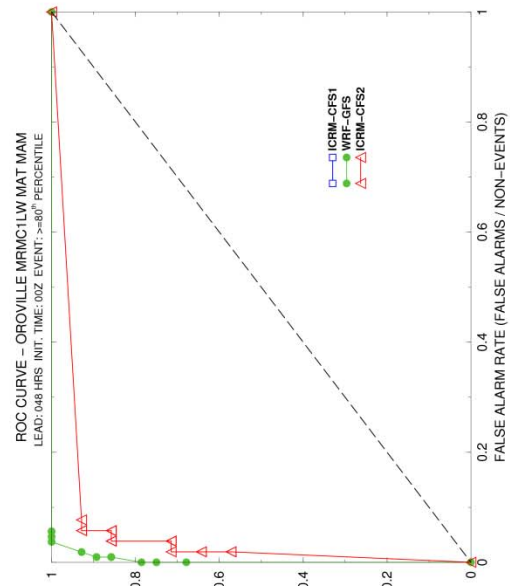
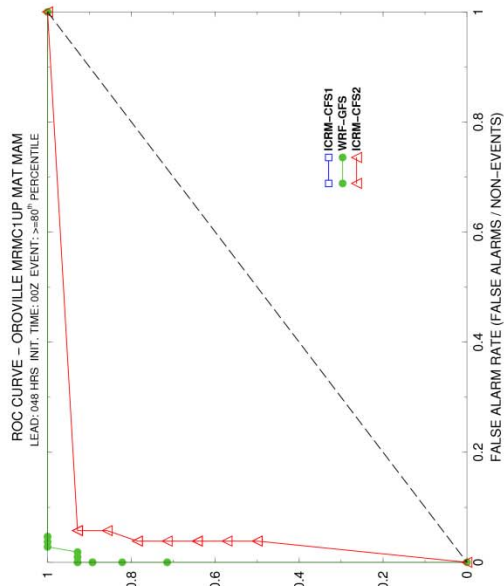


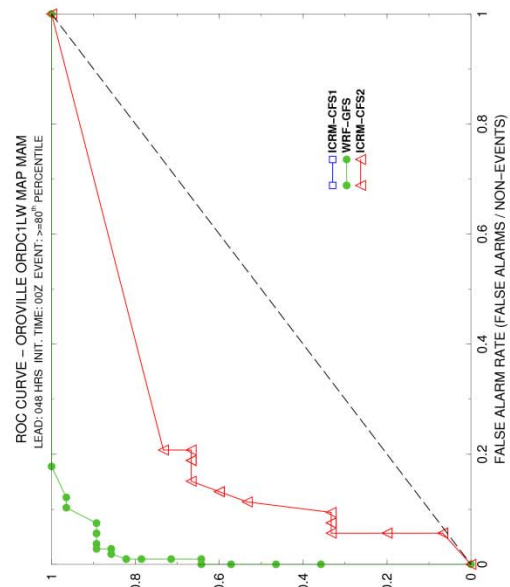
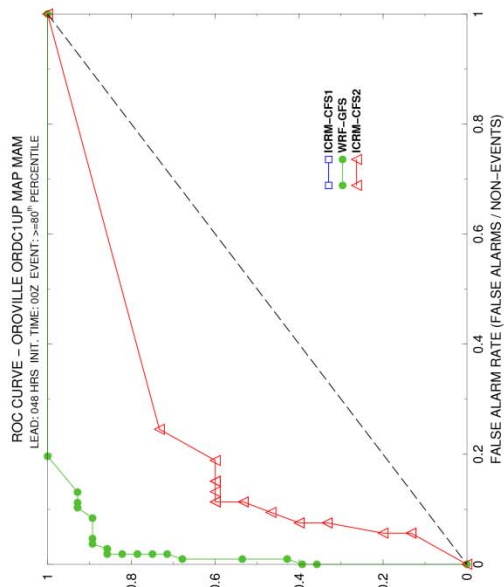
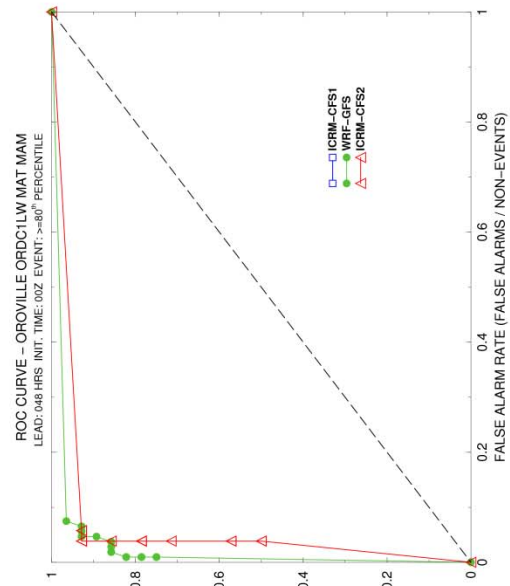
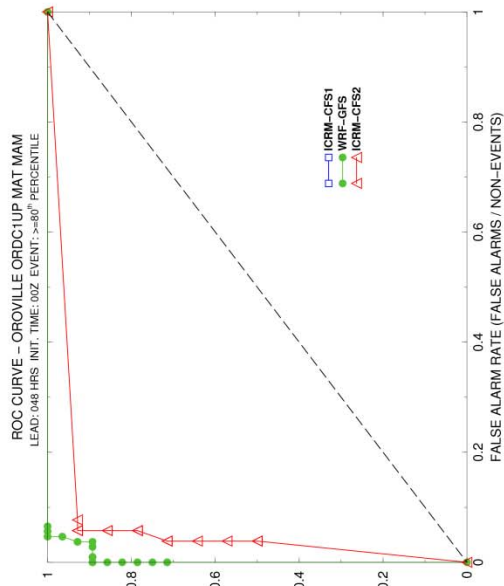


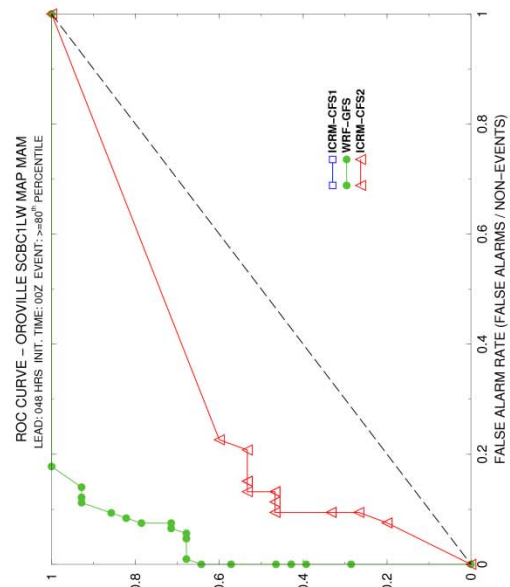
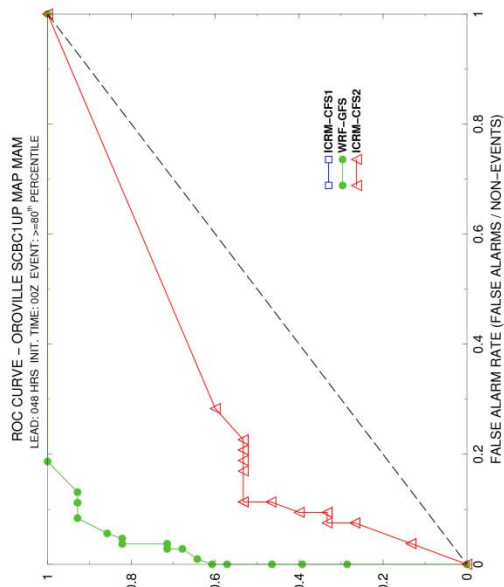
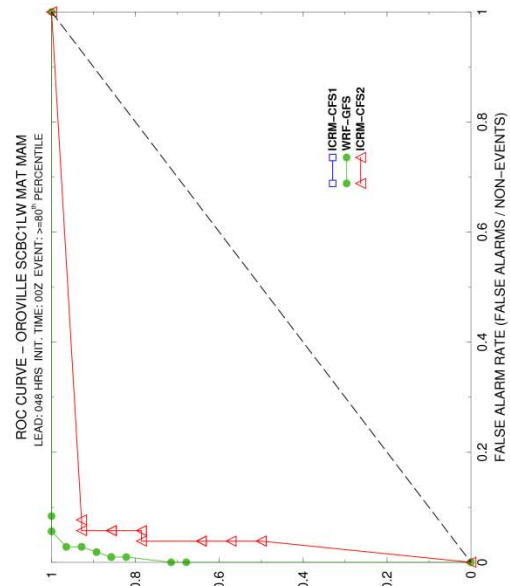
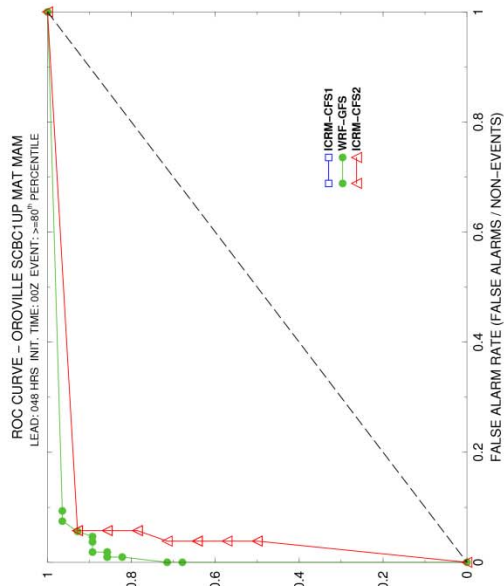


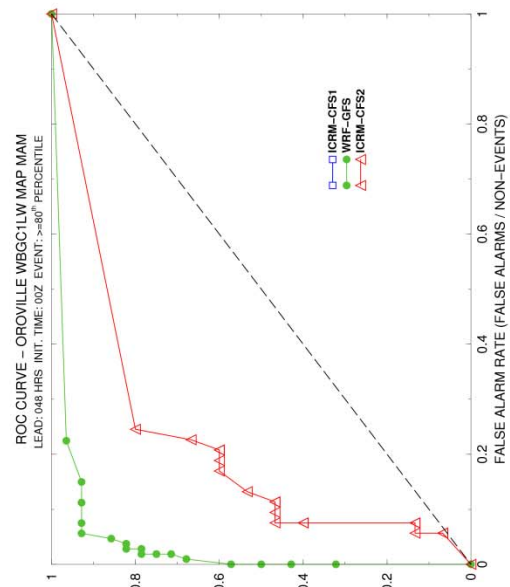
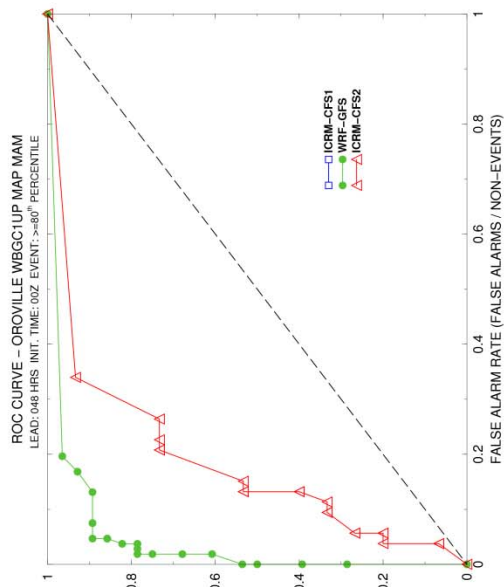
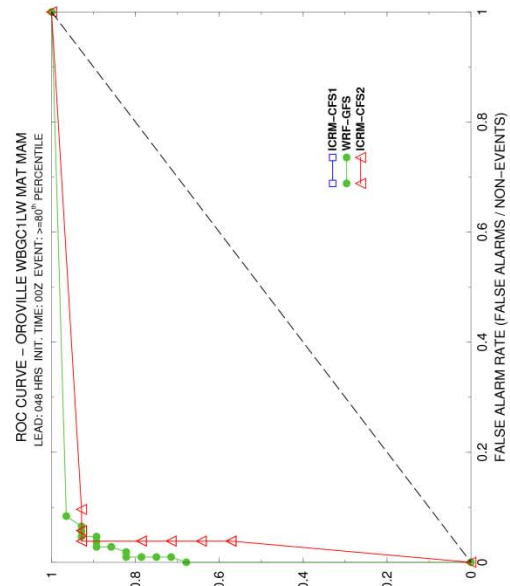
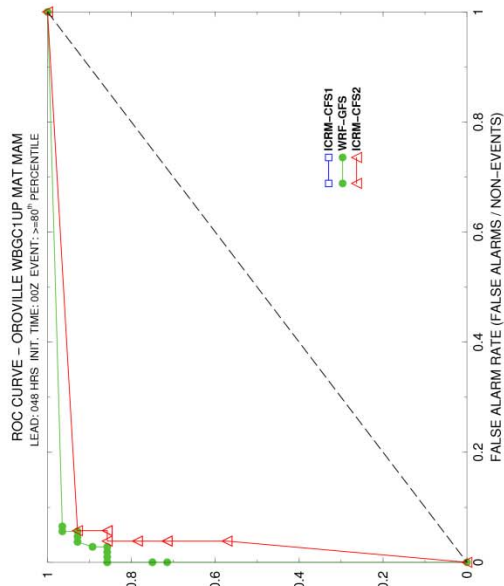


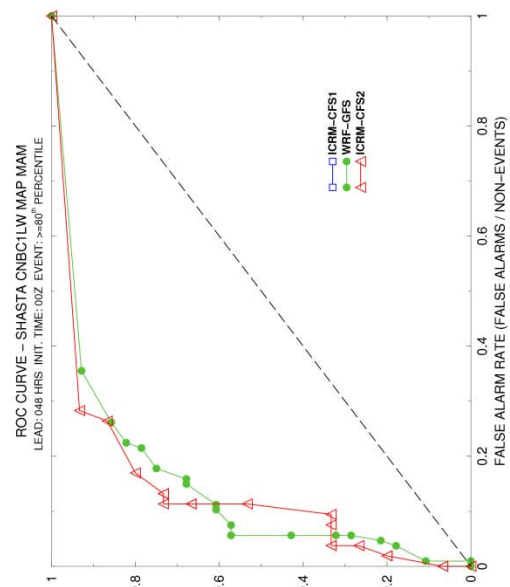
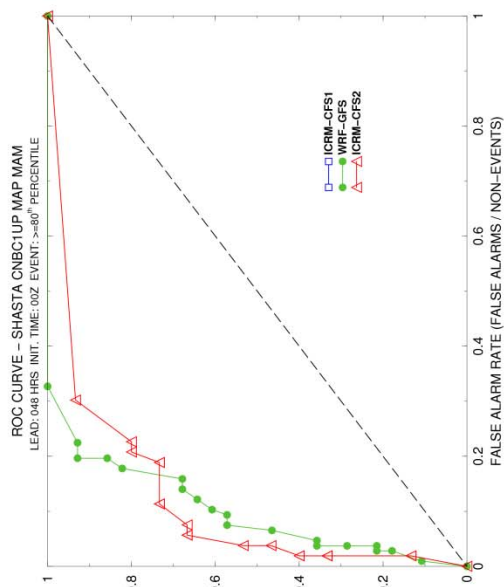
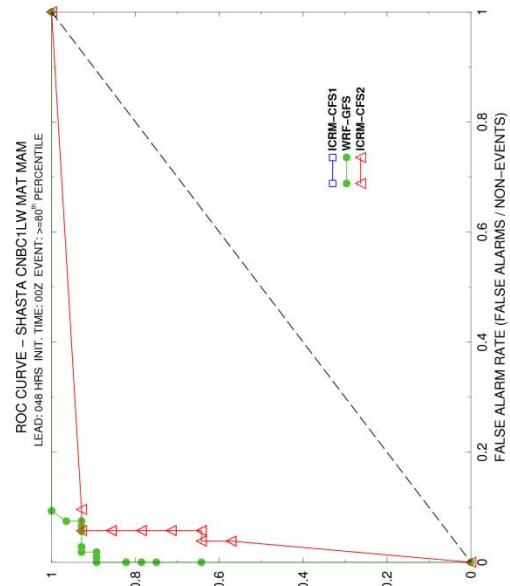
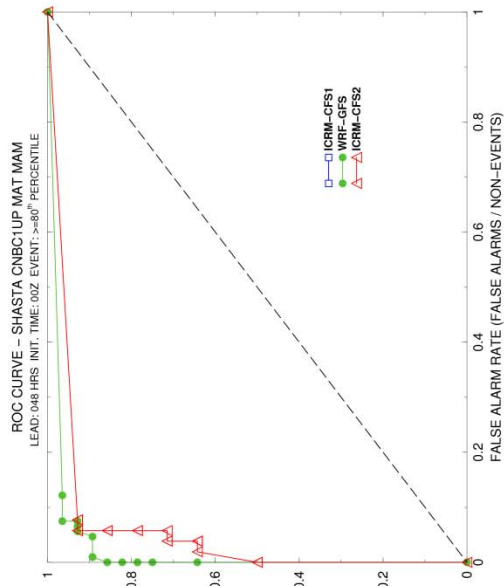


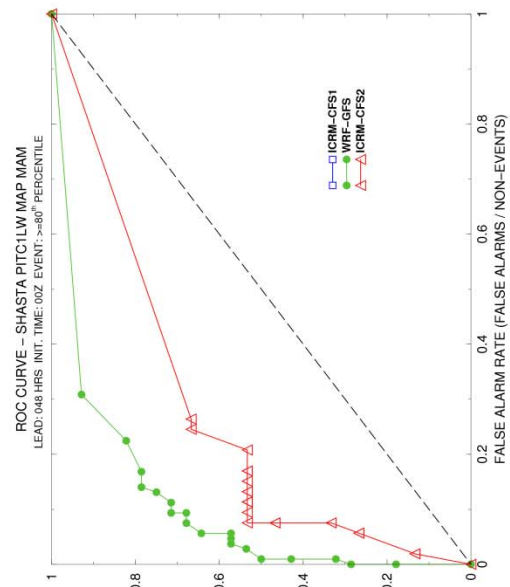
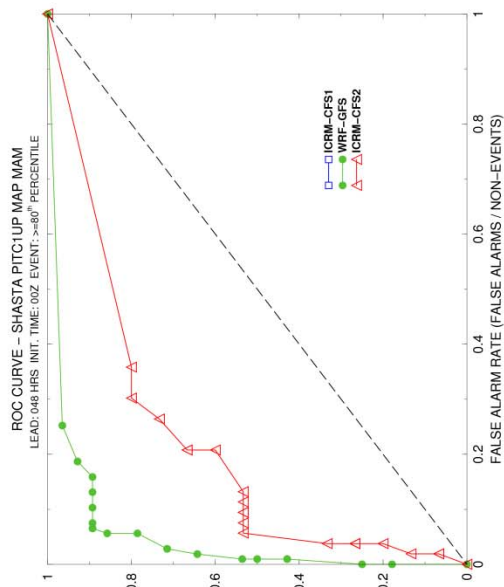
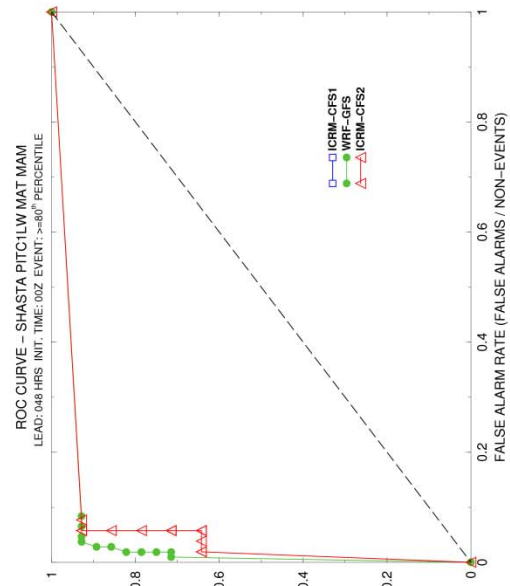
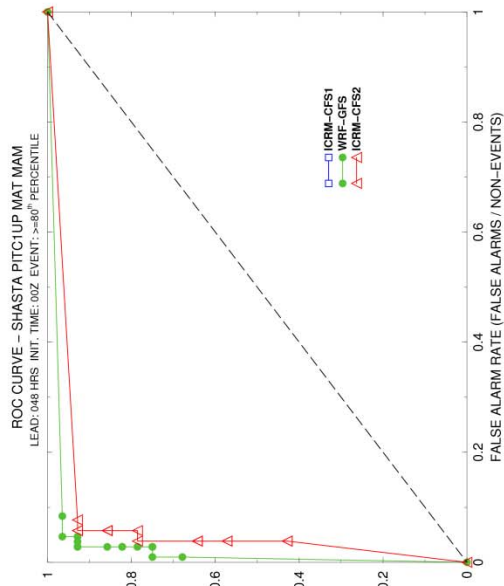


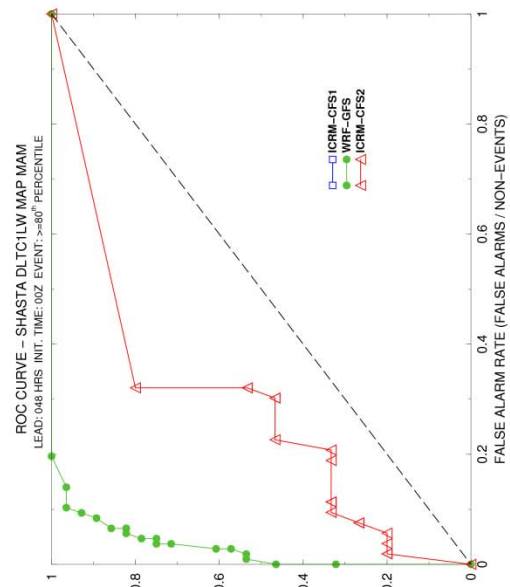
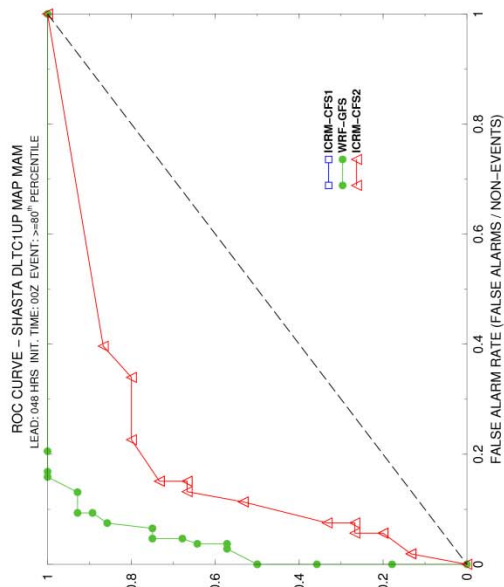
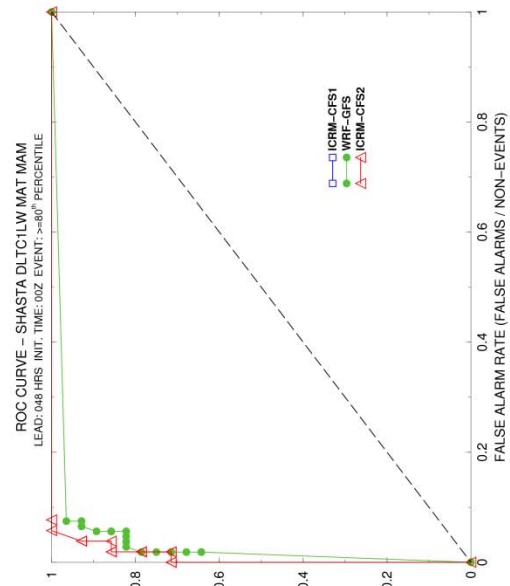
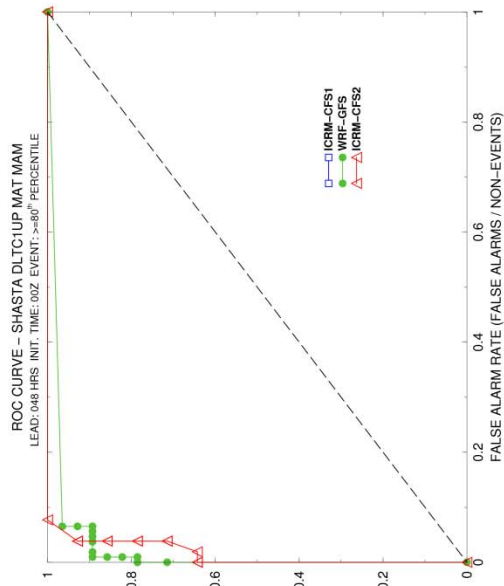


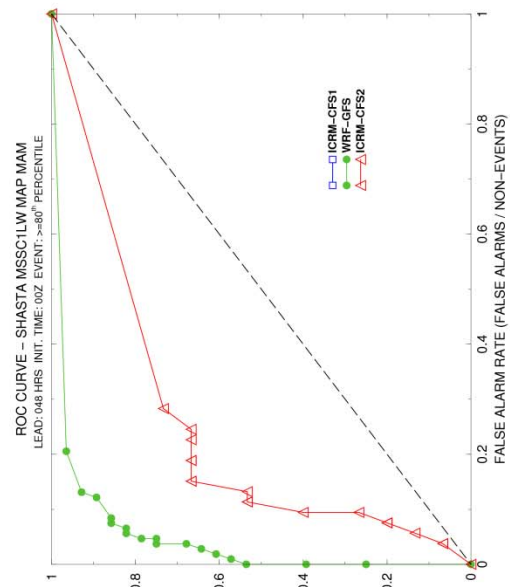
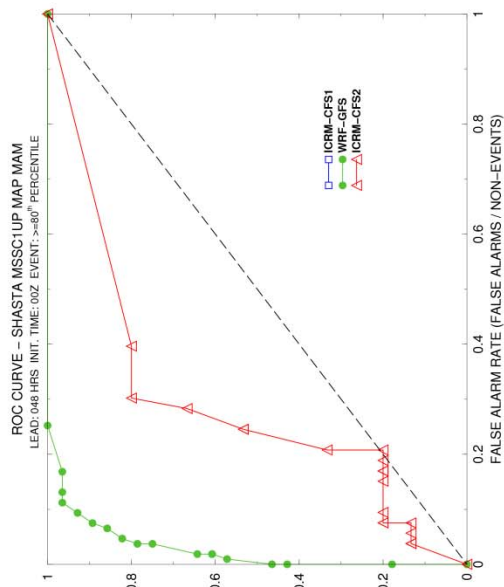
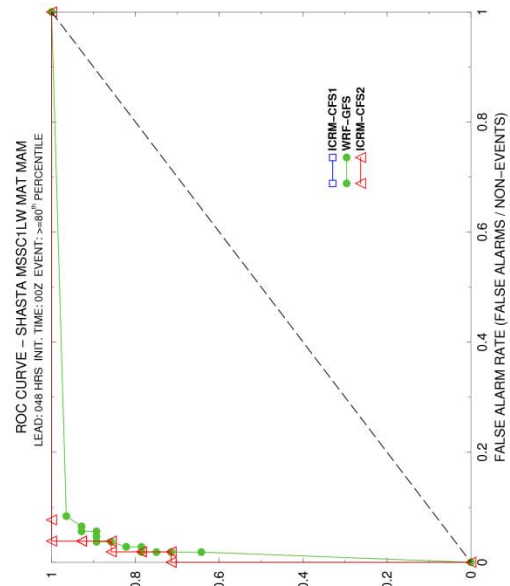
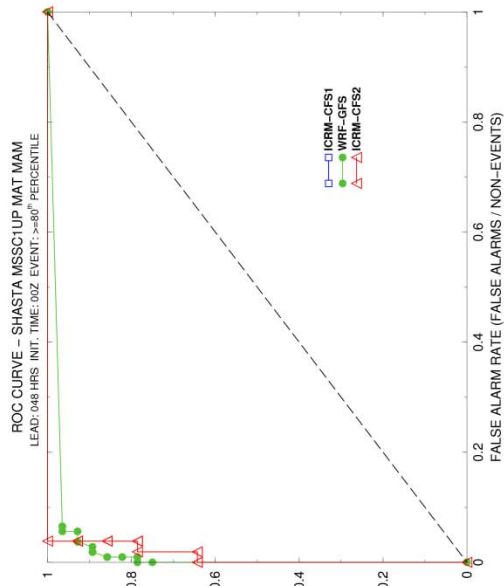


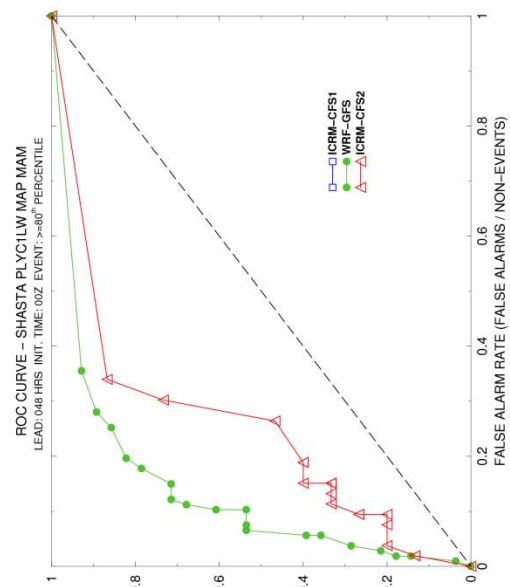
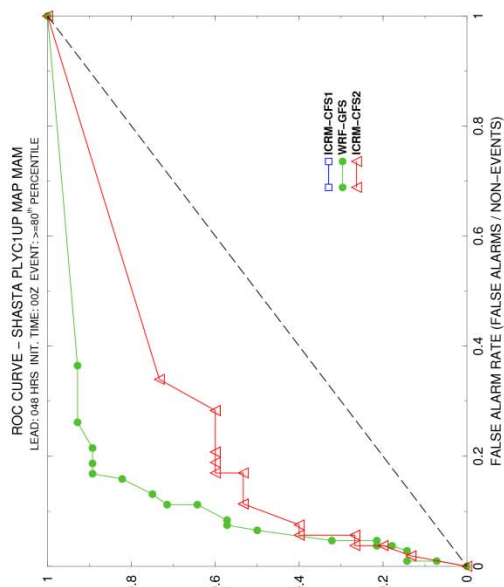
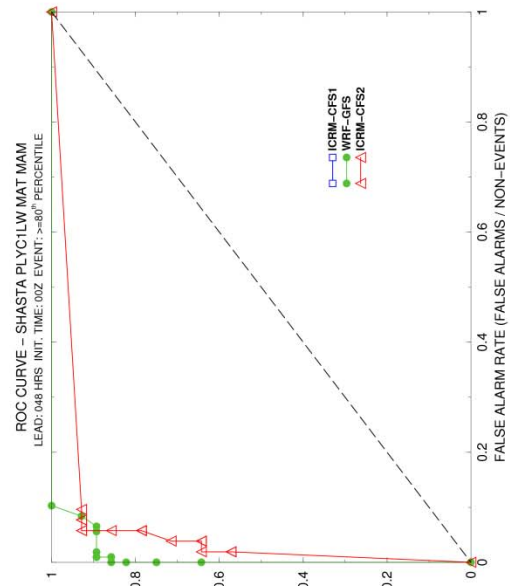
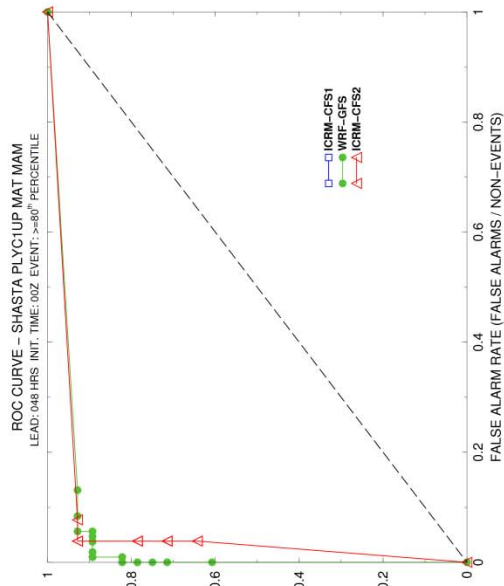


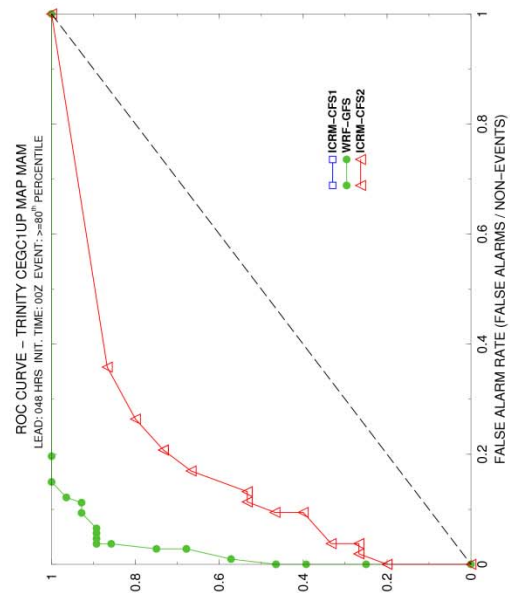
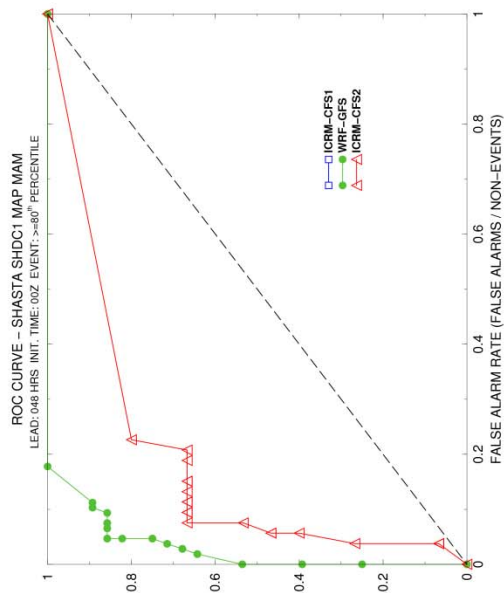
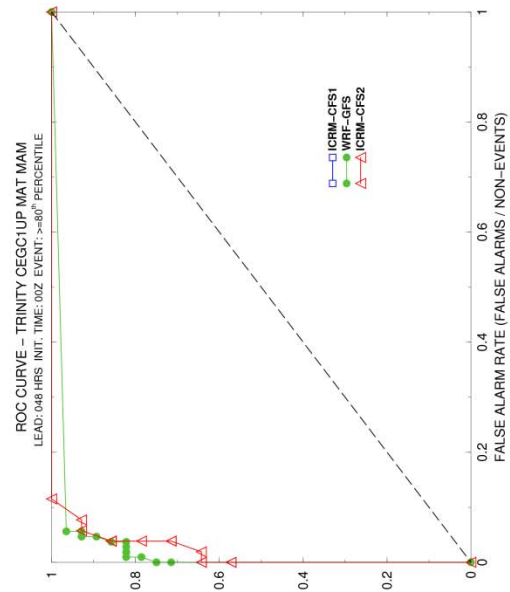
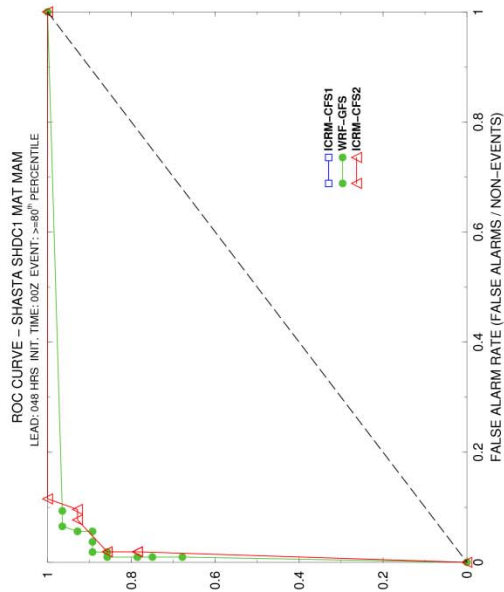


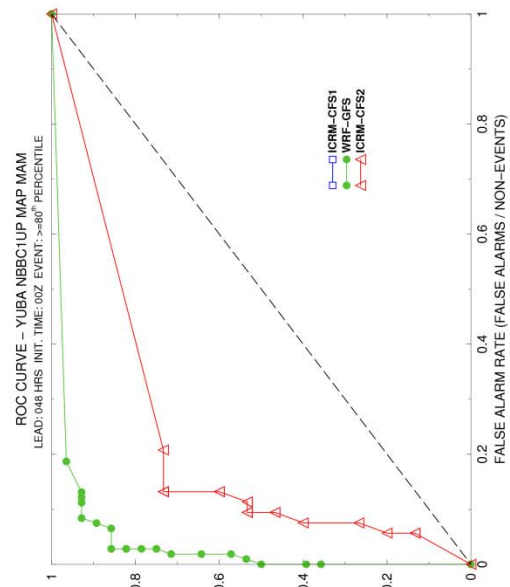
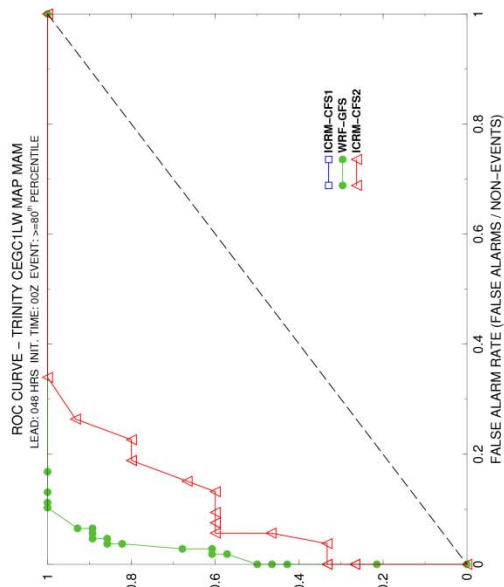
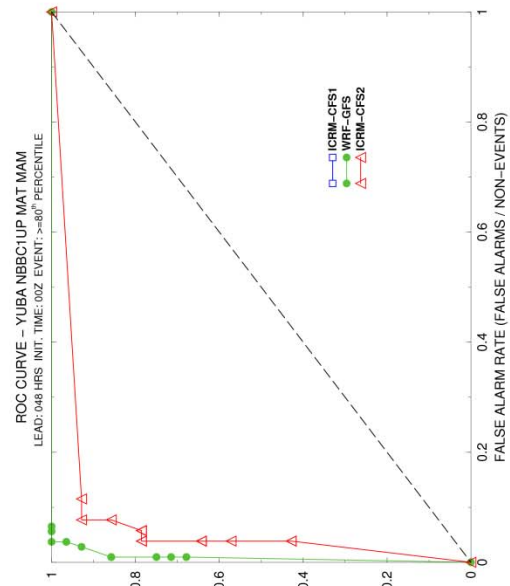
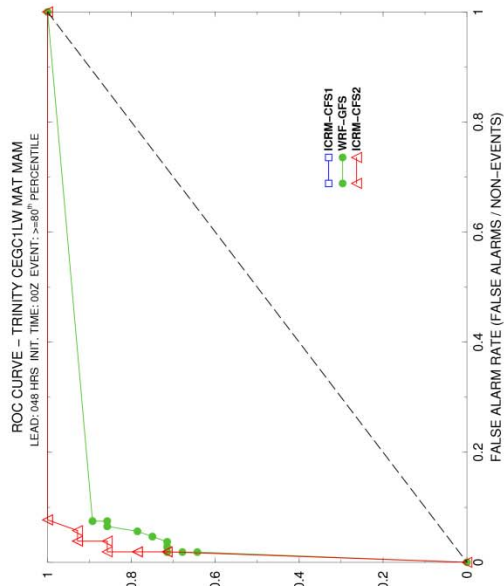


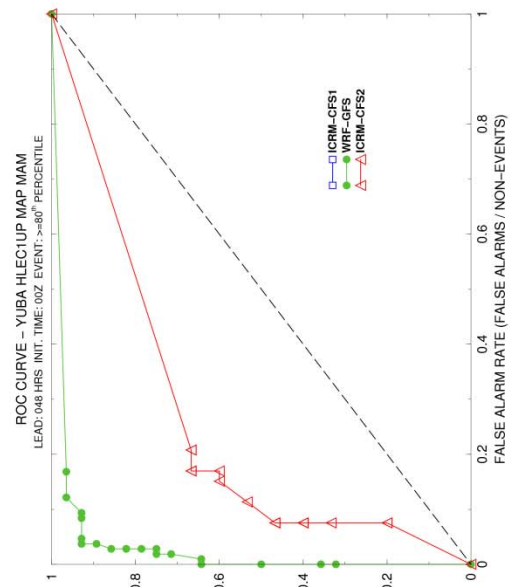
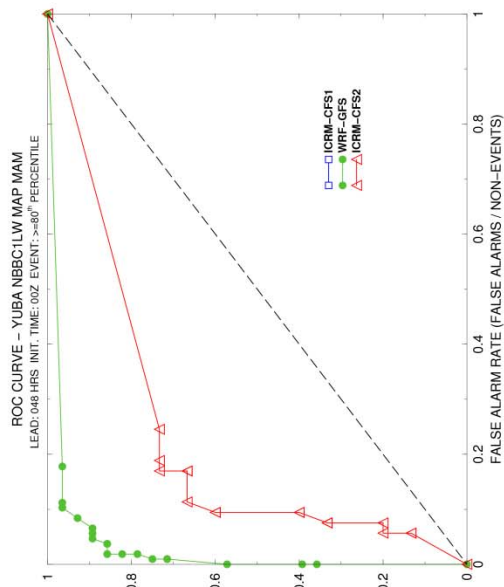
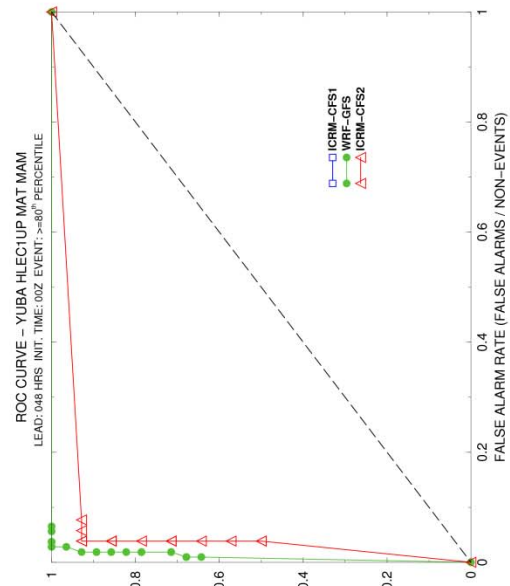
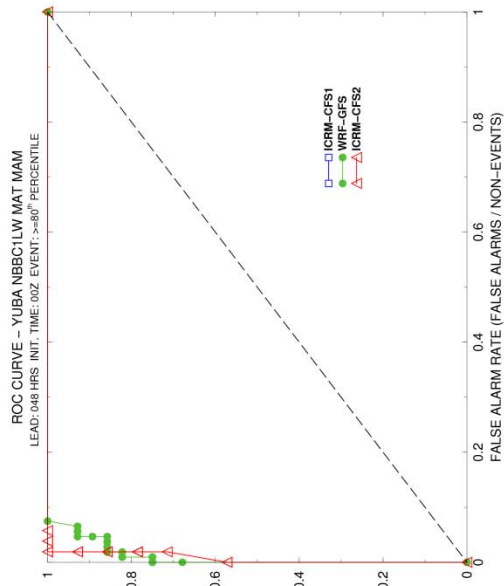


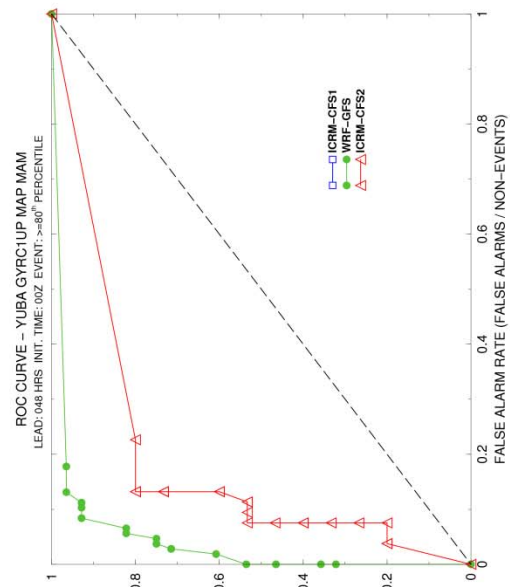
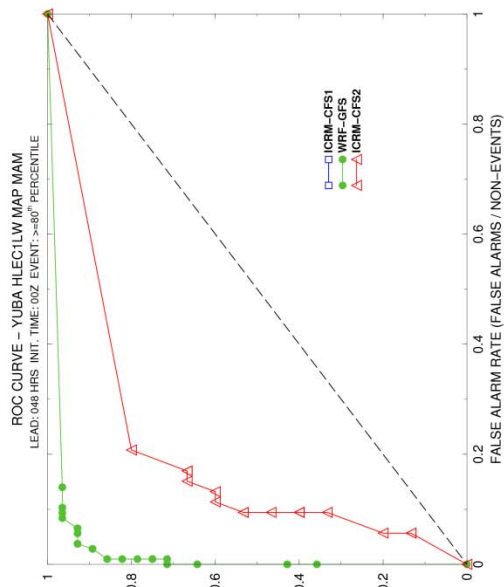
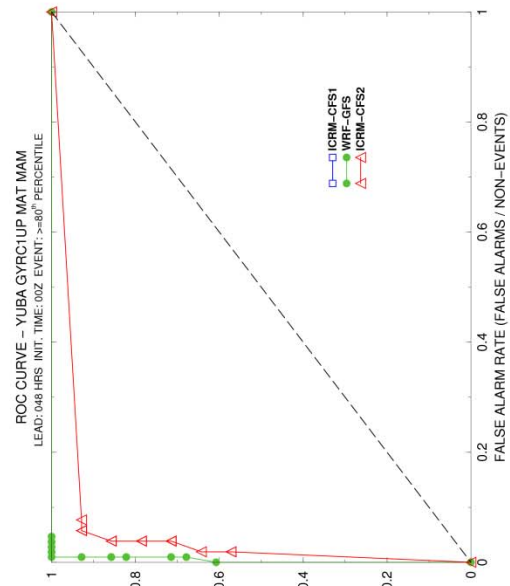
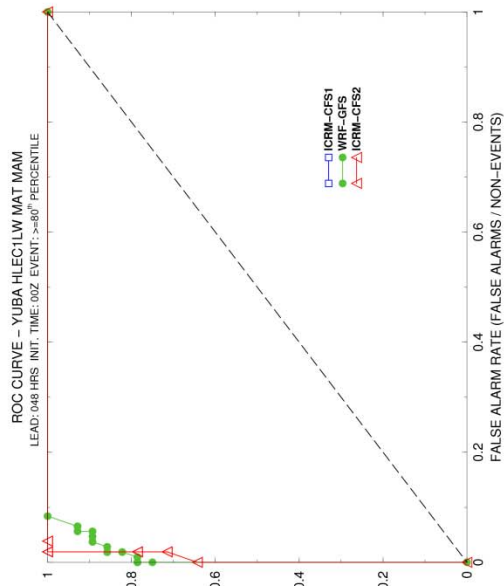








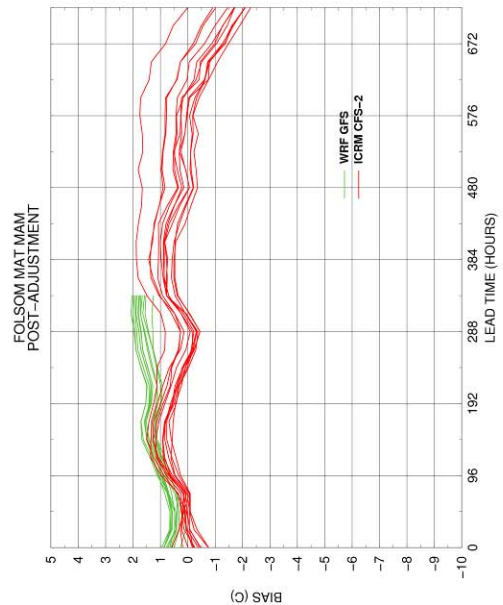
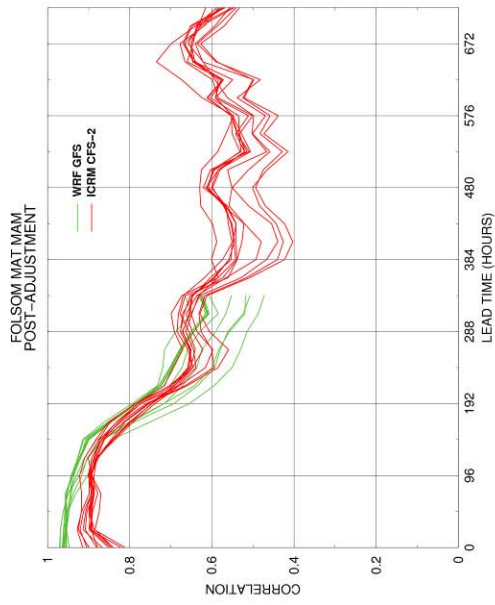
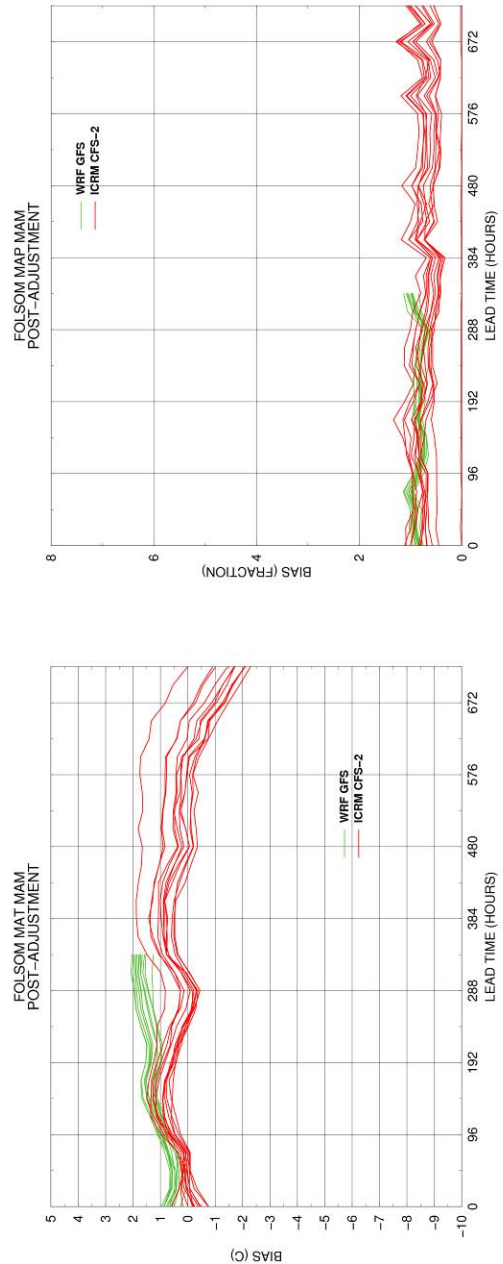
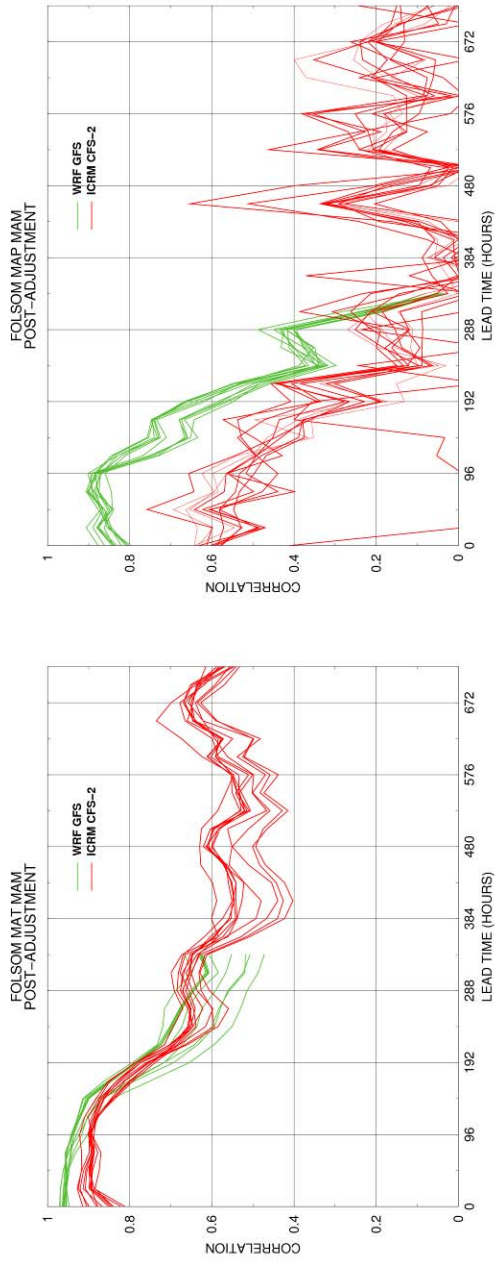


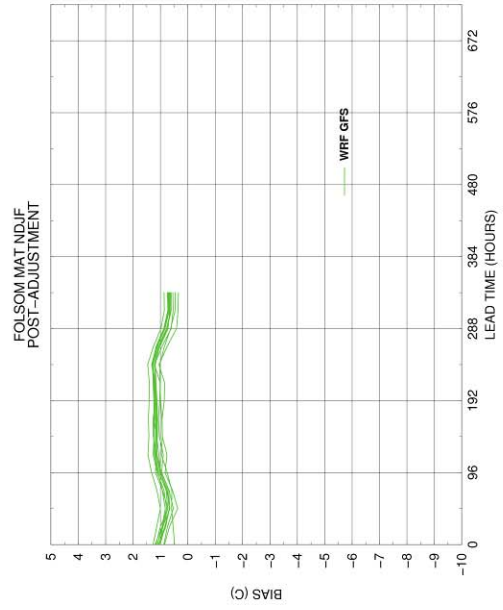
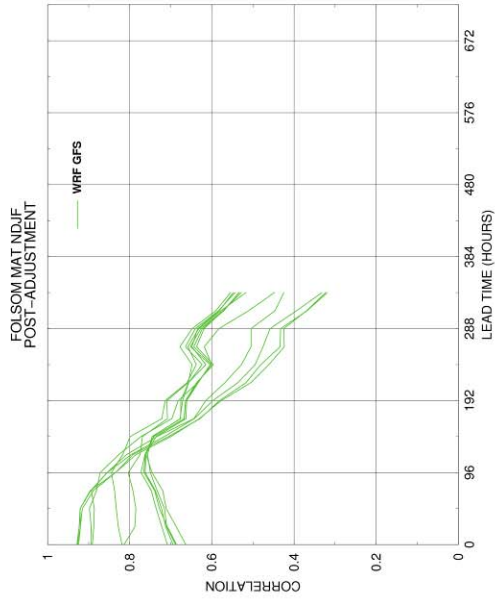
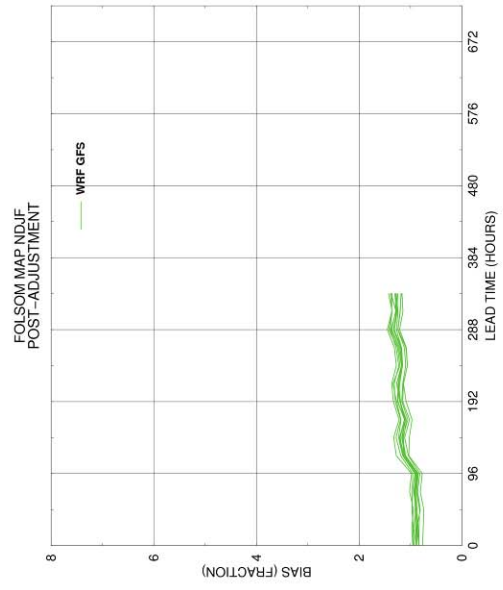
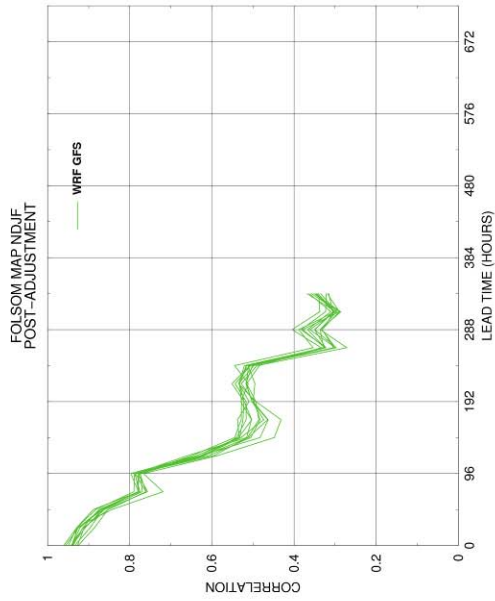


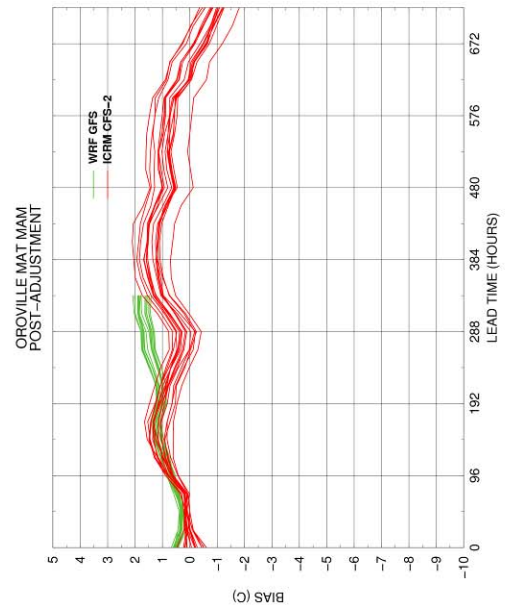
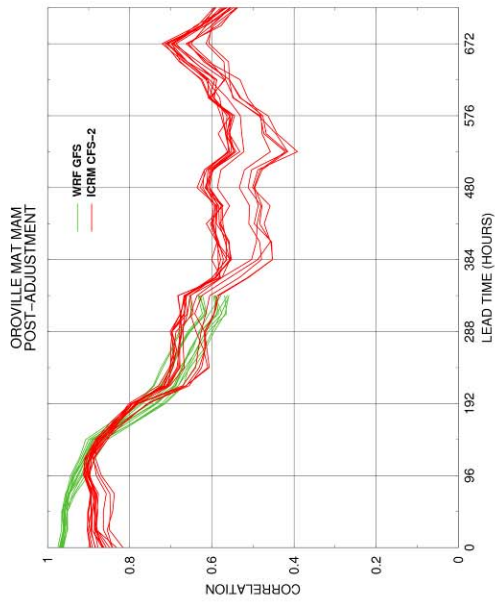
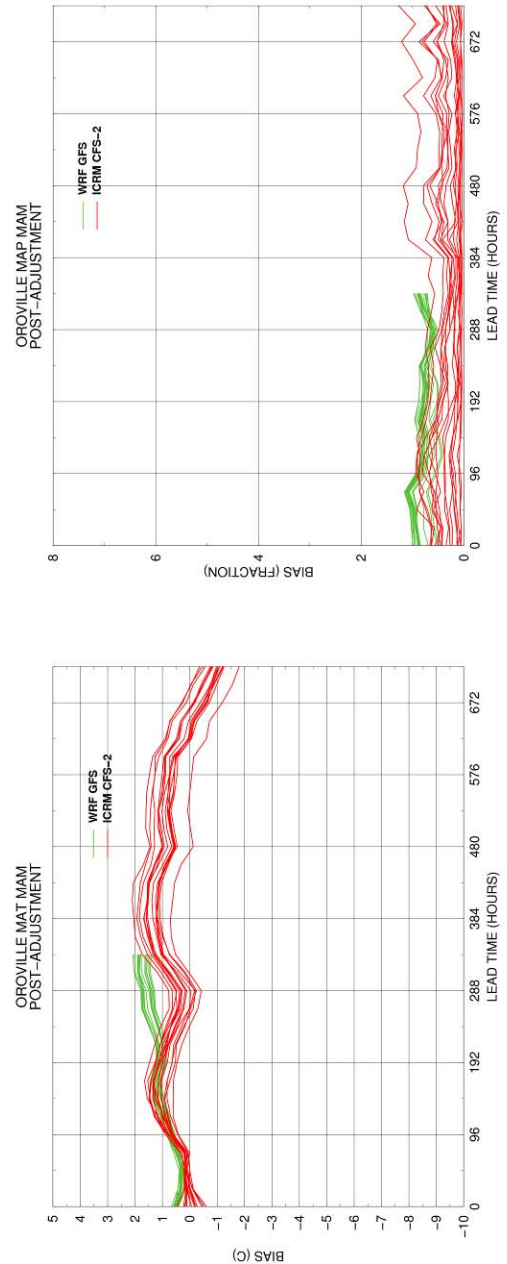
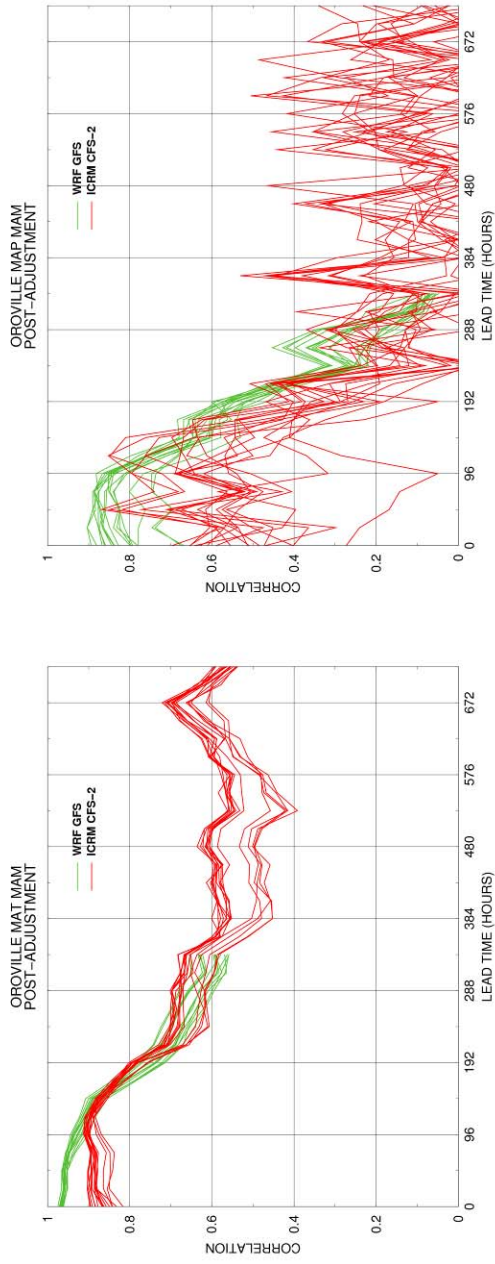
APPENDIX F: Comprehensive Statistical Performance Results after Bias Adjustment

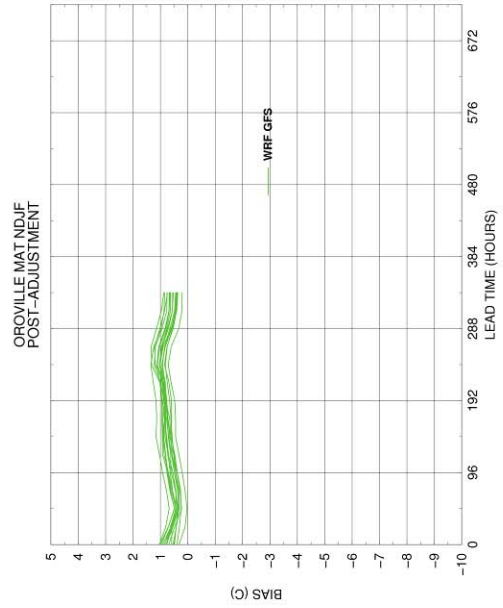
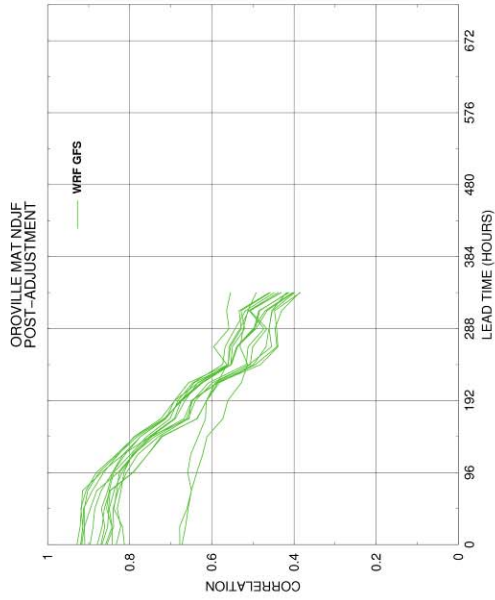
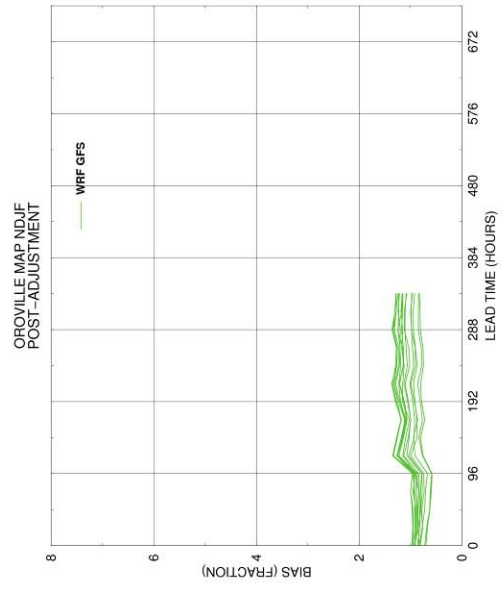
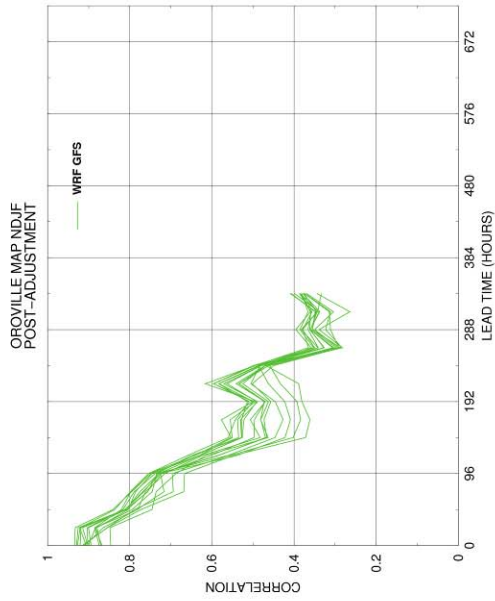
MAP and MAT Forecast Biases and Correlations with Observed

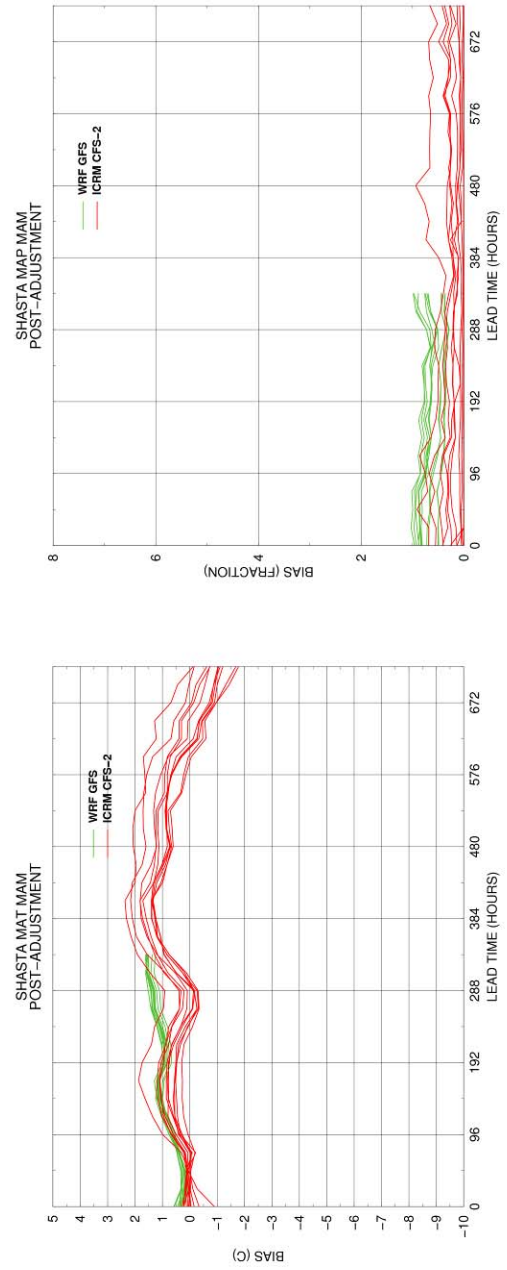
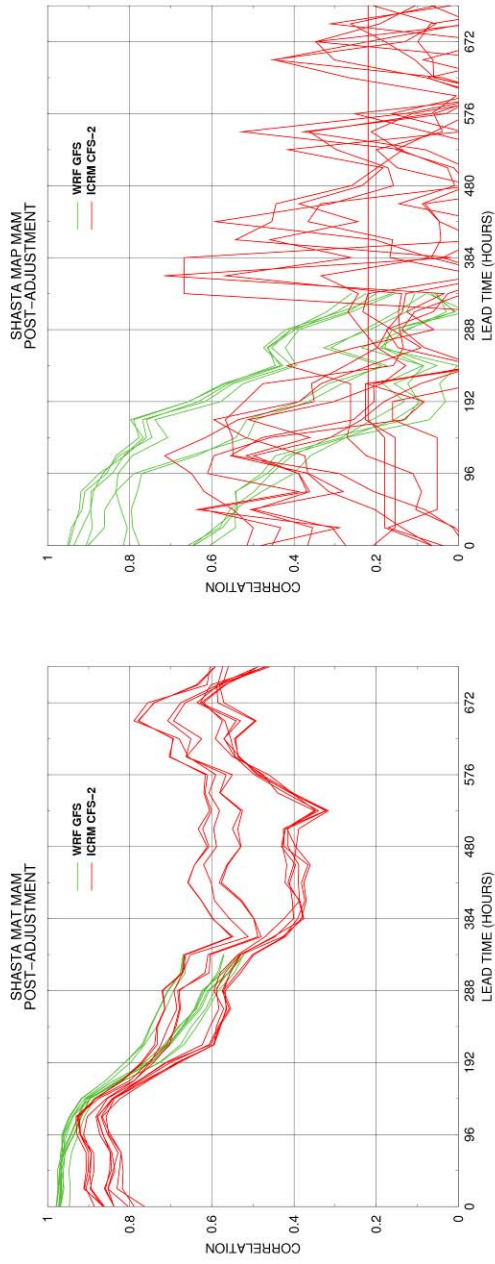
This section of Appendix F presents the results for the bias of the multi-lead forecasts for MAP and MAT as fraction for the MAP and difference for the MAT. It also presents the cross-correlation between the forecasts and observations for the lead times available. These results are presented as plots of bias (or correlation) as a function of lead time, and are for GFS-WRF and CFS2-ICRM ensemble forecasts as described in Chapter 4 (section 4.1.5). Green lines are for the GFS-WRF forecasts and red lines are for the CFS2-ICRM forecasts. Each plot is for a different watershed (drainage of each of the five major reservoirs: Folsom, New Bullards Bar, Oroville, Shasta and Trinity). Multiple lines for each watershed are shown; one for each of the sub-catchments in the watershed (includes upper and lower areas delineated for the snow and soil model). Results for both the accumulation season (NDJF) and the melt season (MAM) are shown in the plots. The NDJF season does not contain any CFS2-ICRM forecasts as they started on 21 February 2012.

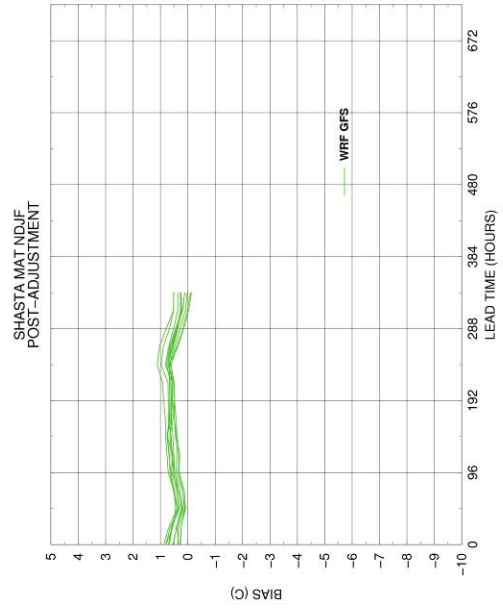
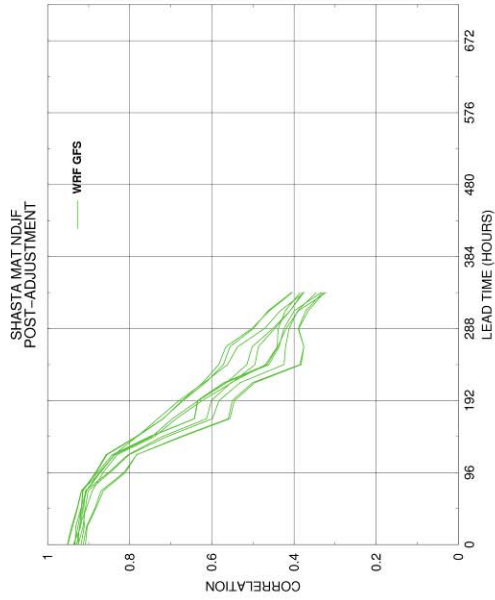
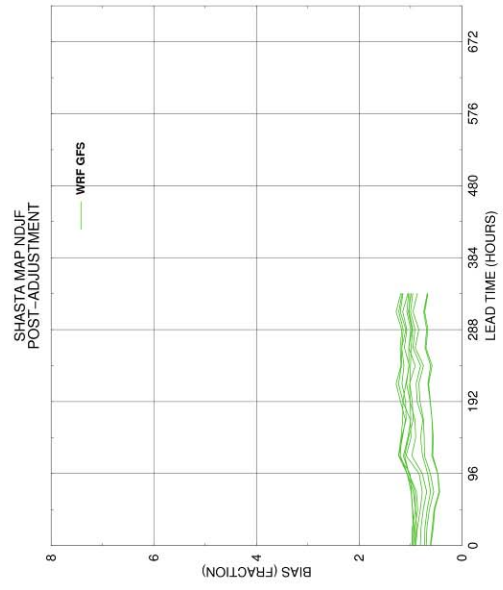
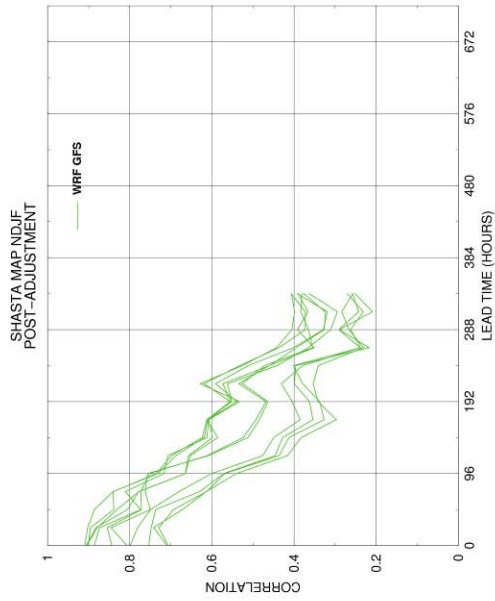


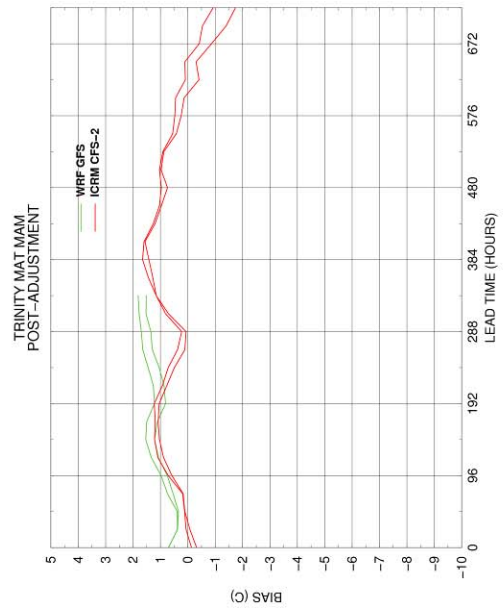
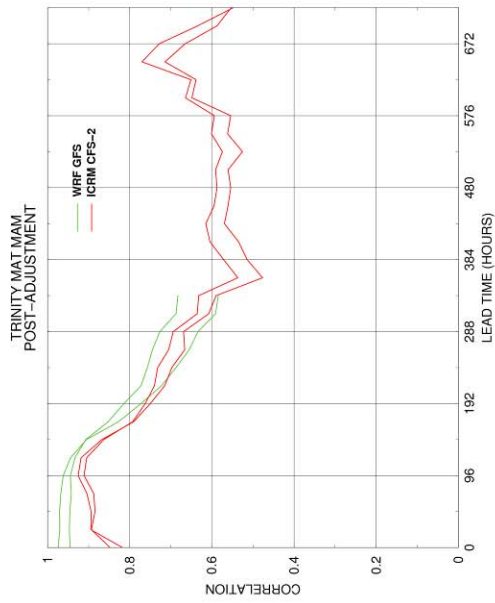
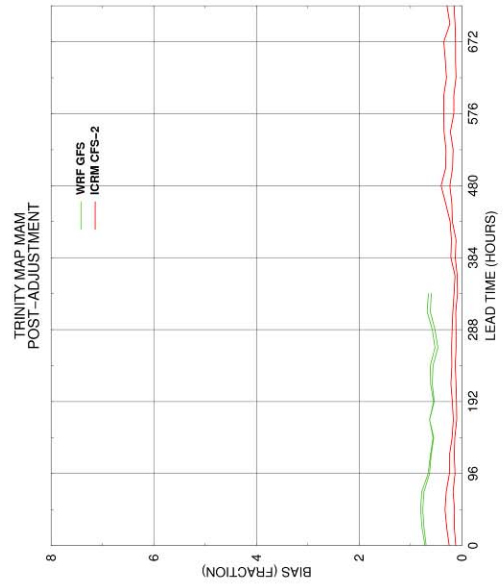
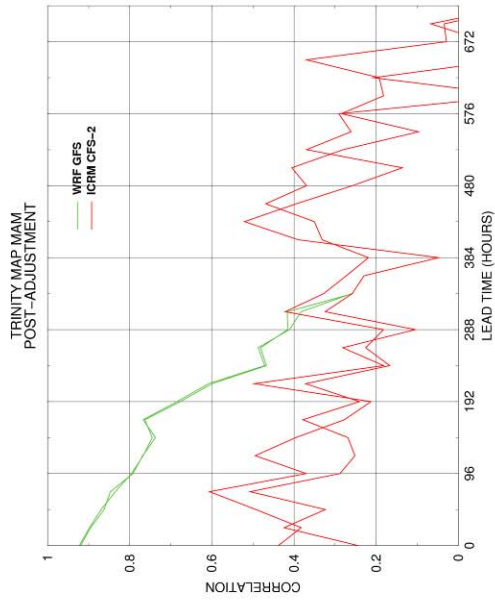


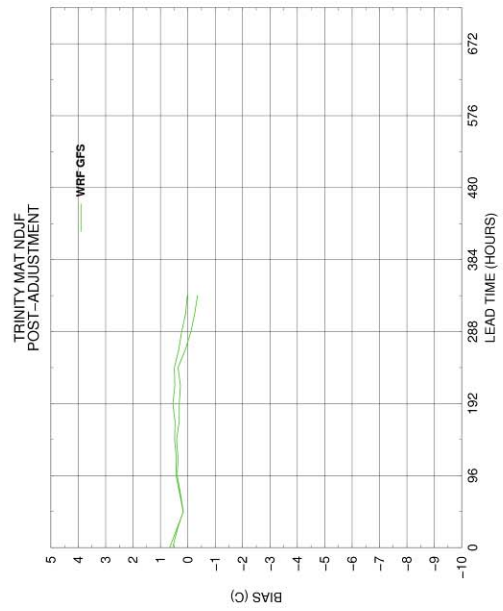
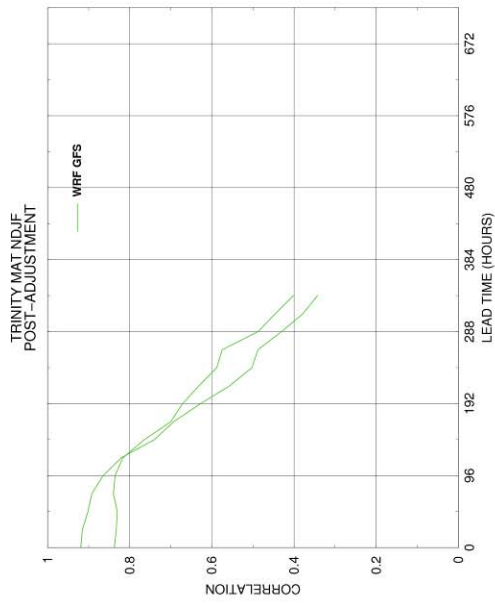
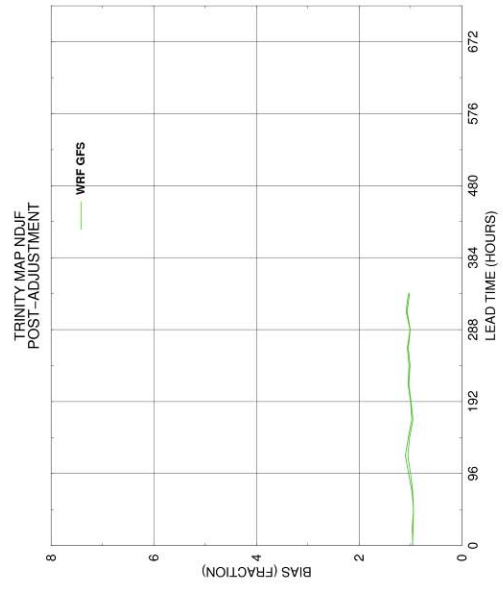
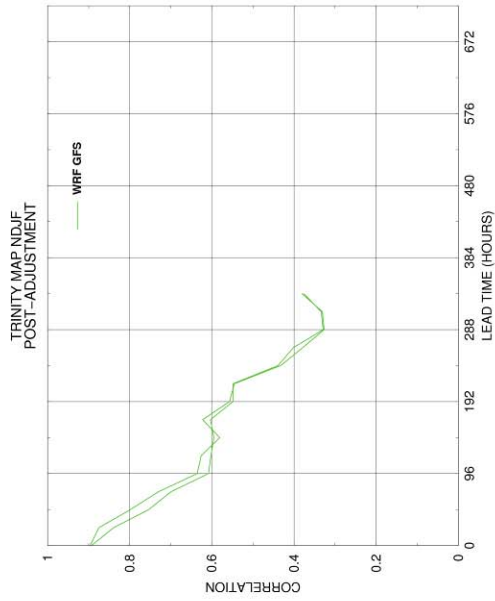


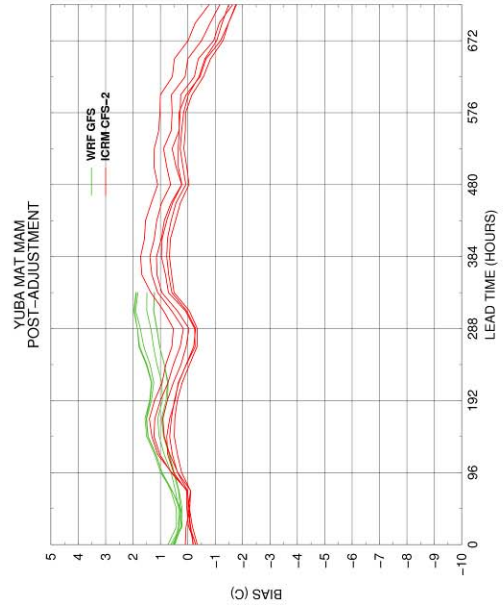
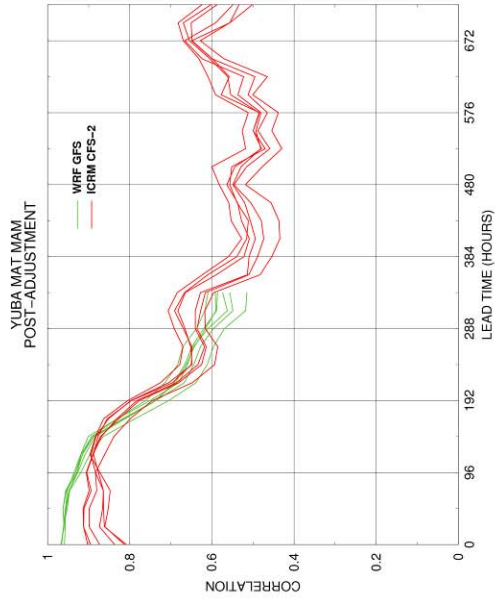
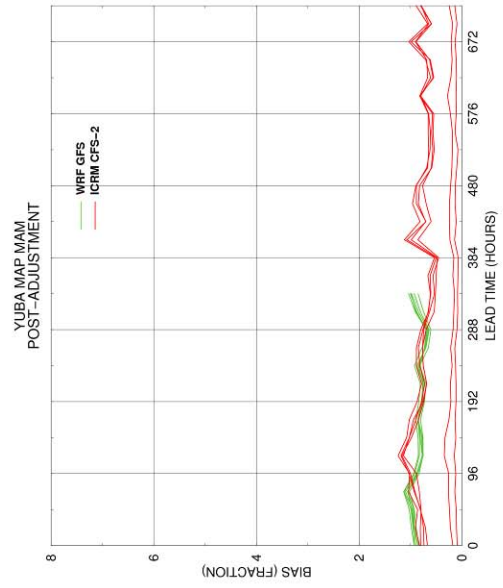
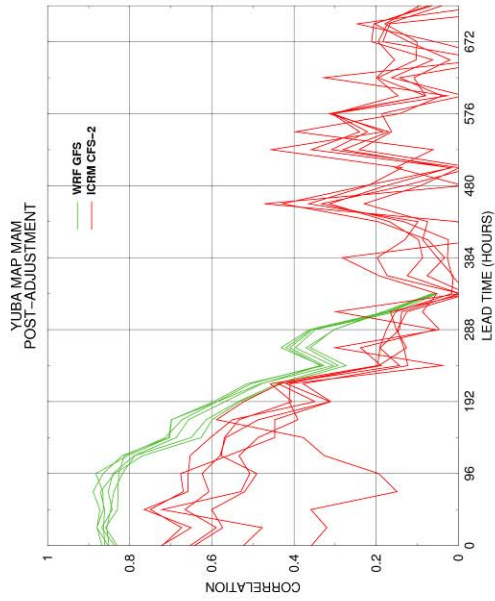


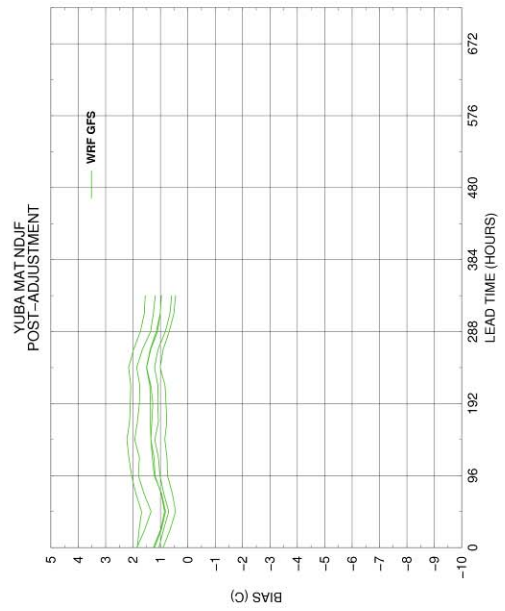
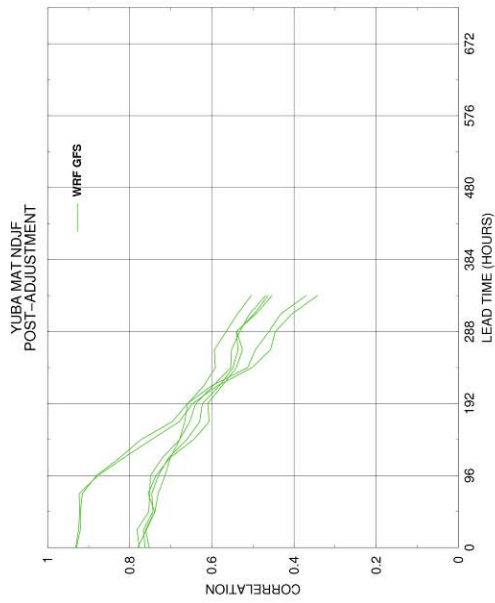
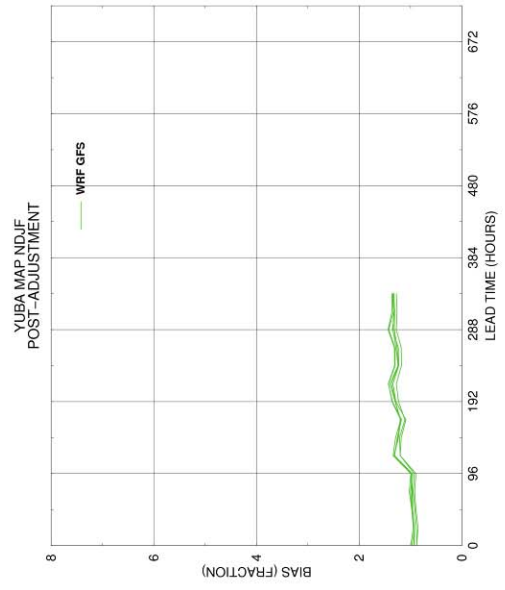
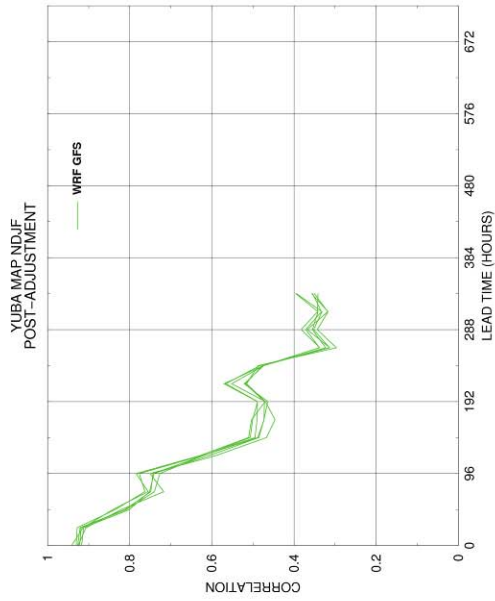






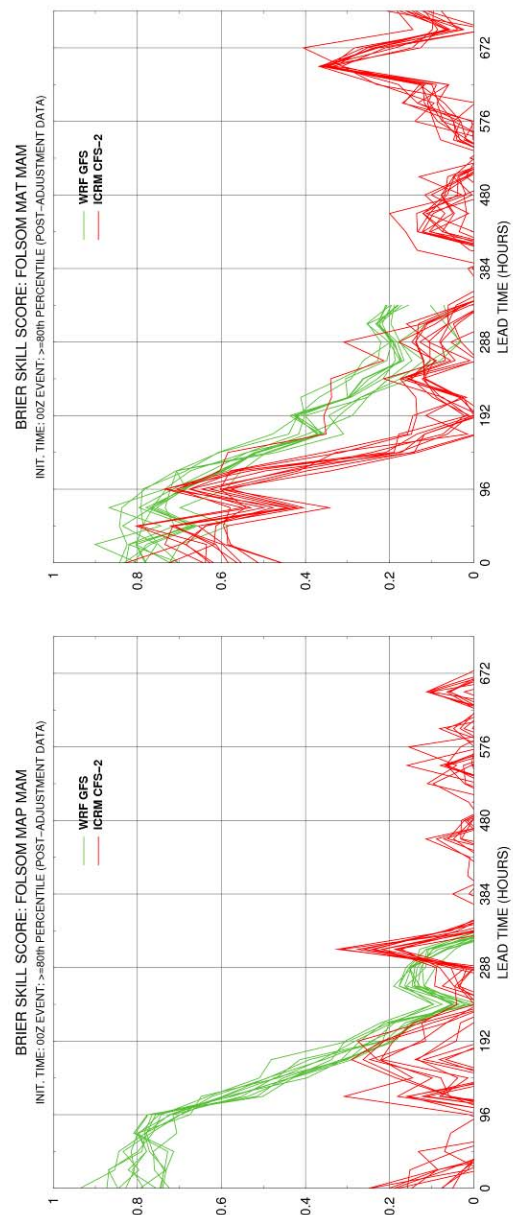
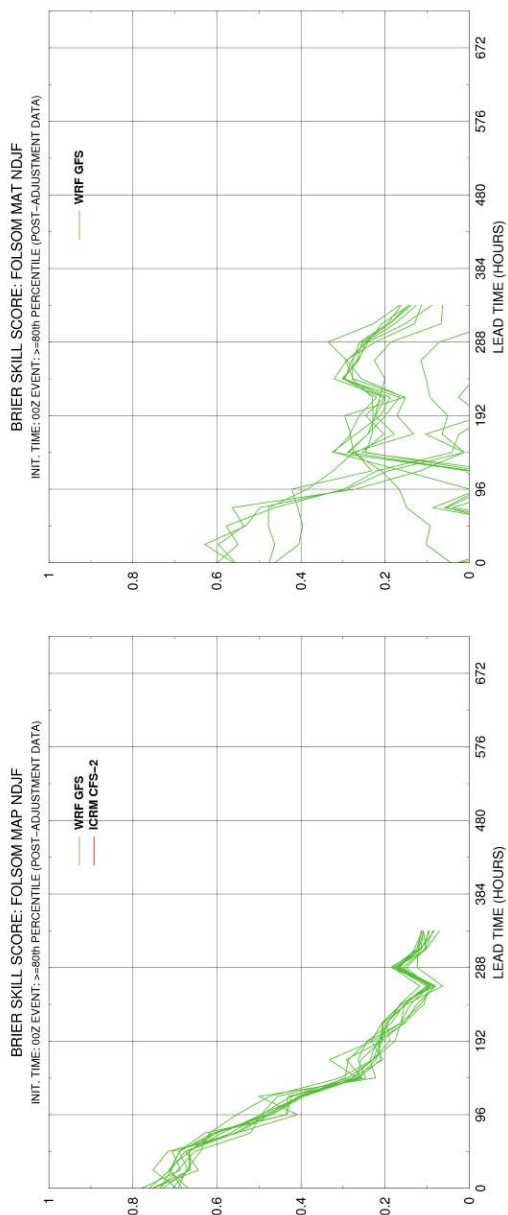


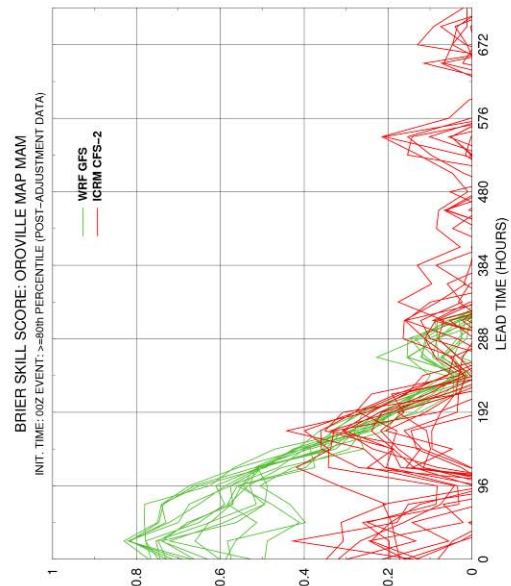
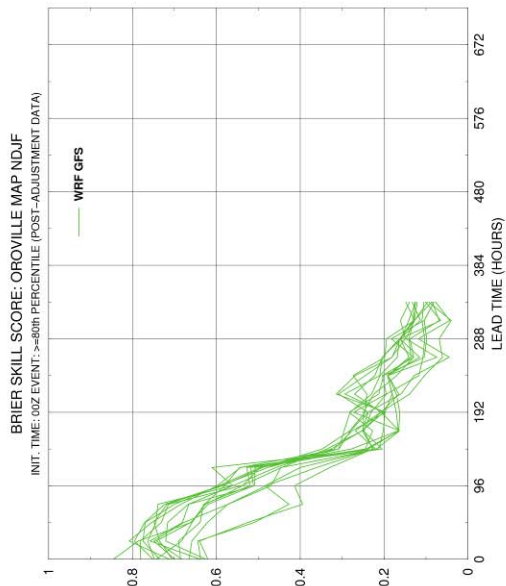
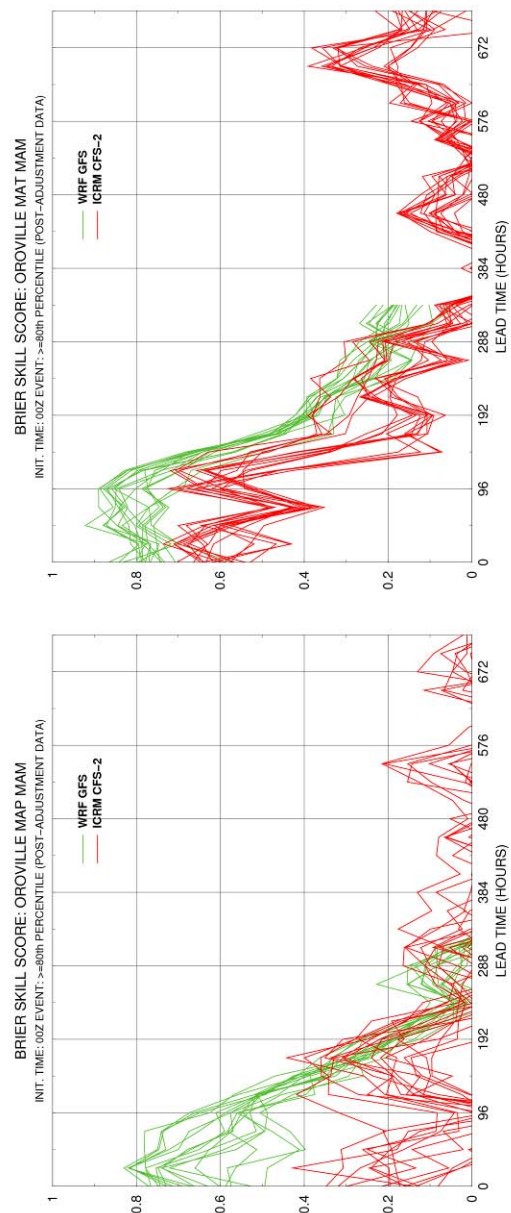
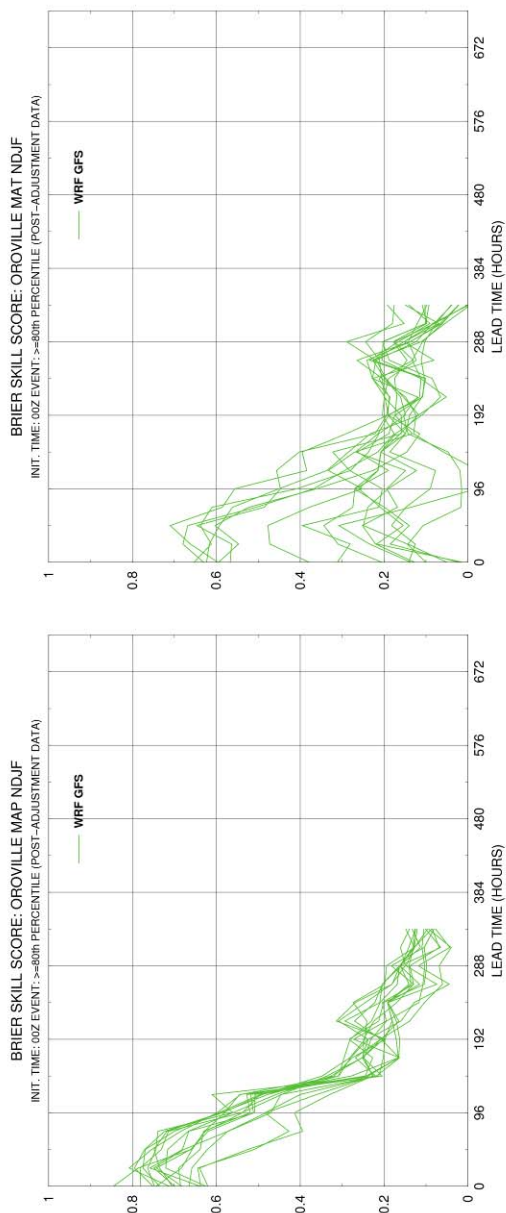


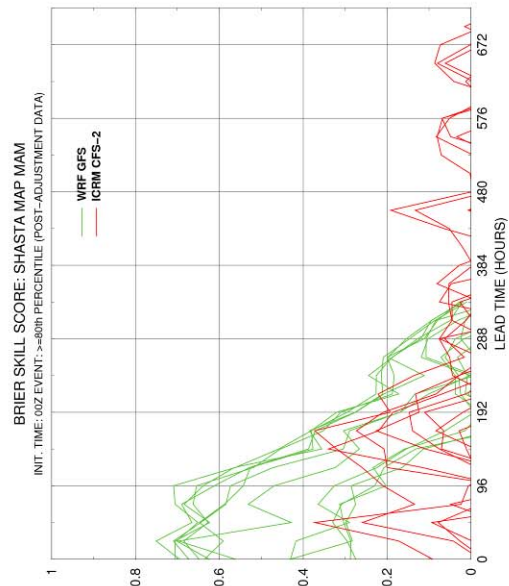
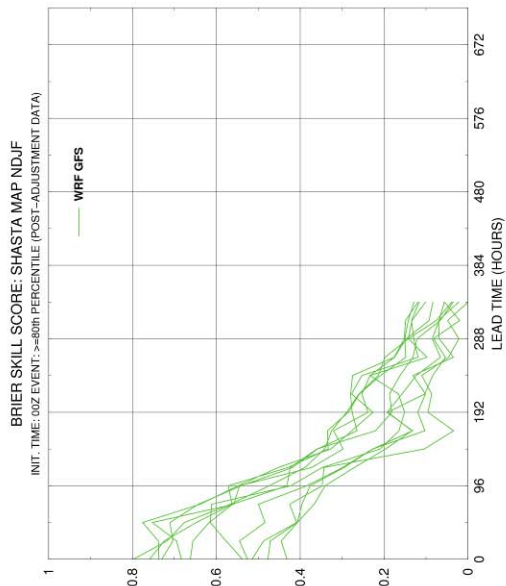
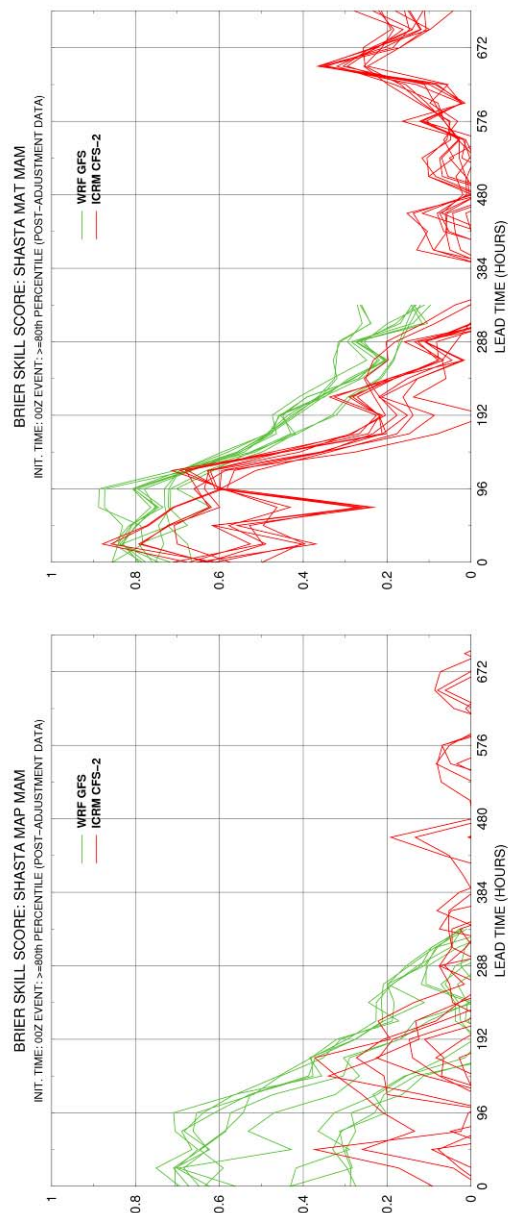
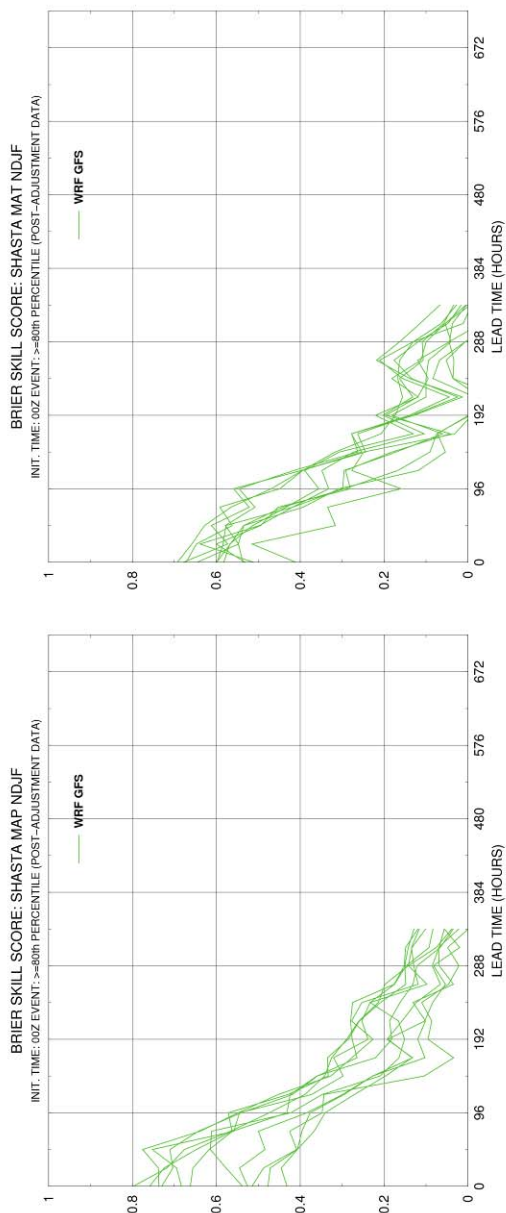


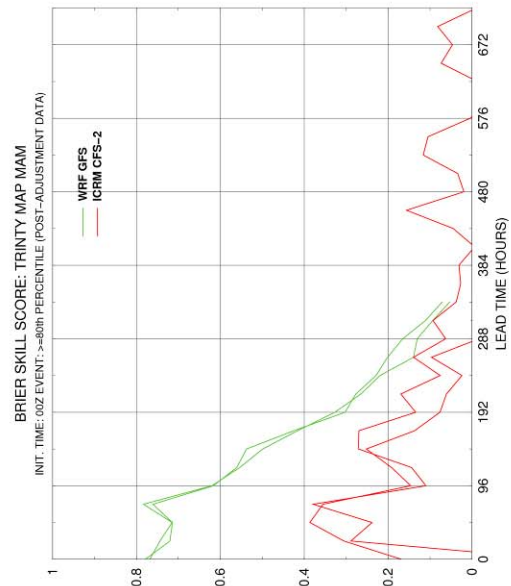
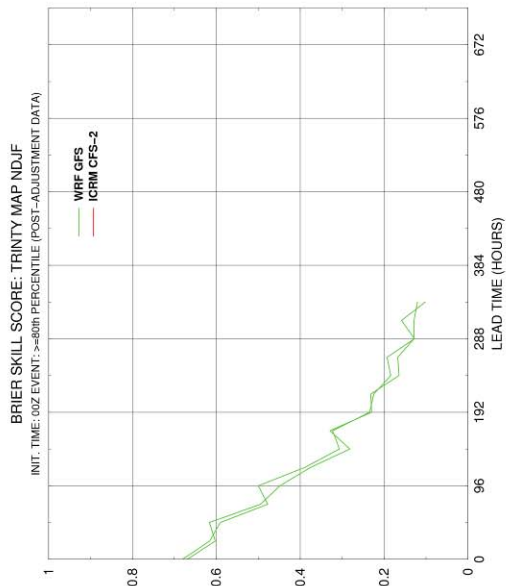
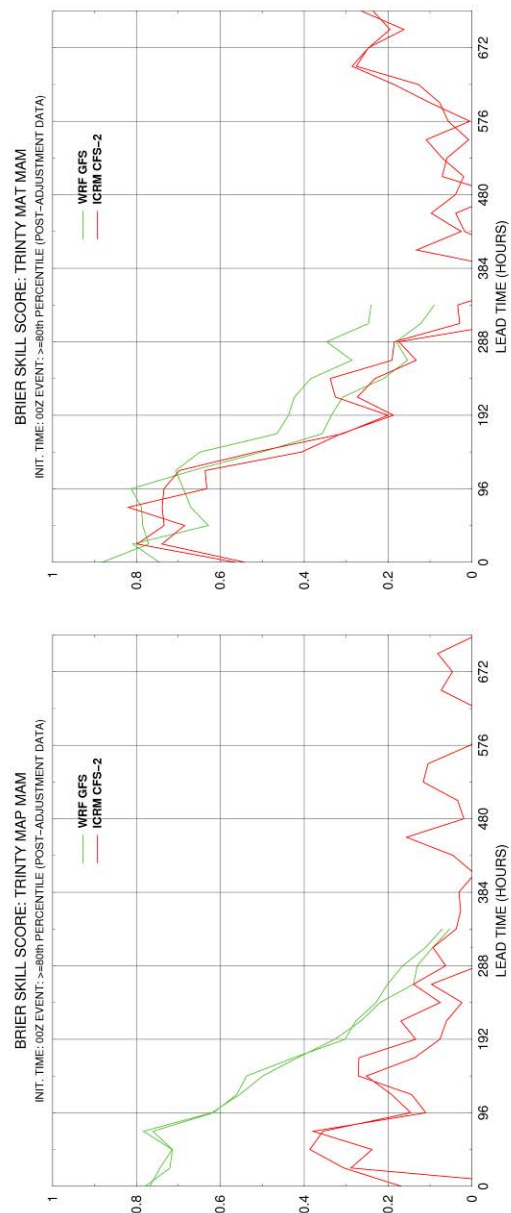
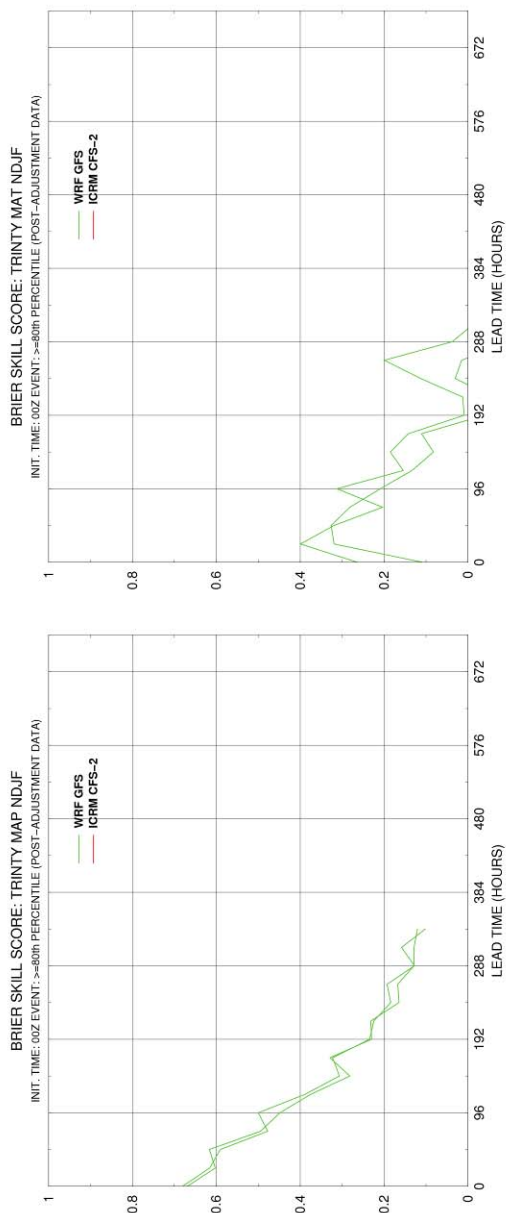
MAP and MAT Reliability Analysis (Post Bias Adjustment)

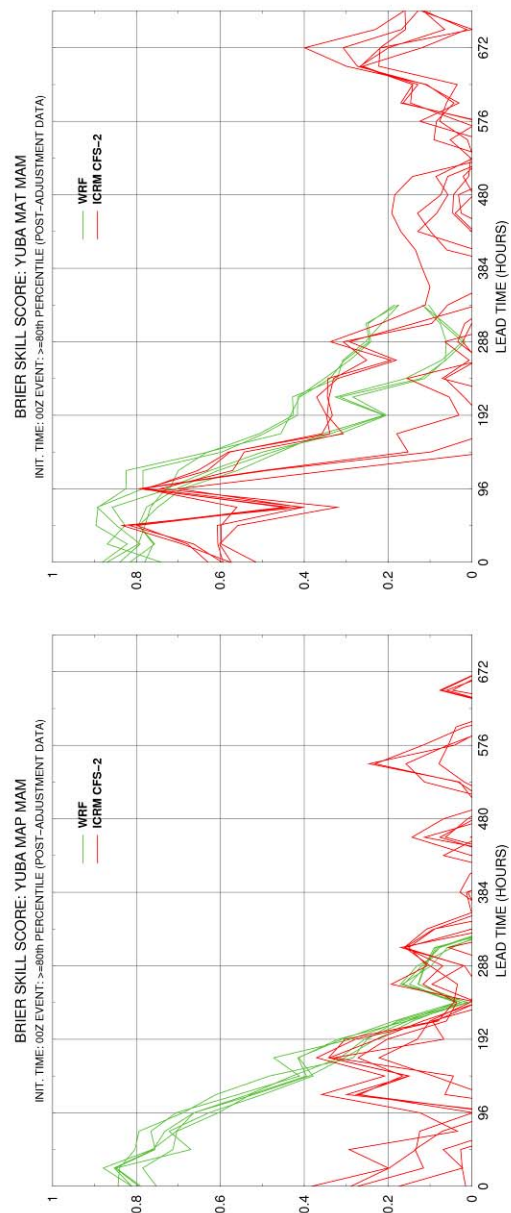
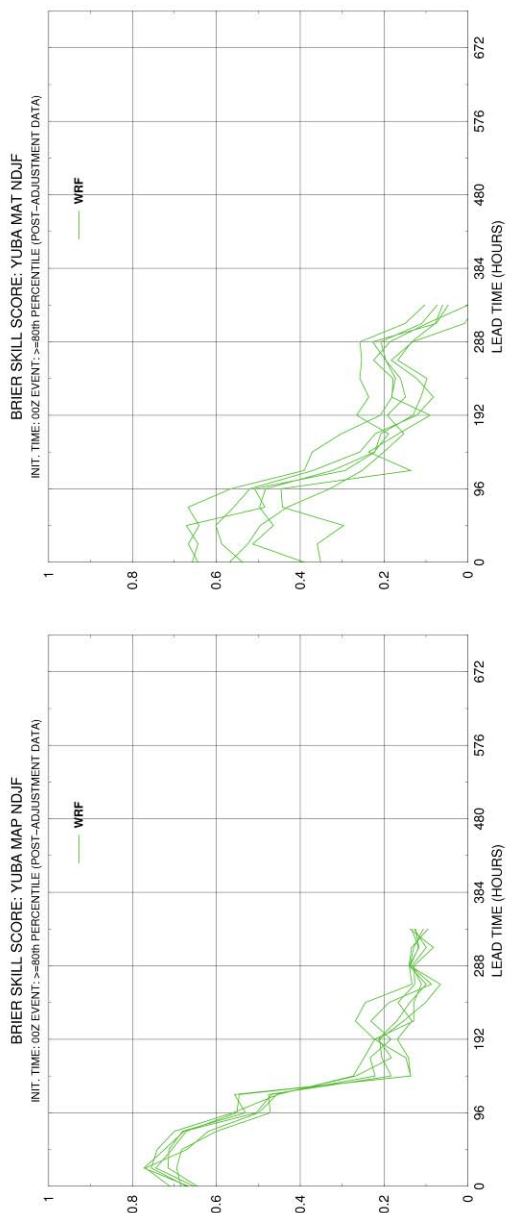
This section of Appendix F presents the Brier Skill Score (BSS) results for multi-lead MAP and MAT ensemble forecasts for all the subcatchments of the INFORM domain watersheds and for both seasons, NDJF and MAM. Following the BSS results, the reliability diagrams of the available 48-hr MAP and MAT ensemble forecasts of the GFS-WRF and CFS2-ICRM models and for NDJF and MAM are shown for individual subcatchments of the INFORM watersheds.

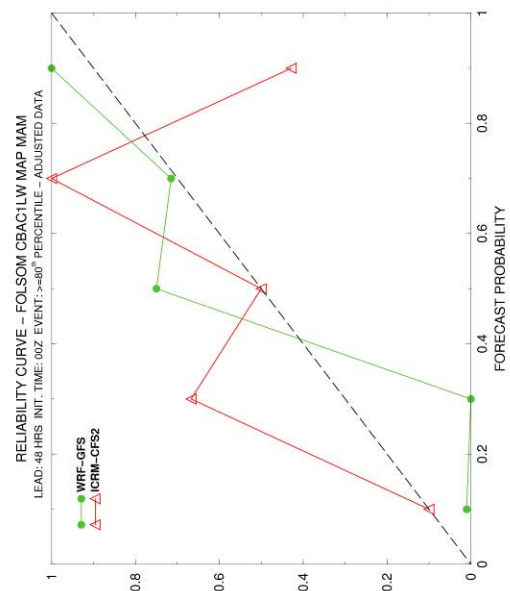
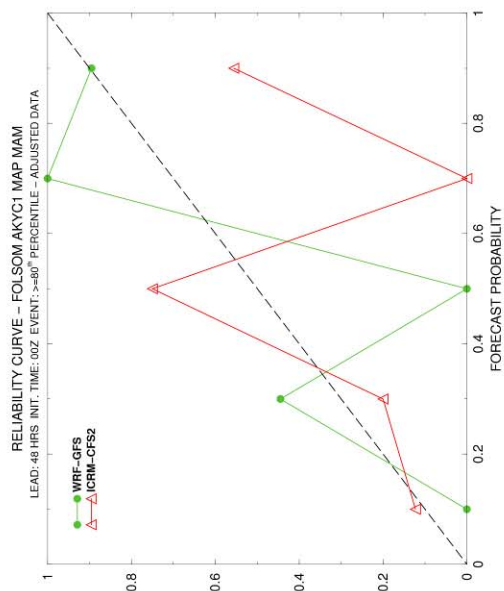
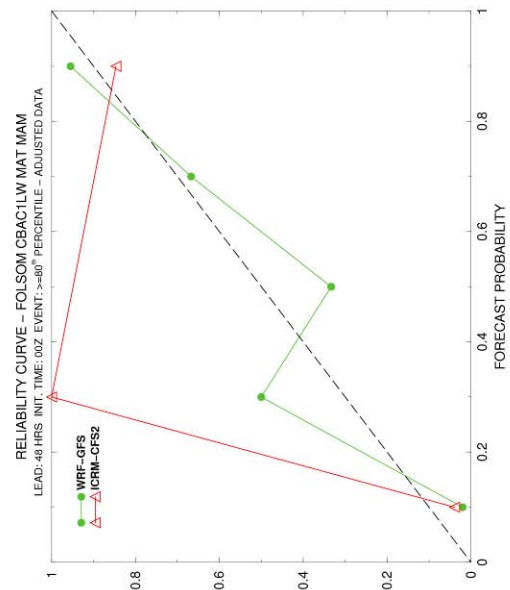
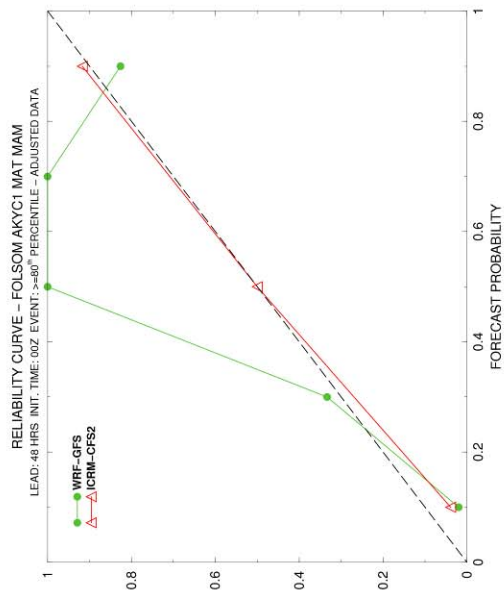


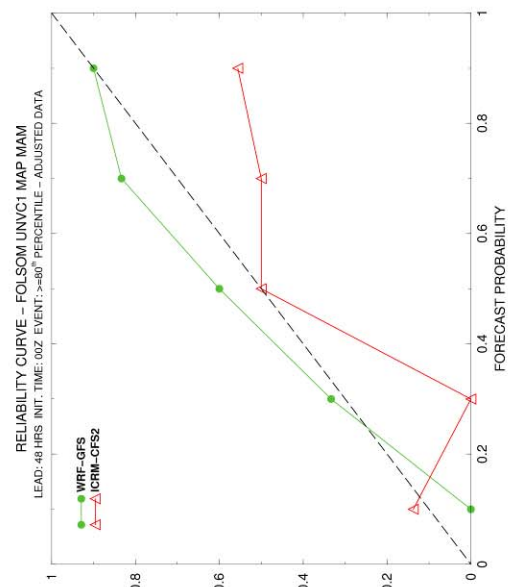
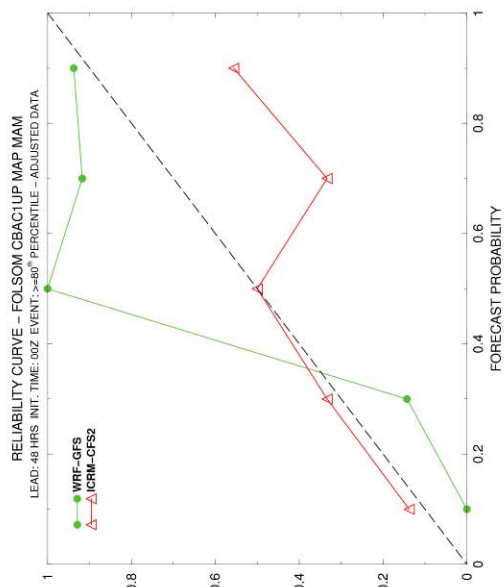
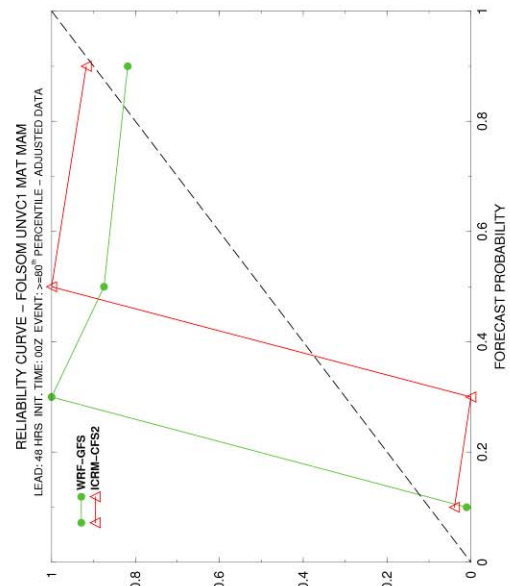
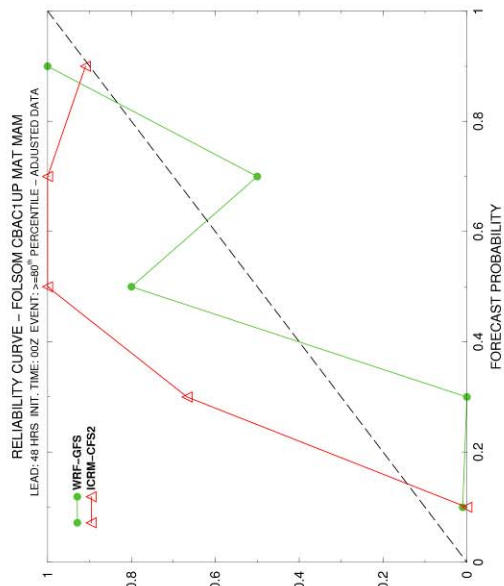


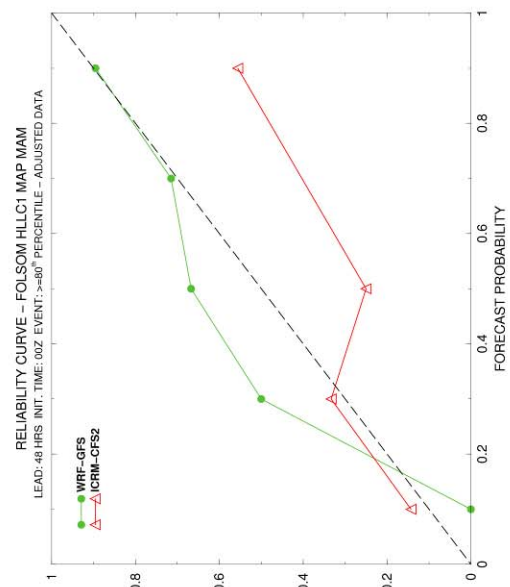
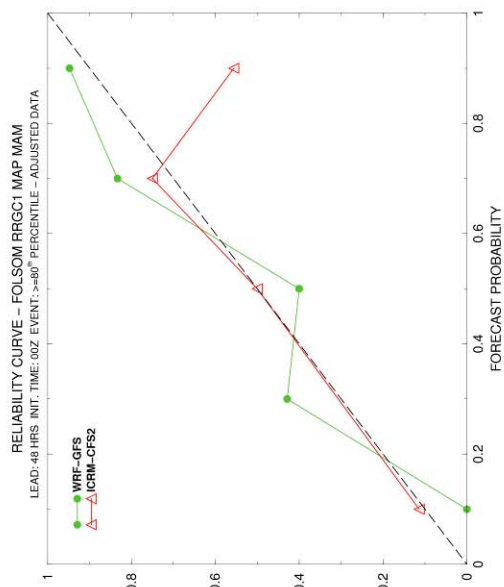
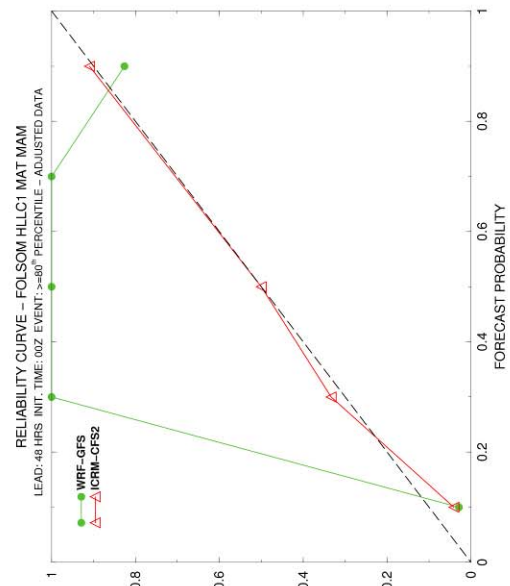
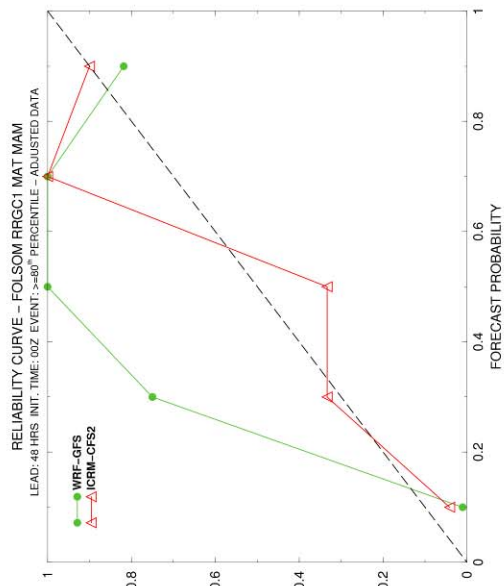


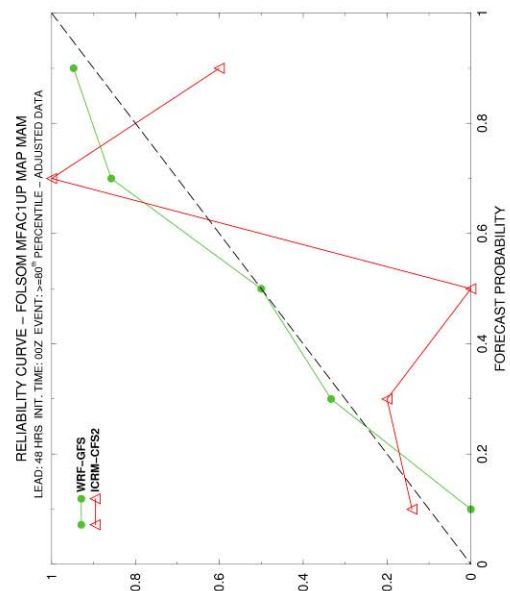
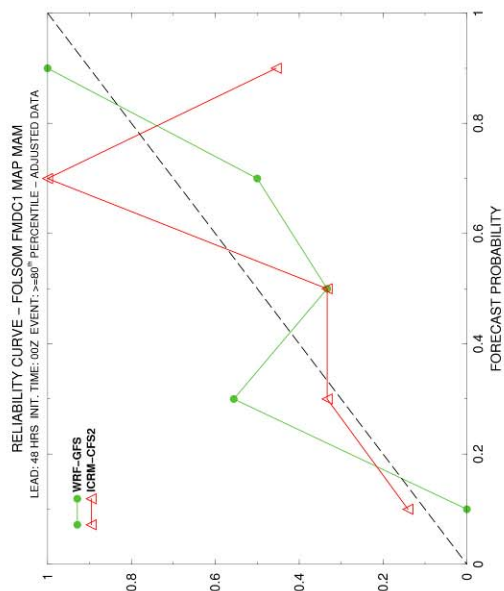
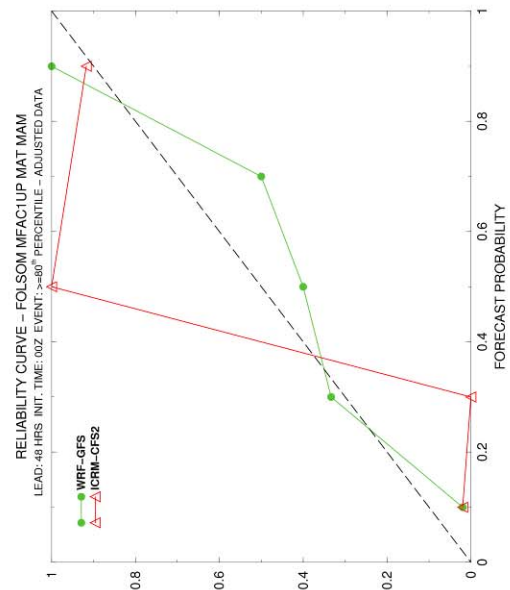
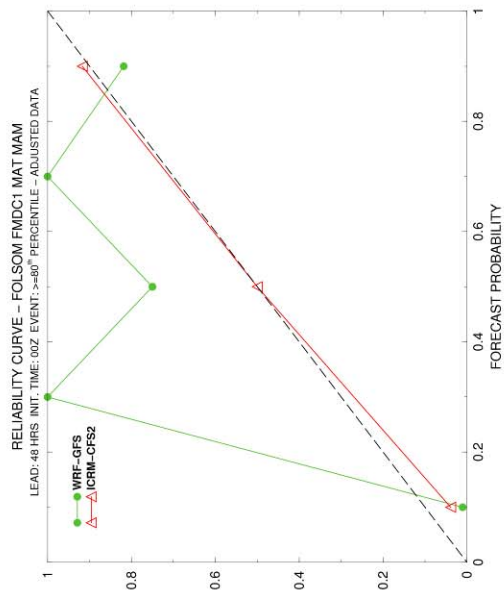


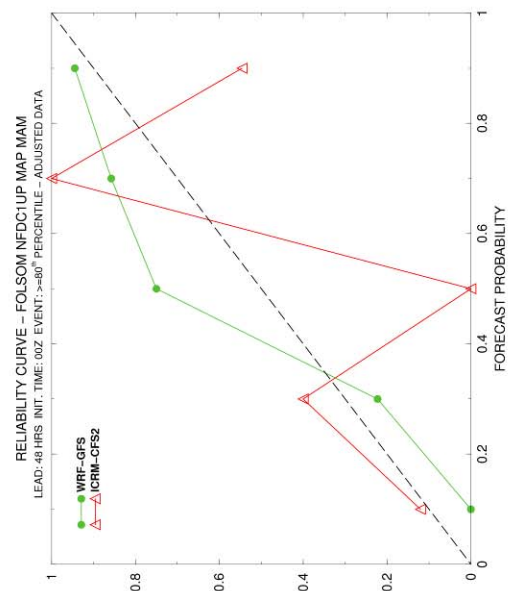
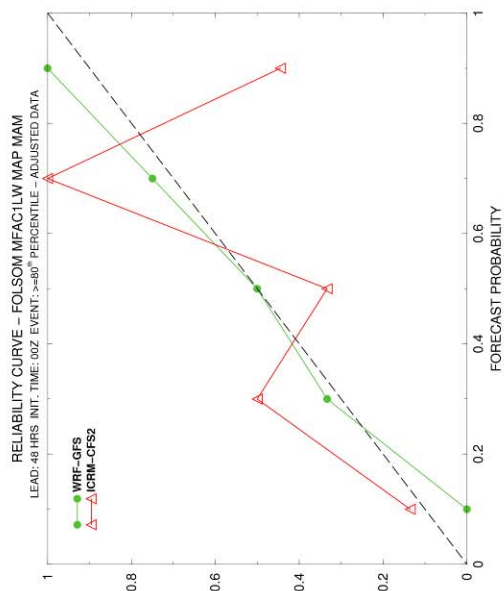
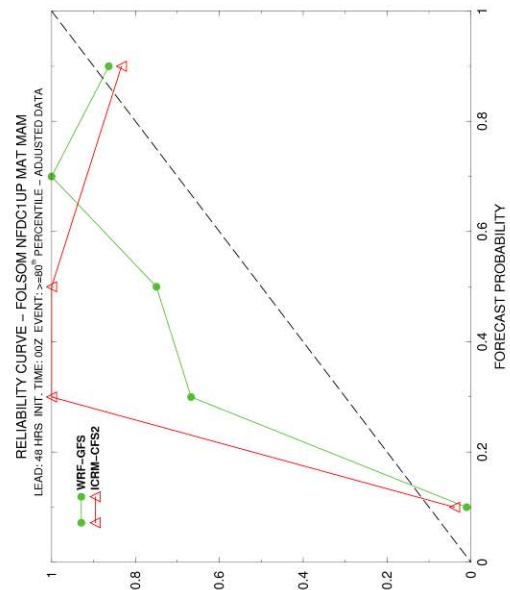
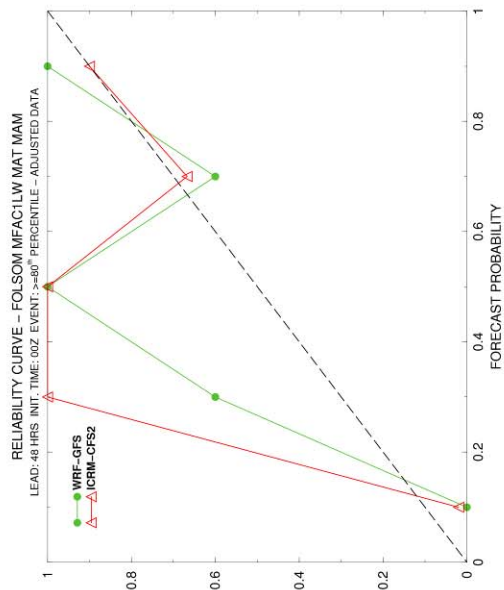


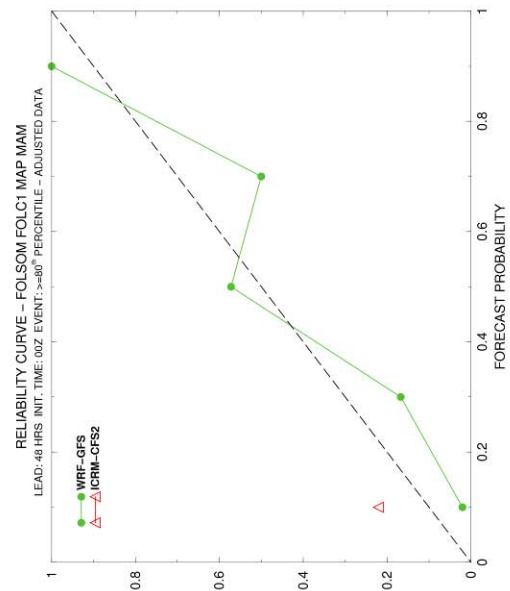
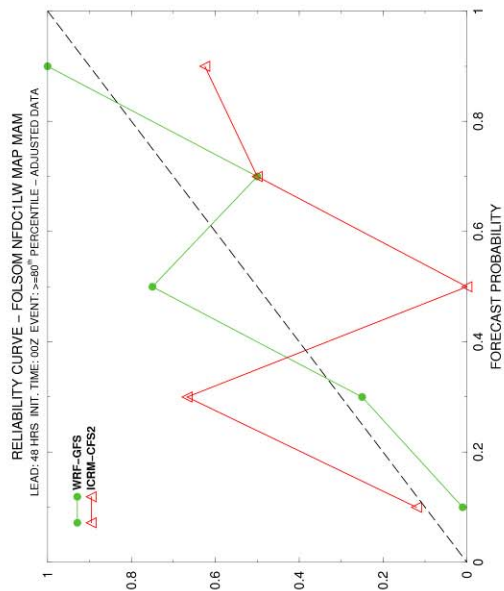
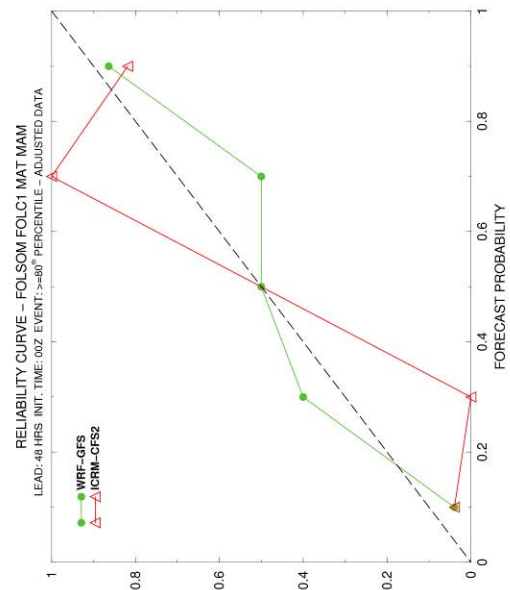
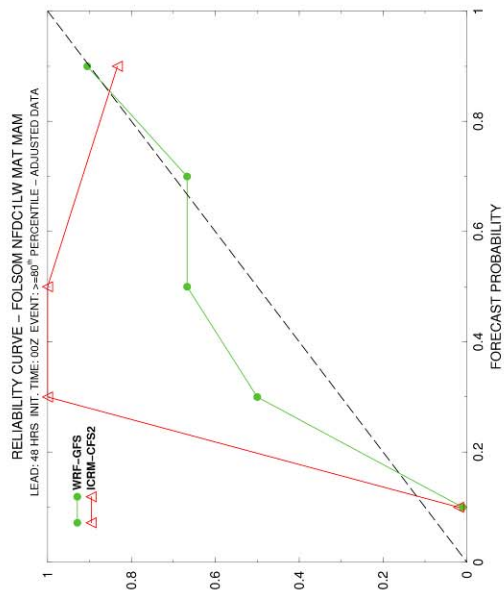


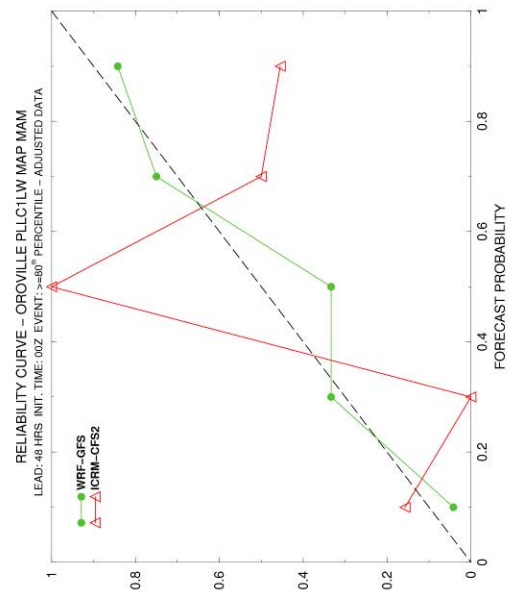
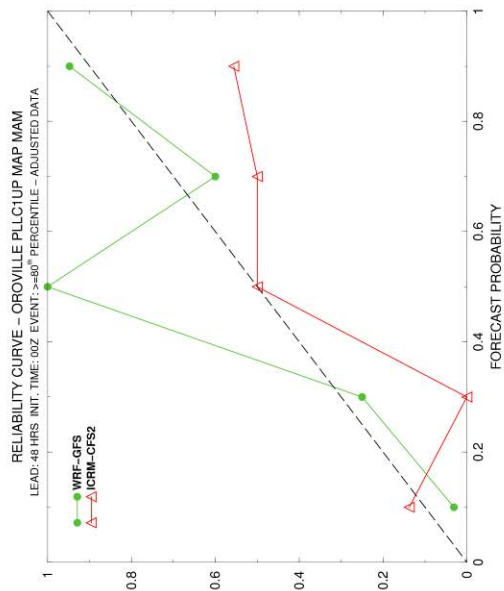
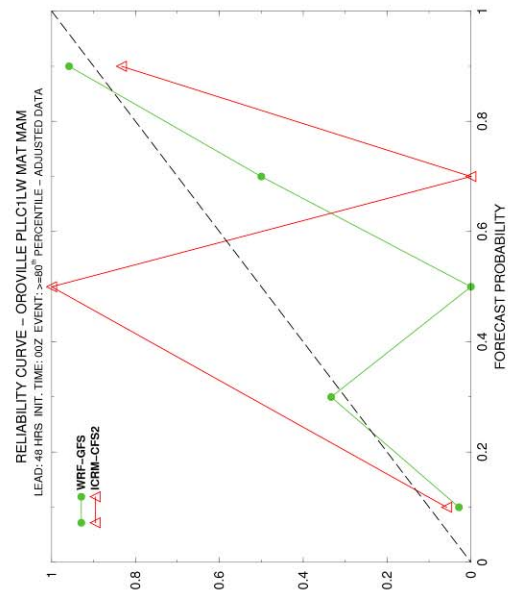
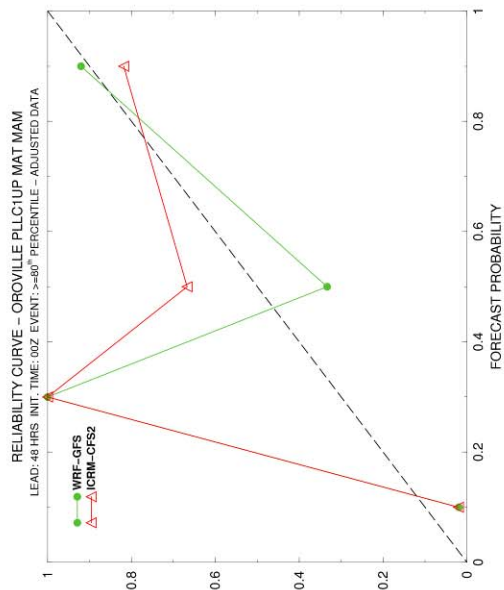


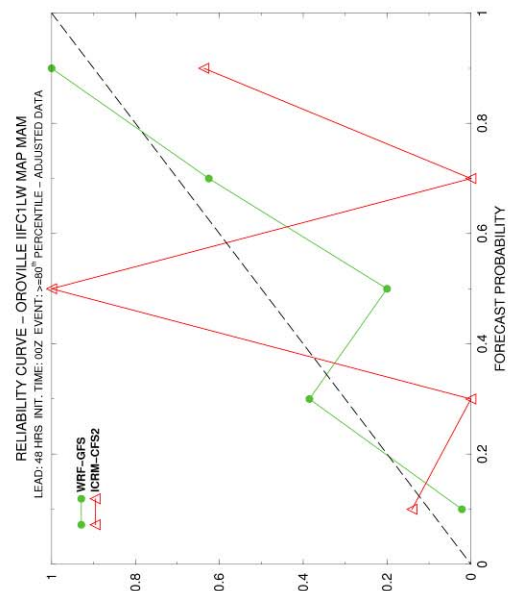
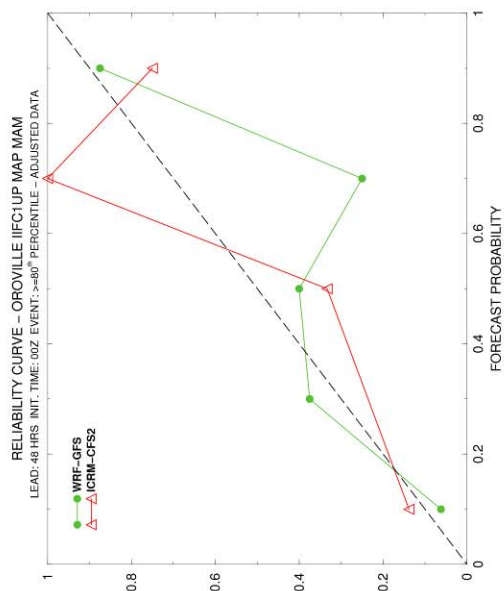
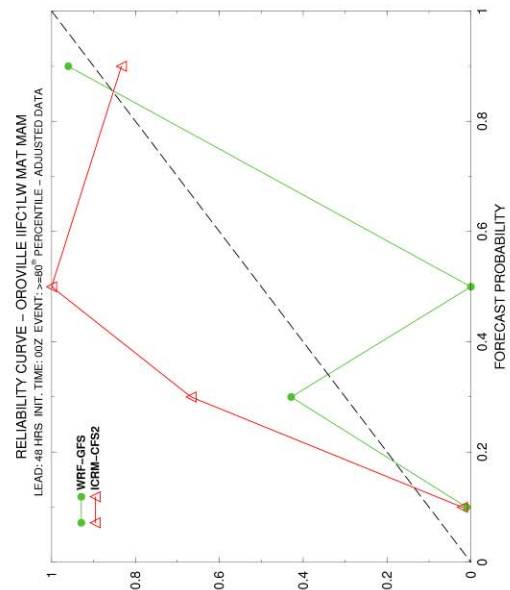
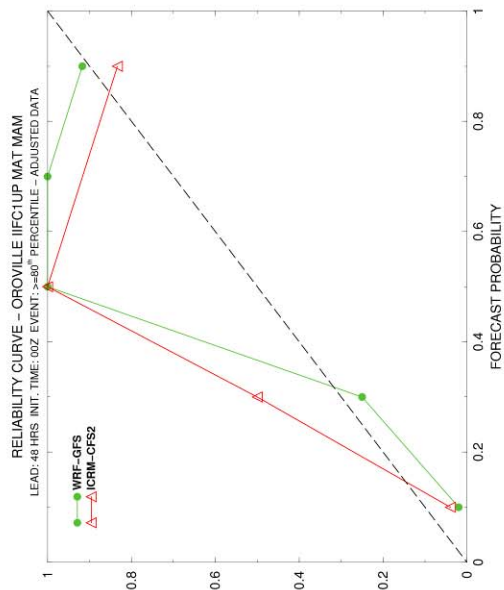


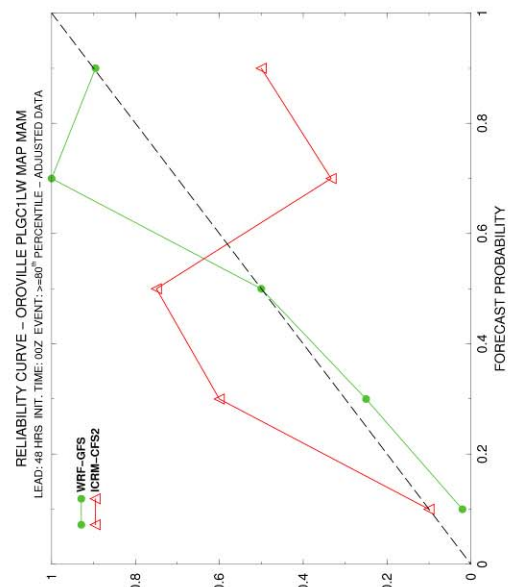
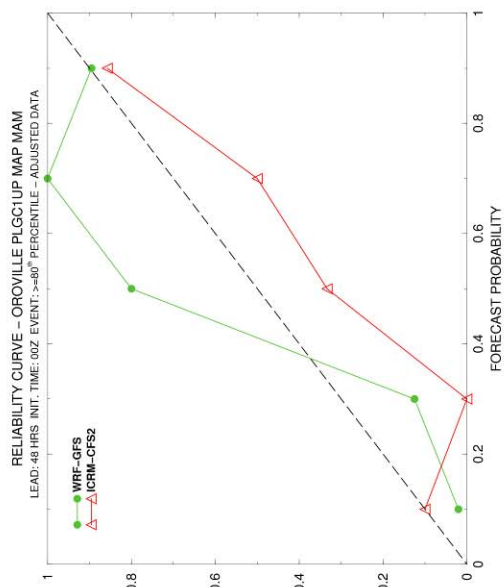
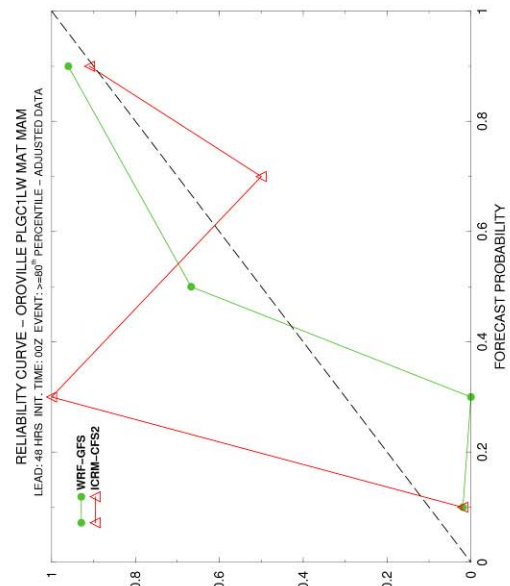
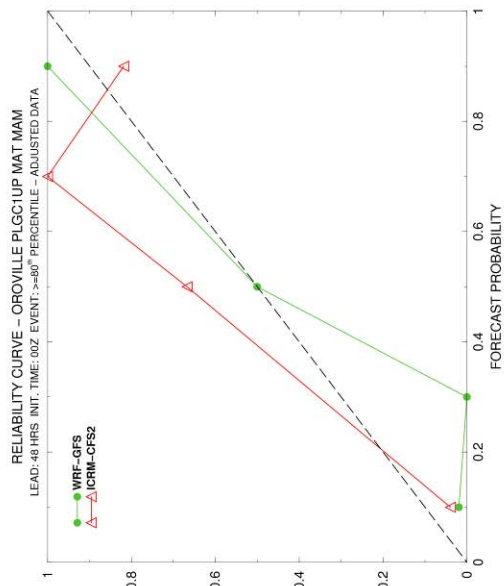


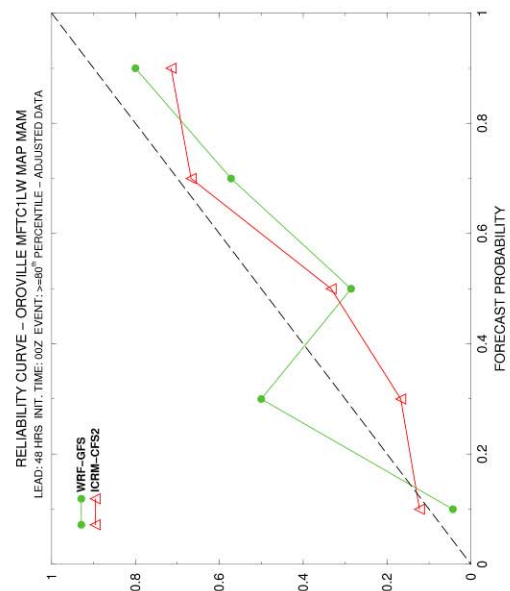
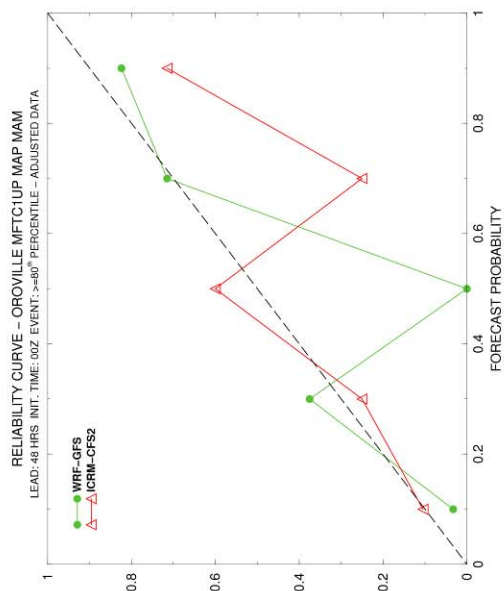
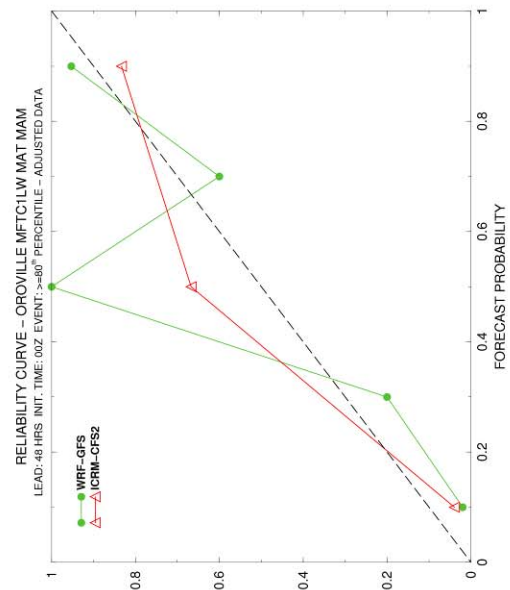
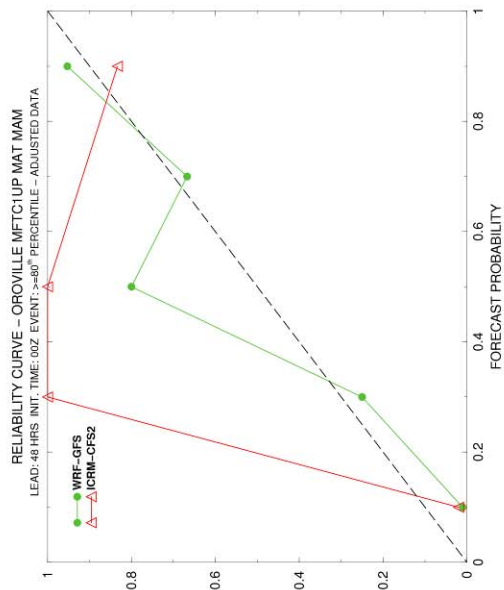


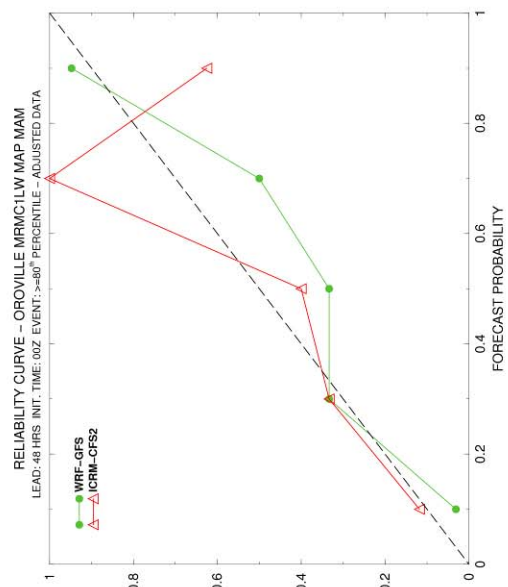
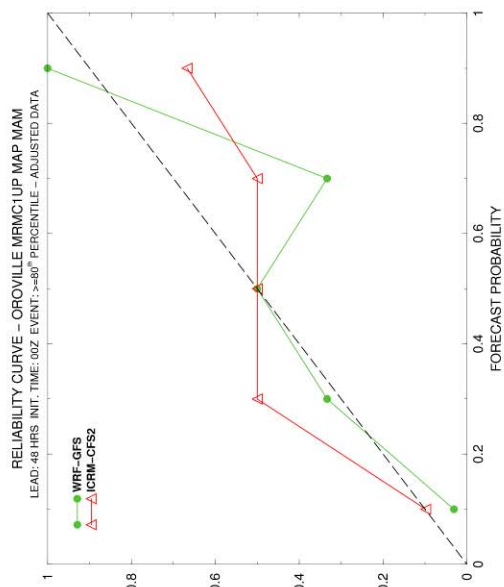
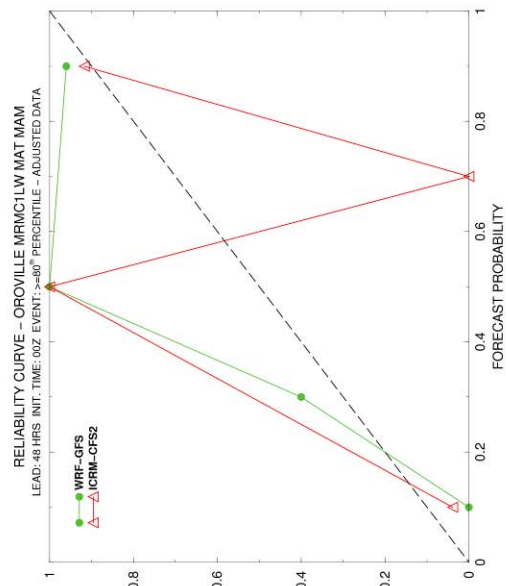
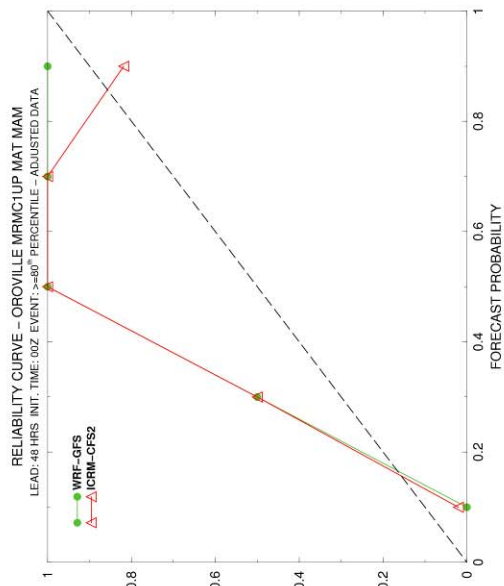


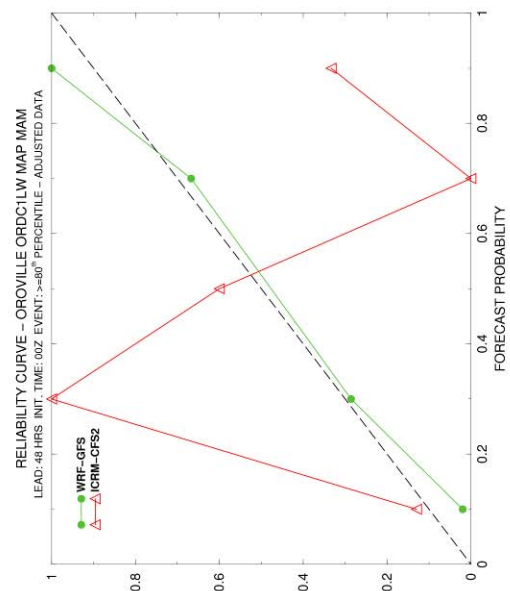
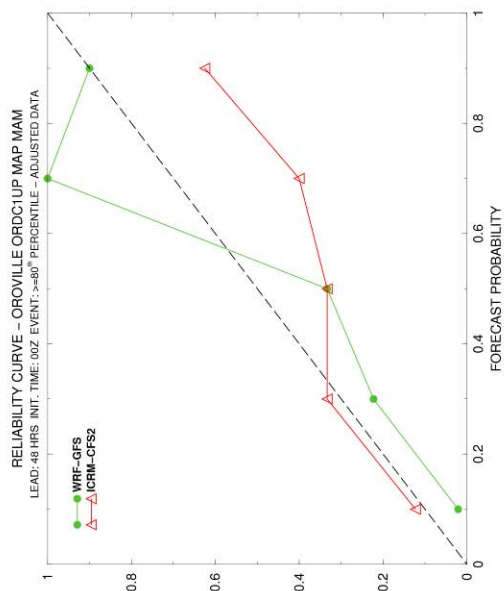
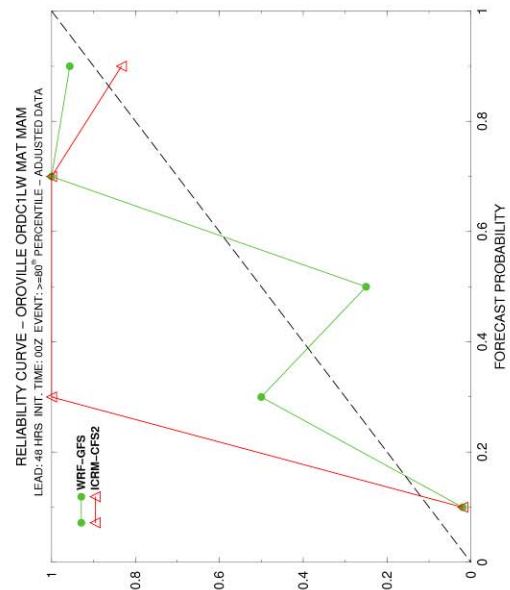
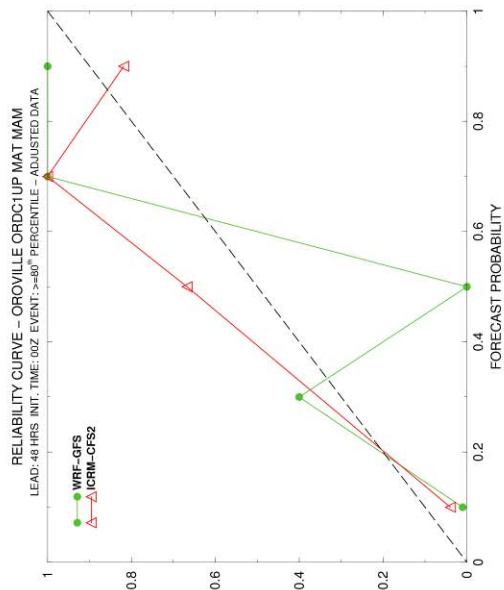


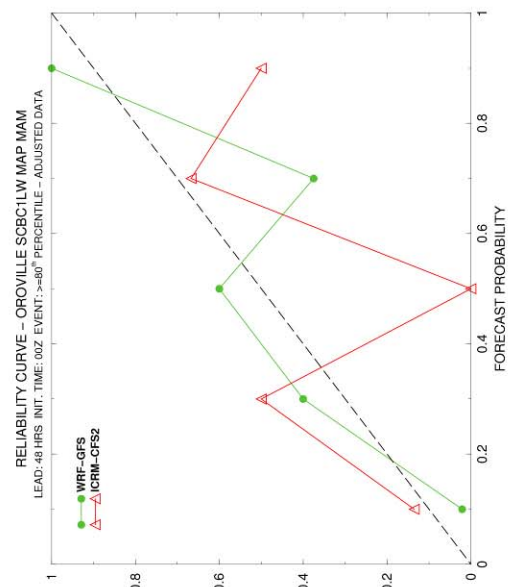
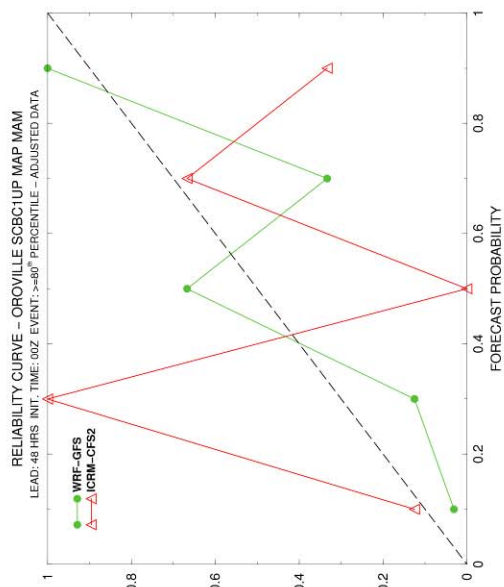
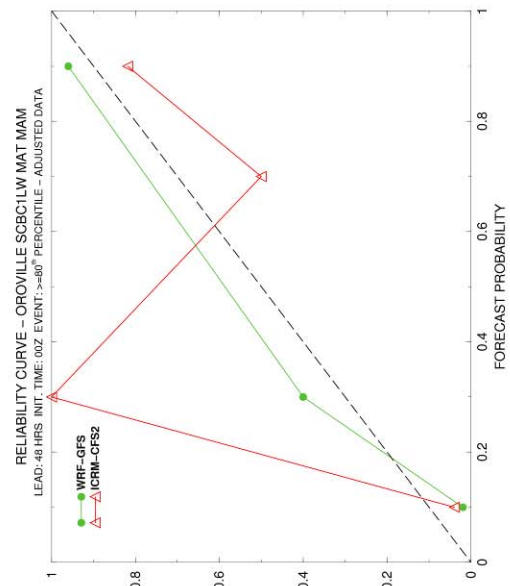
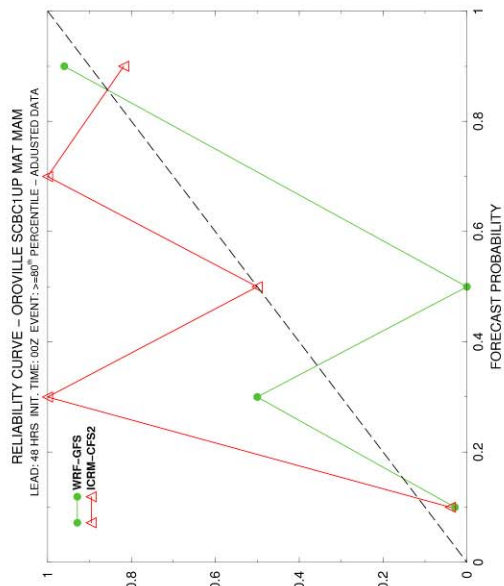


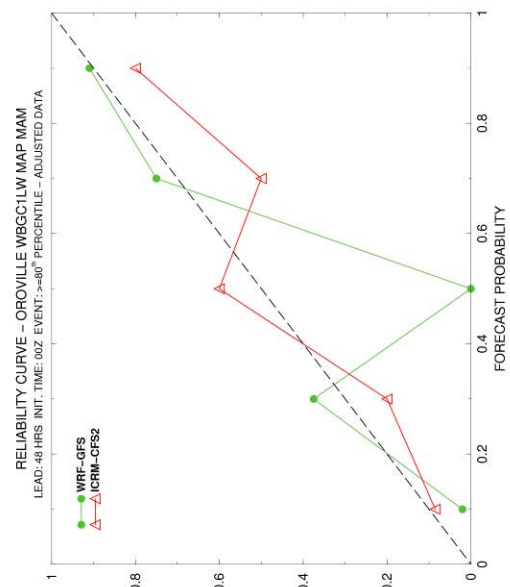
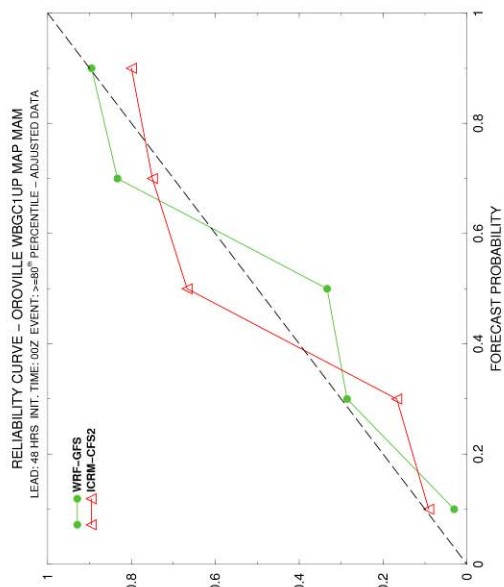
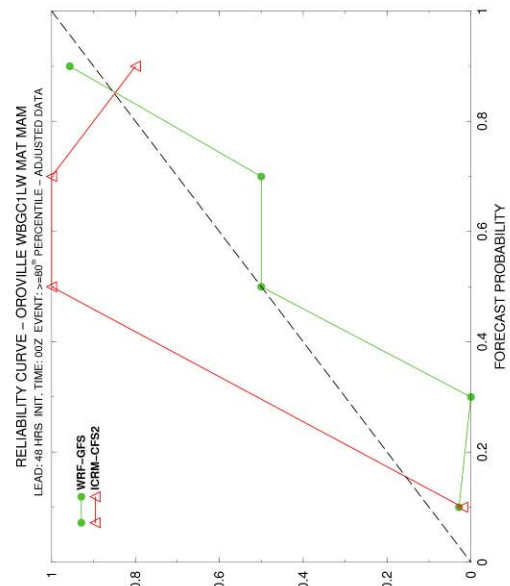
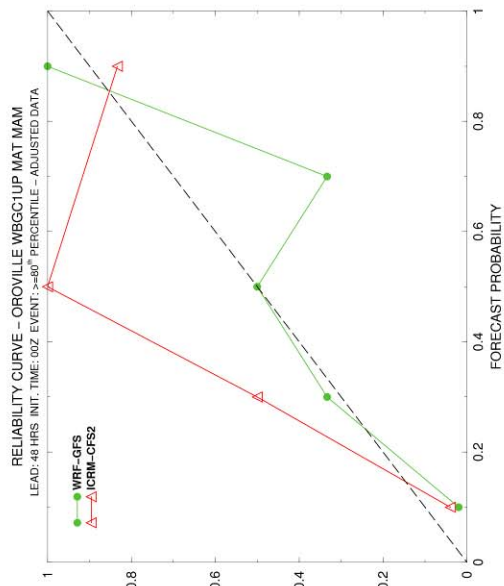


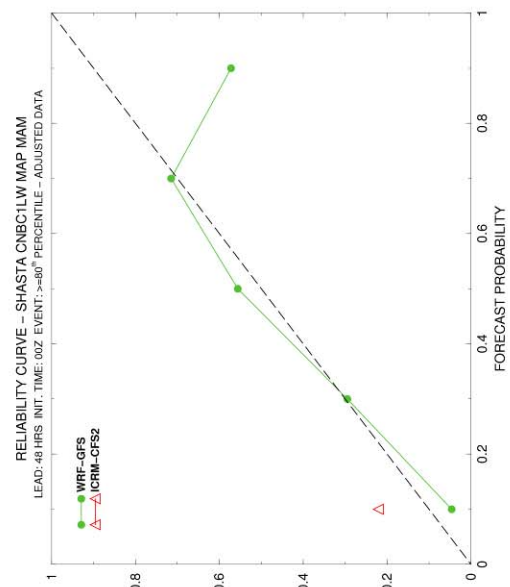
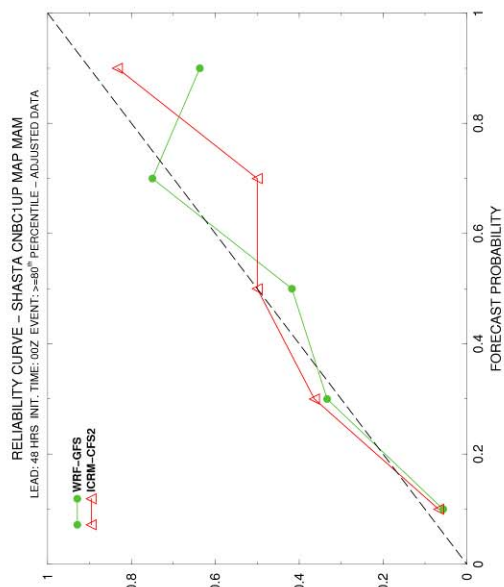
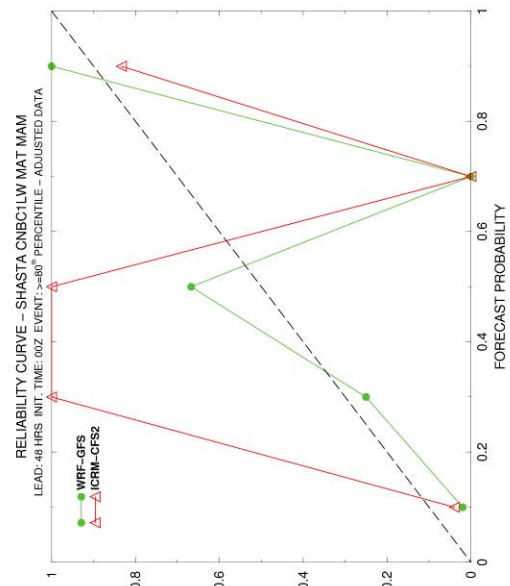
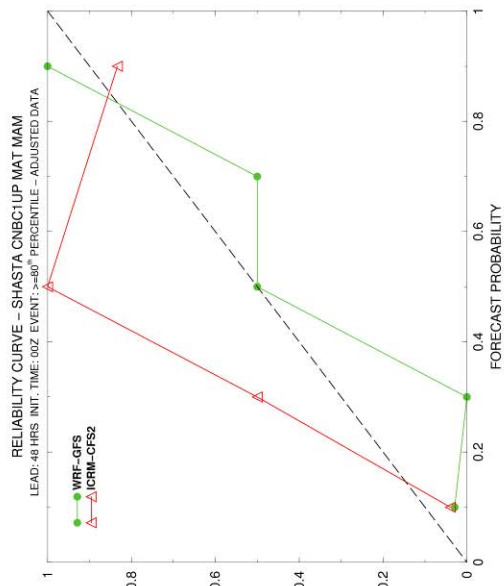


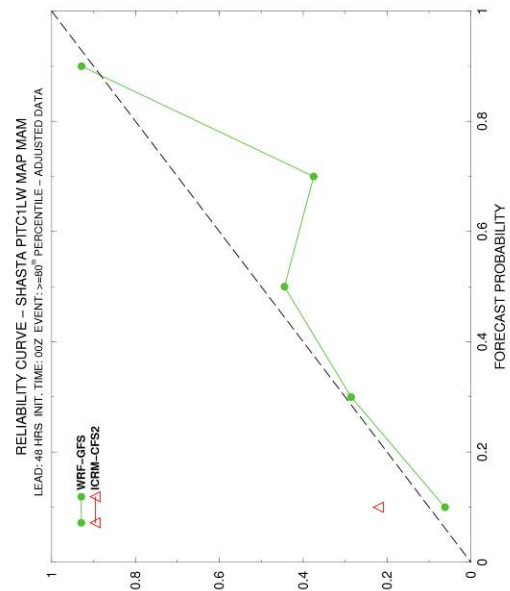
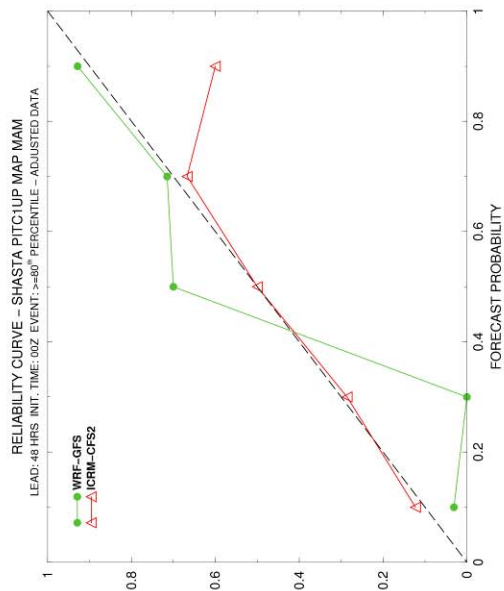
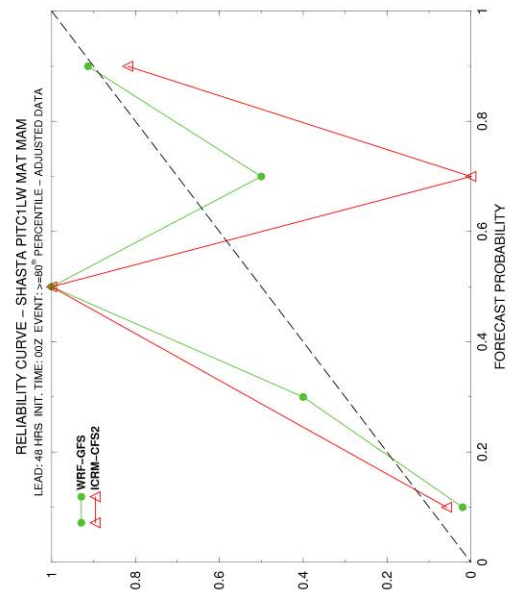
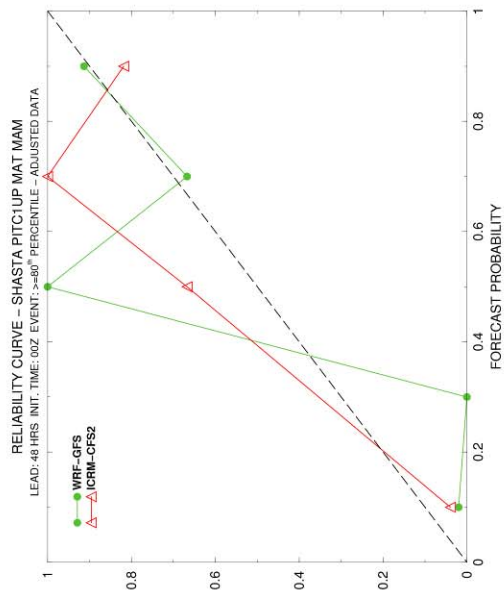


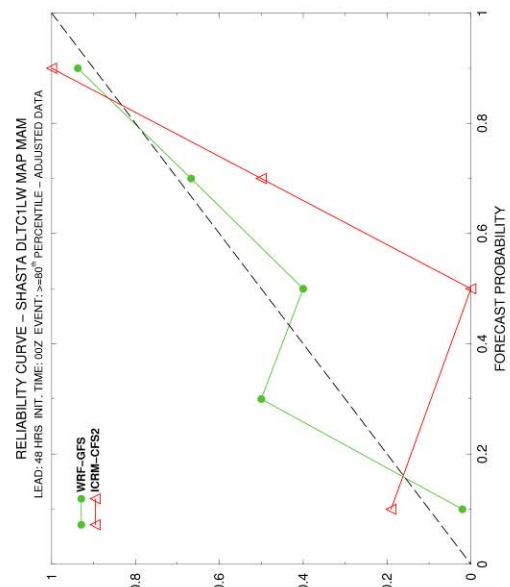
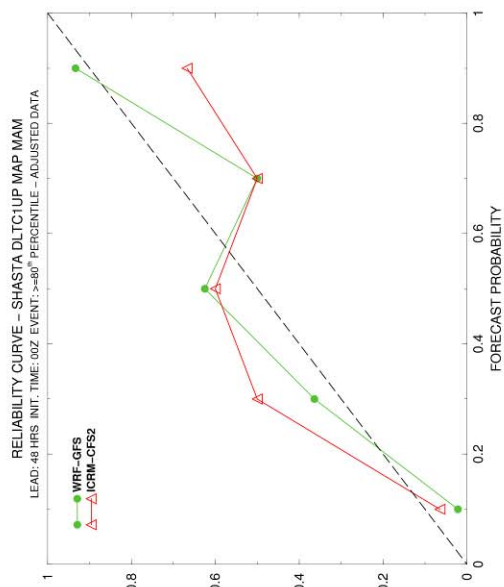
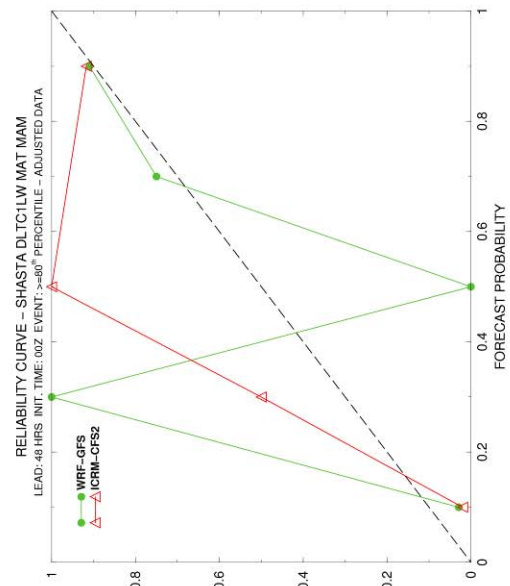
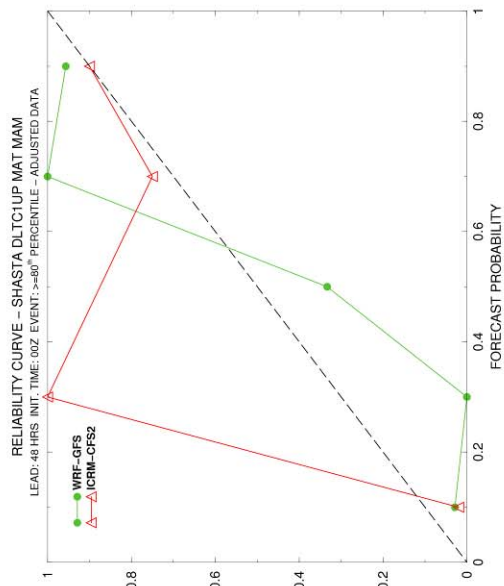


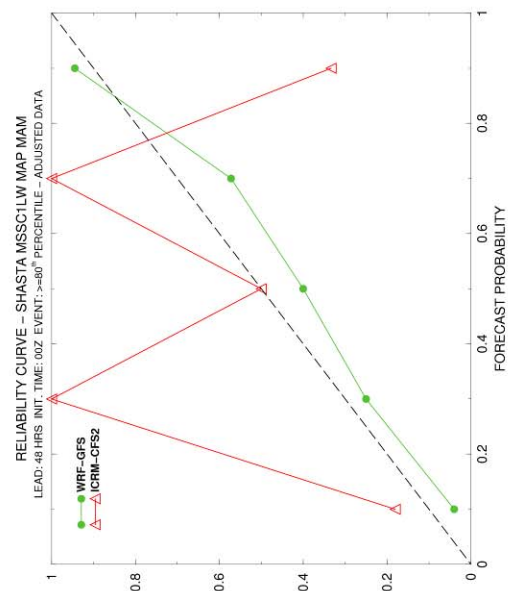
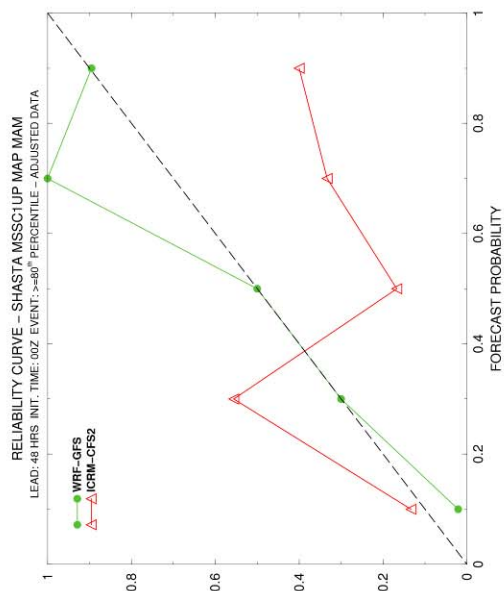
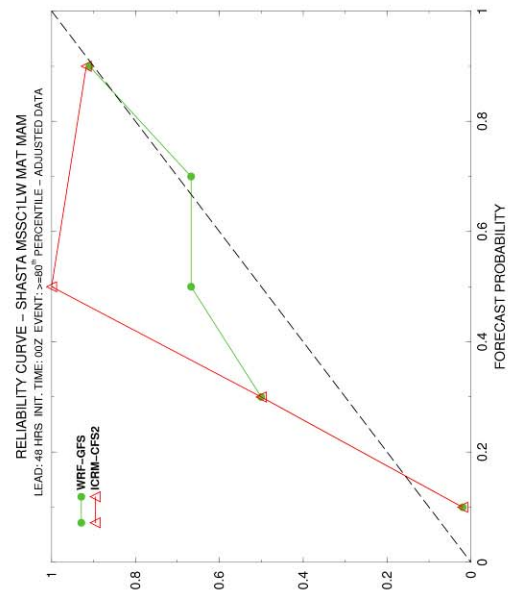
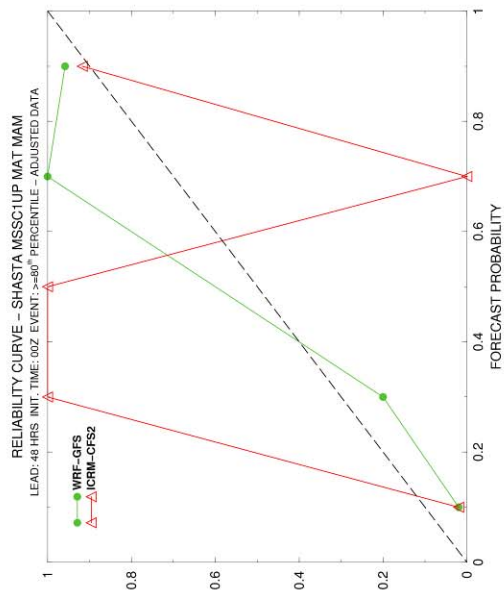


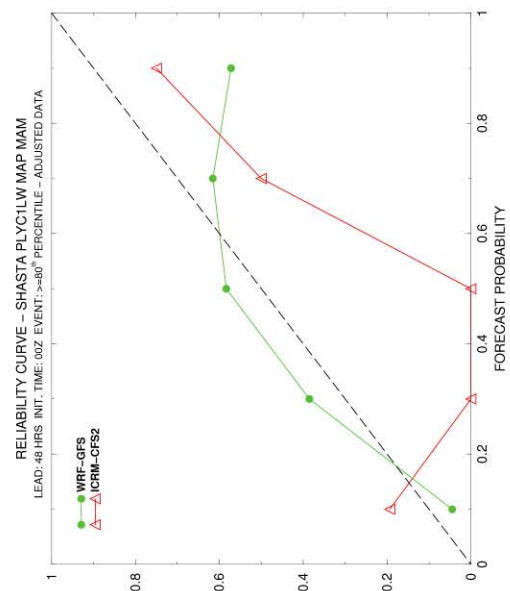
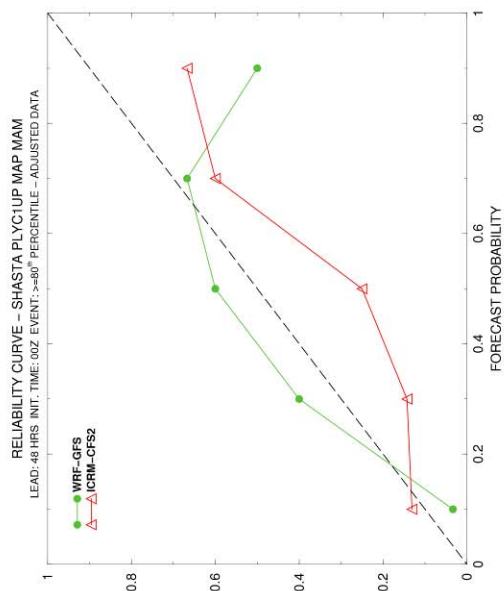
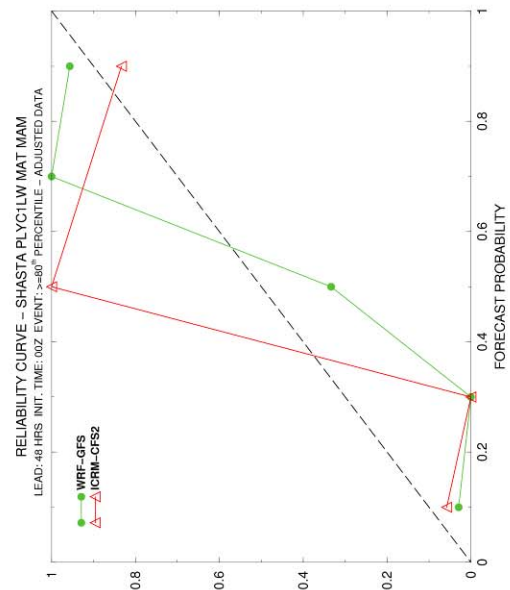
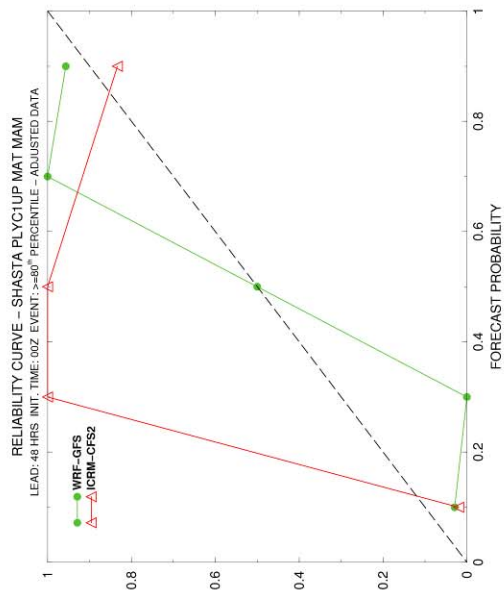


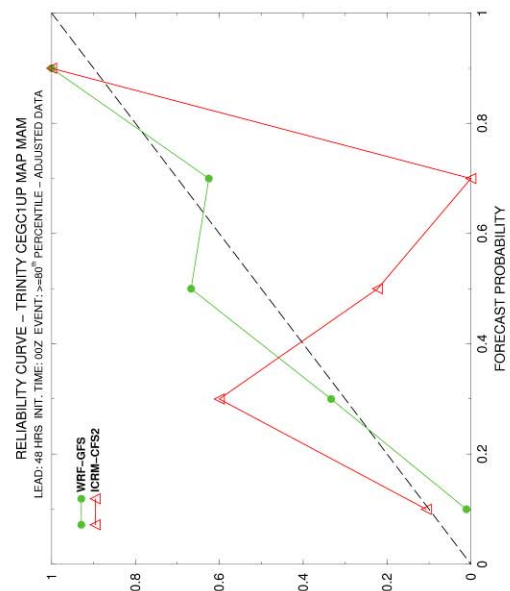
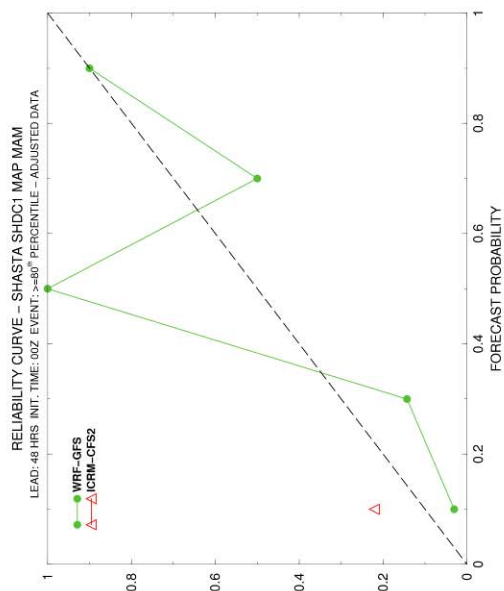
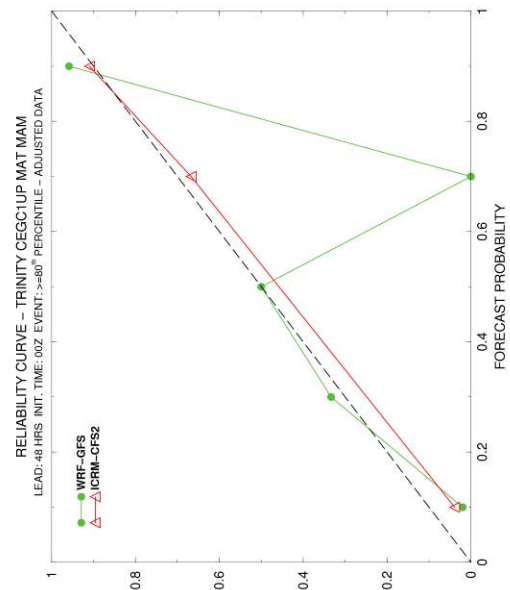
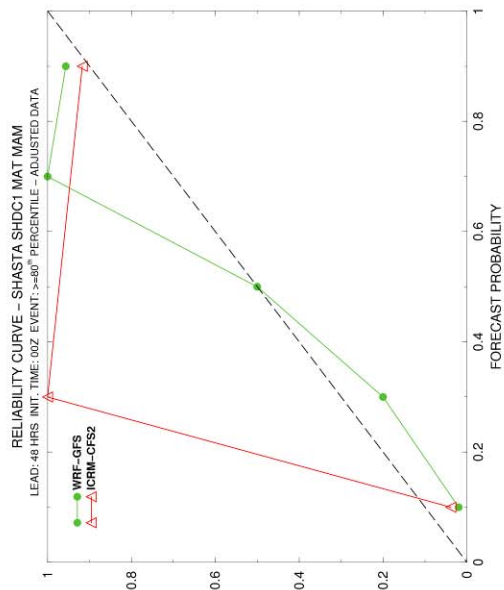


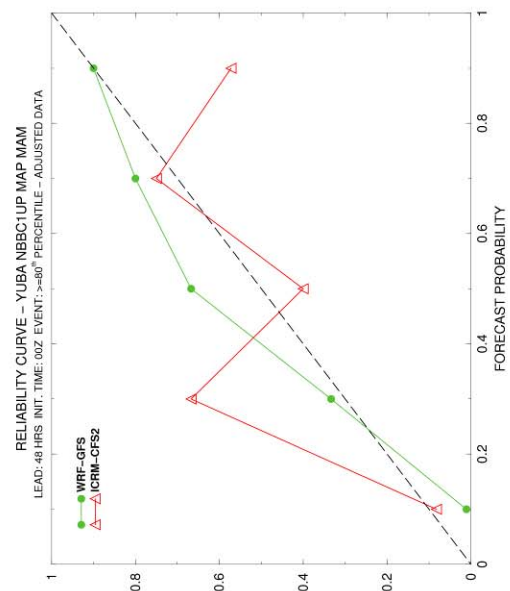
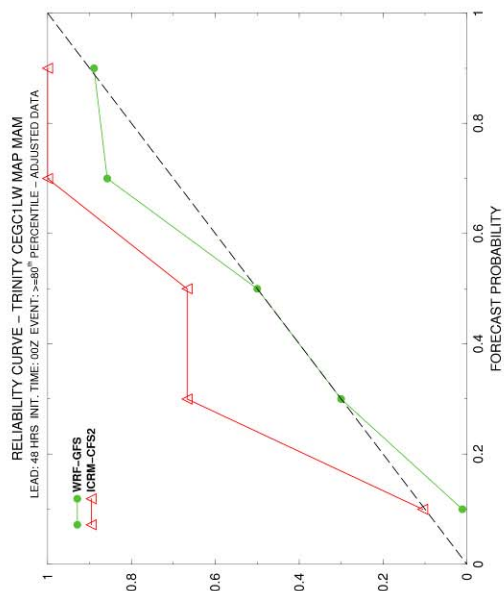
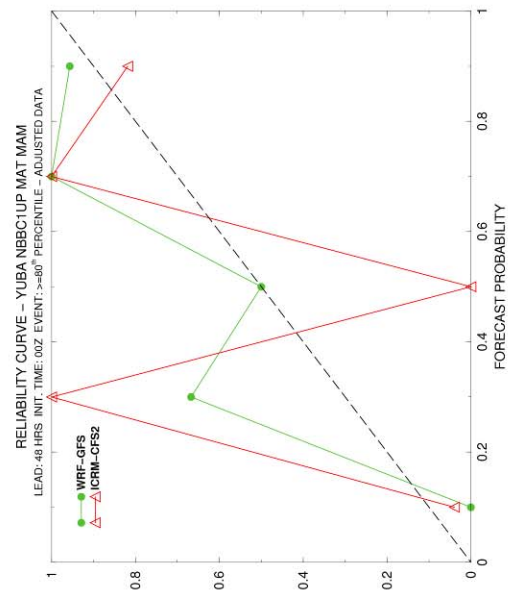
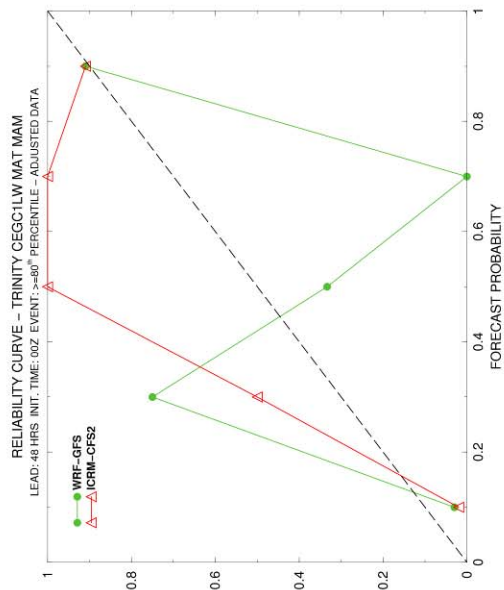


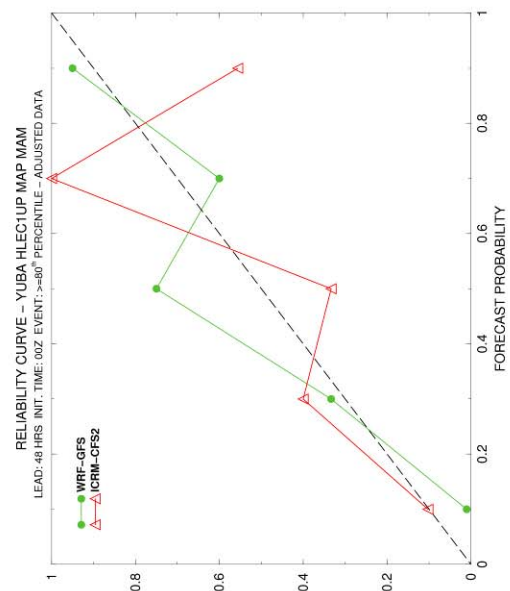
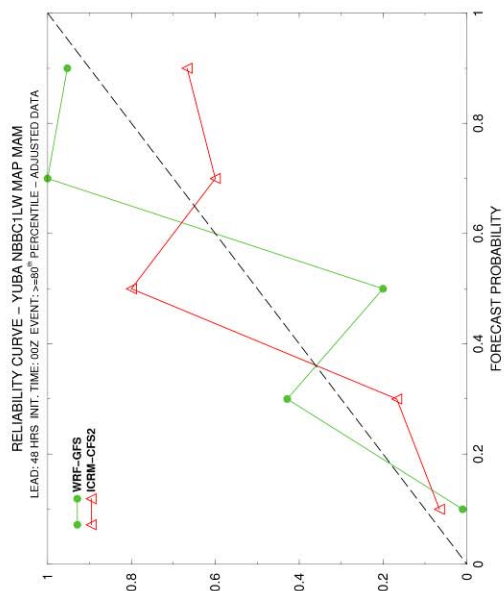
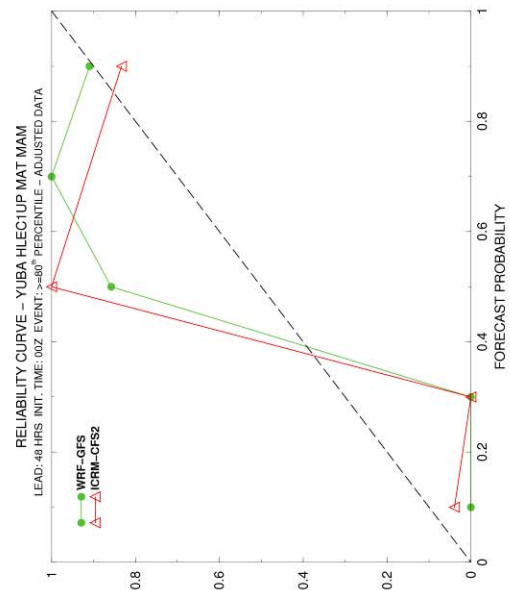
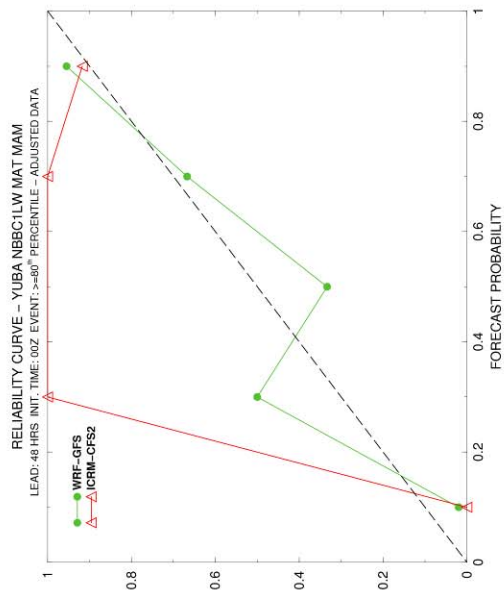


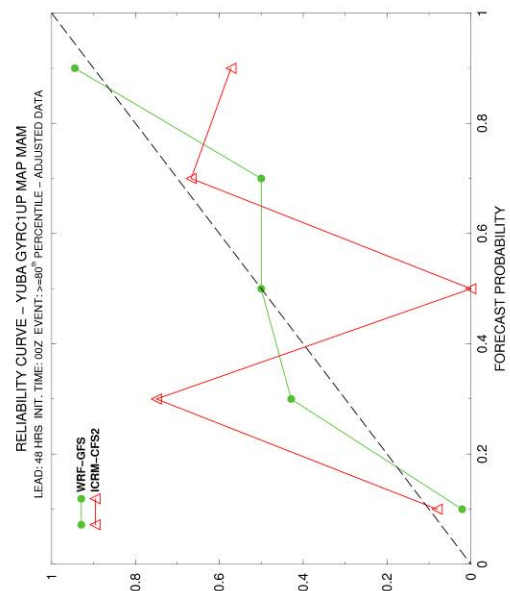
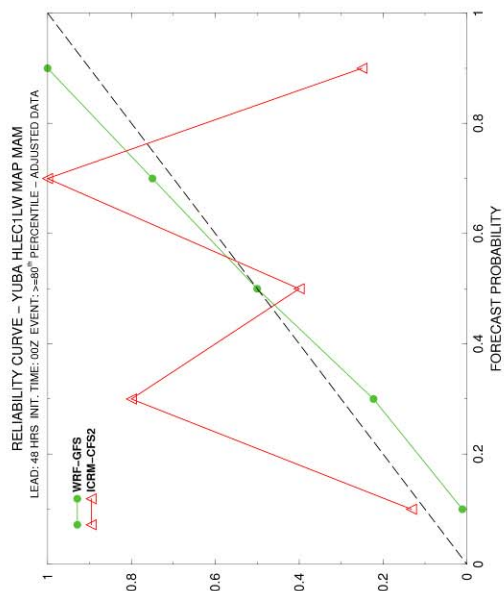
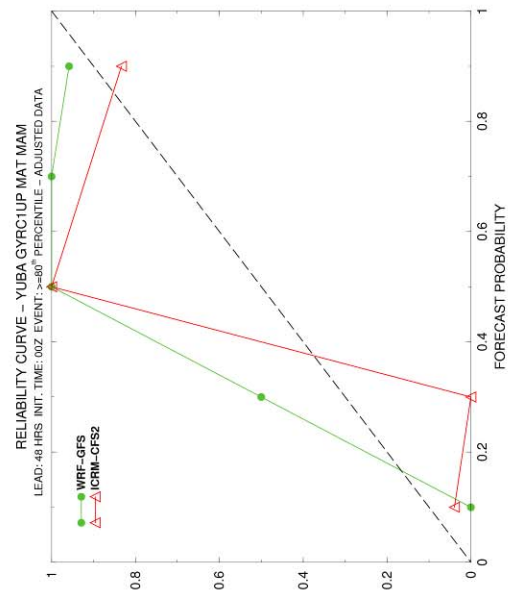
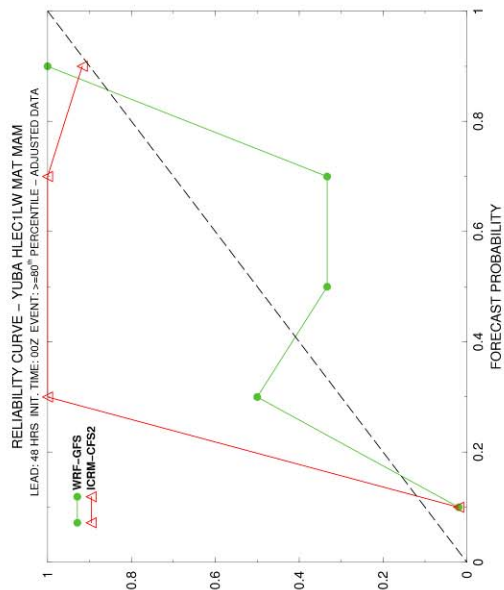


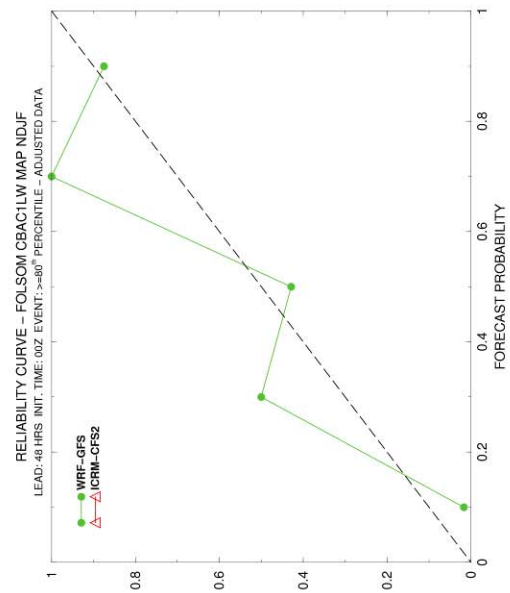
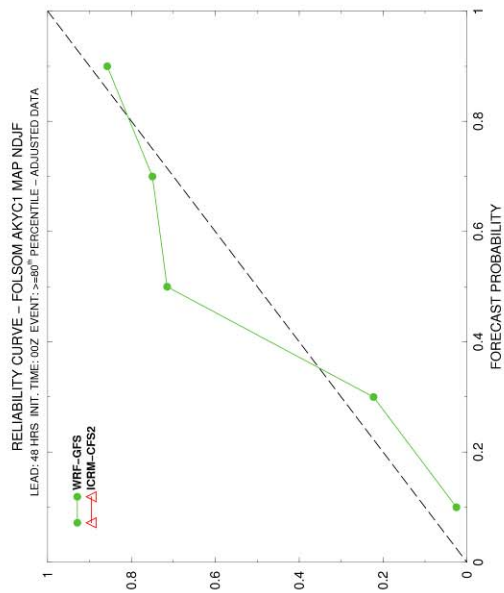
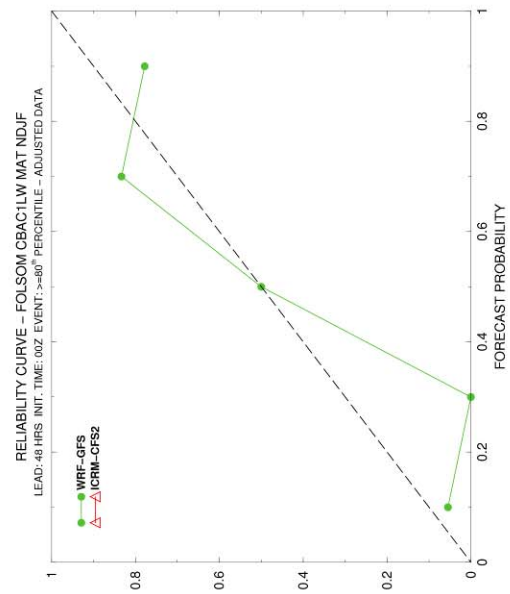
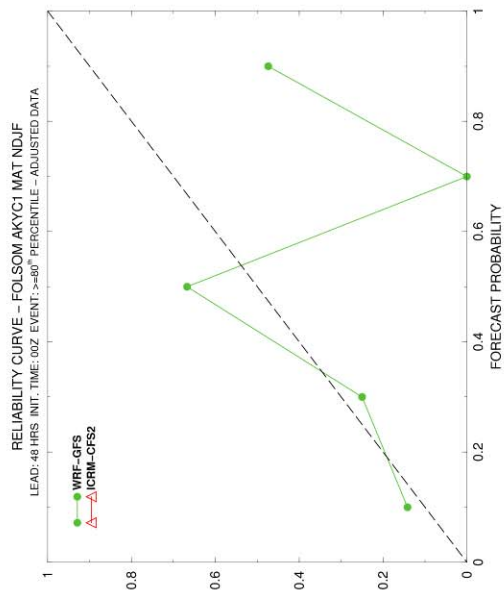


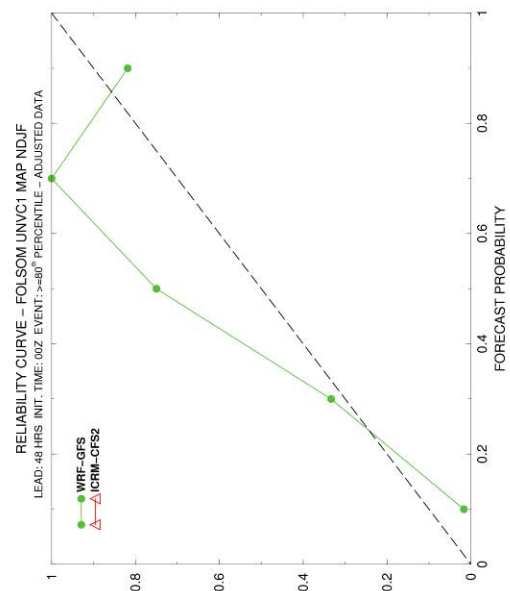
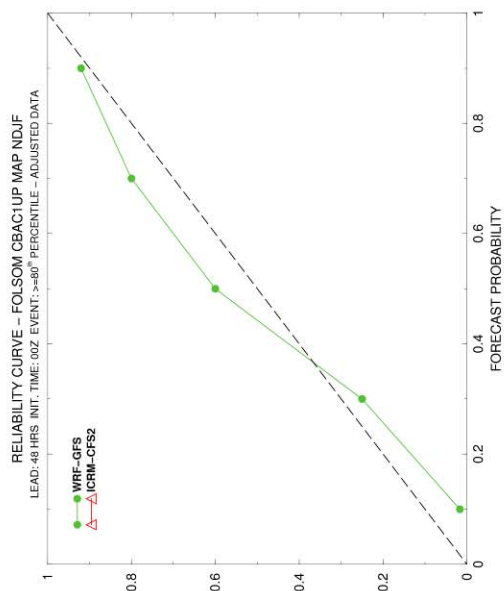
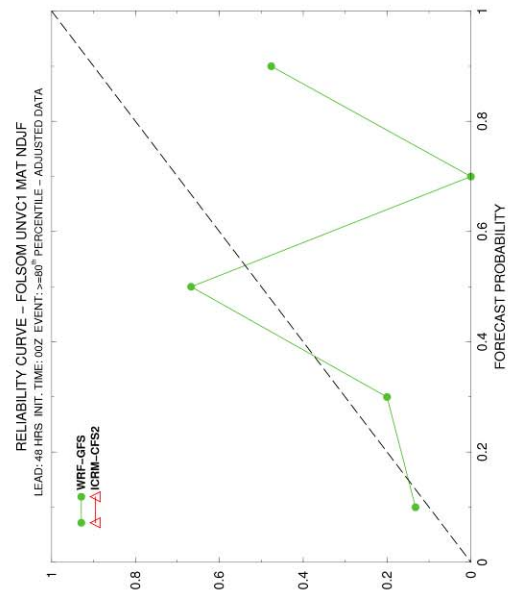
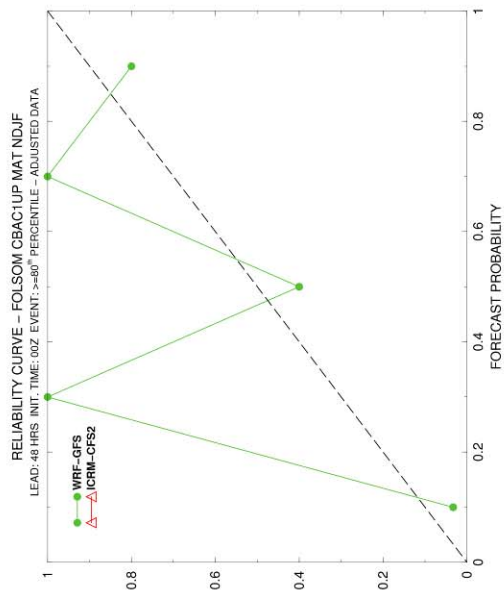


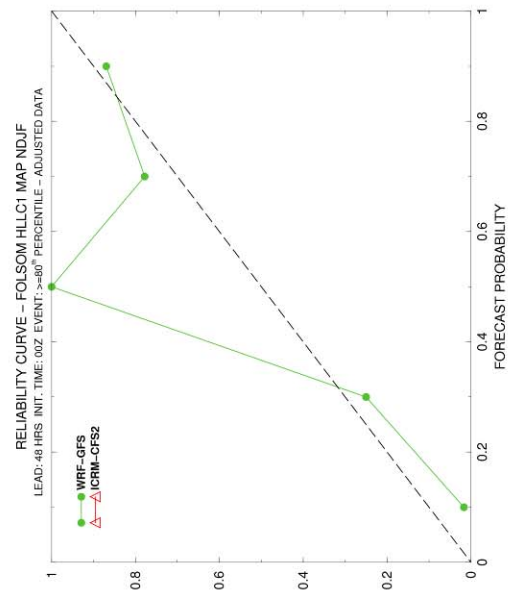
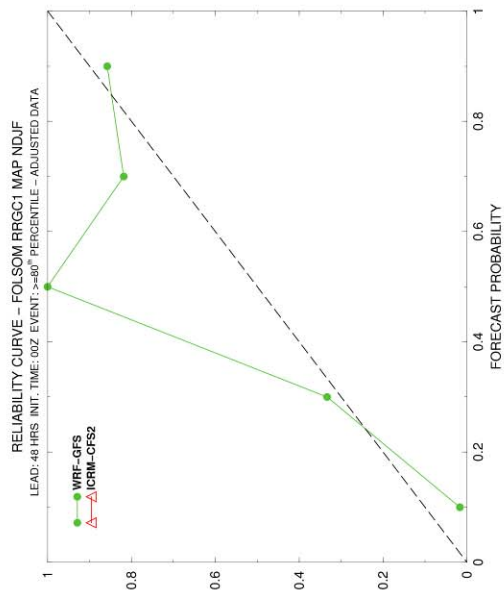
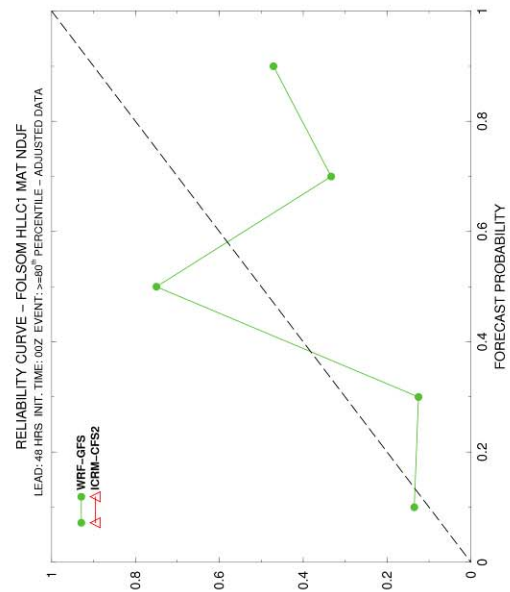
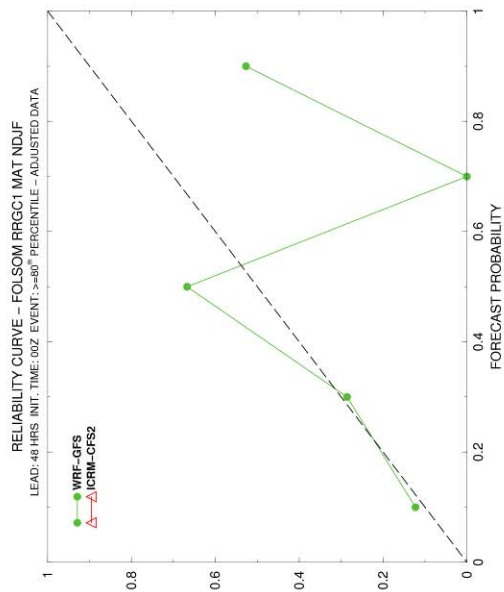


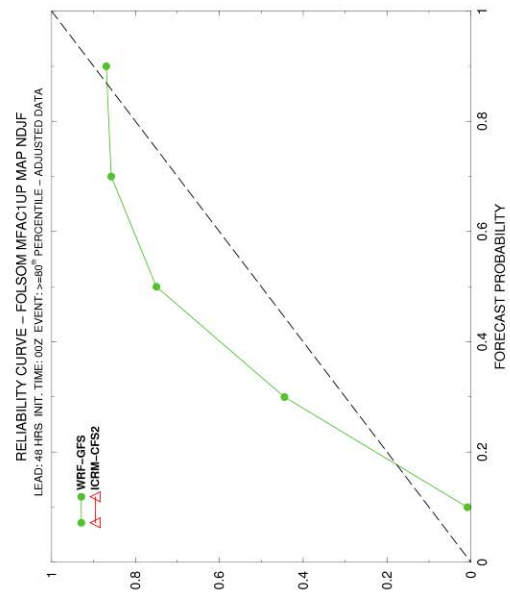
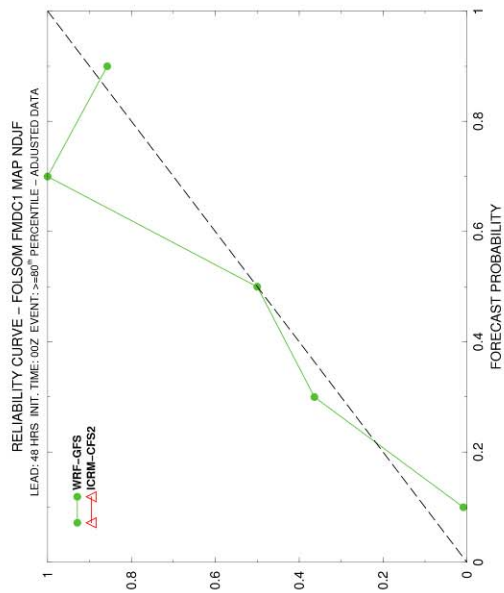
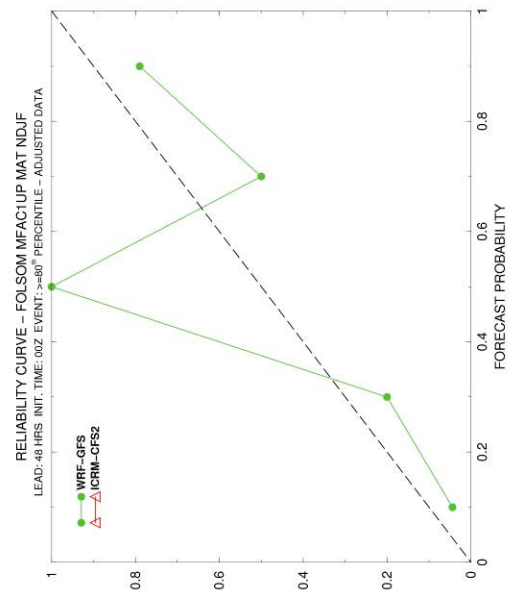
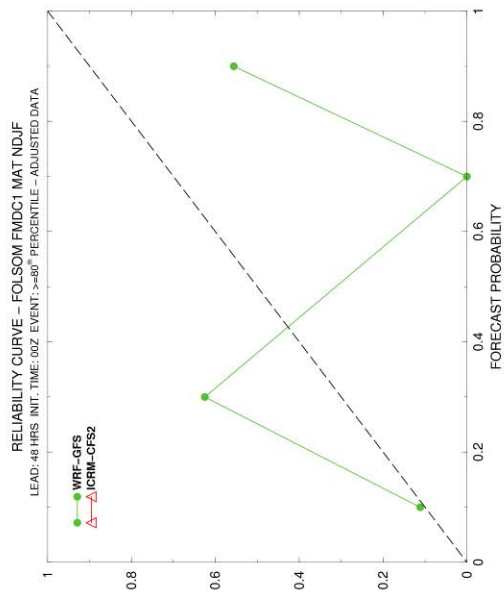


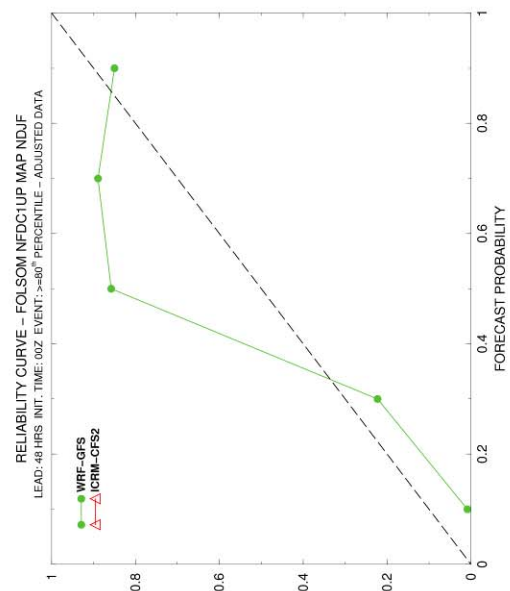
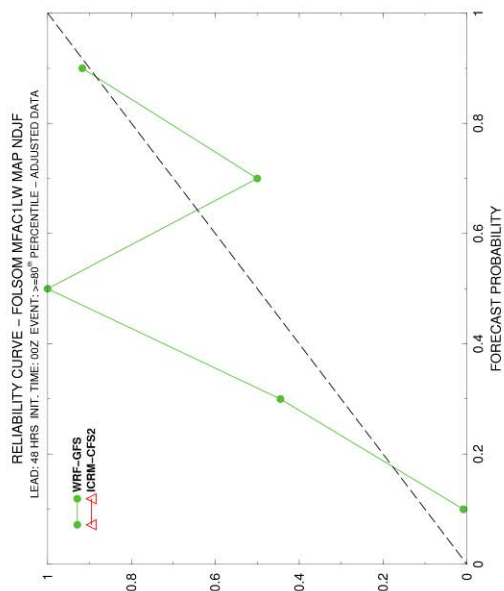
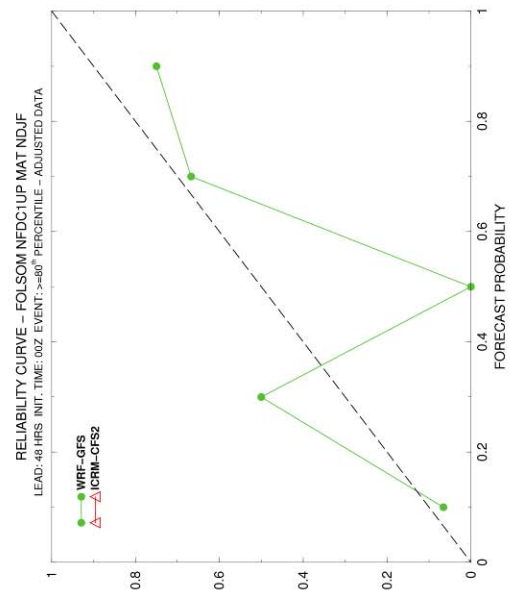
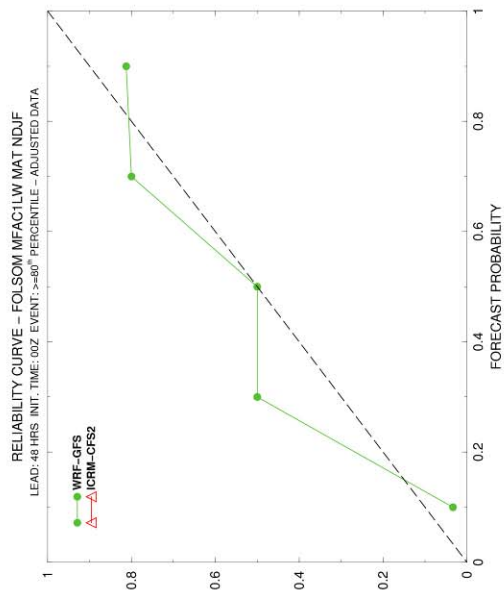


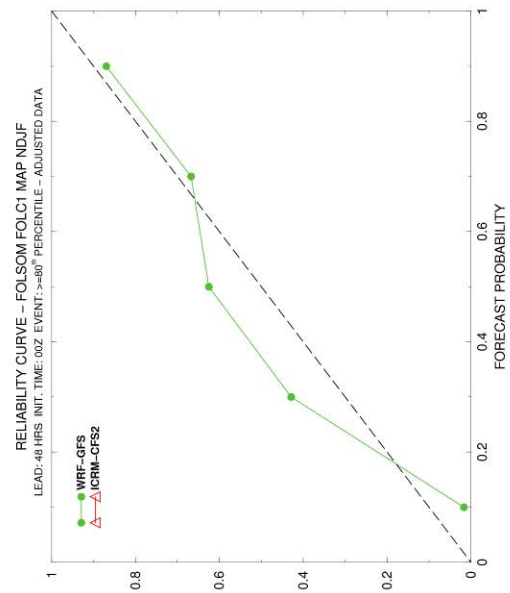
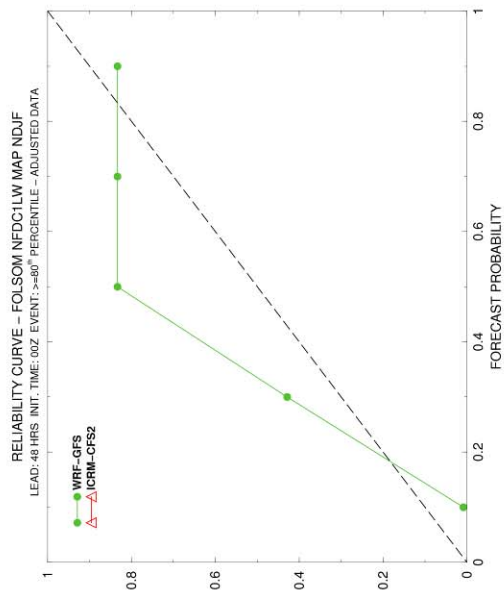
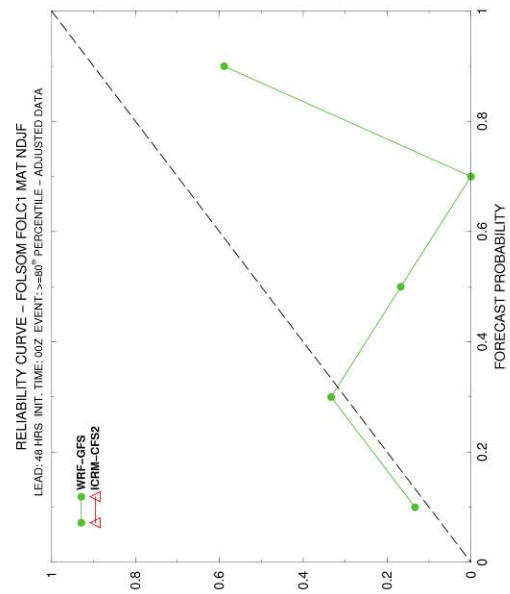
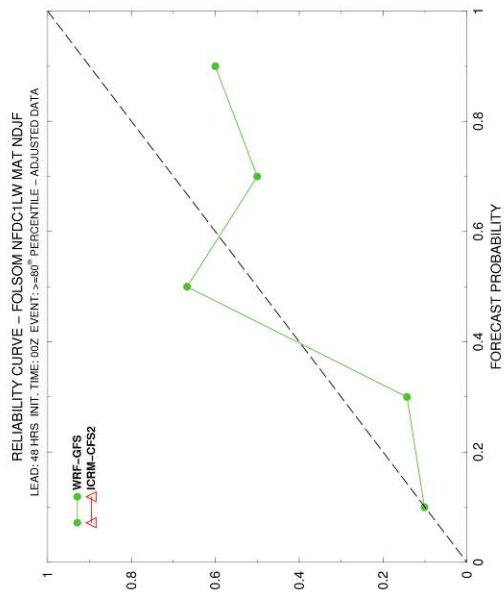


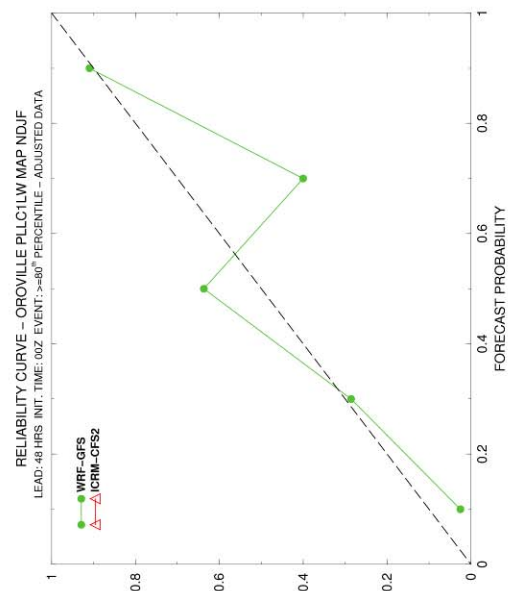
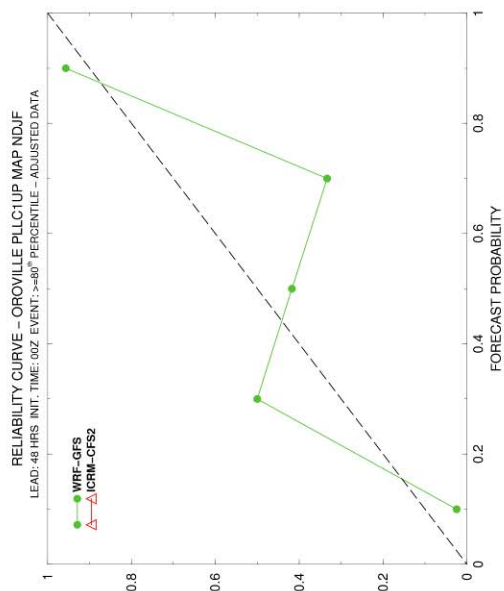
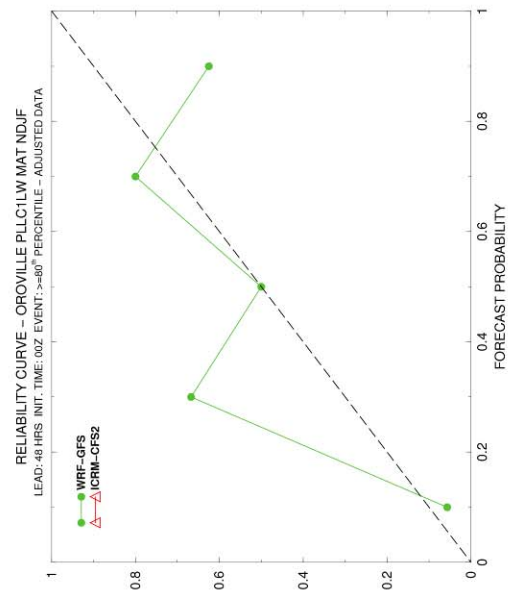
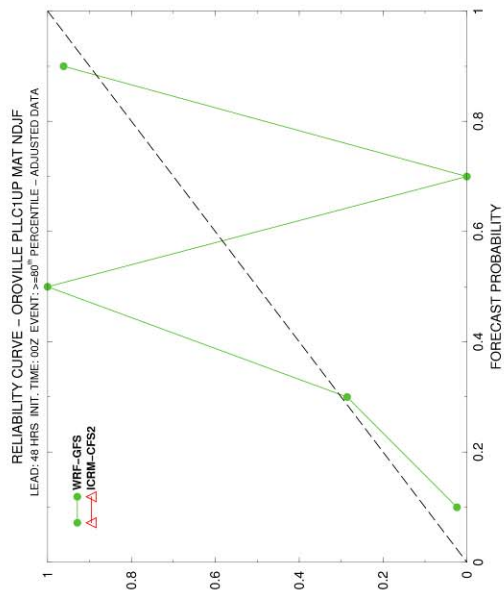


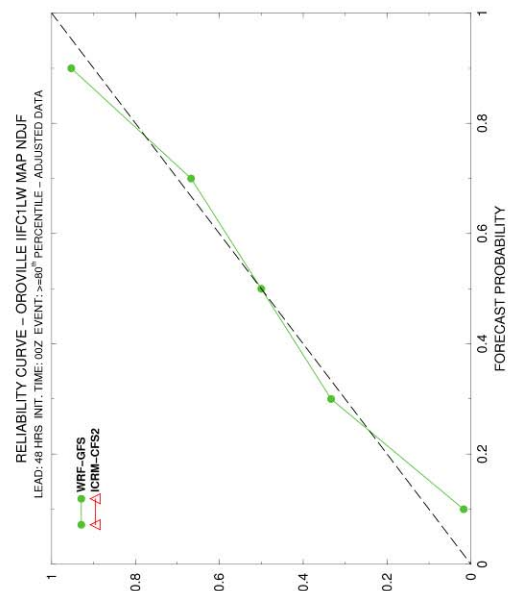
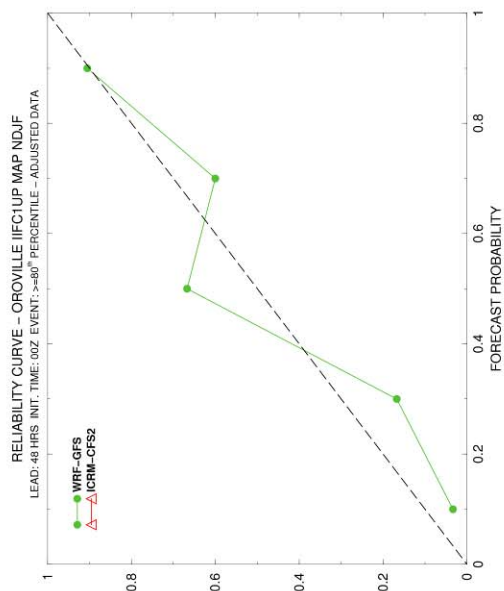
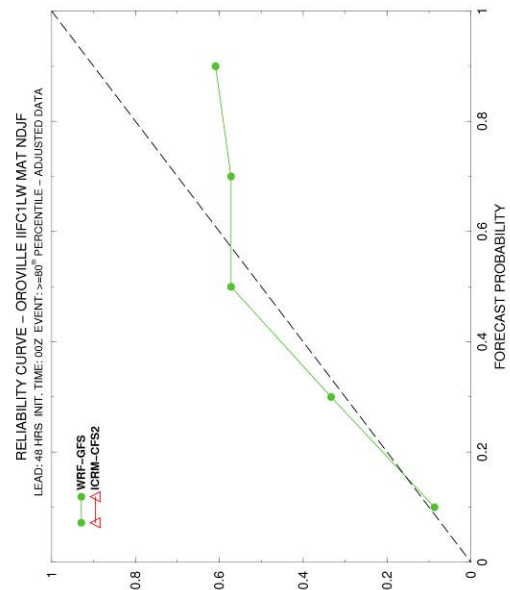
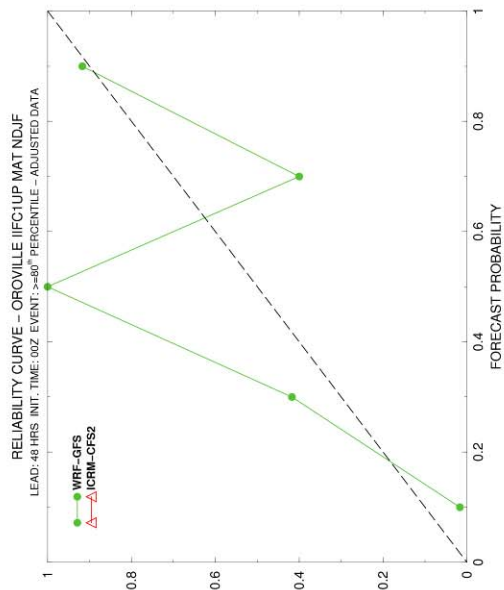


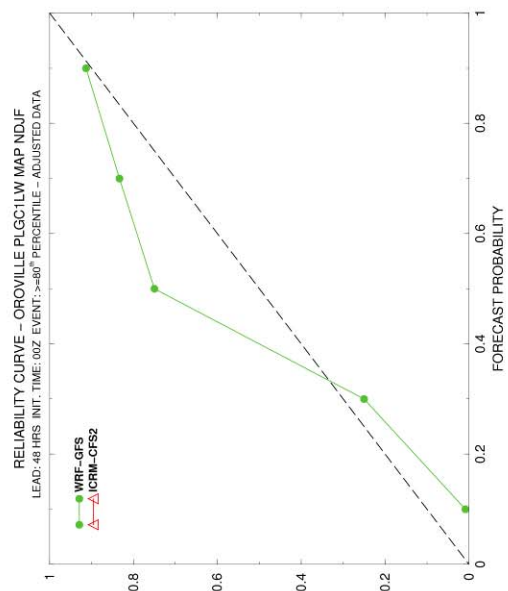
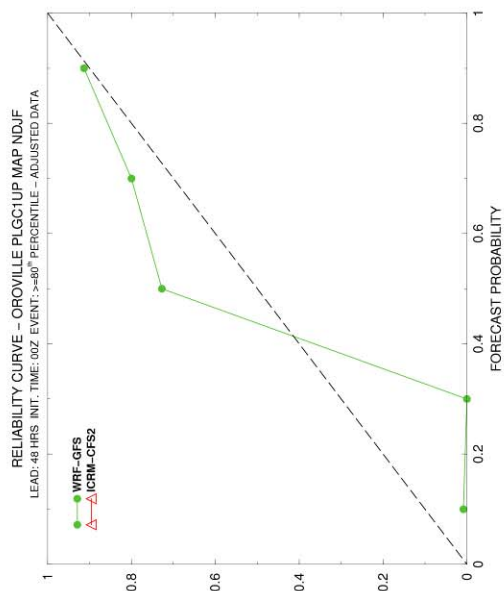
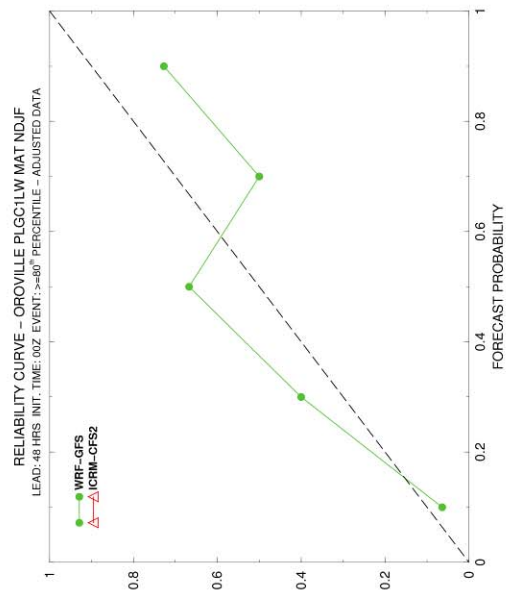
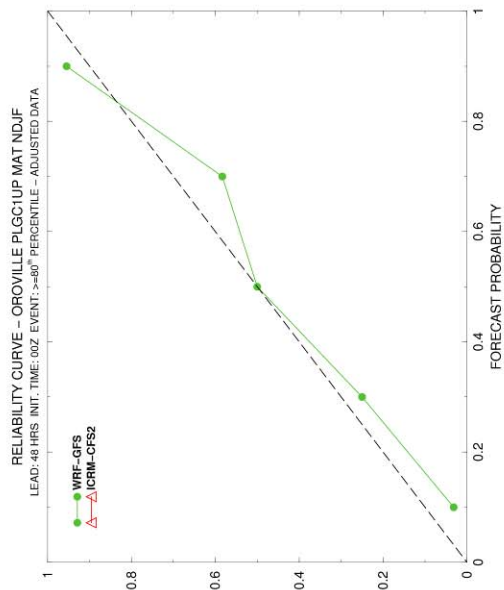


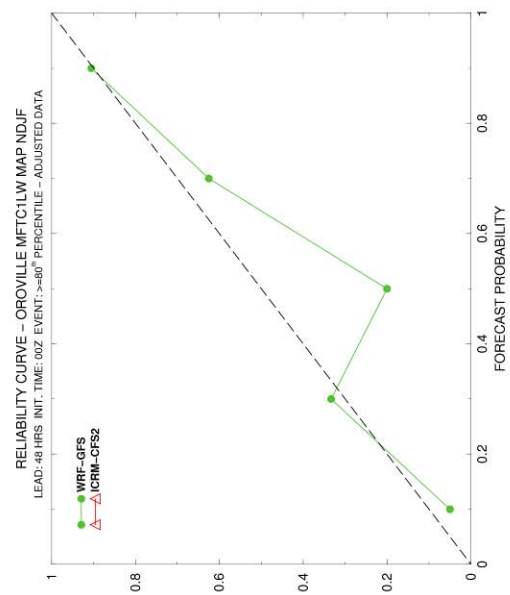
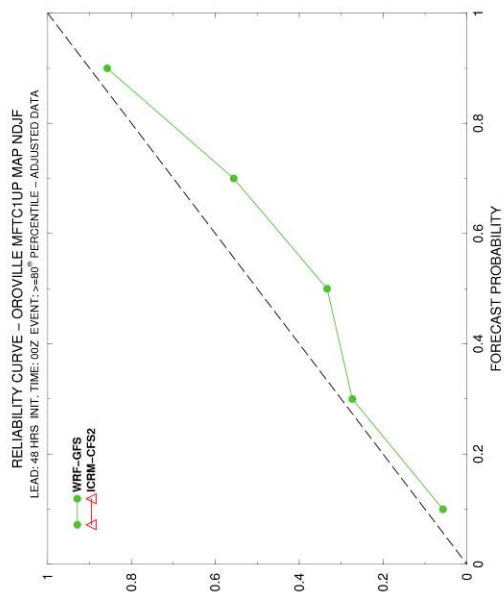
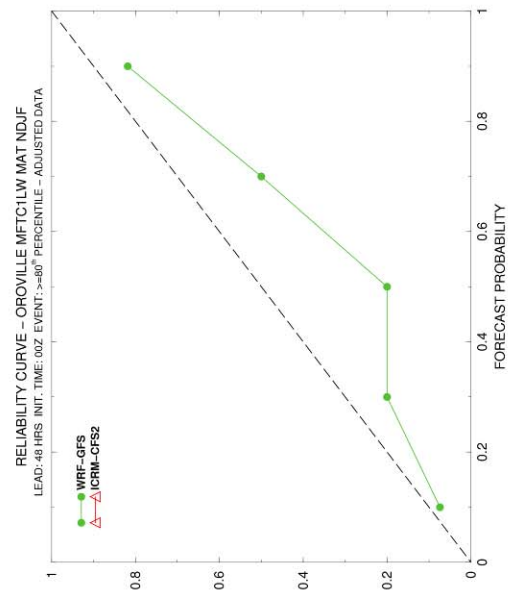
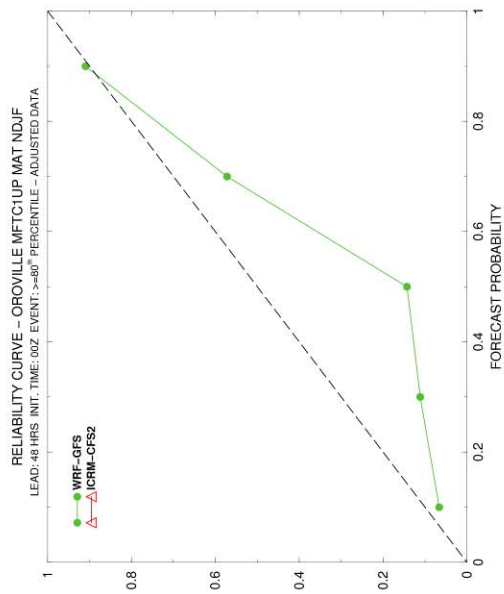


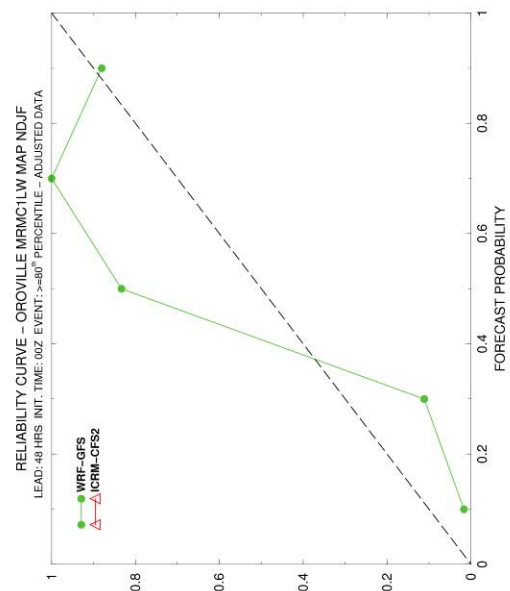
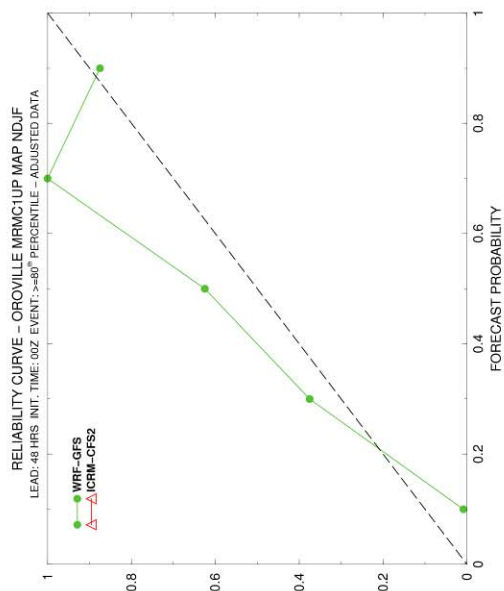
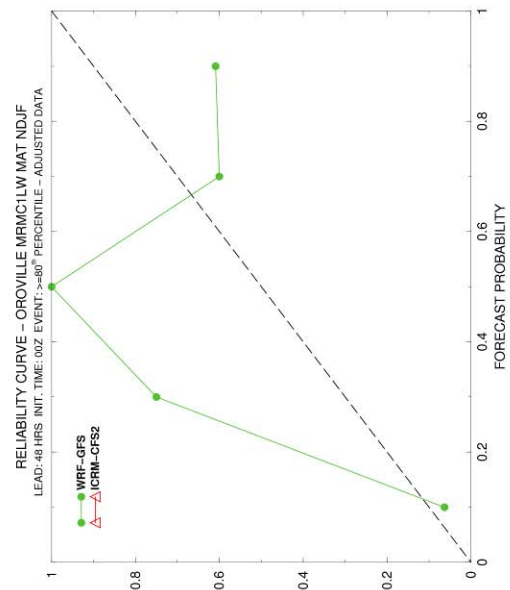
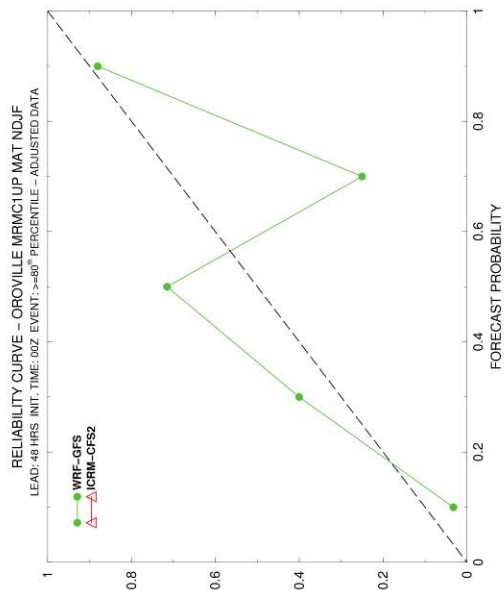


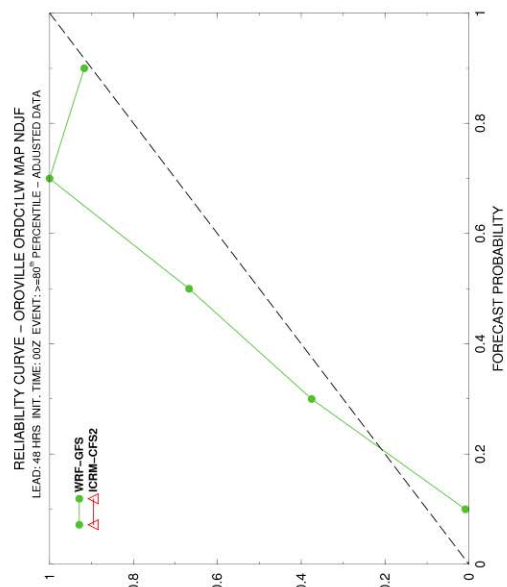
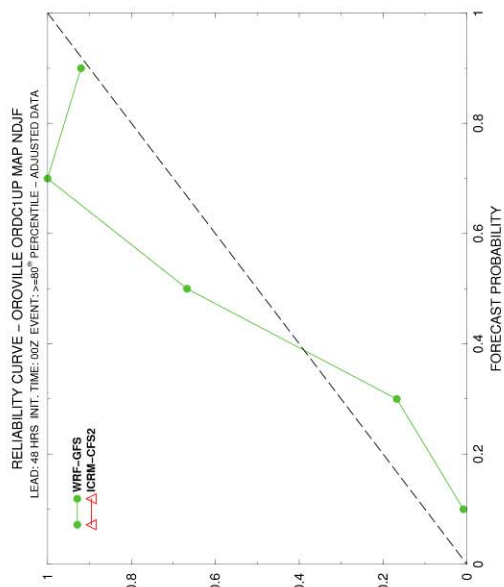
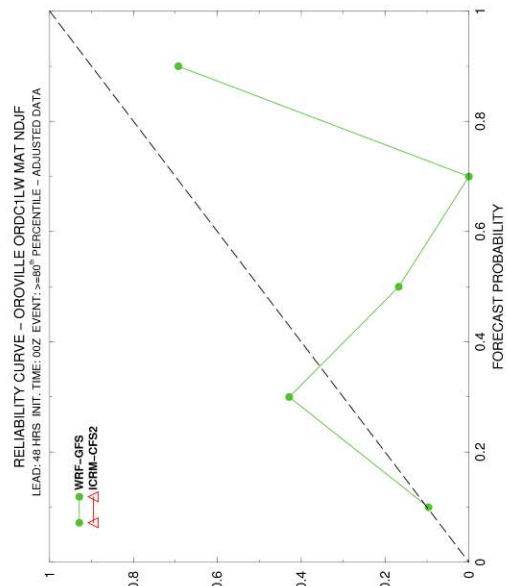
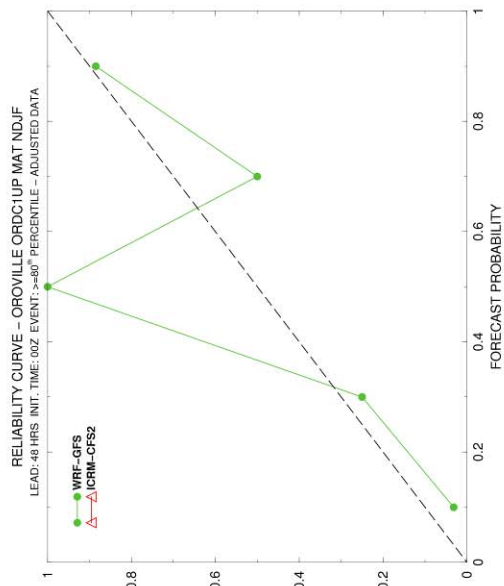


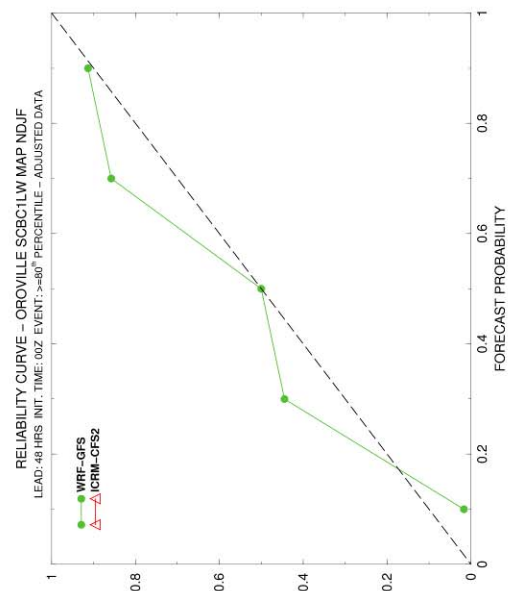
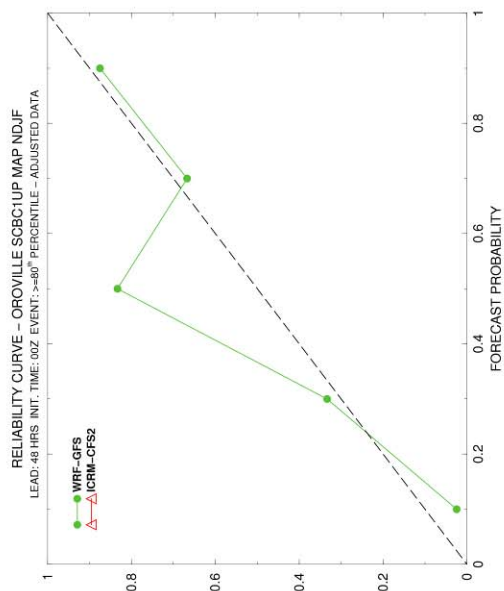
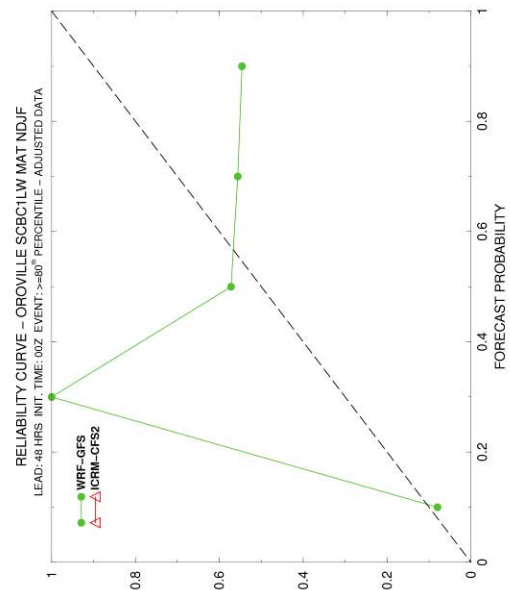
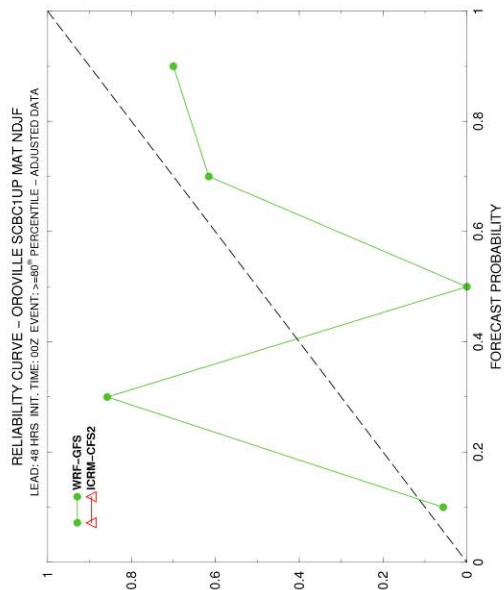


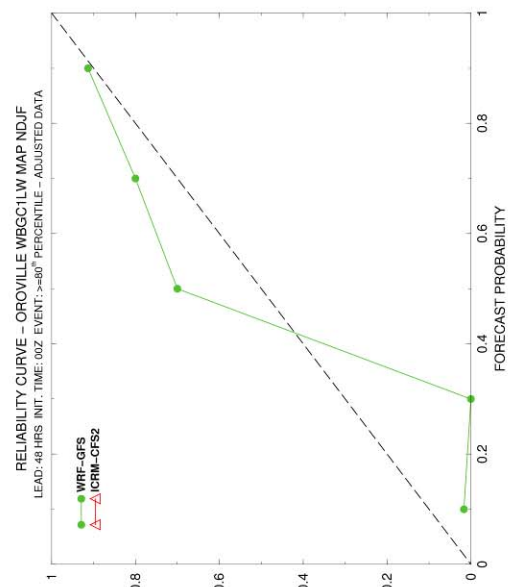
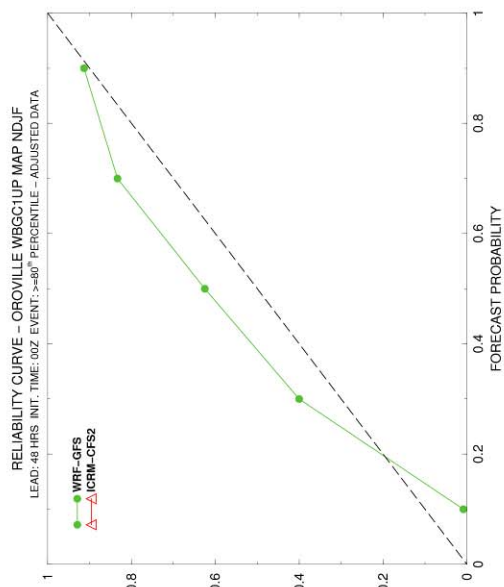
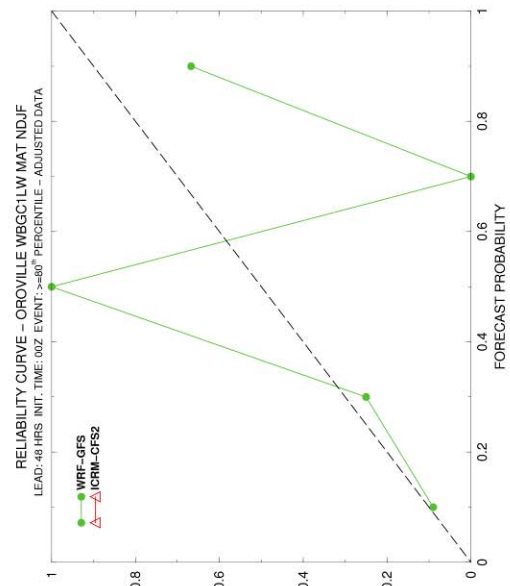
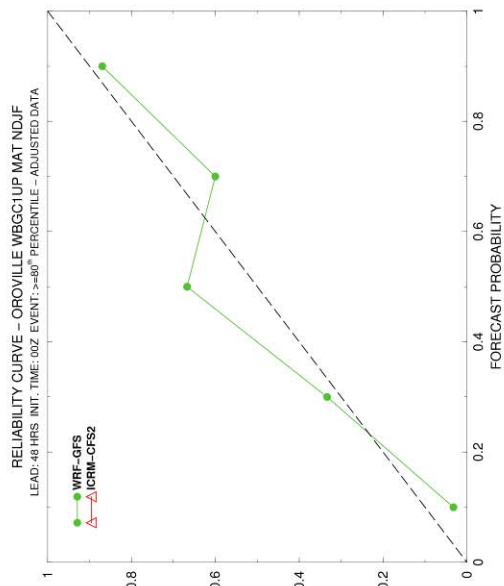


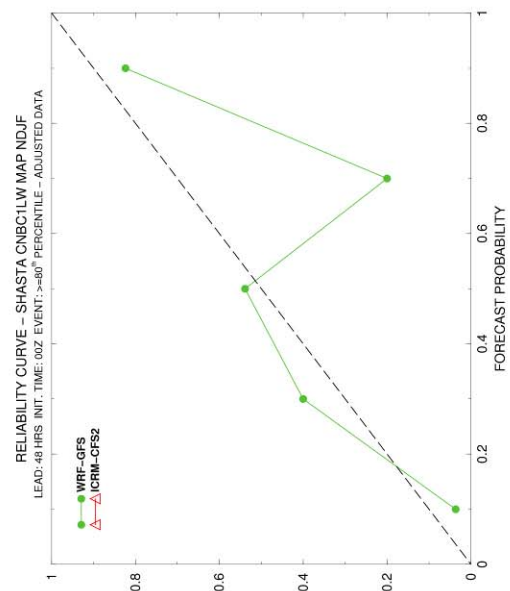
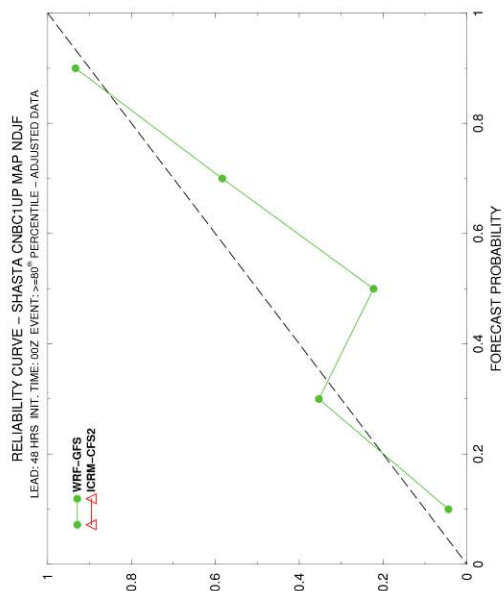
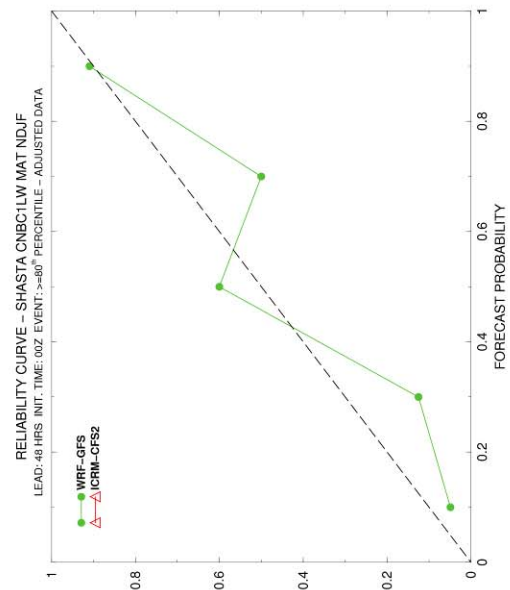
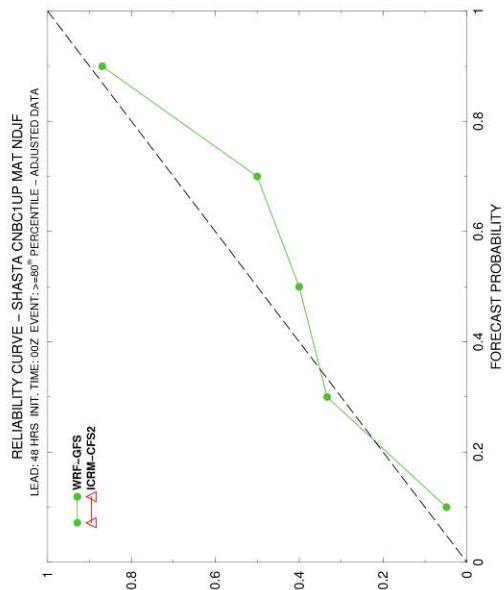


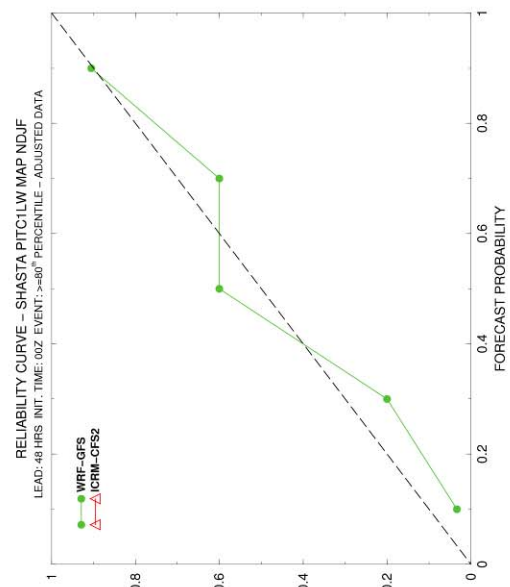
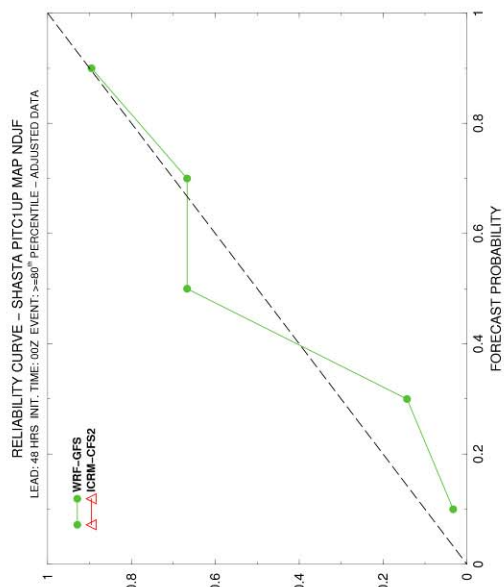
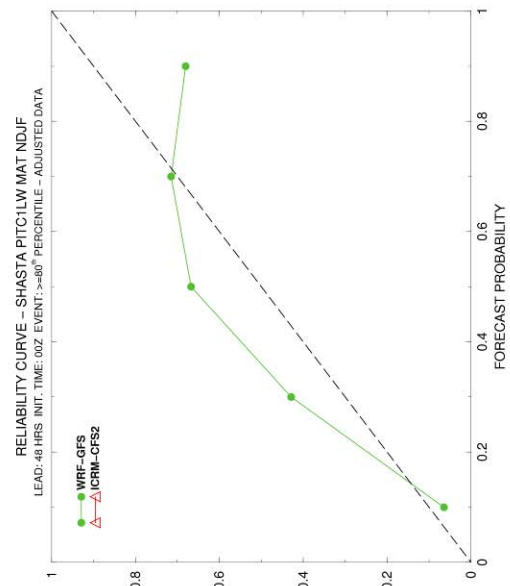
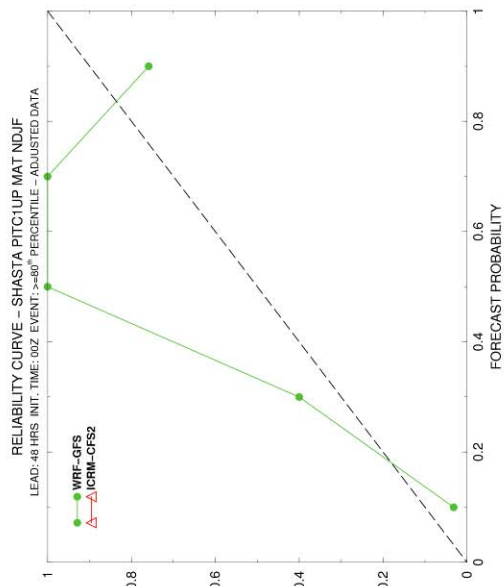


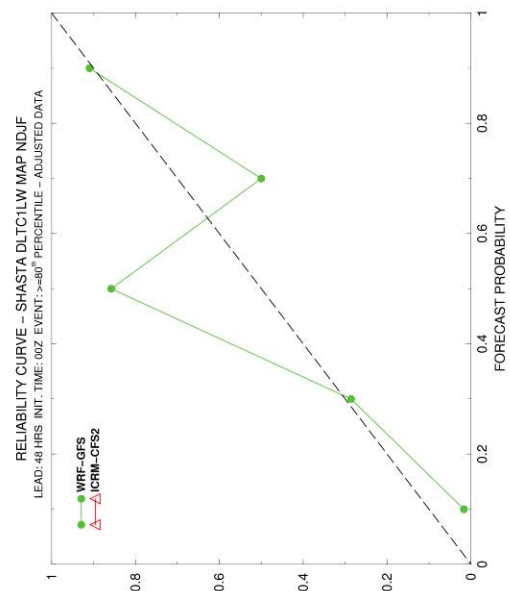
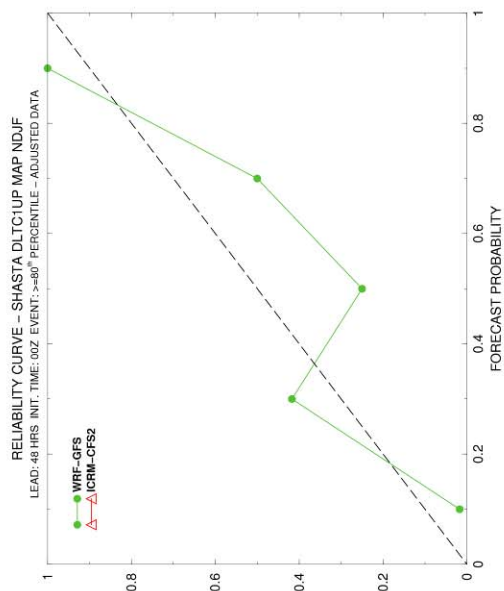
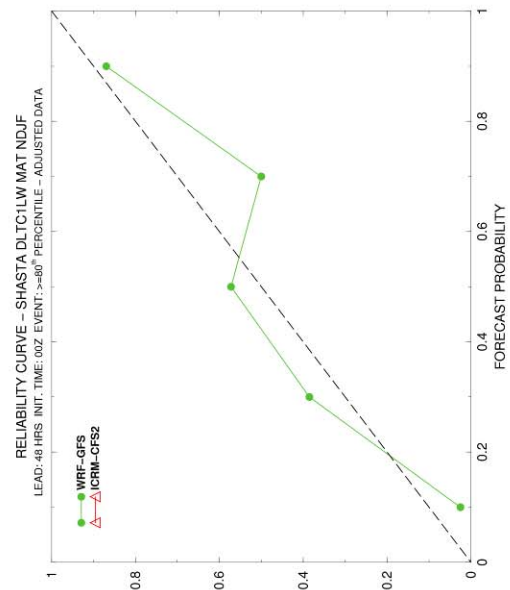
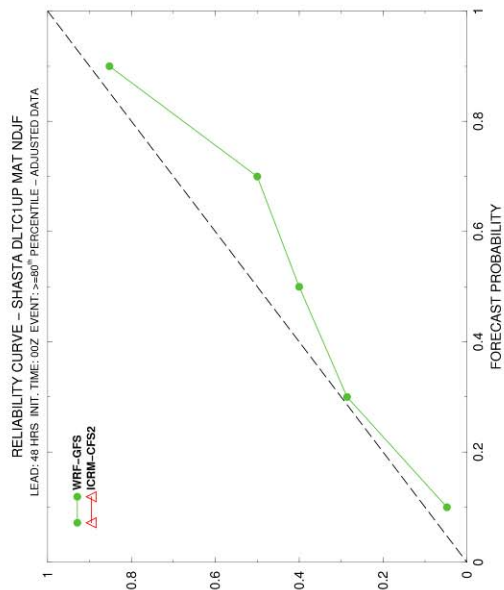


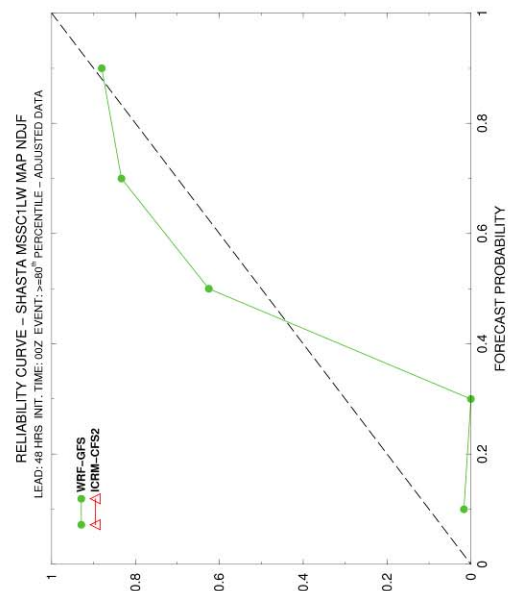
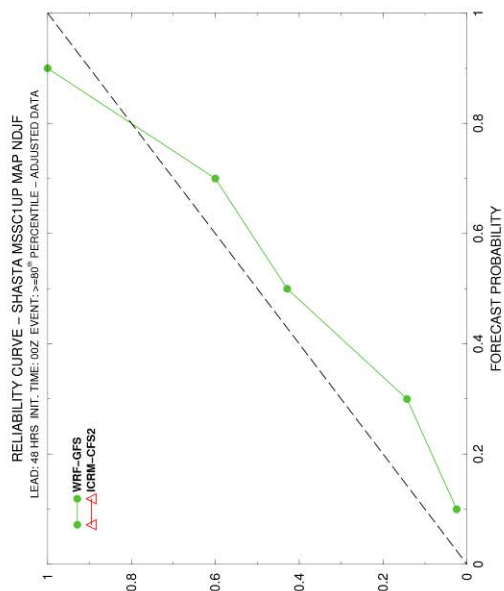
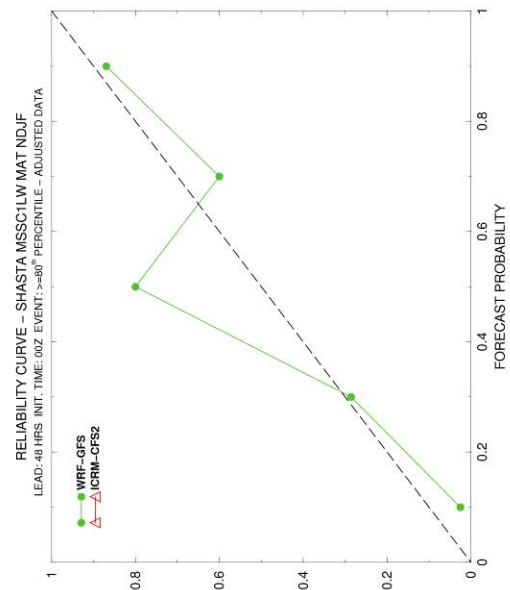
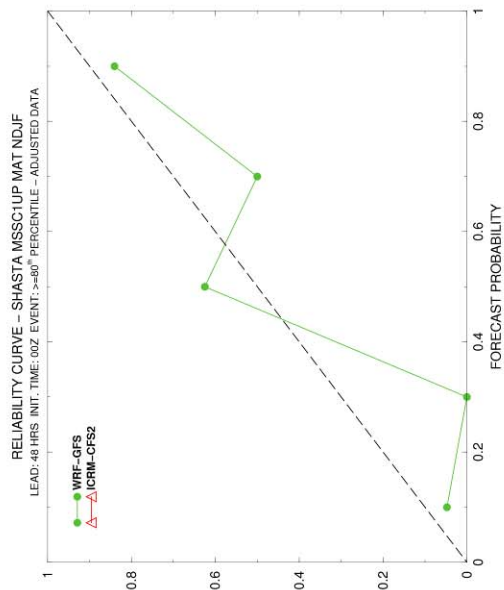


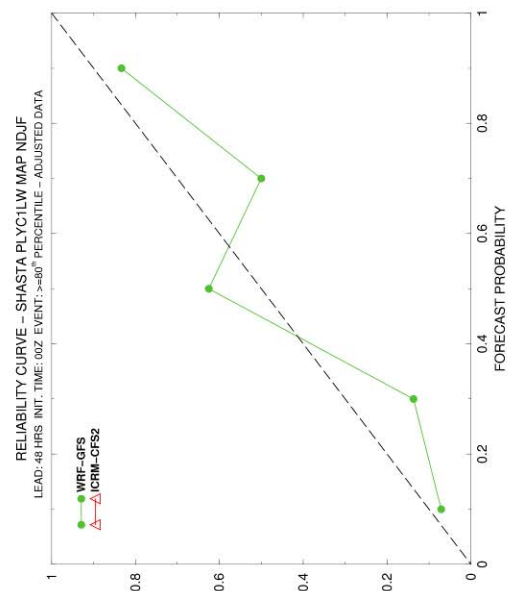
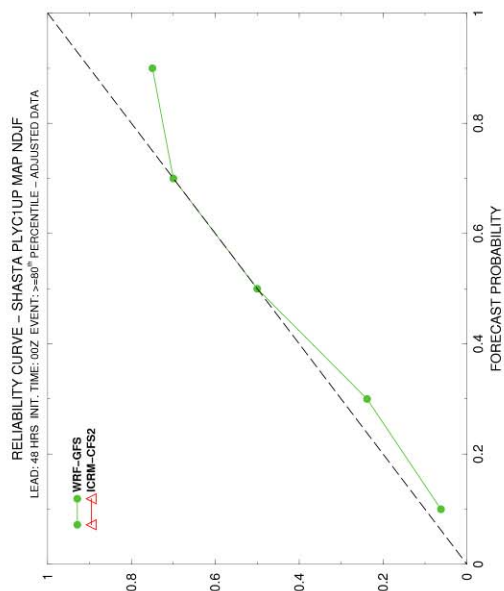
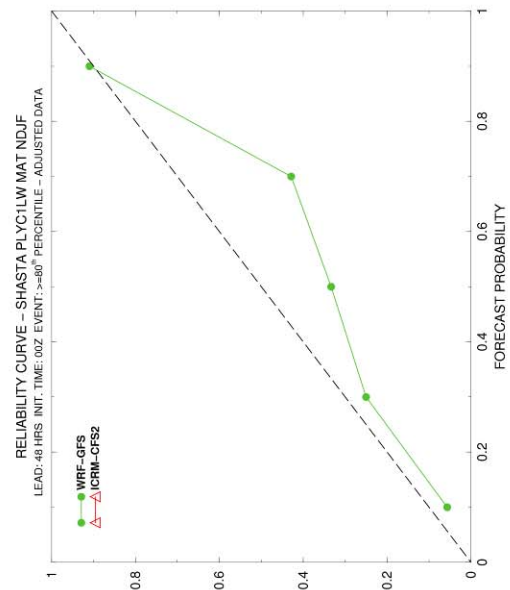
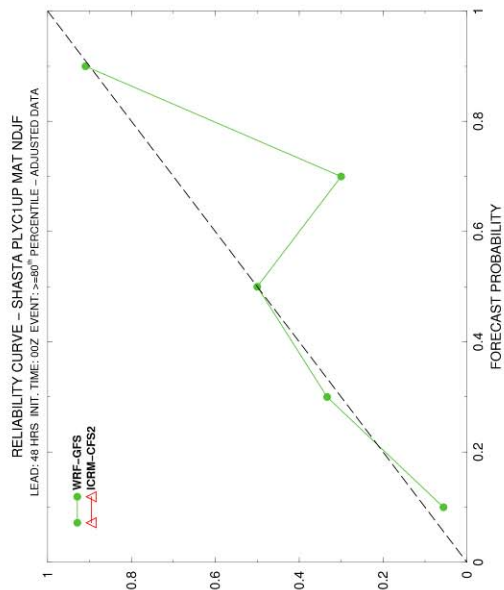


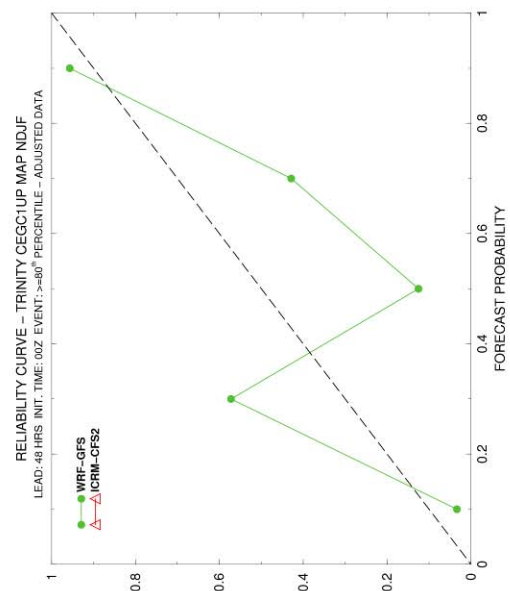
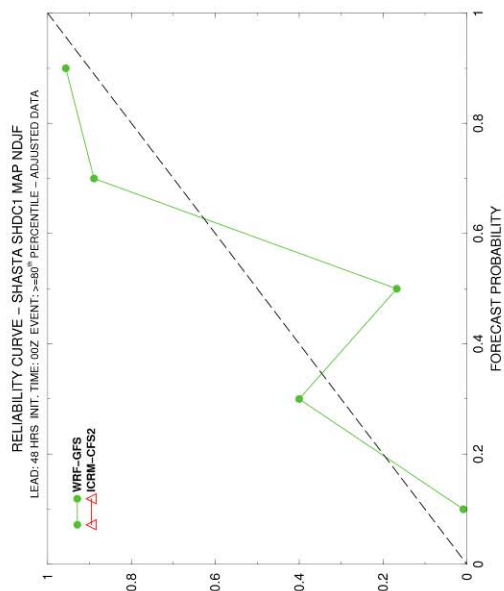
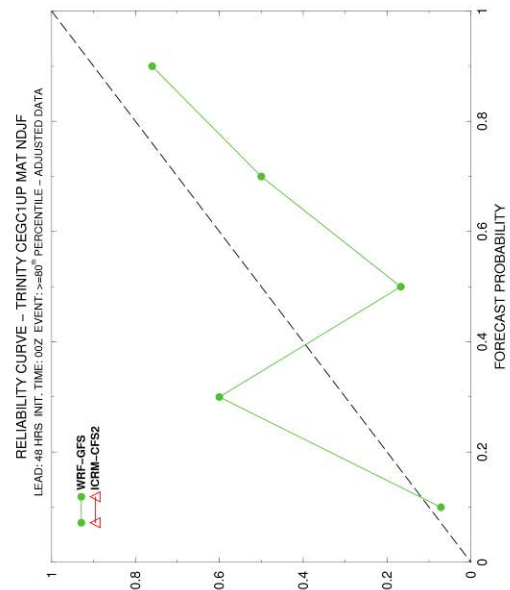
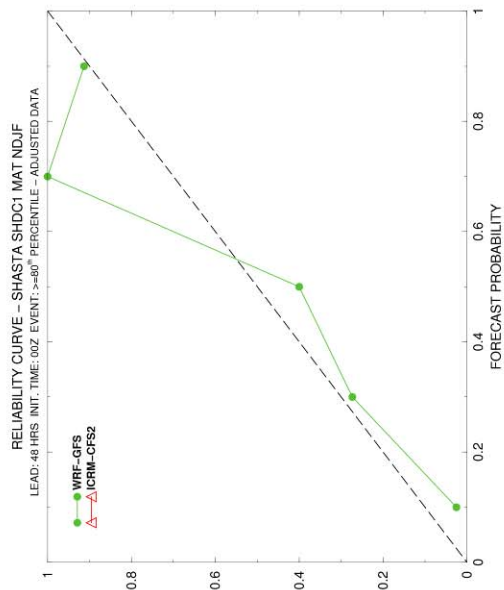


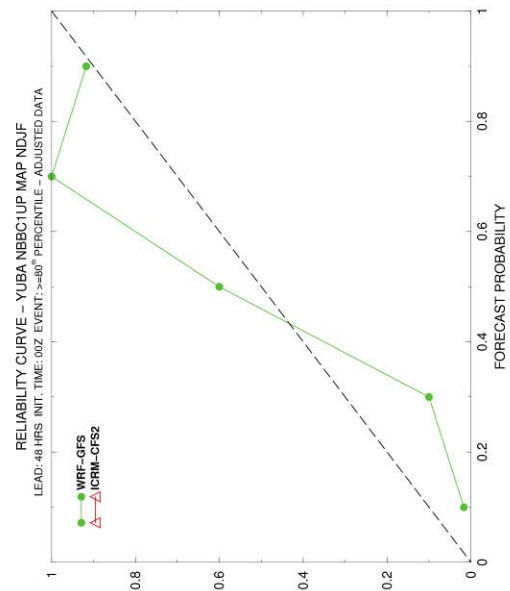
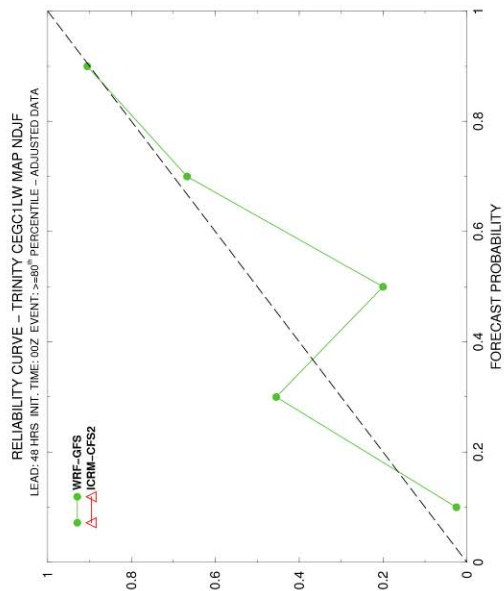
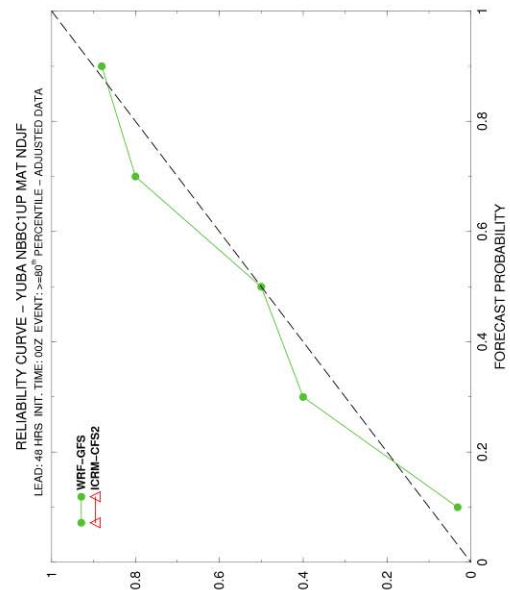
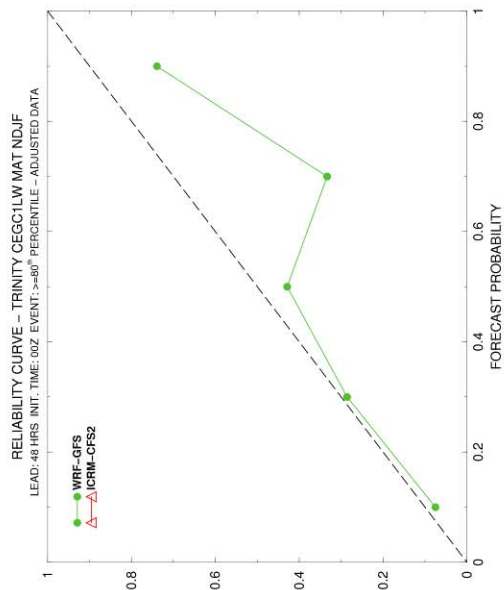


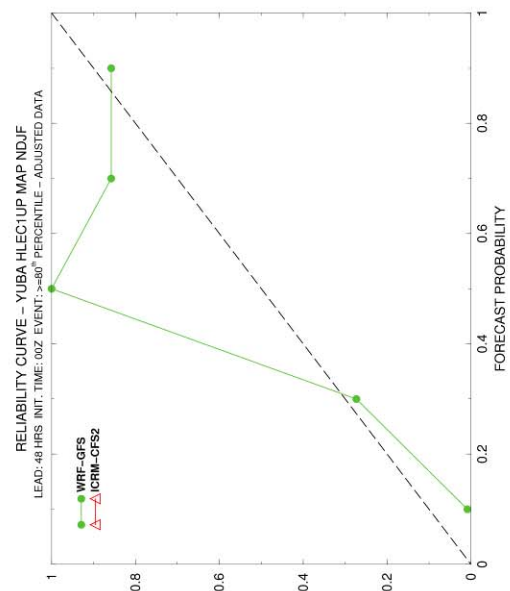
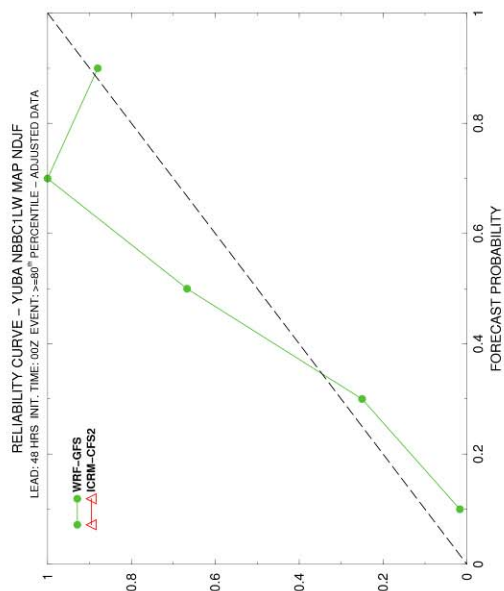
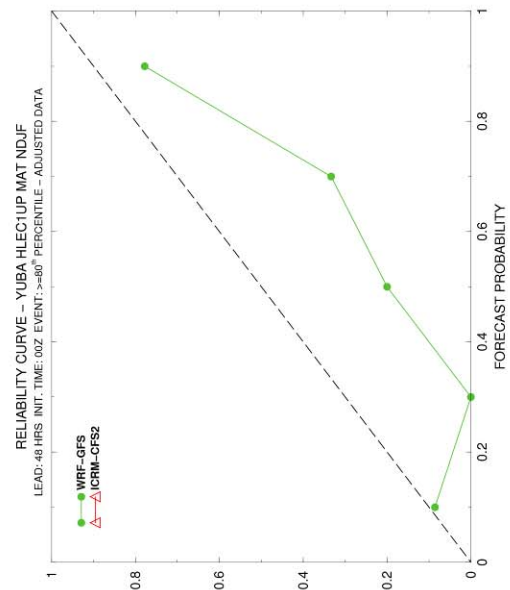
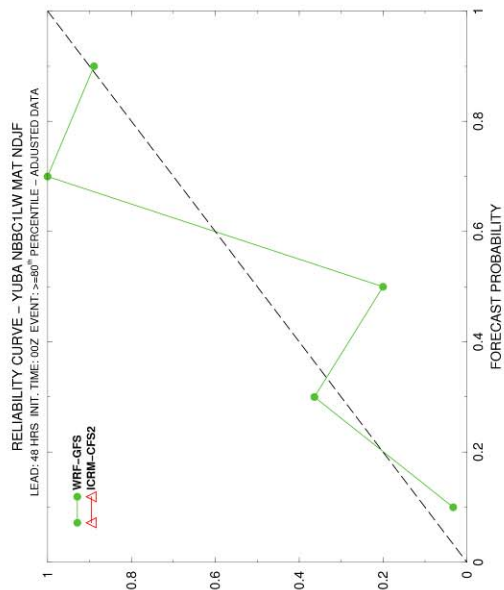


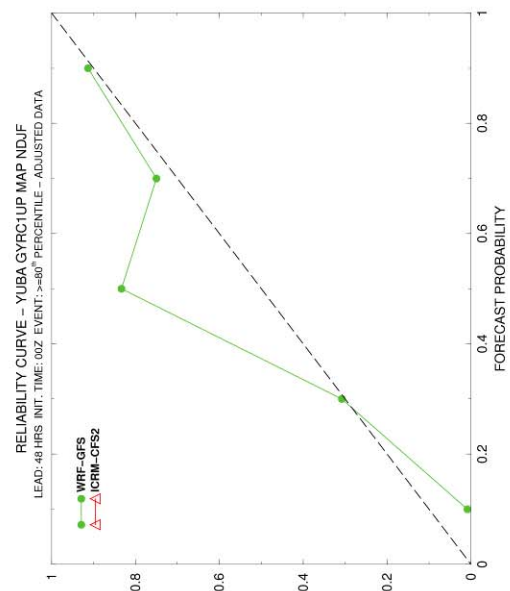
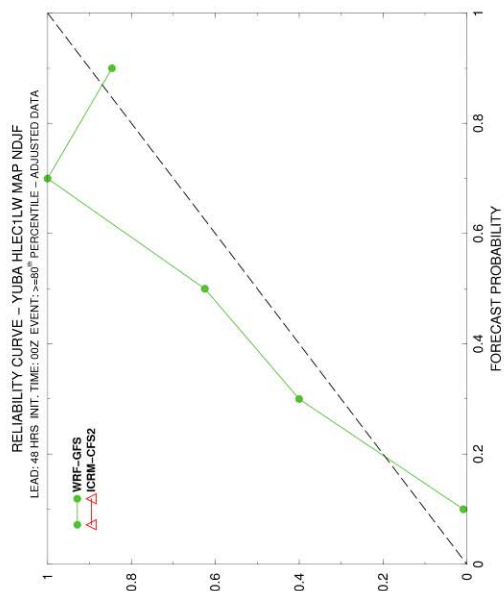
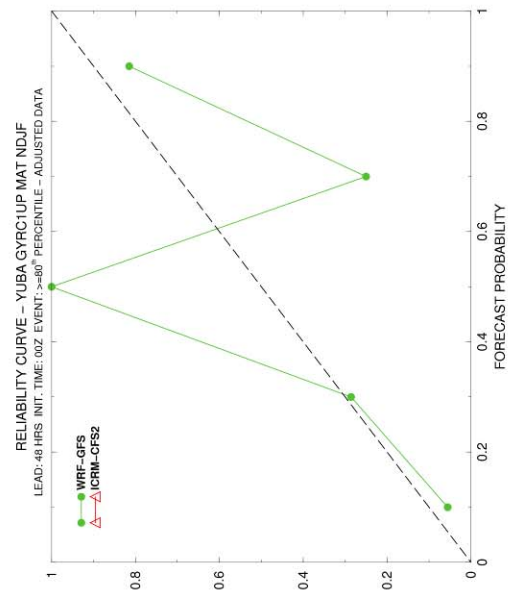
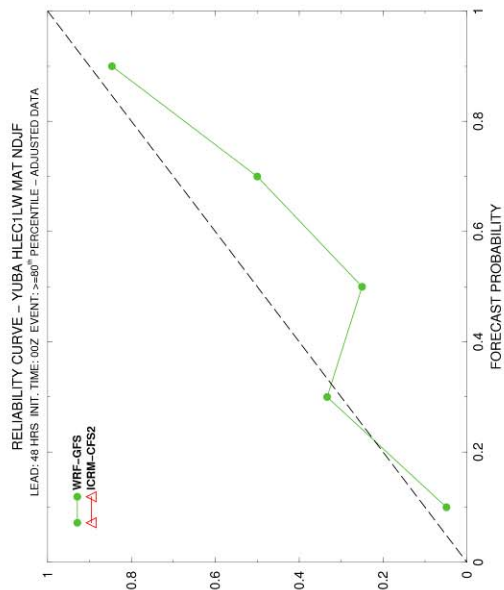












MAP and MAT Relative Operating Characteristic Analysis (Post Bias Adjustment)

In this section, first the plots of the area under the ROC curve (AROC) are presented for all the INFORM domain watersheds, and, subsequently, the individual subcatchment plots showing the ROC curve are shown for all cases available and for both the GFS-WRF and CFS2-ICRM models.

